Investigation of boiling heat transfer on small diameter tubes and tube bundles

by

Ebenezer Adom

A dissertation submitted for the degree of Doctor of Philosophy

School of Engineering and Physical Sciences

Heriot-Watt University

July 2007

ACADEMIC REGISTRY
Research Thesis Submission

Name:	EBENEZER ADOM		
School/PGI:	EPS		
Version: *(i.e. First, Resubmission, Final)*	FINAL	Degree Sought:	PHD

Declaration

In accordance with the appropriate regulations I hereby submit my thesis and I declare that:

1) the thesis embodies the results of my own work and has been composed by myself
2) where appropriate, I have made acknowledgement of the work of others and have made reference to work carried out in collaboration with other persons
3) the thesis is the correct version of the thesis for submission*.
4) my thesis for the award referred to, deposited in the Heriot-Watt University Library, should be made available for loan or photocopying, subject to such conditions as the Librarian may require
5) I understand that as a student of the University I am required to abide by the Regulations of the University and to conform to its discipline.

* *Please note that it is the responsibility of the candidate to ensure that the correct version of the thesis is submitted.*

Signature of Candidate:	A Dwjesc	Date:	20/7/2007

Submission

Submitted By *(name in capitals):*	EBENEZER ADOM
Signature of Individual Submitting:	A Dwjesc
Date Submitted:	20/7/2007

For Completion in Academic Registry

Received in the Academic Registry by *(name in capitals):*	J. TOUGH.		
Method of Submission *(Handed in to Academic Registry; posted through internal/external mail):*	HANDED IN		
Signature:	J. TOUGH.	Date:	20.7.07.

Abstract

Boiling heat transfer on the outside of small diameter tubes in the range of 1.8-3.0mm has been investigated. Pool boiling was investigated at nominal atmospheric pressure for each of the tubes in isolation. The experiment was varied by investigating the effect of bubbles from a second tube mounted below by varying the heat flux on the upper tube. The upper tube diameter was changed from 3.00 to 2.32 and 1.83mm and in each case the lower tube was 3.00mm. Experimental results showed that the upper tube heat transfer coefficient was enhanced due to the combined mechanism of translating bubbles and turbulent convection at low to moderate heat fluxes.

A compact tube bundle made up of 30 stainless steel tubes of outer diameter 3mm, pitch diameter ratio 1.5 and heating length of 50mm was designed to permit the measurement of flow boiling heat transfer coefficient from tubes within the bundle. The heat flux tested was in the range of 4-21 kW/m^2 and mass flux of 5.6-32.8 kg/m^2s using distilled water, R-113 and Flutec PP1 at nominal atmospheric pressure as the working fluids. Results obtained showed that the heat transfer coefficient was predominantly dependent on the heat flux as opposed to mass flux. Macro scale models were compared with the experimental results and none of these models predicted the experimental results well. The Confinement number (C_o) developed for flow boiling inside micro channels was applied to compact tube bundles and it was shown that confinement is expected to be significant for $C_o>0.63$. Photographic studies also showed that the diameter of the bubbles that were generated within the bundle were greater than the tube diameter. As such, the sliding bubbles mechanism played less significant role in contributing to the heat transfer coefficient. The recent three–state correlation developed by Thome et al for flow boiling heat transfer in micro channels was modified to predict the experimental results obtained using a compact tube bundle and it has been shown that the thin film evaporation was the dominant mechanism compared to the nucleate boiling. The results from the twin tube and compact bundle arrangement showed two regions coexist at any point in time; that part of the tube covered with liquid subject to nucleate boiling and the other part completely enveloped with vapour. This latter part is designated by the introduction of a factor p and this has been demonstrated experimentally and theoretically corroborated by a model based on a liquid part $(1-p)$ and vapour part p.

Dedication

This thesis is dedicated to my mum,

Faustina Asiedu,

my sisters,

Florence and Patricia

Acknowledgements

First and foremost I thank Almighty God for making it possible for me to be enrolled for this study. My sincere thanks goes to my advisors Dr Peter Kew and Professor Keith Cornwell who gave me the direction and support throughout this studies, without them this thesis will have not been possible.

I also wish to express my thanks to the entire technicians in the Mechanical and Electrical workshops of the School of Engineering and Physical Sciences for their constant support in the manufacture of my rig especially Richard Kinsella and Andrew Haston. I also acknowledge the financial support from James Watt Scholarship, Heriot-Watt University for the entire period of this research.

To my family, office mates and friends I say a big thank you for your moral support and encouragement and finally to Yaa Addae for your love.

Table of Contents

List of Figures

List of Tables

Nomenclature

A	*surface area (m^2)*
A_x	*cross sectional area (m^2)*
a_l	*liquid thermal diffusivity(m^2/s)*
Bo	*Bond number*
c	*specific heat capacity (J/kgK)*
C_o	*confinement number*
$C_{\delta o}$	*film thickness correction factor*
C_{sf}	*surface finish factor*
d	*diameter (m)*
d_a	*characteristic length (m)*
f	*pair frequency (Hz)*
Δx	*increment in x (m)*
ΔP_{tpf}	*two-phase pressure drop (N/m^2)*
ΔP_l	*liquid pressure drop (N/m^2)*
ΔP_{tps}	*static pressure drop (N/m^2)*
f	*friction factor*
F	*convection enhancement factor*
F_b	*buoyancy force (N)*
F_{PF}	*pressure correction factor*
F_s	*surface tension force (N)*
g	*acceleration due to gravity (m/s^2)*
G	*mass flux (kg/m^2s)*
G_t	*total mass flux (kg/m^2s)*
H	*head (m)*
h	*heat transfer coefficient (W/m^2K)*
h_{fg}	*latent heat of vaporisation (J/kgK)*
I	*current (A)*
k	*thermal conductivity (W/mK)*
l	*length (m)*
L_l	*length of liquid slug (m)*
L_{dry}	*length of dry film (m)*
L_p	*length of pair (m)*
L_{film}	*length of film (m)*

m	*mass flow rate (kg/s)*
M	*molecular mass (kg/mol)*
nf	*heat flux correction factor*
Nu	*Nusselt number*
n	*number of tube rows*
p	*pressure (N/m^2)*
p	*proportion*
p_{crit}	*critical pressure (N/m^2)*
p_r	*reduced pressure*
Pr_l	*liquid Prandtl number*
Pe	*Peclet number*
q	*heat flux (kW/m^2)*
q_o	*reference heat flux (kW/m^2)*
q_g	*heat generated (W/m^3)*
q_{tf}	*heat transfer across film (W)*
Q_{in}	*heat input (W)*
Q_{out}	*heat output (W)*
r	*radius (m)*
R	*resistance (Ω)*
Re	*Reynolds number*
Re_b	*boiling Reynolds number*
Re_l	*liquids Reynolds number*
Re_I	*impeller Reynolds number*
s	*bubble size (m)*
s_I	*transverse pitch (m)*
S	*boiling suppression factor*
t	*time (s)*
t_g	*vapour time (s)*
t_l	*liquid time (s)*
t_{dry}	*dryout time (s)*
T_{sat}	*saturation temperature (K)*
T_{wall}	*wall temperature (K)*
u	*velocity (m/s)*
u_g	*superficial vapour velocity (m/s)*
u_l	*superficial liquid velocity (m/s)*

U_p	*pair velocity (m/s)*
V	*voltage (V)*
v	*specific volume (m^3/kg)*
x	*thermodynamic quality*
X_{tt}	*Lockhart-Martinelli parameter*
z	*axial distance (m)*

Subscripts

b	*boiling*
cv	*convective*
f	fluid
g	*generated*
i	*inside/initial*
lower	*lower tube*
min	*minimum*
nc	*single phase natural convection*
nb	*nucleate boiling*
o	*outside*
out	*out*
sb	*sliding bubble*
sat	*saturation condition*
tf	*thin film*
tps	*two-phase static*
tpm	*two-phase momentum*
tpf	*two-phase friction*
upper	*upper tube*
v	*vapour*

Greek Symbols

α	*heat transfer coefficient ($kW/m^2 K$)*
$\Delta\theta$	*time (s)*
α_{film}	*film heat transfer coefficient (kW/m^2K)*
α_v	*vapour heat transfer coefficient (kW/m^2K)*
α_l	*liquid heat transfer coefficient (kW/m^2K)*
α_o	*ref heat transfer coefficient (kW/m^2K)*
ΔT	*change in temperature (K)*
μ_l	*dynamic viscosity of liquid (Ns/m^2)*
μ_v	*dynamic viscosity of vapour (Ns/m^2)*
ν_l	*kinematic viscosity of liquid (m^2/s)*
ρ_l	*liquid density (kg/m^3)*
ρ_g	*vapour density (kg/m^3)*
δ	*film thickness (m)*
δ_{min}	*minimum film thickness (m)*
δ_o	*initial film thickness (m)*
δ_{end}	*final thickness (m)*
σ	*surface tension (N/m)*
θ	*contact angle*
Φ_l	*two-phase friction factor*

List of Publications by Candidate

1. **Adom E.** , Kew P., Cornwell K., *Experimental Investigation of Boiling on Small Tube Bundles*, Proceedings of the 9th U.K National Heat Transfer Conference, Manchester 2005

2. **Adom E.** , Kew P., Cornwell K., *Experimental Investigation of Boiling Heat Transfer On Two tubes Arranged Horizontally Above Each Other*, Proceedings of the 9th U.K National Heat Transfer Conference , Manchester , 2005

3. **Adom E.,** Kew P., Cornwell K., *Enhancement of Boiling on a Small Diameter Tube Due to Bubbles from Below.*, Proceedings of the 5th International Conference on Enhanced, Compact and Ultra-Compact Heat Exchangers 11-16 September, 2005, Whistler Canada. (Also presented at the 23rd HEXAG Meeting at London South Bank , University)

4. Kew, P., **Adom, E,** Cornwell, K. *Heat Flux Controlled Boiling in Confined Spaces.* Proceedings of the 13th International Heat and Mass Transfer Conference , Sydney, Australia, 2006

5. **Adom E,** Kew. P. Cornwell K. *Boiling on Small Diameter Tube Bundle.* Applied Thermal Engineering (Under Review)

Chapter 1

BACKGROUND

1.1 Introduction

Boiling heat transfer is a widely studied area in engineering due to its profound ability to transfer heat at very low superheat. Early studies in the area of boiling heat transfer concentrated efforts on understanding boiling phenomenon and the derivation of empirical correlations to predict the mechanism of nucleate boiling. Over the years, boiling heat transfer has been applied to the design of industrial components such as the kettle reboiler for the petroleum industries and correlating models have been developed to predict the heat transfer coefficient in such systems. In recent times with the introduction of process intensification, there is the drive towards reducing large industrial components to small units whilst at the same time maintaining the operating duties of such devices. The introduction presents some background information on the following:

- Pool boiling
- Flow boiling
- Applications of boiling heat transfer
- Process intensification
- Compact heat exchangers

1.2 Pool boiling

Pool boiling is distinct from single phase forced convection in that the pool boiling heat transfer coefficient is a strong function of the temperature difference between the heated wall and the bulk liquid. Basically there are three mechanisms occurring during pool boiling and they include the following: (see Figure 1.1), natural convection, nucleate boiling and film boiling.

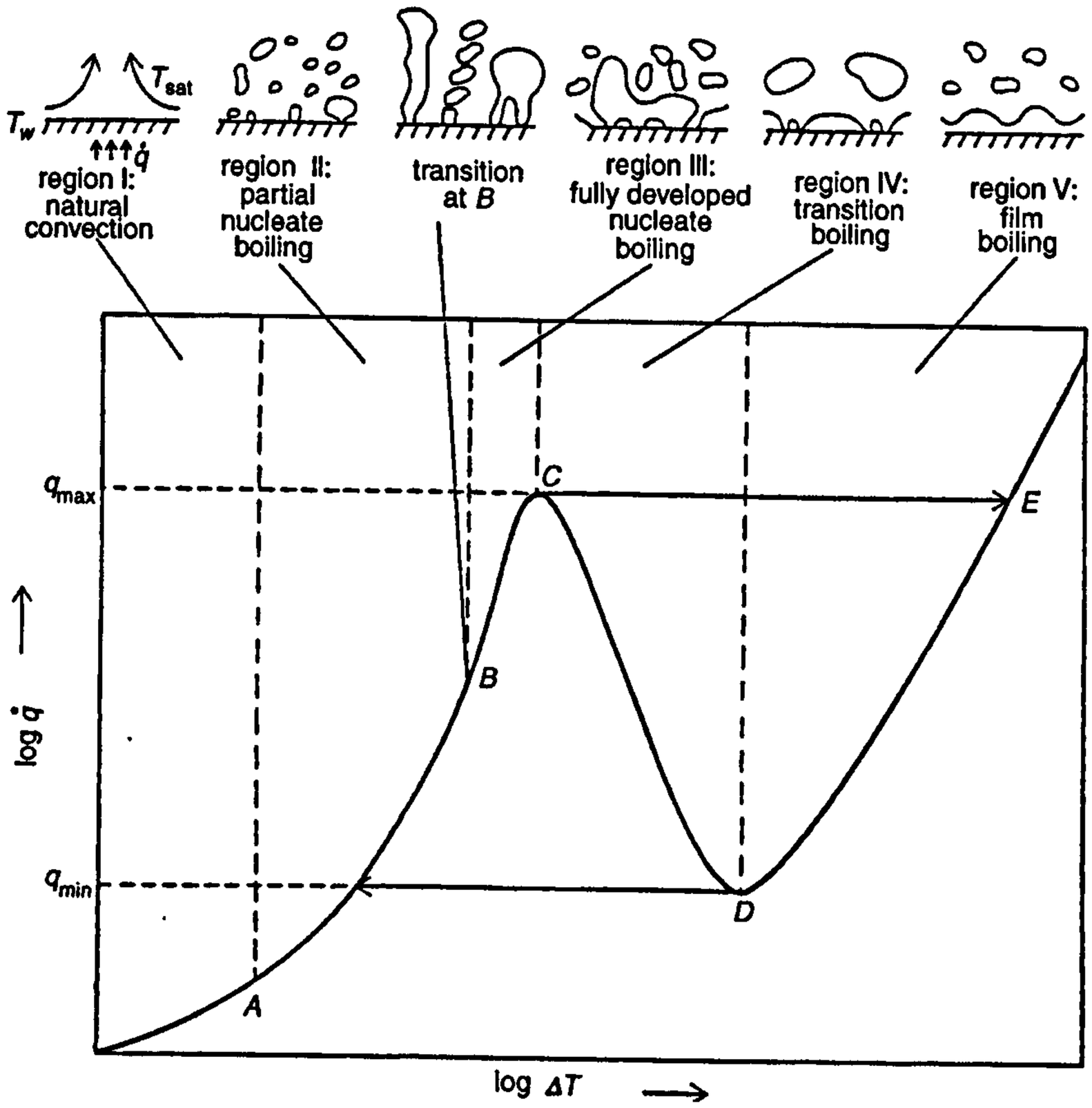

Figure 1.1 Pool boiling graph for a plain smooth tube, Kandlikar [1]

Figure 1.1 represents the boiling curve outside a typical smooth tube in distilled water. As heat is applied to the tube the wall temperature is raised from the initial temperature of zero, thus single-phase natural convection is in effect till nucleation occurs. The wall temperature has to reach a minimum value before boiling occurs and thus natural convection occurs up to this point. Once partial nucleate boiling begins and bubbles begins to grow and depart from the various sites of the heated wall, heat transfer is enhanced by the boiling process and heat flux passing through the heated tube increases to the higher value at point 'B'. At this point fully developed nucleate boiling has been achieved. This regime is characterised by discrete bubbles growing and departing from the heated wall at numerous nucleation sites at low heat fluxes. As the wall superheat continues to rise, a maximum in the heat flux is reached and this point is called the maximum heat flux. This maximum heat flux (q_{max}) is due to hydrodynamic instability in the vapour jets leaving the heated wall which in turn causes a vapour film to form over portions of the heated wall. This regime is characterized partial and intermittent contact of the working fluid with the heated wall and reduces the rate at which heat can be transferred from the fluid to the heated wall. This regime is bounded at high

superheats by point 'D' the minimum heat flux (q_{min}). The region between points C and D on the boiling curve is termed the transition boiling. At this point the liquid is no longer in contact with the heated wall because of the rapid rate of vapour generation in the vapour film covering the surface. The last regime on the curve is the film boiling which is bounded at lower heat fluxes (q_{min}) by the minimum heat flux and at its maximum by the melting temperature of the wall material. The region between D and E is characterised by a stable vapour film that covers the heated wall. This process is inefficient and results in low heat transfer rate and large wall superheats. As a result of vapour blankets, film boiling is avoided in most thermal design.

1.3 Nucleation

Nucleation is a process in which finite size clusters of molecules encompassing properties of the second phase appear in the host liquid. This can be the initiation of bubble formation during boiling. The nucleation process is normally divided into two-categories: homogeneous and heterogeneous nucleation. Homogenous nucleation refers to the formation of vapour-liquid interface (bubble) in superheated liquid in the absence of any pre-existing gas/vapour nuclei and not on any solid surfaces. Heterogeneous nucleation is a process in which bubbles forms discretely on pits, scratches, grooves on a heated surface submerged in a liquid.

1.3.1 Heterogeneous nucleation in pool boiling

The ideal cavity is shown in the Figure 1.2 having a circular opening. As the bubble grows its radius of curvature changes. The minimum radius of curvature of the bubble occurs when the bubble forms a hemisphere at the cavity mouth. The radius of curvature is then, equal to the radius R of the cavity opening.

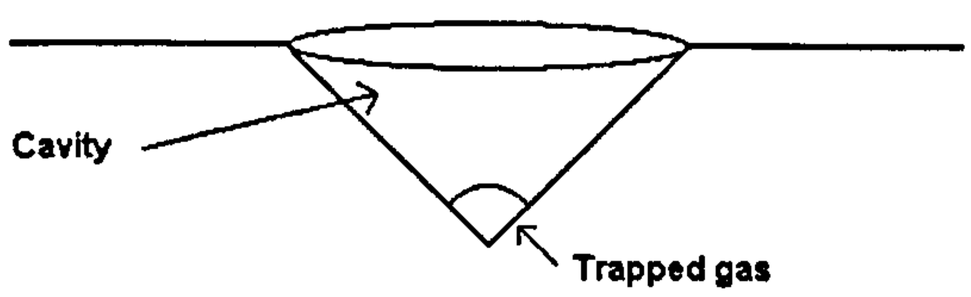

Figure 1.2 Ideal nucleation cavity

If the pressure inside the bubble is p_b (N/m^2), then

$$p_b = p + \frac{2\sigma}{r} \qquad (1.1)$$

Where p is the pressure in the liquid and r is the bubble radius. Now p_b is maximum when r=R (cavity radius). So for the bubble to grow the following condition must hold;

$$T_w > T_{sat} + \frac{dT}{dP}(p_B - p) \qquad (1.2)$$

The slope of vapour pressure curve can be found from the Clausius –Clapeyron equation as depicted in Figure 1.3

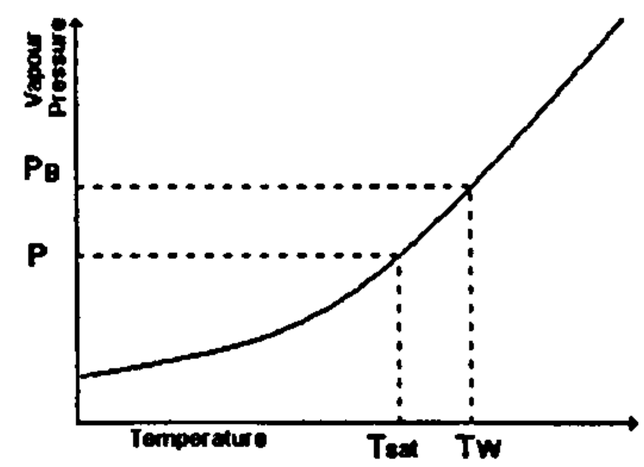

Figure 1.3 Vapour pressure curve superheat required for nucleation.

$$\frac{dp}{dT} = \frac{h_{fg}}{(v_g - v_l)T_{sat}} \qquad (1.3)$$

where h_{fg} is the latent heat of vaporisation, T_{sat} is the saturation temperature and v_g and v_l are the specific volumes of the gas and liquid. Then if $v_g >> v_l$, then

$$\frac{dT}{dp} = \frac{T_{sat}}{h_{fg}\rho_g} \qquad (1.4)$$

And the inequality in equation (1.2) becomes

$$T_w > T_{sat} + \frac{2\sigma T_{sat}}{Rh_{fg}\rho_g} \qquad (1.5)$$

If ΔT_{sat} is the value of $(T_w - T_{sat})$ at which nucleation starts then the cavity radius is given by

$$R = \frac{2\sigma T_{sat}}{\rho_g h_{fg} \Delta T_{sat}} \tag{1.6}$$

Using typical values for water at 1 bar, ΔT_{sat} of 5 K, so substitution values into equation (1.6) we have

$$R = \frac{2 \times 0.059 \times 373}{2257000 \times 0.598} = 6.5 \mu m$$

Thus from the calculation above the cavity size is in the micron range, and if the cavity size of a surface is known then the wall superheat required to start nucleation can be calculated.

1.4 Heat transfer in nucleate boiling

Almost all the models for the calculation of heat transfer start from the fact vapour bubbles are formed from the nuclei that are caused by the roughness of the heating surface. However there are many different opinions concerning how energy is transferred from the heating surface.

Jakob and Linke [2] were among the first researchers in this area. Their model assumed that, by formation, growth and departure of vapour bubbles, strong local flows close to the wall produced can be described by the dimensional numbers with the equations:

$$\frac{\alpha b}{k_l} = 42.4 \left(\frac{q}{\rho_v h_{fg} w} \right)^{0.8} \tag{1.7}$$

where b is the Laplace constant given as ;

$$b = \sqrt{\frac{2\sigma}{g(\rho_l - \rho_g)}} \tag{1.8}$$

The model satisfactorily predicted the boiling heat transfer for water, carbon tetrachloride and several other fluids at atmospheric pressure but it however proved unsatisfactory at other pressures.

One of the first equations to determine the influence of pressure on heat transfer was that of Rosehnow [3]. He agreed with Jakob and Linke [2] in assuming that heat transfer during nucleate boiling is traceable principally to the convective exchange between the heating surface and the adjacent liquid. The turbulent flow in the superheated liquid layer close to the wall necessary for this is produced according to this conception by the vapour bubbles being formed at the heating surface. The convective heat exchange during turbulent flow can be represented by;

$$Nu = c\,\mathrm{Re}^{m}\,\mathrm{Pr}^{n} \tag{1.9}$$

The characteristic length in the Nusselt and Reynolds numbers is the bubble departure diameter according to equation;

$$d_a = 0.851\beta_0\sqrt{\frac{2\sigma}{g(\rho_l - \rho_g)}} \tag{1.10}$$

and velocity of the bubble was given as;

$$v = \frac{q}{\rho_g h_{fg}} \tag{1.11}$$

Forster and Zuber [4] also assumed that heat is transferred principally by convection during nucleate boiling. Like Rosehnow [3], they used the power law which is similar to that of the equation developed by Rosehnow. The characteristics length and velocity were due to that of bubble radius and bubble growth rate.

Han and Griffith [5] subdivided the heating surface into two regions as shown in Figure 1.4 . In the region 1, called the region of 'bulk-convection' is formed by unsteady heat conduction from the heating surface to the adjacent liquid, a superheated boundary layer, which in turn induces bubble formation at nucleation sites of the heating surface. In this region, which corresponds according to Han and Griffiths [5] to twice the bubble

diameter, a bubble displaces the superheated boundary layer from the heating surface. After reaching the departure diameter the bubble frees itself from the heating surface and carries with it the previously dislodged warmer boundary layer liquid into the colder liquid core and mixes itself with this. Simultaneously the colder liquid flows into the heating surface and into the space behind the departed bubble. A thermal boundary layer is formed once again by the intensive heat exchange as a result of unsteady heat conduction. In region 2, outside the range of influence of the bubbles heat is given off by free convection from the heated wall to the liquid. Based on this model, they developed an equation for the estimation of heat transfer coefficient, into which nucleation site density and the dynamic contact angle are were determined experimentally.

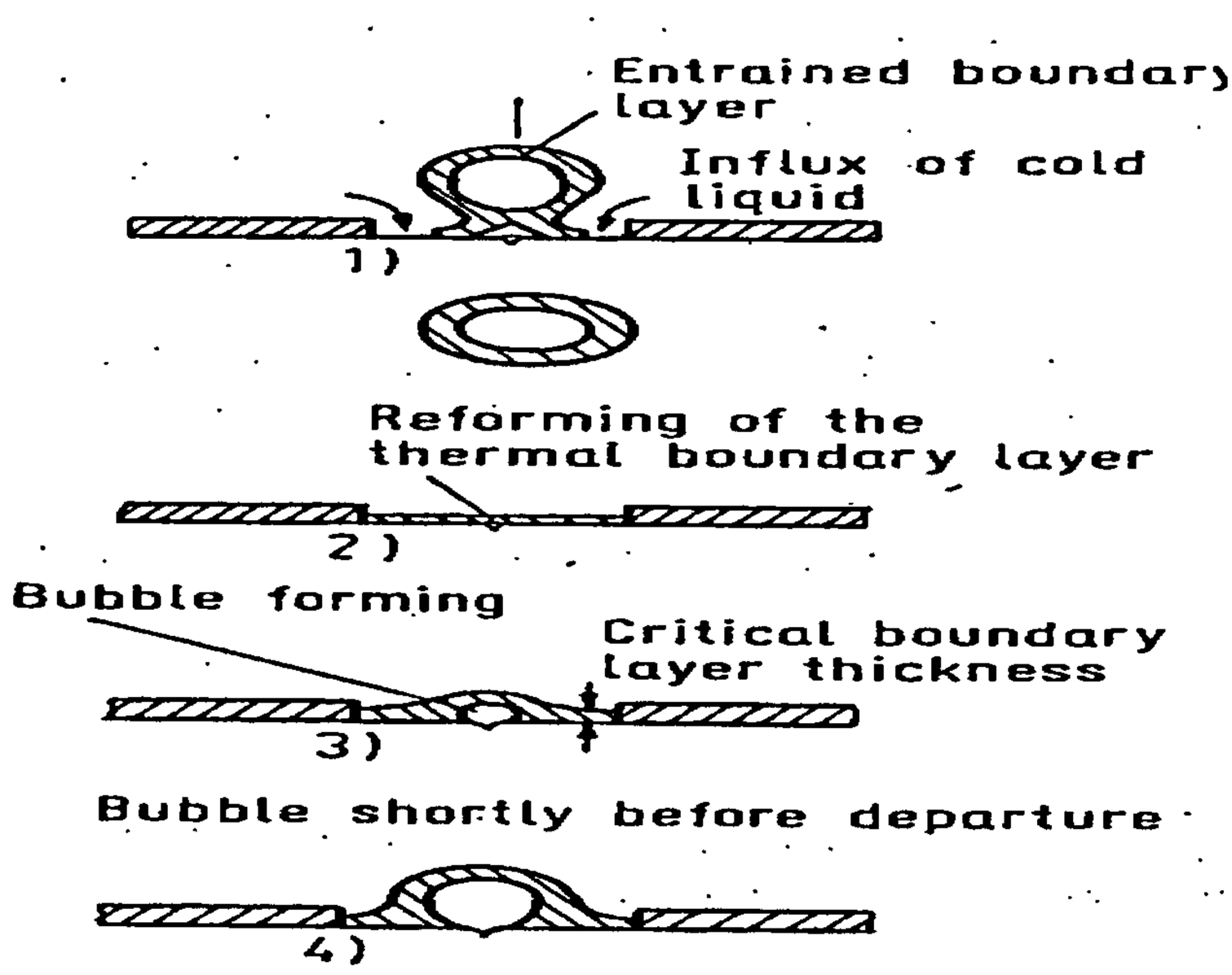

Figure 1.4 Model for heat transfer during nucleate boiling according to Han and Griffith [5]

Beer [6] extended the model of Han and Griffith [5] shown in Figure 1.5 and proved that behind the rising bubble there develops a drift current that exerts a suction effect on the boundary layer. Thus a boundary layer volume of half the size of the bubble volume is removed and intermixed with colder liquid at some distance from the heating surface.

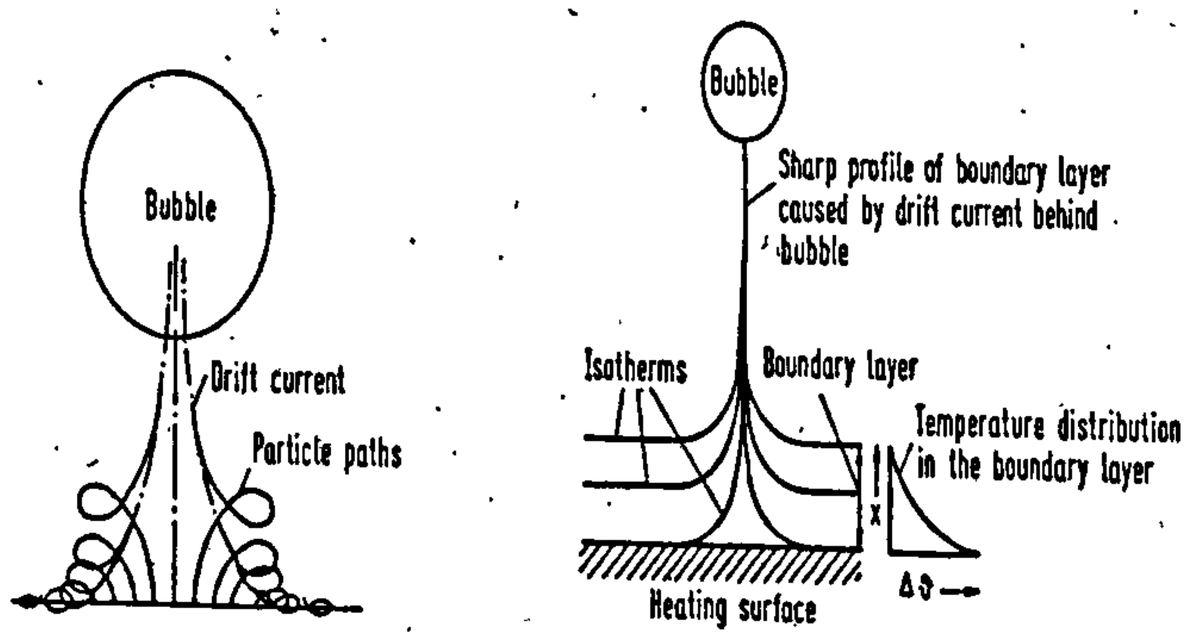

Figure 1.5 Drift flow behind a rising bubble, Beer [6]

Moore and Mesler [7] showed with different methods of testing that the surface of a heated wall exhibits strong temporary fluctuations of temperature during nucleate boiling. For water at atmospheric pressure, a temperature drop of more than 16K was determined within a time span of approximately 2ms. Corresponding to this temperature drop in the heated wall during this short time, is a very large heat flux which is larger by approximately a factor of six than the average heat flux which cannot be explained alone by heat conduction and convective heat exchange to the boiling to liquid. This experimental result was in harmony with the hypothesis that, during the bubble growth, a thin, liquid layer adjacent to the wall is evaporated into the bubble.

Van Stralen [8] developed the 'micro-layer theory'. According to this theory, a part of the bubble is surrounded by superheated liquid, which supplies the enthalpy of vaporisation to the bubble and by so doing cooled itself. After the departure of the bubble the boundary layer at the wall is heated once again, until the next bubble forms at the nucleation site, and the process begins again. The attempt to quantitatively describe these processes by inclusion of the time of dependency of the heat exchange leads, to after a series of assumptions leads to expressions for the velocity of the bubble growth, adhesion time, waiting time, bubble frequency, the departure radius and the peak heat flux for both pure substances and binary mixtures.

Frost and Kipperhan [9] suggested a model for the heat transfer, in which in addition to the convective heat transfer, the mass transfer is also decisive influence. Accordingly a bubble growing at the wall in a superheated boundary layer displaces the superheated liquid, which is then replaced on the upper side of the bubble by colder liquid from the surrounding area. A temperature gradient is thus formed, which makes it possible for

the evaporation from the superheated liquid at the wall into bubble and also the condensation of vapour on the upper side of the bubble. This combined heat and mass transfer is suggested as being responsible for a large part of the entire heat transfer particularly during forced flow.

1.5 Assessment of models of heat transfer during nucleation

Although each of the models to date can describe individual parts of processes, there is no complete theory to describe the whole process. Obviously the heat transfer during nucleate boiling is complicated so that several mechanisms of exchange are active. One of the mechanisms will predominate depending on the prevailing conditions, such as the magnitude of heat flux, pressure, wettability, forced convection subcooling etc. It can be stated fundamentally that previous models contain one or several of the following mechanism for heat exchange:

- Micro-convection in the wall boundary layer as a result of rapid growth of vapour bubbles and also of their collapse in subcooled liquids.

- Displacement of hot liquid from the wall by the growing and departing bubbles and return flow of colder liquid from the interior of the liquid to the wall.

- Vapour formation from the thin, superheated liquid layer under the growing bubble.

It is not rare for heat transfer coefficients calculated according to different equations to deviate by a factor of as much as two compared with the values obtained by experimentation. Such deviations are traceable to the deficiencies in the theory and also by errors in experimental techniques. However, the bubble departure diameter, the wetting angle, and the bubble frequency during fixed conditions are not constant as often assumed, but are also subjected to statistical variations. Empirical correlations that have been developed to predict the heat transfer coefficient in pool boiling would be discussed in Chapter 2 of this thesis.

1.6 Flow Boiling

A boiling curve similar to that in pool boiling is obtained when flow occurs over the tube surface (external boiling) or inside a heated tube (internal boiling) as shown in Figure 1.6.

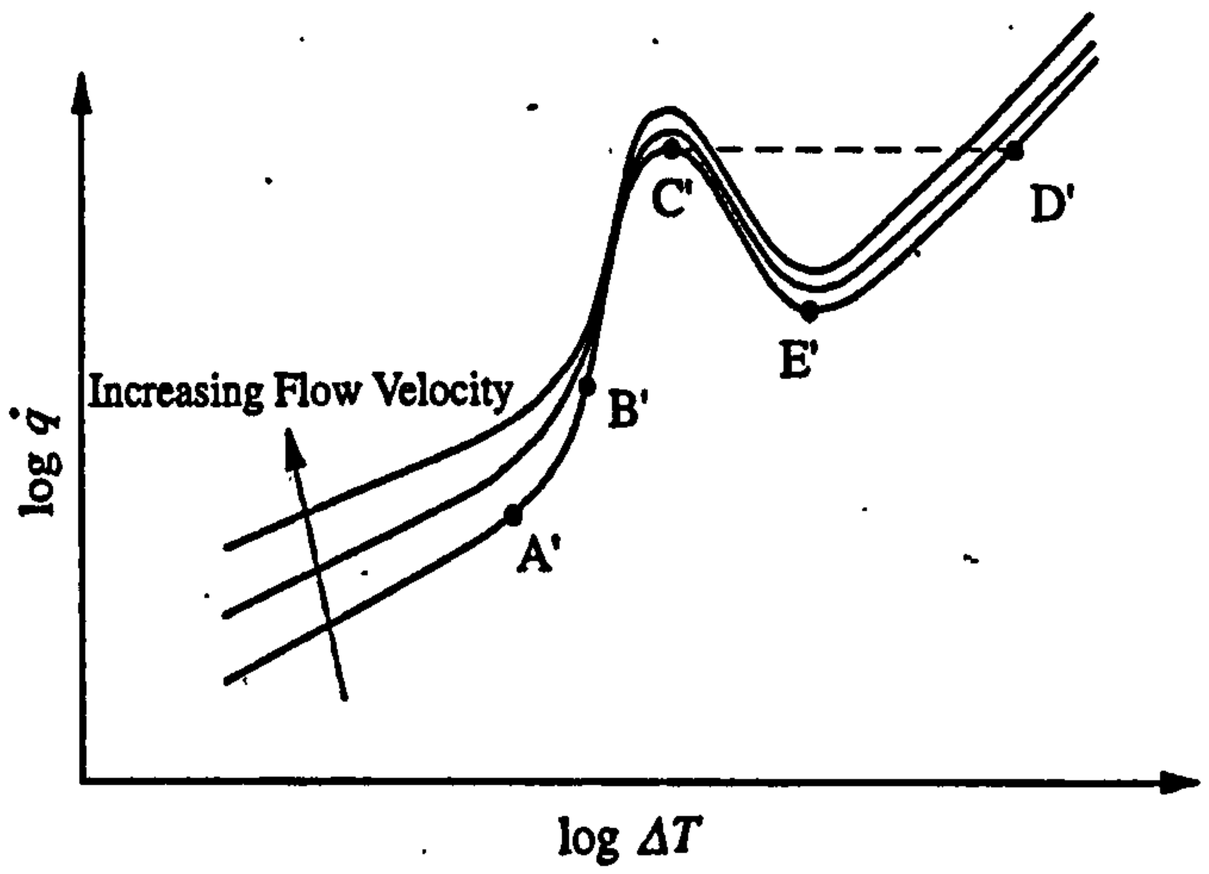

Figure 1.6 Flow boiling curve, Kandlikar [1]

The curve is drawn for a constant total flow rate and a system pressure. The first mode of heat transfer as subcooled liquid enters the tube is single phase forced convection. The magnitude of the heat transfer coefficient depends on the liquid velocity. Since the heat transfer coefficient depends very weakly on the wall superheat in single phase forced convection, the heat flux varies linearly with the wall superheat. After nucleate boiling initiation, an improvement in heat transfer coefficient occurs as the wall superheat is increased. The region $A'B'$ spanning wall superheats from inception to fully developed nucleate boiling is termed partial nucleate boiling. In this region, bubbles are formed discretely on the heated surface, and both single-phase convection and phase change heat transfer contribute to the total heat transfer rate. As a result the dependence of heat flux on the wall superheat is stronger than that for forced convection but weaker than that of fully developed nucleate boiling. Fully developed nucleate boiling curves ($B'C'$) at different velocities generally overlap each other, indicating the dominance of the heat removal by vaporization. In fully developed nucleate boiling; bubble merges and this occurs at the heated surface. However, the phase structure is influenced by the flow regime that exists in the bulk of the working fluid. Possible flow regimes are bubbly, slug and annular. In annular flows when the liquid film on the walls becomes very thin nucleate boiling may be suppressed and the heat removal is through

evaporation at the liquid vapour interface of the thin film. The heat transfer coefficient in very thin annular flow may exceed that given by extension of the pool boiling curve. As a result, for a constant heat flux, the wall superheat in very thin film flow may become smaller than that for fully developed nucleate boiling.

At low flow/heat flux conditions, the critical heat flux occurs when the thin liquid film in annular flow dries out. Such a heat flux is called dry out heat flux and this condition generally occurs in vaporisers such as kettle reboiler. However under high flow/heat flux conditions, the critical heat flux occurs under conditions similar to that of pool boiling. The critical heat flux conditions results when vapour removal rate from the heater surface falls short of the vapour generation rate or the liquid at the heater surface is not replenished fast enough to compensate for the evaporation rate. Critical heat flux is also termed as departure from nucleate boiling, boiling crisis and burnout heat flux. The magnitude of the critical heat flux depends on the local vapour quality, mass velocity and system pressure. For a surface subjected to a uniform heat flux, the critical heat flux condition will first occur at the exit where the local vapour quality is highest. After the occurrence of the critical heat flux, the wall temperature (for a heat flux controlled surface) rises rapidly, and after passing through the regions $C'D'$ and $D'E'$, the surface settles down in film boiling at E'.

1.7 Applications of boiling heat transfer

Boiling is an efficient mode of heat transfer and it is utilised in various energy conversion and heat exchanger systems and in cooling of high energy density electronic components. Boiling heat transfer also finds wide application in chemical, petrochemical, food, refrigeration and other allied industries to generate vapour out of liquid due to it ability to transfer an enormous amount of energy at low temperature gradient. Examples of such applications are in reboilers, heat exchangers (compact and tubular) and heat exchanger reactors (HEX). Majority of boiler and evaporators produced today are based on shell and tube design, with boiling either on the inside of the tubes as in most chemical processes applications. Compact heat exchangers' are becoming more popular in recent times.

1.7.1 Electronic cooling

Since the development of the first electronic computer in the 1940s, the development of faster and denser circuit technologies has been accompanied by increasing heat fluxes.

Most electronic components use air-cooling but with the invention of high-density components with higher heat fluxes it has been recognised that significant amount of the heat fluxes can be removed by liquid cooling. Application of liquid cooling can be categorized as direct or indirect.

Indirect liquid cooling is one in which the liquid does not come into contact with the microelectronic chips nor the substrate upon which it is mounted. Direct liquid offers the opportunity to remove heat directly from the chips with no intervening thermal conduction resistance, other than that between the device heat sources and chip surfaces. Direct liquid immersion cooling offers a high heat transfer coefficient, which reduces the temperature rise of the chip surface above the liquid coolant temperature. The convective heat transfer processes upon which the liquid immersion depends can be explained using the boiling curve in Figure 1.1. From Figure 1.1 the section from the origin to A is the natural convection mode and it offers the lowest heat flux or cooling capability for a given wall superheat. To take advantage of boiling to cool electronic devices it is desirable to operate in the nucleate boiling regime since in this region high heat fluxes can be removed.

1.7.2 Process intensification

Process intensification is a design philosophy that can lead to energy, capital, environmental and safety benefits through the radical reductions in plant size. Cost effective heat transfer is achieved by using smaller innovative heat exchanger designs employing ceramic and polymeric or other novel systems. Process intensification dates back to the late 1970s when ICI first pioneered the concept as a way of reducing the capital cost of a production system. Process intensification is applicable to many industries including chemical, petroleum, power generation, manufacturing, refrigeration etc. In all these areas mentioned, the purpose of the intensification is to make cost savings bearing in mind that the new product/equipment can increase the output of the existing plant using less energy.

At a conference by AIChE's [10] on process intensification several factors were considered as been the motivations for considering process intensification solution. Some of these factors include novel or enhanced product, improved chemistry, enhanced safety, energy and environmental benefits, capital cost reduction. Some of the

areas where process intensification has been used are in the area of compact heat exchangers, catalytic reactors and exothermic reactors.

1.7.3 Vaporizers

Process industries use reboiler to generate vapour for a distillation column. The types of reboiler reviewed here are in line with application to the boiling of small tubes. The selection of vaporizer depends on the evaluation of many factors such as;

- The purpose of vaporisation-to generate a vapour or to cool the heating medium
- The boiling fluid; ie single or multi-component
- The type of heating, gas, radiant or electric.
- The fouling characteristics and blow down requirements
- The operating pressures

The common types of reboilers are based on shell and tube heat exchangers. One fluid flows along the tubes (tube-side fluid) and the other flow is outside the tubes and is contained in the shell (shell side fluid). The shell may, or may not have baffles to direct the flow of the shell side fluid. Various arrangements for a reboiler then arise: the process fluid (that is to be vaporised) can be boiled inside the tubes or outside the tubes, and the process fluid can be separated into liquid and vapour steams in the boiler itself or in the distillation column. Some of the commonest reboilers are kettle reboiler and the thermosyphon reboilers which are described briefly.

1.7.4 Kettle reboiler

Figure 1.7 shows a schematic diagram of a kettle reboiler. In the diagram the process fluid from the distillation column is vaporised on the shell side of the heat exchanger and the separation of the vapour and the liquid is performed in the reboiler shell. The advantages of the kettle reboiler are that the design is simple and control problems are minimised but the heat exchanger is large and therefore expensive. This is a particular disadvantage at high pressure as the shell thickness must be large. Kettle reboilers also

suffer from fouling from the process fluid outside the tubes, and the outside is difficult to clean.

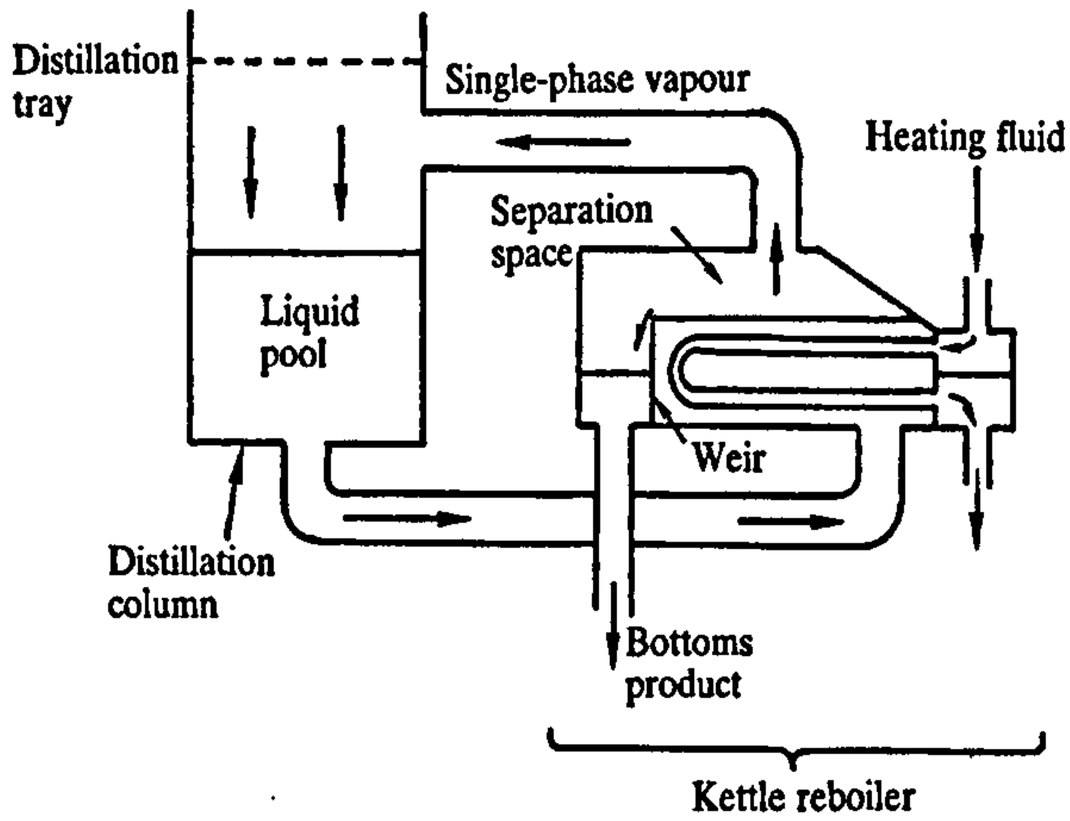

Figure 1.7 Horizontal Kettle reboiler, Whalley [11]

1.7.5 Horizontal thermosyphon reboiler

Figure 1.8 shows the schematic diagram of a horizontal thermosyphon. In this arrangement the process fluid again is vaporised on the shell side, however the reboiler returns a mixture of liquid and vapour to the column inside which is separated. The advantages of a horizontal thermosyphon reboiler are that the shell is now much smaller in diameter and the plant layout is convenient, with the reboiler next to the distillation column. The disadvantages are that the design is now difficult and there may be problems in operation: the reboiler may suffer from instability.

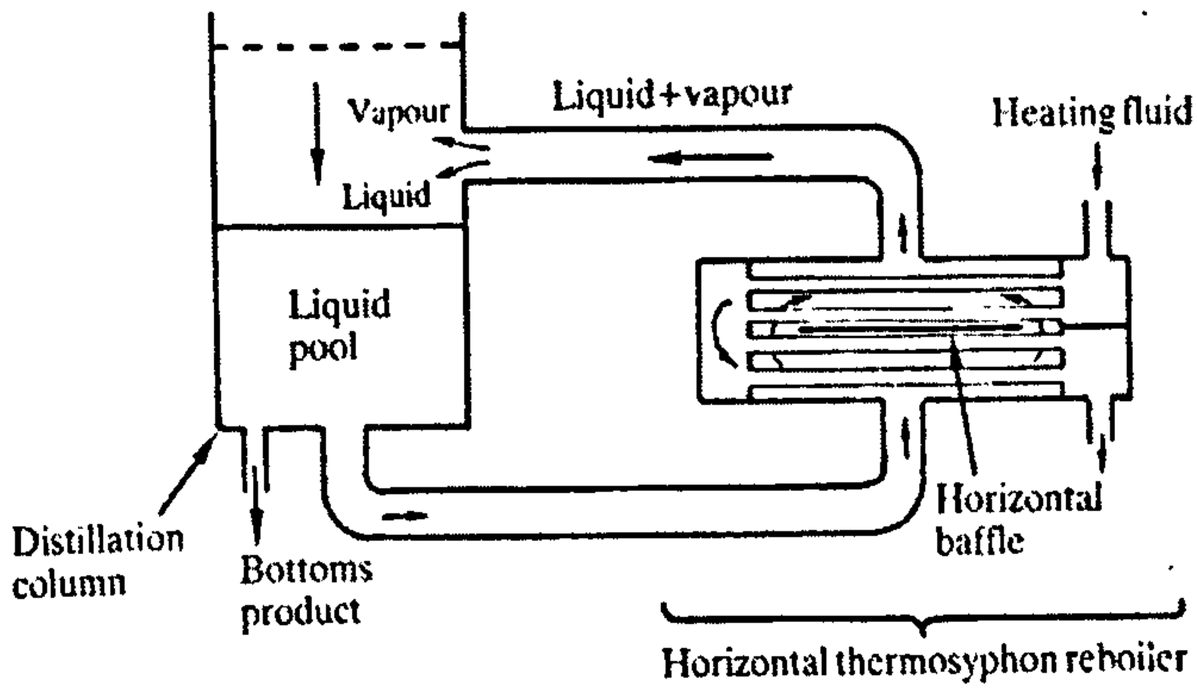

Figure 1.8: Horizontal thermosyphon reboiler, Whalley [11]

1.7.6 Shell and tube heat exchangers

Fig 1.9 shows the schematic diagram of a shell and tube heat exchanger. One fluid flows along the tube (tube side) and the other flow outside the tubes and is contained in the shell. The shell may or may not have baffles to direct the shell side fluid. Typical applications of shell and tube heat exchangers are in the area of petroleum, refrigeration and process industries. The diameter of the tubes used in the shell and tube heat exchangers is in the range of 10-19 mm depending on the system specification. There are some disadvantages to the shell and tube and the commonest one is that of fouling. Fouling increases the resistance of the surface area of the bundle and hence reduces the heat transfer coefficients. Some of the advantages of the shell and tube to that of other heat exchangers are its reliable design methods.

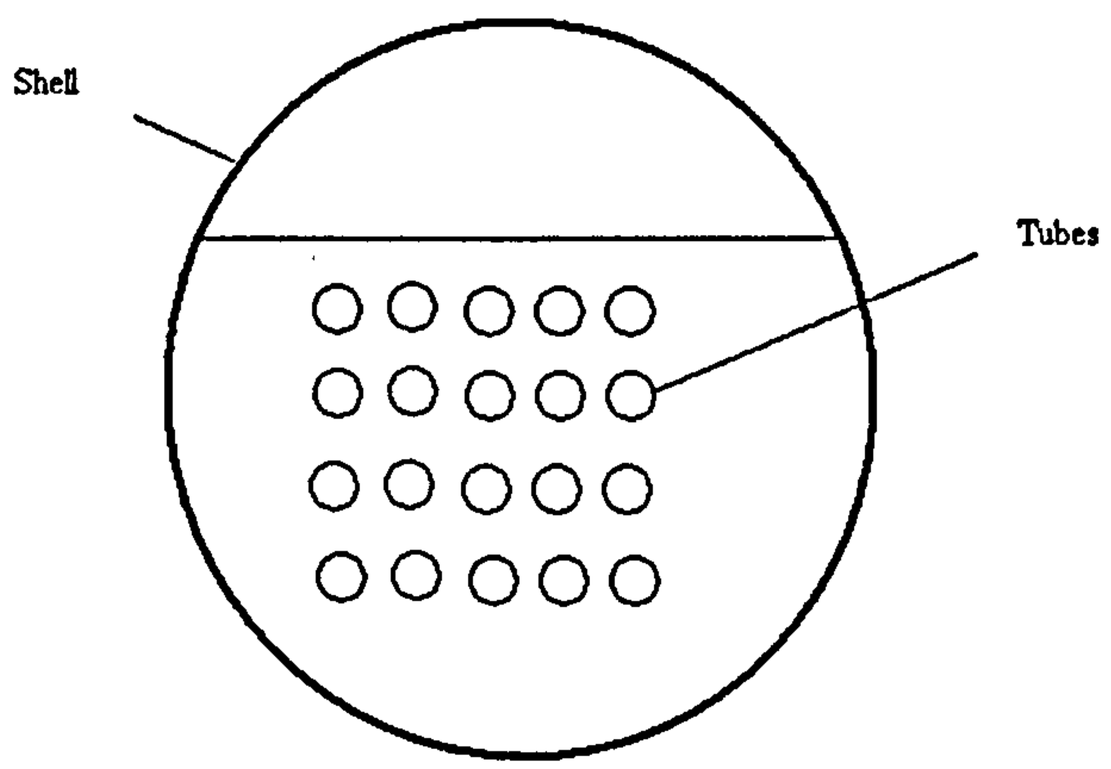

Figure 1.9 Shell and tube heat exchanger

The heat transfer mechanisms occurring in this type of bundle have been examined and appropriate correlations have been developed. Even though a lot has been understood about this type of equipment, once the diameter of the tubes are reduced to the range of 1-3 mm the mechanism occurring will be different. Established correlations are therefore not adequate in predicting the heat transfer coefficient. Detailed review of the mechanism occurring in tube bundle would be discussed in Chapter 2.

1.8 Compact heat exchangers

Heat exchangers may be defined by the compactness in m^2/m^3 and it is generally admitted that values greater than $700m^2/m^3$ characterizes compactness. Compact heat exchanger technologies are advanced but their use and acceptance in the process industry are not yet widespread. Generally, compact heat exchangers include plate heat exchangers and plate fin heat exchanger which have hydraulic diameter between 1 and 10mm. With the advancement of process intensification this compactness can save cost in terms of material (small physical size) and is associated with low installation cost, low fluid inventory that is beneficial in terms of safety as well. Not all compact heat exchangers have been accepted by design engineers due to lack of its benefits and the absence of reliable design methods and conditions under which they operate. It is generally perceived that fouling is a problem associated with small passage sizes in compact heat exchangers. Typical flow regimes and heat transfer mechanism observed in compact heat exchangers would be discussed in Chapter 2.

1.8.1 Plate heat exchangers

Plate heat exchangers (see Figure 1.10) are made of corrugated plates, which are pressed together. The plate size range from $0.02m^2$ to over $3m^2$ with conventional pressing technology. Hydraulic diameters lie between 2 and 10mm for most common plates. To ensure tightness the technologies available are : gaskets, semi-welded or totally welded and brazing. Gasketted PHE is the most common type and the material depends on the fluid temperature etc. For application where high corrosion, pressure are required semi- or totally welded heat exchangers are used. Common applications are OTEC, chemical, petrochemical, and refrigeration industry.

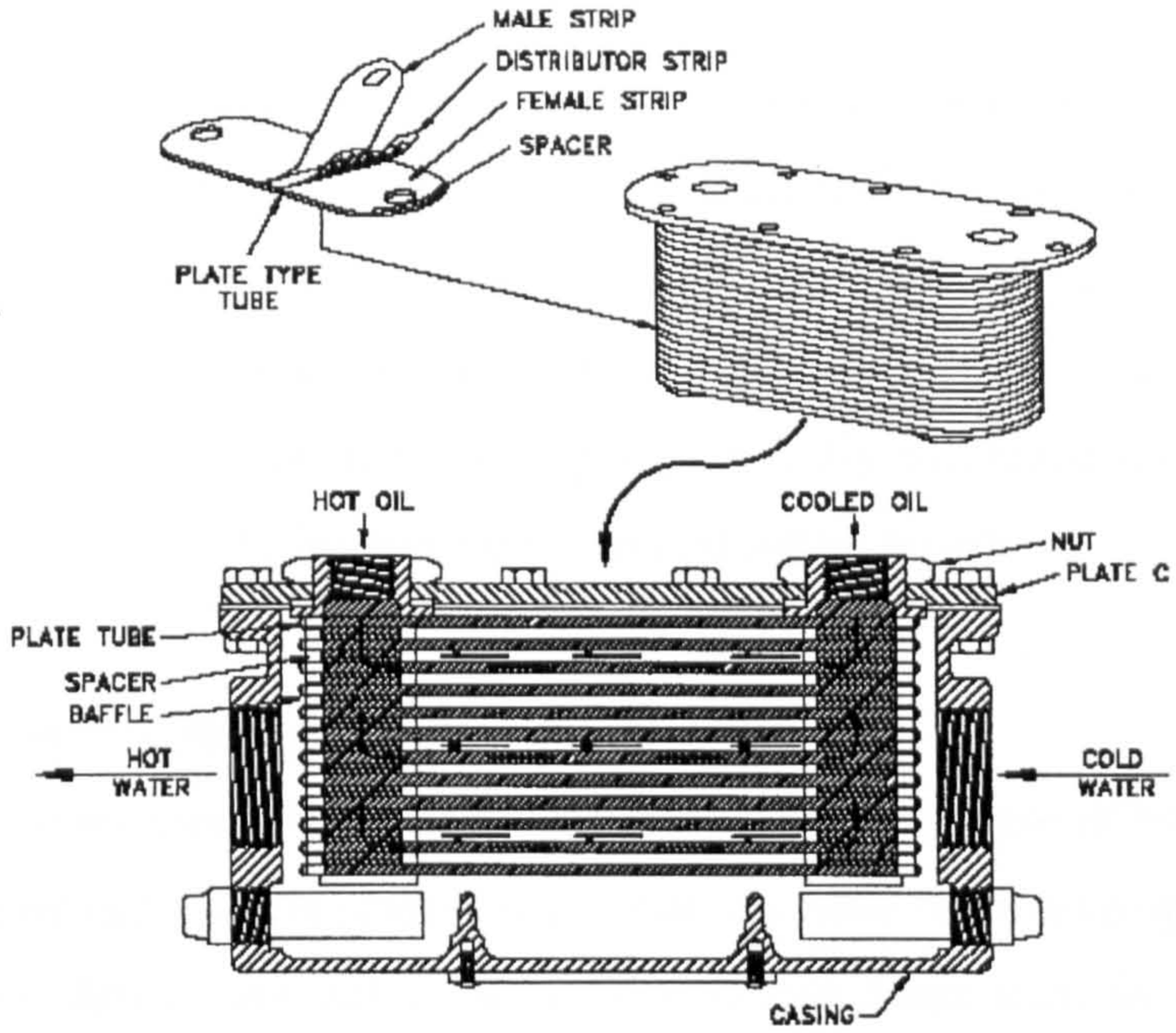

Figure 1.10 Plate heat exchangers, Hesselgreave [12]

1.8.2 Plate and shell exchangers

The principle of the plate and shell heat exchanger is to insert a bundle of plate in a shell. On the plate side, the fluid flows inside corrugated or embossed channels. On the shell side the flow is similar to that of the shell and tube heat exchangers. This technology is applicable for revamping application, as the shell can be kept identical as for a bundle of tubes. It is used in the process industry as boilers (boiling on the shell side) since high pressures can be reached easily on the shell side.

1.8.3 Plate- fin heat exchangers

Aluminium plate fin heat exchangers (PFHE) were initially developed in the 1940s. These provided compact, light and high efficient heat exchanger for gas or gas applications for the aerospace industry. The fluids flow in passages created by 2 plain sheets between which fins are inserted. These heat exchangers can provide secondary surface of up to 90% of the overall heat transfer surface. Several types of fins are available and the selection depends on the application.

1.8.4 Printed circuit heat exchangers

Printed circuit heat exchangers are highly compact, corrosion resistant heat exchangers capable of operating at pressures of several hundred atmospheres and temperature ranges. The printed circuit heat exchangers design offers a unique combination of innovative manufacturing technology and potential application. They are constructed from flat alloy plates with fluid flow passages chemically machined into them. This process is similar to manufacturing electronic printed circuit boards.

1.9 Motivation for the Research

During the 1960s experimental investigations were started in the use of tube bundles in process applications and various empirical correlations have been developed to predict the boiling outside tubes (smooth) as well as enhanced tubes such as finned tubes, coated tubes etc due to its ability to transfer heat at low temperature superheat. In the 1990s research across the UK, the mainland Europe and U.S.A concentrated on reducing the sizes of plants within the process industries. As a result of the process intensification there has been the need to shift our attention from the conventional industrially sized tubes (8-50mm) to those of small sizes such as the order of 3mm. The heat transfer research group of the Heriot-Watt University has done earlier preliminary work boiling on multiple wires arranged in a column. The investigators were not conclusive on the boiling mechanisms occurring in this tube geometry and that is the reason why further studies should be carried out on compact tube bundles. Due to the advent of process intensification it is justifiable for a research to be carried out that would be able to predict the performance of heat transfer in systems such as highly compact reboilers, compact heat exchangers and evaporators using these geometries.

The project would investigate the following;

- The effect of heat transfer coefficient on tube diameter

- Investigate the mechanism occurring in a compact tube bundle using tube diameter of 3.0 mm

- Photographic studies and development of theory to explain the mechanism observed

1.10 Concluding Remarks

The chapter has presented background information on boiling heat transfer and its relevance to industry and some of its limitations and areas that needs further studies. The following remarks are made;

- Boiling heat transfer finds wide application in the refrigeration and cooling industries

- Process intensification in small equipment have been developed and used in the electronic and allied industries

- Compact heat exchangers have been developed for flow boiling inside channels

- Little work has been done on the boiling heat transfer outside small diameter tubes and the scope of intensification for small diameter shell and tube heat exchangers are not documented

- The work in the thesis will present an experimental programme that has been designed to investigate the boiling heat transfer occurring outside small diameter tubes and its applicability to the design of a compact tube bundle.

Chapter 2

LITERATURE REVIEW

2.1 Introduction

This chapter of the thesis presents the literature survey that is available and essential with regards to boiling on small diameter tubes as well as on tube bundles. Pool and flow boiling has been the basis of most industrial components such as reboilers, compact heat exchangers and shell and tube heat exchangers and as such the fundamental studies carried out by previous investigators are reviewed.

The literature survey is subdivided into the following areas:

- Pool boiling on tubes and cylinders
- Pool boiling correlations
- Flow boiling heat transfer on tube bundles
- Heat transfer mechanism in tube bundles
- Flow boiling correlations
- Boiling in confined spaces

2.2 Pool boiling on tubes and cylinders

Since the early work of Nukiyama [13] on boiling heat transfer on a wire, more experimental work has been carried out over the years to establish the pool boiling heat transfer on small diameter tubes. Heat transfer from a smooth tube or surface is governed by parameters such as pressure, surface finish, flow velocity, fluid type and the dimension of the test surface. Boiling heat transfer on single tubes forms the basis of the large tube bundle application. An investigation on the design of large tube bundle considers fundamental studies on single tube or cylinder in pool boiling and would be covered.

Akin and McAdams [14] were among the earliest researchers to have investigated the boiling heat transfer from a 19.5mm diameter nickel plated copper tube to water, n-butanol, isopropanol and isobutnaol at nominal atmospheric pressure. Tubes of similar diameter (19.5mm) were used in a 60 tube evaporator using distilled water. Two different clearances were used in the arrangement. They reported an enhancement of ten times that of a single tube due to the effect of the clearance between the tubes in the bundle. Maximum heat flux of a single tube was reported to be of the same order of magnitude as the bundle.

Bakhru and Lienhard [15] investigated pool boiling from platinum wires of diameter 0.0254, 0.0508, 0.0762 and 0.1016mm in water, benzene, acetone, methanol and isopropanol at a pressure of 1.013 bar. Experimental results that were reported showed an increase in temperature difference and the heat flux increased monotonically without passing through any minimum or maximum on the boiling curve. High speed photographs showed that at high heat fluxes the wires were fully covered with vapour bubbles and there was no contact of liquid to heater. It was concluded that nucleate boiling diminished when the dimensionless radius given in Equation (2.1) is less than 0.01.

$$r' = \frac{r}{\sqrt{\frac{g(\rho_f - \rho_g)}{\sigma}}} \qquad (2.1)$$

However natural convection and film boiling were predicted by conventional methods.

Elrod et al [16] investigated boiling on the outside of a tube with diameter of 19.05 mm for low heat flux for forced and nucleate boiling for both horizontal and vertical tube for four different specimen. They reported that tube material has an effect on the incipient boiling but does not influence the non-boiling heat transfer coefficient at a given surface superheat.

Wege and Jensen [17] investigated the effect of two-phase flow on boiling on a single tube with diameter of 12.7mm with the working fluid being R-113. The parameters that were investigated included vapour quality, mass flux and pressure for heat flux in the

range of 10-50 kW/m^2 , quality 0-20% , p/d 1.16-1.95 and mass flux in the range of 70-1200 kg/m^{2}s. Experimental results showed that the Chen [18] enhancement factor developed for axial flow tends not to be applicable to cross flow boiling but a modification of the correlations predicted experimental results to within 20%.

Yilmaz, Palen and Taborek [19] carried out an investigation to compare the boiling heat transfer performance of an enhanced single tube and that of a plain tube at an atmospheric pressure using p-xylene with the diameter of the tube as 12.7mm. The enhanced tubes were made of Gewa T and thermoExcel surfaces. It was concluded that the single enhanced boiling tubes performed up to an order of magnitude better than the corresponding plain tube. The amount of enhancement depended strongly on the type of enhancement and the physical properties of the fluid to be boiled.

Chou and Lu [20] experimentally investigated the pool boiling heat transfer from a plain tube with outside diameter 17.8 mm made of stainless steel. The working fluids were R-22, R-124, and R-134a at reduced pressures of 0.1 and 0.2. They reported that the Cooper [21] correlation was able to predict their results with a constant of 90. A model proposed by Blochl method (which includes the contribution of latent heat to the total heat transfer rate) was used to predict heat transfer mechanism in terms of the reduced pressure and wall superheat. The model also predicted well the experimental data of other investigators.

Gupta, Agarwal and Varsheney [22] investigated the effects of nucleate pool boiling of liquids with radial flow agitation at atmospheric pressure. The liquids investigated were distilled water, toluene and benzene and the outside diameter of the tube was 32mm. They concluded that superimposition of the radial flow agitation on the boiling of liquids improved the heat transfer depending on the rotational speed of the impeller. A dimensionless correlation was developed for the experimental data given as;

$$Nu = 5.909(Pe)^{0.65}\left(\frac{\rho_g}{\rho_f}\right)^{0.5}(p_r)^{-0.50}(\mathrm{Re}_l)^{0.114} \qquad (2.2)$$

Kumar, Mohanty and Gupta [23] measured experimentally the enhancement due to a lower heating tube on the upper tube. The tube outer diameter was 32 mm, made of copper with heating length of 100mm using distilled water as the working fluid. The heat flux and the pressure range were 19-45kW/m^2 and 35-97 kPa respectively. They reported an increase in the heat transfer coefficient of the upper tube due to vapour bubbles from the lower tube. For all the heat flux range covered the heat transfer coefficient of the lower tube remained unchanged. A correlation was developed to predict the heat transfer coefficient of individual tube in a multi-tube row and bundle heat transfer. The correlation developed was given as;

$$Nu_B = c\,\mathrm{Re}_b^{\,0.7}\,\mathrm{Pr}^{0.4} \tag{2.3}$$

where c is a constant which depends on the liquid surface combination and the Re_b was the boiling Reynolds number. The authors developed a model based on this twin tube to predict the heat transfer coefficient of a tube in a given row of a multi-tubular bundle arrangement using a concept of virtual enhancement which was given as;

$$q_n = q\left(\frac{1-k^n}{1-k}\right) \tag{2.4}$$

where n is the number of tube rows and k is given as ;

$$k = 13.77q^{-0.215} - 1 \tag{2.5}$$

Ribatski and Jabardo [24] investigated the nucleate boiling heat transfer coefficients for halocarbon refrigerants such as R-11, R-123, R-12, R-134a and R-22 using materials of different surface finish and at different reduced pressures. The diameter of the tubes was 19.1mm and thickness 3.1mm made of copper, brass and stainless steel. It was concluded that the nucleate boiling heat transfer of higher pressure refrigerants are higher than those of lower pressure refrigerant and also nucleate pool boiling is affected at reduced pressures and surface roughness. The correlations proposed by Cooper [21], Stephan and Abdelsalam [25] fitted the results within 20% of absolute deviation. Moreover based on the experimental results a correlation was proposed which is of the form;

$$\frac{\alpha}{q^m} = f_w p_r^{\,-0.45}[-\log(p_r)]^{-0.8} Ra^{0.2} M^{-0.5} \tag{2.6}$$

where Ra, M, f_w are arithmetical deviation of the surface profile, molecular mass and surface material parameter respectively.

In summary, work that has been carried out over the years on pool boiling heat transfer on single tubes have shown that heat transfer coefficient obtained is dependent on the surface finish, fluid and conditions at which the experimental work was carried out. These investigations did not take into consideration the effect of the dimensions of the heat transfer surface.

2.2.1 Effect of tube diameter on nucleate boiling heat transfer

Boiling on the outside of tubes is one of the areas that occur in industrial set up such as shell and tube exchangers. Much of the information regarding the effect of diameter is not readily available in open literature and those that were carried out were not conclusive as to the effect of tube diameter on the heat transfer coefficient. The earliest work to consider the effect of diameter on nucleate pool boiling outside a horizontal tube was done by Cornwell [26] in which they investigated the heat transfer coefficient for horizontal tube diameter in the range of 6-30mm for water, refrigerants and organics at nominal atmospheric pressure. It was concluded that the heat transfer coefficient decreases as the diameter increases. A simple correlation was developed to predict the heat transfer with the inclusion of diameter. Later studies by Cornwell and Houston [27] investigated the effect of tube diameter using a convection-based correlation, which is applicable to water, refrigerant and organics. The applicable diameter of the equation was 8-50mm with the operating pressure 0.001-0.8 of the critical pressure. For tubes in the industrial range the equation's applicable and it was concluded that for tubes of diameter more than three times the departure size diameter, the diameter affects the heat transfer coefficient and for tubes with diameter less than about 6mm there was a decrease in the heat transfer coefficient. Moreover the correlation deduced was shown not to be satisfactory with the data set at lower diameter tubes.

Chun and Kang [28] in 1998, reported the parametric effect of surface finish, tube diameter and orientation of nucleate boiling for tube diameters ranging from 9.7- 25.4 mm. It was found out that increased surface roughness increases heat transfer coefficients for both horizontal and vertical tubes. Moreover the heat transfer rate decreased as the tube diameter was increased for both vertical and horizontal tubes. An

empirical correlation was developed. This trend corroborated the earlier work of Cornwell et al [26], [27].

Recent studies by Kew and Houston [29] showed that correlations that indicate inverse relationship between the heat transfer coefficient and the diameter cannot be applied to diameter less than 6mm. Thus data for 8mm tube diameter over predict the heat transfer coefficient for diameter below 3mm. Further experiments carried out on tube diameter ranging from 1-6mm revealed that there was no systematic variation of heat transfer coefficient with the diameters used. Results obtained from their work are shown in Figure 2.1.

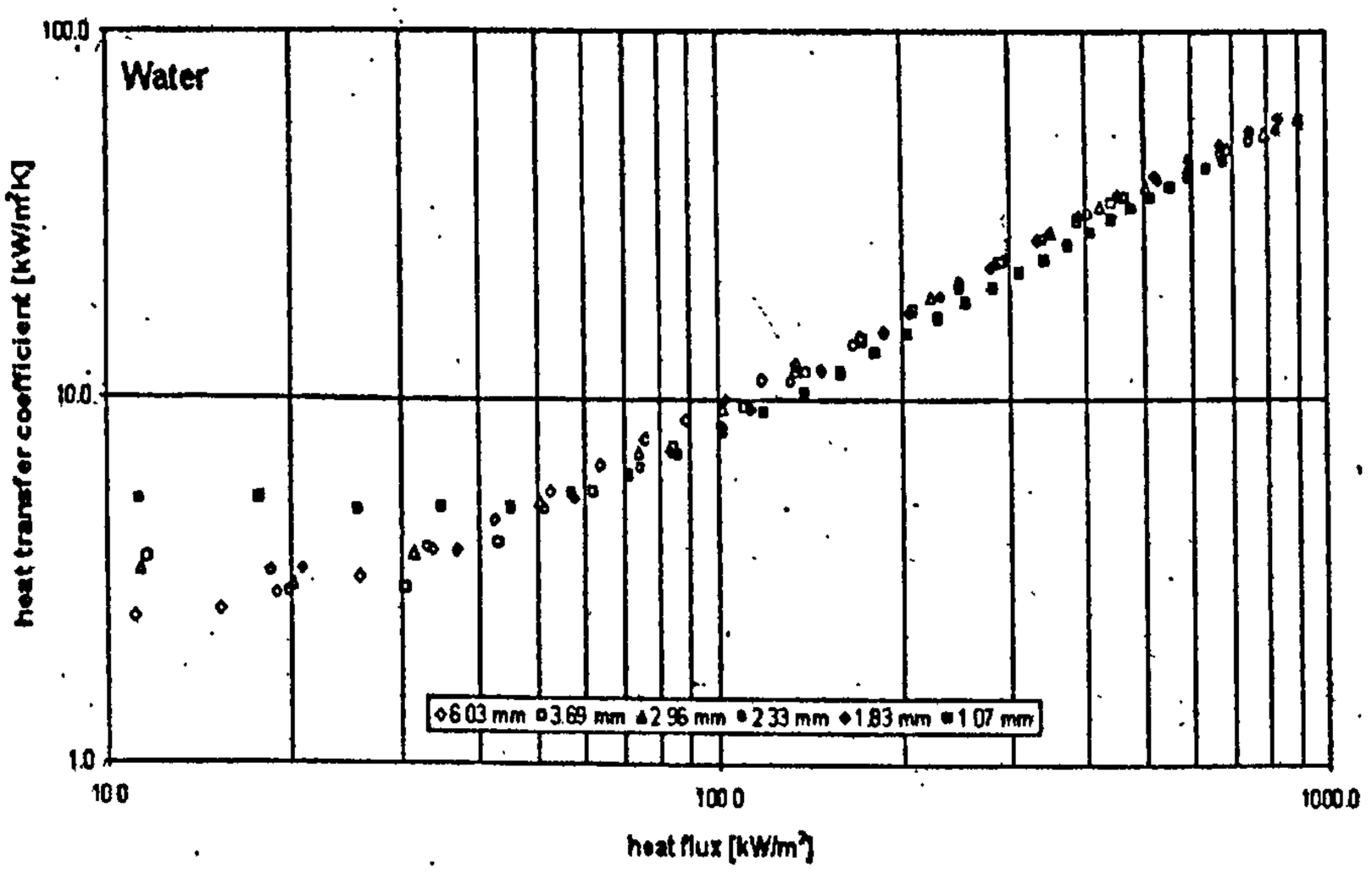

Figure 2.1 Heat transfer coefficient against heat flux, Kew and Houston [29]

Kaupman, Gorenflo et al [30] investigated the effect of pool boiling heat transfer on horizontal tubes of different diameters (4-30 mm). Their results showed that at constant normalised pressure the heat transfer coefficient do not vary much with the tube diameter at intermediate to high heat fluxes. They argued that the influence of tube diameter in their investigations was comparatively small and less compared with correlations in open literature such as those of Cornwell and Houston [27]. Furthermore they also claimed that the heat transfer coefficient for small tubes were greater than that of larger tubes.

Recent studies by Cornwell and Kew [31] on a column of horizontal wires using distilled water and R-113 at nominal atmospheric pressure indicated that there is an increase in heat transfer coefficient upwards but this tends to decrease at the higher position of the wires. Visual inspection of the boiling process showed that bubbles typically of several millimetres diameters passed over the wire enclosing a portion of it with vapour.

In 2004, Das, Putra and Kabelec [32] investigated the effect of diameter for pool boiling for tubes in the range of 4-8mm using distilled water and R-123 as boiling fluids at near atmospheric pressure. It was found out that the usual correlation such as Cooper [21], Stephan [25] developed for the horizontal plate's underestimates the heat transfer coefficient for narrow tubes because of neglecting sliding bubble. However the correlation for large tubes overestimates heat transfer due to considering fully developed sliding bubbles mechanisms. A typical plot of their results is shown in Figure 2.2.

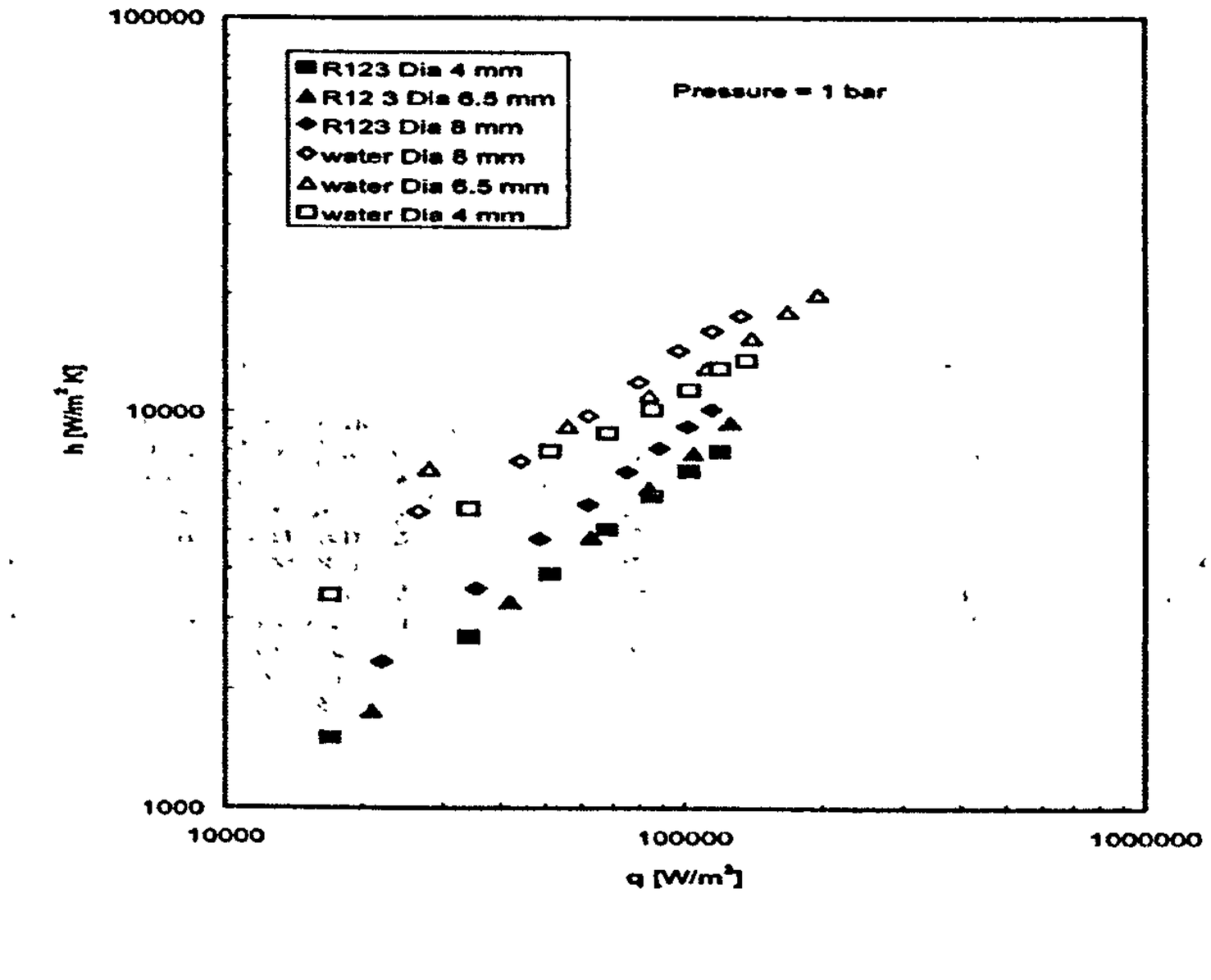

Figure 2.2 Heat transfer coefficient against heat flux at 1 atm, Das, Putra et al [32]

From the literature review, Cornwell and Houston [27] found that there is a relationship between Reynolds number based on vapour generation and for tubes of diameter 6mm upwards. This implies a weak increase of heat transfer coefficient with respect to a decrease in diameter. Studies such as Cornwell [26], Hahne and Shi [33] corroborate

this trend, while investigators such as Kaufaman et al [30] finds no consistent variation above this diameter. As the diameter of the tube reduces to the bubble size it is expected that the sliding bubble component decrease and this result in the reduction of heat transfer coefficient. A sketch summarising these arguments is shown in Figure 2.3. It is noted that there is a danger in relating boiling on wires to boiling on tubes as this comparisons is sensitive to size, fluid and pressure.

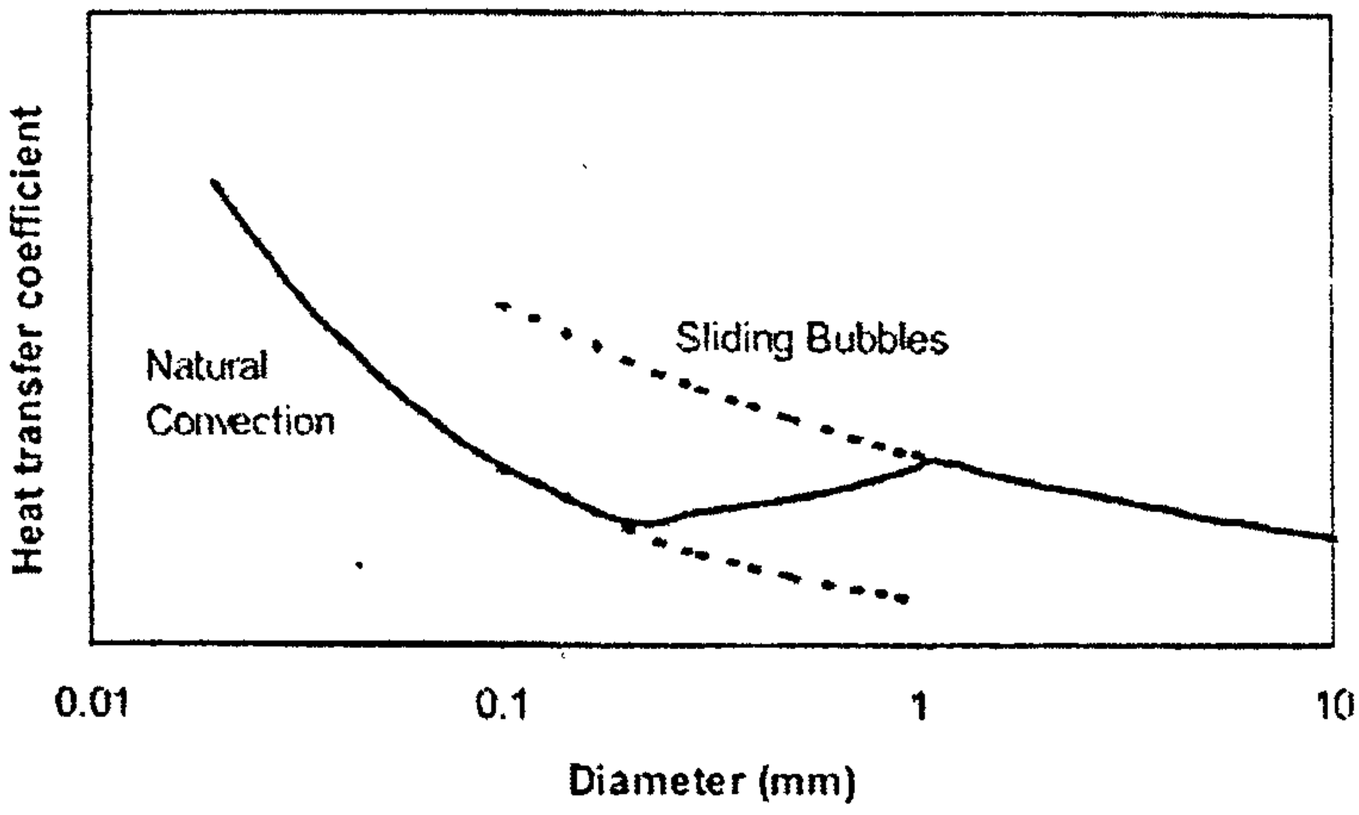

Figure 2.3 Sketch of heat transfer coefficient variation with single tube, Cornwell, Kew et al [34]

2.2.2 Boiling on small diameter tube bundles

The review presented in previous section on boiling on large diameter single tubes has established that there is a difficulty when small diameter tubes (less than 6mm) are intended to be used in a bundle. There is no experimental work that has been published with these tube diameters.

It is clear from the discussion that for boiling on tube bundles, at low quality increase in heat transfer coefficient due to sliding bubbles in large bundle will be absent for small tubes, but the effect of turbulence due to rising bubbles will still lead to an enhancement in heat transfer coefficient. At high vapour quality convective effect are predominant and the small diameter tubes will yield higher values of heat transfer coefficient. From correlation;

$$Nu = 0.211 \mathrm{Re}_f^{0.651} \mathrm{Pr}^{0.34} \tag{2.7}$$

$$\mathrm{Re} = \frac{Gd}{\mu_f}(1-x) \tag{2.8}$$

Thus we have a function of heat transfer coefficient which depends on the diameter of the tube as;

$$\alpha = f(d)^{-0.35} \tag{2.9}$$

The small diameter tubes will yield higher heat transfer coefficient. Premature dryout at intermediate effects are due to the narrow gaps between the tubes which restricts the vapour flow. Dry out has also been reported by Schuller et al [35] for large tube bundles. In miniature tube bundle, dryout would be problematic as it is likely to occur at low vapour qualities. In conclusion the performance of a small tube bundle is likely to be as shown in Figure 2.4

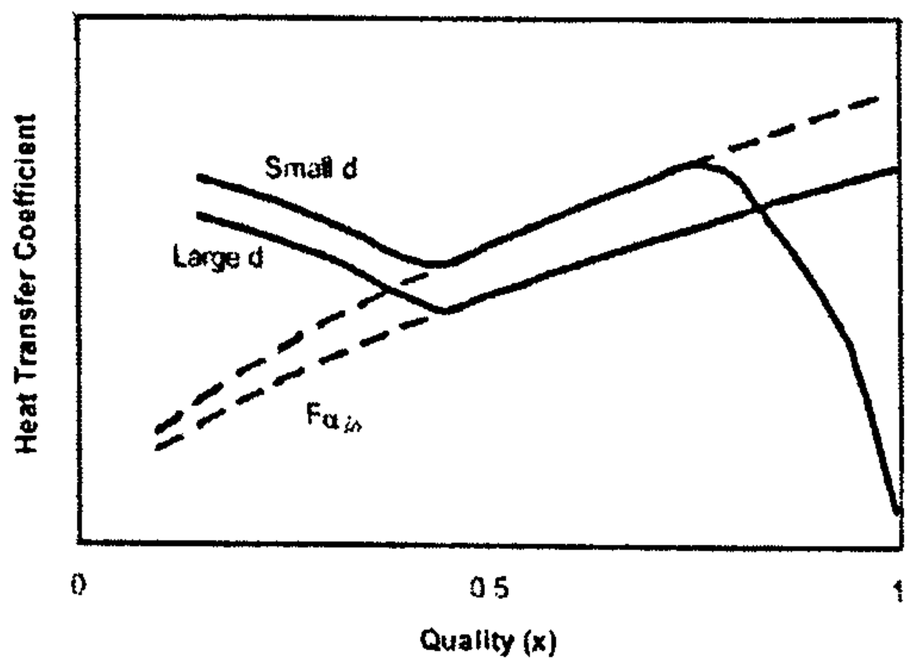

Figure 2.4 Sketch of heat transfer coefficient with quality for tube bundles with large and small diameter tubes, Cornwell, Kew et al [34]

Reduction of tube diameter and pitch from conventional tubes can lead to considerable increase in the heat transfer coefficient. The effect of d on the large tube bundle (889 tubes, p/d 1.33 and d =19.1 mm) have been examined by Cornwell et al [36]. Results from working fluid of R113 at 1 bar and G=450 kg/m^{2}s and q=20kW/m^2 are shown in Figure 2.5. Under the test conditions from d=19.1 mm, p/d=1.33 to d=12.7 mm p/d =1.2 yields an increase over 40% and extrapolation to d=8 mm yielded an increase over 60%. The enhancement due to small gaps where the confinement number (Co greater than 0.5) gap size less than 2.5 mm in water at 1 atm was considerable and generally greater than that due to surface treatment of tubes.

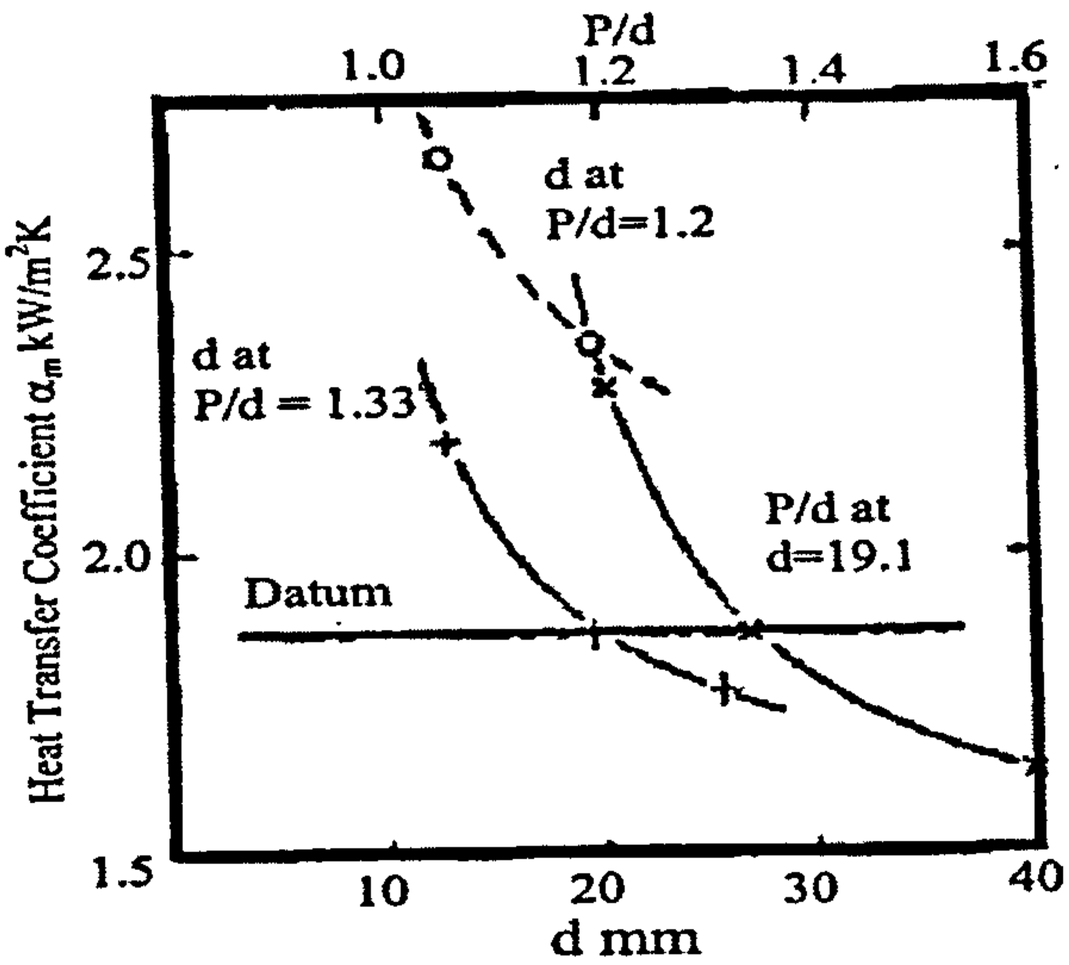

Figure 2.5 The effect of diameter and pitch variation on heat transfer, Cornwell [37].

2.2.3 Nucleate pool boiling correlations

Nucleate boiling correlations are developed by taking into consideration factors such as surface finish, reduced pressures, diameter and the physical properties of the fluid considered. The most widely used correlations are reviewed. Since the early research by Nukiyama [13] for the pool boiling curve for a wire, much research has been carried out to develop appropriate correlation to evaluate the heat transfer coefficient during nucleate boiling. Generally it is very difficult to obtain theoretical expression for the method of calculating heat transfer coefficients during nucleate boiling. This is so because the boiling occurs at nucleation sites and the number of nucleation sites depends on the:

- Condition of the heating surface, and
- How well the liquid wets the surface

Three practical approaches to heat transfer are possible. They are;

- Surface effects
- Fluid properties
- Diameter effects

Pool boiling correlations that are developed are classified into those applicable to flat plates and those to horizontal tubes.

Rosehnow [3] included some effect of the surface in the development of a correlation for the boiling heat transfer from a flat plate. He argued that a single-phase convective heat transfer could be written in the form:

$$Nu = f(\mathrm{Re}, \mathrm{Pr}) \tag{2.10}$$

The correlation takes the physical properties of the liquid by using expressions for velocity and length for the various parameters given as;

$$u = \frac{q}{h_{fg}\rho_l},\ L = \left[\frac{\sigma}{g(\rho_l - \rho_g)}\right]^{1/2} \tag{2.11}$$

Rosehnow [3] correlated his correlation by introducing the surface- fluid constant. C_{sf}. Often the surface- liquid constant is difficult to obtain and this has led to other development of the correlation by different authors. The correlation for the pool boiling heat transfer coefficient is given as;

$$\frac{C_l(T_w - T_s)}{l} = C_{sf}\frac{q}{\mu_l l}\left[\left(\frac{\sigma}{g(\rho_1 - \rho_2}\right)^{1/2}\right]^{1/2}\left(\frac{C\mu}{k}\right)^s \tag{2.12}$$

Pioro [38] recently developed a predictive method for the heat transfer coefficient from a horizontally flat plate. The correlation developed was given as a function of the properties of the fluid which was written as;

$$\frac{\alpha_b l}{k} = C_{sf}\left[\frac{q}{h_{fg}\rho_g{}^{0.5}\left[\sigma g(\rho - \rho_g)\right]^{0.25}}\right]^{2/3} P_r{}^m \tag{2.13}$$

where C_{sf} is a constant that depends on the nature of the heating surface liquid.

Cooper [21] developed a nucleate pool boiling correlation that takes into account the surface roughness parameter, molecular mass and reduced pressure. The data used for

the correlation was taken from about 100 experiments from published sources with a total of 6000 data points. The equations that was obtained after curve fitting was given as;

$$\alpha = 55 p_r^{\,0.12-0.2\log R_p} \left(-\log_{10} p_r\right)^{-0.55} M^{-0.5} q^{0.67} \tag{2.14}$$

with the units as α (W/m^2 K) , q (W/m^2) and R_p in μm. Cooper [21] suggested a constant of 95 be used instead of 55 for horizontal copper cylinders.

The Mostinski's [39] correlation for the nucleate boiling takes into account the effect of reduced pressure and is given by the expression;

$$\alpha_{nb} = 0.1061 q^{0.7} p_c^{0.69} F_p \tag{2.15}$$

F_p is the pressure correction factor, which can be calculated from;

$$F_p = 1.8 p_r^{0.17} + 4 p_r^{1.2} + 10 p_r^{10} \tag{2.16}$$

Labunstosv [40] developed a correlation for the pool boiling heat transfer based on the physical properties of the fluid. The correlation is given as:

$$\alpha_{nb} = 0.075\left[1+10\left(\frac{\rho_g}{\rho_l-\rho_g}\right)^{0.67}\right]\left(\frac{k^2}{\upsilon\sigma(T_s+273.15)}\right)^{0.33} q^{0.67} \tag{2.17}$$

Stephan and Abdelsalam [25] developed a nucleate pool boiling correlation for several classes of pure fluids using regression analysis. The correlation was obtained from 5000 experimental data from over 72 published papers. The fluids were classified into water, refrigerants, hydrocarbons and cryogenic. These correlations are based on the physical properties of the fluid. Their correlation for organic fluids is given as;

$$\frac{\alpha_{nb}}{k_l} = 0.0546\left[\left(\frac{\rho_g}{\rho_l}\right)^{1/2}\left(\frac{qd}{k_l T_{sat}}\right)\right]^{0.67}\left(\frac{h_{fg}d^2}{a_l^2}\right)^{0.248}\left(\frac{\rho_l-\rho_g}{\rho_l}\right)^{-4.33} \tag{2.18}$$

and for water, an expression of the following form was obtained;

$$\frac{\alpha_{nb}d}{k_l} = 0.246\times10^{7}\left(\frac{qd}{k_l T_{sat}}\right)^{0.673}\left(\frac{h_{fg}d^2}{a_l^{\,2}}\right)^{-1.58}\left(\frac{C_p T_{sat}d^2}{a_l^{\,2}}\right)^{1.26}\left(\frac{\rho_l-\rho_g}{\rho_l}\right)^{5.22} \qquad (2.19)$$

For refrigerant their regression analysis's yielded the following expression;

$$\frac{\alpha_{nb}d}{k_l} = 207\left(\frac{qd}{k_l T_{sat}}\right)^{0.745}\left(\frac{\rho_g}{\rho_l}\right)^{0.581}\left(\frac{\nu_l}{a_l}\right)^{0.533}$$

where the bubble departure diameter d is determined by ;

$$d = 0.0146\beta\left[\frac{2\sigma}{g(\rho_l+\rho_g)}\right]^{1/2} \qquad (2.20)$$

All the equations given by Stephan and Abdelsalam [25] are valid within certain ranges of the reduced pressure and absolute deviations.

Cornwell [26] developed a pool boiling correlation that takes into account the effect of diameter. The correlation is applicable to water, refrigerants and organics in tubes with diameter ranging from 6-32mm. The correlation is given as;

$$Nu_b = C_{tb}\,\mathrm{Re}_b^{2/3} \qquad (2.21)$$

where $Nu = \frac{\alpha_{nb}d}{k_f}$ and $\mathrm{Re}_b = \frac{qd}{h_{fg}\mu_f}$ (tube boiling Reynolds number) and C_{tb} is a constant that dependent on the surface, fluid and pressure .

In a later studies described earlier, Cornwell and Houston [27] developed a correlation for pool boiling on horizontal tubes, which was based on a conceptual analysis of convective boiling on tubes. Their analysis was based on the Mostinki's [39] pressure relationship and correlated using experimental data from forty published papers produced:

$$Nu = AF(p)\mathrm{Re}_b^{0.67}\,\mathrm{Pr}^{0.4} \tag{2.22}$$

where $A=9.7(p_c)^{0.5}$ with p_c in bar

$$F(p)=1.8p_r^{0.17}+4p_r^{1.2}+10p_r^{10}$$

More recently Chun and Kang [28] developed a correlation based on the parametric studies of heat exchanger tubes on nucleate boiling. The diameters of the tubes were in the range of 9.7-25.4 mm. This correlation combined the effects of tube diameter, surface roughness and tube orientation. Their correlation was obtained for both horizontal and vertical tubes are given respectively as;

$$q=\frac{0.015R_p^{0.084}\Delta T^{5.508}}{d^{1.318}} \tag{2.23}$$

$$q=\frac{0.024R_p^{0.084}\Delta T^{4.86}}{d^{1.656}} \tag{2.24}$$

Gorenflo [41] and later Gorenflo and Sokol [42], developed an approach for pool boiling heat transfer coefficients which was based on a reference heat transfer coefficient . The correlation obtained for the heat transfer coefficient is thus written as;

$$\alpha=\alpha_o F_{PF}\left(q/q_o\right)^{nf}\left[R_p/R_{po}\right]^{0.133} \tag{2.25}$$

where F_{PF} is the pressure correction factor correlated as;

$$F_{PF}=1.2p_r^{0.27}+2.5P_r+\frac{p_r}{1-p_r} \tag{2.26}$$

which approaches a value of 1 at p_r=0.1. The heat flux correction factor was estimated from;

$$nf=0.9-0.3pr^{0.3} \tag{2.27}$$

The surface roughness of the actual surface R_p was in micrometers and is set to 0.4 for an unknown surface. The expressions given above are for all fluids except water and helium. For water the expression is given as;

$$F_{PF} = 1.73 p_r^{0.27} + \left(6.1 + \frac{0.68}{1 - P_r}\right) p_r^{2} \tag{2.28}$$

$$nf = 0.9 - 0.3 p_r^{0.15} \tag{2.29}$$

In summary, pool boiling correlations developed earlier takes into account the thermophysical properties of the fluid as well as the surface orientation of the tube in question. The only correlations that incorporates tube diameter was that of Cornwell [27] and Kang [43]. These correlations are only able to correlate tubes above 8mm and there was deviation of the correlation when applied to diameter below 8mm.

2.3 Flow boiling heat transfer outside large tube bundles

Flow boiling occurs in industrial components such as the kettle reboiler. In this type of arrangement the flow is externally imposed on the bundle. Investigations have been carried out over the years to predict the performance of tube bundles and to optimise the design of such equipment. In spite of their extensive application such as evaporators in the process industries there are still uncertainties about physical phenomenon controlling the process which is reflected in the marginal accuracy of the correlations used for their design. Tube bundle boiling studies can be classified by the way the experiment was run to obtain the heat transfer coefficients. Typically they are classified as either;

- Local heat transfer coefficient or
- Overall boiling heat transfer coefficient for the bundle

Overall bundle results are obtained by heating a bundle with steam or a hot water source, whereas local bundle boiling coefficient are obtained by instrumenting individual tubes with thermocouples and heating cartridges. Many bundle boiling studies has been carried out without determining the flow rate of the evaporating liquid, such that the vapour quality within the system cannot be evaluated. In those studies the

bundle is immersed in a pool of liquid with a condenser connected above the vapour space. The flow in this arrangement is due to natural convection generated within the pool. Some test facilities utilized a pump through a rectangular channel where the tubes are arranged in the direction of flow, hence the flow rate and vapour quality could be measured from energy balance.

In a typical forced convective boiling rig the liquid is fed at the bottom of the bundle and flows through it by the use of a centrifugal pump. The mass flow rate can be measured at the inlet, and by energy balance the local vapour quality can be evaluated. This experimental arrangement allows associating the heat transfer coefficient to the mass flux and thermodynamic vapour quality. Figure 2.6 shows the flow pattern encountered in such a system with the corresponding heat transfer regimes. Liquid flows up the bottom rows from the inlet pipes, while the liquid is been heated up to near saturation temperature and the wall temperature remains below that necessary for nucleation to occur, the heat transfer mechanism is single-phase convective to the liquid. The heating that are normally used in this type of arrangement are either electric cartridge been inserted into the tubes or by passing saturated vapour through it. When conditions are met for the nucleation to occur the, vapour is generated in the subcooled boiling regime. At some tube row above this point the working fluid reaches its saturation temperature and the saturated boiling regime is attained. In the lower part of the bundle bubbly flow exists similar to that which occurs in nucleate on a single tube. The bubbly flow from the lower tubes forms a two-phase jet which impinges on the tubes above, as the local void fraction increases, large vapour plugs are formed and pass between adjacent tubes trapping thin layers of evaporating liquid on the sides of the tubes. This is the sliding bubble phenomenon reported by Cornwell and Schuller [44] using high speed photographic studies. Higher up in the bundle the vapour becomes a continuous phase and liquid is evaporated from the thin film covering the tubes. At some critical value of the thermodynamic vapour quality, and heat flux dryout of the tubes occurs and this can minimise the heat transfer performance of the bundle.

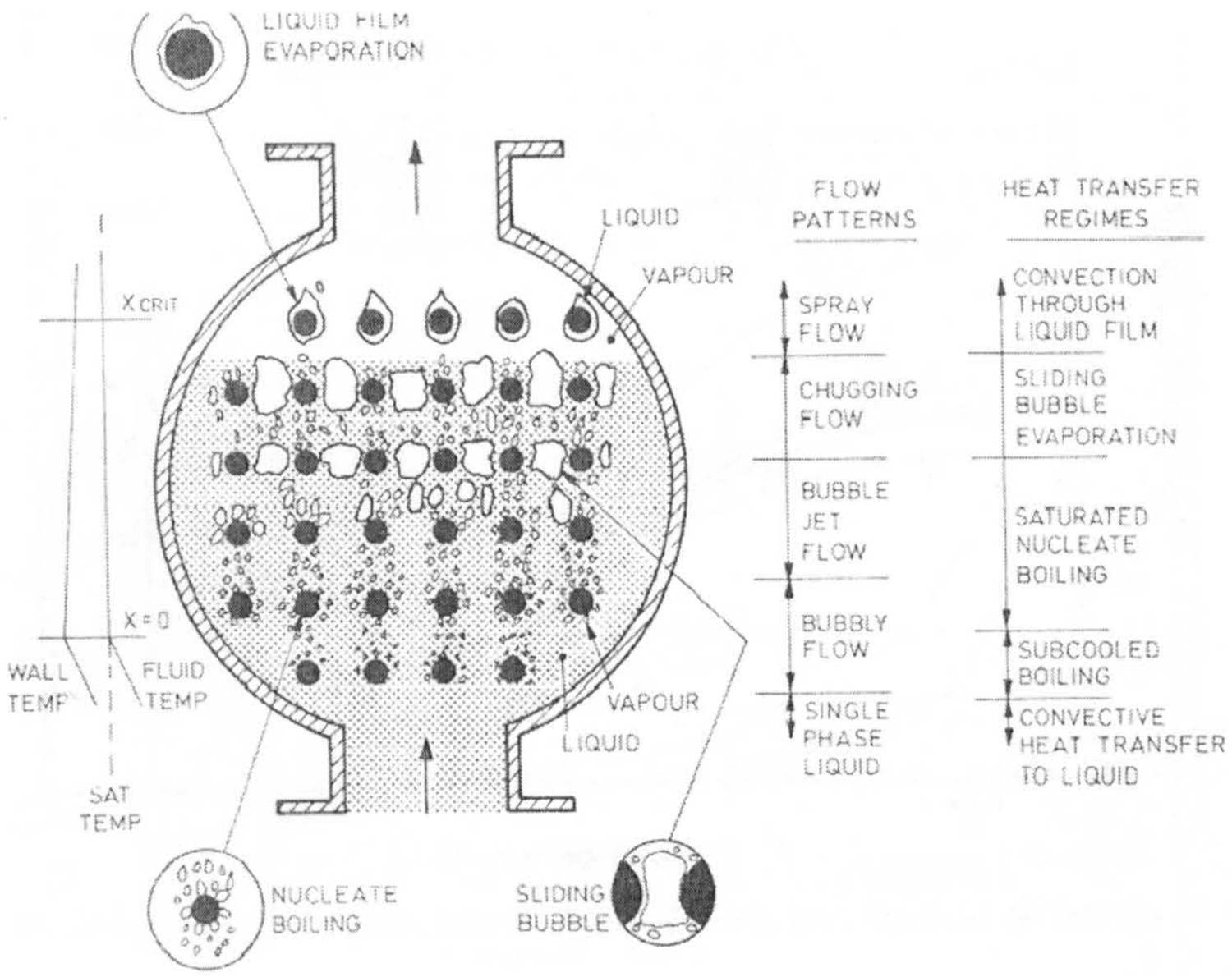

Figure 2.6 The flow pattern and heat transfer regimes in a tube bundle, Collier and Thome [45]

2.3.1 The boiling curve for tube bundles

Heat transfers on the tube side of bundles are generally higher compared to that of single tube when they are subjected to the same flow conditions. A typical graph comparing a single tube to that of a bundle is shown in Figure 2.7. The curve shows heat flux (q) against temperature difference. The slope and general shape of q vs. ΔT curve for bundles was about the same as for single tubes except that the maximum was much flatter. Below the maximum heat flux, the heat transfer rate at a given temperature difference for all bundles tested was considerably greater than that of single tubes. The maximum heat flux for bundles were considerably less than that of single tubes for all the bundles tested. The calculated single tube heat flux in the nucleate boiling regime was obtained by using the Mostinki's correlation whereas the maximum heat flux was evaluated using the equation given below;

$$\frac{q_{\max}}{p_c} = 803\left(\frac{p}{p_c}\right)^{0.35}\left[1-\left(\frac{p}{p_c}\right)\right]^{0.9} \qquad (2.30)$$

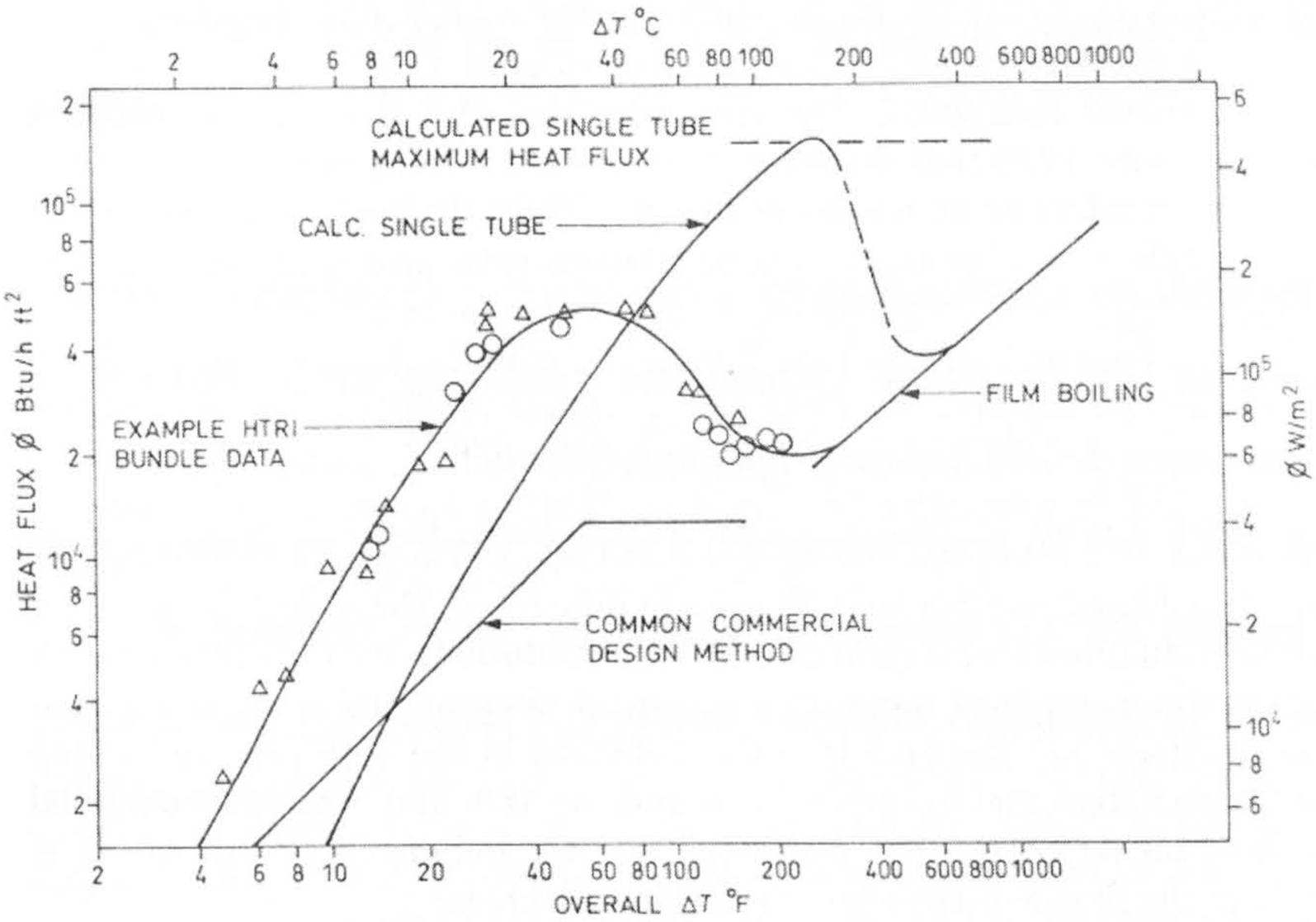

Figure 2.7 Tube bundle boiling data compared to a single tube, Palen, Yarden et al [46].

2.3.2 Bundle Effect

Myers and Katz [47] investigated boiling on the outside of four horizontal tubes in a vertical row to determine the effect of tube position and the behaviour of the lower tubes measured. The boiling heat transfer coefficients for the top tubes were higher than the lower tube and it was greatest at small temperature differences. A correlation of data considered factors such as tube dimensions and the physical properties of the fluids used. They assumed that the boiling heat transfer is a function of the thermal conductivity of the liquid, surface tension of the fluid, density of the liquid, latent heat of vaporisation and viscosity. In a later studies , Palen, Yarden et al [46] carried out an experimental investigation into the boiling outside tube bundle for commercially sized kettle reboilers. They found out that the maximum heat transfer for a tube bundle was a strong function of the bundle length–diameter ratio and the tube spacing or tube layout density. Moreover the average boiling side heat transfer coefficient for tube bundles increases with pressure and usually higher than the nucleate boiling coefficient for a single tube.

Wall and Park [48] investigated the bundle effect in an array of five tubes arranged vertically with outside diameter being 26.6mm, boiling over n-pentane-hexane and several different mixtures. They found out that the effect of tubes at the bottom of a vertical array on the tubes at the top are similar irrespective of whether a pure

component or a mixture was been boiled. This increase is restricted at low nucleate boiling heat fluxes.

In a similar studies, Nakajima [49] investigated the enhancement on the upper tubes of a tube bundle with tube diameter 25mm and heating length of 300 mm using electric heating and hot water heating. The test bundles consisted of 3 rows and 3 different staggered arrangements of 3, 5 and 20 on a triangular pitch of p/d 1.38. According to theoretical and experimental investigations they concluded that the passing period of a bubble observed on the tube surface is almost constant regardless of the vapour flow rate from visual observation.

Leong and Cornwell [50] tested a 241 tube bundle heated electrically. The tests were run with R-113 at atmospheric pressure with plain tubes of diameter 19.05 mm on a square pitch. Their iso-contour is shown in Figure 2.8 for the heat flux of 20 kW/m^2. The bundle was simulated with an oversized shell. The coefficient at the bottom of the bundle was comparable to those predicted by the single tube correlation whiles two-phase circulation up the bundle increases the boiling coefficient substantially. A typical boiling photo is shown in Figure 2.9.

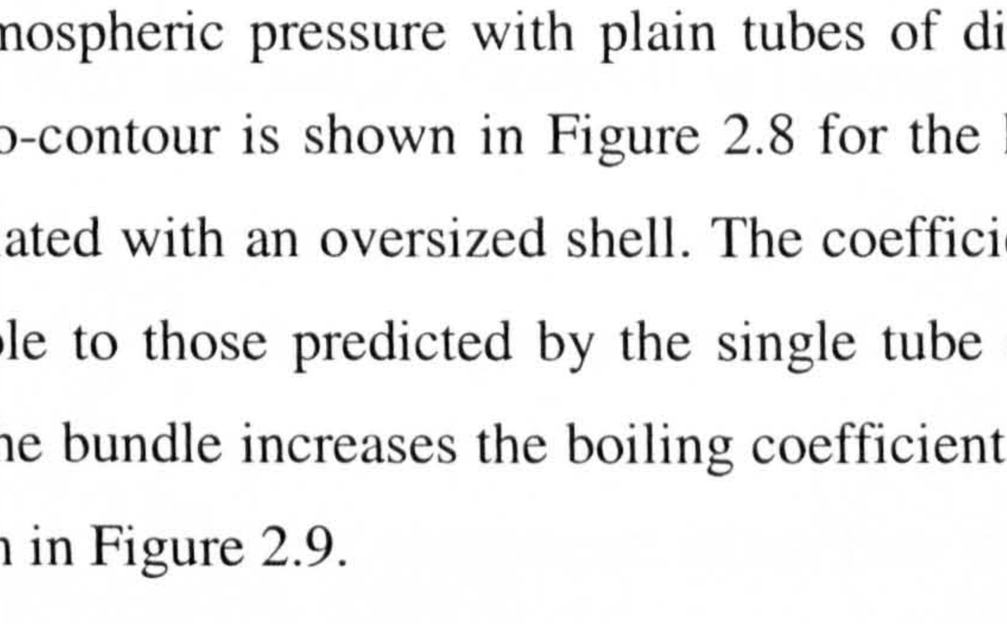

Figure 2.8 Variation of heat transfer in a horizontal kettle reboiler, Leong and Cornwell [50]

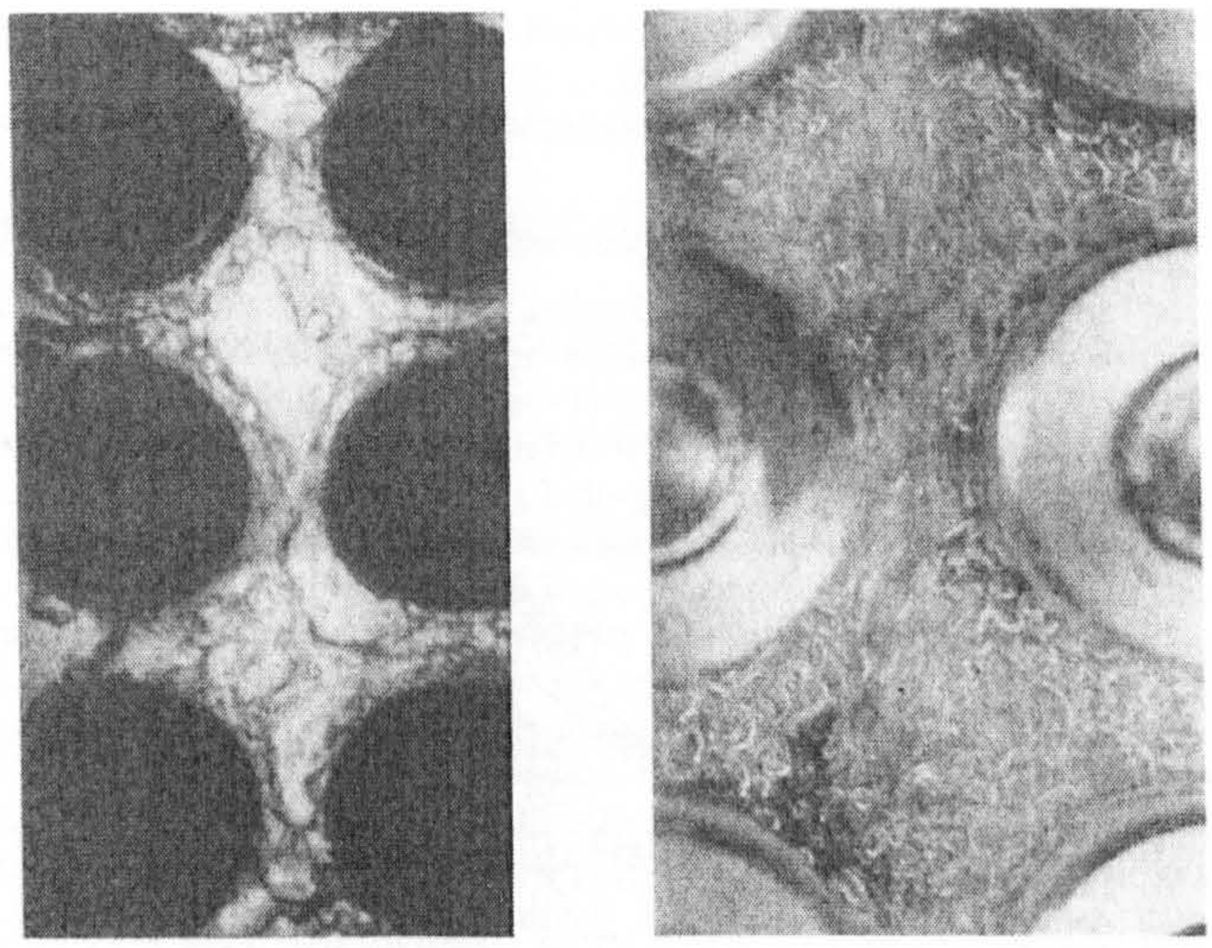

(a) (b)

Figure 2.9 Boling on a horizontal tube bundle : a) water at 1 bar, 50kW/m^2 and x=0.05 b) R-113 at 1 bar, 15 kW/m^2 and x=0.05, Cornwell and Leong [50]

Scoones [51] investigated experimentally the boiling heat transfer on plain and low finned tube bundles using R-113 at various pressures. They concluded that the heat transfer coefficient increased up the tube bundle and this was due to quality which resulted in a two-phase convective component. Mass flux was found to have little influence on the heat transfer coefficient at any given heat flux, at higher quality heat transfer coefficient was increased for both the plain and low finned tubes.

Rebrov, Bukin and Danilova [52] investigated the local boiling heat transfer on a 30 and 50 tubes vertically stacked tube bundle with the diameter of the tubes as 22 mm and a p/d ratio of 1.45 using R-12/R-22 with heat flux in the range of 1-15 kW/m^2. Their results showed that the heat transfer coefficient increased with the tube rows. At the heat flux of 10 kW/m^2 the heat transfer coefficient at the 16th row was 33% higher than that at the second row and the 48th and 50th rows were 100% higher. Thus the bundle effect does level off after the first five or six rows but continues to increase.

Danilova , Dyundin and Soloviyov [53] investigated the local boiling coefficient for a 5 row tube bundle of hexagonal arrangement with p/d ratio of 1.35 and the diameter of the tube as 20mm using R-717/R-22. The heat flux was in the range of 1 to 10 kW/m^2. It was found that there was an increase of heat transfer coefficient with the tube position.

Fujita et al [54], [55] investigated the tube bundle effect in nucleate boiling outside horizontal tubes of diameter 25mm and heating length 120mm using R113 at pressures ranging from 0.1 to 1.0 MPa. A model was proposed based on the Mikic and Rosehnow pool boiling correlation. The model incorporated the convection due to the generating bubbles on the tube of interest and convection due to rising bubbles from the tubes below. The model was used to determine the enhanced heat transfer coefficients due to bundle effect calculated from the volumetric flow of rising bubbles and the population density of the active nucleation sites. The model was able to predict the heat transfer coefficient for the variation of tube arrangement, heat flux distribution and the system pressure. Typical observation of bubbles that were observed is shown in Figure 2.10.

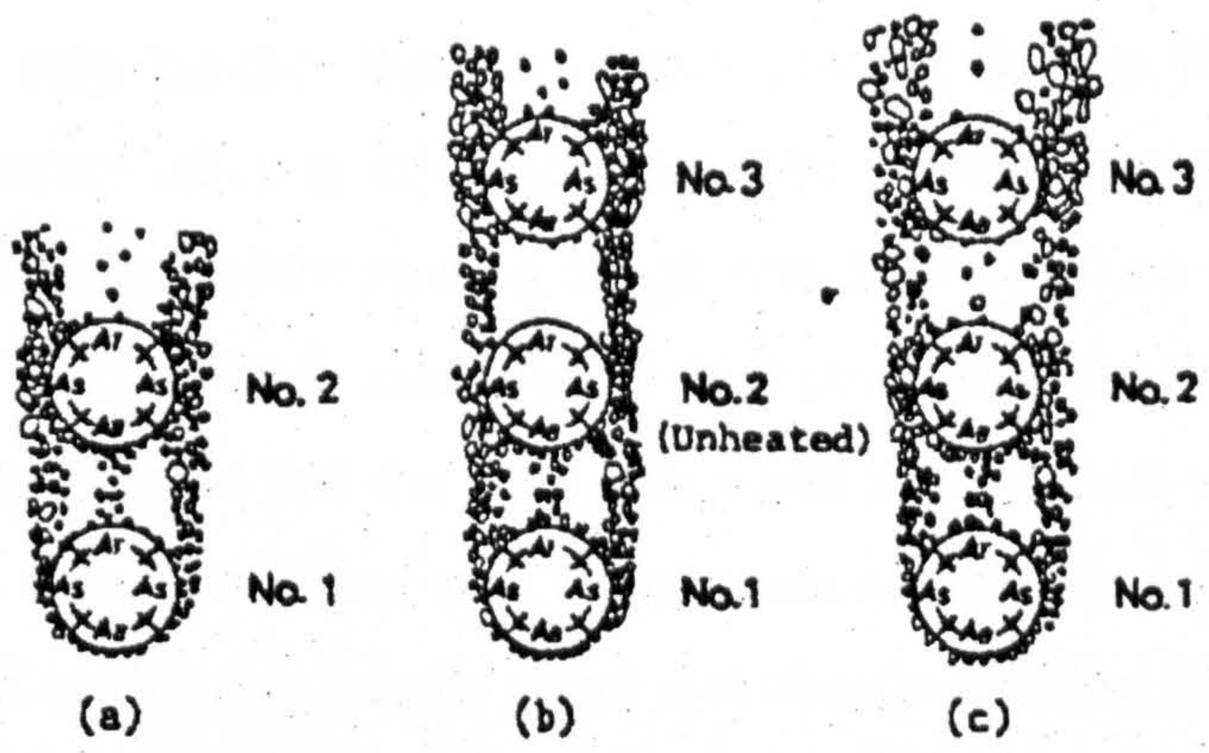

Figure 2.10 Sketches of bubbles behaviour around tubes, Fujita [55]

Jensen and Hsu [56] investigated the parametric study on the boiling heat transfer in a 27 horizontal tube bundle in an upward flow with R-113 as the working fluid using stainless steel tubes with diameter of 7.94 mm/7.62 mm. The parameters investigated were pressure 200,400 500kPa, mass flux 50-675kg/m^{2}s, quality 0-0.36 and heat flux 1.6- 44.1 kW/m^2 on heat transfer coefficients. They found that at low heat fluxes and mass velocities there was only a slight increase in heat transfer coefficient from the bottom tube row. Mass velocity and heat flux had the strongest influence on the heat transfer coefficient while the effect of quality was minor.

Grant and Henry [57] investigated the maximum heat flux for a slice of a small kettle reboiler made up of 177 tubes and tube diameter of 19 mm using R-12 as the working fluid. Their experimental results indicate that the nucleate boiling heat transfer was the

dominant mechanism that was observed and also there was no indication of shell-side dryout.

Hsu, Lin and Jensen [58] investigated the boiling heat transfer mechanisms on a tube bundle to determine the heat transfer of a tube in a heated tube bundle with heating and without heating. The test section consisted of a 5×27 square arrangement with the working fluid being R-113. Test was carried out for heat flux 3-47 kW/m^2, mass flux 45-460 kg/m^{2}s, pressure 206-517 kPa and quality of 0.014-0.136. Experimental results from the analysis of the circumferential variation for heat transfer indicate that possible mechanisms were that of bubble agitation and liquid thin film formation on the surface of the tube.

Recent studies by Robinson and Thome [59] investigated the boiling heat transfer of R-134a outside a 20 tube bundle that used water flowing through the tubes as a heat source with temperature taken at axial locations. The outside diameter of the tube was 18.7 mm made of copper and the heating length was 1027mm. Test were carried in the range of heat flux 2-35 kW/m^2, mass flux 5-41 kg/m^{2}s and vapour quality 0.1-0.87. Experimental results showed that the local heat transfer coefficient increased with heat flux for a constant mass flux. There was a dependence of heat transfer coefficient with mass flux or vapour quality, but bundle effect was observed within the bundle.

2.3.3 Effect of pressure on boiling heat transfer coefficient

Available data shows that heat transfer coefficient in nucleate boiling increases with increasing pressure. This is apparently due to a decrease in surface tension, which permits smaller bubbles to be formed at a given superheat and to a decrease in latent heat which causes a greater vapour generation rate and the presence of more agitation for a given heat flux. Similar effects are observed for multi-tube bundles.

2.3.4 Effect of velocity and mass flux

Boiling on a single tube with an externally imposed flow is a simplified configuration relative to a tube bundle and this has been studied by a lot of researchers. It has been described in Chapter 1 using the Figure 1.6 that velocity has effect on the boiling inside or outside a tube.

Yilmaz and Westwater [60] obtained the boiling curves for R-113 at 1.01 bar with steam heated horizontal tubes of diameter 6.4mm and velocities from 0 to 6.8 m/s. The effect of velocity was shown to be important in all the boiling regimes: nucleate transition and film boiling. These effects has also been corroborated by Singh et al [61] by using R-12 for low velocities at 0.013m/s. For R-13/11 mixtures, Fink et al [62] found similar trends for a 25 mm diameter electrically heated copper cylinder. Figure 2.11 depict their data.

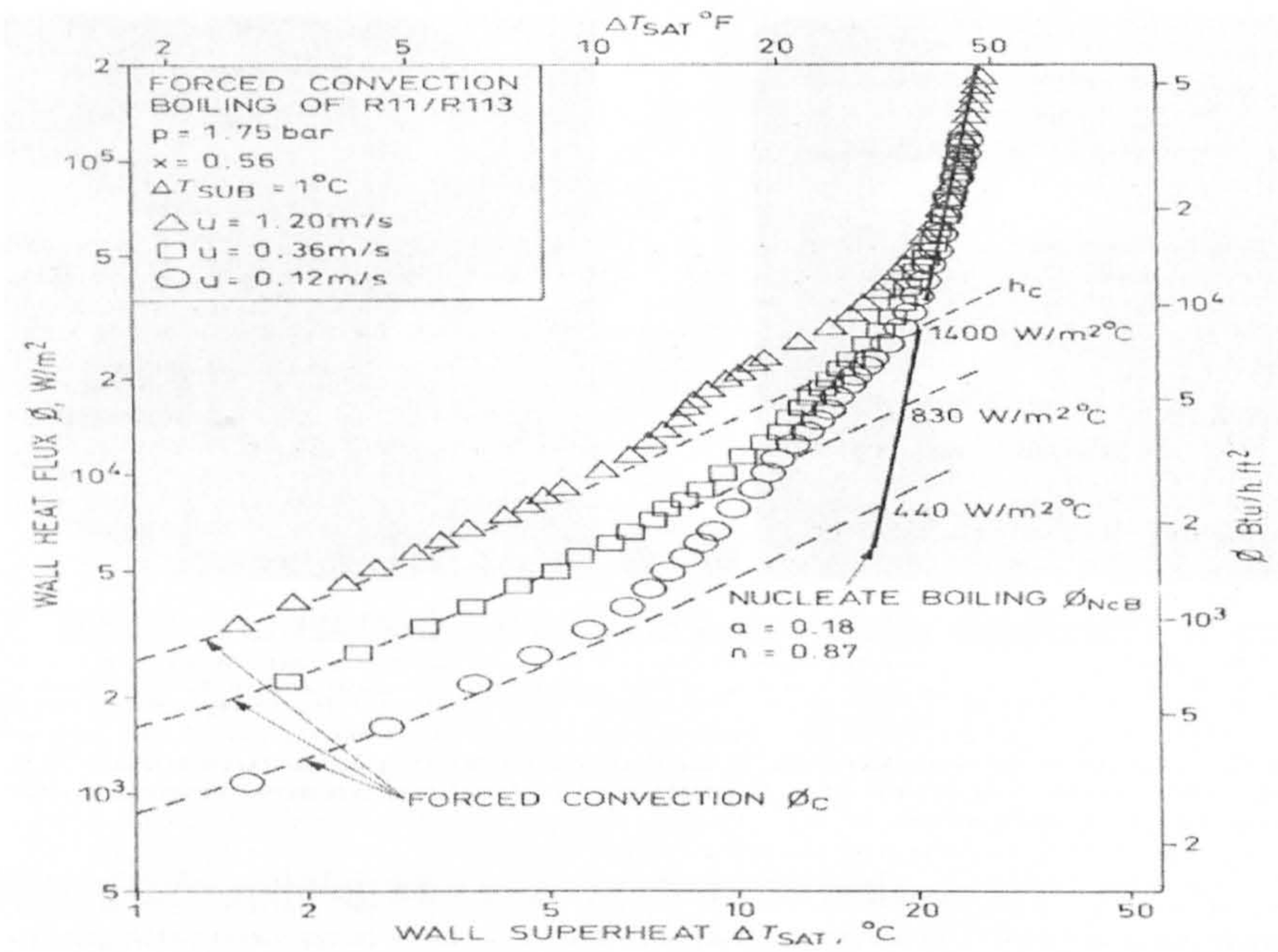

Figure 2.11 Effect of cross flow on boiling on a single tube, Fink et al [62]

Hwang and Yao [63] carried out experimental studies on a horizontal tube at various mass fluxes, local flow qualities and geometric arrangement (heated tube in a channel, heated tube in a non-heated tube bundle and heated tube in a heated tube bundle). It was found out that the single-phase convection heat transfer coefficient of a single tube is the lowest. Also the modified Chen's [64] correlation was able to predict the experimental values within 20% accuracy. At any point in the bundle the boiling heat transfer was found to be mainly dependent on the local flow velocity and the local quality.

Gupta [65] reported experimental studies of a 5 by 3 in-line bundle in pool and flow boiling using distilled water as the working fluid at nominal atmospheric pressure. The tube diameter used in the test was 19.05 mm with pitch to diameter ratios of 1.5 and 3,

heat flux 10-40 kW/m^2 and mass flux 0-10 kg/m^{2}s. Results obtained shown in Figure 2.12 indicates that at low mass flux and low heat flux there is an effect of cross flow velocity on the heat transfer coefficient whereas at higher mass flux and heat flux there was no significant change in the heat transfer coefficient observed. A Chen [18] correlation was developed to predict their experimental results to within ±30%.

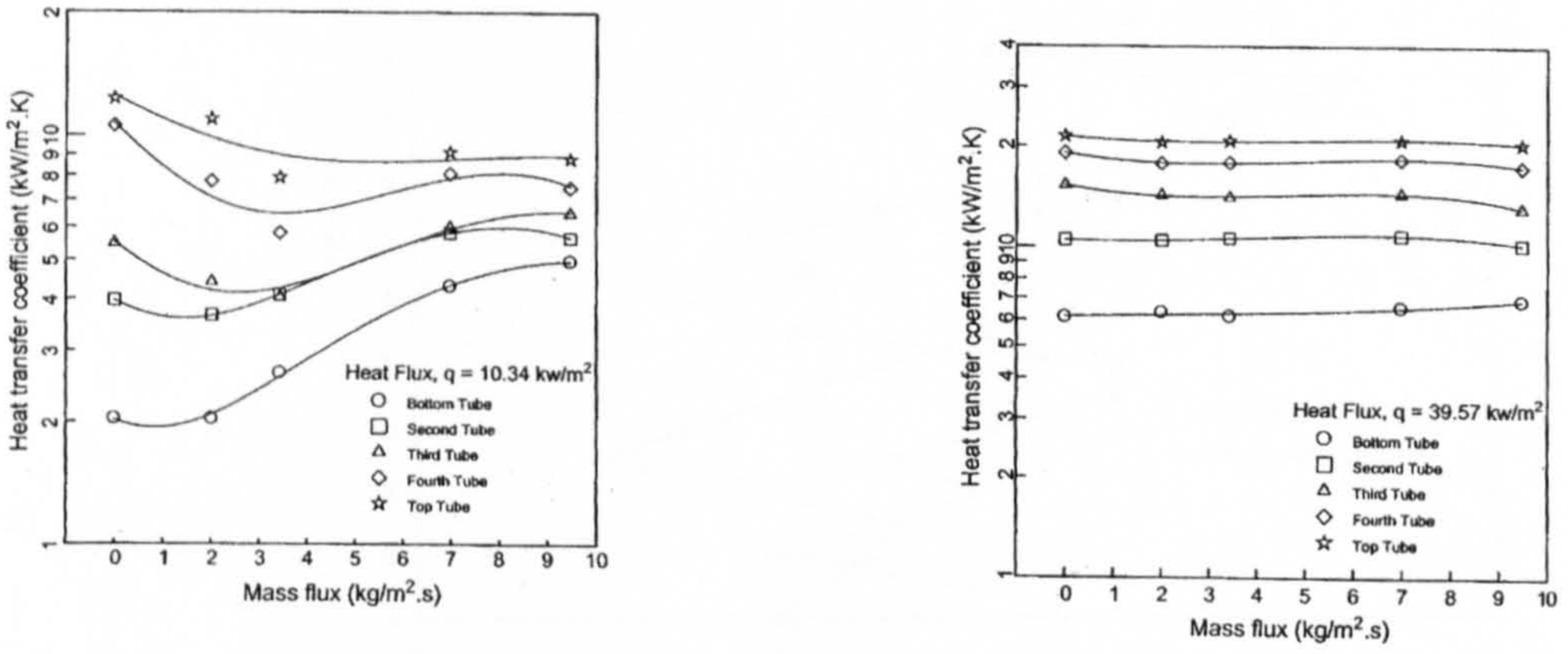

Figure 2.12 Effect of cross-flow velocity on heat transfer coefficient on central tubes, Gupta [65]

2.3.5 Effect of tube spacing and pitch to diameter ratio

The configuration of a bundle is classified as either an in-line, triangular or square arrangement. The heat transfer coefficient obtained in a bundle depends on the arrangement of the tubes and also the spacing between them. The smaller the clearance, the higher the heat transfer coefficient expected to be observed. The proceeding paragraph reviews experimental studies that have been carried out with bundle configuration in mind. Cornwell, Einarson and Andrews [66, 67] investigated a 34 tube bundle in–line and staggered tube arrangement with R-113 at 1 atmosphere. The heat flux range considered was 10-30 kW/m^2. It was inferred from the experimental results that there was no difference between the total heat transferred in staggered and in line bundle under the same conditions for both constant temperature and constant heat flux. A correlation satisfactorily predicted the experimental results were proposed as;

$$Nu = 0.4\,\mathrm{Re}_f^{\,0.60}\,\mathrm{Pr}_f^{\,0.36} + 150\,\mathrm{Re}_b^{\,0.67} \qquad (2.31)$$

Typical results obtained are shown in Figure 2.13 indicates there is no substantial variation between inline and rotated tube bundles.

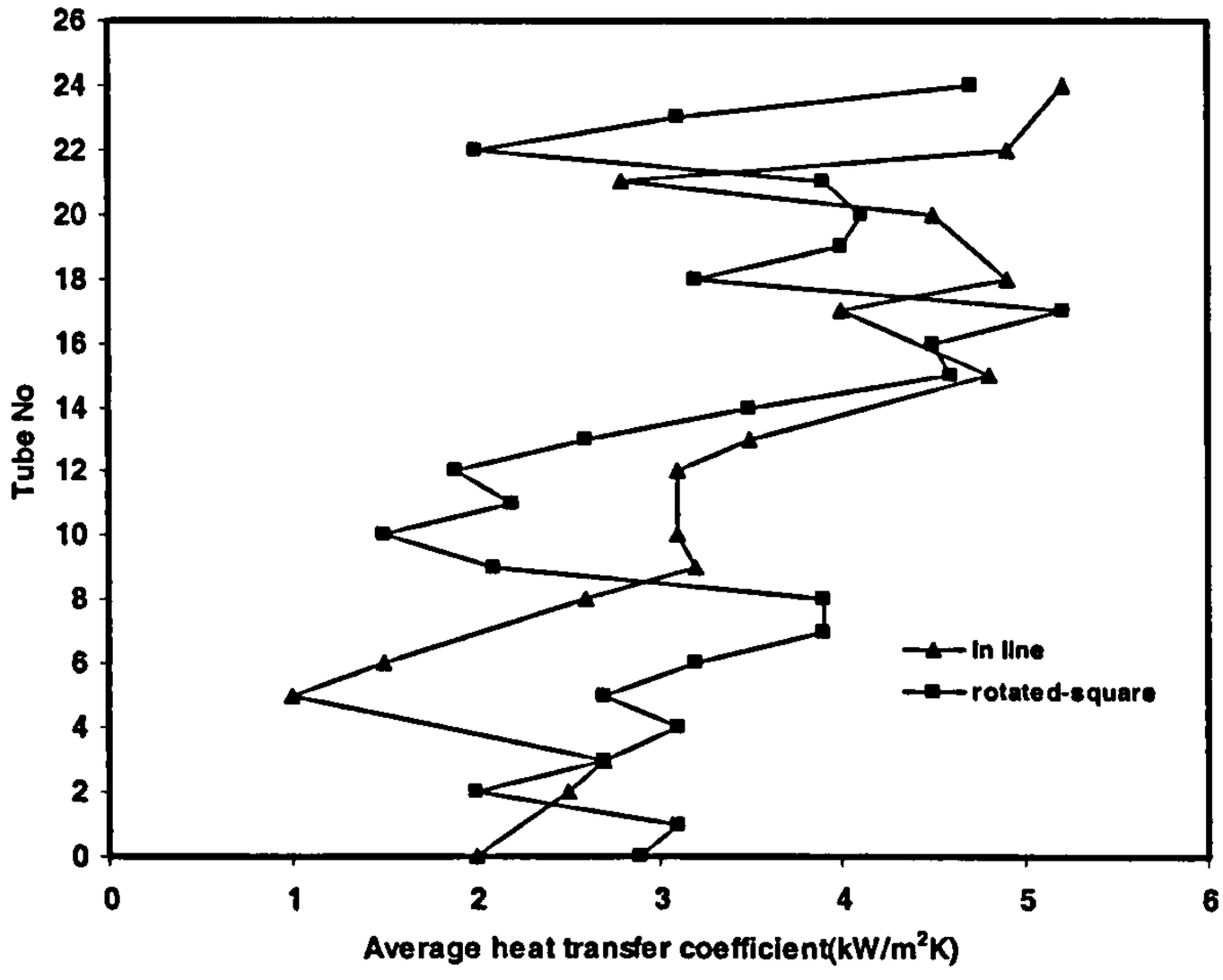

Figure 2.13 Comparison of rotated square and in-line bundles for q=20 kW/m^2, Cornwell, Einarsson et al [66]

Ivanov, Mamchenko et al [68] investigated the boiling heat transfer of refrigerant on a tube bundle with tube diameter of 10mm and p/d ratio of 1.4 using R-12 and R-22 with the heat flux in the range of 1-20 kW/m^2. A correlation was developed to predict the experimental results which included the p/d ratio and the boiling pressure. The correlation that was developed is as shown;

$$\alpha = Aq^{0.65} P_0^{0.25} \left[s/d \right]^{-0.45} \qquad (2.32)$$

where 'A' is a constant that depends on the type of the fluid, and P_o accounts for the operating pressure of the system. The value of 'A' was 3.98 and 4.65 for R-12 and R-22 respectively.

Slesarenko, Rudakova et al [69] investigated the boiling heat transfer on a tube bundle with p/d ratio 1.25-2.0 using distilled water as the working fluid. Heat flux and pressure were in the range of 22-135 kW/m^2 and 6-101 kPa respectively. Results indicated that

the heat transfer coefficient increased with height and bundle configuration ceased to have any effect at high heat flux.

In a related study, Hsu and Jensen [70] investigated the effect of pitch to diameter ratio on forced convective cross flow boiling in an inline tube bundle using R-113 with p/d ratio of 1.70 and 1.30. It was found out that at low heat fluxes the tube bundle with higher p/d ratio had a higher heat transfer coefficient. At moderate to high heat fluxes there were not significant differences in the heat transfer coefficients from the pitch-diameter ratios used. Moreover the heat transfer coefficients from each bundle have the same trend with respect to heat flux, mass velocity, pressure and vapour quality.

Marto and Anderson [71] investigated the effect of tube position upon the incipient boiling point and any hysteresis effect common to nucleate boiling processes for a 15 electrically heated copper tube bundle with outside diameter of 15.9 mm, which was subjected to aging processes. All tests were performed at atmospheric pressure. They showed that during natural convection heated lower tubes do not have much influence on the heat transfer from the upper tubes and the presence of the heated lower tubes enhanced the heat transfer coefficients of the upper tubes at lower heat fluxes and the enhancement leads to a bundle factor that depends upon heat flux and the number of heated tubes in the bundle. They went on to show that average bundle heat transfer coefficient of a smooth tube bundle was larger than that obtained for a single tube.

Gupta, Saini and Varma [72] carried out an investigation to determine the local heat transfer coefficient in a small tube bundle 5×3 with tube diameter of 19.05mm. The working condition used in their setup was heat flux in the range 10-40 kW/m^2, mass flux of 0-40 kg/m^2s with distilled water at nominal pressure. They found out that heat transfer characteristics of the lowermost tubes in the tube bundle was independent of the presence of the bundle, and there was no significant effect of bundle geometry on the heat transfer coefficient of the bottom tube compared with that of a single tube. Vapour bubbles rising from the lower tubes and agitating the liquid around the upper tubes increased the heat transfer coefficients on the upper tubes. A Chen [64] type correlation was able to predict the experimental data within reasonable degree of accuracy. The correlations developed from their experimental results are given in the following set of equations. The total heat transfer coefficient was given as;

$$\alpha = F\alpha_l + \alpha_{mic} \tag{2.33}$$

The heat transfer coefficient due to convection was that of Whitaker which was obtained as;

$$\alpha_l = \frac{k_l}{d}\left[0.4\mathrm{Re}_l^{1/2} + 0.06\mathrm{Re}_l^{2/3}\right](\mathrm{Pr}_l)^{0.36}\left(\frac{\mu_l}{\mu_v}\right)^{0.25} \tag{2.34}$$

The micro convection heat transfer was estimated from;

$$\alpha_{mic} = 13.0355(\Delta T_e)^{2.881} \tag{2.35}$$

The enhancement factor E was obtained as;

$$E = 938.53(B_o)^{0.710}\left(s/d\right)^{0.186} n^{0.463} \tag{2.36}$$

This correlation proposed was able to predict their experimental data to within 20%.

King and Jensen [73] investigated the heat transfer and flow pattern in a 75 electrically heated tube bundle with R-113 as the working fluid. It was found out that there was a small increase in heat transfer coefficients against position at low to moderate heat fluxes. A bubbly plume of mixture existed at the top of the bundle and the flow was found to be generally vertical between the columns of the bundle whiles some horizontal flow was also observed. Local flow patterns were found to be made up of single phase, bubbly, frothy and droplets in two-phase flow throughout the bundle.

Fujita [74] experimentally investigated the effects of tube bundles on nucleate boiling and critical heat flux using a fifty tube bundle of tube diameter 14mm using Freon-113 as the boiling fluid for two different set of arrangements. The p/d ratios were 1.3 and 1.5. From their experimental results it was concluded that heat transfer enhancement by the tube bundle effect was remarkable in the low to medium heat flux regions and the enhancement increased for tubes at higher location due to bubbles from the tubes

beneath it. The Hahne [75] prediction method was able to model their experimental values offering a fairly good agreement.

Liu and Qiu [76] investigated experimentally the enhancement effects by the restricted spaces in a compact tube bundle and enhanced tubes for boiling of pure water and salt mixtures under atmospheric pressure. The bundle was made of 17 tubes made of copper with outer diameter and inner diameter of 18 and 12 mm respectively. The spacing between the tubes was varied from 0.5 to 4 mm. The experimental results shown in Figure 2.14 indicated that the small gaps between the tubes enhanced the heat transfer coefficient for the compact tube bundle. For compact tube bundles with smooth tubes the heat transfer coefficients increased with decreasing tube spacing and for increasing heat fluxes the enhancement decreased and disappears.

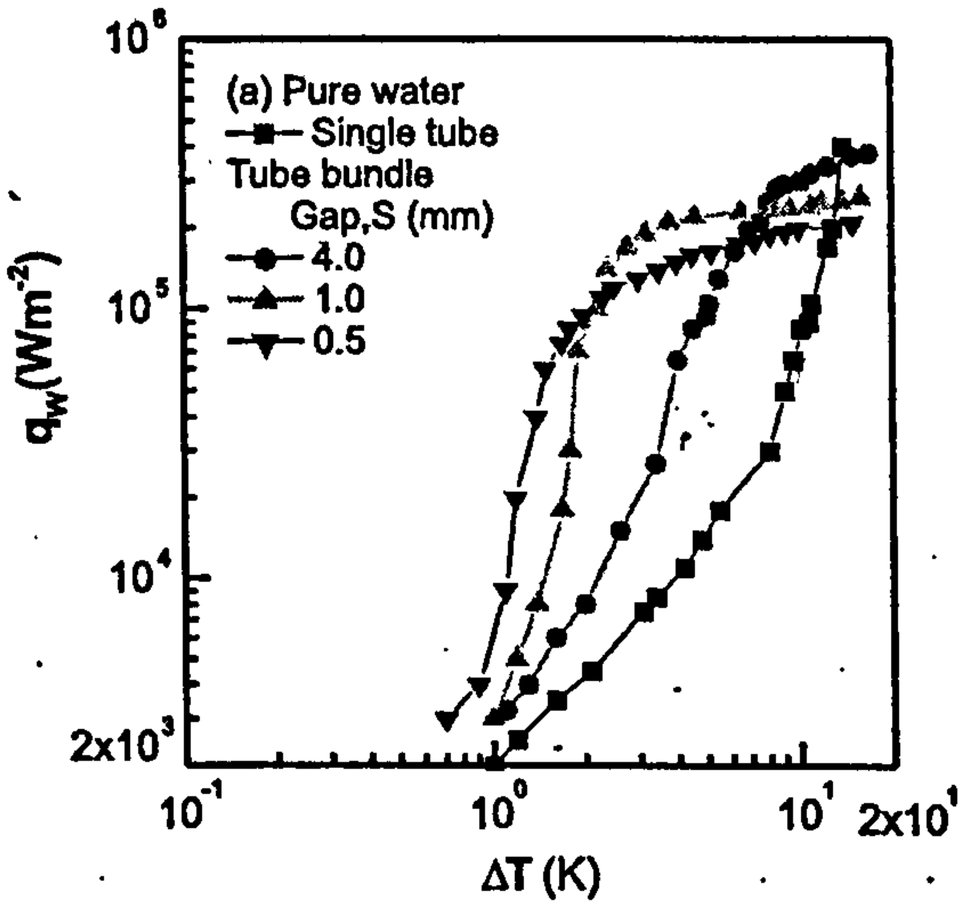

Figure 2.14 Boiling heat transfer results for compact smooth tube bundle, Liu and Qui [77]

Qiu and Liu [78] experimentally investigated the effect of tube spacing, pressure and positions of tubes in an 18 staggered tube bundles. The tube diameter was 18mm and made of copper. During the investigation it was concluded that for boiling in compact tube bundles the tube spacing had significant effect on the heat transfer coefficient. With a spacing of 3mm the bundle has a high heat transfer coefficient in the low and moderate heat flux region and at higher heat fluxes the effect decreases. Moreover the position of the tubes did not have any significant effect on the boiling heat transfer

coefficient but the heat transfer increases as the test pressure increases. Results obtained in their set up are given in Figure.2.13.

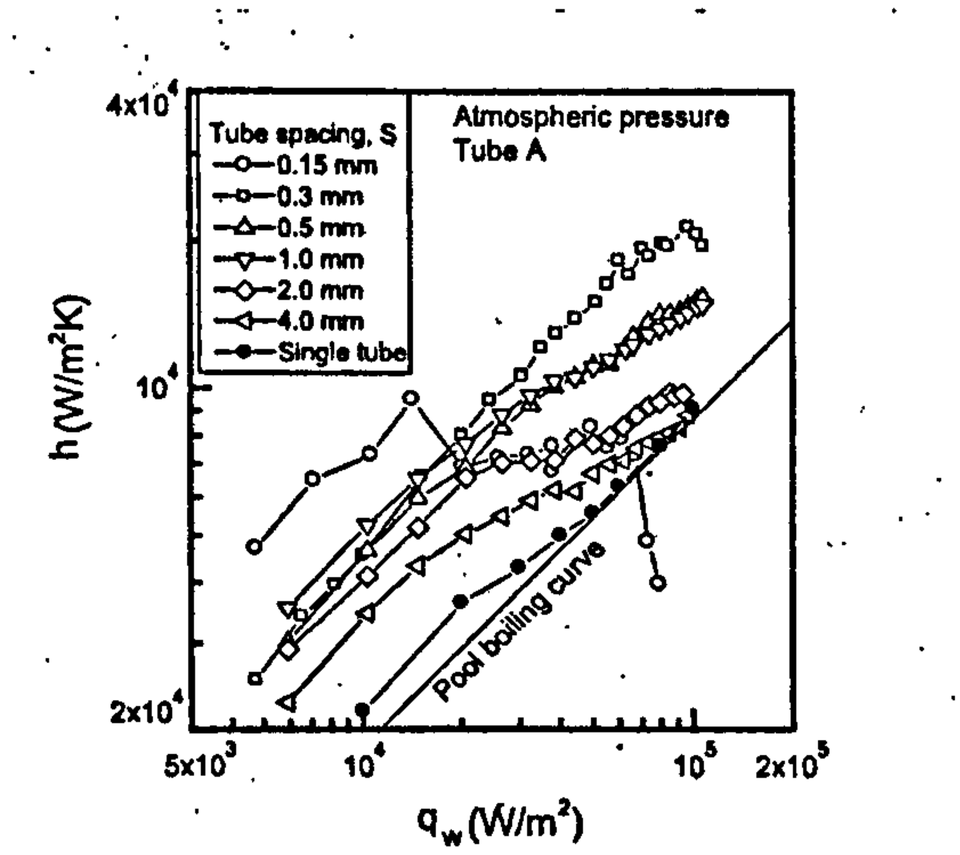

Figure 2.15 The effects of tube spacing on tube bundle, Qiu and Liu [78]

2.4 Heat transfer mechanisms associated with large tube bundles

Heat transfer mechanism occurring in a tube bundle has been shown to be made up of nucleate and a convective component occurring simultaneously on a tube surface. Investigation into the anomalous increase in heat transfer coefficient in the upper tubes has resulted in the general conclusion that sliding bubble contributes to the enhancement that has been observed and reported in literature. The sliding bubble effect and film thickness are reviewed in this section. Cornwell and Schuller [44] investigated the increase in heat transfer coefficient in the upper tubes of a bundle. A photographic study of boiling outside the tubes near the top reveals multiple bubbles sliding up the side of the tube as shown in Figure 2.16.

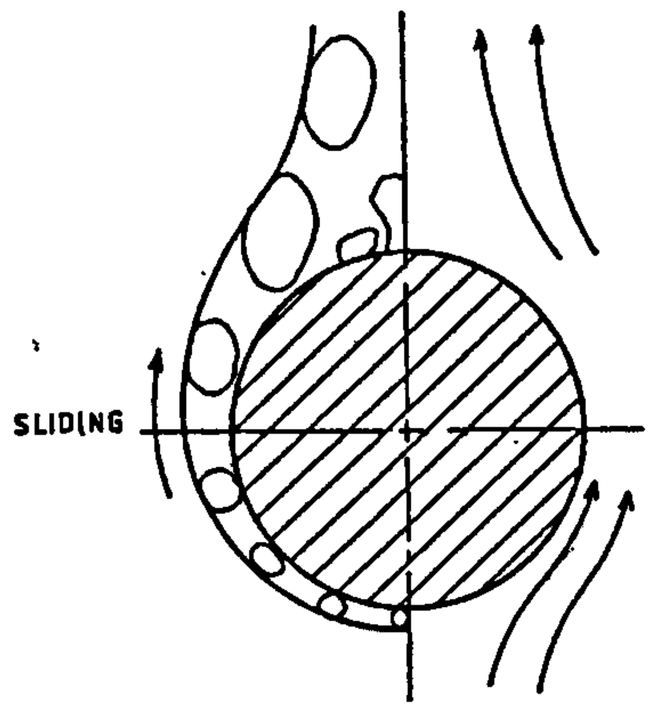

Figure 2.16 Sliding bubbles on a horizontal tube, Cornwell and Schuler [44]

It was found out that sliding bubbles account for the heat transfer in tube and bundles. A model based on the evaporation of the film layer beneath the bubble was used to explain the enhancement in heat transfer coefficient. A force balance analysis of the bubble reveals that the velocity of the sliding bubble is sensitive to the liquid properties and the contact angle.

In a later studies, Cornwell [79] carried out an experimental investigation to distinguish between the mechanisms that increases heat transfer coefficient in a tube bundle during bubbly flow using R-113. The heat transfer mechanism observed is a combination of forced convection, sliding bubbles and nucleate boiling, which is illustrated by the expression;

$$\alpha = \alpha_c + \alpha_{sb} + \alpha_{nb} \tag{2.37}$$

The liquid convection term was obtained by using the appropriate Nusselt number equation, whereas the sliding bubbles was due to the heat flow to a tube as a results of bubbles existing in the free stream. The nucleate boiling terms was due to bubbles which nucleate and grow on the surface of the tube.

Moreover the boiling heat transfer was determined on the surface of the tubes and the sides of the tubes were shown to exhibit high heat transfer due to sliding bubbles. In a similar studies, Cornwell [80] investigated the role of sliding bubbles in boiling on tube bundle using R113 at atmospheric pressure. He argued that the heat transfer coefficient within a bundle is determined from;

$$\alpha_{total} = \alpha_b \text{ for } \alpha_{total} > F\alpha_c \tag{2.38}$$

or

$$\alpha_{total} = F\alpha_c \text{ for } \alpha_{total} > \alpha_b \tag{2.39}$$

where α_b was the summation of the nucleate and sliding bubbles. Moreover it was inferred that tubes in the upper section of the bundle does not have any enhancement due to nucleation rather it is due to liquid convection and sliding bubbles alone, but tubes in the lower column experienced nucleation due to low quality and voidage of the fluid. They concluded that sliding bubbles play an important role in heat transfer in tube bundles and simple addition of boiling and convective mechanism are inadequate and a proper model should incorporate the quality. In another work, Cornwell and Houston [81] carried out experimental studies on a test tube within a bundle to investigate the effect of sliding bubbles during the heat transfer mechanism that occur at the outside tubes. He concluded that the enhancement was due to sliding bubbles rather than nucleation. Moreover, there was conduction through a thin film of liquid on the surface of the tube.

An attempt to study the heat transfer to bubbles under a horizontal tube by Addlessee [82] revealed that neither bubble sweeping mechanism nor layer evaporation alone are responsible but both mechanism must be included in analysis involving the local heat transfer coefficient. It has been shown that there was a thin film of layer under the bubbles that caused enhancement of the heat transfer coefficient. The size of the thin film had effect on the heat transfer coefficient that was predicted. Analytical model was developed by Addlessee and Cornwell [83] to predict the liquid film thickness above a bubble rising under an inclined plane. By using boundary layer of the adiabatic case the analysis yielded an estimated film thickness in the range of 200-300μm for fluids under normal room conditions. An experimental and theoretical studies by Kenning et al [84] , on the heat transfer to a sliding vapour bubble underneath a sloping plate has been verified. They found out that local variation in wall temperature was consistent with evaporation from a micro layer of 50-70 μm but accounted for only 35% of the total heat flow into the bubble deduced from its rate growth. Later, Addlessee and Kew [85] developed a model to estimate the liquid film thickness above a sliding bubble. The model considered the mechanics of the flow around the bubble and the method allowed

for the change of velocity profile and film thickness. Predicted values of the film thickness were compared with estimates obtained by thermal analysis of the measured temperature transients due to a steam of bubble sliding along a heated plate. The model was consistent with film thickness of 50-100μm.

In summary sliding bubbles play an important role in the transfer of heat from a surface in nucleate boiling and they are generally accepted in literature that it accounts for a proportion of the enhancement observed on tubes in bundles. There tends to be an argument on the exact size of the film thickness beneath an evaporating bubble. Some investigators predict 50-70μm as the film thickness beneath the bubble. Moreover experimental studies by Cornwell and Kew [31] using wire indicates that sliding bubbles cannot contribute to the enhancement on small tubes arrangement.

2.5 Pressure drop across large tube bundle

It is a conventional practice in tube bundle experimental arrangement to determine the pressure drop across the tube bundle. The pressure drop across the bundle is made up of the frictional component, acceleration component and the two-phase component. Mathematically it is written as:

$$\rho g H = \Delta P_f + \Delta P_a + \Delta P_{tp} \tag{2.40}$$

For a tube bundle it is assumed that the liquid frictional drop is negligible. The acceleration pressure drop is also assumed to be negligible. The two-phase pressure drop across the tube bundle is the most significant. The pressure drop in the liquid zone is essentially composed only of static head. The length of the liquid zone depends on the amount of the sub-cooling of the fluid entering the bottom of the bundle and the rate of heat transfer to the fluid. The amount of subcooling is a function of the static head and the operating pressures.

2.5.1 Two-phase pressure drop

The two-phase pressure drop across a tube bundle is made up of the following which has described by Palen and Yang [86]:

$$\Delta P_{tp} = \Delta P_{tps} + \Delta P_{tpm} + \Delta P_{tpf} \tag{2.41}$$

The static head term is calculated as;

$$\Delta P_{tps} = \rho_{tp} g \Delta l \tag{2.42}$$

where

$$\rho_{tp} = \rho_f R_f + \rho_f \left(1 - R_f\right) \tag{2.43}$$

The liquid volume fraction is calculated from a theoretical relationship with the two-phase shear term which is given as;

$$R_l = \left(\frac{1}{\phi_l^{\,2}}\right)^m \tag{2.44}$$

The friction term was calculated as follows;

$$\Delta P_{tpf} = \phi_l^{\,2} \Delta P_l \tag{2.45}$$

where

$$\phi_l^{\,2} = 1 + \frac{C}{X_{tt}} + \frac{1}{X_{tt}^{\,2}} \tag{2.46}$$

The value of C depends on the geometry and flow regime and is correlated for best agreement with data

The single-phase pressure drop was given as;

$$\Delta P_l = \frac{2 f G_t (1-x) N}{\rho_l} \tag{2.47}$$

The friction factor f is based on the Reynolds number for the liquid phase alone. The momentum term is calculated as;

$$\Delta P_{tm} = G_t^2 \left\{ \left[\frac{(1-x)^2}{\rho_l R_l} + \frac{x^2}{\rho_v (1-R_l)} \right] - \left[\frac{(1-x)^2}{\rho_l R_l} + \frac{x^2}{\rho_v (1-R_l)} \right] \right\} \tag{2.48}$$

2.6 Large tube bundle boiling heat transfer correlations

Similar to boiling inside a tube, a mechanistic approach to the formulation of a bundle boiling model requires a single phase correlation for the convective contribution to the heat transfer. The heat transfer from forced convective boiling across a tube bundle bank is dependent on the flow velocity, bundle diameter and fluid properties. Experimental results are normally correlated in the form;

$$Nu = c\,\mathrm{Re}^{m}\,\mathrm{Pr}^{n}\left(\mathrm{Pr}/\mathrm{Pr}_{w}\right)^{0.25} \tag{2.49}$$

where the empirical constant c and exponents m and n are dependent on the Reynolds number and the tube layout.

2.6.1 Average bundle boiling correlations

A method for estimating the bundle boiling heat transfer coefficients has been presented by Palen and Yang [86] for a tube bundle. The average heat transfer coefficients have been obtained by the contributions of the boiling and natural convections components as;

$$\alpha_b = \alpha_{nb} F_b F_c + \alpha_{nc} \tag{2.50}$$

where α_{nb} is the nucleate boiling coefficient , F_b is the bundle boiling factor and F_c is the mixture boiling correction factor and α_{nc} is the single phase natural convection . The nucleate pool boiling was calculated using a suitable correlation whiles F_c accounts for the degradation of α_{nb}. The factor F_b is an empirical multiplier that ranges from 1 to 3 at heat fluxes above 50 kW/m^2.

An empirical correlation has been developed by Rebrov, Bukin et al [52] for tube bundles with 5, 6, 18, 30 and 50 vertical tube rows. Their boiling expression for the average bundle heat transfer coefficient was determined from the expression;

$$Nu_f = 0.04 e^{0.087N}\,\mathrm{Re}_f^{\,(0.7-0.0078N)}\,K_p^{\,(0.6-0.0058N)}\,\mathrm{Pr}_f^{\,0.4} \tag{2.51}$$

where the boiling Nusselt number was defined as ;

$$Nu_f = \frac{\alpha_b \left[\sigma / g(\rho_f - \rho_g) \right]^{1/2}}{k_f}, \tag{2.52}$$

and the boiling Reynolds number was defined as ;

$$\mathrm{Re}_f = \frac{q\left[\dfrac{\sigma}{g(\rho_f - \rho_g)} \right]}{h_{fg}\rho_f \nu_f} \tag{2.53}$$

K_p was the pressure correction factor determined as;

$$K_p = \frac{p_{sat}}{[\sigma g(\rho_f - \rho_g)]^{1/2}} \tag{2.54}$$

This correlation was applicable for heat fluxes in the range of 1 to 15 kW/m^2, tube pitch of 1.45, n from 1 to 50 and the saturation temperature T_{sat} from -30°C to 10°C

2.6.2 Local bundle boiling models

A large number of correlations have been proposed for boiling on tube bundle. However, many of these are restricted and could only be applied to the experimental fluid used in the development of such correlations. In this section the models that have been developed would be reviewed in conjunction with its applicability to boiling on tube bundle.

An early correlation for saturated boiling still generally quoted is that of Chen [64] who divided the heat transfer into two parts: a micro convective nucleate boiling on the tube surface and a nucleate pool boiling. Forster and Zuber [4] correlation was used for the nucleate pool boiling component and the single phase macro convective component based on the Dittus–Boetler correlation. The F factor is greater than unity and reflects the much higher velocities and the suppression factor reflects the lower effective superheat available in forced convective pool boiling as opposed to pool boiling due to the thinner boundary layer. The model is given as;

$$\alpha = \alpha_{fc} F + \alpha_b S \tag{2.55}$$

where

$$\alpha_{nb} = 0.00122 \left(\frac{k_l^{0.79} C_{pl}^{0.45} \rho_l^{0.49}}{\sigma^{0.5} \mu_l^{0.29} h_{fg}^{0.24} \rho_g^{0.24}} \right) \Delta T_{sat}^{0.25} \Delta p_{sat}^{0.75} \tag{2.56}$$

as the Foster and Zuber [4] correlation for nucleate boiling component.

Clapeyron's equation may be used to determine from;

$$\Delta p_{sat} = \frac{h_{fg} \Delta T_{sat}}{T_{sat} \left(\frac{1}{\rho_g} - \frac{1}{\rho_l} \right)} \tag{2.57}$$

The natural convection component of the Chen [64] correlation was given as;

$$\alpha_{fc} = \frac{k}{d} 0.023 \mathrm{Re}_l^{0.8} \mathrm{Pr}_l^{0.4} \tag{2.58}$$

For the Chen [64] correlation the enhancement factor was defined as a function of the Martinelli parameter as ;

$$F = 2.35 \left(\frac{1}{X_{tt}} + 0.213 \right)^{0.736} \tag{2.59}$$

whereas the suppression factor was given as;

$$S = \frac{1}{1 + 2.53 \times 10^{-6} \mathrm{Re}_l^{1.17}} \tag{2.60}$$

and the Reynolds number as;

$$\mathrm{Re}_l = \frac{m(1-x)d}{\mu_l} \tag{2.61}$$

The model used by Hwang and Yao [63] for the development of their correlation was based on the Chen [64] superposition model. The purpose was to redefine the enhancement and the suppression factors used in a tube bundle. Three different geometries were studied namely a heated tube in a channel, a heated tube in a non heated in line tube bundle and a heated tube in a heated in-line tube bundle. The expression for the model was given as follows;

$$\alpha = S\alpha_{nb} + F\alpha_c \tag{2.62}$$

The nucleate boiling was determined from their experimental results by correlating the single tube results as;

$$\alpha_{nb} = 0.2086q^{0.75} \tag{2.63}$$

Heat transfer due to the convective boiling was determined as;

$$\alpha_l = \alpha_c[1 - x_{loc}]^{0.6} \tag{2.64}$$

Their suppression factor was based on the correlation of the Bennett [87] as;

$$S = \frac{k_l}{F\alpha_l Y}\left[1 - \exp\left(\frac{-F\alpha_l Y}{k_l}\right)\right] \tag{2.65}$$

where

$$Y = 0.0205\left(\frac{d}{R^*}\right),$$

and R^* was given as;

$$R^* = \frac{d}{2}\left[\frac{\sigma}{g(\rho_f - \rho_g)}\right]^{-1/2} \tag{2.66}$$

And the enhancement factor was obtained as a function of the void fraction as;

$$F = \left(\frac{1}{1-\varepsilon}\right)^{0.744} \tag{2.67}$$

where ε_m was the modified void fraction which was given as

$$\varepsilon_m = \frac{0.833x}{x + (1-x)\left(\rho_g / \rho_f\right)} \tag{2.68}$$

At any point within the bundle the local heat transfer coefficient was found to be dependent on the mass flux and thermodynamic quality.

Nakajima [49] proposed that the bundle boiling coefficient was the summation of nucleate boiling and film thin evaporation. The general expression for the local bundle boiling heat transfer coefficient on the nth row from the bottom of the bundle was given as;

$$\alpha_b = (1-\varepsilon)\alpha_{nb} + \varepsilon\alpha_{tf} \tag{2.69}$$

At low void fraction nucleate boiling was dominant mechanism whereas at high void fraction the thin film evaporation becomes the controlling mechanism. The film thin heat transfer coefficients were given by the equation;

$$\alpha_{tf} = 2326 + 151\exp\left[-\left(0.556/u_g\right)\right]^{1.5} \tag{2.70}$$

The superficial vapour velocity was calculated from the energy input of the lower tube row as;

$$u_g = \sum_{N}^{N-1} \frac{q\pi d}{h_{fg}\rho_g N s_1} \tag{2.71}$$

where s_1 was the transverse tube pitch. No convective heat transfer contribution was considered, thus the limit when the void fraction is 1 the model breaks down and predicts thin film evaporation to occur when no liquid is present.

Cornwell, Duffin et al [88] developed a model to predict the local heat transfer coefficient within a tube bundle. The model was made up of the summation of the convective and the boiling heat transfer coefficients. The convective component of the boiling for in tube bundles was obtained from the Zaukukas [89] correlation for an in-line tube bundle as;

$$Nu_f = 0.27\,\mathrm{Re}_f^{\,0.63}\,\mathrm{Pr}_f^{\,0.36} \tag{2.72}$$

For the variation of the velocity in the bundle the Lockhart–Martinelli model for separated flow was used despite being derived for flow in pipes. Hence the convective Nusselt numbers was found from the method developed by Cornwell, Duffin et al [88] which was given as:

$$Nu_f = \frac{\alpha_f d}{k_f} \tag{2.73}$$

And the liquid Reynolds number as;

$$\mathrm{Re}_f = \frac{\rho_f U_f d}{\mu_f} \tag{2.74}$$

The liquid velocity was determined from the relation;

$$U_f = U_g\left(\frac{\varepsilon}{1-\varepsilon}\right)\left(\frac{\rho_g}{\rho_f}\right)\left(\frac{1-x}{x}\right) \tag{2.75}$$

and the vapour velocity was estimated as;

$$U_g = \frac{m_i x}{\rho_g A_i \varepsilon} \tag{2.76}$$

But from Cornwell, Duffin et al [88] the void fraction was calculated using the Martinelli parameter as;

$$\frac{1}{1-\varepsilon} = 1 + \left(\frac{6}{X_{tt}}\right)^{0.71} \tag{2.77}$$

The constant mass flow rate was estimated from the liquid flow into the test section and the parameters were calculated from the bottom to the top of the bundle.

Webb and Chien [90] proposed a correlation for the boiling on plain tube bundles based on their own data using R-113 and R-123. The bundle was made of copper tubes of diameter 16.8 with a triangular pitch .They correlated their results using the asymptotic model with boiling suppression set to unity and the asymptotic exponent set to 3. For the single–phase convective component the Zaukauskaus [89] correlation was used. Their asymptotic model was able to predict their database within -50% and +75% while Chen [64] predictions gave from -40% to +95%.

Gupte and Webb [91] assumed that S=1 and validated it experimentally. They derived their expression from the momentum heat transfer analogy. They presented the two-phase boiling heat transfer as:

$$\alpha = \left[(F\alpha_l)^n + (\alpha_{nb})^n\right]^{\frac{1}{n}} \tag{2.78}$$

And the enhancement factor was obtained as;

$$F = C_1\left[\frac{\phi_l(\mathrm{Pr}_l + 1)}{2}\right]^{C_2} \tag{2.79}$$

The two-phase friction factor used was based on the correlation developed by Ishihara, Palen et al [92]. The single phase heat transfer in the above expression was based on the Zaukakas [89]. C_1 and C_2 were obtained from experimental data. For a selected value of n, the root mean squared error and the mean deviation were calculated in order to select the suitable value of n. Their model was validated against measurements of Cornwell and Scoones [93] for R-113 on plain banks tubes and their own experimental data. For n=3 and S=1, they obtained C_1=18.2 and C_2=0.229. The model predicted 84% of their data with an accuracy of ±20% for low finned and enhanced tube banks.

In summary, there are various boiling methods available in open literature but none of them have been able to predict an independent data that is not included in its developments. Most often the methods described does not reflect the boiling mechanisms observed.

2.7 Circulation boiling models

The studies by Cornwell and Leong [94] in an oversized shell indicated that there was recirculation in the bundle. Thus the flow rate must be determined by balancing the pressure drops (two-phase) with the static head of the liquid. This recirculation has been found to have an effect on the local as well as mean boiling heat transfer coefficient. Various models discussed have been developed to account for these effects.

Brisbane, Grant and Whalley [95] developed a simpler recirculation model to predict the local heat transfer coefficient inside a kettle reboiler and also quality with position in the bundle. The model considered the flow as one dimensional and also boiling occurred only below the tube bundle whiles the liquid and vapour phase are considered to be in equilibrium. Their model was used to predict the experimental results of Cornwell and Leong [94] which predicts an increase in bundle size. This required an iterative procedure as the thermal and hydraulic of the system are closely linked. This simplified model required pressure drop, void fraction and heat transfer correlations for one-dimensional two-phase flow across the tube bundles. Whalley and Butterworth [96] presented a method for calculating the recirculation flow in a vertical thermosyphon and kettle reboiler. The method used the two-phase homogeneous model for prediction using explicit equations which were functions of the outlet quality.

Palen and Yang [86] extended the earlier work of Brisbane, Whalley et al [95] and co-workers and developed a circulation model in order to predict the local heat transfer coefficient at low temperature differences and also to account for both enhanced surfaces and finned tubes. The model considered the pressure drop balance across the bundle.

A modification of these model Palen and Yang [86], Brisbane [95] has been proposed by Jensen [97]. The bundle was considered as multiple 1D column, which allowed a better representation of the geometric configuration of the bundle in the shell. Jensen

[97] developed a one-dimensional model to estimate the recirculation flow in a kettle reboiler. The factors considered in his model are the effect of bundle size, pressure drop and heat flux. The model was able to predict the heat transfer coefficient for the bundle work of Leong and Cornwell [50]. The model was an attempt as it did not include the transverse flow that occurs in between columns, hence a two–dimensional approach was needed which would incorporate it.

Cornwell, Duffin et al [88], King and Jensen [73] have shown that the variability of the heat transfer coefficient in the bundle is not only effective in the vertical direction (the well known bundle effect), but is also significant in the horizontal direction. Consequently, the two-dimensional flow in the bundle must be taken into account for an accurate thermal design of the reboiler. Furthermore, King and Jensen [73] have shown that the recirculation in the shell is more complex than a simple cell of the liquid, and it involves different patterns of the two-phase flow with one or several flow cells.

Kumar, Jain et al [98] developed a hydrodynamic model to determine the pressure drop, vapour quality , recirculation rate , boiling regime and heat transfer coefficient for various rows in a kettle reboiler using physio-thermal properties of the liquid and also liquid vapour mixture as well as empirical correlations. The model is able to predict the results of Leong and Cornwell [50] to an accuracy of ±20% shown in Figure 2.17.

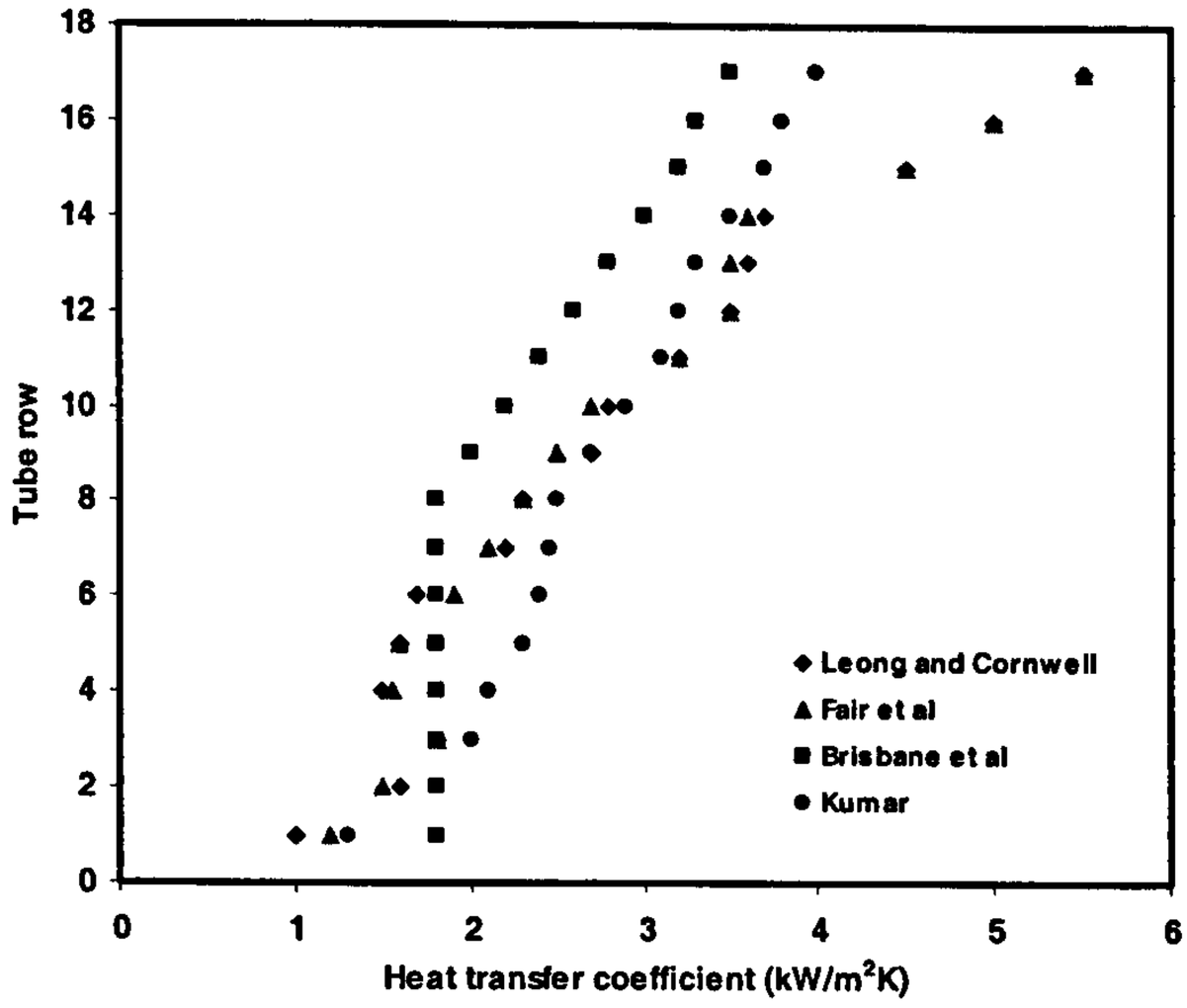

Figure 2.17 Comparison of model with data of Leong and Cornwell [50], Kumar, Jain et al [98].

2.8 Boiling in confined spaces

Several investigations have been carried out on nucleate boiling in confined spaces formed by either annuli or narrow gaps between flat plates. Nucleate boiling can be the dominant mechanisms and useful information can be obtained about the boiling mechanism in application to compact heat exchangers.

Ishibashi and Nishikawa [99] investigated the boiling mechanisms in a confined space using different fluids for various arrangement of the test section at different heat flux and pressures. Their results clarified the effect of restriction on the nucleate boiling heat transfer phenomena. They reported the boiling heat transfer coefficients against heat flux for different gap size and pressures. Results showed that the restriction enhanced the heat transfer coefficient.

Fujita, Ohta et al [100] investigated nucleate pool boiling heat transfer and critical heat flux for saturated water in a confined narrow space bounded by a vertical copper rectangular heating plate and an unopposed unheated parallel rectangular plate. Three different experimental results were obtained. The first was an open periphery where four edges of a confined space were open to the bulk liquid, second was a closed side periphery where both sides of the edges were closed and the top and bottom edges open to the bulk liquid. Heat transfer measurements and still photographs were obtained to explain the observed mechanisms. Gap sizes considered in the tests were 5, 2, 0.6 and 0.15 mm with the working fluid being distilled water at atmospheric pressure. Heat flux was varied from inception to critical heat flux. Experimental results showed that heat transfer coefficient increased to a certain maximum with decrease of the gap size. At moderate heat flux whiles with further decrease of gap size there was degradation of heat transfer coefficient.

Hung and Yao [101] presented a data base for pool boiling heat transfer in horizontal annuli with various gap sizes and provided the explanation of physical phenomena and a correction factor was developed to correct the critical heat flux in annular crevices. The data presented investigated the effect of fluid properties, gap sizes , crevice length and sub-cooling all at saturated conditions and at atmospheric pressure for gap size of 0.32, 0.80 and 2.58 mm with distilled water, Freon and acetone as the working fluid. Results showed that boiling heat transfer at the top was due to thin film evaporation and more effective nucleate boiling was observed when the gap sizes were reduced. Critical heat

flux always occurred at the top centre of the heated tube. Semi-analytical correlation has been established which was comparable to the experimental data.

Kang and Han [102] investigated the effect of gap size on the pool boiling heat transfer coefficient (3.9-44.3 mm). Their investigation concluded that the gap size has effect on the heat transfer coefficient. The smaller the gap sizes the higher the heat transfer coefficient. It depends on the geometry of the bottom of the annuli, this can be either closed or open. For the case of closed bottom more complicated bubble and liquid mixing occurs. As the gap size is small the liquid supply is not sufficient due to interruption by bubble slugs. Abrupt bubble slug formation is observed around the tube surfaces even at low heat fluxes. This bubbles resulted in the deterioration of the heat transfer coefficient. Kang [103] investigated the effect of subcooling on the boiling heat transfer in a confined annular space with closed bottom. The gap size was 7.05 mm. The experiments were carried out at saturation condition and the working fluid was distilled water. The level of subcooling ranged from 0 to 50 K. Experimental results indicated that increase in subcooling results in an enhancement of the heat transfer coefficient, but as the subcooling decreased there was a deterioration of the heat transfer coefficients. The mechanism of boiling is that restricted spaces form a stable and stagnant superheated thermal boundary layer on the heated surfaces, which initiates boiling at low heat flux. Huge coalesced bubbles generated in the restricted spaces displace completely the superheated boundary and fresh liquid dashes into the space periodically hence the high heat transfer obtained at low heat flux. When the restricted space is small the temperature of the liquid in the restricted spaces increases due to the small mass of fluid. A compact tube bundle where the tube spacing is so small, the gap size has a strong effect on the heat transfer coefficient at low to medium heat flux. At higher heat flux this enhancement is exceeded. Tube position within a bundle has little effect on the heat transfer coefficient.

2.8.1 Characteristics of nucleate flow boiling in confined spaces

Nucleate boiling is observed to be the predominant mechanism occurring in confined spaces. Flow regimes that occur in tubes have been the subject of intense debate for the past two decades. Such a flow occurs when a liquid is been vaporised inside. The actual two–phase flow inside a tube or channel depends on the relative values of the physical properties of the fluid. Generally most researchers classify flow patterns into four classes such as stratified flow, intermittent flow, annular flow and bubbly flow.

An analysis of the effect of tube diameter on vertical two-phase flow has been presented by Chen, Tian et al [104] using diameter of 1.01, 2.01, 2.88 and 4.26 mm with R-134a as the working fluid. The test was carried out at a pressure of 10 bar. Seven flow patterns were observed under the experimental conditions shown in Figure 2.18 and Figure 2.19. They concluded that the flow regimes observed for the 2.88 and 4.26 mm diameters were similar to that of large diameter. When the tube was further reduced to 1.10 mm confined bubbles was dominant which indicated that surface tension was significant. In general the results were grouped into the following;

- Bubbly flow: in this case the bubble size is not comparable to the tube diameter
- Confined bubble: the bubble is of the same size as the tube diameter and the restrained by the tube wall
- Slug: bubble develop into bullet shapes due to the restriction of the walls
- Churn: bullet bubbles begins to distort and small bubbles in the liquid slug coalesce with an increase in velocity
- Annular: the gas phase becomes dominant

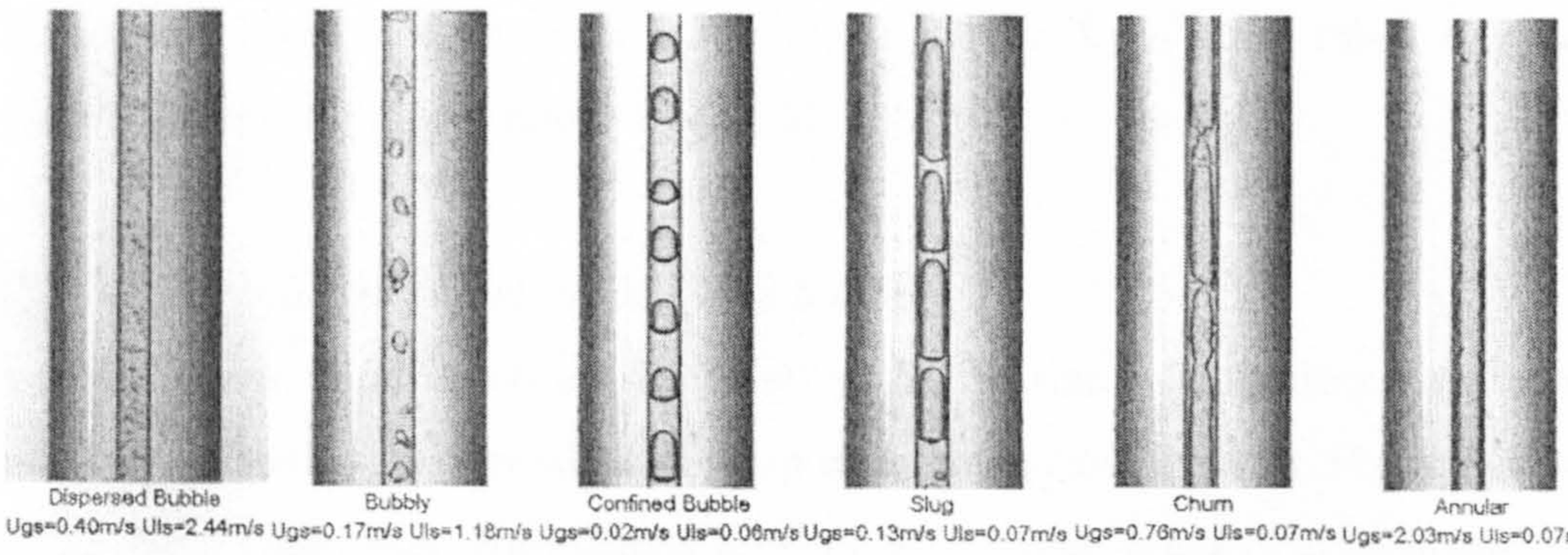

Figure 2.18 Flow patterns observed in 1.10 mm diameter tube at 10 bar , Chen , Tian et al [104]

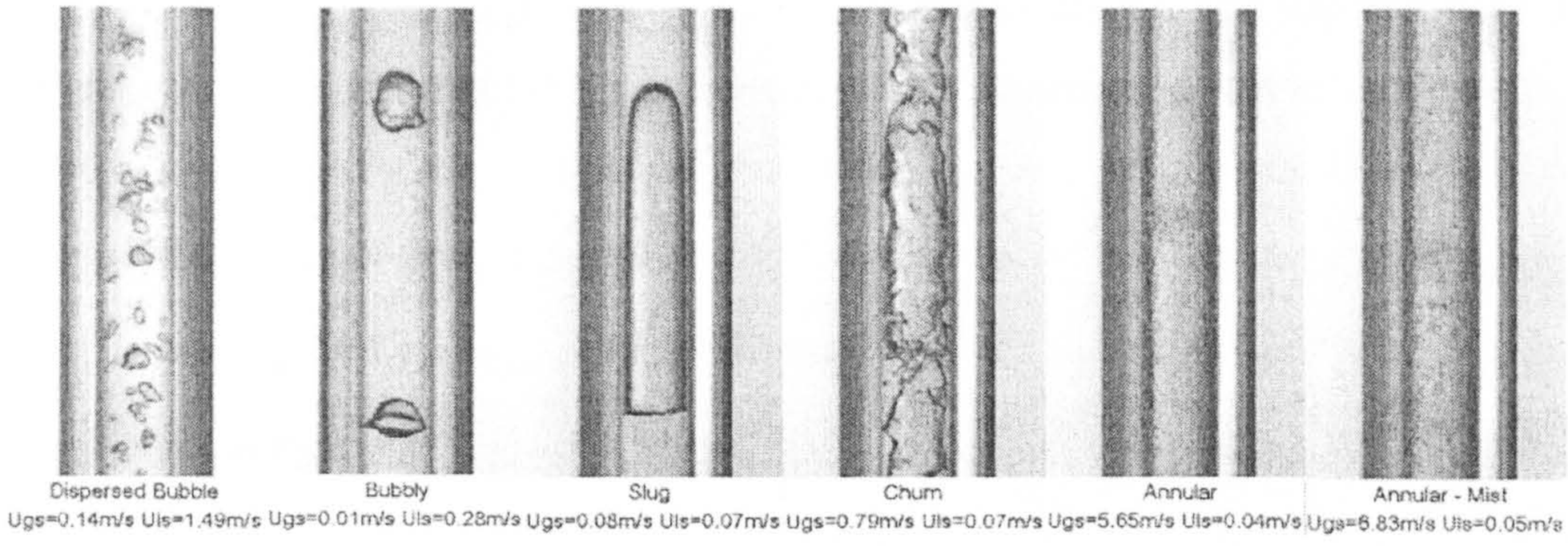

Figure 2.19 Flow patterns observed in 2.88 mm diameter tube at 10 bar , Chen , Tian et al [104]

2.8.2 Confinement number

Confinement number Co has been used by Kew and Cornwell [105] for the heat transfer associated with a small channel. They suggested that confinement has effect for channel dimension having hydraulic diameter in the excess of 0.5. This criterion enabled the determination of the critical size of the channel defining the shift from isolated bubble regime to confined bubble regime for a given fluid pressure. The confinement number C_o defined by Cornwell and Kew [106] for flow in tubes was given as ;

$$C_o = \frac{\sqrt{\sigma / g(\rho_l - \rho_g)}}{d} \tag{2.80}$$

The C_o has been used to differentiate the transition from large tubes from micro-channels by several investigators such as Thome [107].

2.8.3 Heat transfer models in confined boiling

In compact tube bundles where there is effect of gap size, heat transfer correlations are complicated due to the dependence of gap size on the flow regimes. For large channels or gap sizes established correlations are available which predicts experimental results fairly. Experimental investigations such as those of Chen [64] and several others inside channels have distinguished two types of mechanisms governing the heat transfer coefficient namely nucleate and convective boiling. Correlations for flow boiling in conventional large tube have been based on nucleate and convective component heat transfer coefficient. There are three main models that exist in literature as reviewed by

Gupte et al [108], superposition, asymptotic and enhancement. The superposition model was given as the addition of the mechanisms with a suppression factor S given as;

$$\alpha = S\alpha_{nb} + F\alpha_{cv} \tag{2.81}$$

Suppression factor was due to that of Chen [64] which takes into consideration the effect of velocity.

Liu and Winterton [109] developed a correlation based on the asymptotic model for vertical and horizontal flow in tubes and annuli. The data bank for the development of the correlation contains 4200 data points. The nucleate boiling component was based on that of Cooper [21]. Suppression factor in the superposition expression was given as;

$$S = \left[1 + 0.055E^{0.1}\ \mathrm{Re}_l^{\,0.16}\right]^{-1} \tag{2.82}$$

The enhancement E was determined from;

$$E = \left[1 + x\,\mathrm{Pr}_l\left(\rho_l/\rho_g - 1\right)\right]^{0.35} \tag{2.83}$$

The convective part of the correlation was determined from;

$$\alpha_{cv} = E\alpha_{tl} \tag{2.84}$$

Recent interests in the development of a model to predict the local boiling heat transfer coefficient in small circular tube has led to the development of a two-state model by Jacobi and Thome [110]. Jacobi and Thome modelled [110] and developed a method to predict the heat transfer coefficient in small circular tube. It was assumed that the heat transfer coefficient observed in flow boiling was due to an elongated bubble in which transient evaporation was taking place. They concluded that the heat transfer coefficient in the laminar flow of the liquid was negligible compared to the thin film coefficient thus making the model a one–zone model. Parametric studies showed that the model predicted several independent data quite well when it was assumed that the film thickness lies in the range of 10-20μm for channel size of 2.5mm.

Thome, Dupont et al [111] developed a three–zone model shown in Figure 2.20 which was an extension of the Jacobi model to predict the heat transfer coefficient inside micro tubes. Their model predicted the heat transfer coefficient at fixed location in a channel.

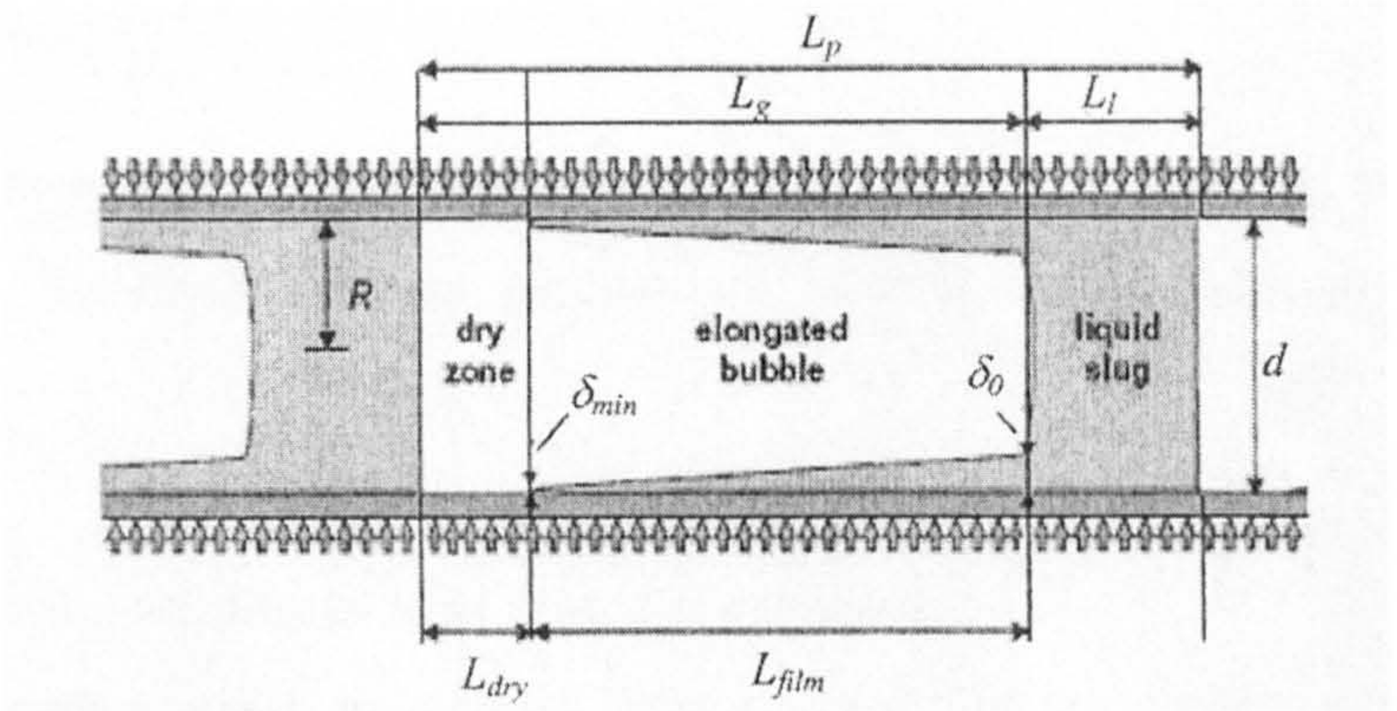

Figure 2.20 Diagram illustrating the three zone model of Thome, Dupont et al [111]

The model was given for the time averaged local heat transfer coefficient was given as;

$$\alpha(z) = \frac{t_l}{\tau}\alpha_l + \frac{t_{film}}{\tau}\alpha_{film}(z) + \frac{t_{dry}}{\tau}\alpha_v(z) \tag{2.85}$$

The time periods used in the above model were given as;

$$t_l = \frac{\tau}{1+\frac{\rho_l}{\rho_g}\frac{x}{1-x}},\ t_g = \frac{\tau}{1+\frac{\rho_g}{\rho_l}\frac{1-x}{x}} \text{ and } t_{dry\ film}(z) = \frac{\rho_l h_{fg}}{q}\left[\delta_o(z) - \delta_{\min}\right],\ f = \frac{1}{\tau}$$

The average heat transfer coefficient through the elongated bubble was obtained using the following set of equations:

$$\alpha_{film}(z) = \frac{k_l}{\delta_o - \delta_{end}}\ln\left(\frac{\delta_o}{\delta_{end}}\right) \tag{2.86}$$

$$\delta(z,t) = \delta_o(z) - \frac{q}{\rho_l h_{fg}}t \tag{2.87}$$

$$\frac{\delta_o}{d} = C_{\delta_o}\left(3\sqrt{\frac{\nu_l}{U_p d}}\right)^{0.84}\left[\left(0.07Bo^{0.41}\right)^{-8} + .1^{-8}\right]^{-1/8} \tag{2.88}$$

$$U_p = G_{total}\left[\frac{x}{\rho_g} + \frac{1-x}{\rho_l}\right] \tag{2.89}$$

This model showed that the heat transfer coefficient due to the liquid and vapour slug are negligible, but the dominant mechanism is evaporation through the elongated bubble.

2.9 Visualisation studies in heat transfer research

Visualisation studies are an interdisciplinary science that researchers used in obtaining additional information. Such studies are applicable in heat transfer in areas such as bubble dynamics, two-phase flows etc. In heat transfer studies on the outside of tube when the interest of bubble size and flow regimes are paramount then visualisation techniques are of great importance in interpreting heat transfer results. In the study by Cornwell and Schuller [44] to determine the effect if sliding bubbles, a Hadland Hyspeed rotating prism camera was used to explain the bubble motion around the periphery of the tube. Huo, Chen et al [112] investigate the flow boiling and boiling regimes inside tubes of diameter 2.01 and 4.26 mm at pressures range of 8-12 bar with mass flux in the range of 100-150 kg/m^{2}s and heat flux between 13-150 kW/m^2 with R-134a as the working fluid. A glass tube was connected at the downstream of the test section. The two-phase flow patterns were observed and recorded using a digital high speed camera model Phantom V4 B/W, 512×512 pixels resolution, 1000 pictures per second with full resolution and maximum 3200 pictures per second. Similar studies by Chen , Tian et al [104] using the same apparatus as that of Huo, Chen et al [112] was also used to determine the flow pattern with the diameters in the range of 1,10, 2.01, 2.88 and 4.26 mm. The results obtained were used to distinguish between the flow patterns observed.

2.10 Concluding remarks

The chapter began to present the state of the art information on the boiling heat transfer occurring outside small diameter tubes. The following remarks are made;

- Boiling heat transfer on the outside of diameter (1-3mm) tube bundles are scarce in the open literature. There is no firm conclusion on the effect of diameter below 8mm as reported by Cornwell and Houston [27] , Kew and Houston [29] and more recently by Das, Putra et al [32]. Pool boiling correlations that are used for plates are inappropriate to these diameter range

- Macro scale model developed by Chen [18] has been adapted to model heat transfer on the outside tube bundles. This approach has not been able to predict independent data

- Mass velocity and mass flux has been shown to have effect on the heat transfer coefficient at low to medium heat flux

- Sliding bubbles could not account for the heat transfer occurring outside miniature bundles but has been shown to contribute to the enhancement in large diameter tube bundles

- The pitch to diameter ratio has effect on the heat transfer coefficient at low to medium heat flux thereby increasing the enhancement, however there is no variation at high heat flux

- The recent model developed by Thome, Dupont et al [111] has shown that the dominant heat transfer mechanism in mini channel is that of thin film evaporation

A summary of the literature review is shown in, Table 2.1 and Table 2.2

Table 2.1 : Summary Pool boiling correlations

Author	Correlations	Key Parameters	Remarks
Rohsenow [3]	$\frac{C_l(T_w - T_s)}{l} = C_{sf}\frac{q}{\mu_l l}\left[\left(\frac{\sigma}{g(\rho_1 - \rho_2}\right)^{1/2}\right]^{1/2}\left(\frac{C\mu}{k}\right)^s$	Pressure, fluid heating, flat plate	Surface fluid constant depends on both the surface and fluid
Mostinski [39]	$\alpha_{nb} = 0.106q^{0.7}p_c^{0.69}F_p$	Physical properties of the fluid.	Does not incorporate surface finish
Stephan and Abdelsalam [25]	$\frac{\alpha_{nb}}{\lambda_l} = 0.0546\left[\left(\frac{\rho_v}{\rho_l}\right)^{\frac{1}{2}}\left(\frac{qd}{\lambda_l}\right)\right]^{0.67}\left(\frac{h_{fg}}{a_l^2}\right)^{0.248}\left(\frac{\rho_l - \rho_v}{\rho_l}\right)^{-4.33}$	Physical properties of the fluid(horizontal flat plate and tubes	Fluid: water, organics and refrigerants.
Cornwell [26]	$Nu = C_{tb}\,\mathrm{Re}_b^{0.67}$	Diameter	Fluid; water refrigerants and organics Pressure<0.1p_c, Tube diameter:6-32mm Surface: commercial finish
Cooper [21]	$\alpha = 55p_r^{0.12-0.2\log R_p}(-\log p_r)^{-0.55}M^{-0.5}q^{0.67}$	Surface roughness Liquid property	Orientation: horizontal flat plates
Cornwell and Houston [27]	$Nu = AF(p)\mathrm{Re}_b^{0.67}\,\mathrm{Pr}^{0.4}$	Diameter	Fluid: water, organics and refrigerants Diameter:8-50mm Surface: machined or drawn
Kang [28]	$q = \frac{0.015R_p^{0.084}\Delta T^{5.508}}{d^{1.318}}$	Diameter Surface orientation	Fluid: Water Pressure: 0.1Mpa Heat flux:0<q<160kW/m^2 Tube diameter: 9.7-25.4mm

Table 2.2: Summary of boiling on bundles

Authors	Parameters	Fluid	Diameter of tube	Remarks
Akin and McAdams [14]	Bundle effect	Water at atmospheric pressure.	12.7 mm, chrome plated copper tubes. 60 tubes.	Variation in heat transfer with height observed
Myers and Katz [47]	Tube position and behaviour of lower tube	Freon 12,methyl chloride, propane, sulphur dioxide and normal butane	19.05 mm plain and finned tubes. Four horizontal tubes.	Heat transfer coefficient varies up the bundle.
Palen, Yarden et al [46]	Bundle geometry, pressure, surface conditions	Pentane, heptane, paraxylne, acetone, Freon113, isopropyl alcohol	9.525mm-19.05mm	Clearance between tubes and bundle diameter are significant.
Wall and Park [48]	Bundle effect	n-pentane and other mixtures	26.6mm	Lower tubes have effect on upper tubes. Increase of heat transfer coefficient is at low heat fluxes
Nakajima [49]	Bundle effect	Freon 11	25 mm with triangular pitch to diameter ratio of 1.38	Boiling coefficient of bundle is greater than single tubes.
Leong and Cornwell [50]	Bundle effect	R-113 at atmospheric pressure	19.05 mm,241 tube bundle	Rise of heat transfer up the tube bundle.
Hwang and Yao [63]	Mass flux, flow qualities.	Freon-113	19.1 mm stainless steel tubes.	Boiling heat transfer is founds to depend local flow velocity and quality.
Andrews [113]	Tube bundle orientation ,tube bundle length on local heat transfer	R-113 at atmospheric pressure	241 stainless steel tubes of diameter 19.05 mm	Large variations of heat transfer coefficient were detected.
Scoones [114]	Effect of mass flux and quality	R-113	Plain tubes and finned tubes	Bundle effect is observed. Mass flux is found to have effect on the heat transfer coefficient

Fujita, et al [100]	Effect of pressure and position of tubes	Freon 114 at pressures of 0.1,0-1.0 MPa	25mm , copper tube	A model is proposed to account for the bundle effect.
Jensen and Hsu [56]	Mass velocity, quality and pressure	R-113	7.94/7.62mm stainless steel	Mass flux significant at higher heat flux.
Rebrov, Bukin et al [52]	Bundle effect	R-12 and R-22	22 mm smooth steel tubes.	A correlation is developed to predict the heat transfer with the position of the tube.
Marto and Anderson [71]	Effect of tube position on incipient boiling	R-113 at atmospheric pressure	15.9mm smooth copper	Lower tube has effect on upper tube
Danilova ,Dyundin, et al [53]	Local boiling heat transfer	R-717 and R-22	20mm steel tubes	Increment of heat transfer coefficient with height
Memory, [115]	Bundle effect	R-113	15.9 mm	Lower tubes does not have effect on upper tubes in natural convection
Gupta, Saini et al [72]	Heat flux, cross flow velocity and tube geometry	Distilled water	19.05 mm	Enhanced turbulence of vapour bubbles increases heat transfer coefficient
Fujita [74]	Bundle effect	Freon 113	50 tubes, OD 14mm	Bundle effect observed.
Liu and Ishibashi [77]	Effects of tube spacing, positions of tubes	Water salt mixture	18mm copper tubes	Space between tubes has considerable effect
Qui and Liu [78]	Effects of tube spacing, position of tubes and pressure	Water	Copper tube of outside diameter 18mm	Results shows that tube spacing has a significant effect on boiling heat transfer coefficient.
Robinson and Thome [59]	Local two phase flow data	R-134a	20 tube bundle mad of copper alloys of OD 18.87mm	No bundle effect observed

Chapter 3

EXPERIMENTAL PROGRAMME

3.1 Introduction

The experimental rigs used in obtaining data are described in this chapter. Two rigs are used in this study, Rig I for a twin tube arrangement whereas Rig II was for the compact tube bundle arrangement. The various components of the rigs are described. The two rigs described are for the purpose of investigating the following:

- Nucleate pool boiling

- Convective flow boiling on a small diameter compact tube bundle

The study of pool boiling on single tubes complements the studies on the compact bundle arrangement.

3.2 Pool boiling (Rig I)

The purpose of the pool boiling rig was as follows;

- Experimental investigation of heat transfer coefficient on a single tube heated alone for diameter of tubes ranging from 1.83-3.00mm using distilled water and Flutec PP1

- Experimental investigation of the enhancement of upper tube due to bubbles produced by boiling on a 3.00mm tube diameter beneath

- Photographic studies to investigate the mechanism on the upper tube and provision of visual data to assist in the development of a model

3.3 Convective boiling on a small diameter tube bundle (Rig II)

The literature survey showed that boiling heat transfer has been carried out for large diameter tube bundles with different pitch to diameter ratios at different operating conditions. The trends in the experimental set-ups are normally that of a forced convective and it has been shown in the literature survey in Chapter 2 that at upper tubes of the bundle the heat transfer coefficient depends on sliding bubbles as well as two-phase convection. The experimental investigation of the boiling on the compact tube bundle was designed in respect to the following;

- Effect of position on heat transfer coefficient
- Effect of heat flux on heat transfer coefficient
- Effect of mass flux on heat transfer coefficient
- Provision of data for the comparison of large tube correlations with that of confined geometry

3.4 Description of test section (Rig I)

The test section consists of an aluminium vertical channel of dimension 150mm wide, 12mm deep and 380mm high as shown in Fig 3.1 and a photograph of the whole rig in Figure 3.2. The test section was connected to a condenser at the top and a condensate line back to the bottom of the test section. In front of the test section there was a glass window to aid in the visualization studies. At the back of the test section, two guard heaters were inserted which was connected to a variac to control the power supplied. A 500W DC power supply was connected to the test tubes and there were voltage tappings at the end of the tubes for the recording of the voltage drop. Type K thermocouples were inserted inside the tube to measure the internal temperature of the tubes which was connected to a data logger. Two other type K thermocouples were also inserted at the top and bottom of the test section to give an average of the saturation temperature of the working fluid.

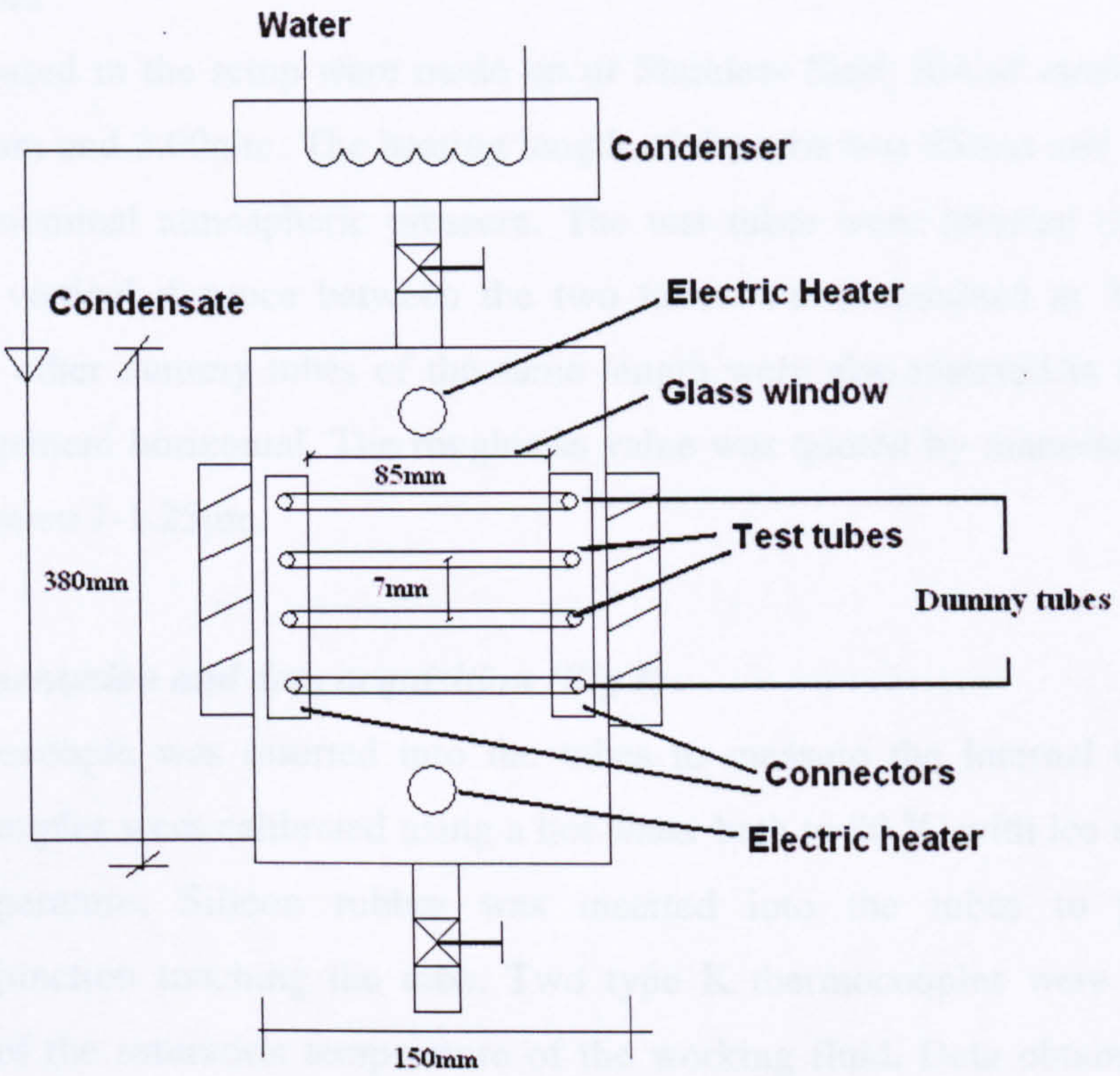

Figure 3.1 Schematic diagram of experimental set up for Rig I

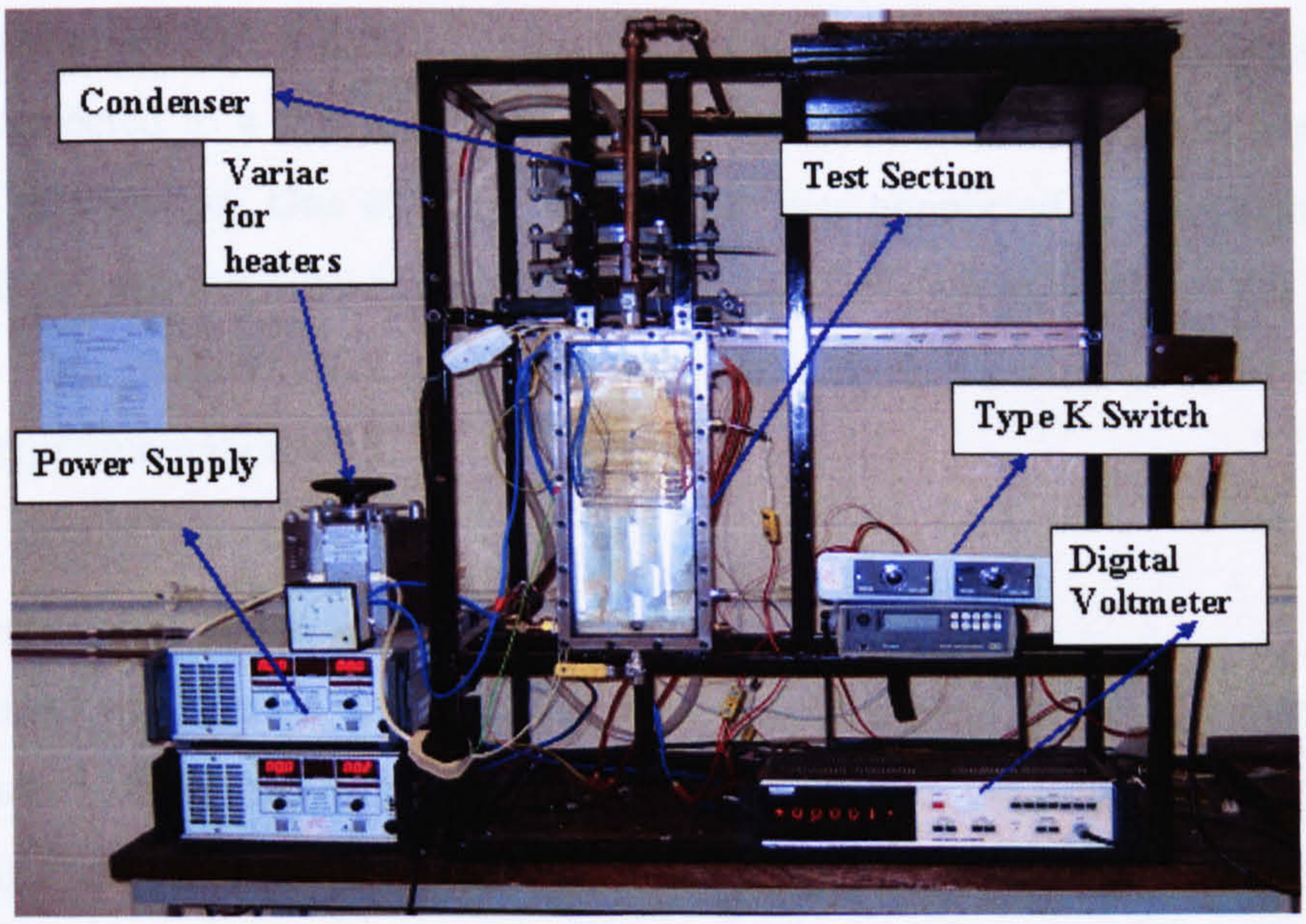

Figure 3.2 Photograph of Rig I showing major components

3.4.1 Test tubes

The test tubes used in the setup were made up of Stainless Steel 304 of outside diameter 1.83mm, 2.32mm and 3.00mm. The heating length of the tube was 85mm and the test was carried out at nominal atmospheric pressure. The test tubes were inserted in a terminal block and the vertical distance between the two tubes was maintained at 7mm (centre distance). Two other dummy tubes of the same length were also inserted in the block to keep the arrangement horizontal. The roughness value was quoted by manufacturer of the tubes to be between 1-1.25μm.

3.4.2 Instrumentation and data acquisition (Rig I)

Type K thermocouple was inserted into the tubes to measure the internal temperature. These thermocouples were calibrated using a hot water bath to 80 °C with ice at 0°C as the reference temperature. Silicon rubber was inserted into the tubes to prevent the thermocouple junction touching the tube. Two type K thermocouples were used in the determination of the saturation temperature of the working fluid. Data obtained from the thermocouples were recorded using software called Easyest. The two test tubes used were connected to separate power supply. The power supply was a 500W rated DC supply with a maximum current of 80A at 6.25V. Voltage tappings were soldered at the ends of the tubes and were connected to a digital voltage meter. Two guard heaters were connected to the back of the test section. One of the guard heaters was connected at a distance of 10mm from the base of the test section and the other heater inserted vertically at the back of the test section. These heaters were connected independently to a variac which was controlled during the experimental process.

3.4.3 Experimental procedure for Rig I

The experiment was carried out by filling the test section with the test fluid to two-thirds full. The variacs connected to the heaters at the back of the test section were switched on. The working fluid was heated to reach its saturation temperature and also allowed to boil for 3minutes to ensure that condensable gases escape from the test section whiles the cooling water connected to the condenser was turned on. The power supply to the single tube was switched on and temperature was measured after a steady state has been observed i.e. between 1-2 minutes. This steady state was achieved by observing that the temperature

on the on the display remained constant. The temperature in the tube as well as the working fluid temperature was recorded on the data logger. One hundred temperature data points were recorded on the data logger and the average temperature values were used in the computation of the heat transfer coefficient. The experiment was first performed with distilled water from the lowest power input to the highest and then carried out in the reverse directions to eliminate the possibility of hysteresis. The repeatability of the experiments was checked by conducting the experiments within time intervals.

The high speed video camera was used to record the motion of bubbles generated on the test tube. After obtaining results for isolated tube, the twin tubes experiment was carried out. In this particular case the upper tube heat flux was varied while the lower tube remained constant. The current, voltage and temperature readings were thus obtained. The experimental run was repeated by varying the diameter of the upper tube from 1.83, 2.32 and 3.0 mm. The test section was drained and compressed air was used to dry the components before another working fluid was used in the experimentation. Heat flux covered in the test run is as shown in Table 3.1.

Diameter of tube (mm)	**Heat flux range using distilled water (kW/m^2)**	**Heat flux ranged using Flutec PP1 (kW/m^2)**
1.83	13-243	6-150
2.32	11-218	6-150
3.00	6-192	6-169

Table 3.1 Range of parameter tested for single and twin tube arrangement

3.5 General description of Rig II

The rig was designed to investigate the heat transfer in the central column of a 3x10 tube bundle. The rig shown in Figure 3.3 and Figure 3.4 essentially consists of a test section, a condenser, flow meter, heating tank, power supplies, pre-heater and a guard heater. The detailed descriptions of the major components are discussed. A heating element was submerged in a fluid tank so as to heat the fluid to its saturation temperature. The liquid was allowed to boil continuously before been pumped to the test section. There was also a bypass from the pump to control the amount of the fluid entering the tank because of the

volume of the test section. A centrifugal pump was used to pump the liquid from the heating tank through a flow meter to the test section. Since the discharge from the pump was high, the bypass was used to control the flow. There was also a drain connected to the end of the pump to drain the whole rig in order to change the working fluid being used. A rotameter (0-0.5l/min) was connected to the test section prior to fluid entering the test section. Calibration of the flow meter is shown in the appendix A.2.

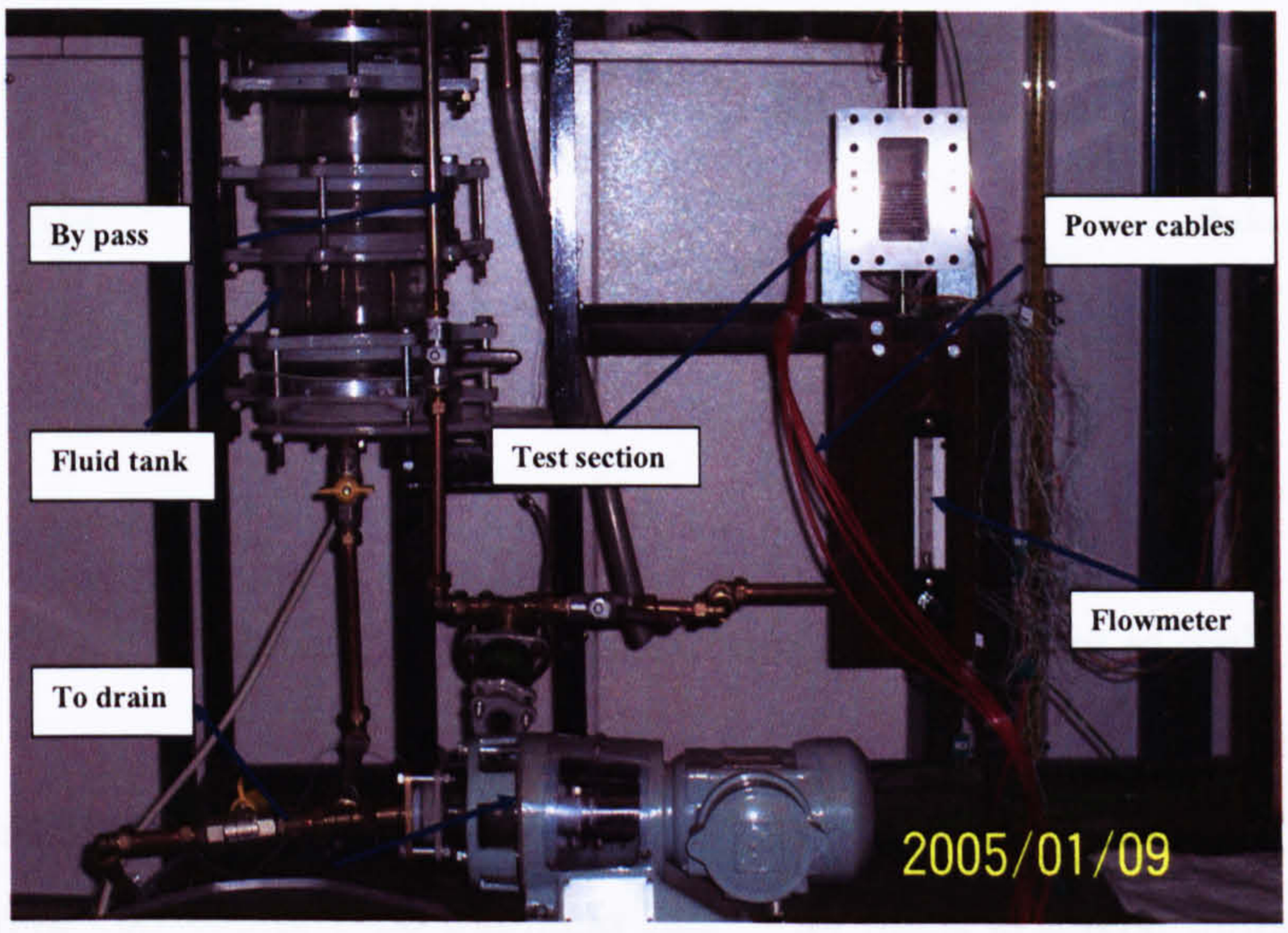

Figure 3.3 A photo of the test arrangement for the bundle (Rig II)

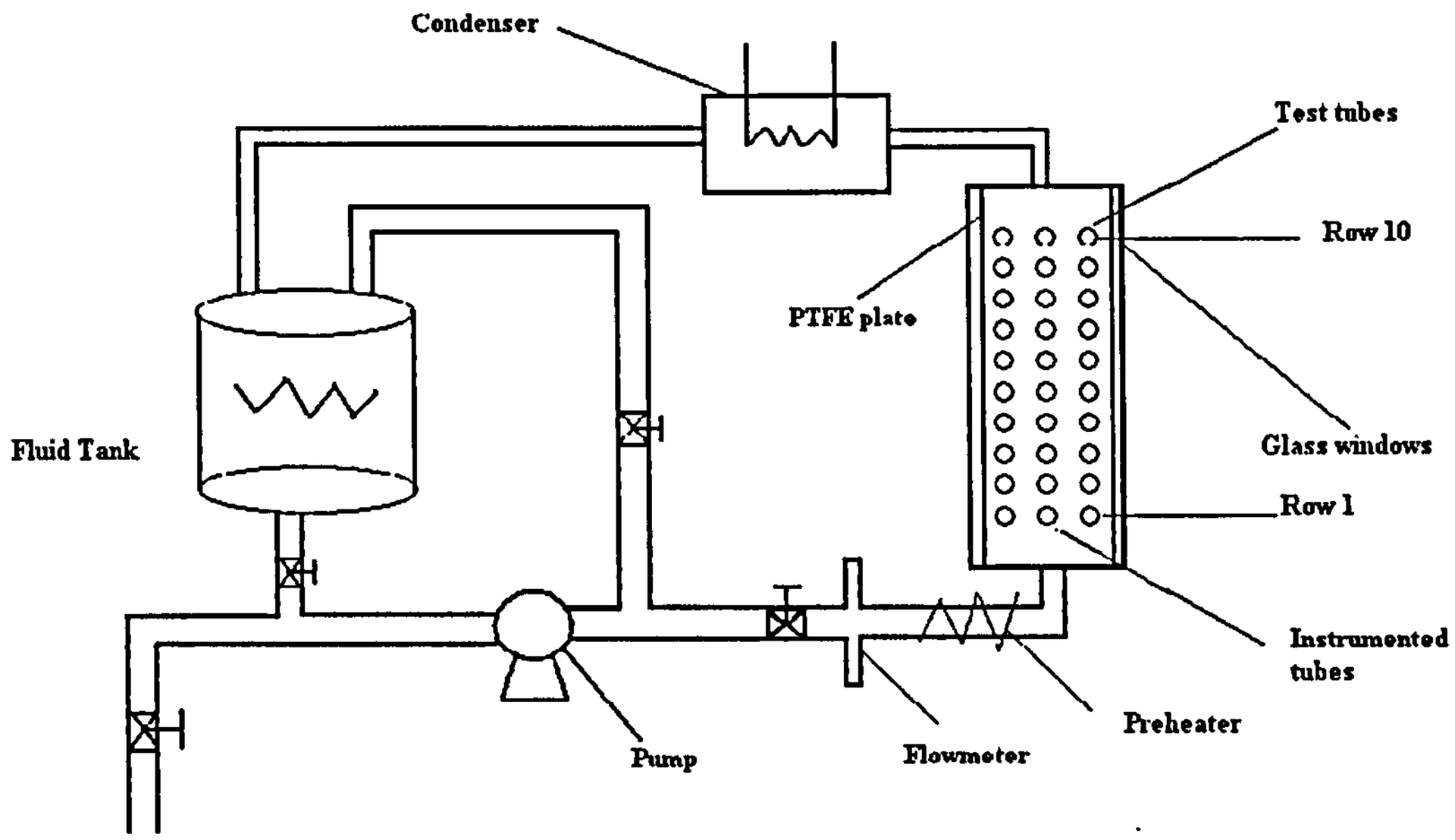

Figure 3.4 Schematic diagram for the compact bundle (Rig II) (not to scale)

3.5.1 Test section

The test section consists of a 30 Stainless Steel 304 tubes arranged inline with a pitch to diameter ratio of 1.5 (Figure 3.5 and Figure 3.6) with the tube numbered from the lowest as tube 1 to the topmost tube as 10. The heating length of the tube was 50 mm with the outer diameter of 3.00mm. The tubes were inserted inside a PTFE ends of length 100mm and width 15mm which is shown in Figure 3.7 and the length of the inlet to the first tube was 15mm. The length from the tube number 10 to the exit of the test section was 45mm. The PTFE ends were mounted on a stainless steel plates with standard pipe fittings. Glass windows were clamped in front and back of the test section to aid in the visualization studies. The test section to the top was connected to a condenser and the bottom was connected in series with the flow meter. Paper gaskets with hylomar were used to seal the test section. The hylomar was allowed to cure for at least 48 hours before tests were carried out.

PAGE NUMBERING AS ORIGINAL

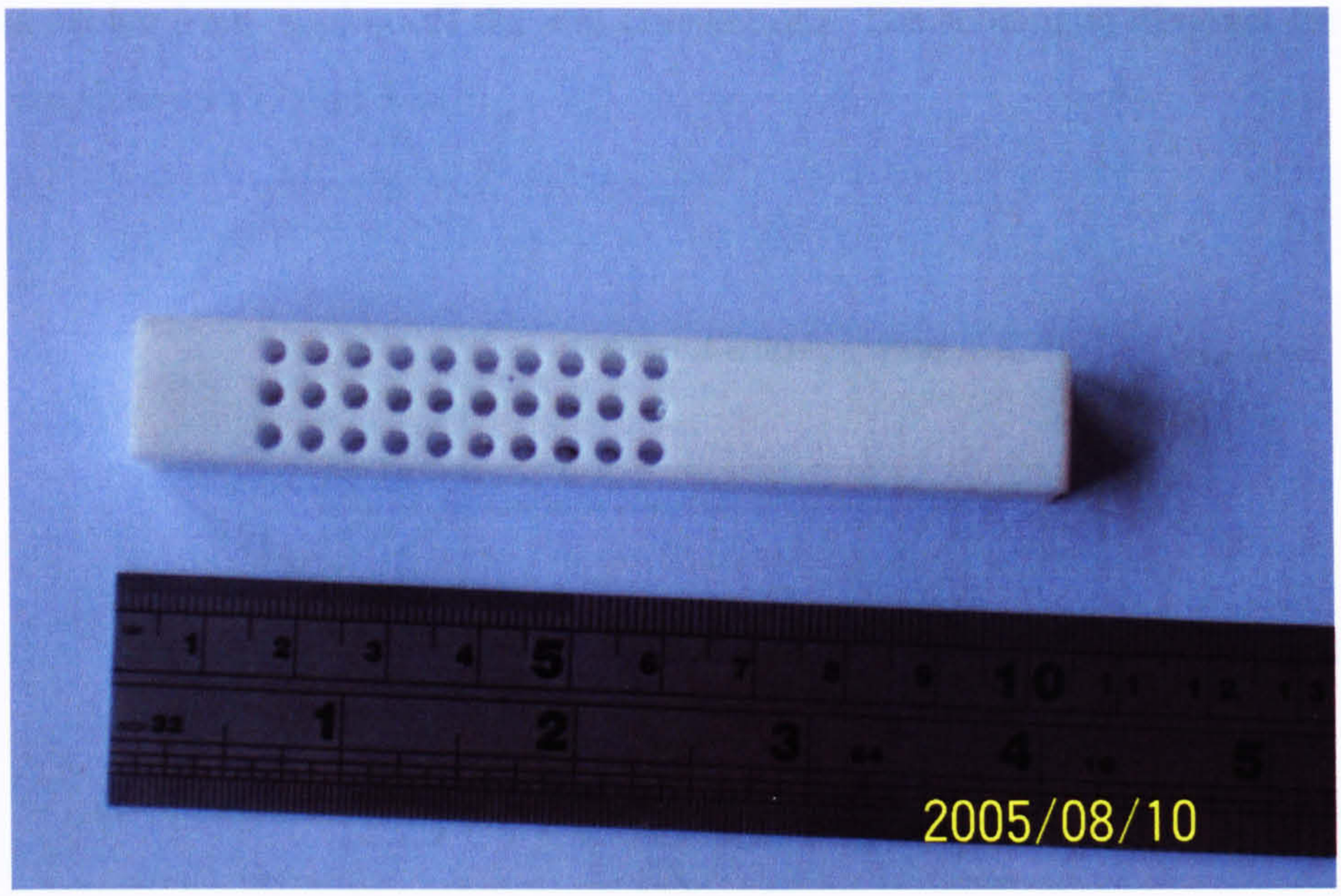

Figure 3.7 Photo of the PTFE ends of the tube bundle

3.5.2 Instrumentation of Rig II

Type K thermocouple was coated with an insulating varnish prior to its insertion it into the tubes. This was done to prevent it from been overheated and being short circuited. PTFE sleeves of length 50mm were also inserted into the tubes in order to prevent the thermocouples from touching the walls of the tube. The arrangement of the thermocouple through the copper inserts is shown in Figure 3.8. The thermocouples were then connected to the Easyest data logger to record the temperature of the inside of the tubes. Two other type K thermocouples were inserted at the inlet and the exit of the test section to record the saturation temperature of the working fluid. One hundred temperature readings were obtained using the Easyest software and the average was used in the computation of the heat transfer coefficient. Copper pipes in the test section were covered with insulation material to prevent heat loss from the pipe. This was done in order to get the temperature at the inlet to near saturation. An electrical heating tape, which was connected to a variac was wound round the inlet pipe so as to keep the temperature of the working fluid close to within 0.1-0.2 K of saturation temperature. Brass inserts were designed so as to serve as the connection to the main tubes in the bundle. These were done in order to prevent the power

supplies cables from ripping off the end connections. The schematic diagram for the brass inserts are shown in Figure 3.8 .

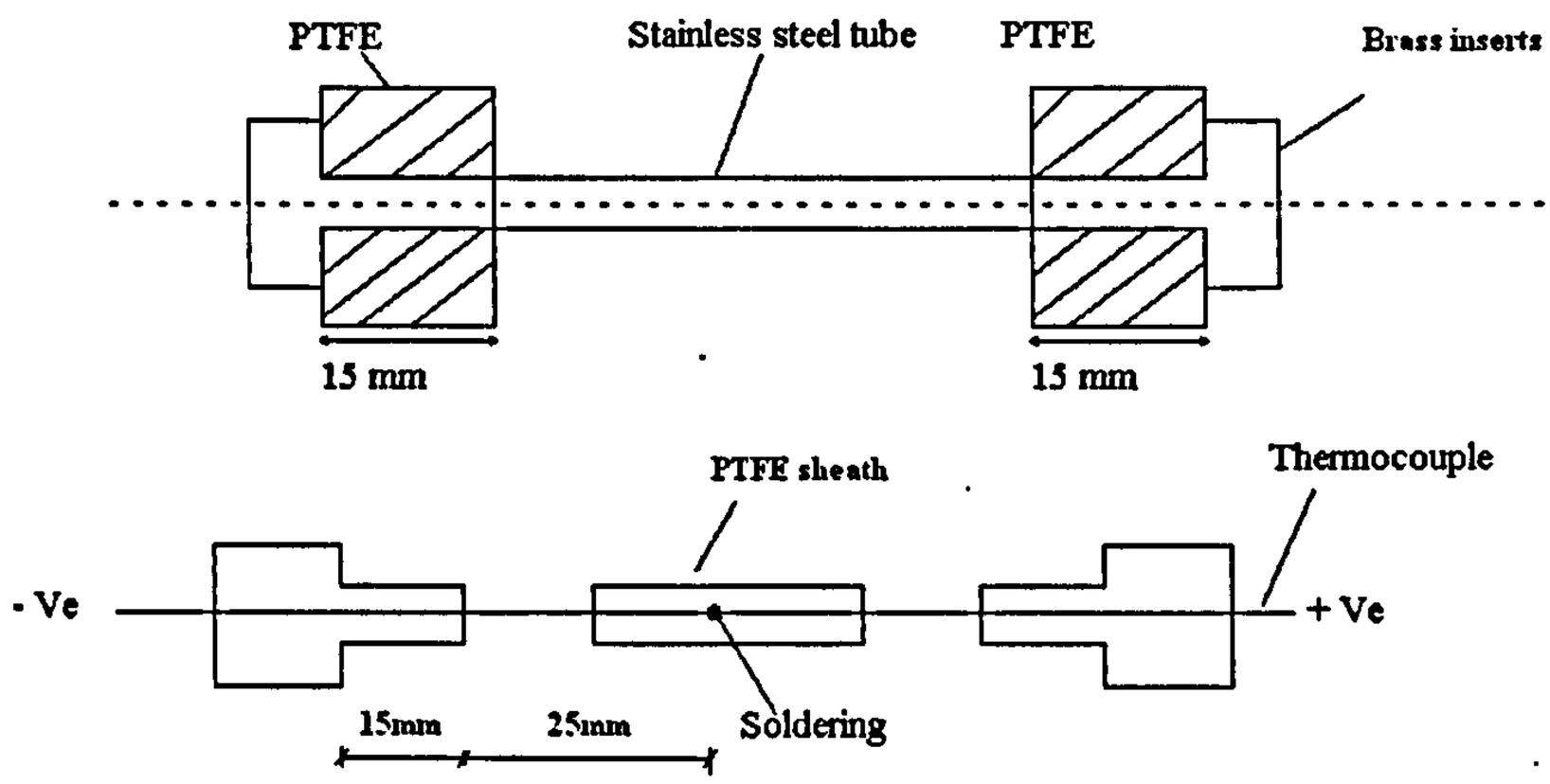

Figure 3.8 A schematic diagram of the electrical inserts used in the tube bundle (not to scale)

A differential pressure transducer was connected across the test section to measure the pressure difference between the inlet and outlet of the bundle. The transducer has operating range of 0-5psi. The transducer was connected to a data logger which used the Easyest software. The transducer was powered by a 9 V DC battery and was calibrated by inputting a known pressure at one port and the other open to the atmosphere. The height of the fluid was increased and the corresponding voltage signal was logged on the data board. Three different sets of test were made and there was repeatability of results. Results obtained are shown in the appendix of this thesis. Uncertainty analysis showed that the results were reliable to within 5%. A power supply model PS1540S which was capable of variable voltage between 3-15 V and a maximum current of 40A was connected to the centre tubes which were connected in series. The ripple noise of is $10mV_{rms}$ and an efficiency of over 80%.There was also an LCD screen which indicates the voltage and the corresponding current through the tubes. The first and third columns were connected to a similar model PS 1540S power supply. This power source was in turn connected to the tubes, which was connected in series.

3.5.3 Experimental procedure for Rig II

The experiment was carried out by switching on the heater connected to the fluid tank. The working fluid in the heating tank was allowed to boil before the pump was switched on. Once the fluid enters the test section, the power supplies to the tubes were switched on. This was allowed for a steady state to be reached before readings were taken. Single phase experimental studies were carried out to check for the repeatability of the results. The steady state was determined by ensuring that the temperature readings by the thermocouples remained constant. The experiments was varied for various flow rates and in each case the heat flux, pressure and thermocouples readings were recorded on the data logger using the Easyest software. Pressure drop across the bundle was also noted for corresponding heat and mass fluxes. The range of heat flux (chosen for low heat flux as most industrial devices operate to avoid burnout), and mass flux for each fluid used are shown in Table 3.2.

Fluid	**Heat flux q (kW/m^2)**	**Mass flux G (kg/m^2s)**	**Saturation temperature (^oC) at 1 atmosphere**
Distilled water	6-21	5.6-27.8	100.0
R113	4-14	13.1- 32.8	48.2
Flutec PP1	4-13	17-26.0	57.0

Table 3.2 Parameters investigated for the compact tube bundle

The velocity of the working fluid as it enters the compact tube bundle was obtained using the continuity equation is shown in Table 3.3. It was observed from the literature review that the effect of velocity is significant on the heat transfer coefficient. This has been corroborated by Singh, Saini et al [61] in his work. As a result the compact tube bundle was designed with these velocities in mind with velocities in the range of 0-0.1 m/s.

Flow rate(l/min)	**Velocity (m/s)**
0.1	0.021
0.2	0.042
0.3	0.063
0.4	0.084
0.5	0.106

Table 3.3 Velocities used in the compact tube bundle

3.6 Photographic studies

3.6.1 Direct visual observation

Direct observation of the movement of bubbles from the boiling tube was possible for the test section. The glass window in front of the test section permitted the observer to view the mechanisms occurring in the boiling process. The major restrictions of direct observation are the record of such short duration events.

3.6.2 Flash photography

Flash photography was used as this provides clear pictures of either the localised areas or the entire mechanisms occurring. Various photos of the twin heating tubes were obtained. The photos were taken by varying the diameter of the upper tube whiles keeping the lower tube constant. This photos not shown here although were clearer than the high speed video, it was not appropriate as the motion of bubbles could not be traced.

3.6.3 Video recording

High-speed video camera was used as this techniques gives an idea about the passage of bubble as it moves past the upper tube. The images obtained by the high speed camera are not of high resolution as that of the flash photography but gives an indication of the mechanism occurring at a particular area. This method was useful in studying bubble growth. For the purpose of this thesis the high speed video were carried out at 240 frames per second as it gave good images. The exposure rate of the lens was set at 1/2000 or 1/240sec and the camera was capable of recording for 8sec. The videos were recorded on a video cassette and this was played back to analyse the motion of the bubbles. A laminated sheet of paper was placed at the back of the test section to aid in the capture of the bubbles so as not be blurred. Preliminary tests were carried out by changing the lighting used in the high speed video until the appropriate images have been obtained. Typical photos obtained for a twin tube and tube bundle are shown in Figure 3.9 and Figure 3.10.

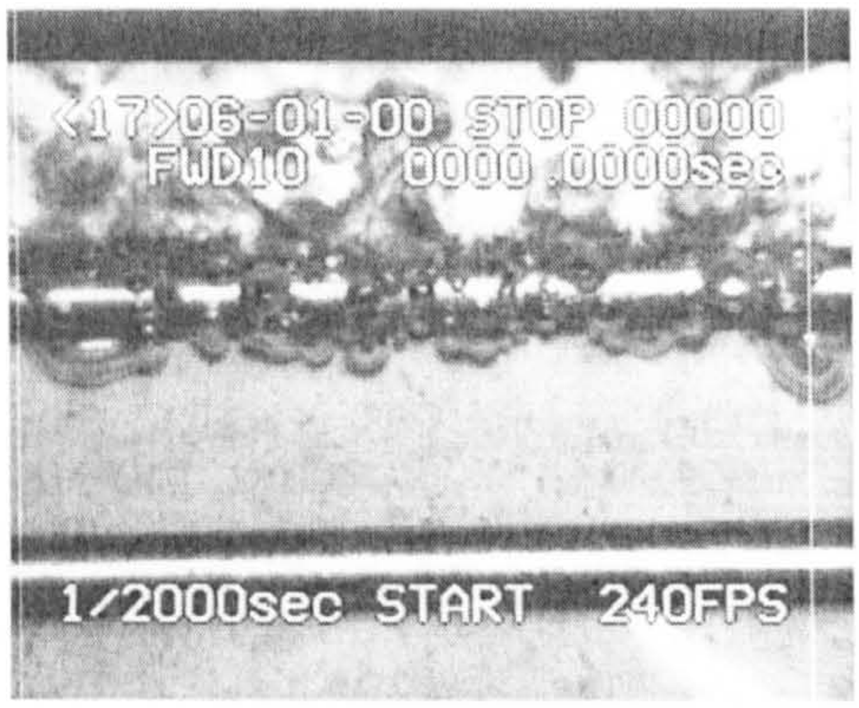

Figure 3.9 Typical photo of boiling on 3.0 mm tube at 169 kW/m^2 with distilled water

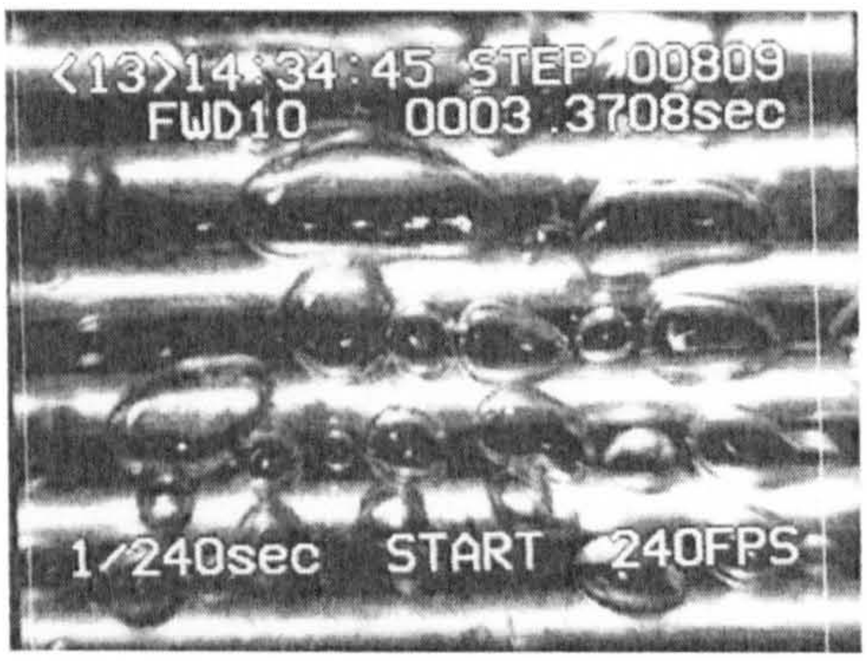

Figure 3.10 Typical photo for tube bundle with distilled water

3.7 Evaluation of heat transfer data

The data obtained from the experimental setup was evaluated as follows. The heat flux was calculated from;

$$q = \frac{IV}{\pi d_o l} \tag{3.1}$$

Equation (3.1) was used for Rig I as the ends of the tubes were connected to a voltmeter to measure the voltage drop. The heat flux for the bundle rig (Rig II) was calculated from equation (3.2) with the resistance of the stainless tube obtained using Ohm's law as;

$$q = \frac{I^2 R}{\pi d_o l} \tag{3.2}$$

The heat transfer coefficient was evaluated from;

$$\alpha = \frac{q}{T_{wall} - T_{sat}} \tag{3.3}$$

The surface temperature was evaluated by considering cylindrical conduction through the tube. In this case the heat generated was considered in the temperature profile. The surface temperature is thus given as;

$$T_{wall} = T_i - \frac{q r_o^{\,2}}{2k}\left[\frac{1}{2}\left(1 - \frac{r_i^{\,2}}{r_o^{\,2}}\right) + \frac{r_i^{\,2}}{r_o^{\,2}} \ln \frac{r_i}{r_o}\right] \tag{3.4}$$

Derivation of the Equation (3.4) is shown in Appendix A.

The mass flux of fluid through the bundle was given as;

$$G = \frac{\dot{m}}{A_{\min}} \tag{3.5}$$

The minimum flow area of the bundle was evaluated from;

$$A_{\min} = 50 \times [15 - 3 \times 3] = 300 mm^2 \tag{3.6}$$

The thermodynamic quality in the bundle is evaluated by using an energy balance of the entire bundle. Based on the tube position the local quality at each tube was also evaluated. The thermodynamic quality is thus given as;

$$x = \frac{m_v}{m_v + m_l} \tag{3.7}$$

where m_l is the mass flow rate of liquid and m_v is the mass flow rate of the vapour.

The uncertainty in the heat flux was given as;

$$\left[\frac{U_q}{q}\right]=\left[\left(\frac{U_Q}{Q}\right)^2+\left(\frac{U_{do}}{d_o}\right)^2+\left(\frac{U_l}{l}\right)^2\right]^{1/2} \tag{3.8}$$

Details of the uncertainty analysis are shown in Appendix A. Error analysis on the heat transfer coefficient gave an average of 14%. Details of this uncertainty analyses are shown in appendix A.

3.8 Validation of results

Single phase experimental work was carried out using the rigs used in this thesis. The heat transfer coefficients obtained were compared with the Churchill, Thehen [116] correlation for natural convection. This result shown in Figure 3.11 agreed within a deviation of 16% and is of the same order for that of the 2.32 and 1.8mm diameter tubes. The results for the single and twin tube were validated using the correlation of Churchill for natural convection over a horizontal cylinder. Their correlation is given as;

$$\sqrt{Nu}=\sqrt{0.360}+\left[\frac{\frac{Gr\,\mathrm{Pr}}{300}}{\left(1+\left(\frac{0.5}{P_r}\right)^{9/16}\right)^{16/9}}\right]^{1/6} \tag{3.9}$$

where the Grashof number is given as;

$$Gr==\frac{d^3g\rho^2\beta|T_w-T_\infty|}{\mu^2}=\frac{0.003^3\times9.81\times958^2\times210\times10^{-6}|T_w-T_\infty|}{\left(2.76\times10^{-4}\right)^2}=670.14\times|T_w-T_\infty|$$

Substitution values gives;

$$\sqrt{Nu}=\sqrt{0.36}+\left(\frac{3.8022|T_w-T_\infty|}{2.0610}\right)^{0.1666} \tag{3.10}$$

Similarly the above expressions were also used to obtain the relations for the 1.83 and 2.32 diameters respectively as;

$$\sqrt{Nu} = \sqrt{0.36} + \left[4.366\times10^{-4}(T_w - T_\infty)\right]^{0.1666} \tag{3.11}$$

$$\sqrt{Nu} = \sqrt{0.36} + \left[0.8532(T_w - T_\infty)\right]^{0.1666} \tag{3.12}$$

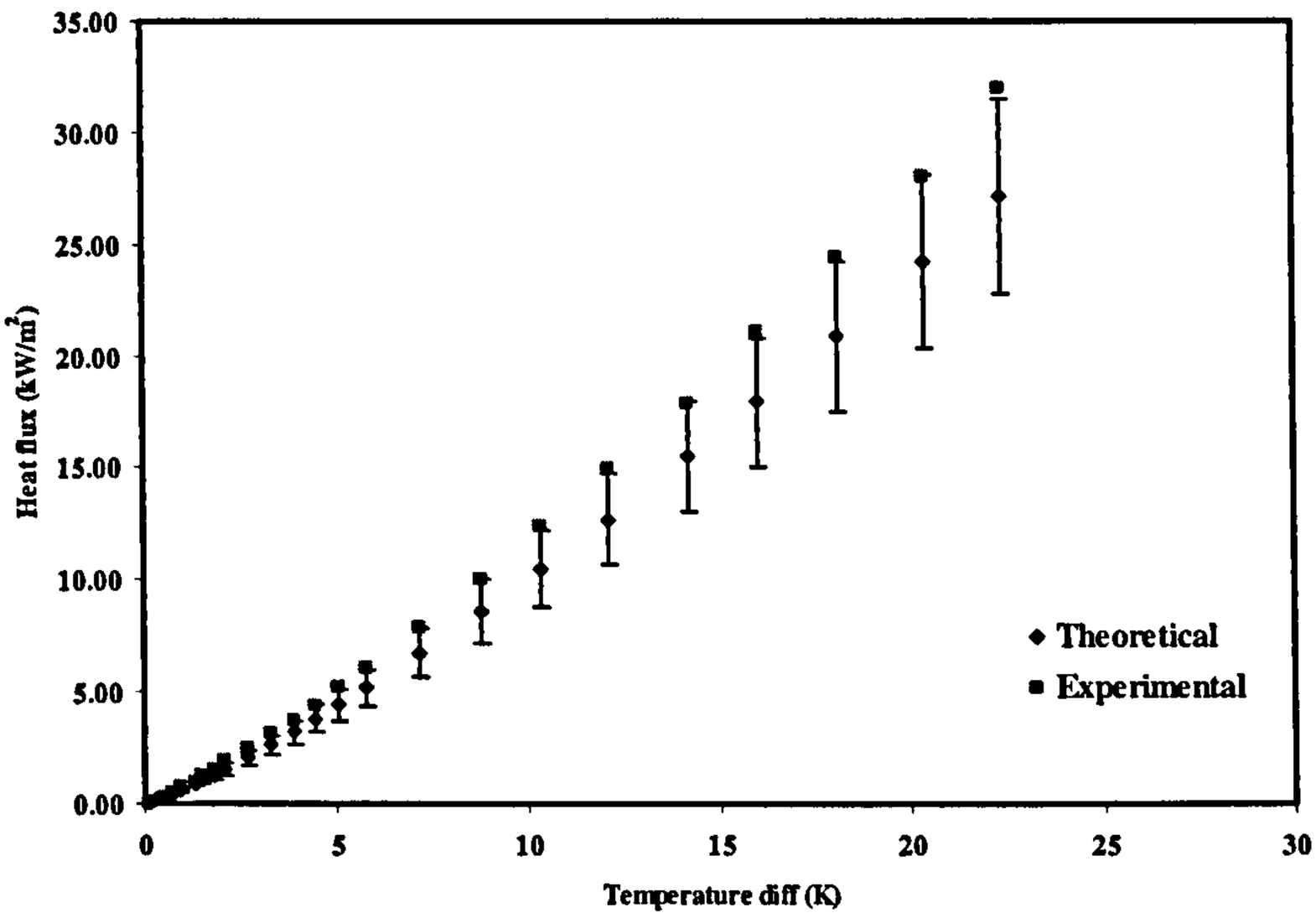

Figure 3.11 Validation: Experimental versus theoretical result for 3.00mm tube using distilled water

3.9 Concluding remarks

Experimental rigs have been designed for the investigation of boiling heat transfer on small diameter tubes and bundle at nominal atmospheric pressure.

- Two rigs were designed in order to complement the results obtained from each other.

- Rig I results helps to better understand the mechanism occurring in a bundle using the same diameter.

- Heat transfer results obtained using the two rigs designed in this section would be discussed in Chapter 4.

Chapter 4

EXPERIMENTAL RESULTS AND HEAT TRANSFER MECHANISMS

4.1 Introduction

This chapter discusses the experimental results obtained from Rigs I and Rigs II. Single and twin tube pool boiling experimental results is presented for both distilled water and Flutec PP1 at nominal atmospheric pressure. The mechanisms observed using photographic studies are also discussed. Boiling correlations for large tubes and plates reported in Chapter 2 are compared with the experimental results obtained for the single tubes.

Experimental results obtained from Rig II (compact bundle) are discussed in respect to the effect of heat flux, vapour quality and bundle effect on local heat transfer coefficient. Photographic studies are presented for a section of the compact bundle in the concluding part of the chapter to determine the effect of confinement on the bubbles as it travels up the bundle.

4.2 Single tube experimental results and discussion

The single tube pool boiling experiments are shown in Figure 4.1-Figure 4.2 . The plots show the heat flux against the wall superheat for the diameters of 1.83-3.0mm for distilled water and Flutec PP1. The observed results of the single tubes for the diameters considered follow the form of the traditional pool boiling data. Natural convection was observed at low heat flux, followed by incipient boiling. At incipient boiling, small bubbles were observed to be developed at the nucleation sites on the surface of the tube. The sizes of the bubbles observed were comparable to the diameter of the tubes. Once nucleate boiling was fully developed, more bubbles were generated on the tube surface and the frequency of bubble generation was high.

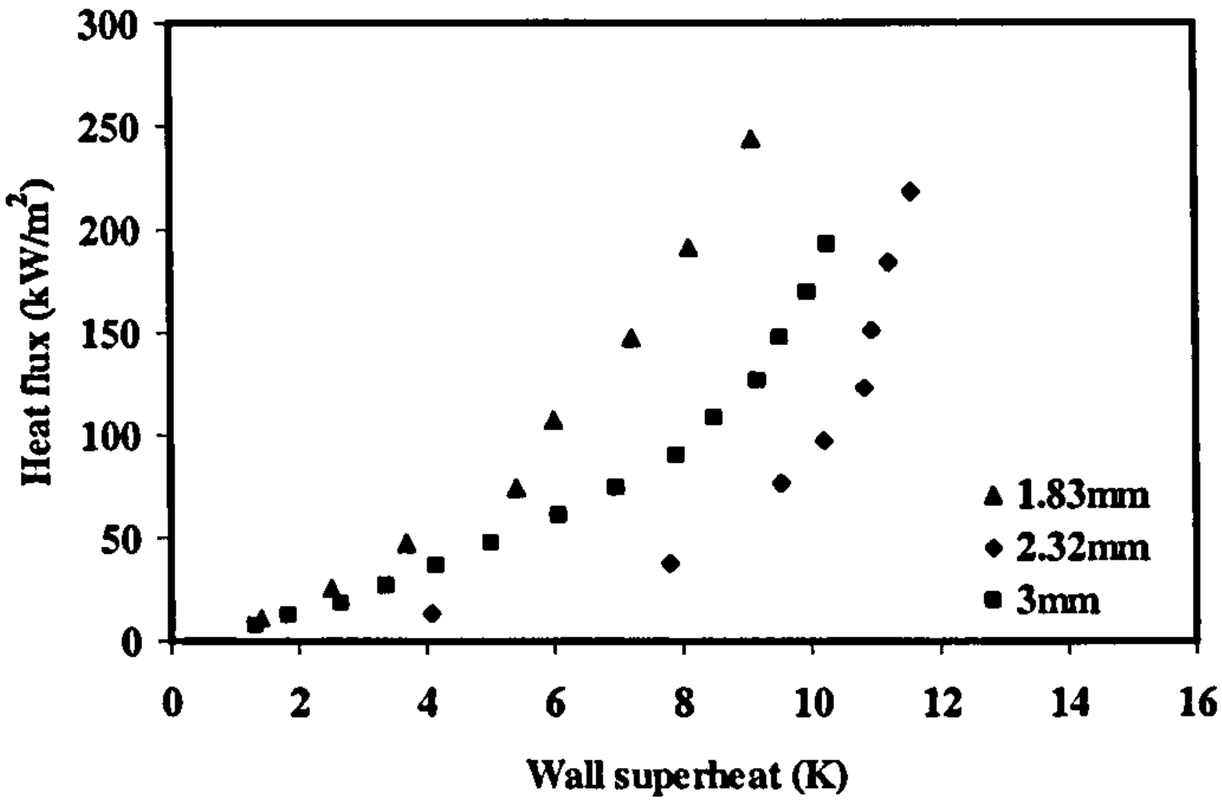

Figure 4.1 Heat flux against wall superheat for 1.83, 2.32 and 3.0 mm tubes with distilled water

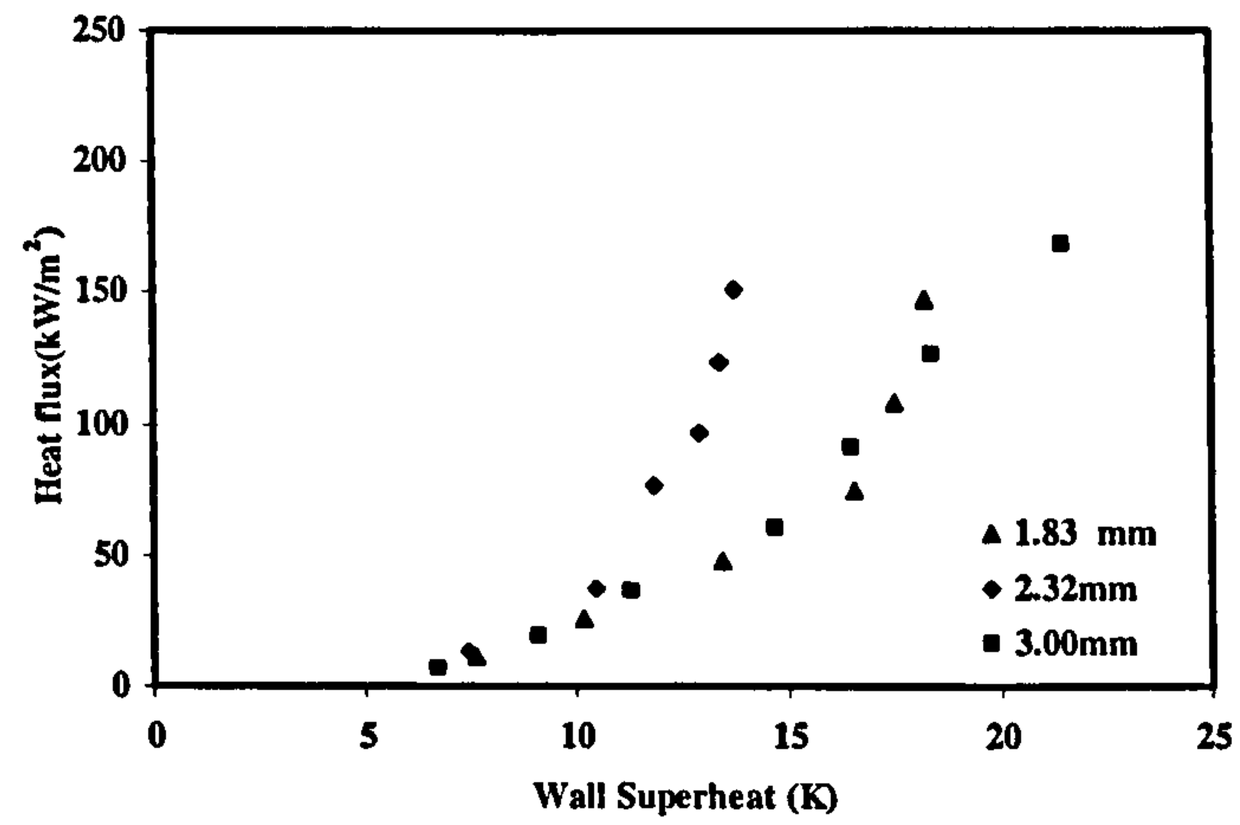

Figure 4.2 Heat flux against wall superheat for 1.83, 2.32 and 3 mm tubes with Flutec PP1.

The experimental results of the heat transfer coefficient against heat flux are shown in Figure 4.3-Figure 4.4 for both distilled water and Flutec PP1. The results from the experiments show a power curve fit. Interestingly, the high heat transfer coefficient obtained here is due to translating bubbles that translates over the surface of the tubes. Direct visual observations and also by using high speed video camera were used for the pool boiling on the narrow tubes that were considered with respect to heat transfer coefficient to establish the trends as well as the mechanisms that occurs. For boiling on the tubes using distilled water at nominal atmospheric pressure, the bubbles observed on the smallest tube (1.83mm) were large compared to the tube diameter. At the bottom of the tube buoyancy played an important role thereby allowing the bubbles to stuck to the surface. As heat flux was increased more bubbles were generated and the size of the bubble

decreased as the nucleation site density increased. The translating bubbles mechanism observed changed with respect to the diameter of the tubes tested and it decreased as the diameter of the tube decreased. The bubbles observed on these tubes were minimal and it was observed that there was a direct departure of bubbles from the surfaces of the tubes and even where there were sliding bubbles their contact area were small. This mechanism was also observed by Houston and Cornwell [117] for boiling on large tube bundles and also by Das et al [32] for diameters in the range of 4-8 mm at nominal atmospheric pressure.

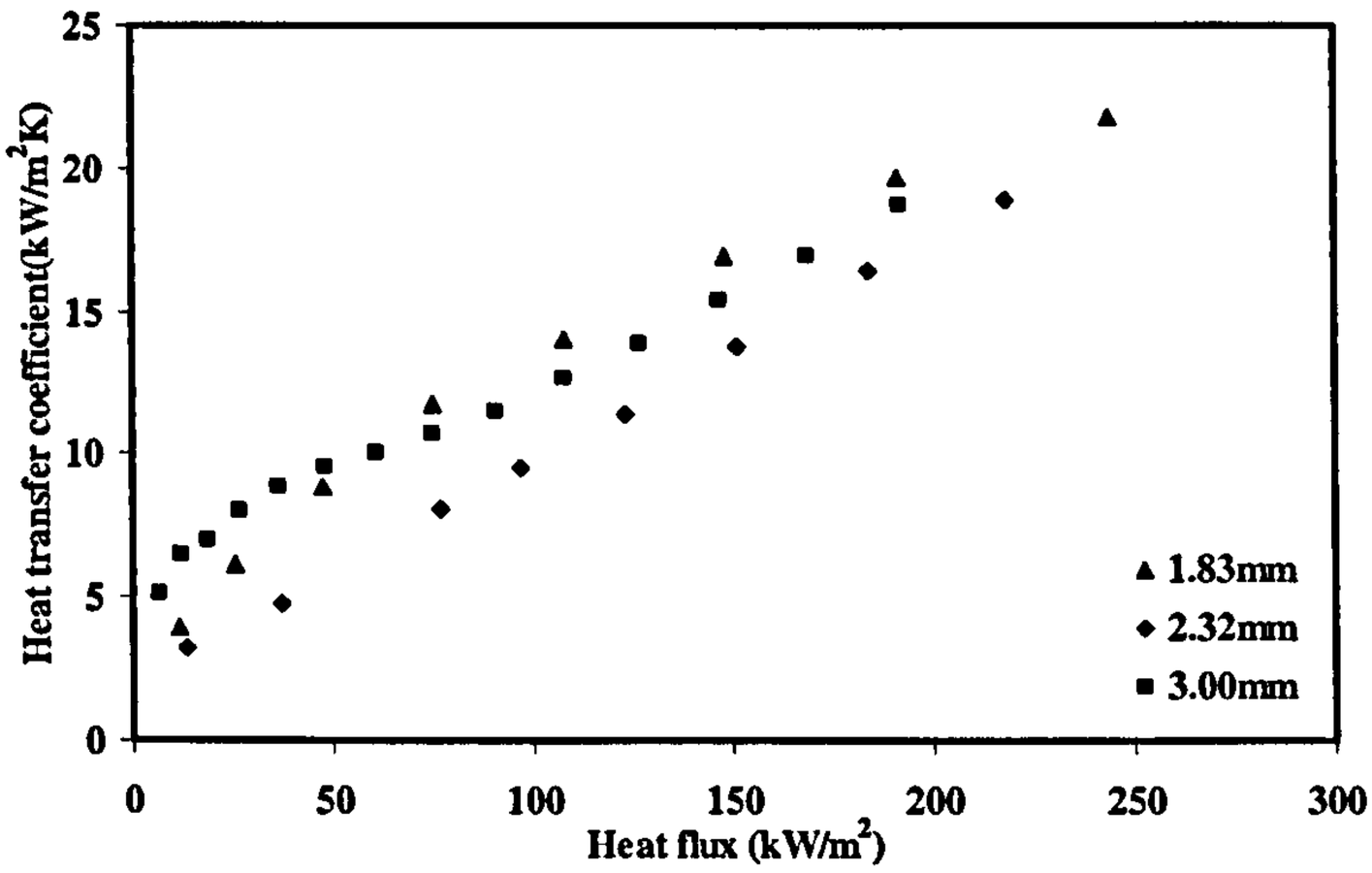

Figure 4.3 Heat transfer coefficient against heat flux for 1.83, 2.32 and 3.0 mm with distilled water.

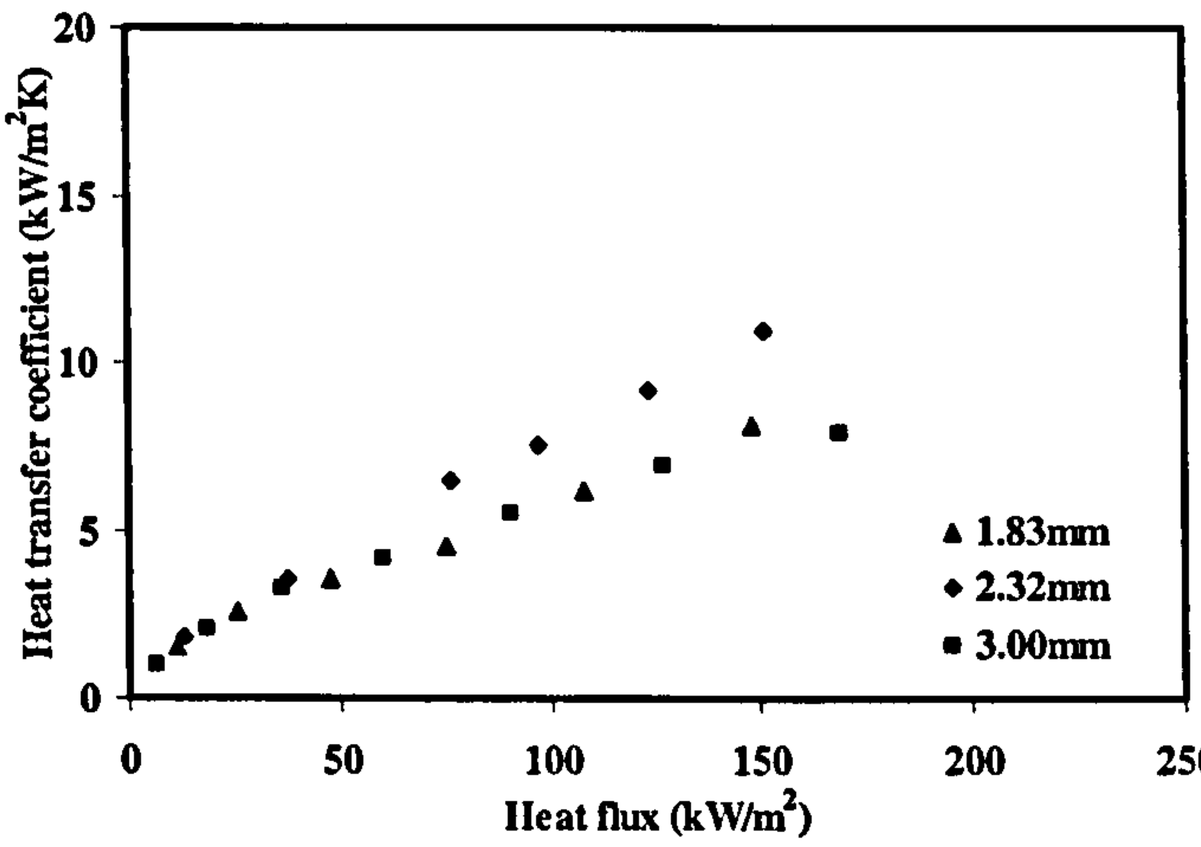

Figure 4.4 Heat transfer coefficient against heat flux for 1.83, 2.32 and 3.0 mm with Flutec PP1.

4.2.1 Discussion of effect of tube diameter

The results from the three different tubes diameters were plotted to compare the effect of diameter on the heat transfer coefficient as shown in Figure 4.3-Figure 4.4 . Also the Nusselt number and the boiling Reynolds number were plotted on the same graph as this dimensionless parameter has diameter in its development (Figure 4.5-Figure 4.6). In pool boiling the convection was driven by vapour bubbles at the surface creating liquid movement while in forced convection the liquid movement is caused by external flow. Pool boiling for a large tube induces a bubbly layer around the tube in which local transfer from the surface was largely due to liquid convection and evaporation under the sliding bubble. The driving force for both mechanisms was the bubble production rate and hence the mean mass flux at the surface. This approach has been used by Cornwell and Houston [27] and Das, Putra et al [32]. Thus the boiling Reynolds number becomes;

$$\mathrm{Re}_b = \frac{qd}{\mu_f h_{fg}} \tag{4.1}$$

and the Nusselt number as;

$$Nu = \frac{\alpha d}{k_f} \tag{4.2}$$

In boiling on horizontal tubes observation showed that the nucleation occurred at the underside of the tube and the bubble slide along before departure (large tubes). This was not a significant process on small tubes as the bubble diameter approached the tube diameter. The plots using the Nusselt number and the Reynolds numbers shows that as the diameter decreased from 3.00 to 1.83mm there was no significant change in the heat transfer coefficient at high heat flux (127-169 kW/m^2) for distilled water and for Flutec PP1 the difference was not appreciable.

Photographs taken (Figure 4.7) at various heat fluxes on the pool boiling experiments indicated that there was a translating bubble on the tube but these bubbles tend to leave the surface of the tube compared to the mechanism observed on a large tube where bubbles slides over the surface and sides. As the heat flux was increased on the tubes used in the

experiment, a point was reached for the 3.00mm diameter at heat flux of 169 kW/m^2 where the bubbles merged together on departing from the surface. Beyond such heat fluxes it was impossible for bubbles to slide on the surface or underside of the tube. The results also indicated that there was no systematic variation of heat transfer on the tubes observed, there was a decrease in the heat transfer coefficient from the 3.0 mm diameter to 2.32 mm. There was no difference between the heat transfer coefficients observed at higher heat fluxes which was also observed in the data of Kew and Houston [29], Das, Putra et al [32] for a diameter range of 4-8mm with distilled water at 1 bar.

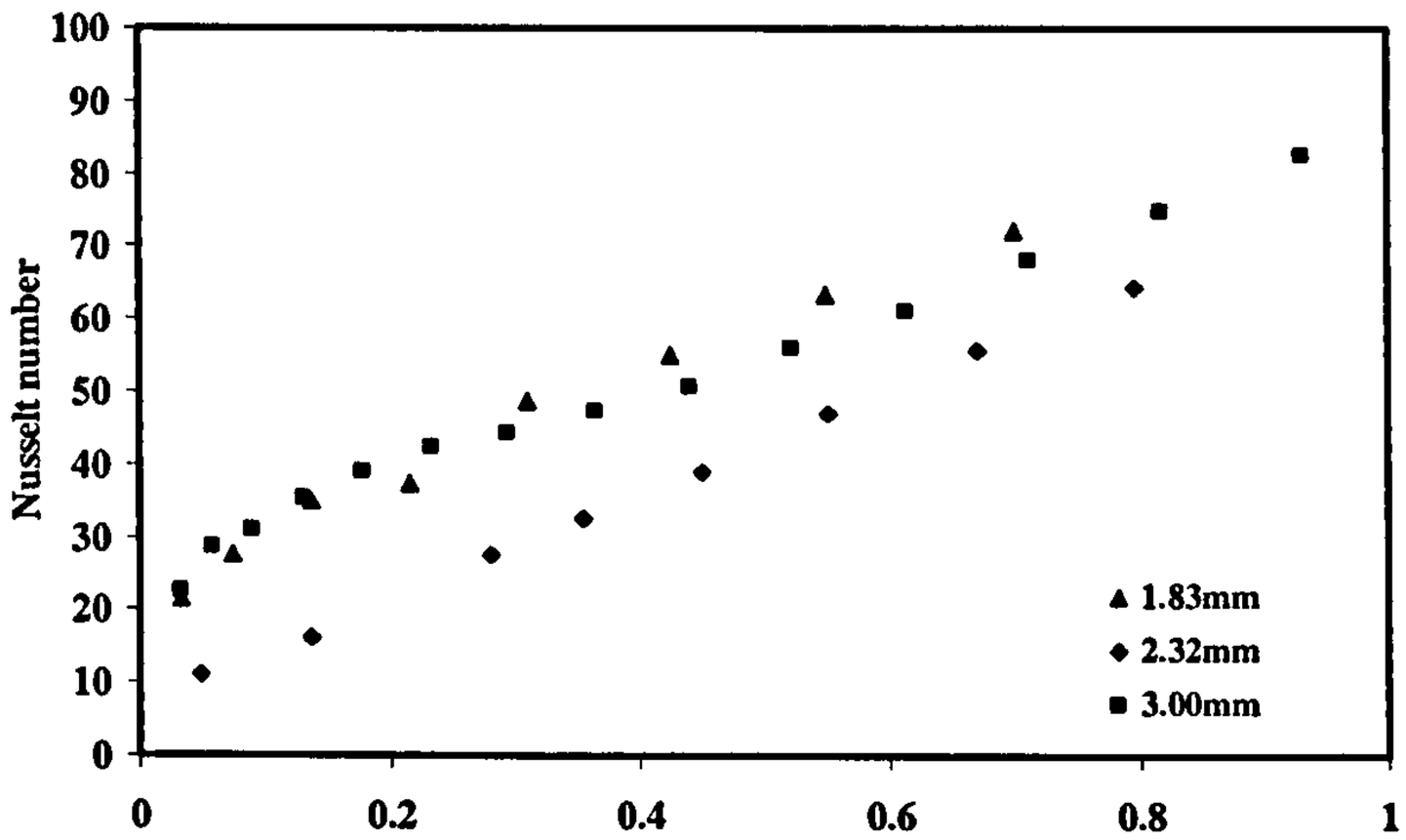

Figure 4.5 Nusselt number against boiling Reynolds number with distilled water.

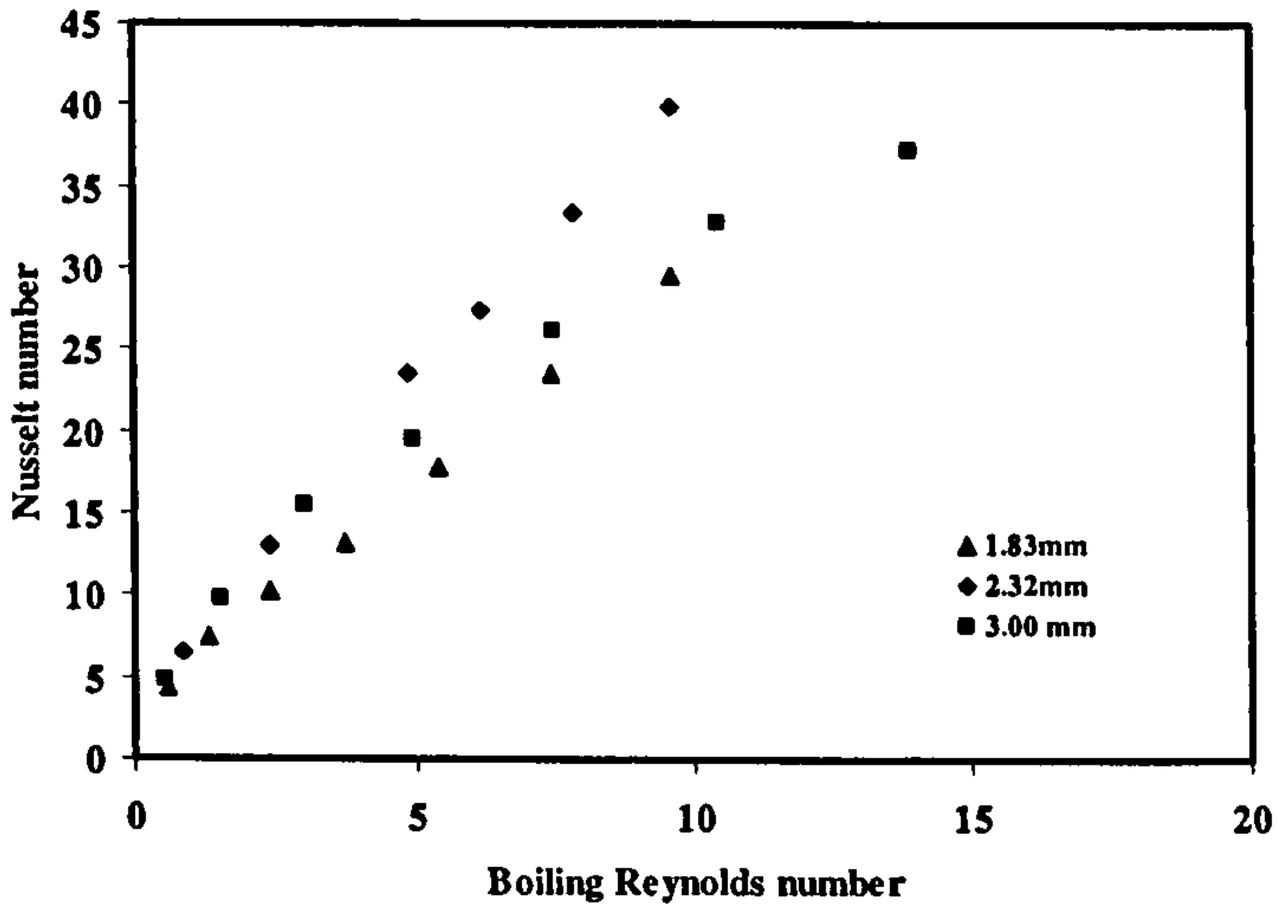

Figure 4.6 Nusselt number against boiling Reynolds number with Flutec PP1.

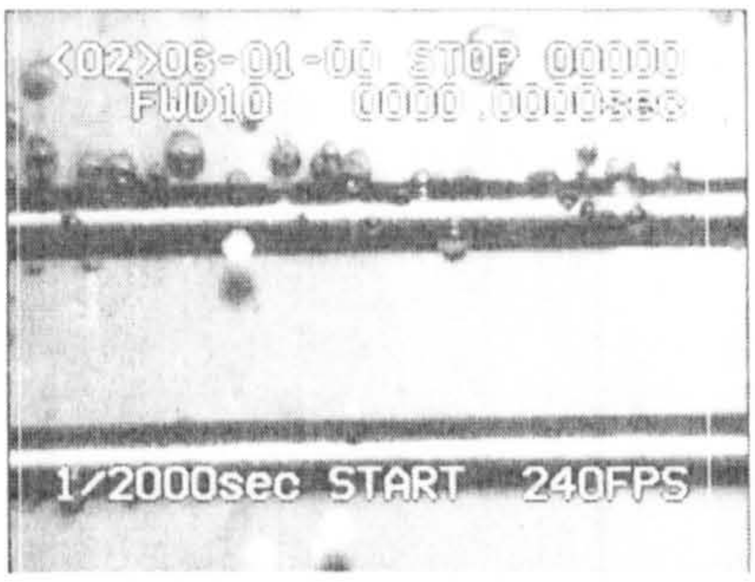

3.00mm at 37 kW/m^2

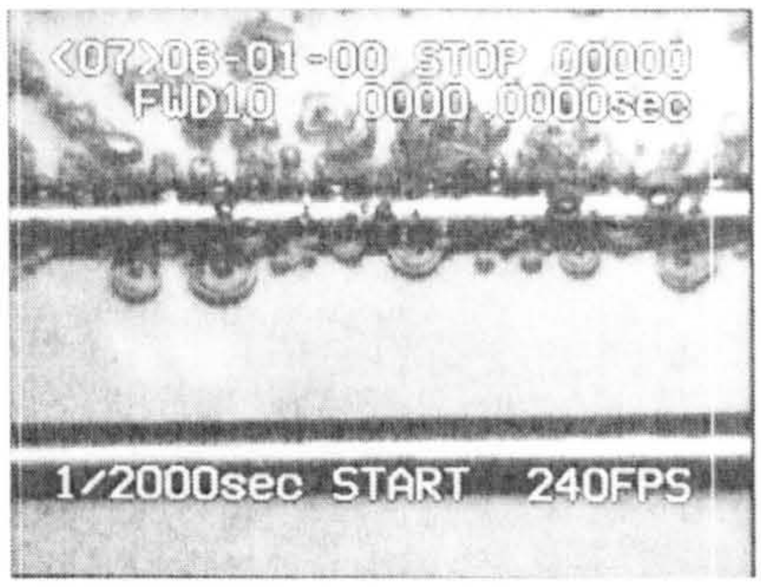

3.00mm at 91 kW/m^2

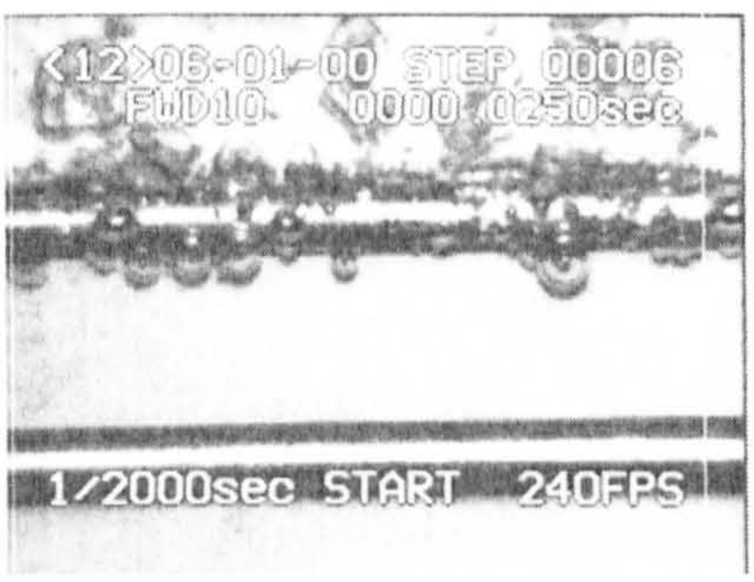

3.00mm at 127kW/m^2

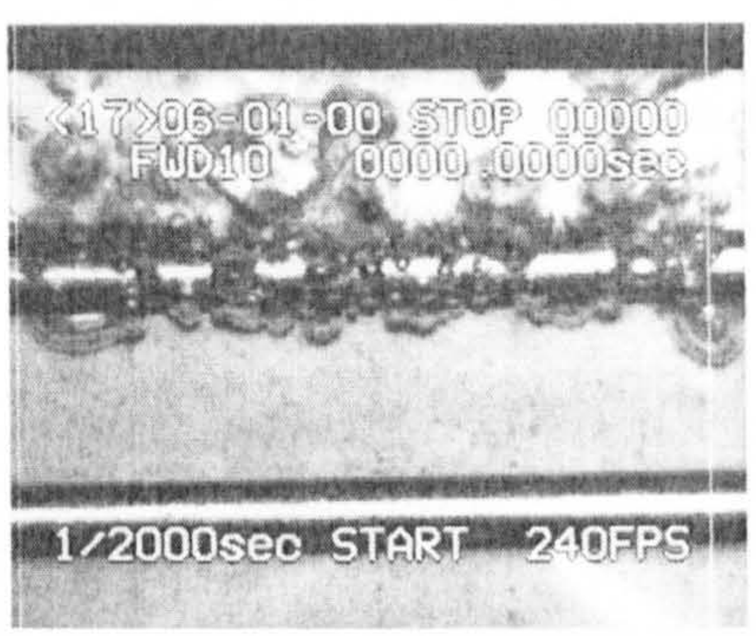

3.00mm at 169 kW/m^2

Figure 4.7 Typical photos of boiling on the 3.00mm diameter tube with distilled water as working fluid

Figure 4.8 shows the comparison of heat transfer coefficient reported for the diameters 1.83, 2.32 and 3.00mm with those found in literature such as Kew and Houston[29], and Das, Putra et al [32] for distilled water. The results showed that at high heat fluxes of 100 kW/m^2 the effect of tube diameter diminishes. However in the low to medium heat flux below 100 kW/m^2 there was an inconsistency in the effect of diameter. This would be due to the bubble departure diameter approximately equal to the tube diameter. As such the effect of sliding bubbles becomes minimal.

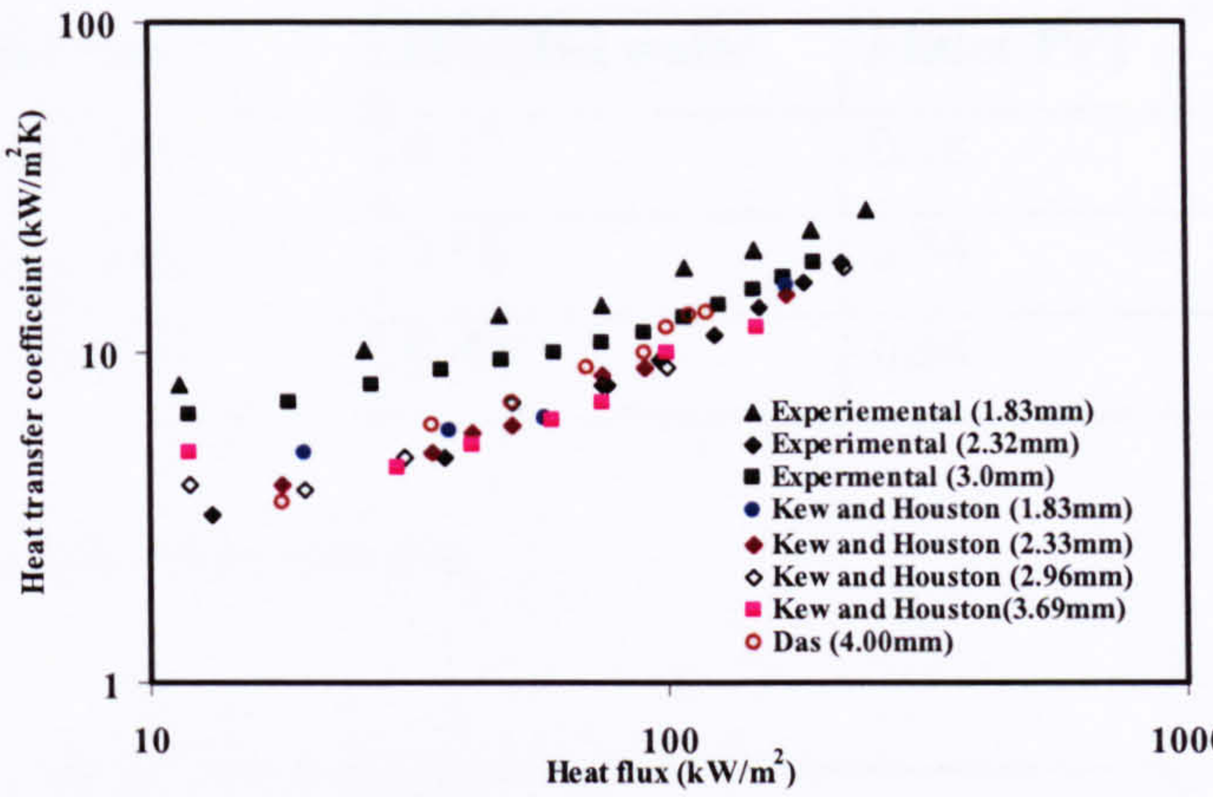

Figure 4.8 Comparison of heat transfer results from Kew and Houston [29], Das, Putra et al [32] with experimental results

4.2.2 Comparison of pool boiling with selected nucleate pool boiling correlations

The pool boiling results obtained were compared with selected correlations from literature for those of large tube diameter and flat plates to elucidate the differences of the use of these models. The earliest correlation of Mostinki's [39], Stephan and Abdelsalam [25] Cornwell and Houston [27] and Cooper's [21] were used for the comparison. For the Cooper correlation a surface roughness factor of unity was applied. Comparisons of the results for experimental data are shown Table 4.1 and in Figs 4.8 – 4.12. Typical pool boiling correlations are of the form;

$$\alpha = Cq^n \tag{4.3}$$

for large tubes n lies in between 0.67-0.70. The constant C depends on the fluid properties and the surface effect of the tube.

Diameter	n	
	Distilled water	Flutec PP1
1.83 mm	0.47	0.68
2.32 mm	0.64	0.74
3.00 mm	0.49	0.64

Table 4.1 Values of n from experiment

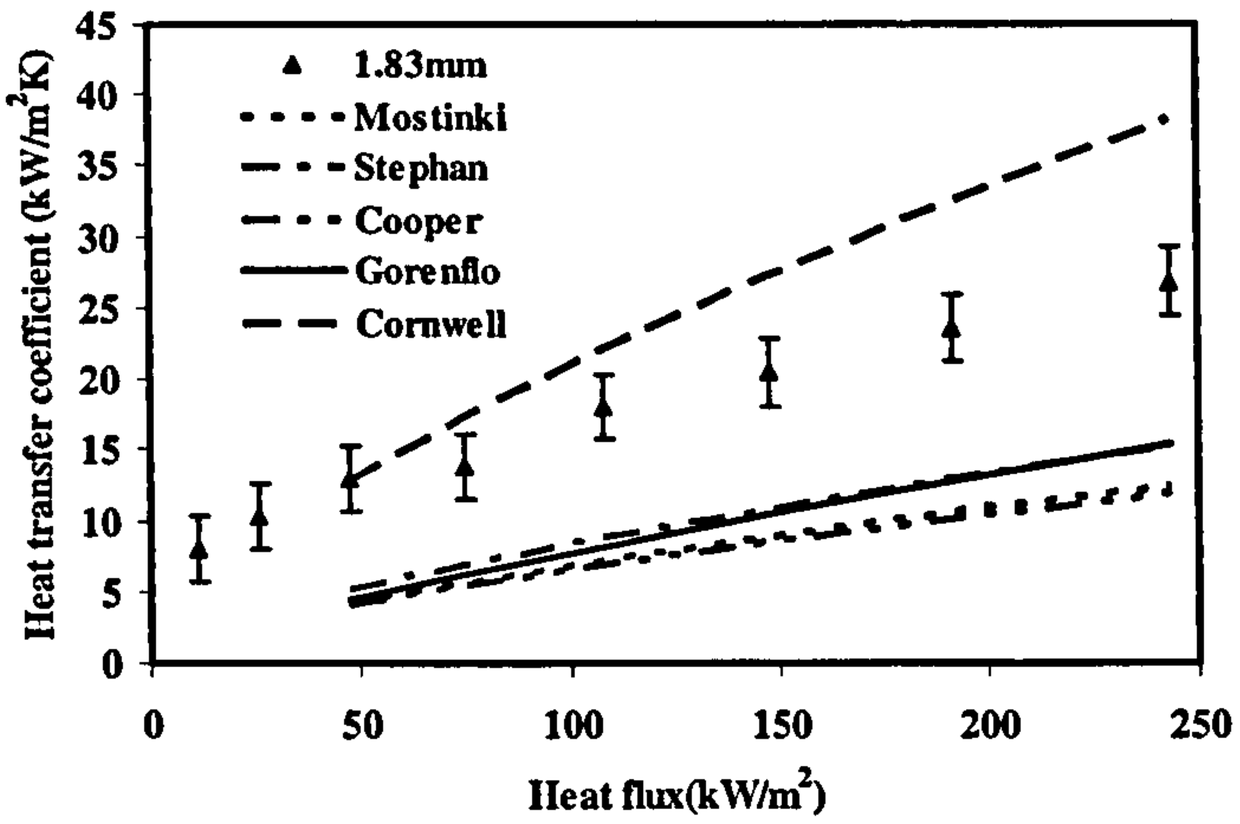

Figure 4.9 Comparison of experimental results with large tube correlations for 1.83mm tube with distilled water.

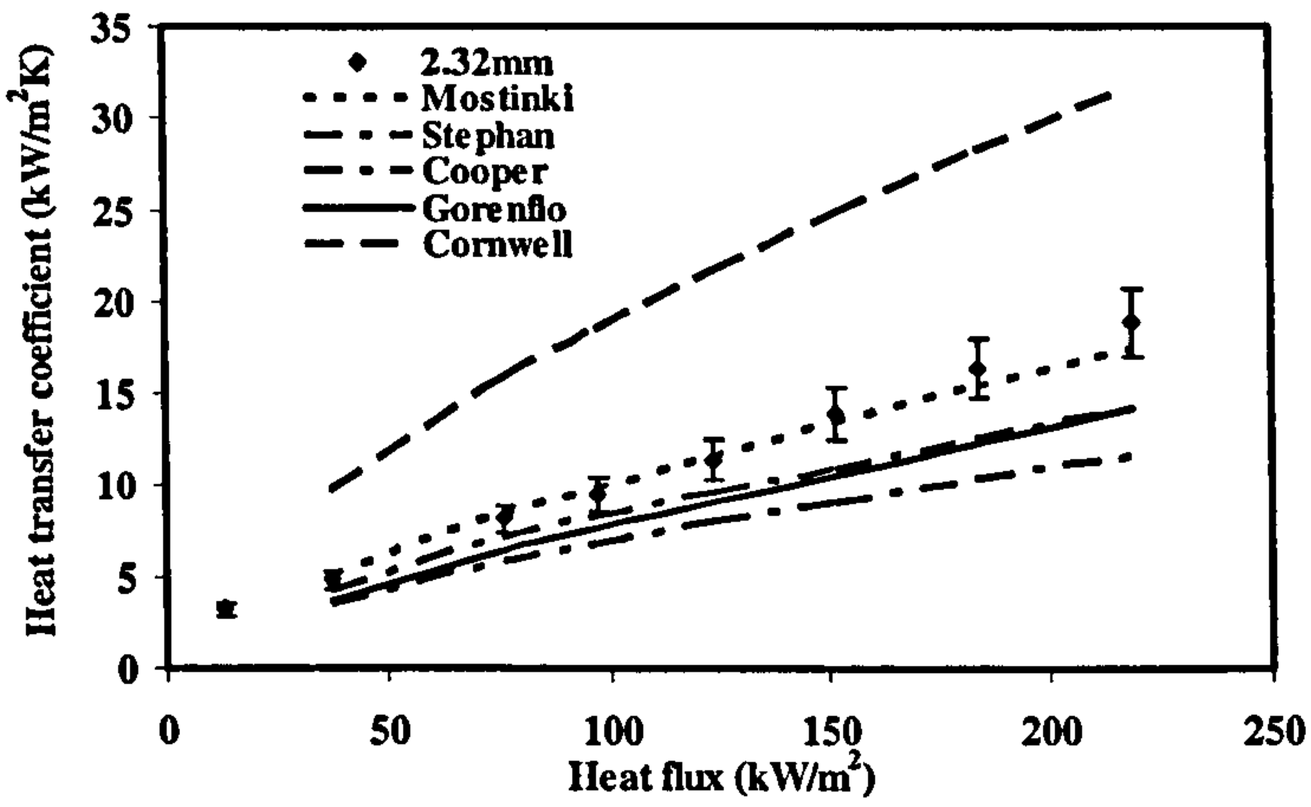

Figure 4.10 Comparison of experimental results with large tube correlations for 2.32mm tube with distilled water

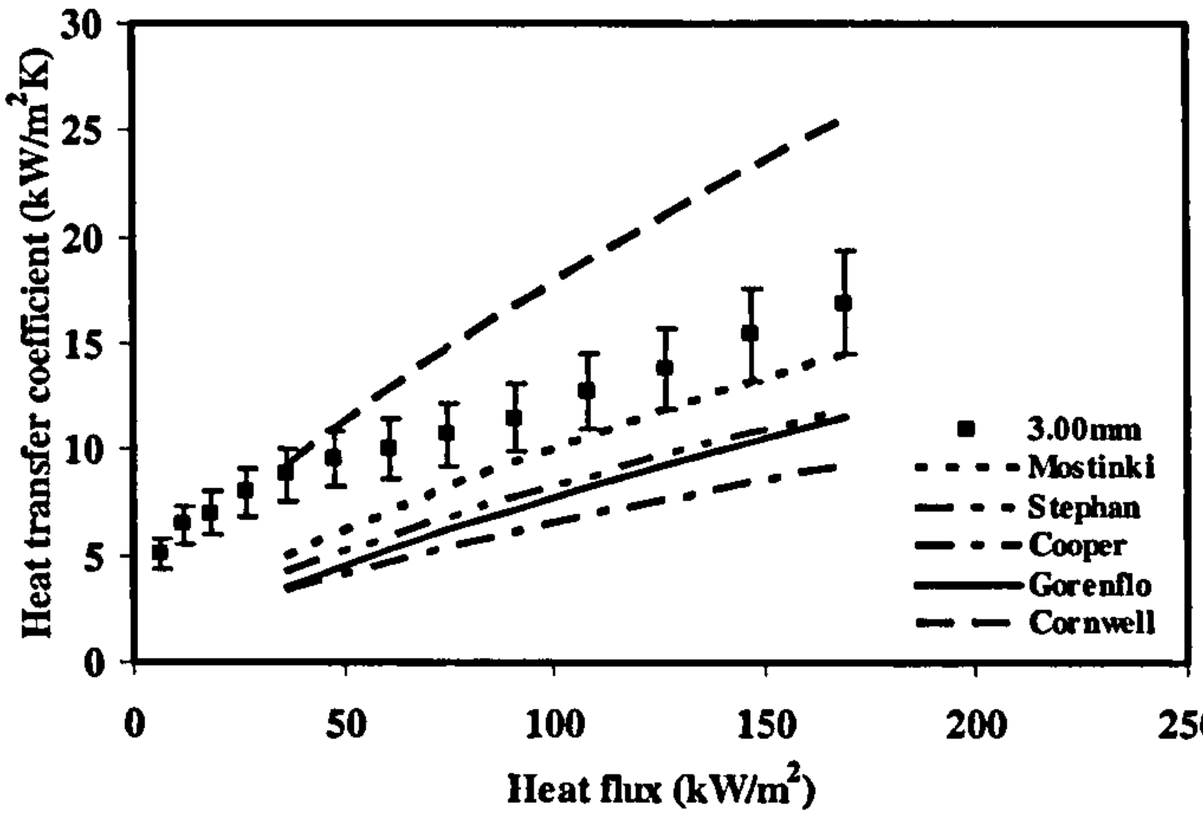

Figure 4.11 Comparisons of experimental results with large tube correlations for 3.00mm tube with distilled water

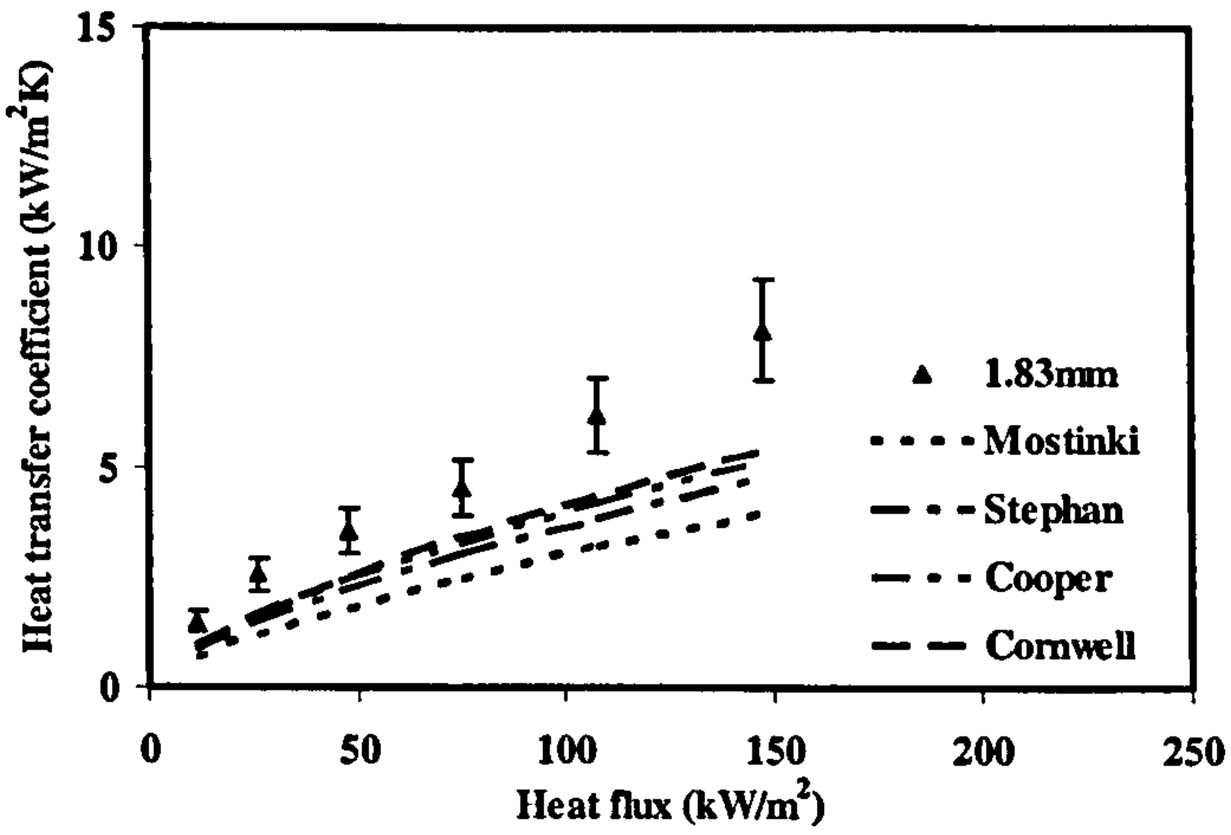

Figure 4.12 Comparison of experimental results with large tube correlations for 1.83 mm with Flutec PP1

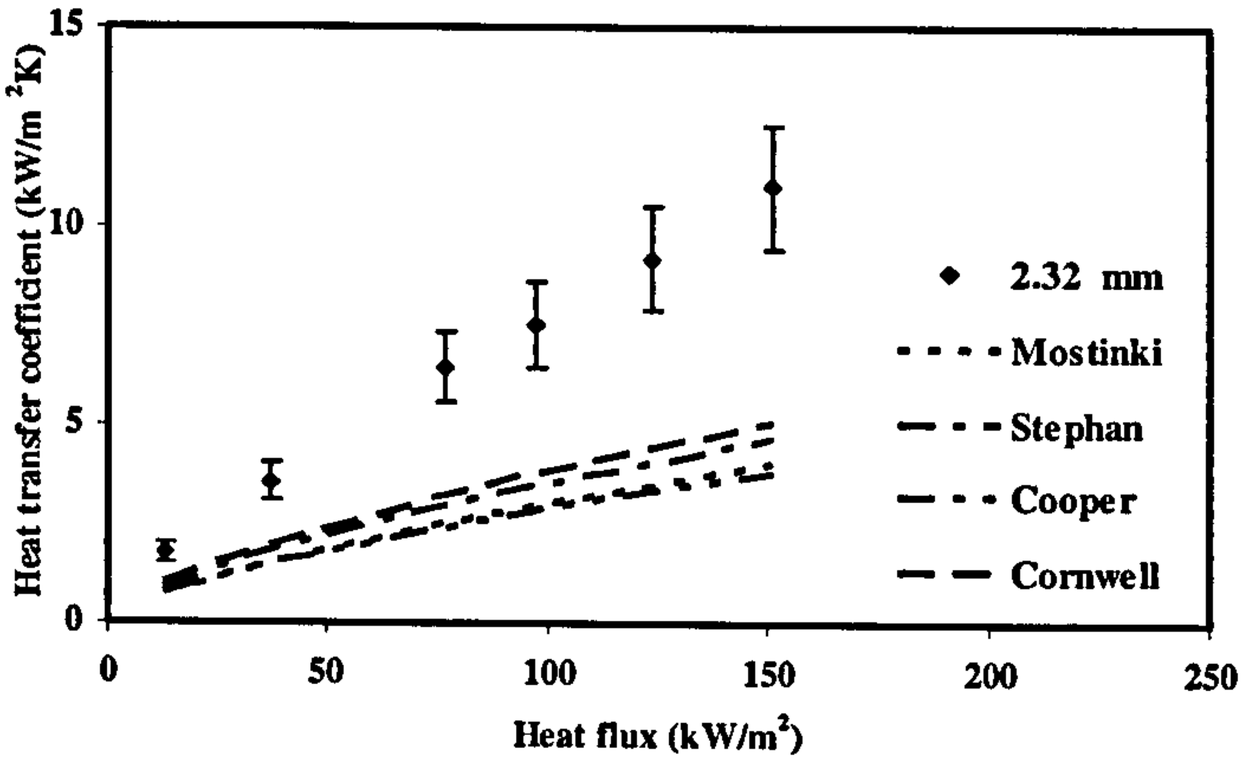

Figure 4.13 Comparison of experimental results with large tube correlations for 2.32mm with Flutec PP1

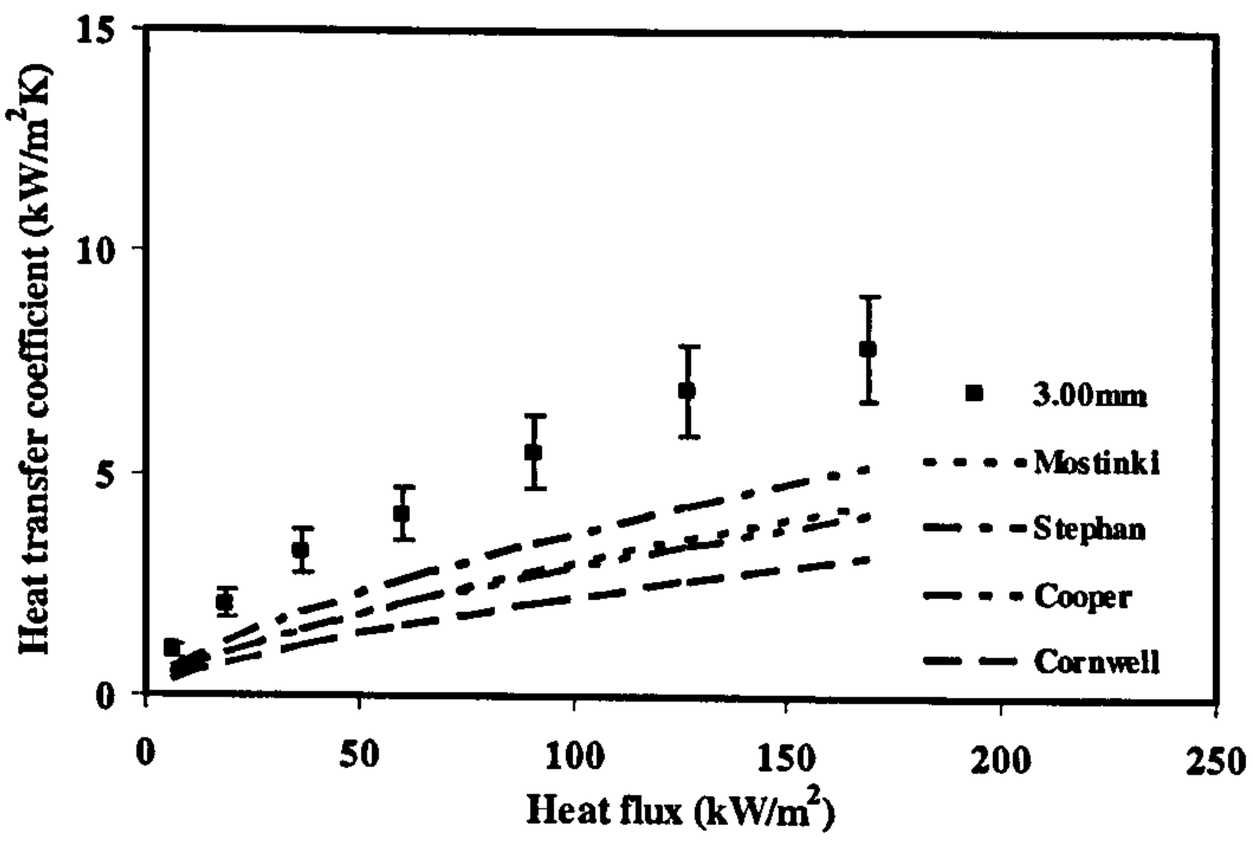

Figure 4.14 Comparison of experimental results with large tube correlations for 3.00mm tube with Flutec PP1

Root Mean Square Error Analysis (RMSE)

Error analysis was estimated using RMSE to compare the deviation of the experimental results against the pool boiling correlations used. Table 4.2 showed the deviation obtained for the correlations used in the comparison. The mean deviation was calculated from;

$$\text{Mean Error} = \frac{\alpha_{\text{exp}} - \alpha_{pred}}{n\alpha_{\text{exp}}} \qquad (4.4)$$

$$RMSE = \sum \left[\left[\frac{\left(\Delta p_{\exp} - \Delta p_{pred} \right)}{n \Delta p_{\exp}} \right]^2 \right]^{1/2} \tag{4.5}$$

Correlations	Deviation using Distilled Water			Deviation using Flutec PP1		
	3.00mm	2.32mm	1.83mm	3.00mm	2.32mm	1.83mm
Cooper [21]	0.49	0.53	0.65	0.33	0.48	0.35
Mostinki's[39]	0.37	0.12	0.63	0.50	0.61	0.51
Cornwell and Houston [27]	0.41	0.83	0.62	0.62	0.50	0.33
Stephan and Abdelsalam [25]	0.36	0.28	0.56	0.40	0.11	0.36
Gorenflo [42]	0.41	0.44	0.59	-	-	-

Table 4.2 Deviation of correlations with experimental results

4.2.3 Comment on pool boiling correlations

The comparison of the large diameter tube correlations with that of the experimental results showed that none of the models were able to predict the results satisfactorily. The Cornwell and Houston [27] correlation which included the effect of diameter in the derivation had the highest deviation. The correlation was developed for data base of diameter in the range of 8-50mm. The Stephan and Abdelsalam [25] correlation was developed using regression analysis for different fluids such as water and refrigerants. It was based on the bubble departure diameter and most of the analysis in the development of the correlation was obtained from experiments using boiling on tubes. As such it was expected to be able to predict the heat transfer coefficient at higher heat flux where the effect of diameter was less important.

4.3 Twin tube experimental results

This section presents the results obtained when the arrangement was that of a twin tube with the upper tube diameter been varied from 1.83-3.00mm while the lower tube was kept

constant at the diameter of 3.00mm. The experimental results presented here were obtained by using distilled water Flutec PP1 as the working fluids at nominal atmospheric pressure. The results obtained was divided into three categories namely, low heat flux, medium heat flux and high heat flux. Figure 4.15-Figure 4.20 shows the plot of heat flux against wall superheat for the twin tube arrangement. The plots shows that by keeping the lower tube heat flux constant and varying the heat flux on the upper tube enhancement observed on the upper tube is identical to that of a single tube. The presence of the lower tube bubbles shifts the boiling curve to the left on the graph. The plot showing the heat flux against the wall superheat for the 1.83mm tube showed a marked shift in the pool boiling curve. Nucleate boiling was observed to commence at 4.38 K (47 kW/m^2) when there was no heat input on the lower tube. Once the heat flux on the lower tube was varied from 37, 61, 91 127 and 169 kW/m^2 the wall superheat on the 1.83 mm upper tube reduced to 4.68, 3.58, 3.48 and 2.88 K respectively. At medium heat flux of 147 kW/m^2 on the upper tube, the wall superheat was greater than that of the single tube. This indicated that the bubbles from the lower tube were not having any contribution to enhancing the heat transfer coefficient. Similarly at higher heat flux as in the 1.83mm tube fully covered with nucleate bubbles of its own, the bubbles from the lower tube suppressed any enhancement on it. This results in a minimum in the observed heat transfer coefficient. For the 2.32 mm, tube the wall superheat for nucleate boiling to commence was 7.8 K at a heat flux of 37 kW/m^2. The presence of the bubbles on the lower tube caused the heat flux to decrease the wall superheat of the upper tube to 7.11 K when the heat flux was 76 kW/m^2 and that of the lower being 37 kW/m^2. At higher heat fluxes of 183 kW/m^2 and above the boiling curve were close to each other irrespective of the bubbles generated on the lower tube. Fully developed nucleate boiling was observed to have occurred on the upper tube and hence the enhancement becomes insignificant. Thus, the presence of the lower tube bubbles shifts the curve to the left.

Nucleate boiling was observed to start at a wall superheat of 4.2 K for the 3.0 mm tube with distilled water as the working fluid. Once the heat flux on the lower tube was increased from 37 -167 kW/m^2, the boiling curve shifted to the left which corresponds to a decrease in the wall superheat from 3.96, 3.6, 3.35 and 2.59 K for a heat flux of 37 kW/m^2 on the upper tube when the lower tube was at 37, 91, 127 and 169 kW/m^2 respectively. At medium

heat flux of 91 kW/m^2 such reduction was also observed on the upper tube. With the heat flux on the upper tube increased to 169 kW/m^2 the single tube performed better as shown by the shift of the wall superheat to the left of the curve.

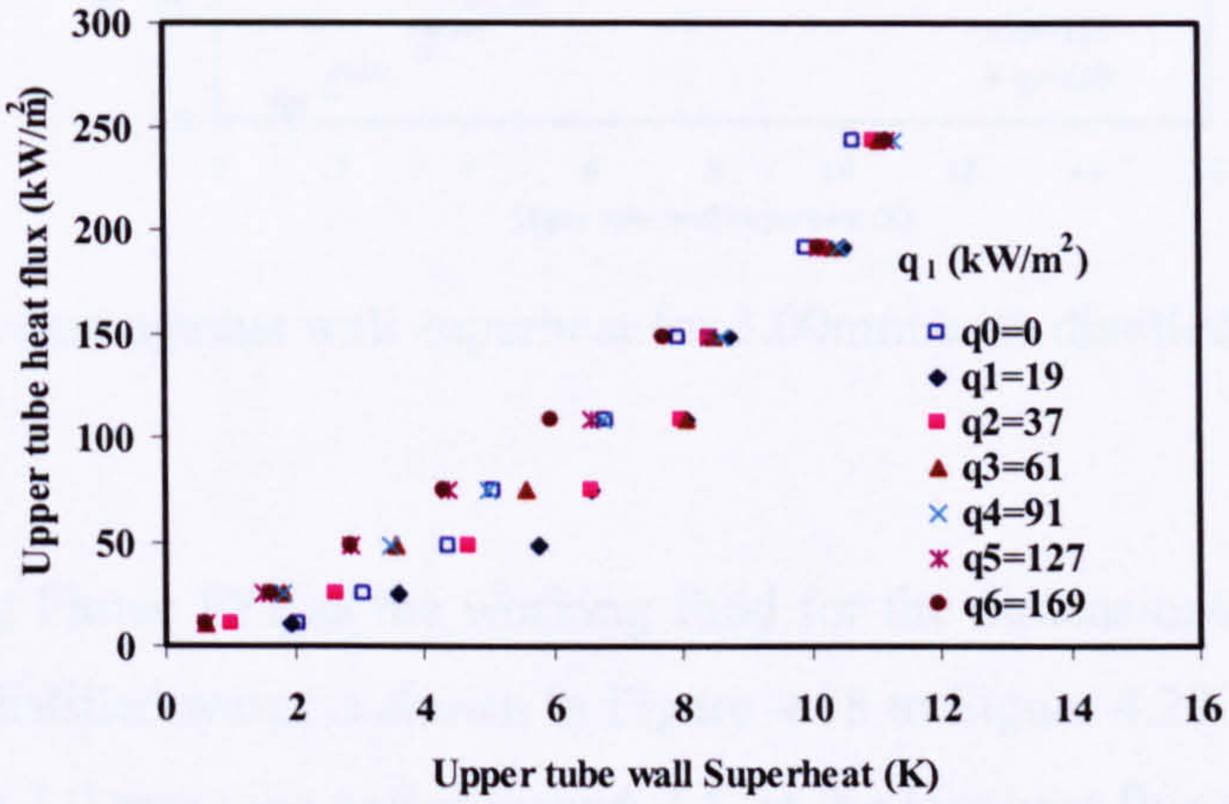

Figure 4.15 A plot of heat flux against wall superheat for diameter of 1.83mm with distilled water due to bubbles from below

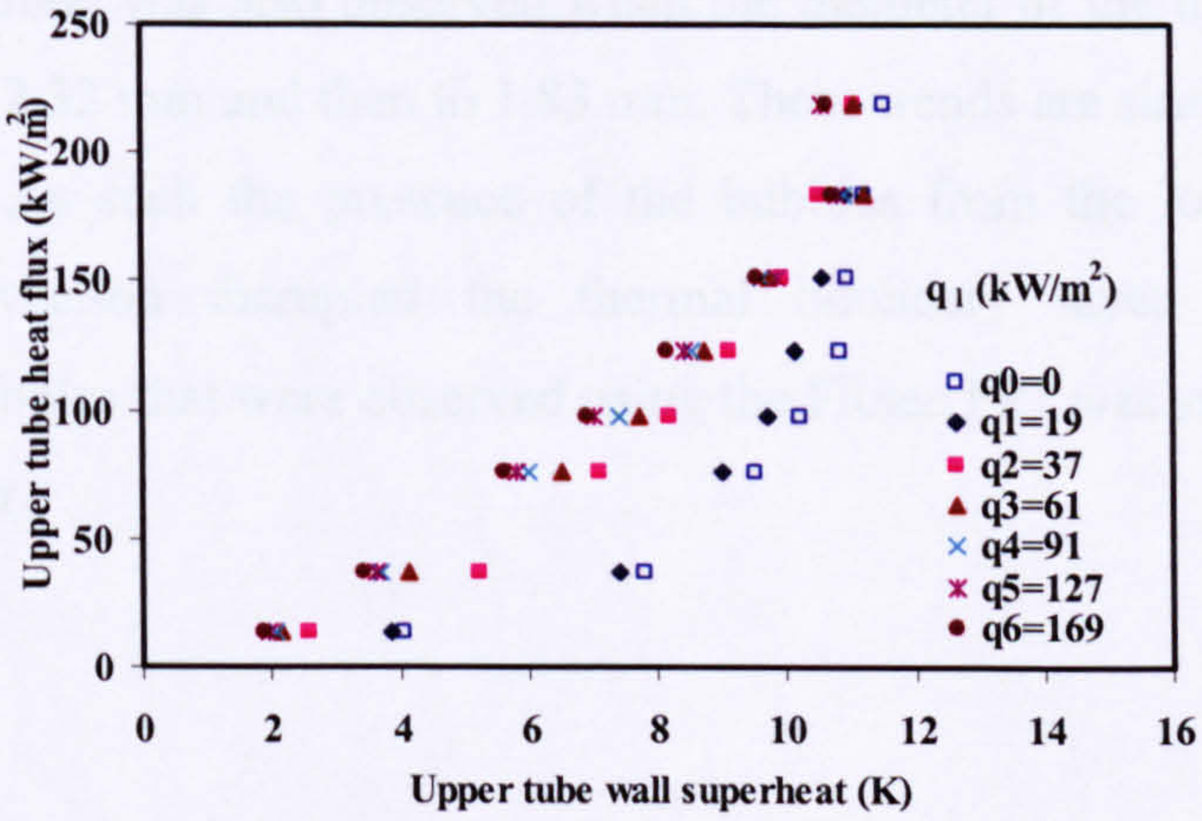

Figure 4.16 Heat flux against wall superheat for 2.32mm tube with distilled water due to bubbles from below

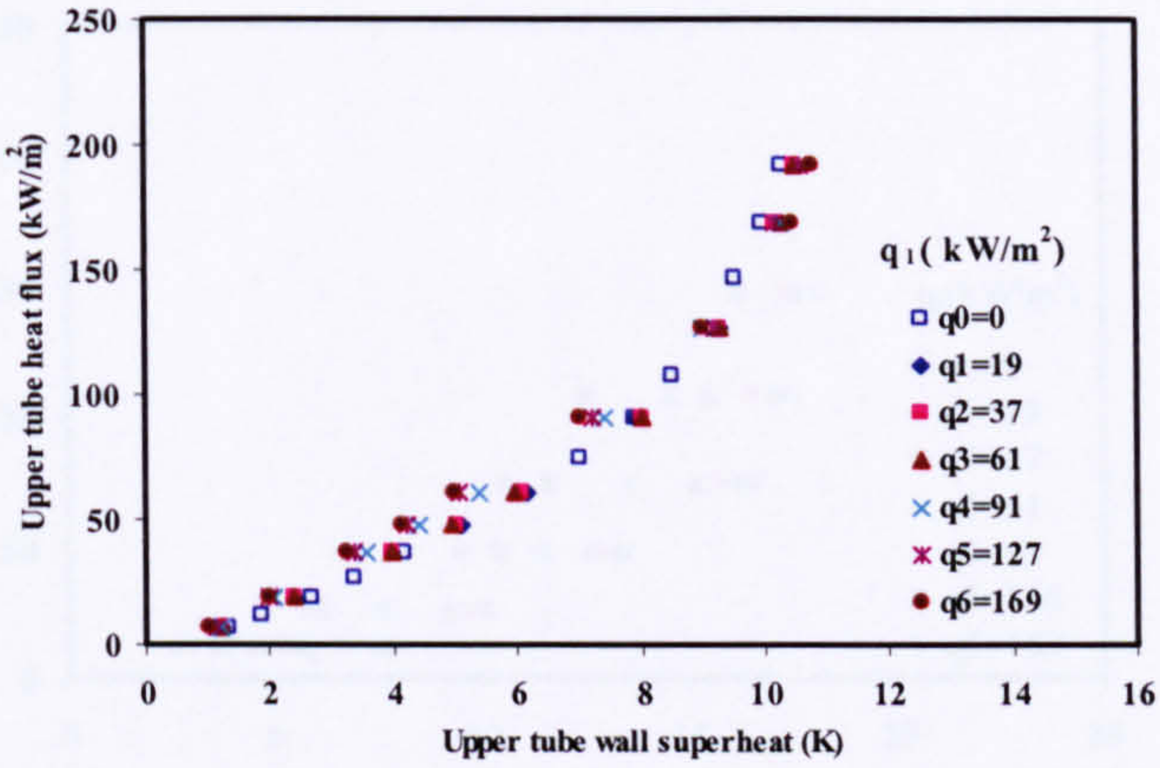

Figure 4.17 Heat flux against wall superheat for 3.00mm with distilled water due to bubbles from below

The results using Flutec PP1 as the working fluid for the dimensions of tube had been the same as that of distilled water is shown in Figure 4.18 to Figure 4.20 . The single tube wall superheat for the 3.0 mm tube varies from 6.7 K at the low heat flux to 21.5 K at high heat flux of 169kW/m^2. Once the bubbles are generated from the lower tube, this shifts to the left of the boiling curve. For instance when the heat flux on the lower tube was varied from 19 kW/m^2 the wall superheat was reduced from 4.52K at low heat flux to 20.8 K at high heat flux. This trend was also observed when the diameter of the upper tube was changed from 3.0 mm to 2.32 mm and then to 1.83 mm. These trends are similar to that observed for distilled water. As such the presence of the bubbles from the lower tube and also the turbulence convection disrupted the thermal boundary layer thereby reducing the temperature. Bubbles that were observed using the Flutec PP1 was smaller compared to that of distilled water.

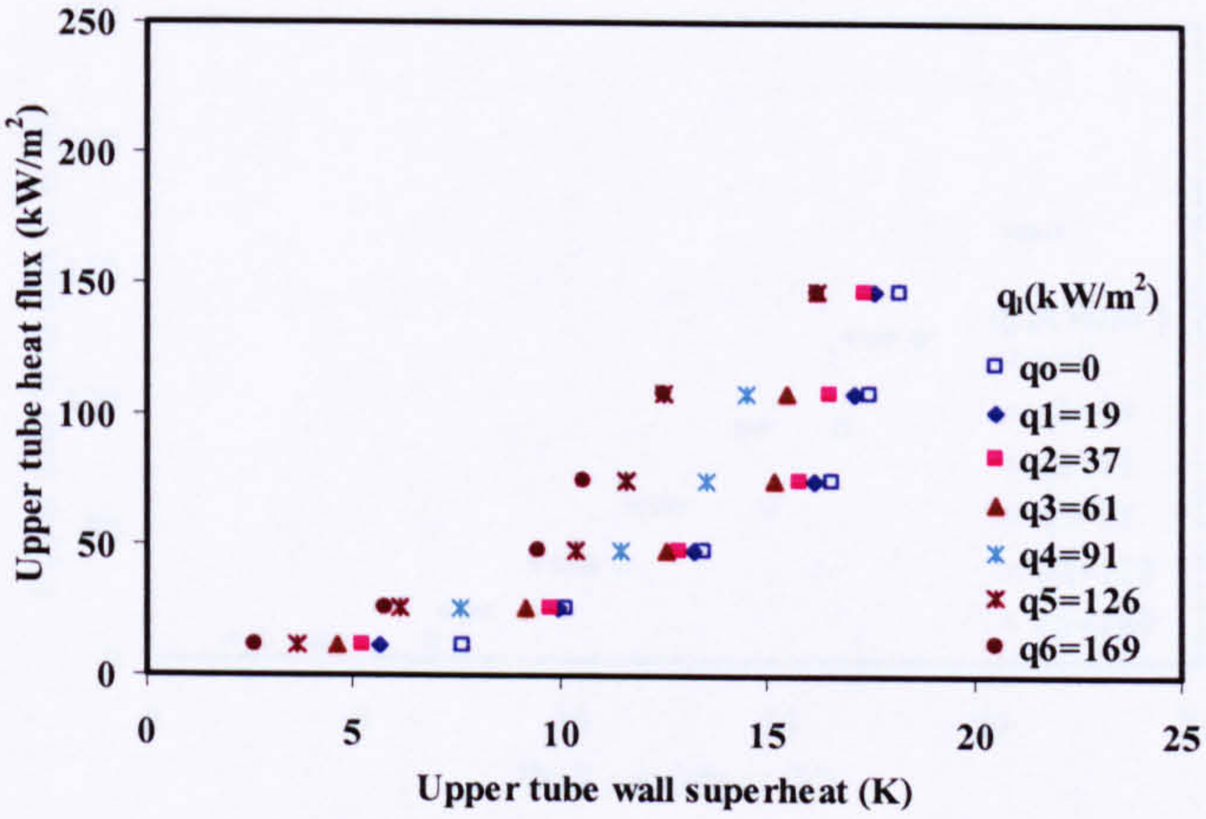

Figure 4.18 Heat flux against wall superheat for 1.83mm tube with Flutec PP1 due to bubbles from below

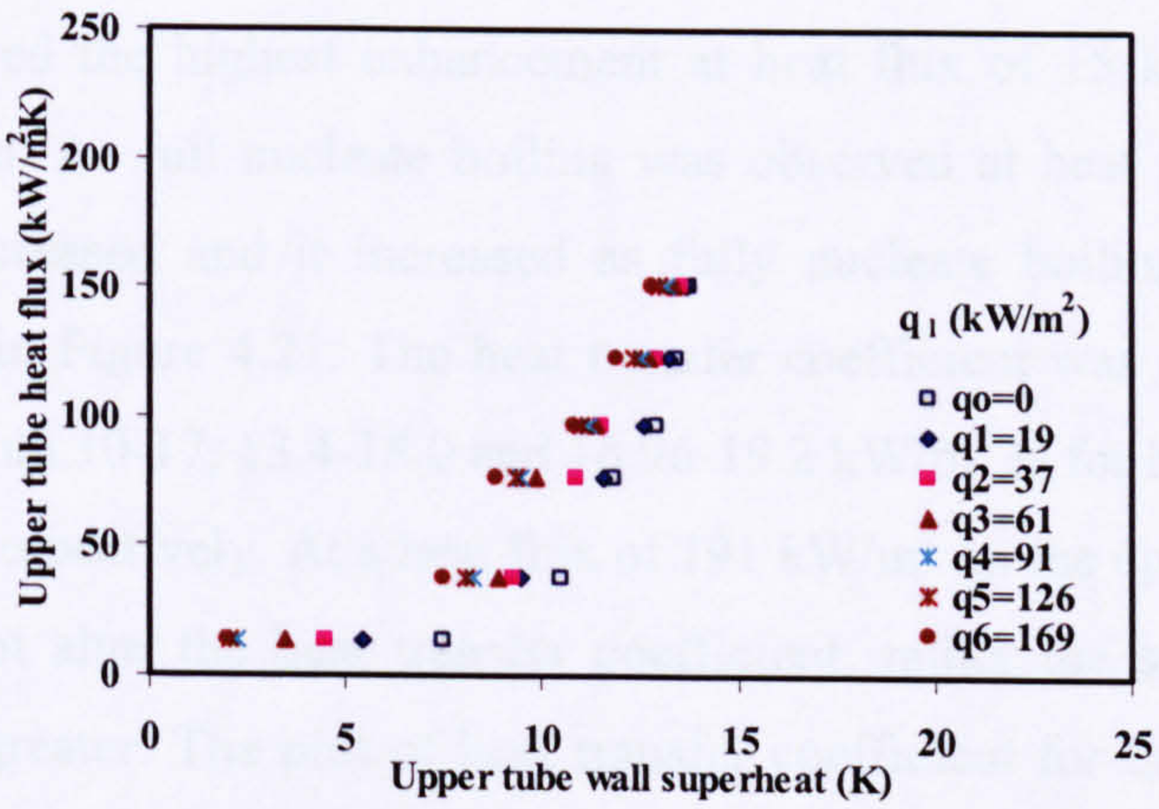

Figure 4.19 Heat flux against wall superheat for 2.32mm tube with Flutec PP1 due to bubbles from below

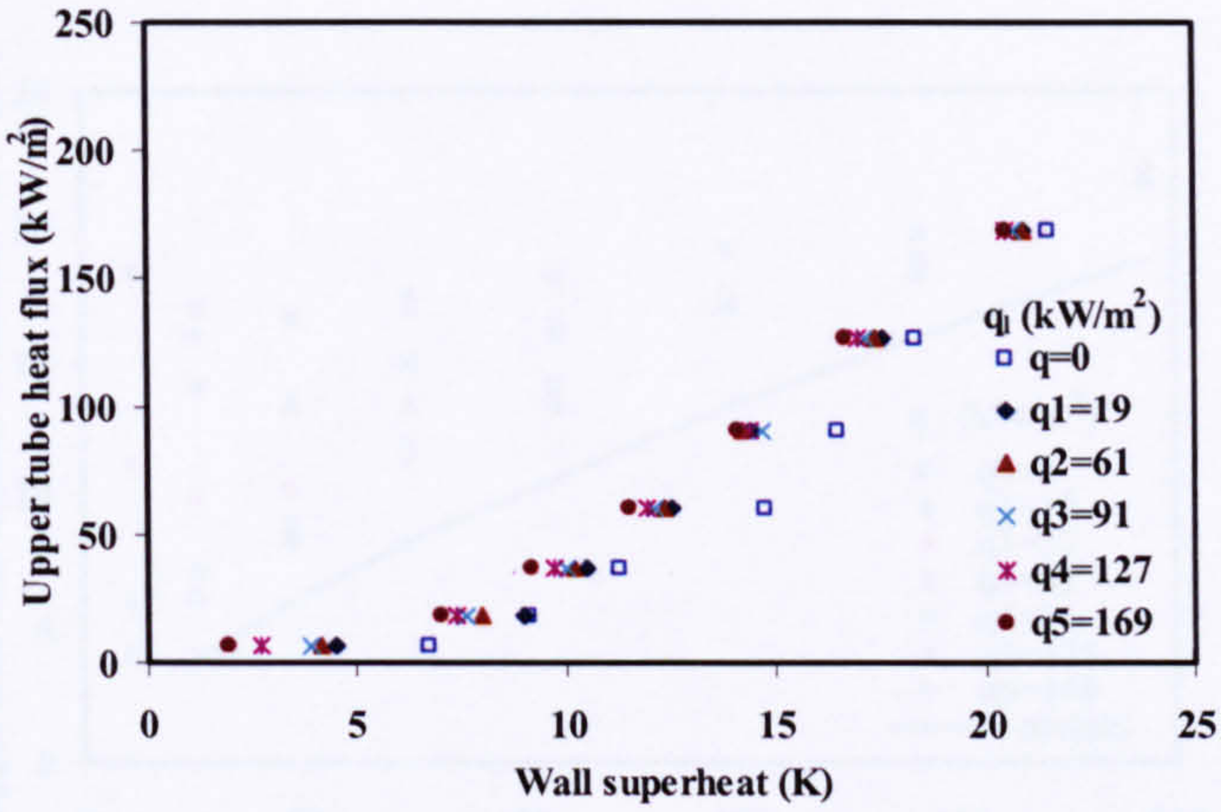

Figure 4.20 Heat flux against wall superheat for 3.00mm tube with Flutec PP1 due to bubbles from below

The plots of heat transfer coefficient against heat flux for the upper tube are shown in Figure 4.21-Figure 4.26 for the distilled water and Flutec PP1. The plots for the 1.83 mm upper tube showed the highest enhancement at heat flux of 15 kW/m^2 where there was patchy nucleation. As full nucleate boiling was observed at heat flux of 191 kW/m^2, the enhancement decreased and it increased as fully nucleate boiling occurred on the tube which is shown in Figure 4.21. The heat transfer coefficient was observed to increase on the upper tube from 10-17, 13.4-18.0 and 16.96-19.2 kW/m^2 K for heat fluxes of 47, 74,107 and 147 kW/m^2 respectively. At a heat flux of 191 kW/m^2 on the upper tube the presence of the lower did not alter the heat transfer coefficient; rather the single tube heat transfer coefficient was greater. The plot of heat transfer coefficient for the 2.32 mm is shown in Figure 4.22. It was observed that the heat transfer coefficient increased from 7.15-10.92, 10.75-13.86, and 16.38-17.45kW/m^{2}K at heat flux of 37, 76 and 183 respectively when the lower tube was varied from 19-169 kW/m^2. At higher heat fluxes the enhancement was observed to decrease due to vapour blanketing on the tube. Similarly, for the 3.0 mm diameter tube, an increase in enhancement was observed in the region of 37-127 kW/m^2. At the heat flux of 37 kW/m^2 the heat transfer coefficient increased from 10.17-12.21 kW/m^{2}K. This enhanced from 11.32-12.94 kW/m^{2}K at 91 kW/m^2 whereas at 127 kW/m^2 there was 0.46 kW/m^{2}K increment. Mostinki's[39] correlation was used in the comparisons the RSME was better compared to the other correlations.

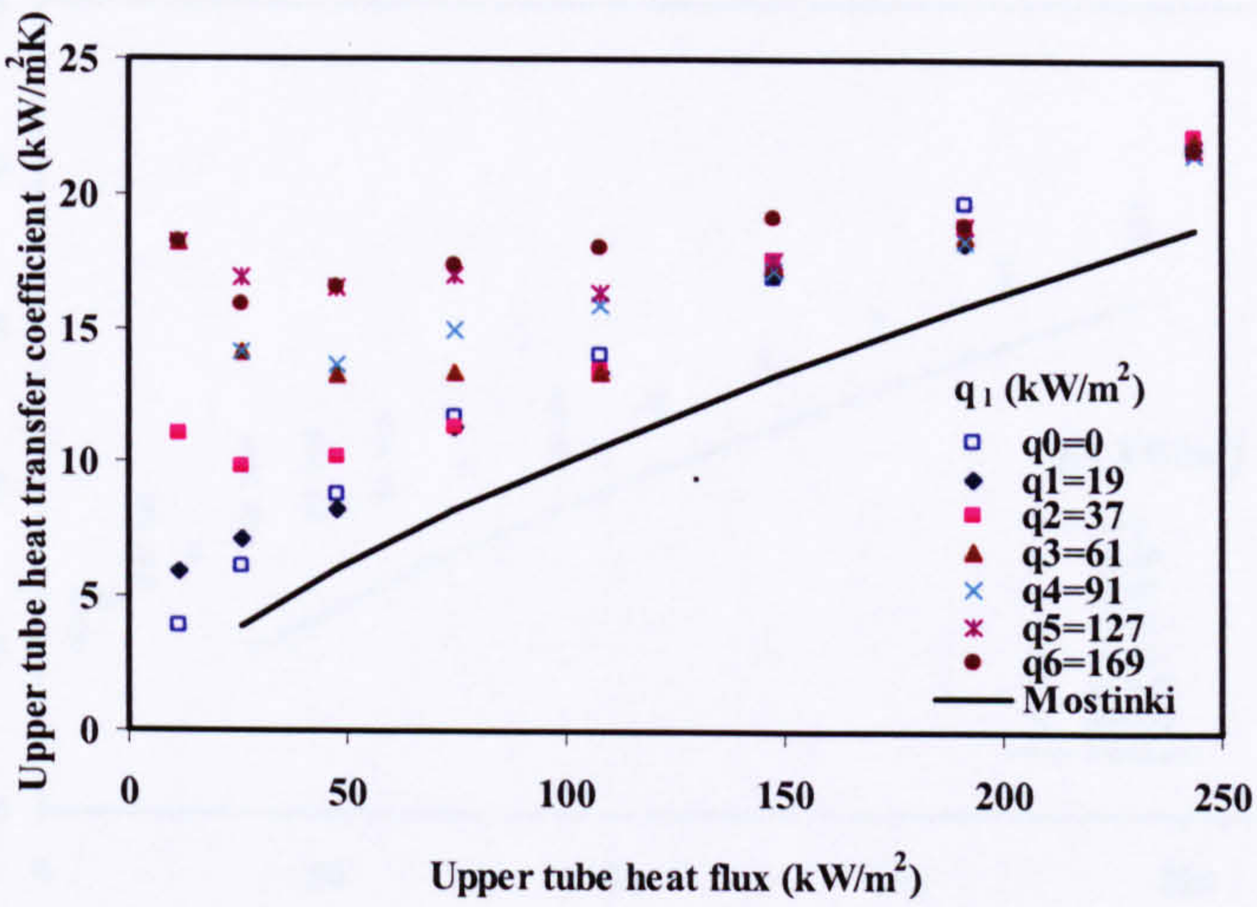

Figure 4.21 Heat transfer coefficient against upper tube heat flux (1.83mm) with distilled water due to bubbles from below

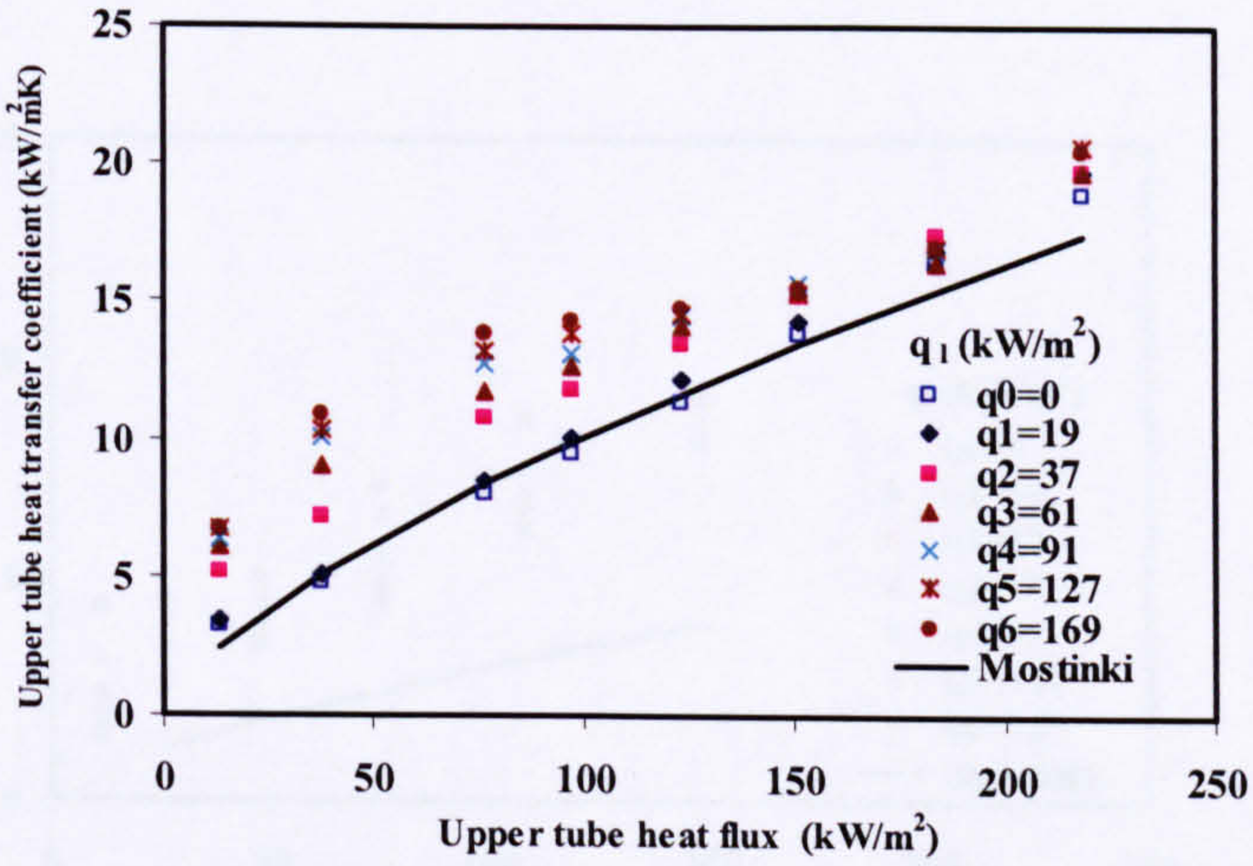

Figure 4.22 Heat transfer coefficient against upper tube heat flux (2.32mm) with distilled water due to bubbles from below

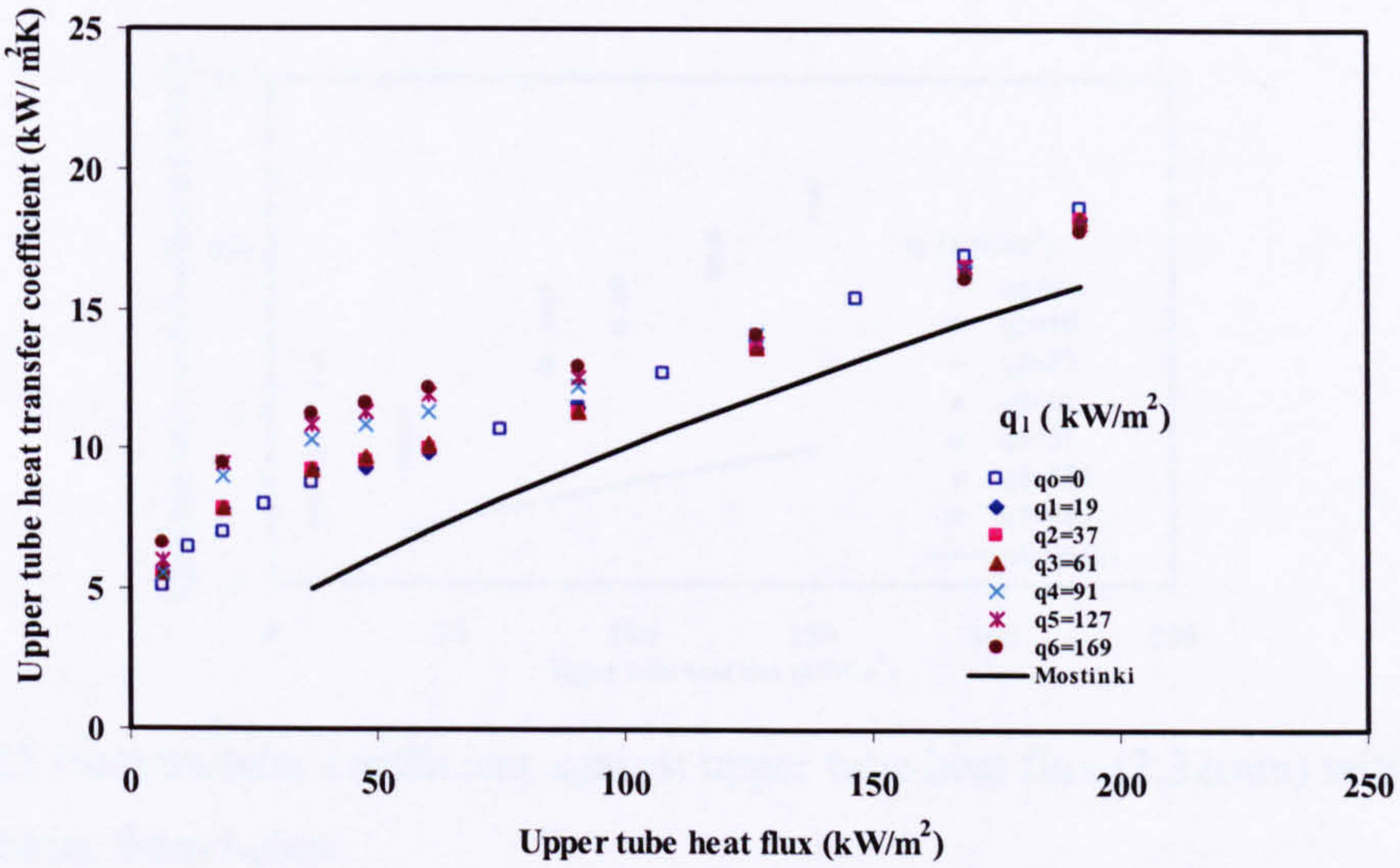

Figure 4.23 Heat transfer coefficient against upper tube heat flux (3.00mm) with distilled water due to bubbles from below

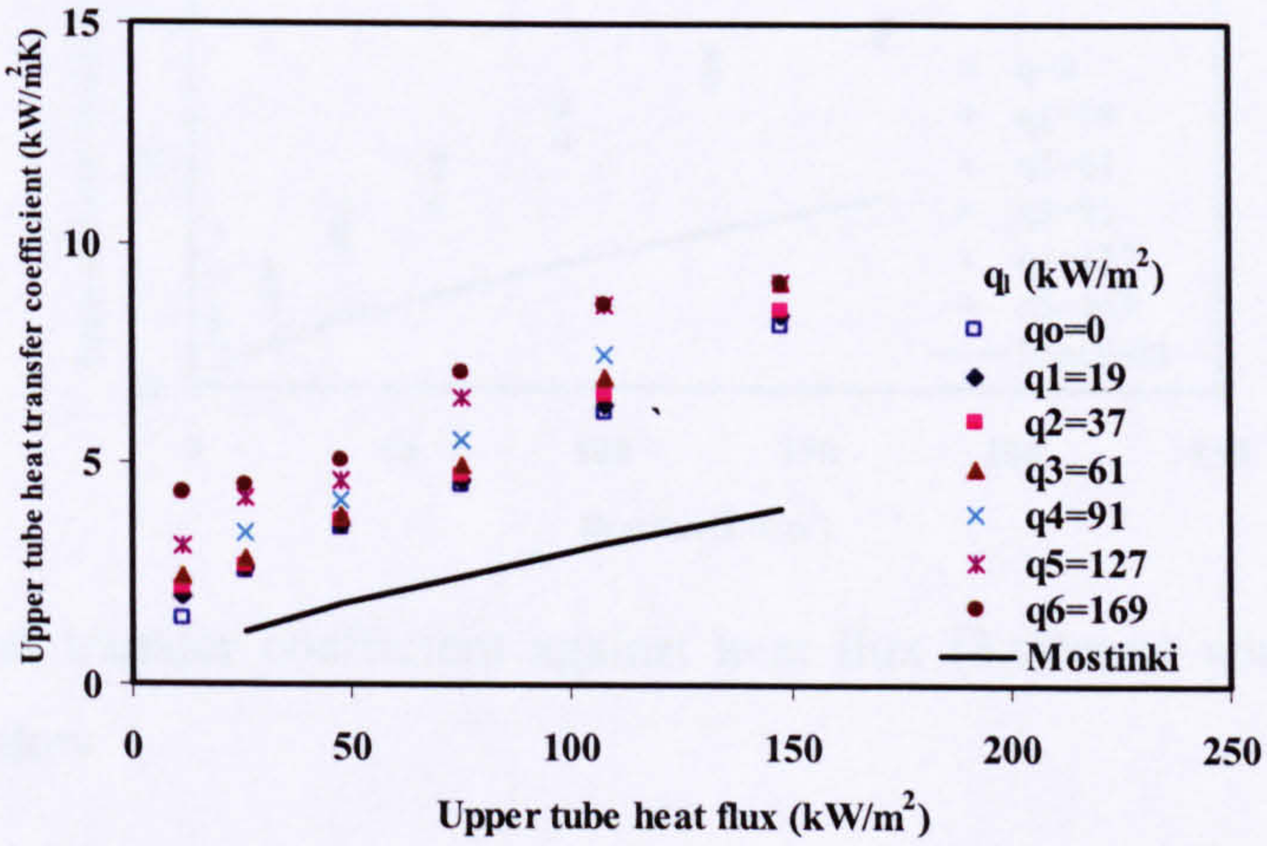

Figure 4.24 Heat transfer coefficient against upper tube heat flux (1.83mm) with Flutec PP1 due to bubbles from below

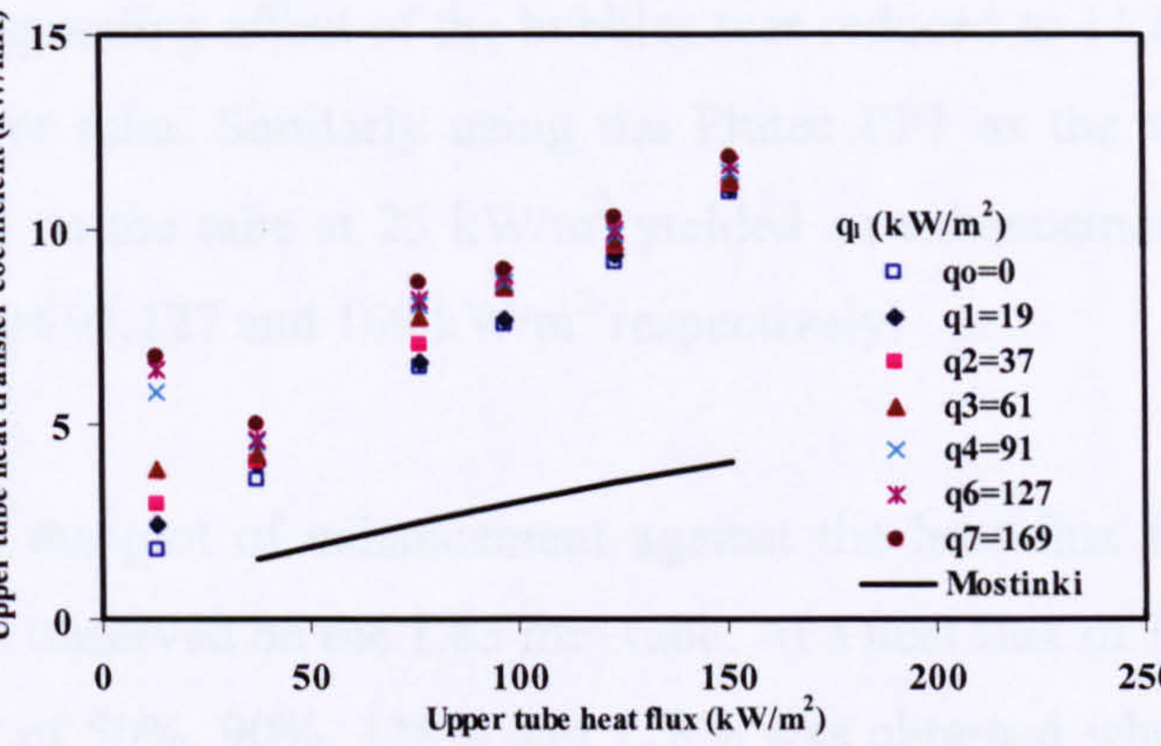

Figure 4.25 Heat transfer coefficient against upper tube heat flux (2.32mm) with Flutec PP1 due to bubbles from below

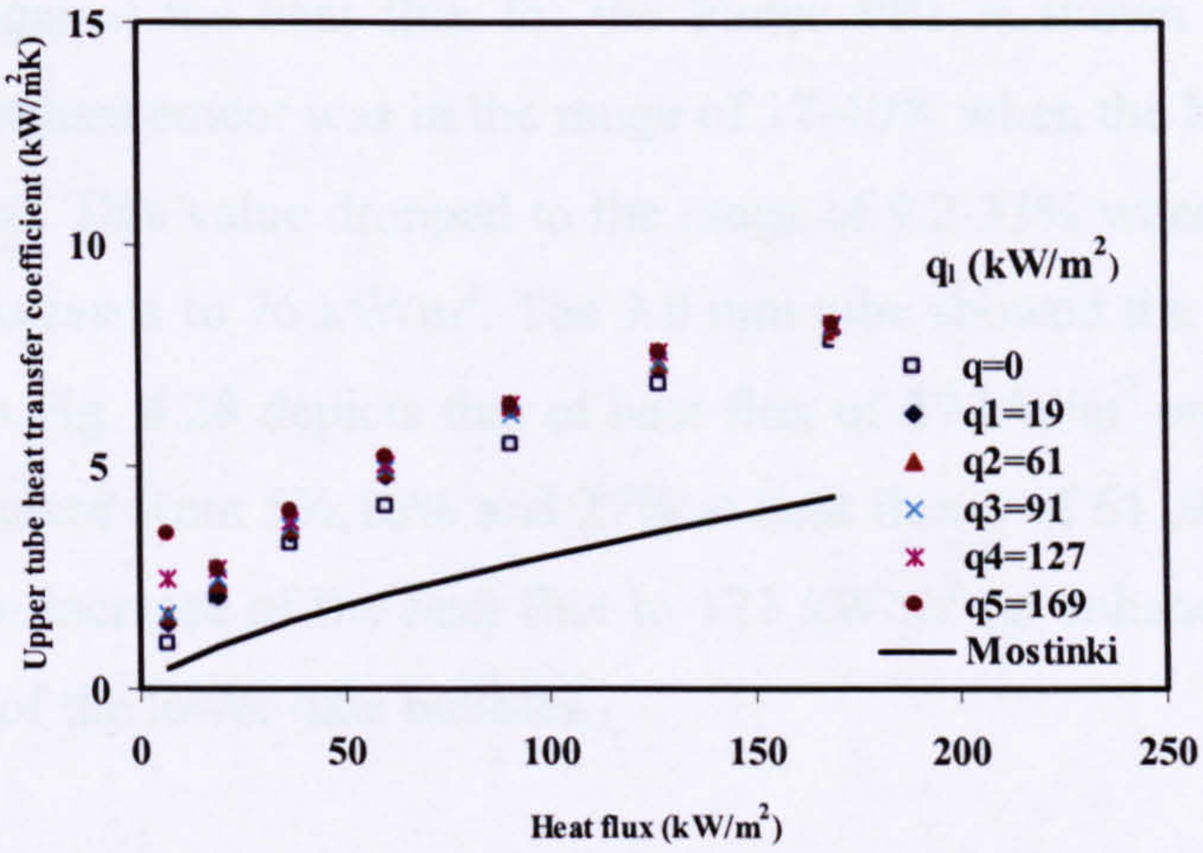

Figure 4.26 Heat transfer coefficient against heat flux (3.00mm) with Flutec PP1 due to bubbles from below

Figure 4.27 to Figure 4.32, shows the plot of enhancement on the upper tube against heat flux. The enhancement was the difference between the single tubes when there was heat input on the lower tube. The enhancement starts to rise in the natural convection region in the first instance, until discrete nucleate boiling was observed. In the case of the 1.83 mm tube which is shown in Fig. 4.26, there is an increment of 15%, 50%, 54% and 86% for heat fluxes on the lower tube at 37, 61, 91 and 169 kW/m^2 respectively, when the upper tube was at 47 kW/m^2. At a heat flux of 74 kW/m^2 on the upper tube and varying the lower tube heat flux from 61, 91,127 and 169 kW/m^2 showed an increase of 14%, 27%, 45% and

48% respectively. It was observed from the plots that as the heat flux on the upper tube was increased the corresponding effect of the bubbles was reduced to 11.6% at heat flux of 169 kW/m^2 on the lower tube. Similarly using the Flutec PP1 as the working fluid, (Figure 4.30), the heat flux on the tube at 25 kW/m^2 yielded an enhancement of 31%, 61.5% and 70% at heat fluxes of 91,127 and 169 kW/m^2 respectively.

Figure 4.28 shows the plot of enhancement against the heat flux for the 2.32 mm tube. Similar trends were observed on the 1.83 mm tube. At a heat flux of 37 kW/m^2 on the upper tube, enhancement of 50%, 90%, 118% and 128% was obtained when the heat flux on the lower tube was varied from 37, 61, 91 and 169 kW/m^2 respectively. This enhancement decreased as the heat flux on the tube was varied to a medium value of 97 kW/m^2. At a higher heat flux of 123 kW/m^2, the enhancement decreased to an average of 21%. The plot of enhancement against the heat flux for the Flutec PP1 is shown in Fig. 4.30. It was observed that the enhancement was in the range of 17-40% when the heat flux on the upper tube was 37 kW/m^2. This value dropped to the range of 9.2-33% when the heat flux on the upper tube was increased to 76 kW/m^2. The 3.0 mm tube showed the lowest enhancement. The plot shown in Fig. 4.28 depicts that at heat flux of 37 kW/m^2,on the upper tube , the enhancement increased from 5%,16% and 27% at heat fluxes of 61 ,91 and 169 kW/m^2 on the lower tube. An increase of the heat flux to 127 kW/m^2 no enhancement was observed with the presence of the lower tube bubbles.

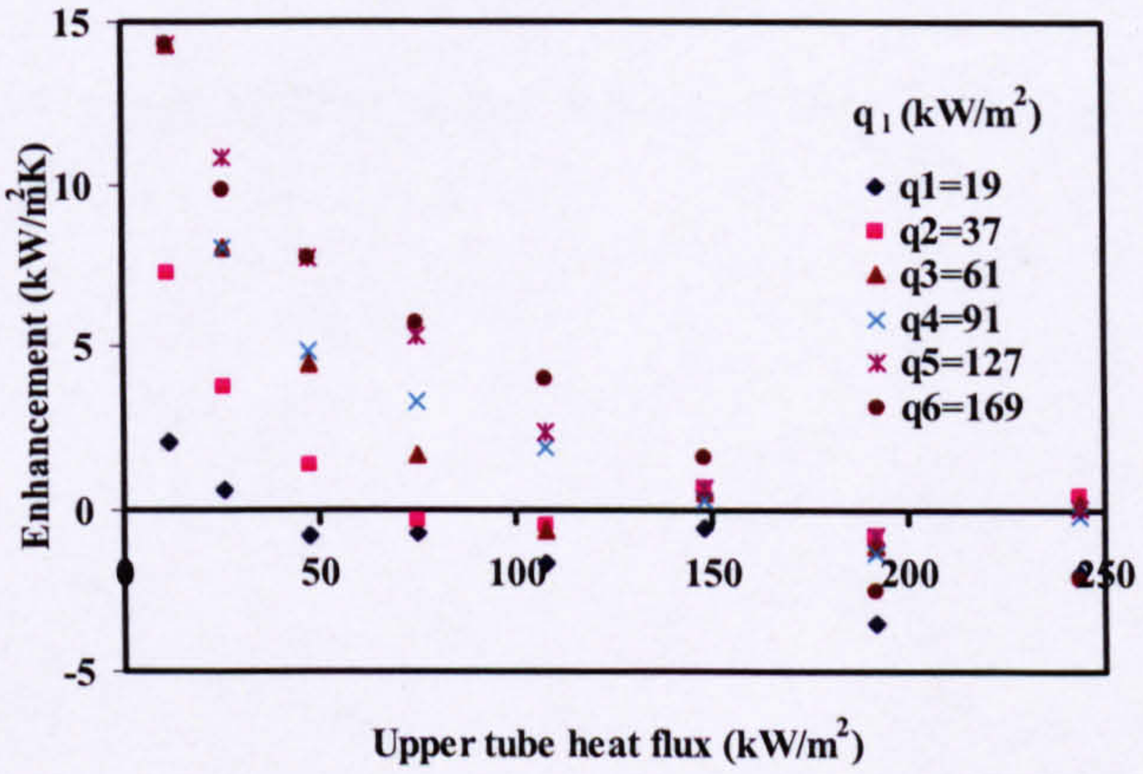

Figure 4.27 Enhancement against upper tube heat flux (1.83mm) with distilled water due to bubbles from below.

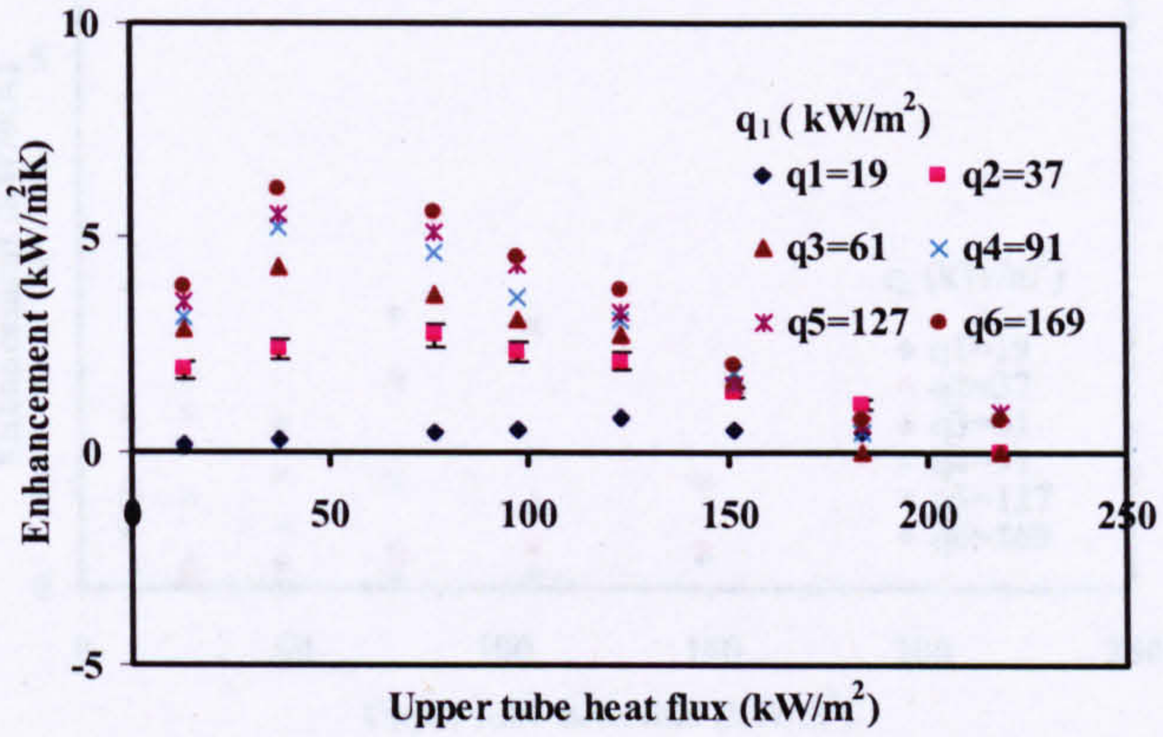

Figure 4.28 Enhancement against upper tube heat flux (2.32mm) with distilled water due to bubbles from below

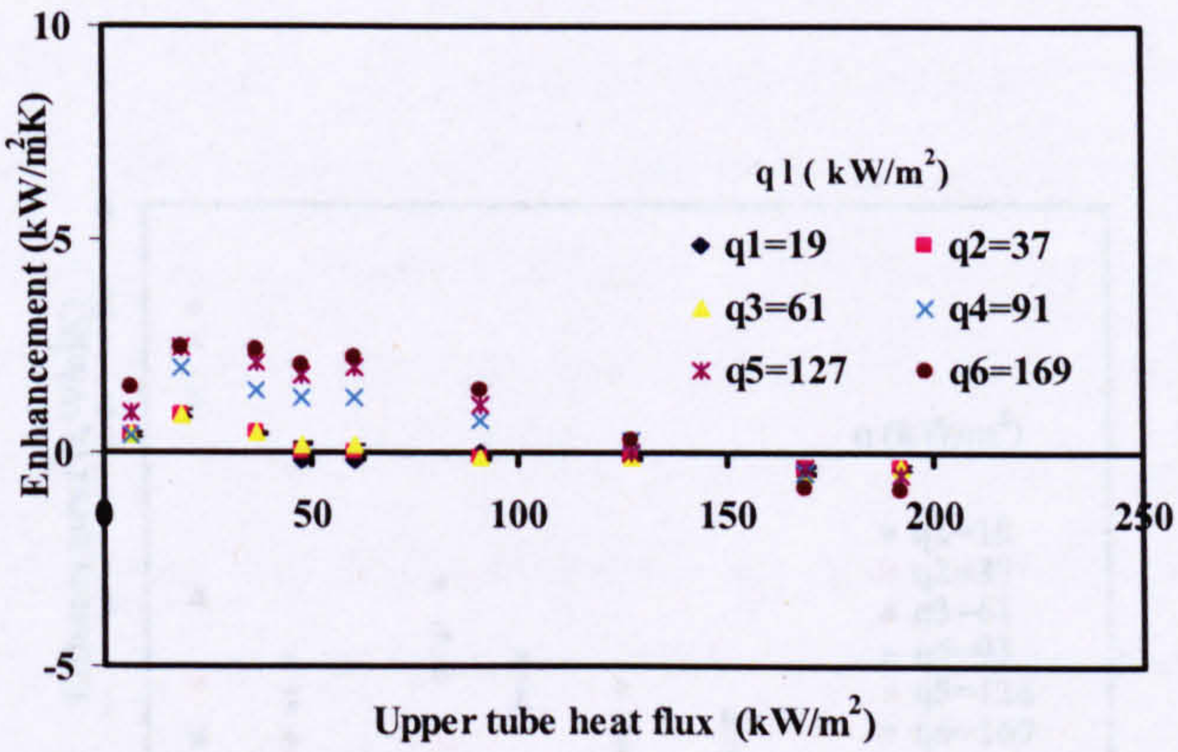

Figure 4.29 Enhancement against upper tube (3.00mm) with distilled water due to bubbles from below

.

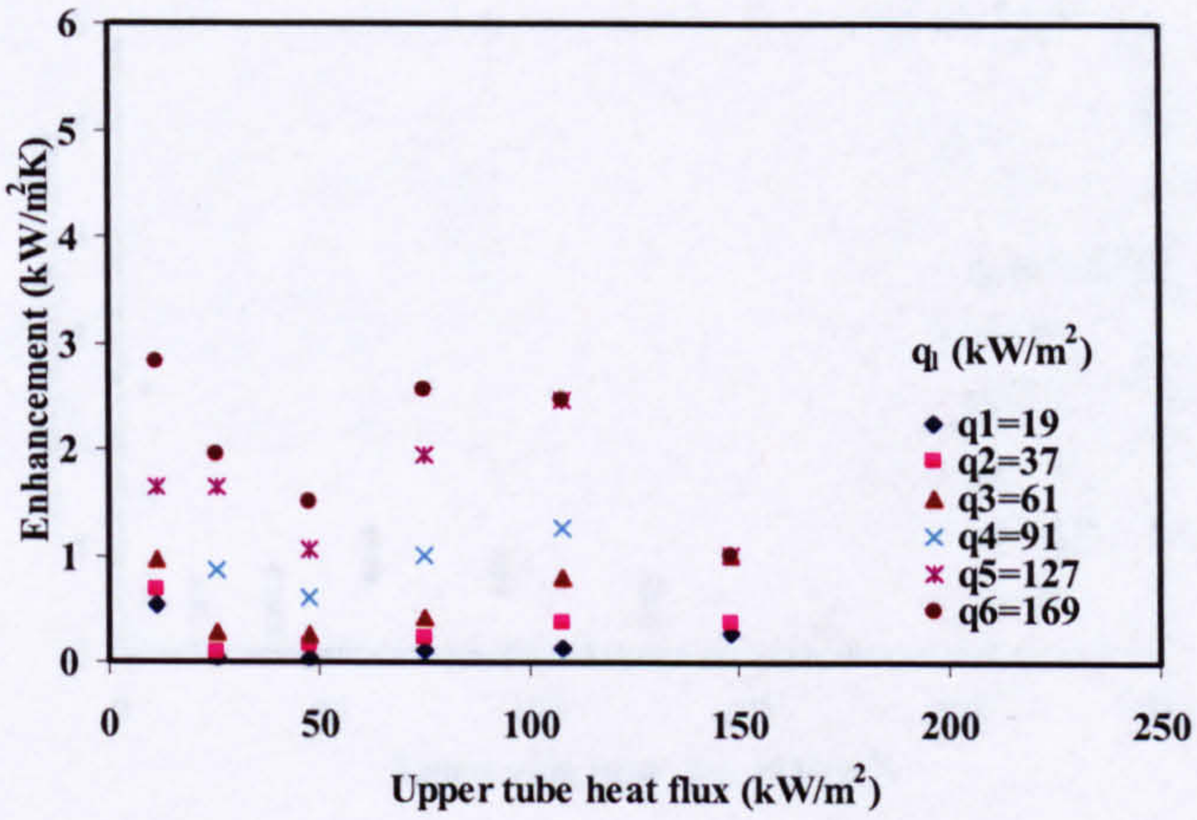

Figure 4.30 Enhancement against upper tube (1.83mm) with Flutec PP1 due to bubbles from below

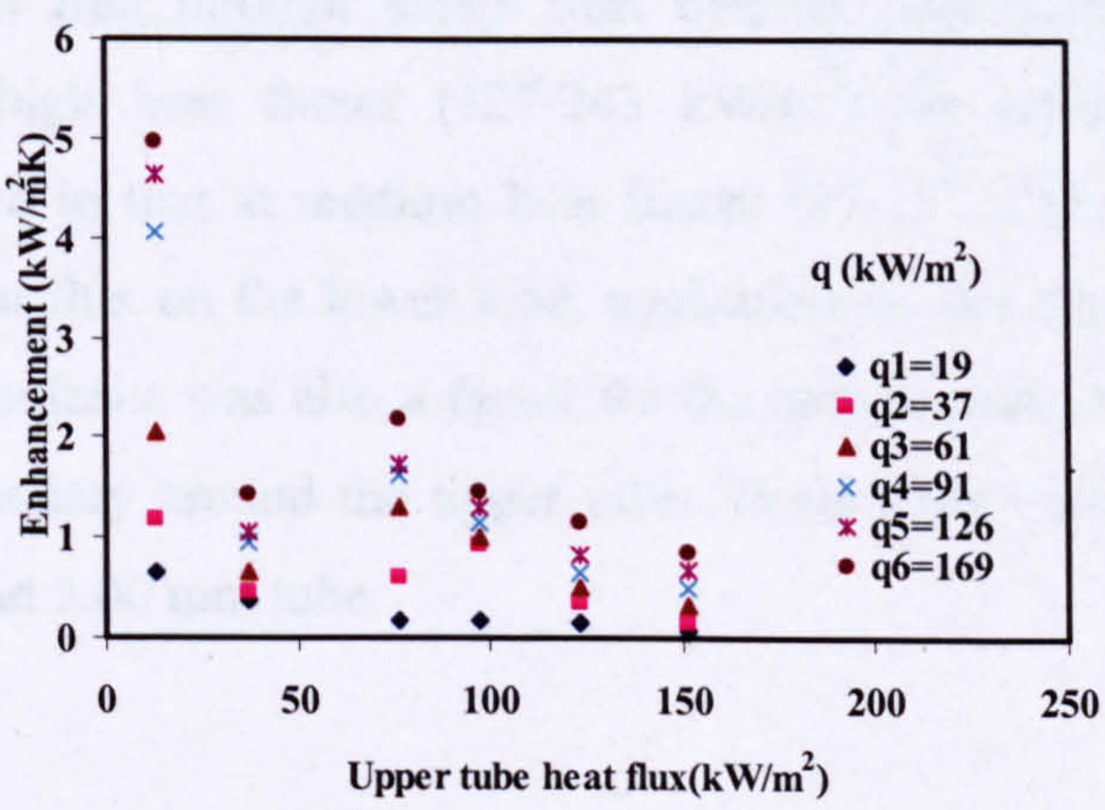

Figure 4.31 Enhancement against upper tube (2.32mm) with Flutec PP1 due to bubbles from below

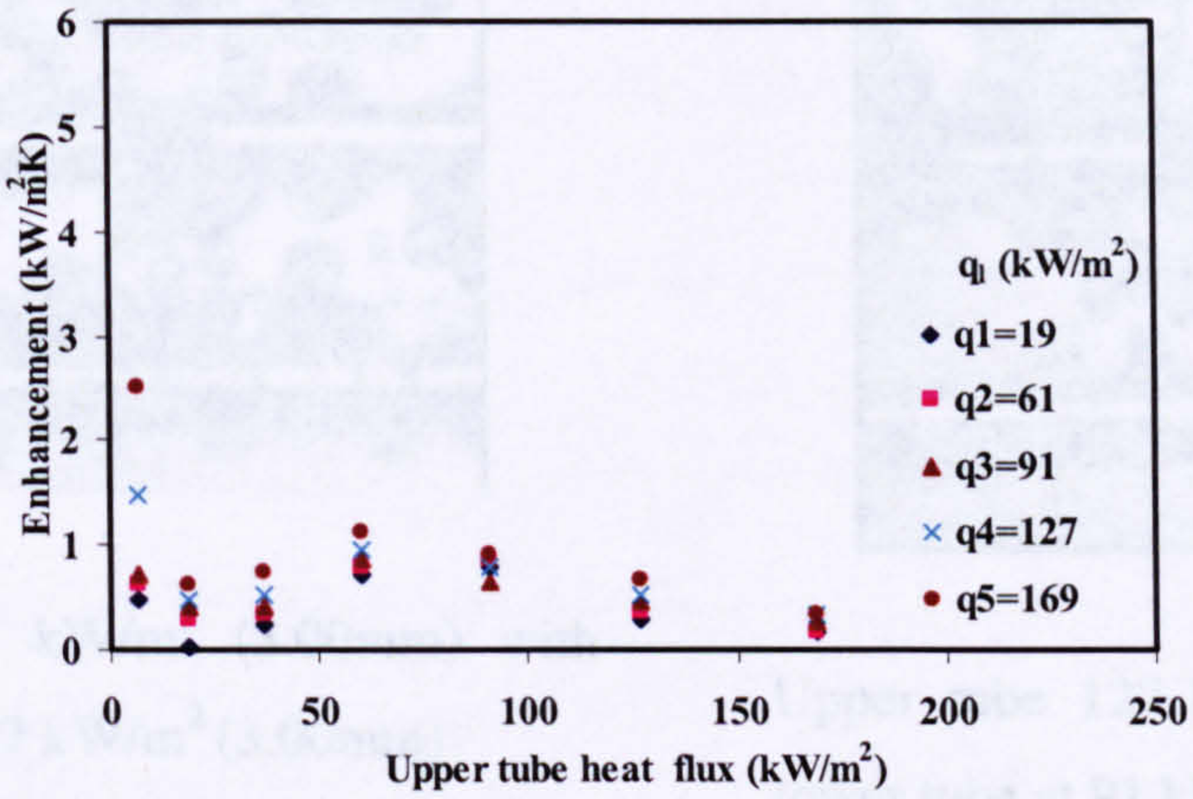

Figure 4.32 Enhancement against upper tube (3.00mm) with Flutec PP1 due to bubbles from below

Photographic studies showed that portion of the upper tubes was covered by translating bubbles from the lower tube whiles other portion were undergoing nucleate boiling. This bubbles laid a thin film through which heat transfer coefficient occurred. It was also observed that at high heat fluxes (127-243 kW/m^2) the enhancement observed was negligible compared to that at medium heat fluxes (37-127 kW/m^2) for the 3 mm upper tube. At higher heat flux on the lower tube, nucleation on the upper tube was suppressed, and convective turbulence was also a factor for the enhancement as there was a disruption of the thermal boundary around the upper tube. These observations are shown in Figure 4.33 for the 1.83 and 3.00 mm tube.

Upper tube 37 kW/m^2 (3.00mm) with lower tube at 127 kW/m^2 (3.00mm)

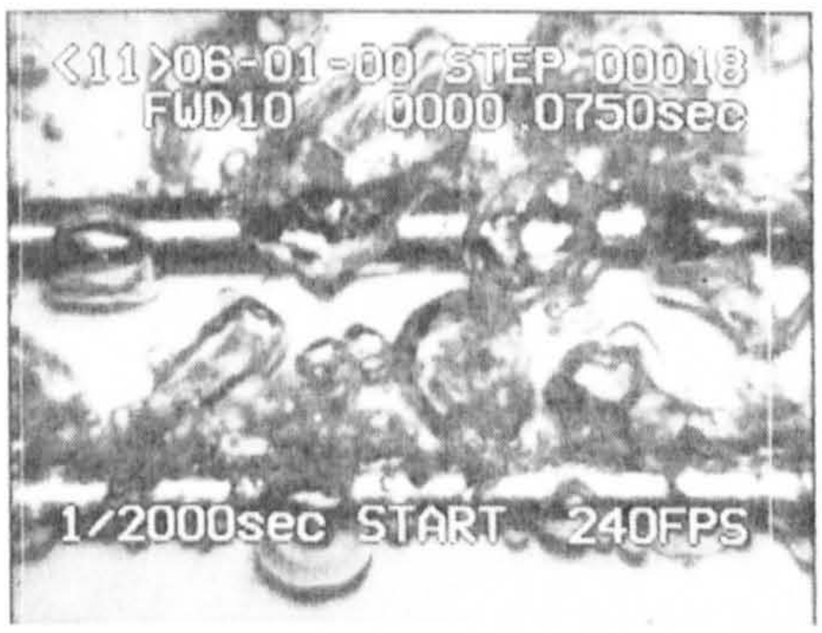

Upper tube 91kW/m^2 (3.00mm) with lower tube at 169 kW/m^2 (3.00mm)

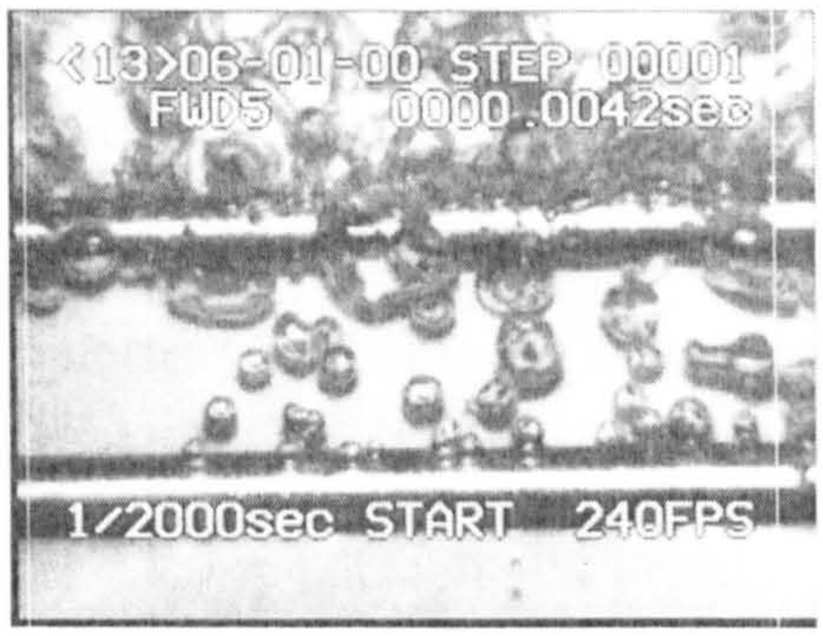

Upper tube 127 kW/m^2 (3.00mm) with lower tube at 91 kW/m^2 (3.00mm)

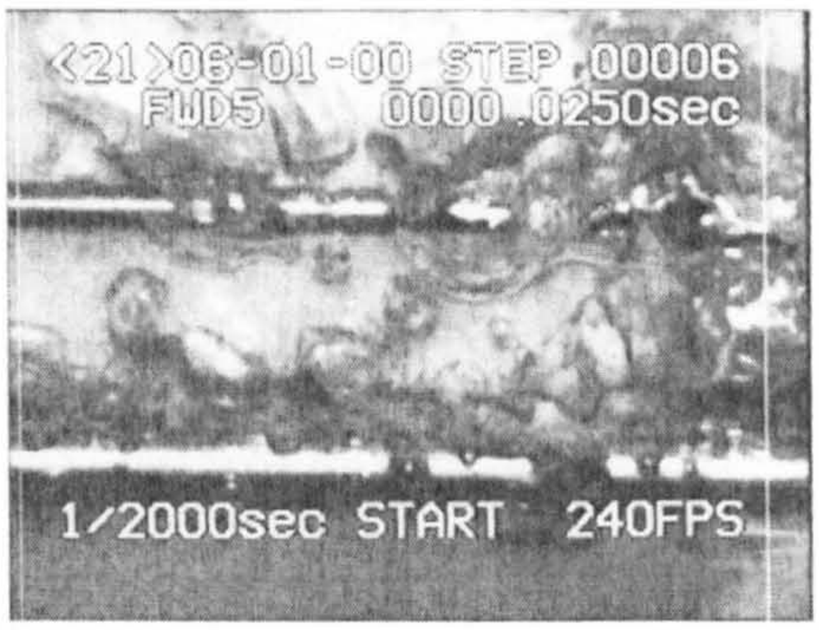

Upper tube at 191 kW/m^2 (1.83mm) with lower tube at 169 kW/m^2 (3.00mm)

Figure 4.33 Typical photos of bubbles on twin tube for distilled water

4.4 Comparison of results with the work Boinnet

Boinnet [118] investigated the heat transfer coefficient for tube diameters in the range of 1.1-3.0mm undergoing natural convection using distilled water as the working fluid. The set up was made up of a stainless steel of tube length 49 mm. Compressed air was passed through a flow meter of similar tube with holes beneath the tube above. This compressed air was used to simulate the natural convection occurring on the upper tube. The temperature of the distilled water in the basin was kept at 20 ^{o}C. Flow rates of air were

varied from 0-20 litre/min. For a constant heat input of the upper tube, airflow through the lower tube was varied. Heat flux was in the range of 8-28 kW/m^2. Results obtained are shown in Figure 4.34 and Figure 4.35. It is shown that the presence of the air bubbles enhances the heat transfer coefficient. As the flow rate was increased the enhancement levels at 7.5 kW/m^{2}K for 2.32 mm and 3.0 mm upper tubes respectively.

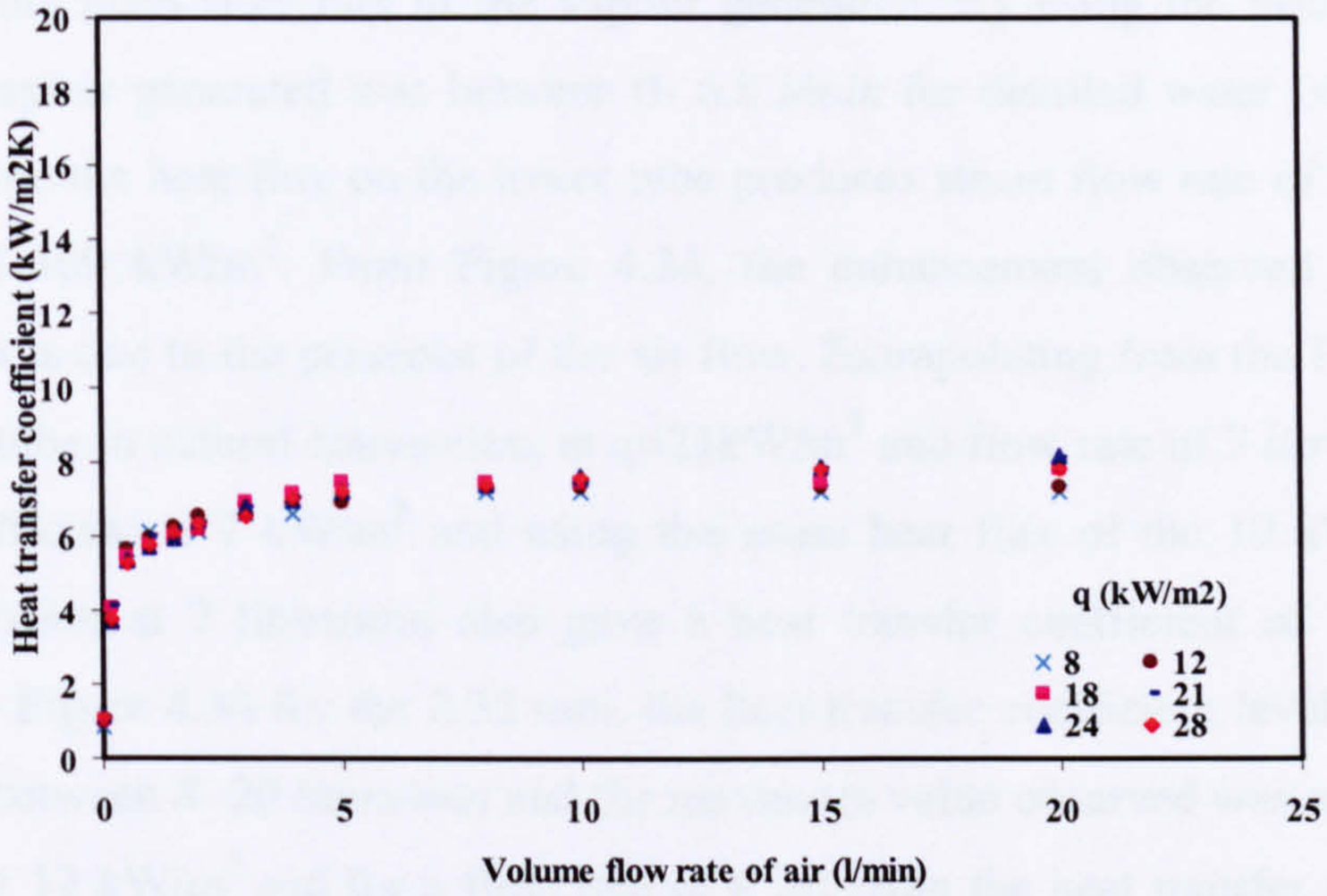

Figure 4.34 Heat transfer coefficient against volume flow rate of air (l/min) for 2.3mm tube with distilled water

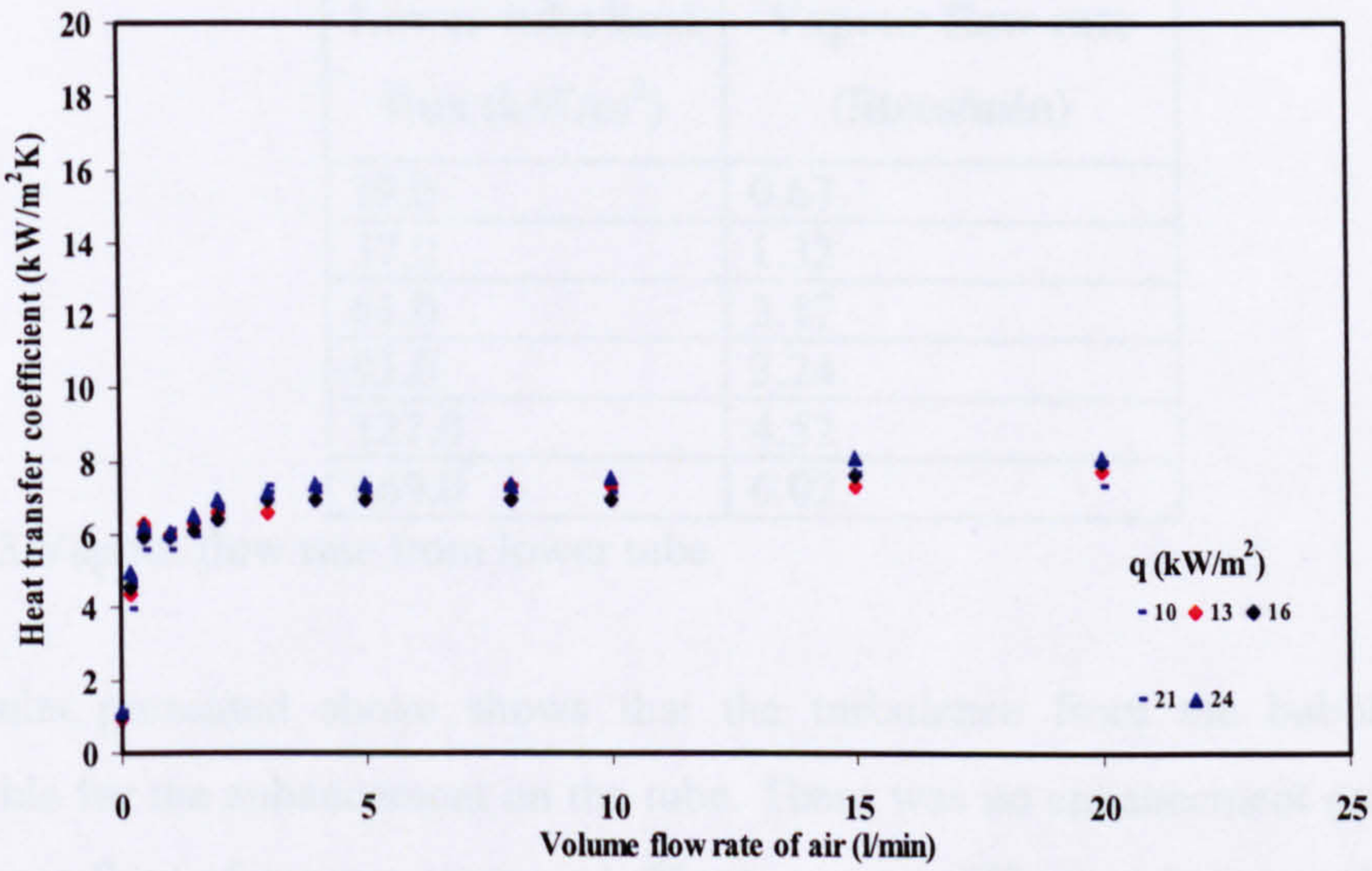

Figure 4.35 Heat transfer coefficient against volume flow rate of air (l/min) for 3.00mm tube with distilled water

The heat flux on the lower tube can be converted to determine the amount of vapour that was generated using the 3.00mm as the reference diameter. Energy balance on a tube of length l with a heat flux q is given as;

$$qA = mh_{fg} \tag{4.6}$$

where m is the mass flow rate of the vapour generated. By using the Equation (4.6) the amount of vapour generated was between 0- 6.8 *l/min* for distilled water (shown in Table 4.3). Therefore the heat flux on the lower tube produces steam flow rate of 7 l/min for the heat flux of 169 kW/m^2. From Figure 4.34, the enhancement observed in the natural convection was due to the presence of the air flow. Extrapolating from the Figure 4.35, for the 3.0 mm tube in natural convection, at q=21kW/m^2 and flow rate of 7 *litres/min* the heat transfer coefficient is 7 kW/m^2 and using the same heat flux of the 19 kW/m^2 with the steam generation at 7 litres/min also gave a heat transfer coefficient of 7.88 kW/m^{2}K. Referring to Figure 4.34 for the 2.32 mm, the heat transfer coefficient levels off when the flow rate is between *8- 20 litres/min* and the maximum value observed was approximately *7* kW/m^{2}K. At 12 kW/m^2 and for a flow rate of 6 litre/min the heat transfer coefficient is 7 kW/m^{2}K. Comparing the same heat flux on Figure 4.35, a value of 7.07 kW/m^{2}K was obtained for heat flux of 13 kW/m^2.

Lower tube heat flux (kW/m^2)	**Vapour flow rate (litres/min)**
19.0	0.67
37.0	1.32
61.0	2.17
91.0	3.24
127.0	4.52
169.0	6.02

Table 4.3 Vapour flow rate from lower tube

The results presented above shows that the turbulence from the bubbles below was responsible for the enhancement on the tube. There was no enhancement on the upper tube as the mass flow of air was increased. There was no difference between the heat transfer coefficient observed for the 2.32mm and 3.00mm tube.

4.5 Compact tube bundle results

Experimental results obtained from the compact tube bundle are presented in this section. Factors such as mass flux, vapour quality, tube position and bundle effect are discussed in relation to the heat transfer coefficient. The tubes are numbered from position 1 on the lowest tube to position 10 which is the highest. Photographic studies are also presented to examine the effect of rising bubbles in this compact arrangement. The confinement number which would be shown later in Chapter 5 of this thesis is given as;

$$C_o = \frac{\sqrt{\sigma / g(\rho_l - \rho_g)}}{s} \tag{4.7}$$

For each of the fluid used the confinement number was calculated using Equation (4.7) as shown in Table 4.4. The distance ***s*** is the clearance between the tubes which in this case is given as 1.5 mm. Using theory which would be discussed in Chapter 5 shows that for the compact bundle, for a bubble to be confined, C_o should be greater than 0.63. This value is consistent with that of internal flow previously developed for micro channels.

Fluid	**Confinement number (C_o)**
Distilled water	1.67
R113	0.67
Flutec PP1	0.58

Table 4.4 Confinement numbers for working fluids

4.5.1 Effect of tube position

Figure 4.36 to Figure 4.45 shows the plot of heat transfer coefficient against tube position. The results indicated that the heat transfer coefficient increased with the heat flux by an appreciable amount. At high heat flux the nucleation occurred and more bubbles was generated. This trend of results is typical of boiling in tube bundles and is similar to that obtained by Andrews and Cornwell [113] in their large tube bundle even though their results showed an increase in heat transfer up the bundle. The plots (Figure 4.36 to Figure 4.40) shows the increase of heat transfer coefficient from tube 1 to tube 4 for the working

fluid being distilled water, Flutec PP1 and R-113 and then a decrease in the heat transfer coefficient in the mid of the bundle (5-10). Similar trends were observed for the results using R-113 and Flutec PP1 which are shown in Figure 4.41 to Figure 4.45.

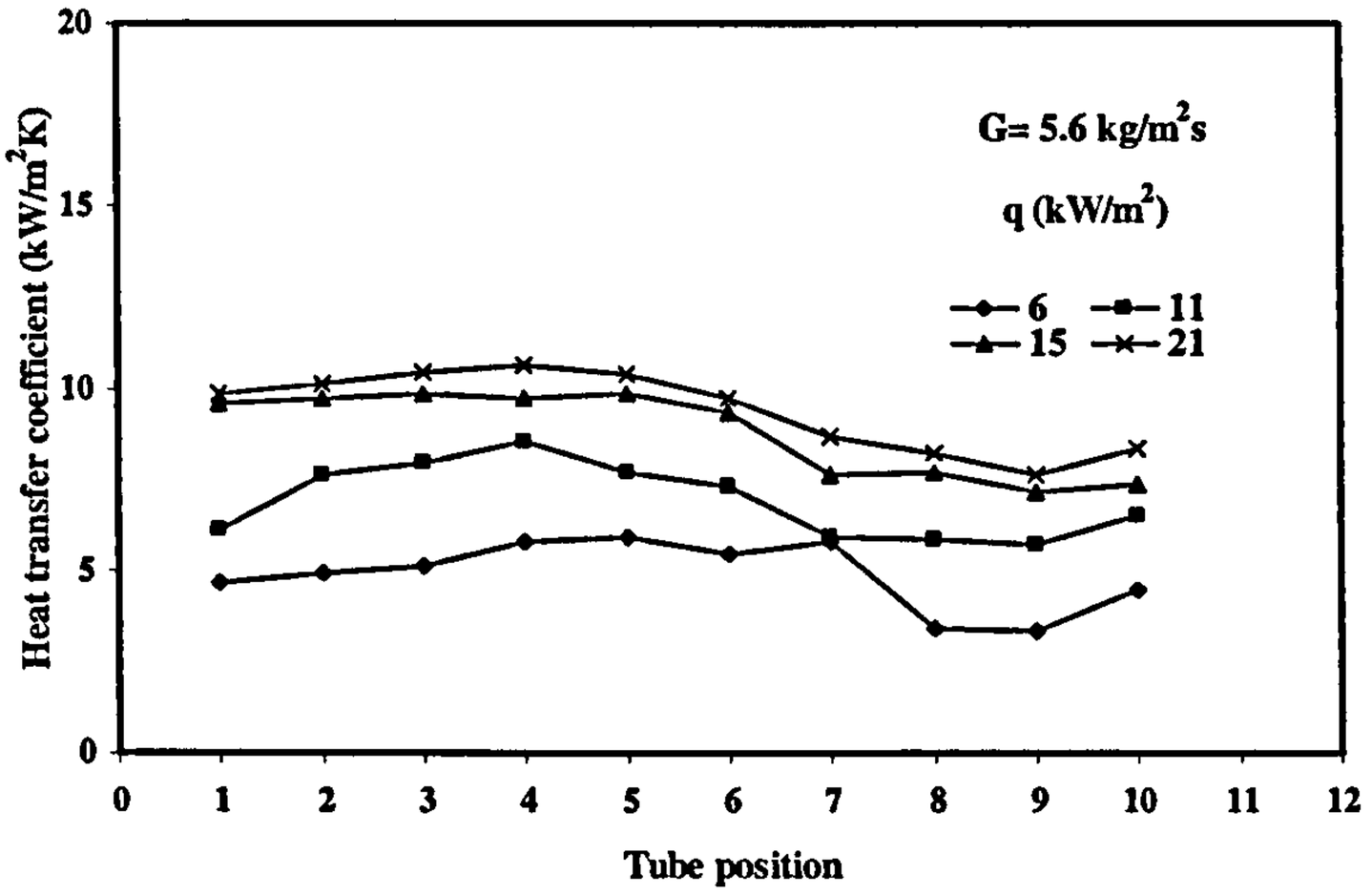

Figure 4.36 Heat transfer coefficient against tube position for G=5.6 kg/m^{2}s with distilled water

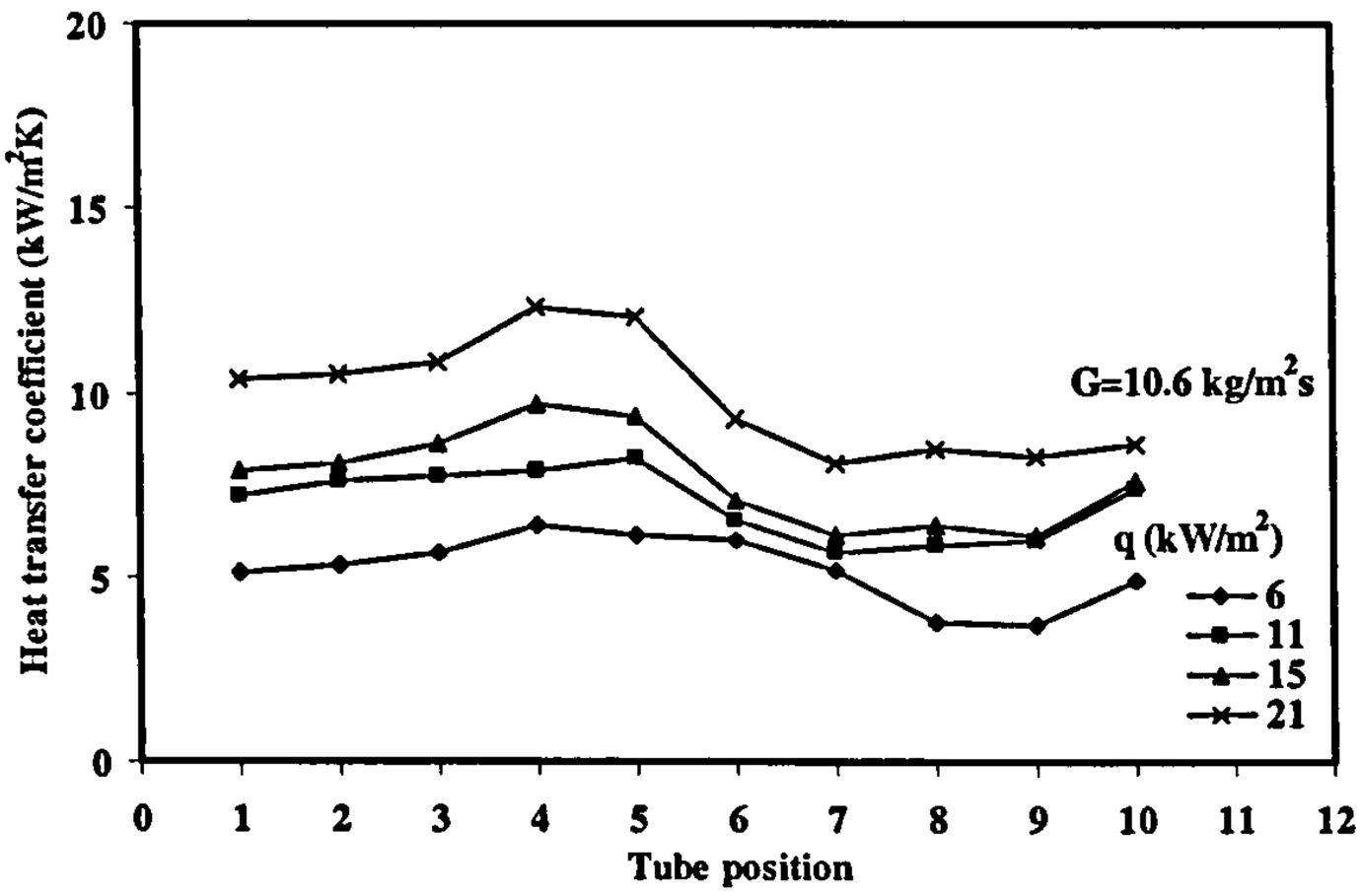

Figure 4.37 Heat transfer coefficient against tube position for G=10.6 kg/m^{2}s with distilled water

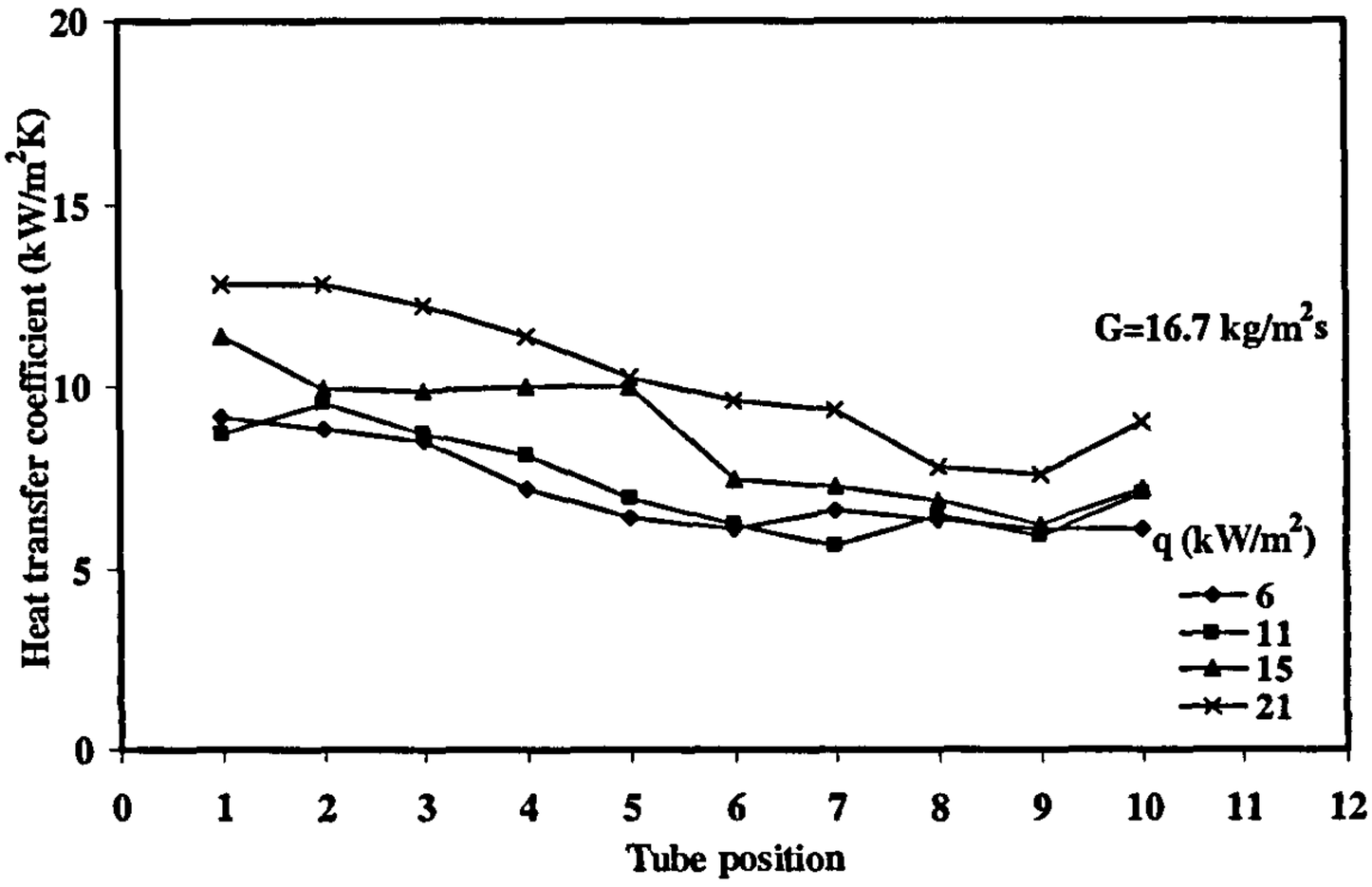

Figure 4.38 Heat transfer coefficient against tube position for G=16.7 kg/m^{2}s with distilled water

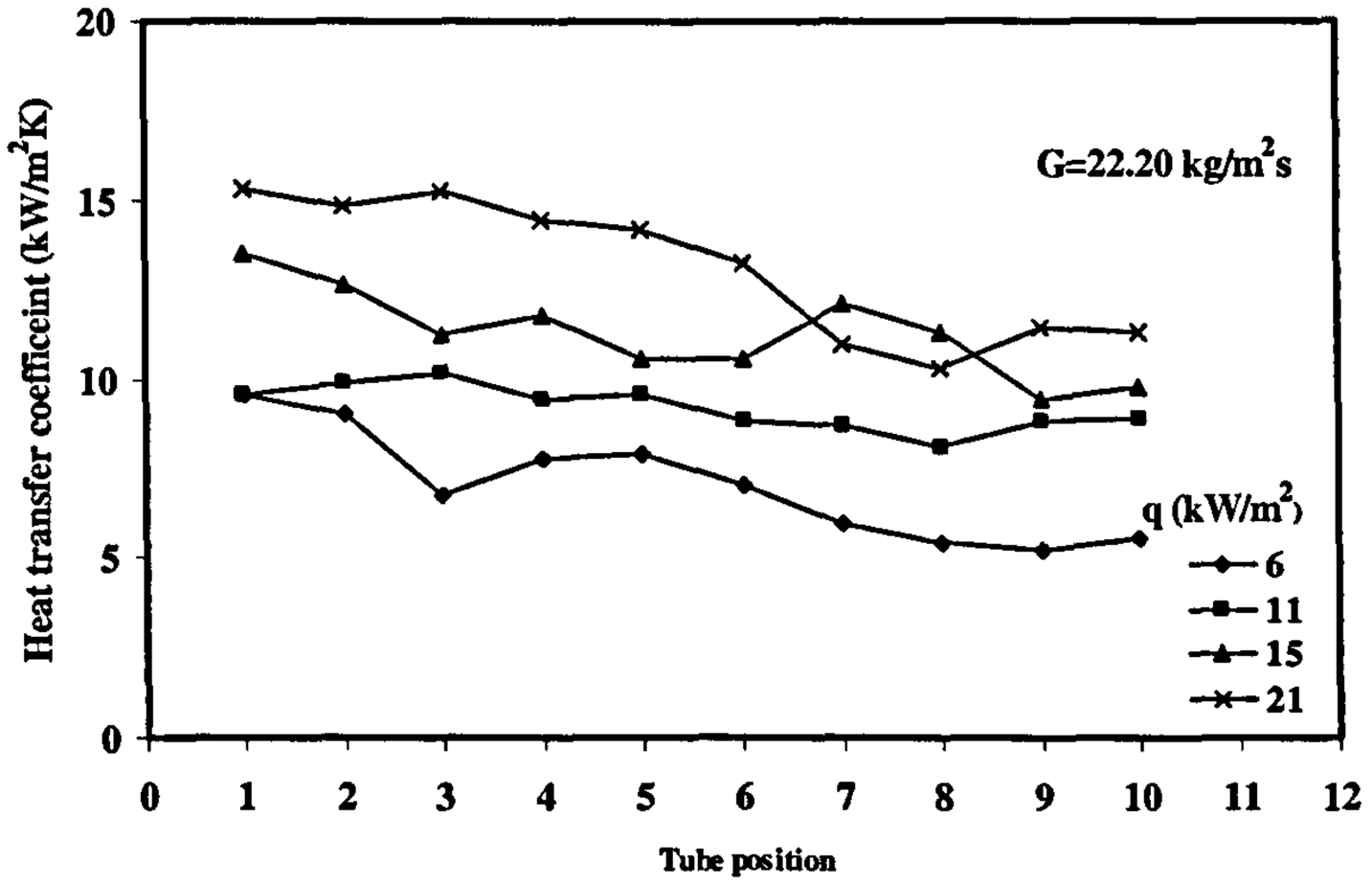

Figure 4.39 Heat transfer coefficient against tube position for G=22.20 kg/m^{2}s for distilled water

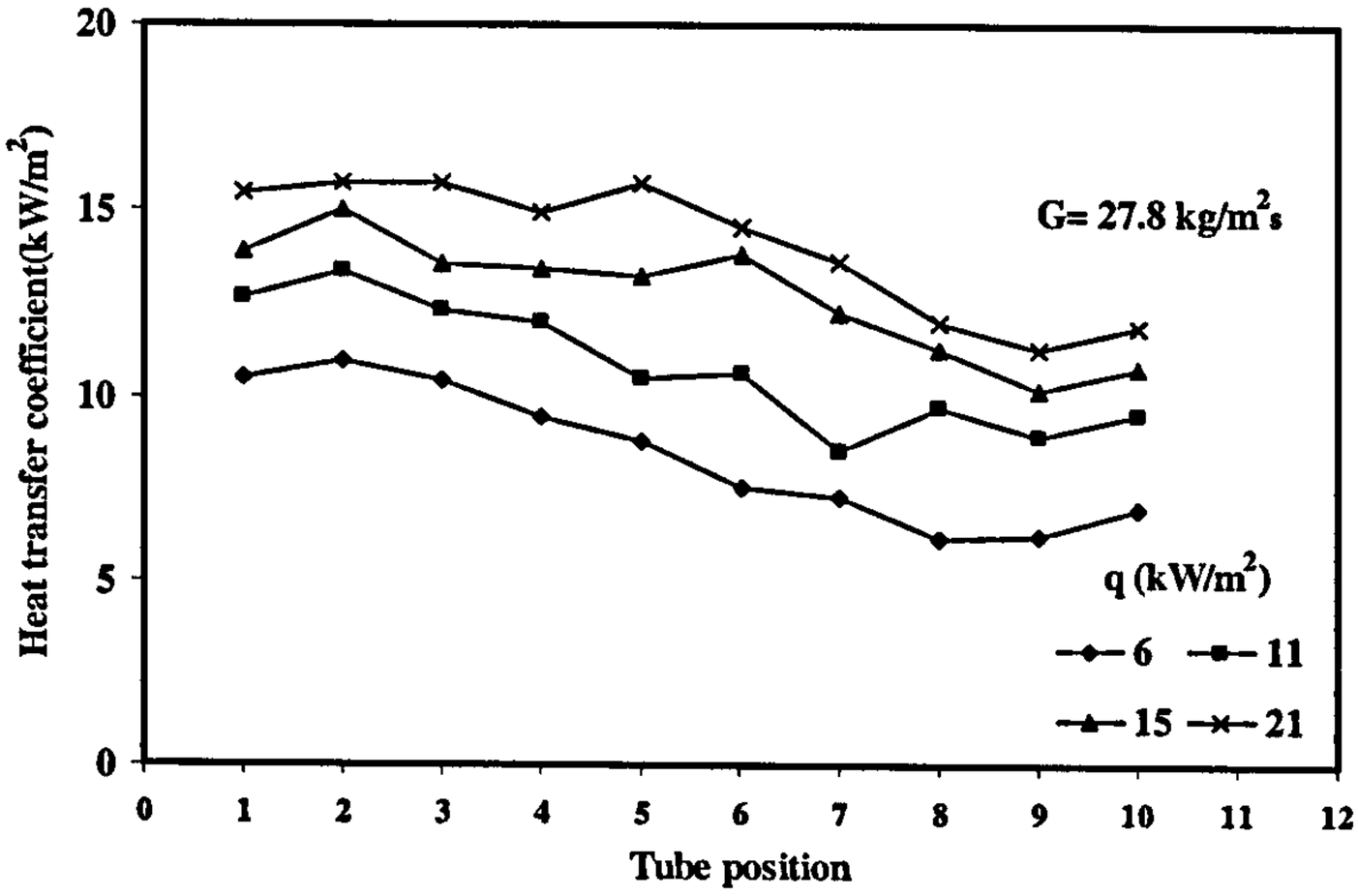

Figure 4.40 Heat transfer coefficient against tube position for G=27.8 kg/m^{2}s with distilled water

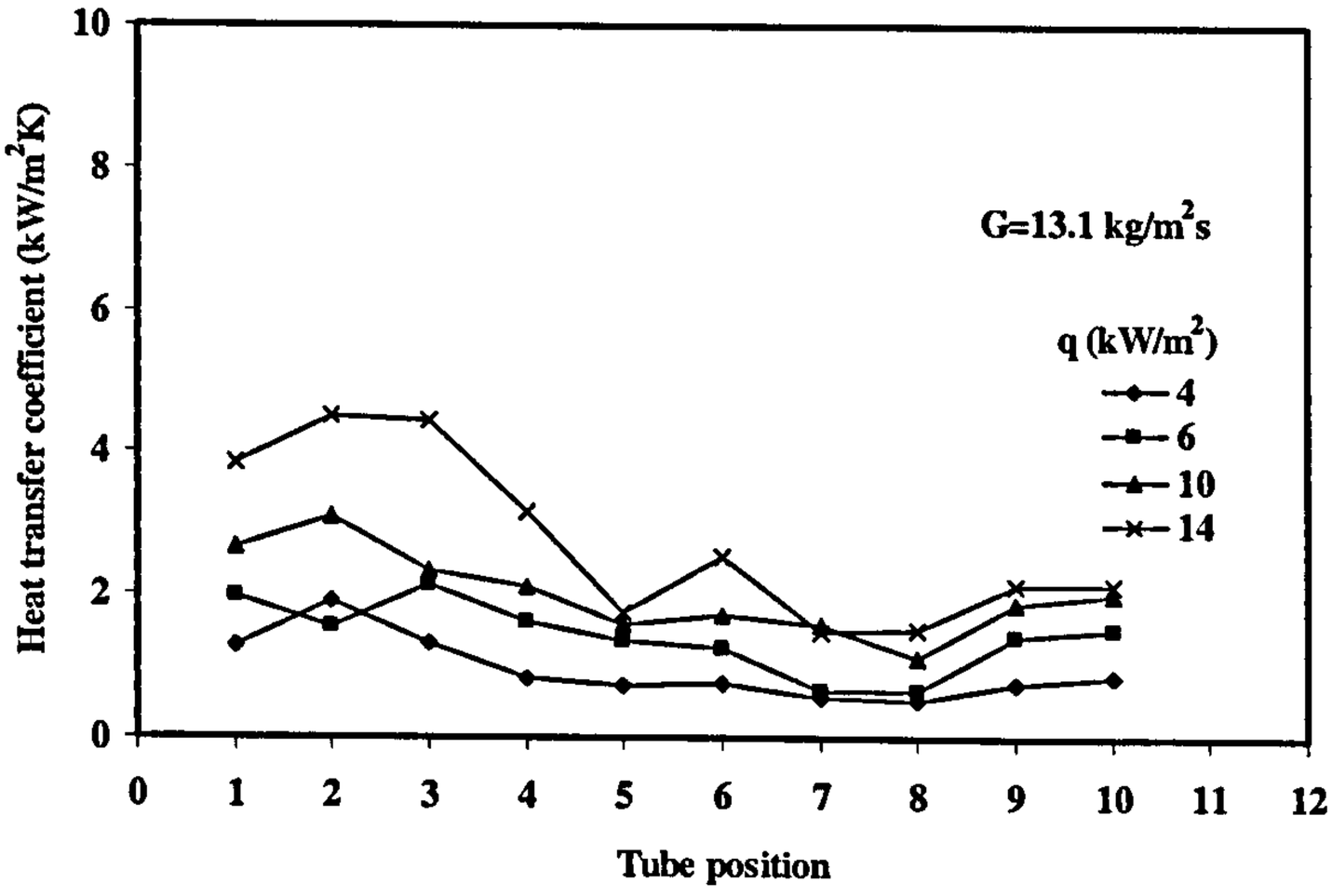

Figure 4.41 Heat transfer coefficient against tube position for G=13.1 kg/m^{2}s with R-113

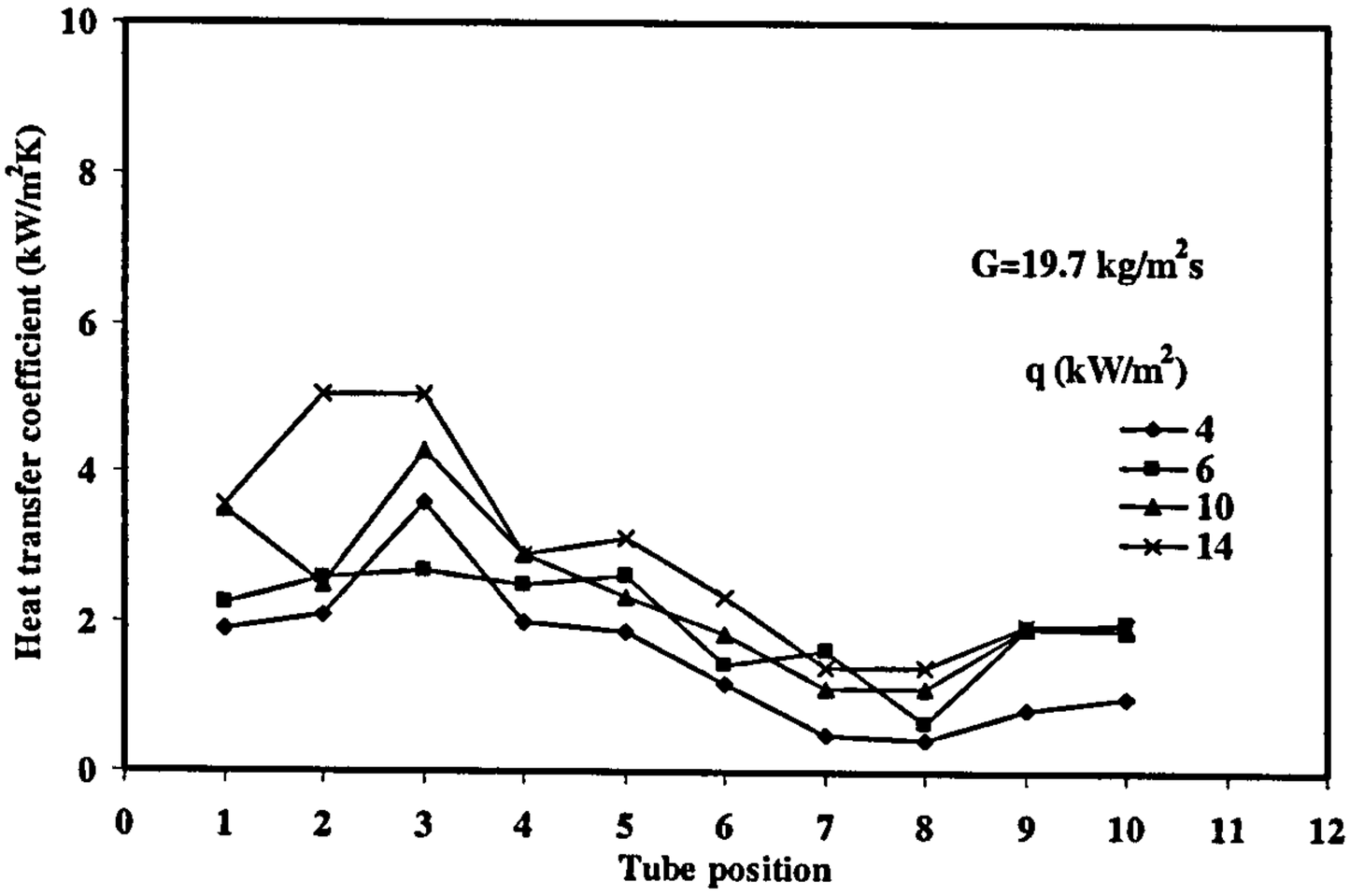

Figure 4.42 Heat transfer coefficient against tube position for G=19.7 kg/m^{2}s with R-113

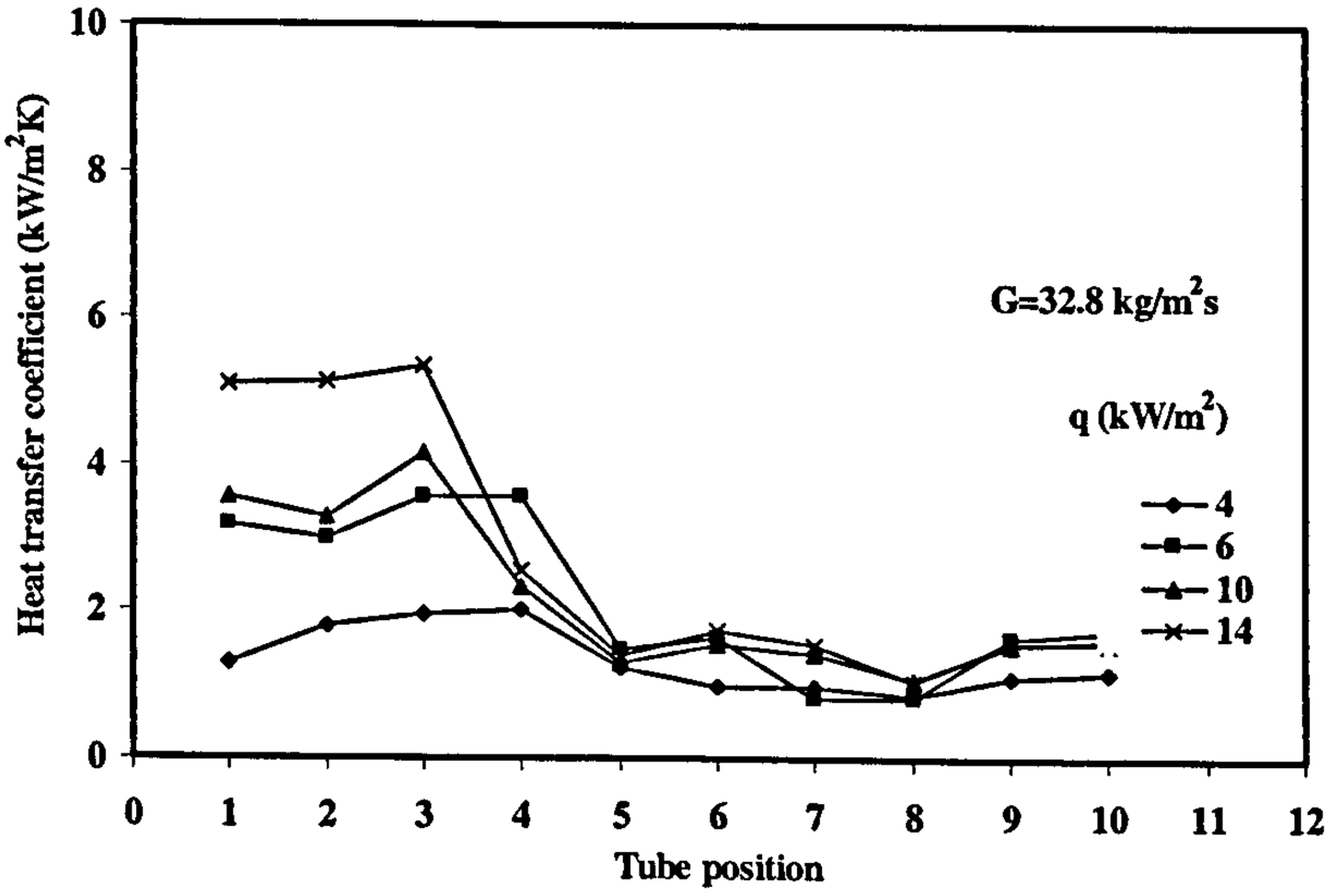

Figure 4.43: Heat transfer coefficient against tube position for G=32.8 kg/m^{2}s with R-113

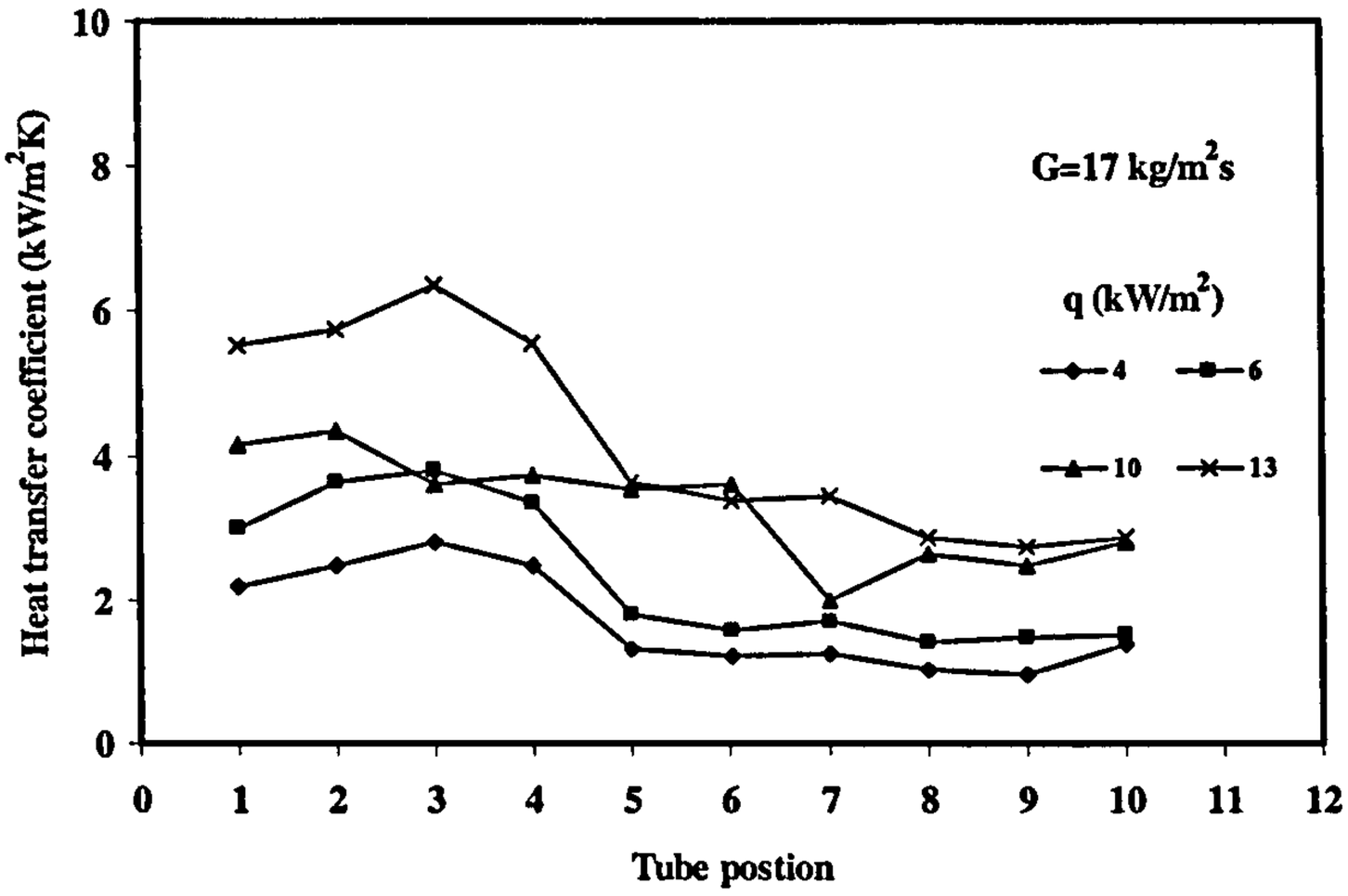

Figure 4.44 Heat transfer coefficient against tube position for G=17 kg/m^{2}s with Flutec PP1

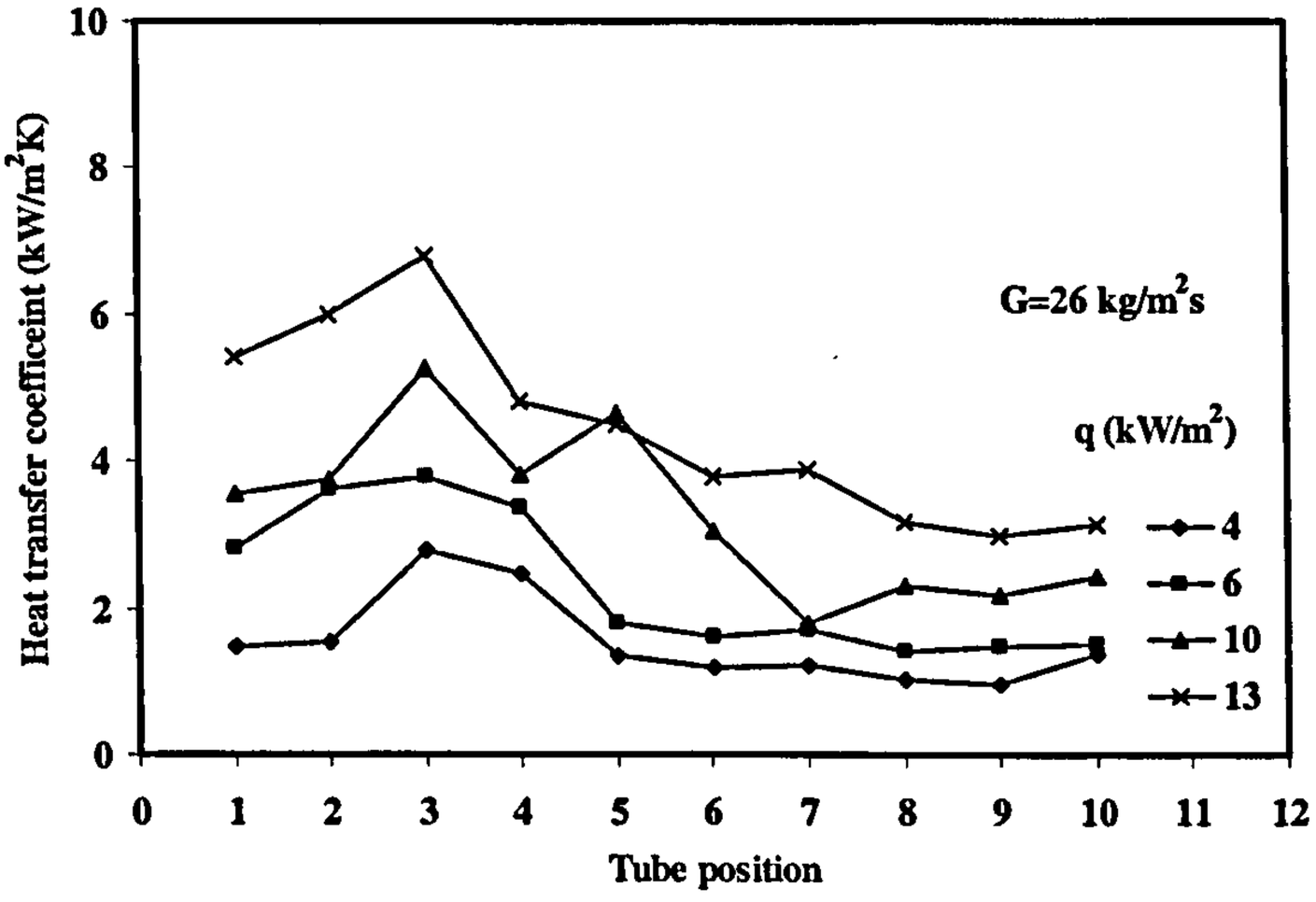

Figure 4.45 Heat transfer coefficient against tube position for G=26 kg/m^{2}s with Flutec PP1

4.5.2 Effect of mass flux

The local quality at each position of the tube was evaluated for all the working fluids. Energy balance was used for the control volume of each tube to determine the local quality.

The plots of heat transfer coefficient against local vapour quality are shown in Figure 4.46 to Figure 4.55. From theory, the local quality increases with the position of the tube. The results for all the working fluid indicated that there was an effect of mass flux on tubes 1-5. As the quality increased the heat transfer coefficient decreases at the upper tubes. The results of distilled water show a slight dependence of the heat transfer coefficient with mass flux between zero and 0.1 for distilled water. It is suggested that the decrease in the heat transfer coefficient in the upper tubes was due to intermittent partial dryout as bubbles generated on the lower tubes thus (1-5) were not able to influence those of the upper tubes (5-10).

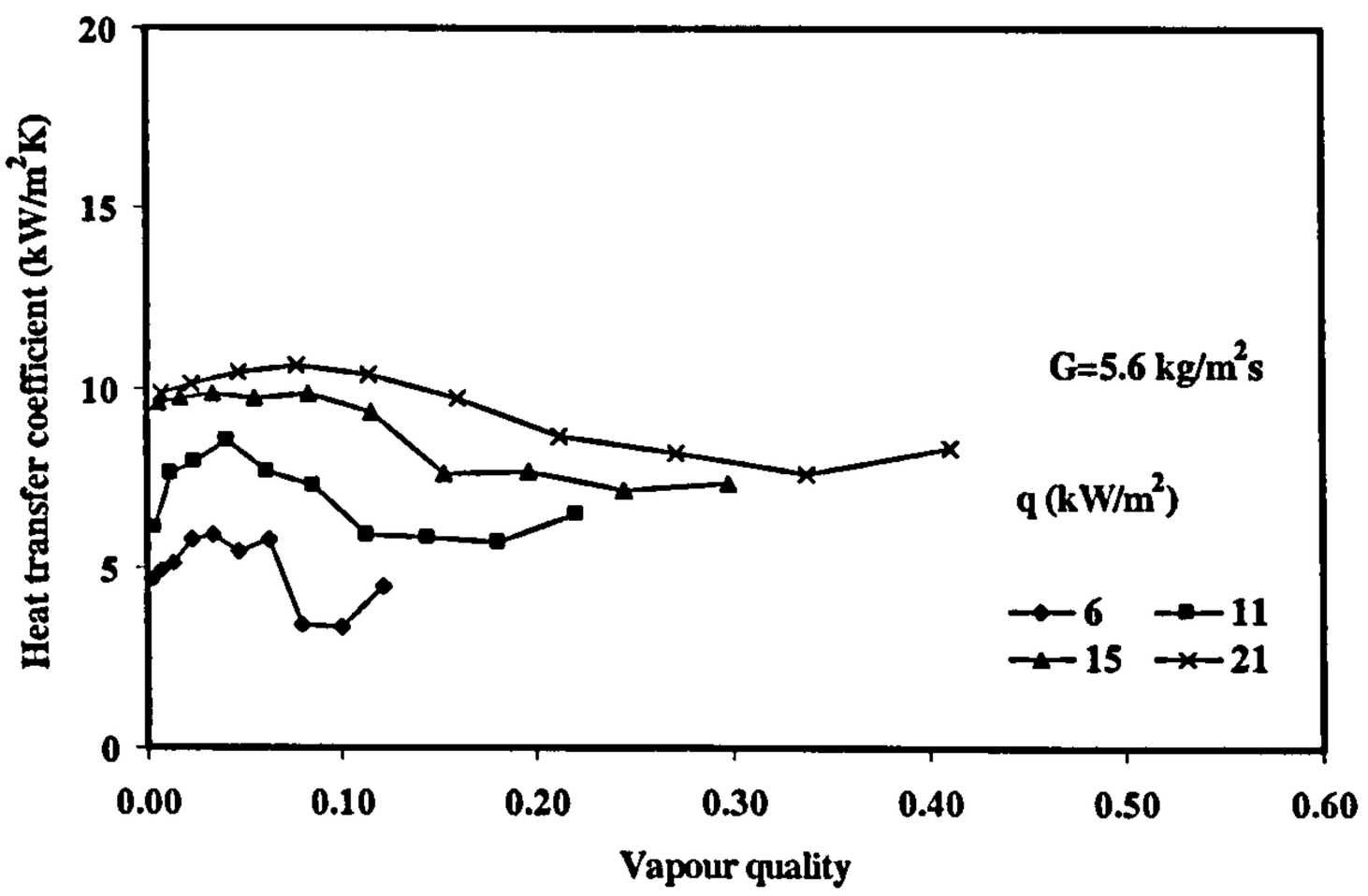

Figure 4.46 Heat transfer coefficient against vapour quality for G= 5.6 kg/m^{2}s with distilled water

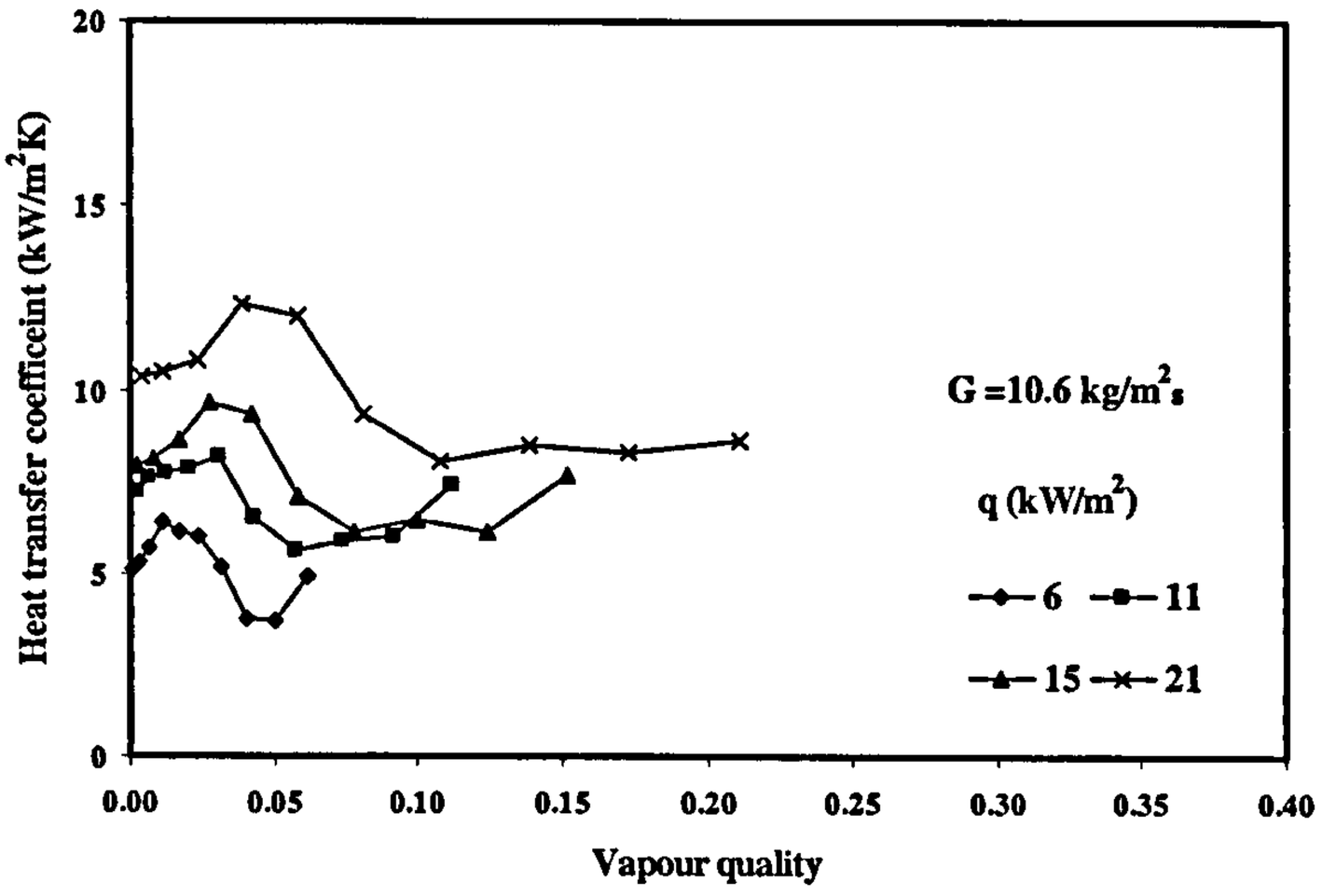

Figure 4.47 Heat transfer coefficient against vapour quality for G= 10.6 kg/m^{2}s with distilled water

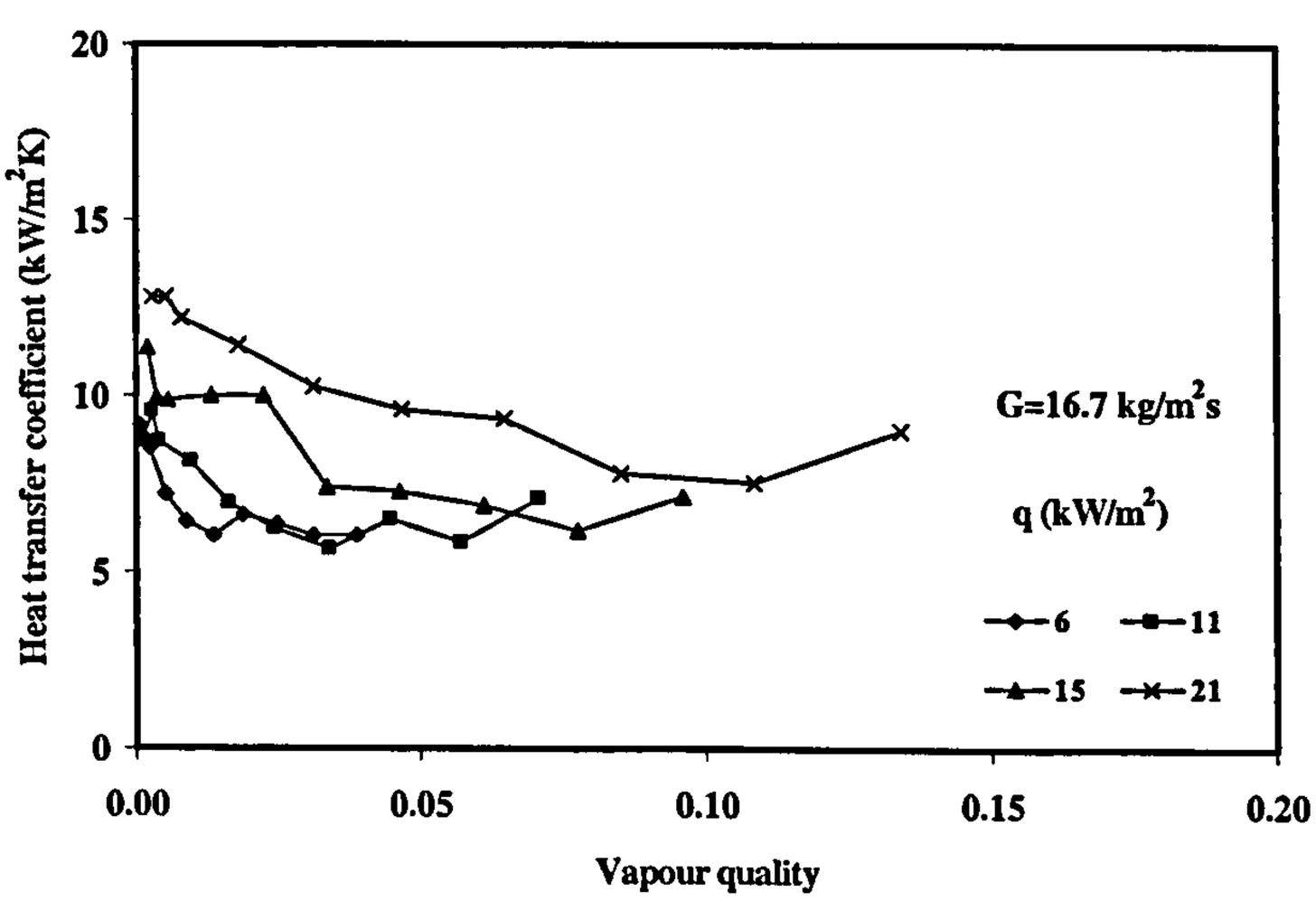

Figure 4.48 Heat transfer coefficient against vapour quality for G=16.7 kg/m^{2}s with distilled water

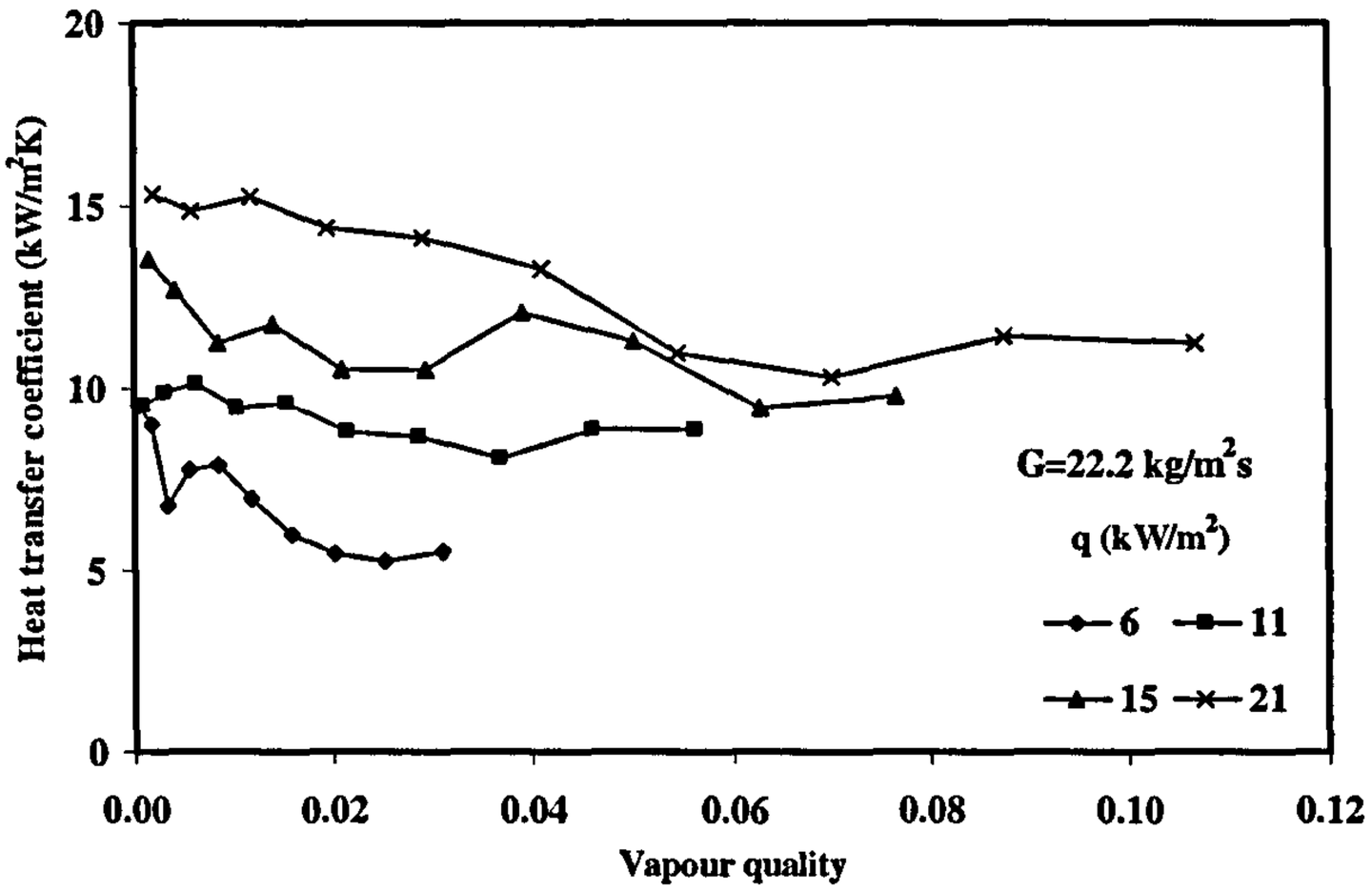

Figure 4.49 Heat transfer coefficient against vapour quality for G=22.20 kg/m^{2}s with distilled water

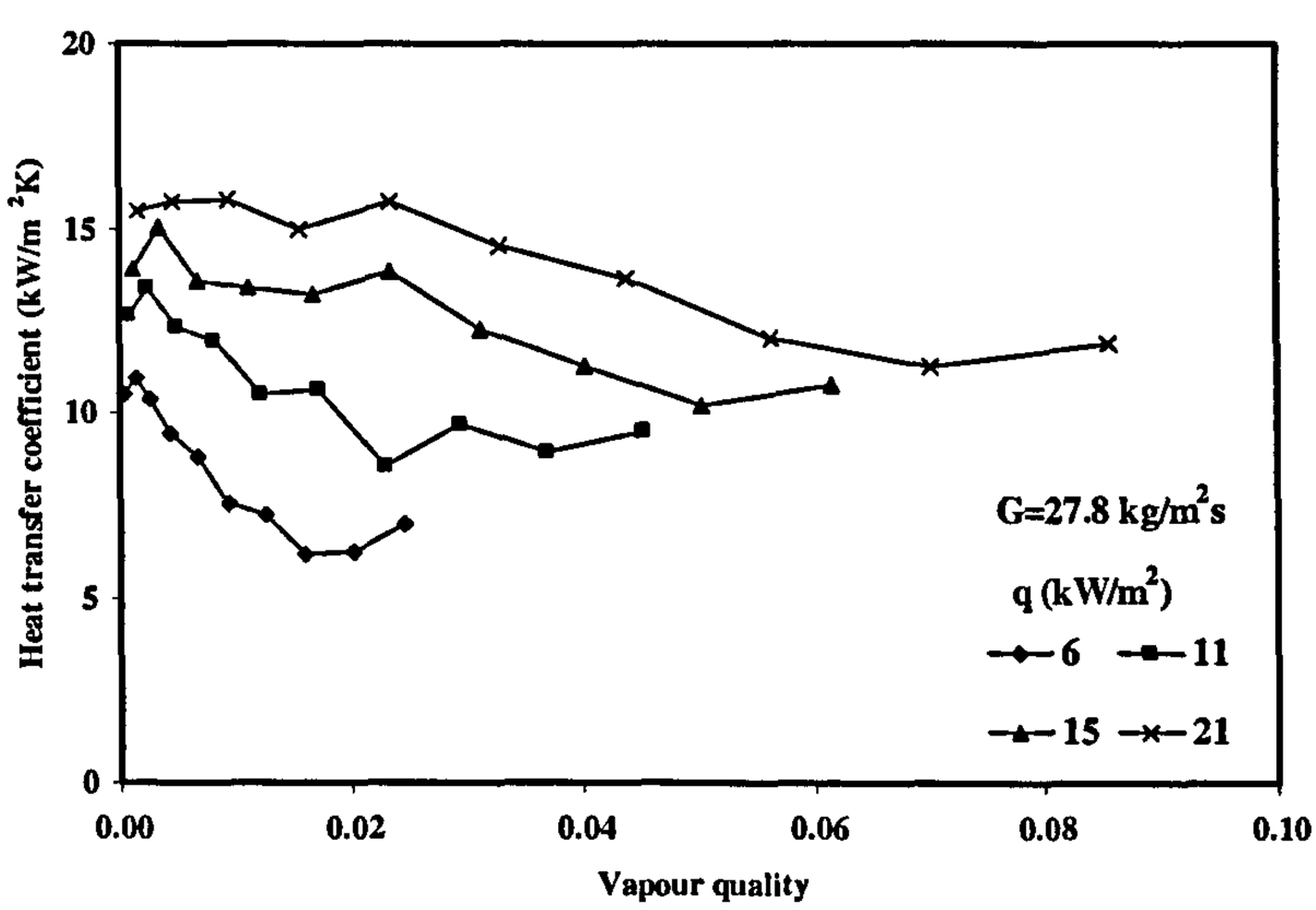

Figure 4.50 Heat transfer coefficient against vapour quality for G=27.8 kg/m^{2}s with distilled water

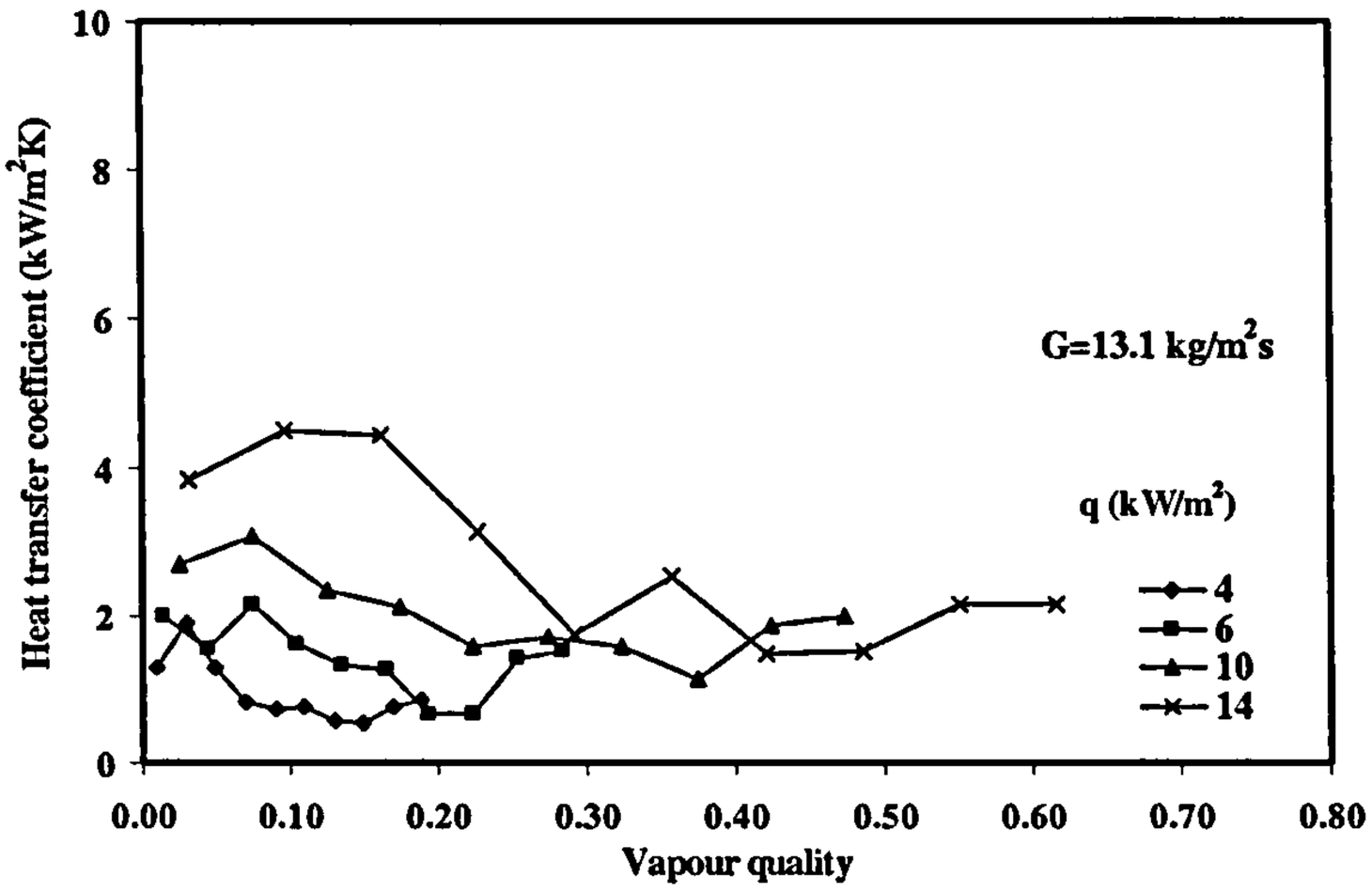

Figure 4.51 Heat transfer coefficient against vapour quality for G=13.1 kg/m^{2}s with R-113

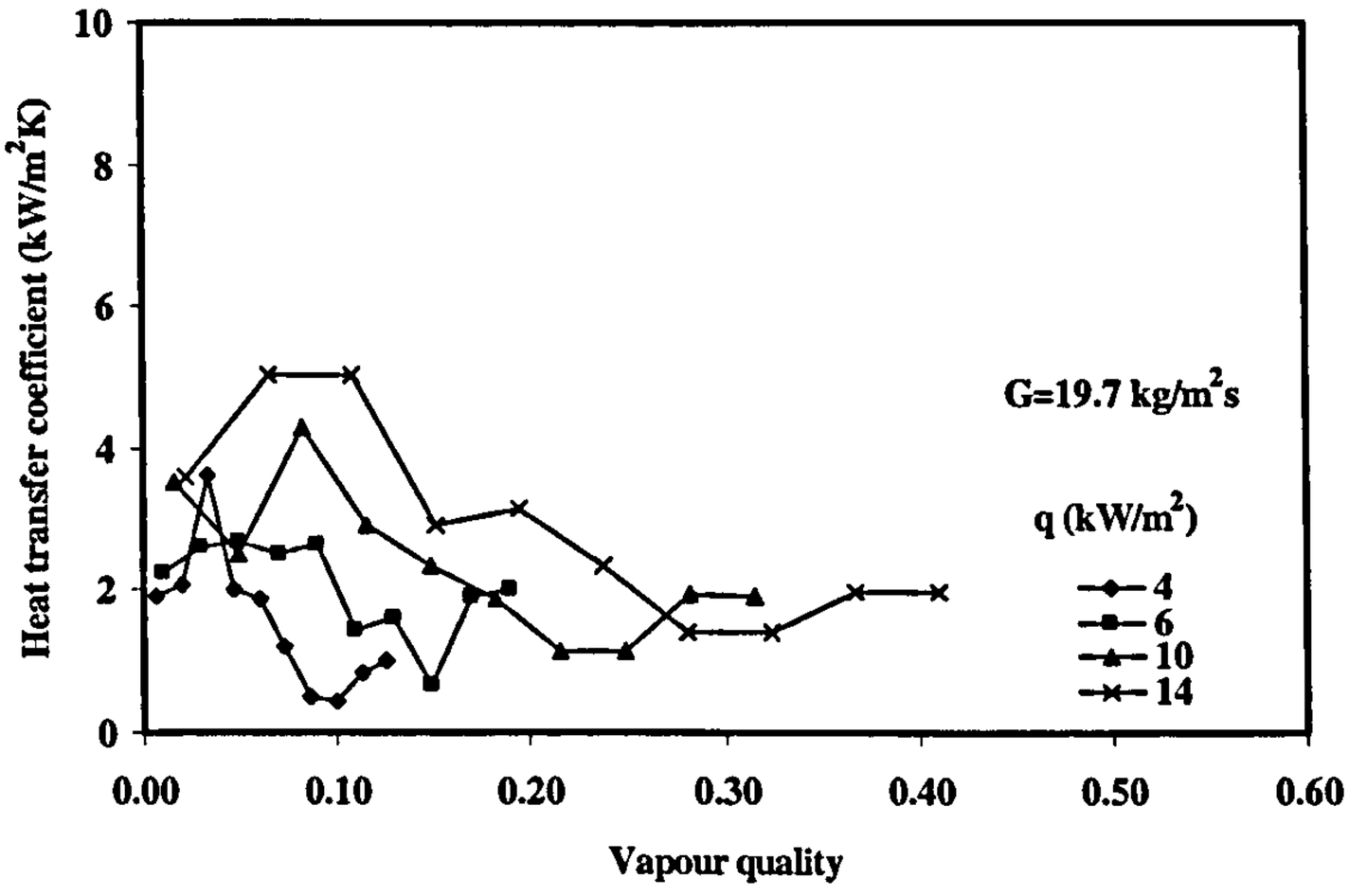

Figure 4.52 Heat transfer coefficient against quality for G=19.7 kg/m^{2}s with R-113

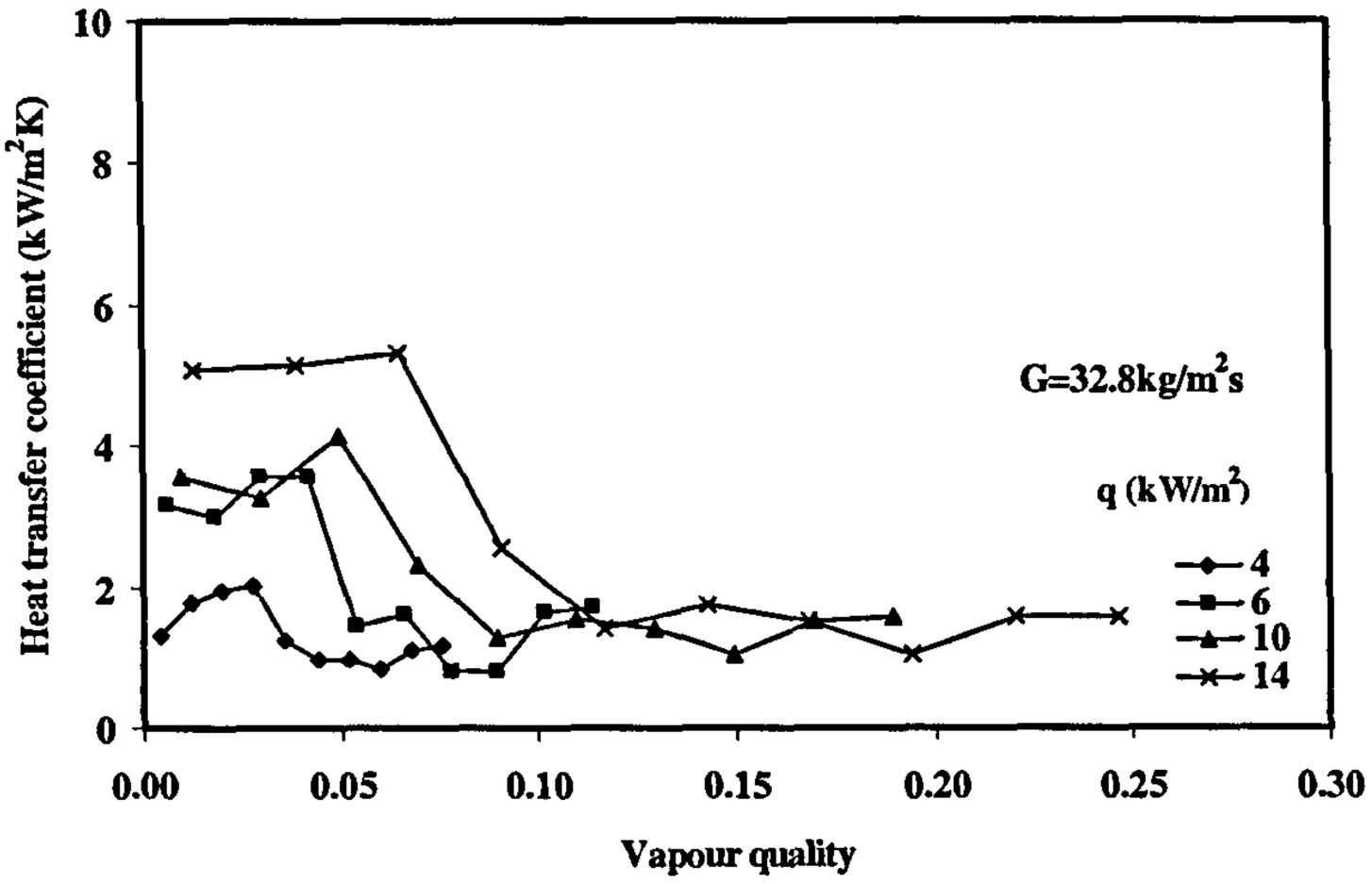

Figure 4.53 Heat transfer coefficient against vapour quality for G=32.8 kg/m^{2}s with R-113

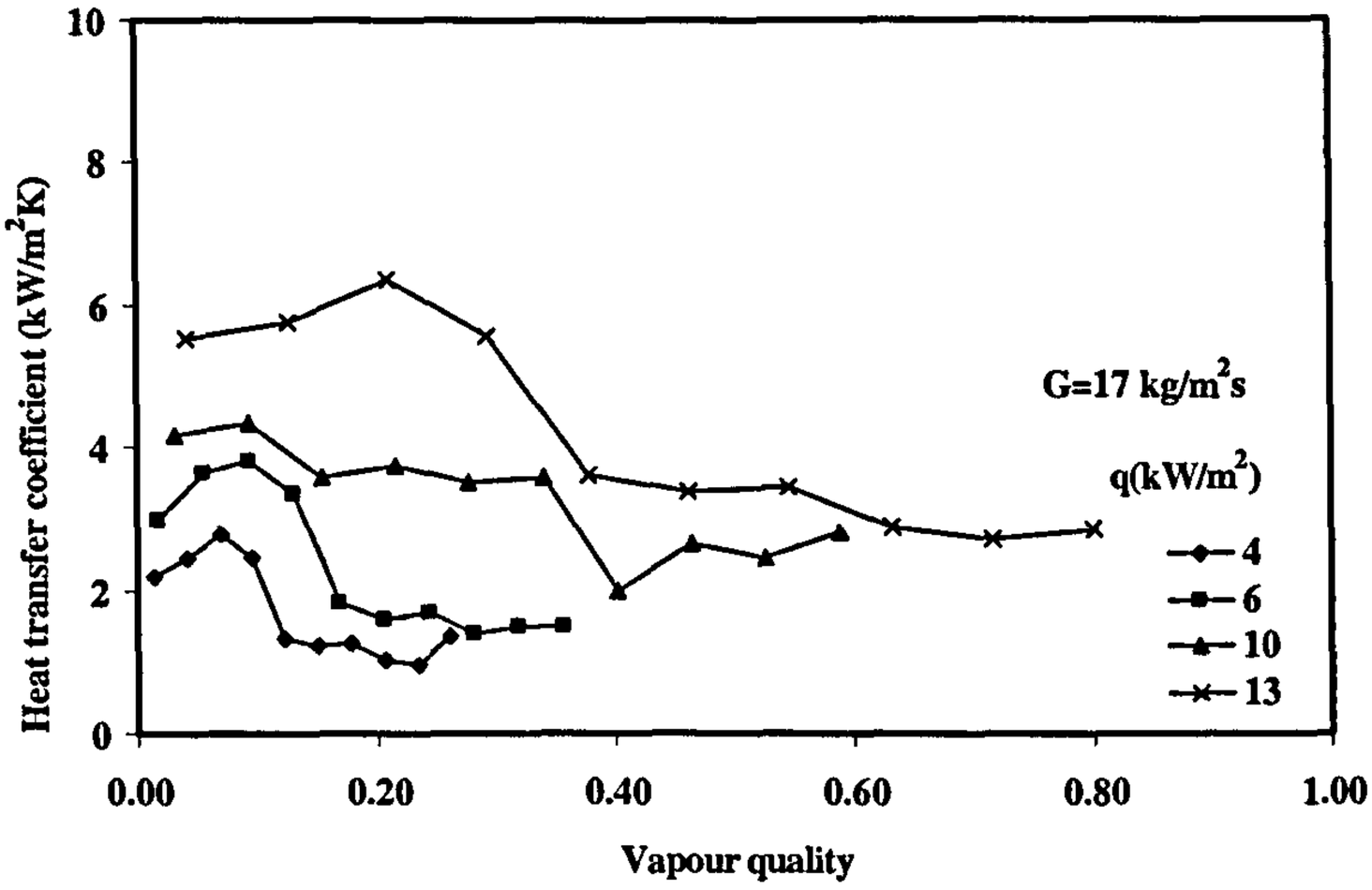

Figure 4.54 Heat transfer coefficient against vapour quality for G=17 kg/m^{2}s with Flutec PP1

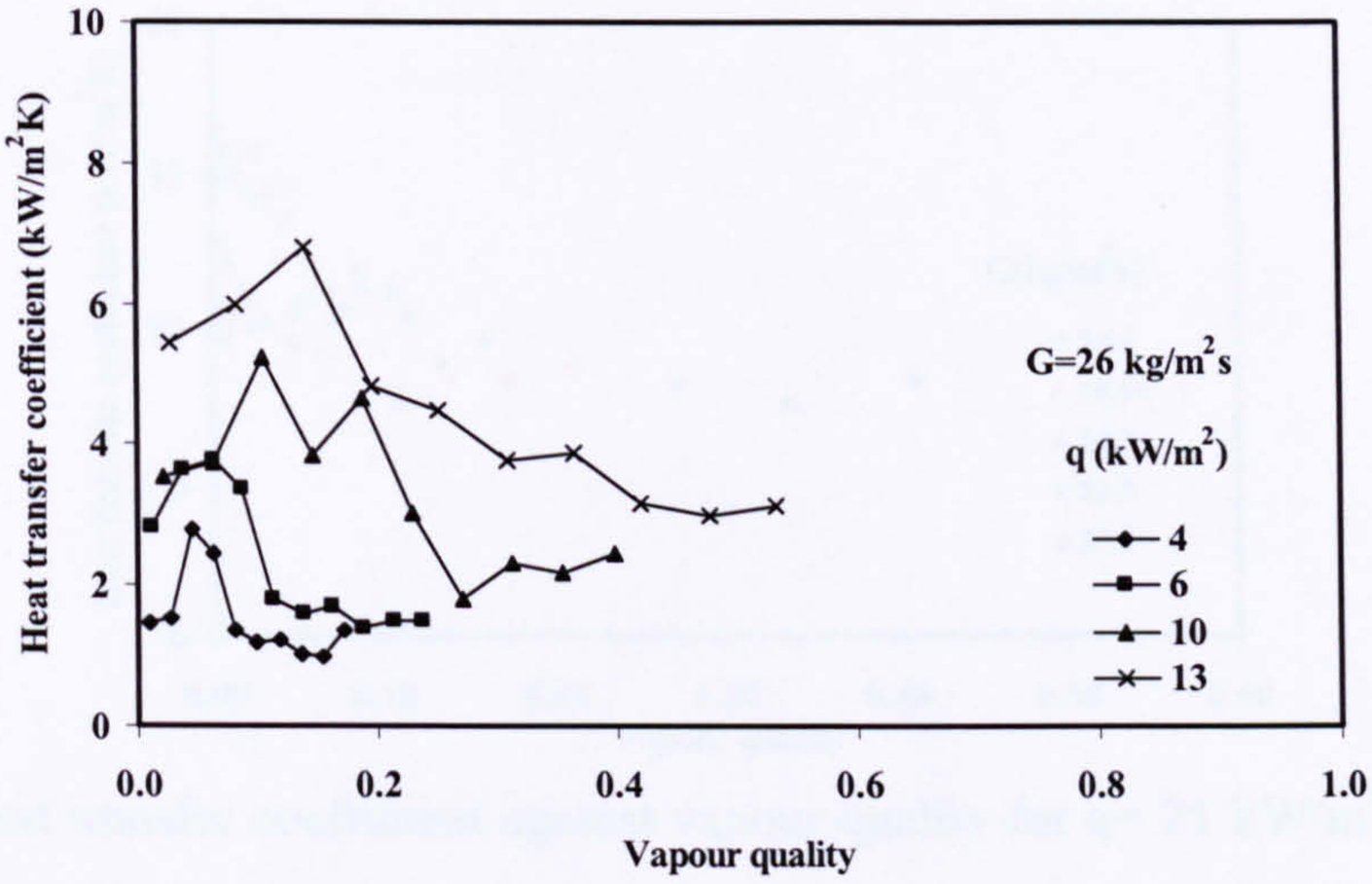

Figure 4.55 Heat transfer coefficient against vapour quality for G=26 kg/m^{2}s with Flutec PP1

Figure 4.56 to Figure 4.57 shows plot of heat transfer coefficient against vapour quality for the mass flux tested using distilled water. The plot clearly indicates that the effect of local quality is significant between 0 to 0.2. However at values greater than 0.2 the effect is less important.

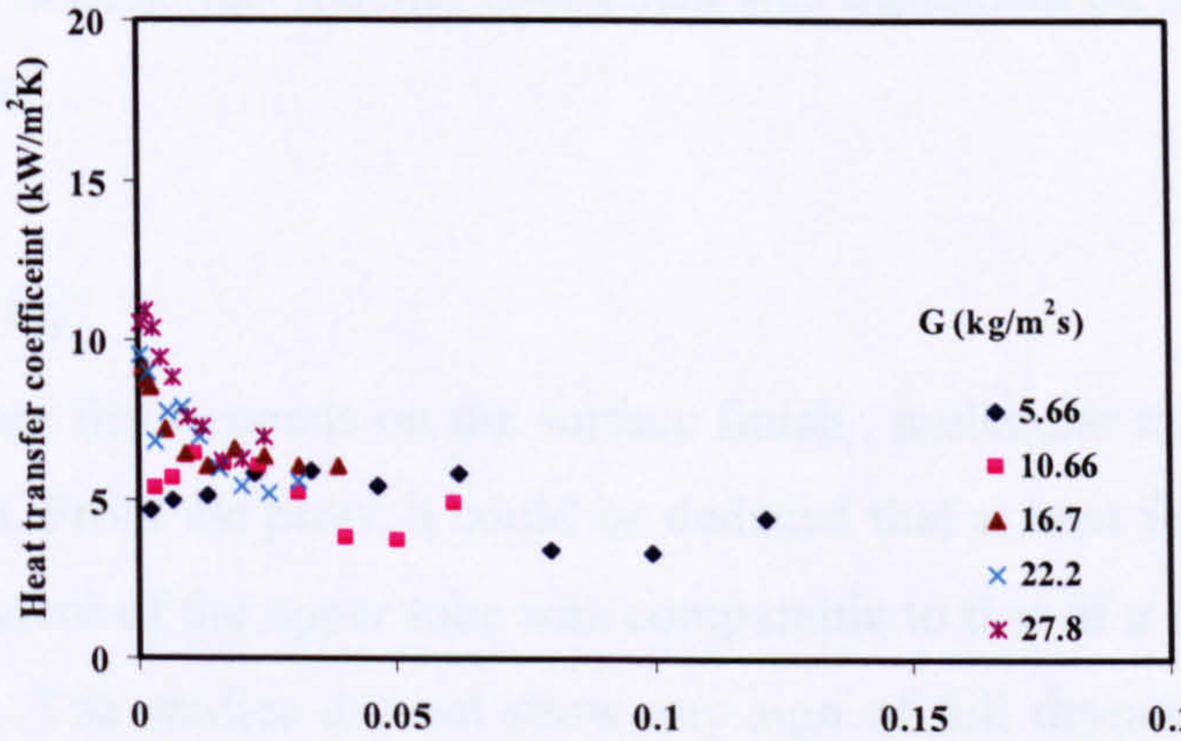

Figure 4.56 Heat transfer coefficient against vapour quality for q= 6 kW/m^2 with distilled water as the working fluid

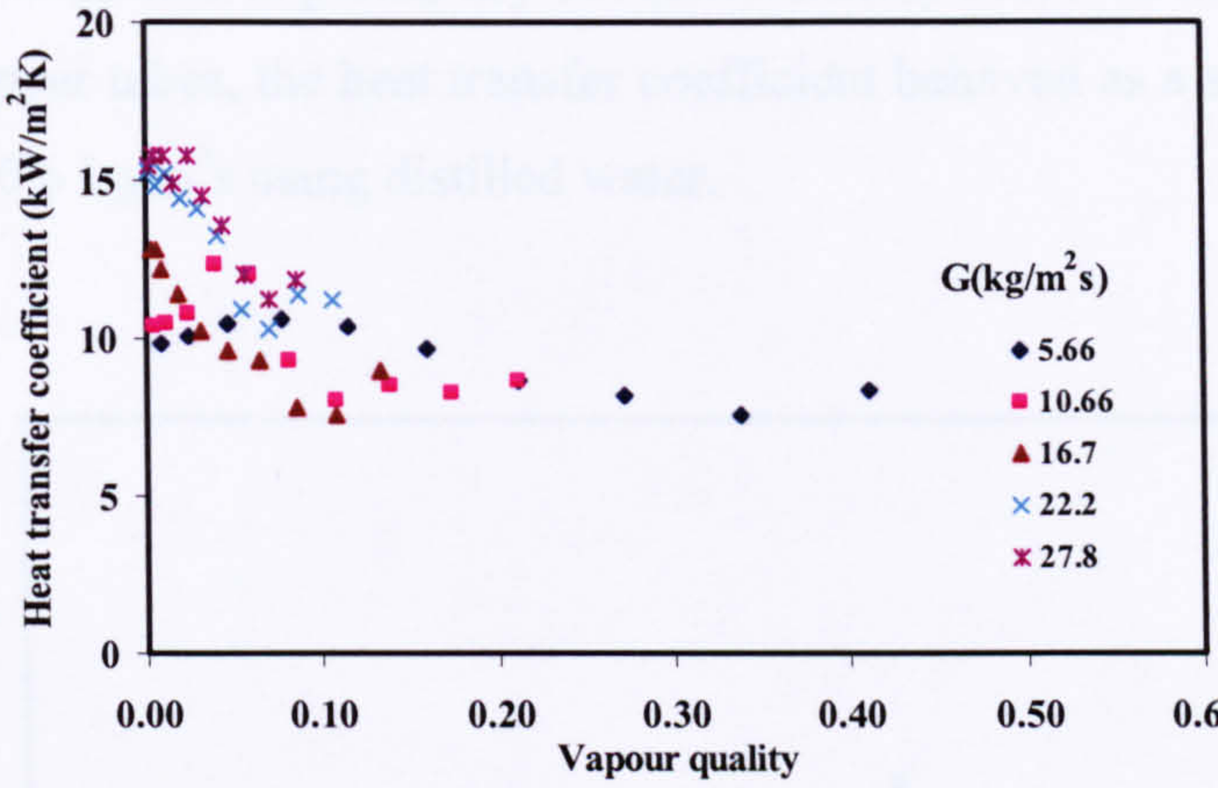

Figure 4.57 Heat transfer coefficient against vapour quality for q= 21 kW/m^2 with distilled water as the working fluid

4.5.3 Effect of heat flux

The plots of heat transfer coefficient against heat flux are shown in Figure 4.58 to Figure 4.67 for all the working fluids used. Heat transfer coefficient increased with the applied heat flux. The distilled water plots in Figure 4.58-Figure 4.62 showed that the heat transfer coefficient increased from 4 -6 kW/m^{2}K at q=6 kW/m^{2}K and increased from 8-12 kW/m^{2}K when the mass flux was 10.6 kg/m^{2}s. These results when compared with that of large tube bundles are in what is termed the apparent nucleate boiling regime. It has been shown in section 4.2, that the boiling heat transfer coefficient was dependent on the heat flux and was typically of the form;

$$\alpha = Cq^n \qquad (4.\ 1)$$

where C is a constant that depends on the surface finish , molecular mass of the fluids and the critical pressure. From the plots, it could be deduced that at heat flux of 21 kW/m^2, the heat transfer coefficient of the upper tube was comparable to that of a single tube boiling at the same heat flux. The studies did not show any sign of full dryness during the boiling process. The sudden drop of heat transfer coefficient at the upper tubes was attributed to inability of the bubbles to move up the bundle. The result in effect showed variation of the heat transfer coefficient from the first tube to the tenth tube. The results showed that there was a variation of heat transfer coefficient with the position of the tube. The heat transfer increased from the first tube and there is drop and an increase at the top. This cyclical

variation could be attributed to partial dry out (intermittent) observed in the bundle. It was observed that at upper tubes, the heat transfer coefficient behaved as a single tube for mass fluxes of 5.6and 10.6 kg/m^{2}s using distilled water.

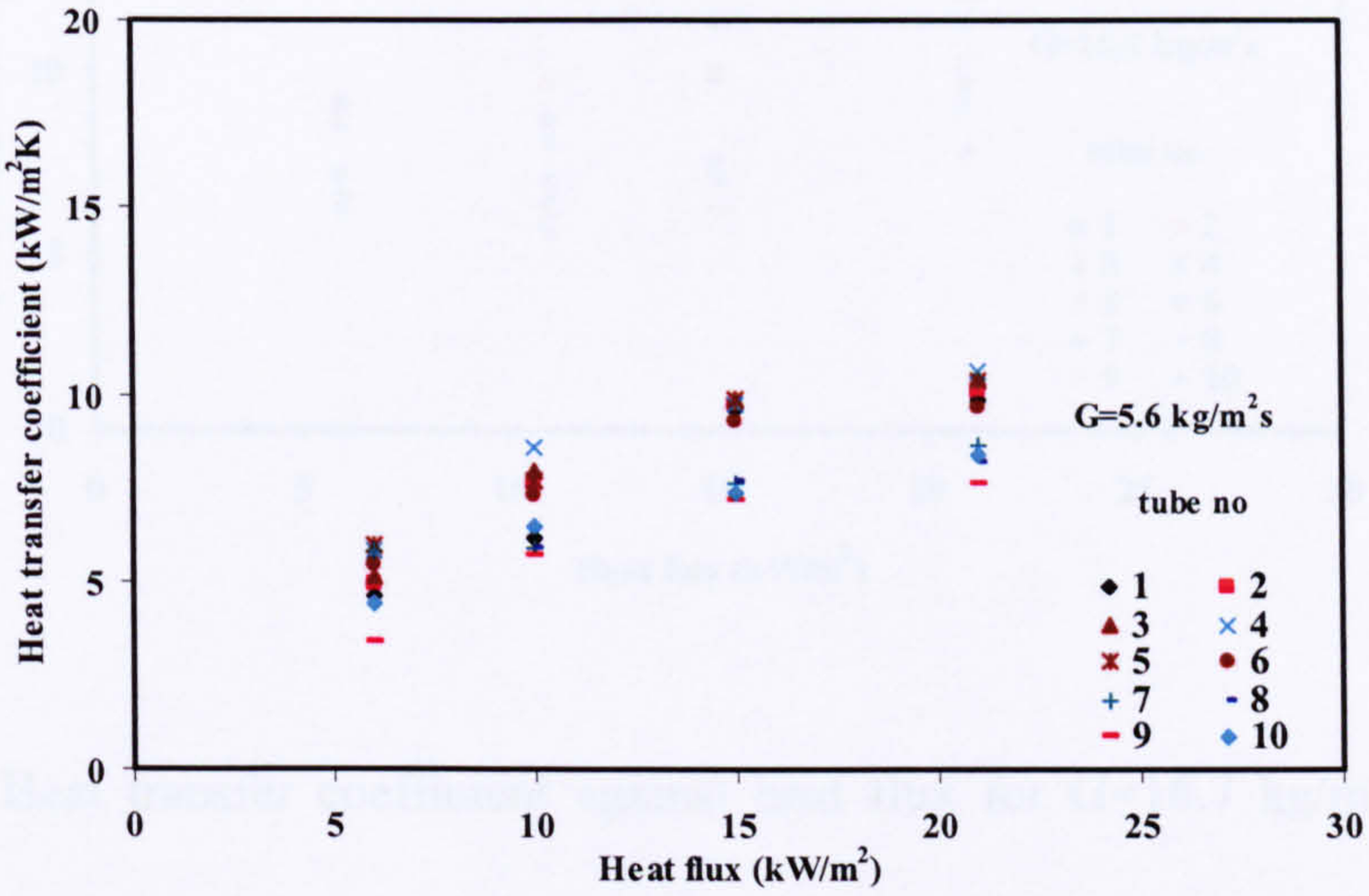

Figure 4.58 Heat transfer coefficient against heat flux for G=5.6 kg/m^{2}s with distilled water

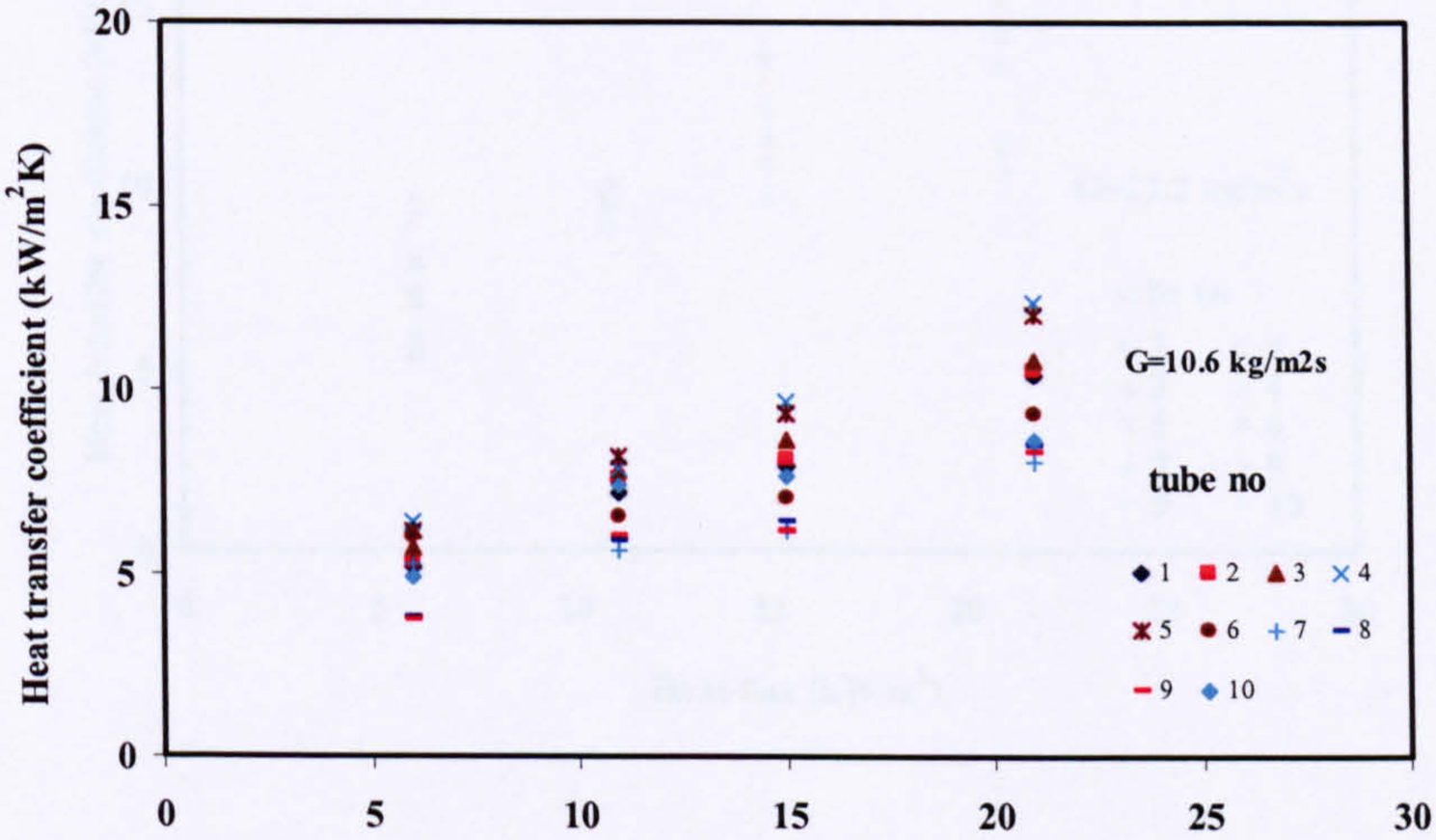

Figure 4.59 Heat transfer coefficient against heat flux for G=10.6 kg/m^{2}s with distilled water

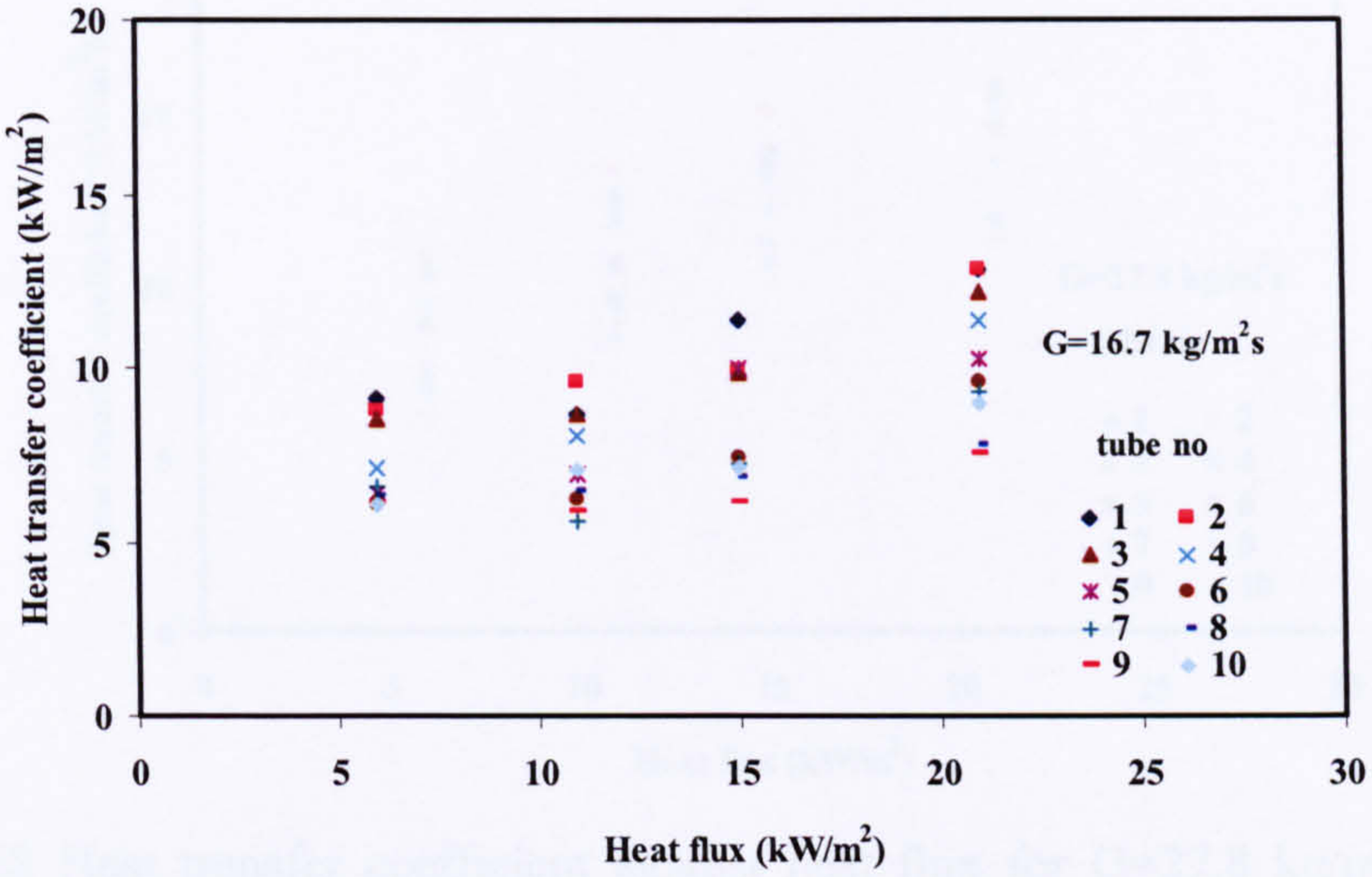

Figure 4.60 Heat transfer coefficient against heat flux for G=16.7 kg/m^{2}s with distilled water

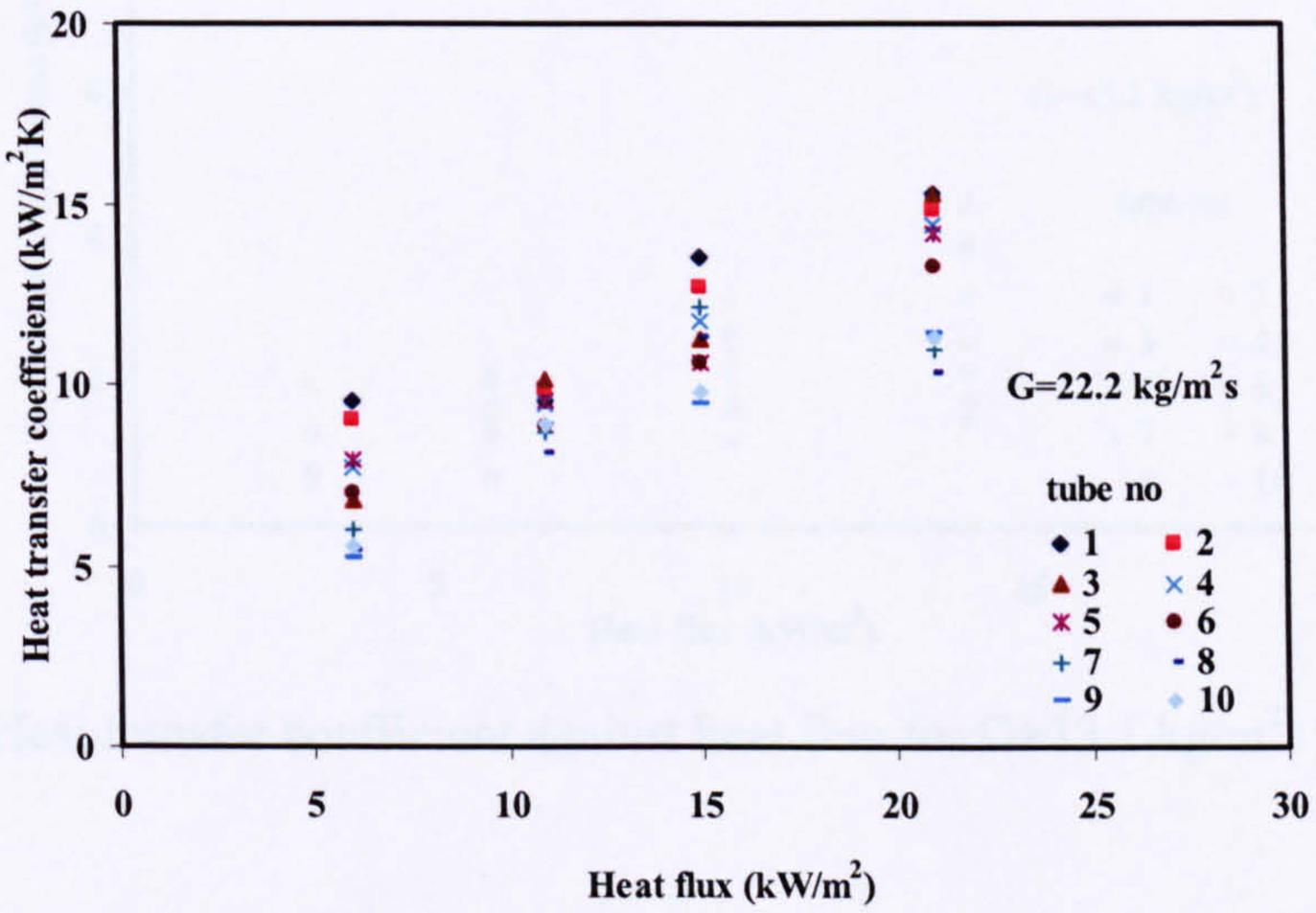

Figure 4.61 Heat transfer coefficient against heat flux for G=22.20 kg/m^{2}s with distilled water

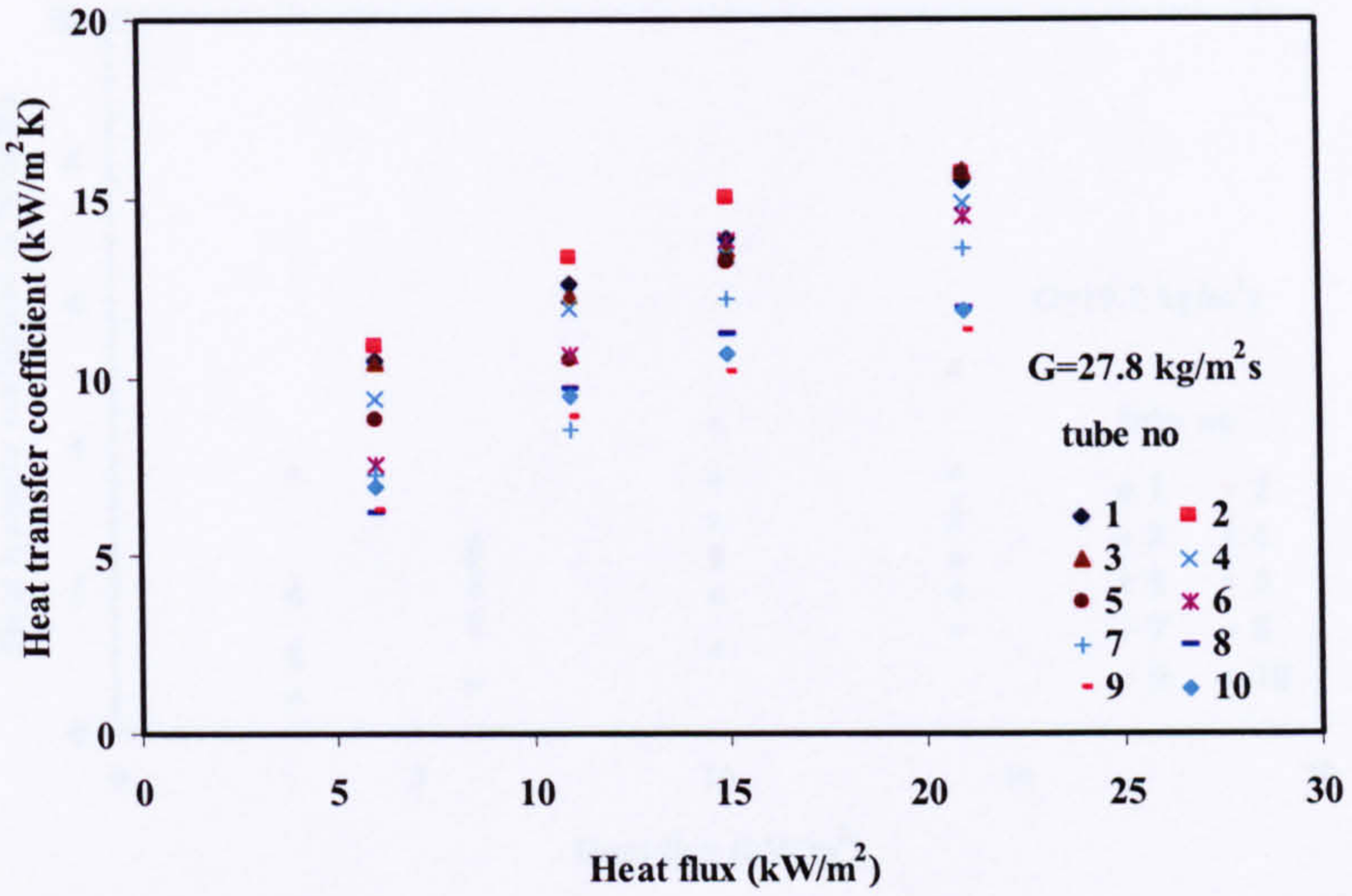

Figure 4.62 Heat transfer coefficient against heat flux for G=27.8 kg/m^{2}s with distilled water

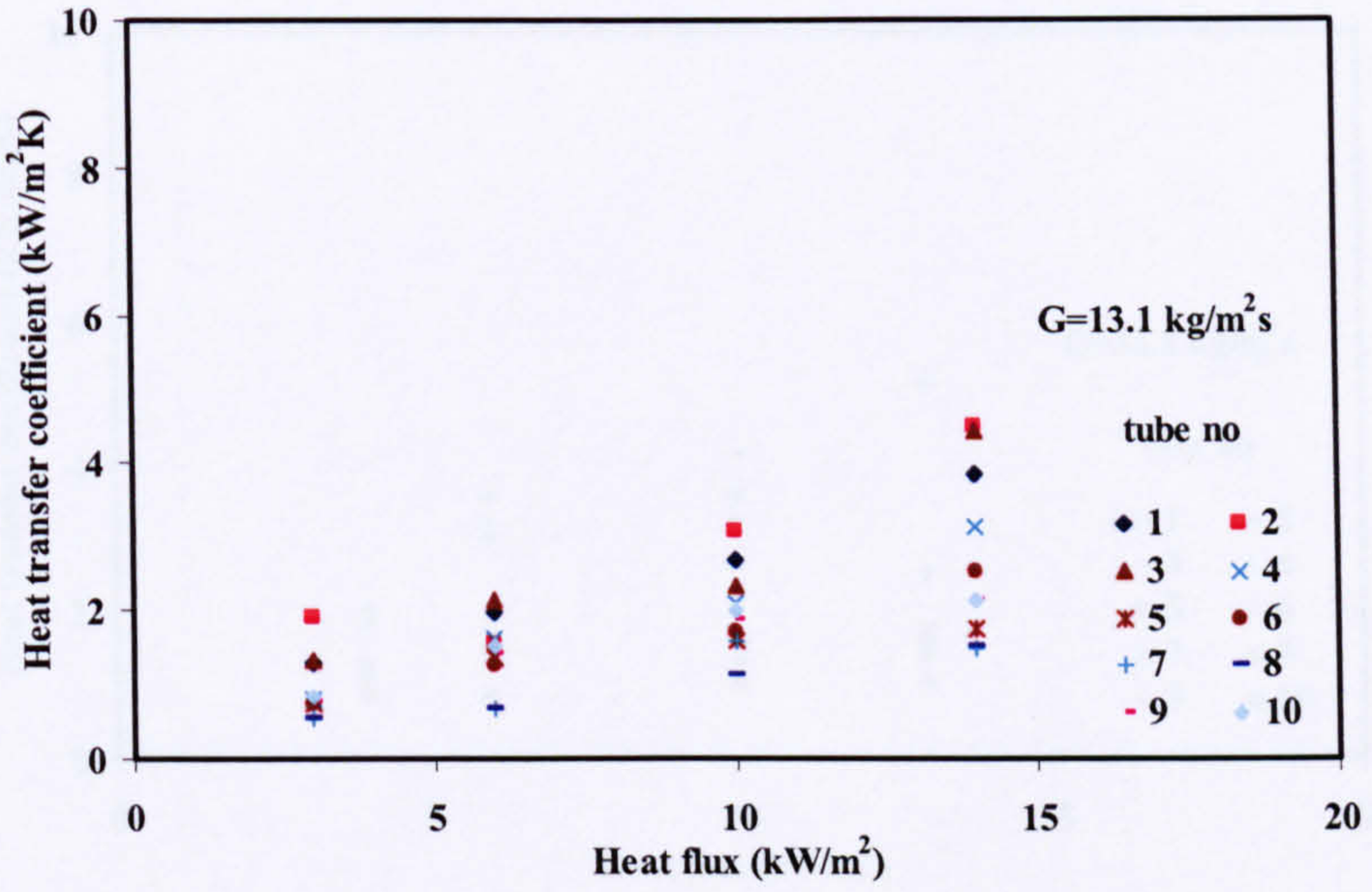

Figure 4.63 Heat transfer coefficient against heat flux for G=13.1 kg/m^{2}s with R-113

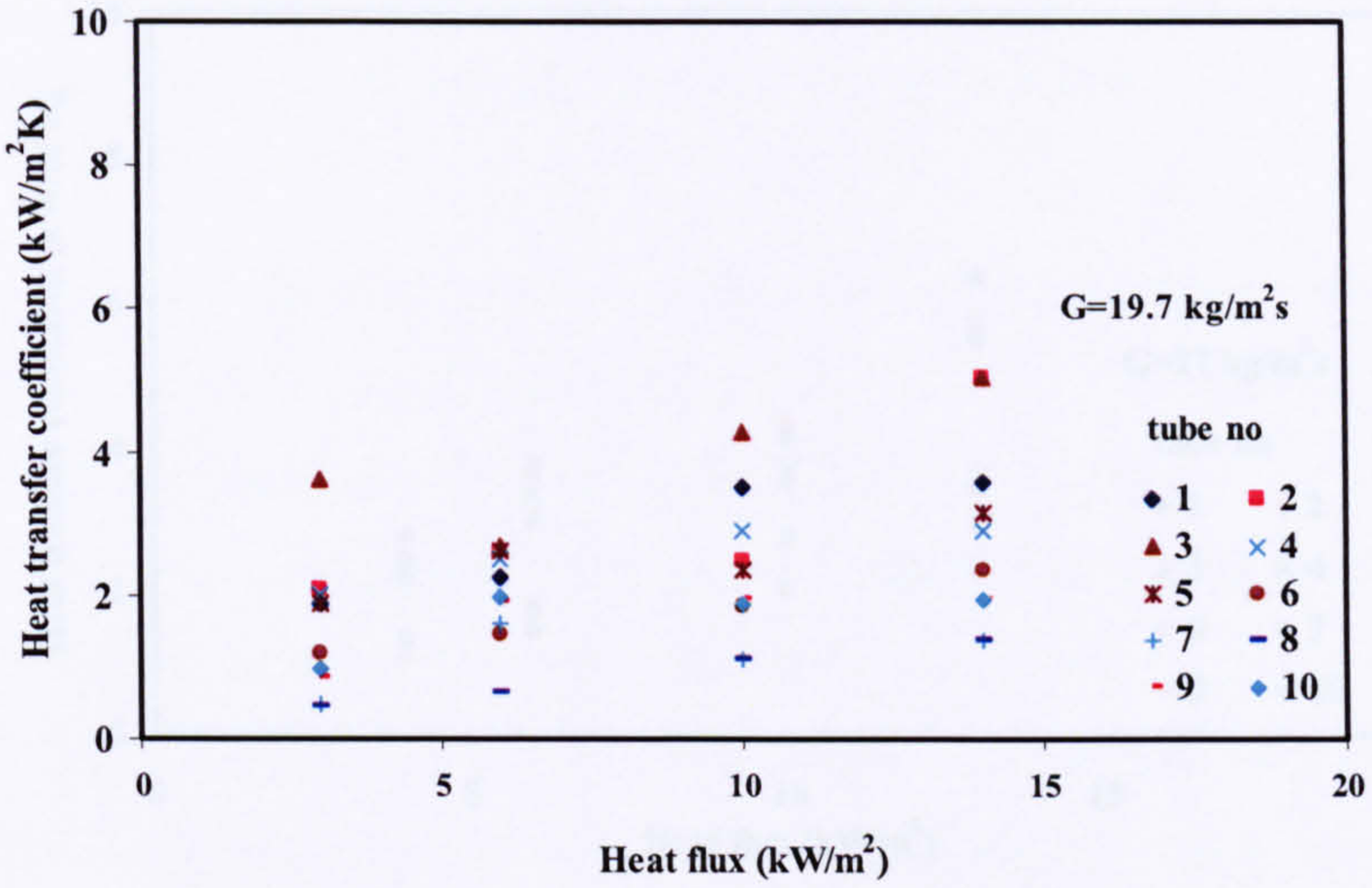

Figure 4.64 Heat transfer coefficient against heat flux for G=19.7 kg/m^{2}s with R-113

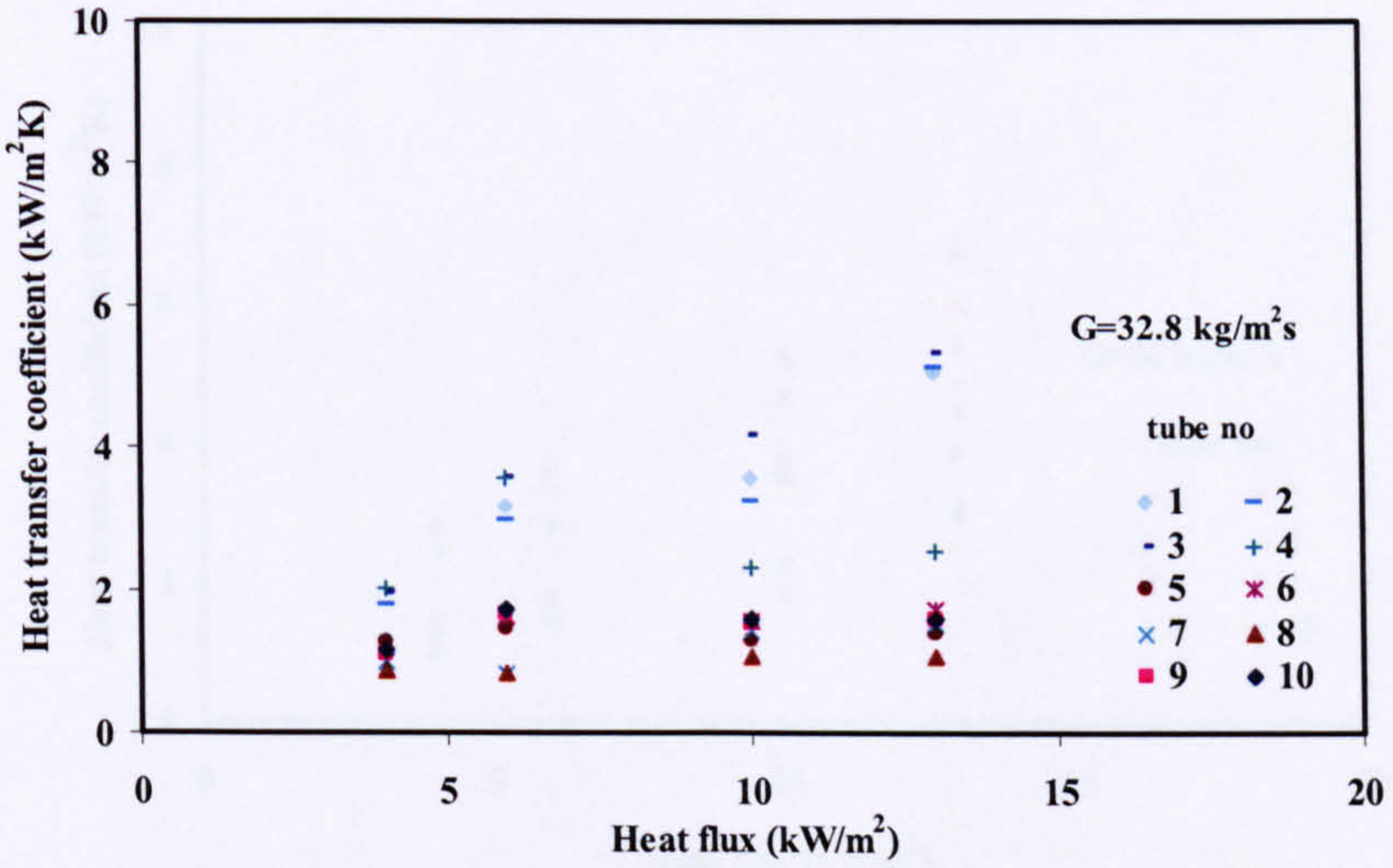

Figure 4.65 Heat transfer coefficient against heat flux for G=32.8 kg/m^{2}s with R-113

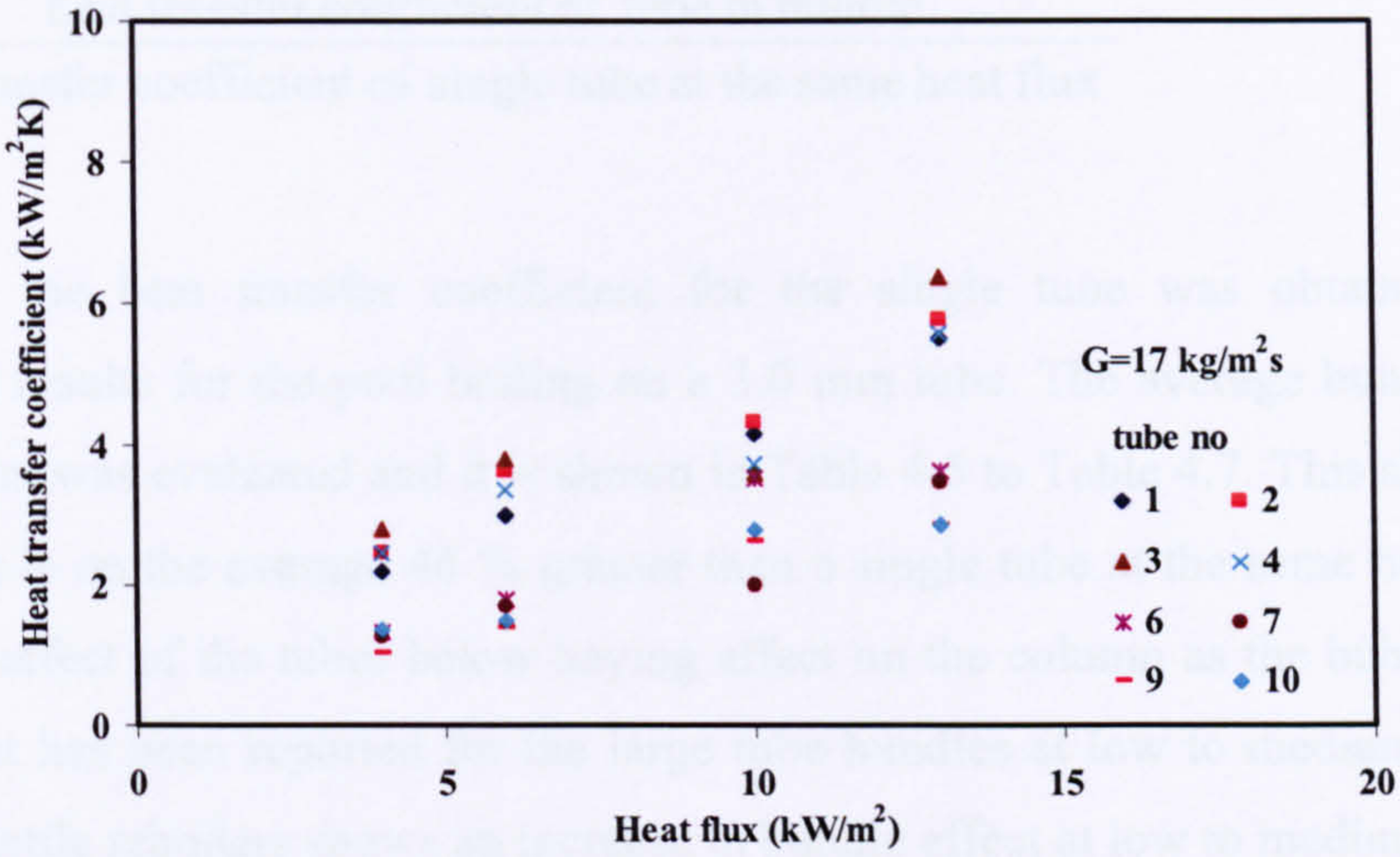

Figure 4.66 Heat transfer coefficient against heat flux for G=17 kg/m^{2}s with Flutec PP1

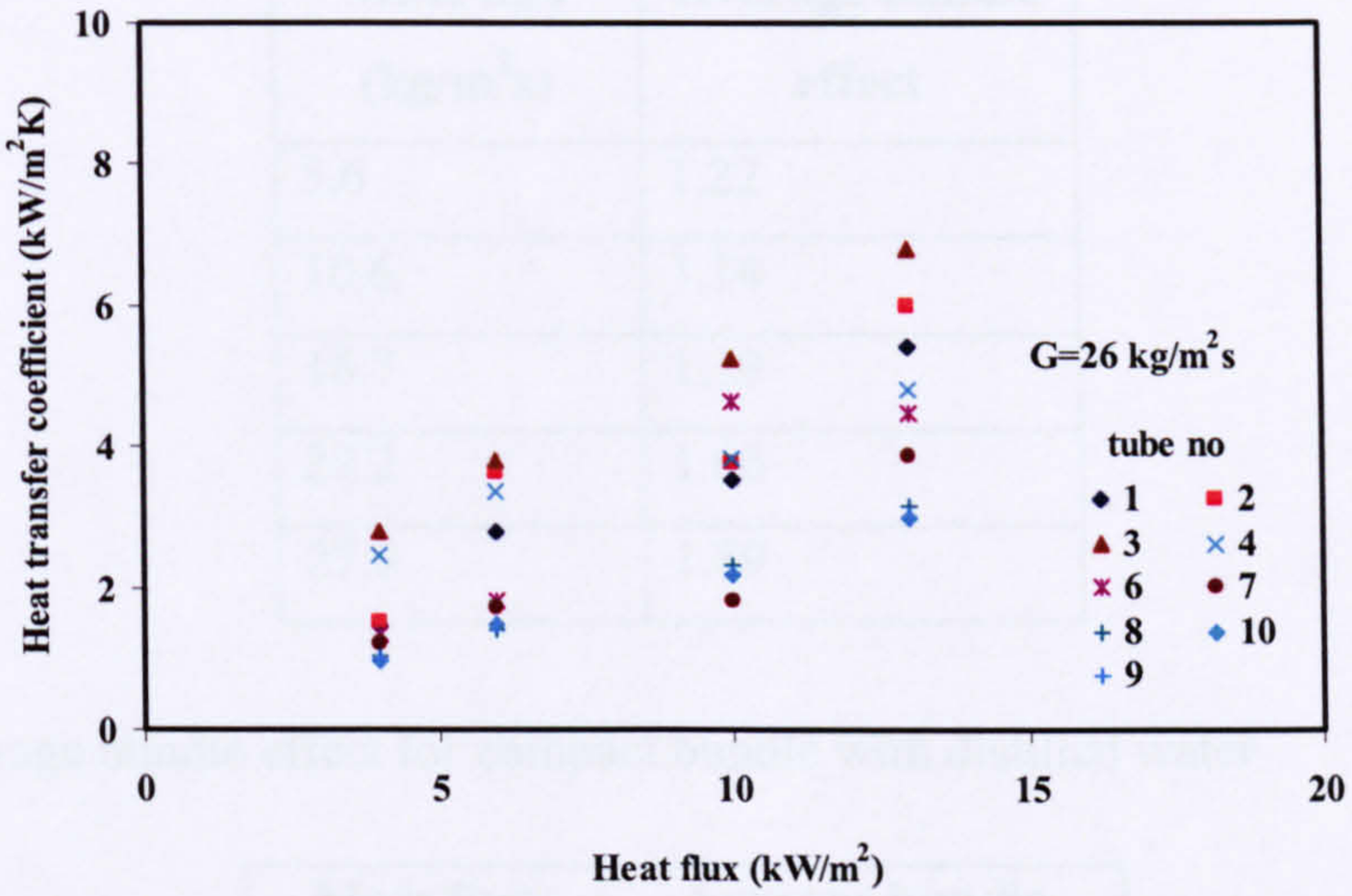

Figure 4.67 Heat transfer coefficient against heat flux for G=26 kg/m^{2}s with Flutec PP1

4.5.4 Bundle effect

The bundle effect is explained as the effect of bubbles from the lower tube on the upper tube thereby increasing the heat transfer coefficient. This effect is comparable assuming the tube is heated alone in pool boiling. The bundle effect plot for the mass fluxes is shown in Figure 4.68 to Figure 4.77. The bundle effect is computed as;

$$BE = \frac{\text{heat transfer coefficient of tube in bundle}}{\text{heat transfer coefficient of single tube at the same heat flux}}$$

In this case the heat transfer coefficient for the single tube was obtained from the experimental results for the pool boiling on a 3.0 mm tube. The average bundle effect for each mass flux was evaluated and it is shown in Table 4.5 to Table 4.7. This shows that the bundle effect is on the average 46 % greater than a single tube at the same heat flux. This explains the effect of the tubes below having effect on the column as the bubbles rises up. Similar effect has been reported for the large tube bundles at low to medium heat fluxes. Traditional kettle reboilers shows an increase in bundle effect at low to medium heat fluxes, contrary the small tube bundle shows a rise from the lower to mid sections of the bundle. The tube spacing is attributed for the dis-enhancement on the upper section.

Mass flux (kg/m^2s)	Average bundle effect
5.6	1.22
10.6	1.14
16.7	1.39
22.2	1.66
27.8	1.89

Table 4.5 Average bundle effect for compact bundle with distilled water

Mass flux (kg/m^2s)	Average bundle effect
17.0	2.19
26.0	2.32

Table 4.6 Average bundle effect for compact bundle with Flutec PP1

Mass flux (kg/m^2s)	Average bundle effect
13.1	2.78
19.7	3.71
32.8	3.42

Table 4.7 Average bundle effect for compact bundle with R-113

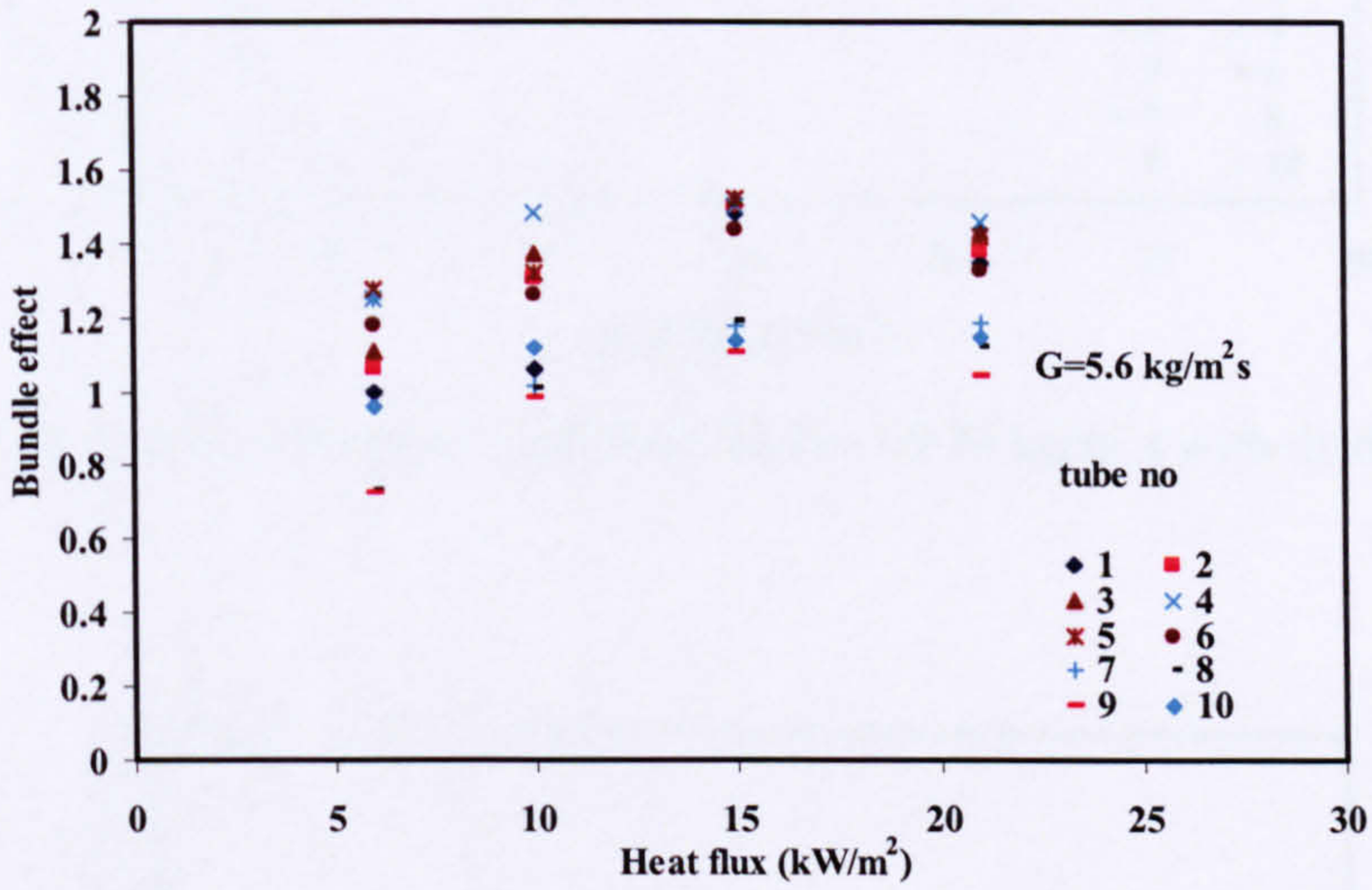

Figure 4.68 Bundle effect against heat flux for G= 5.6 kg/m^2s with distilled water

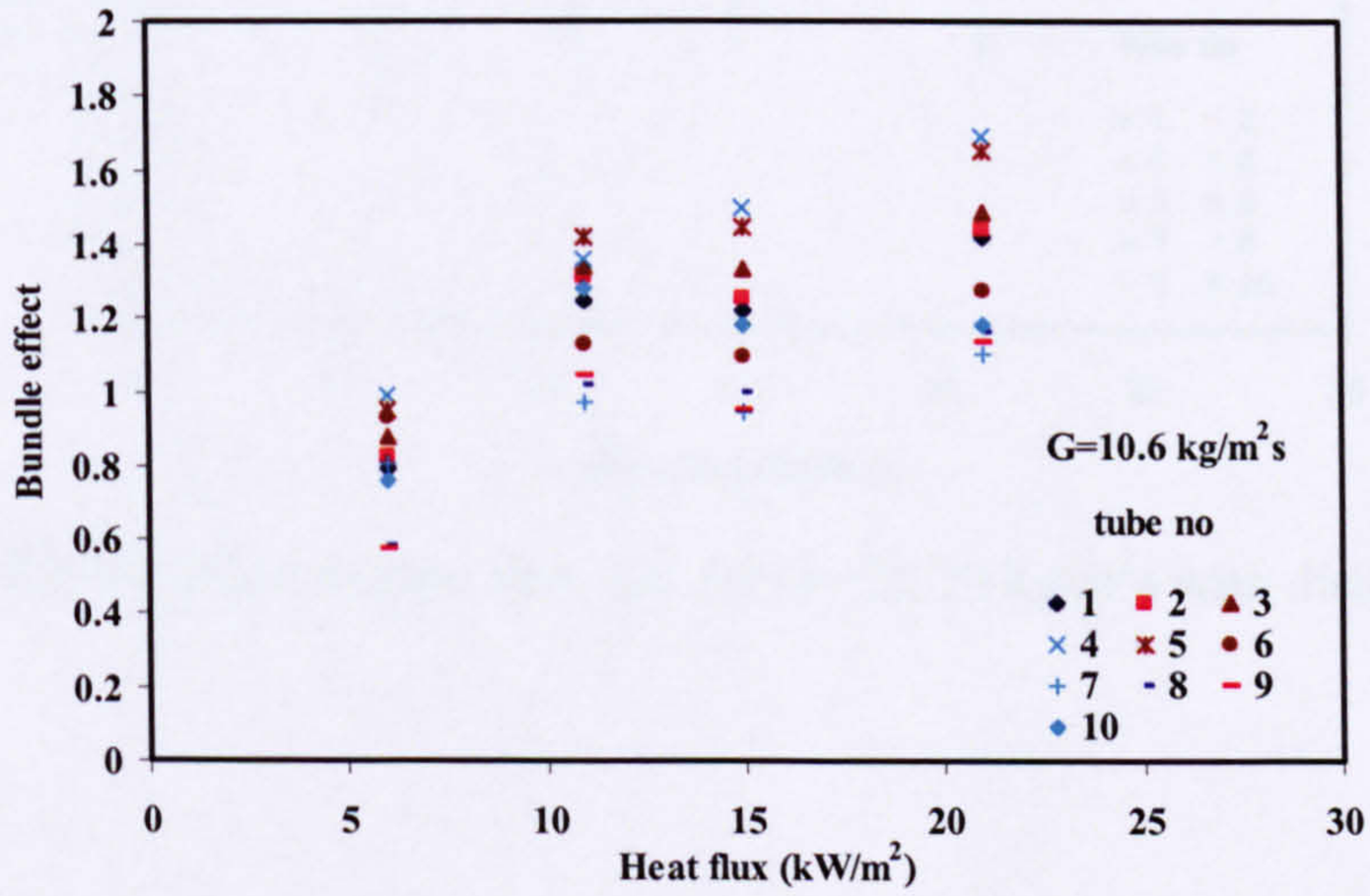

Figure 4.69 Bundle effect against heat flux for G= 10.6 kg/m^2s with distilled water

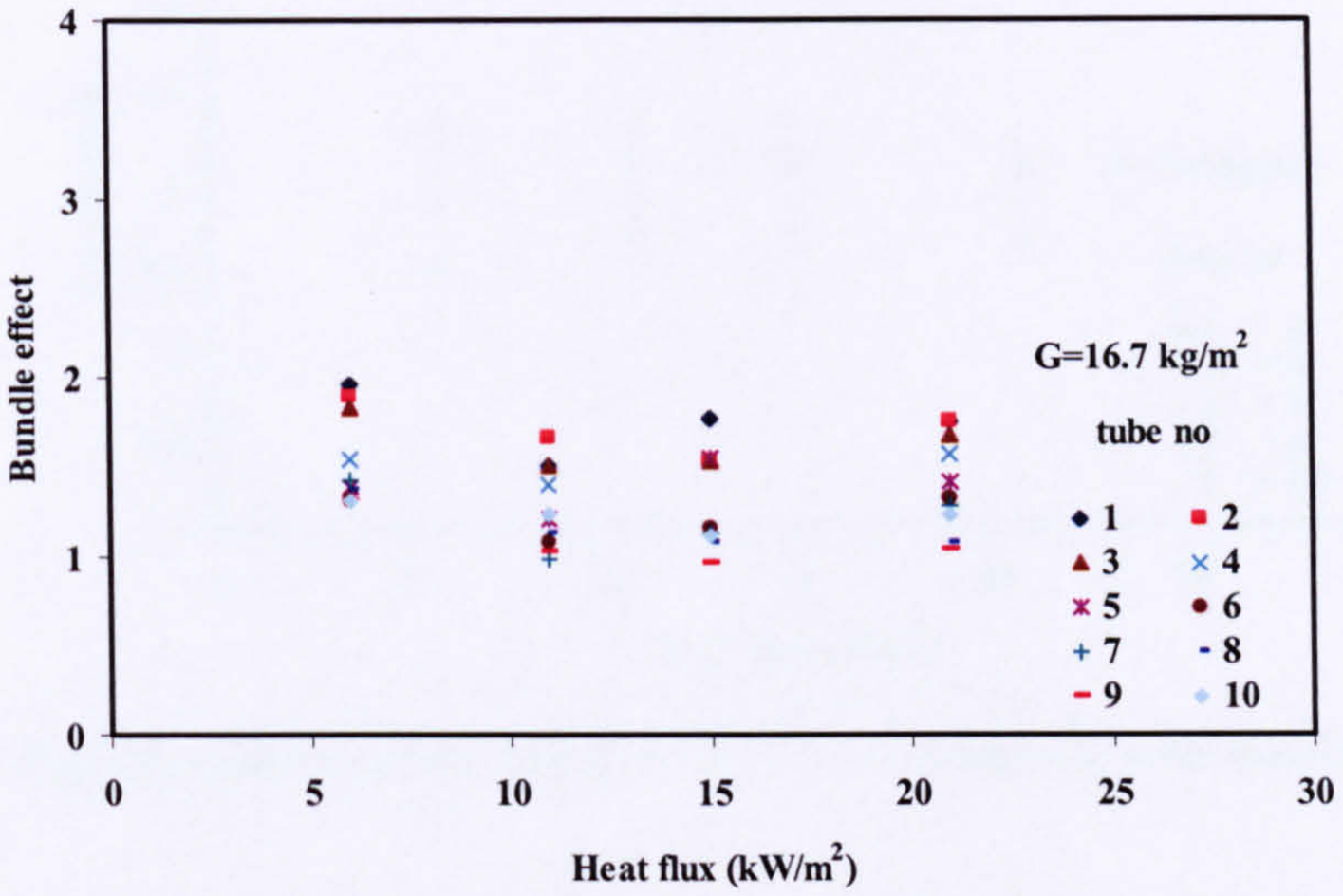

Figure 4.70 Bundle effect against heat flux for G= 16.70 kg/m^{2}s with distilled water

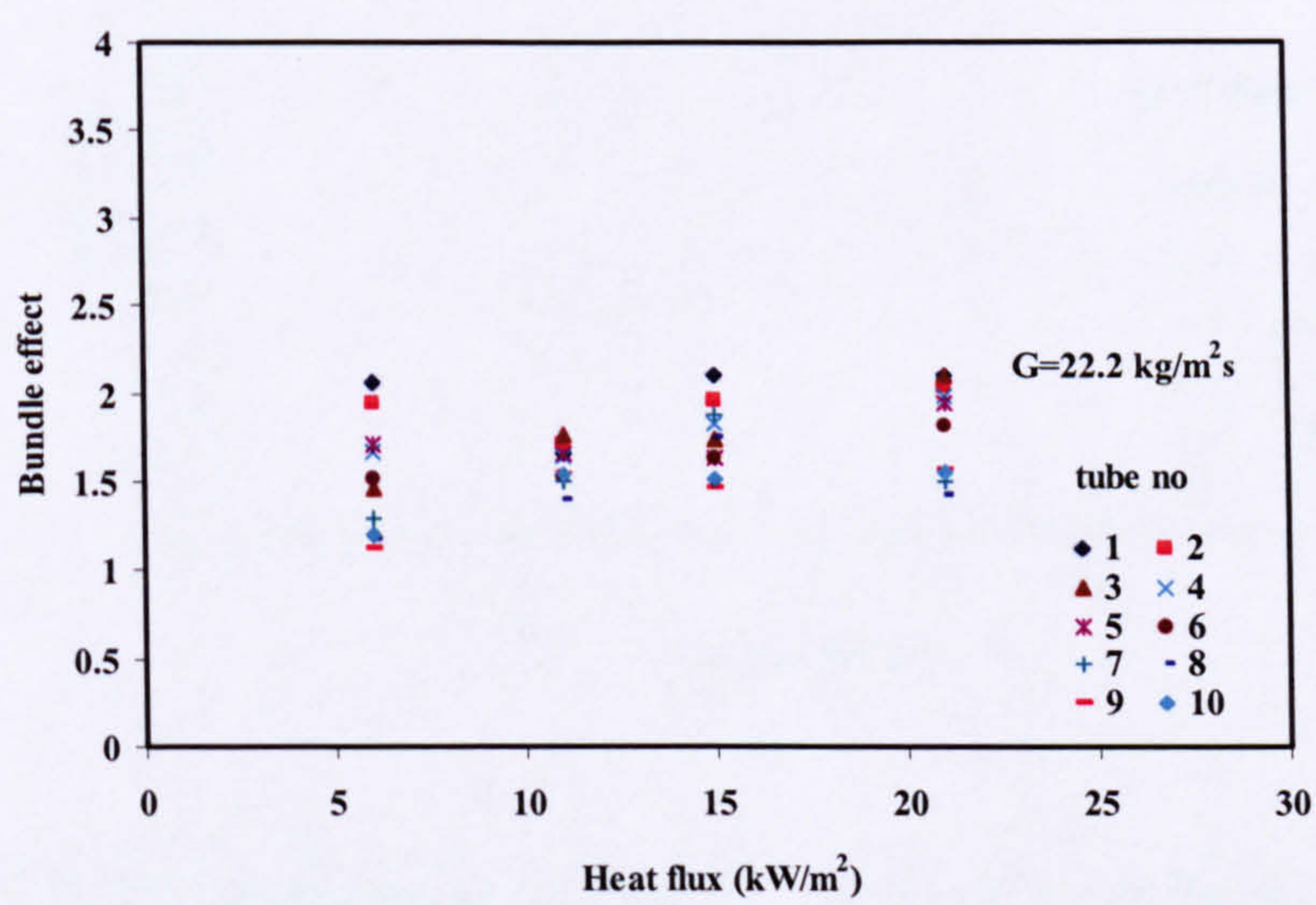

Figure 4.71 Bundle effect against heat flux for G= 22.20 kg/m^{2}s with distilled water

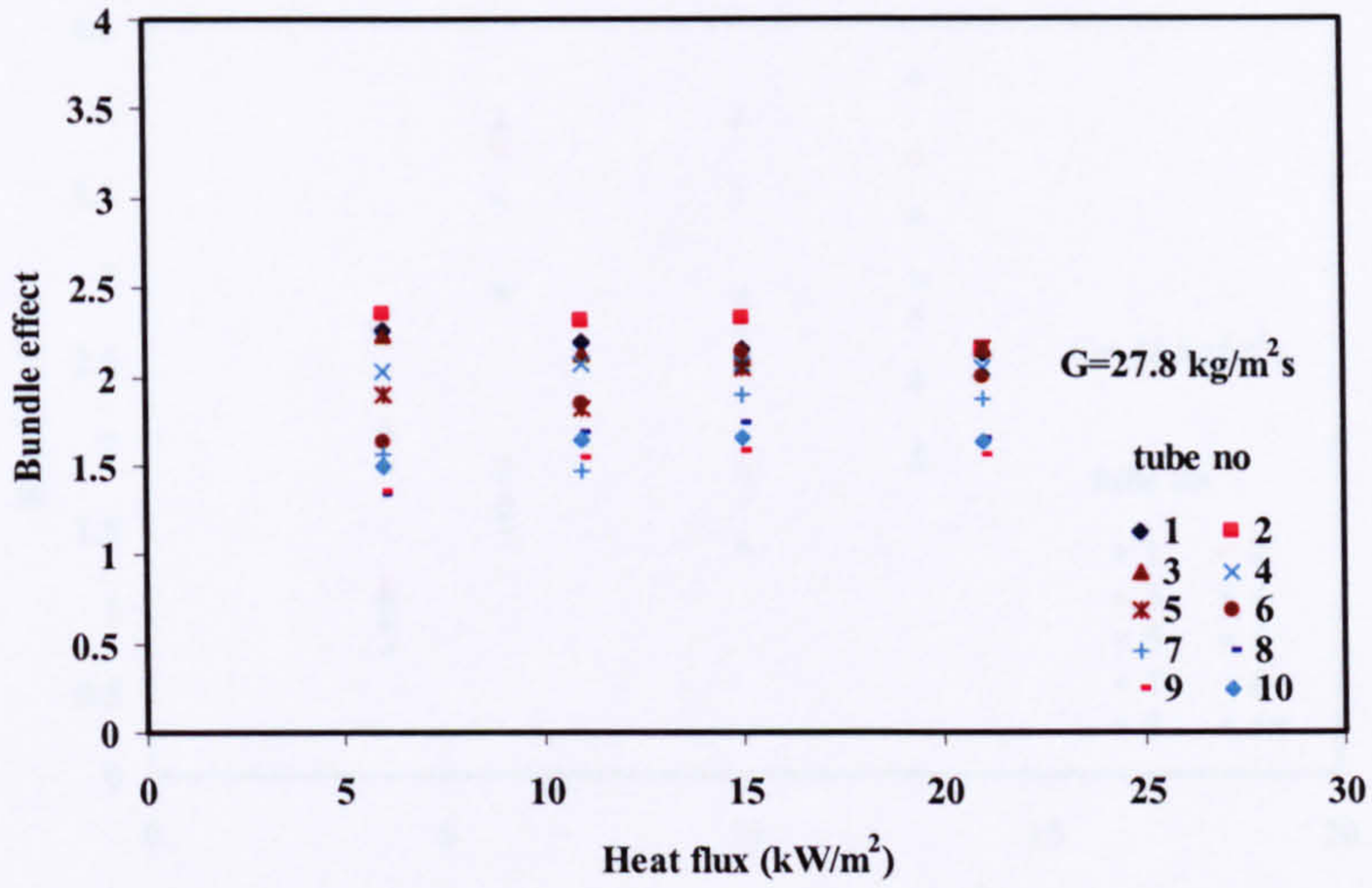

Figure 4.72 Bundle effect against heat flux for G= 27.8 kg/m^{2}s with distilled water

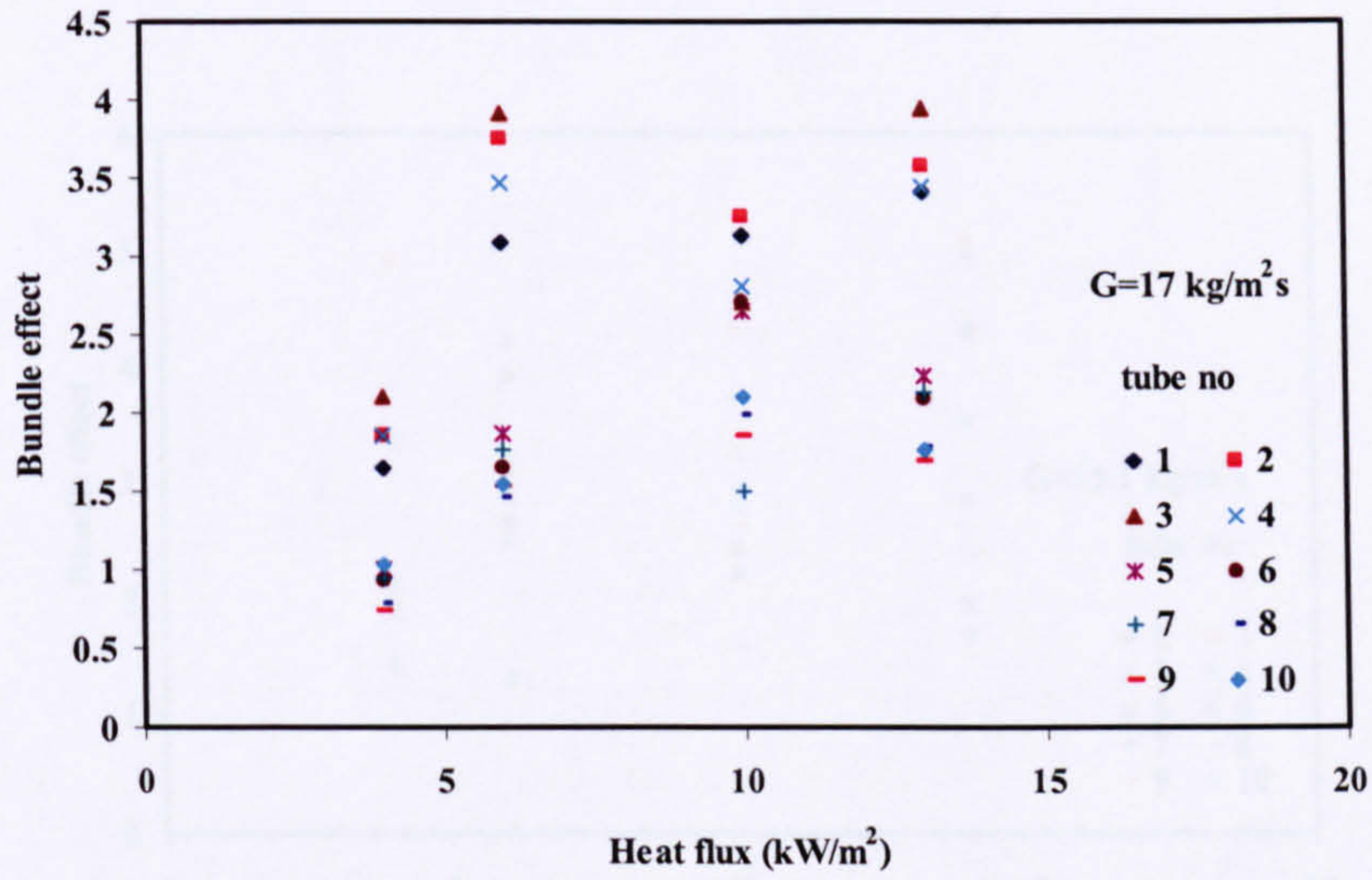

Figure 4.73 Bundle effect against heat flux for G=17 kg/m^{2}s with Flutec PP1

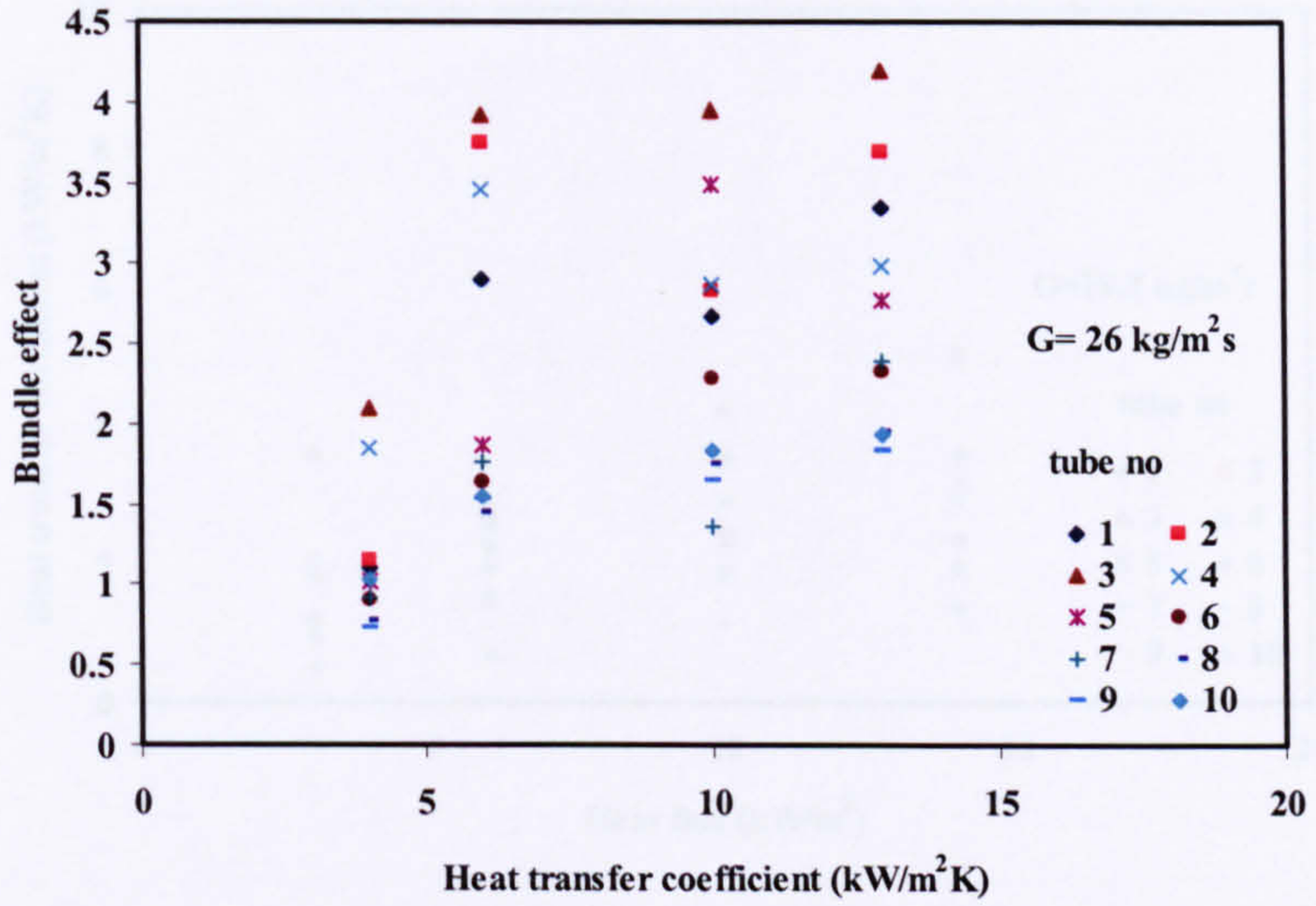

Figure 4.74 Bundle effect against heat flux for G= 26 kg/m^{2}s with Flutec PP1

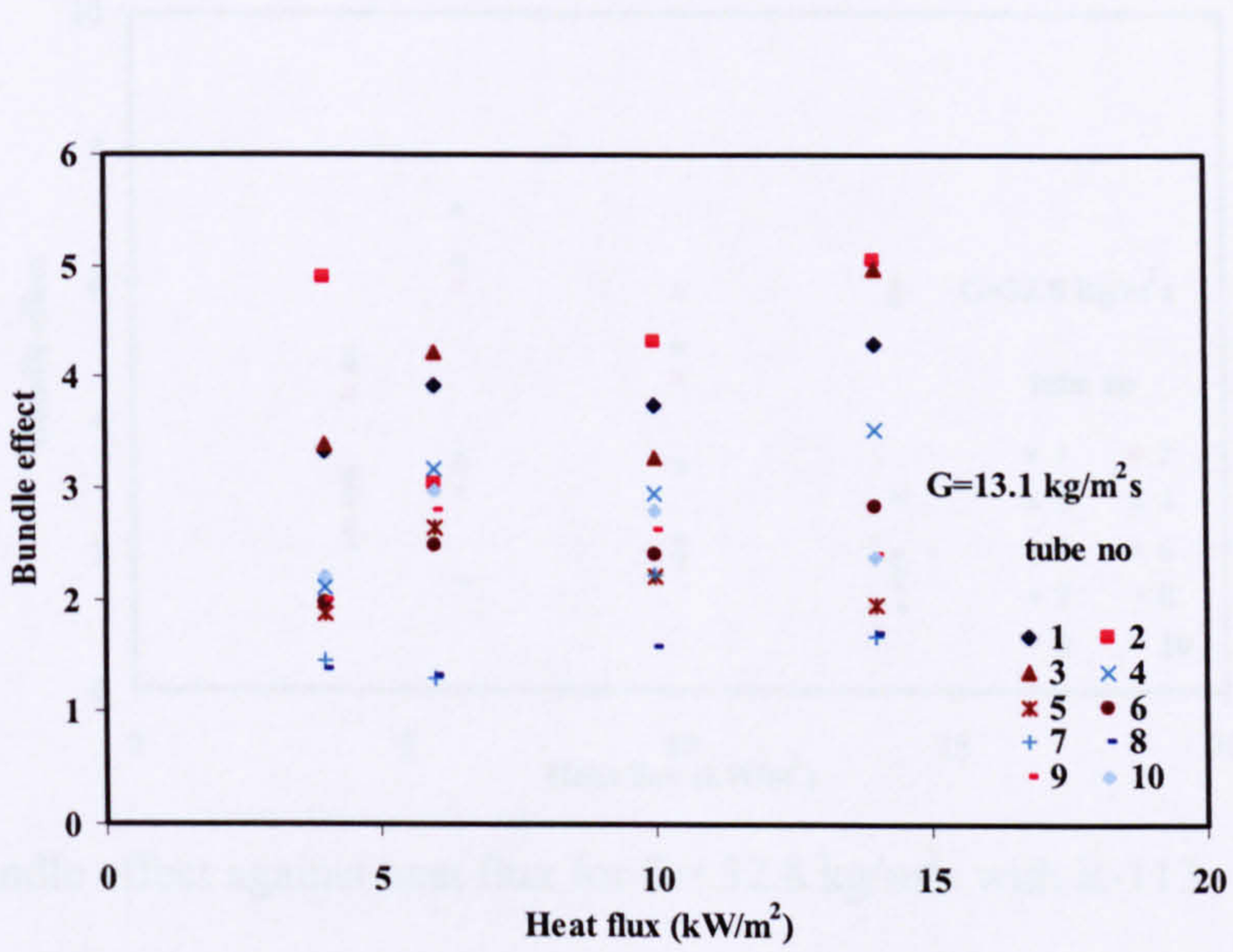

Figure 4.75 Bundle effect against heat flux for G= 13.1 kg/m^{2}s with R-113

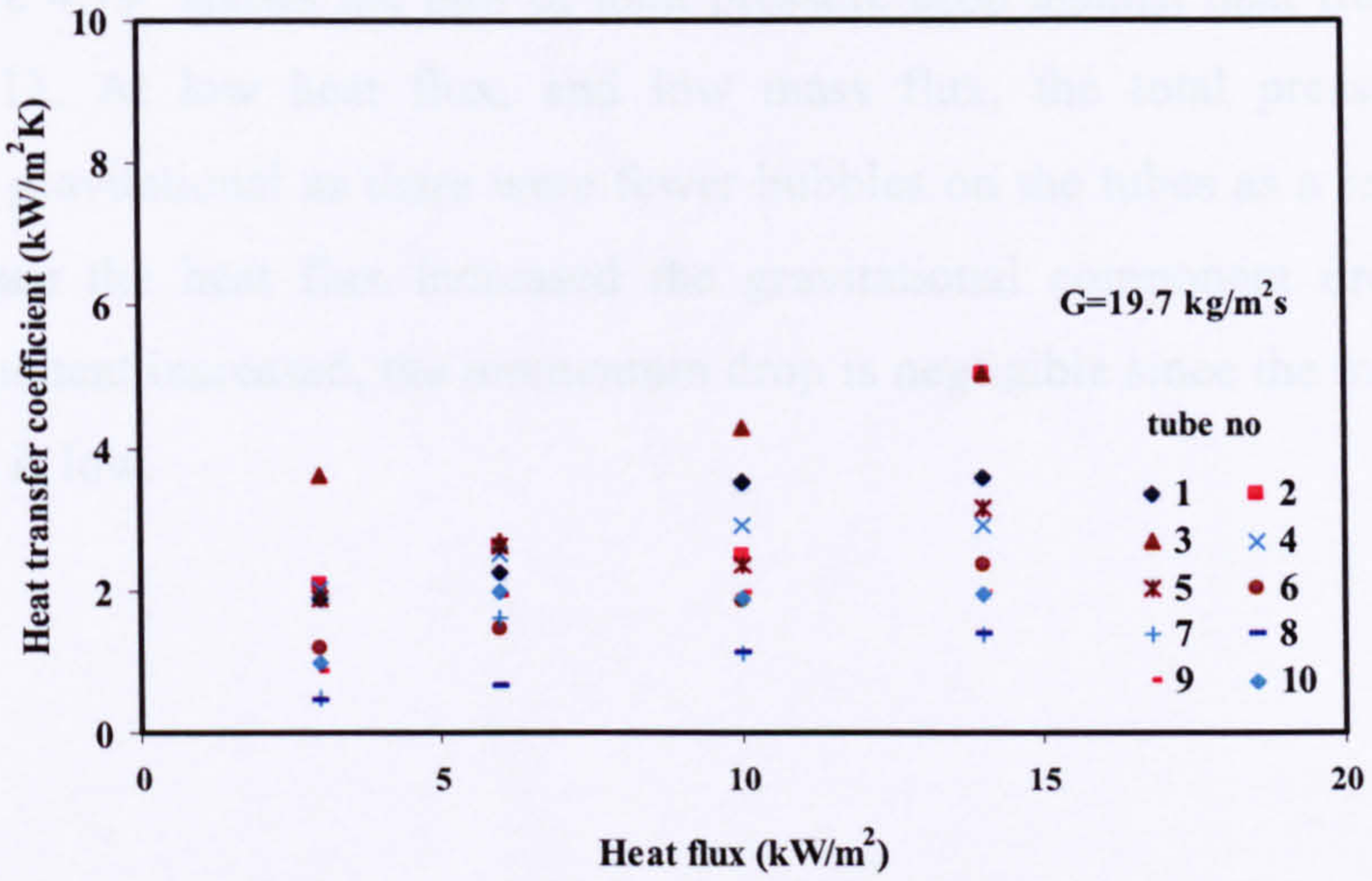

Figure 4.76 Bundle effect against heat flux for G= 19.7 kg/m^{2}s with R-113

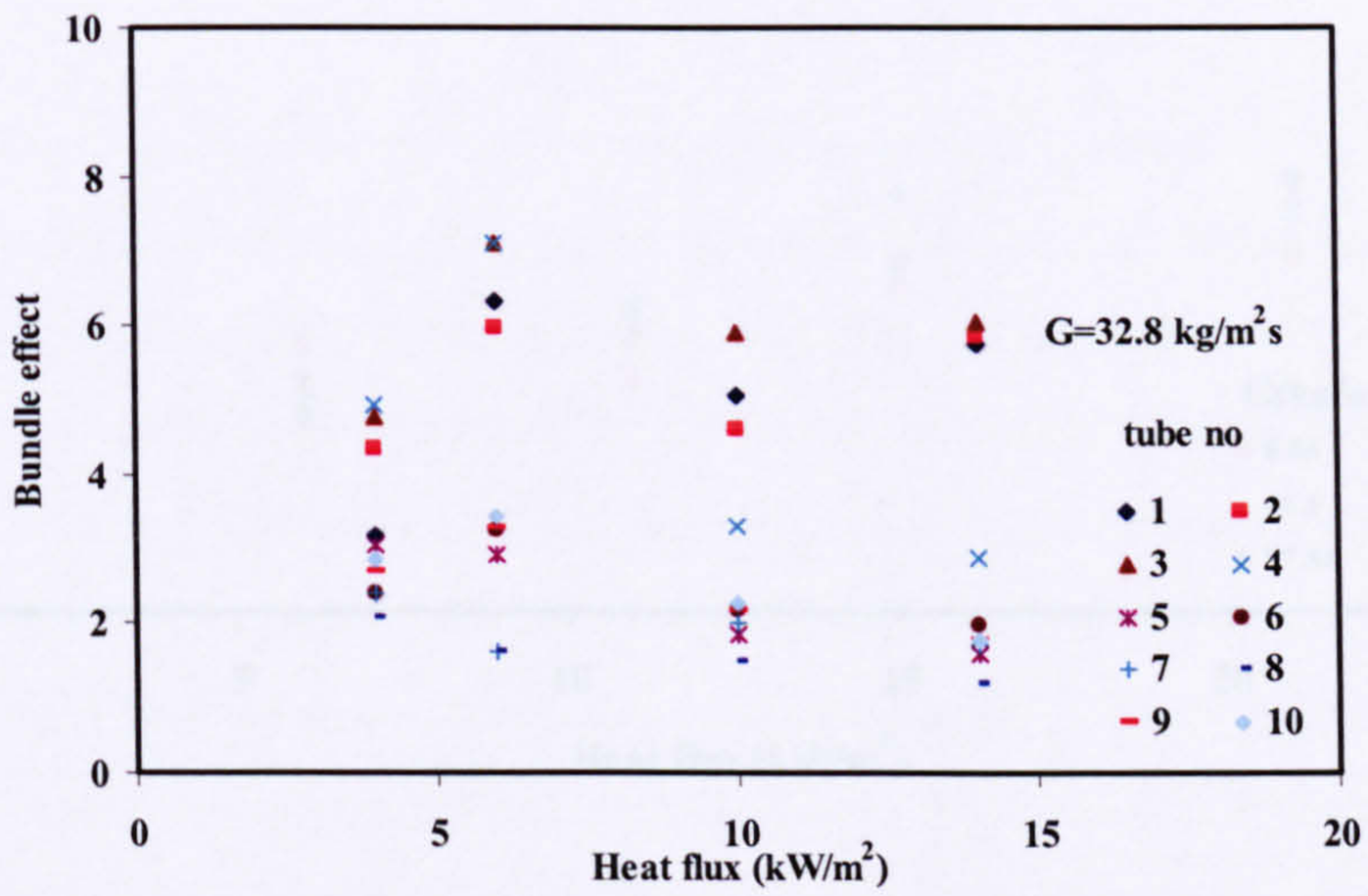

Figure 4.77 Bundle effect against heat flux for G= 32.8 kg/m^{2}s with R-113

4.5.5 Pressure drop results

Pressure drop tapping were inserted at the top and bottom of the test section to measure the total drop across the bundle. The total pressure across the bundle was that due to inlet and exit of the test section. It is well known from two-phase theory studies that pressure drop is due to gravitational, frictional and acceleration components. Results presented here are the sum of these three components. Review of the available correlations for large tube bundle has been presented in the literature review and as such will not be elaborated here. Figure

4.78 and Figure 4.79 shows the plot of total pressure drop against heat flux for distilled water and R113. At low heat flux, and low mass flux, the total pressure drop was predominantly gravitational as there were fewer bubbles on the tubes as a result of patchy nucleation. Once the heat flux increased the gravitational component drops while the frictional component increased, the momentum drop is negligible since the mass flux of the working fluids is low.

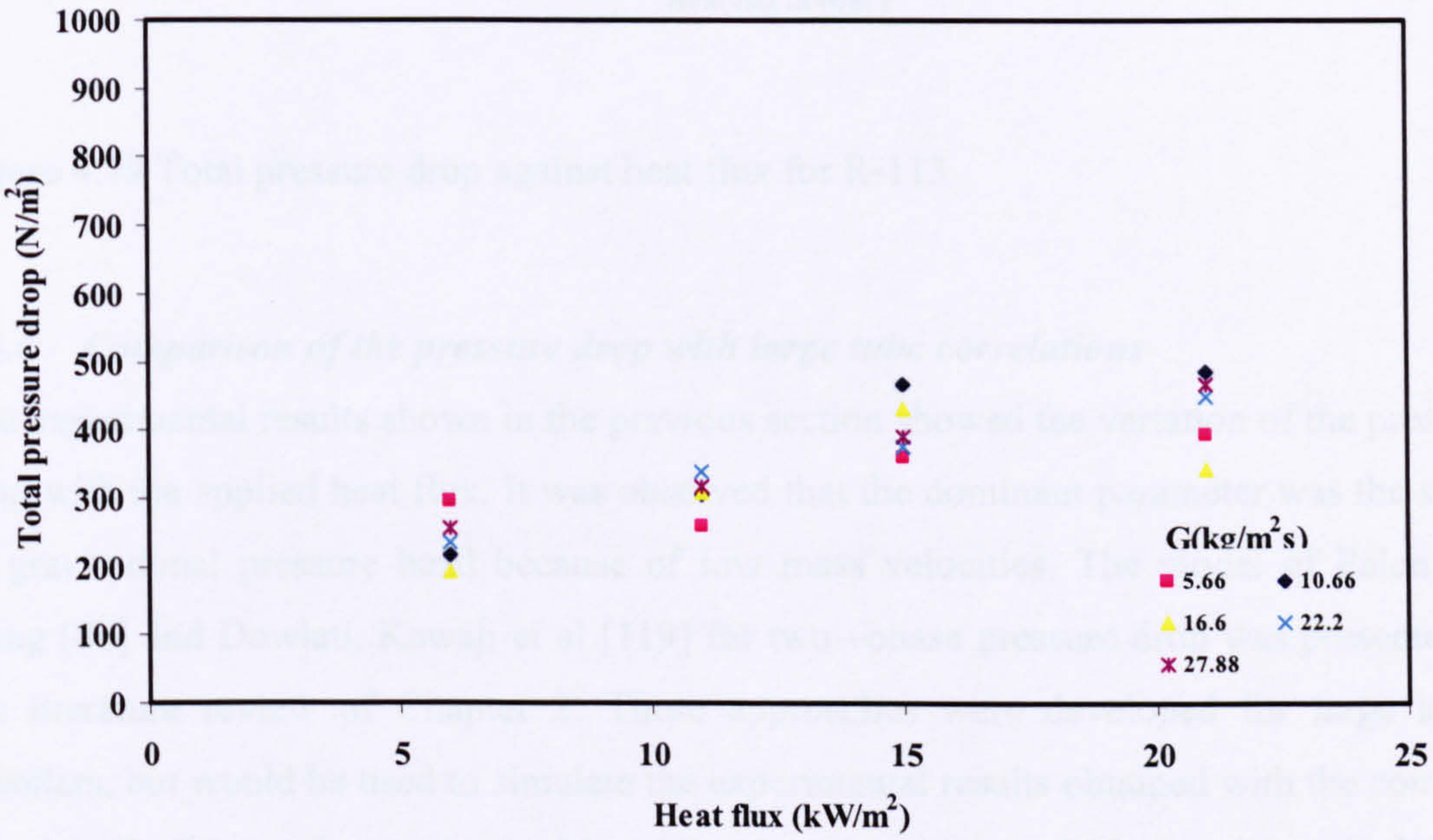

Figure 4.78 Total pressure drop against heat flux for distilled water.

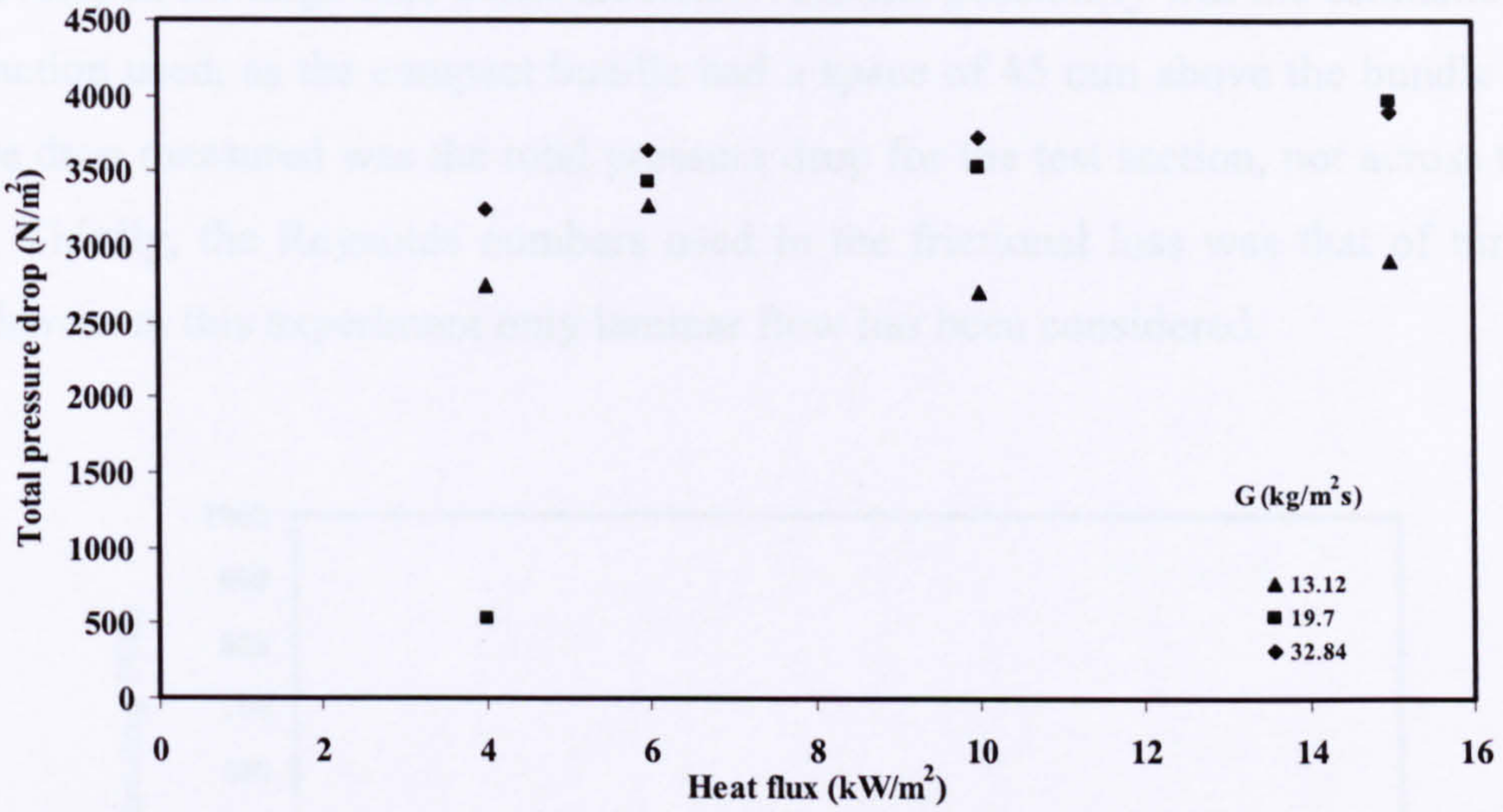

Figure 4.79 Total pressure drop against heat flux for R-113

4.5.6 Comparison of the pressure drop with large tube correlations

The experimental results shown in the previous section showed the variation of the pressure drop with the applied heat flux. It was observed that the dominant parameter was the static or gravitational pressure head because of low mass velocities. The model of Palen and Yang [86] and Dowlati, Kawaji et al [119] for two –phase pressure drop was presented in the literature review of Chapter 2. These approaches were developed for large kettle reboilers, but would be used to simulate the experimental results obtained with the compact tube bundle. It must be emphasised here that there was a gap of 45 mm above the bundle which would affect the pressure drop results; however it would give us an estimate using the models. Figure 4.80 to Figure 4.83 shows the plot of total pressure drop against heat flux for R113 and distilled water. The results shows a mean deviation of 0.6914 for G=13.1 kg/m^{2}s, 0.6061 for G=19.7 kg/m^{2}s with the model of Palen and Yang [86]. Similar trends were observed using the model of Dowlati, Kawaji et al [119] however this showed a mean deviation of 0.6275 for G=13.1 kg/m^{2}s. Using distilled water as the working fluid showed a mean error of 0.2129, at 10.6 kg/m^{2}s and 0.2129 at 5.6 kg/m^{2}s using the model of Palen and Yang [86], whereas Dowlati, Kawaji et al [119] yielded a mean deviation of -0.3925 and -0.5723 for mass fluxes 5.6 and 10.6 kg/m^{2}s respectively. The differences in the experimental results compared to the model was due to the fact that Palen and Yang [86]

were developed for large tube kettle reboilers. Another possibility was the estimation of the void fraction used, as the compact bundle had a space of 45 mm above the bundle and the pressure drop measured was the total pressure drop for the test section, not across the tube bundle. Thirdly, the Reynolds numbers used in the frictional loss was that of turbulence flow whereas in this experiment only laminar flow has been considered.

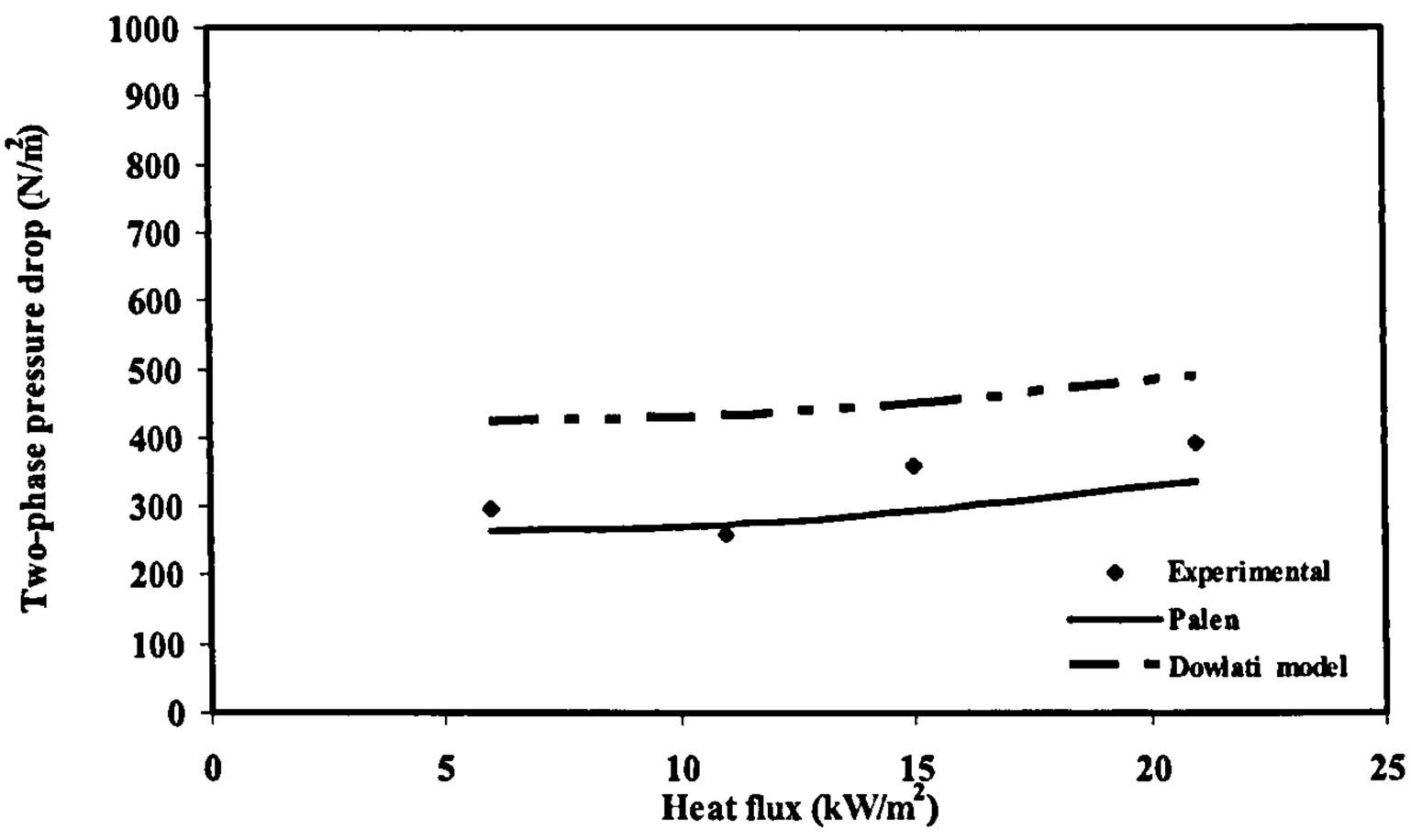

Figure 4.80 Comparison of total pressure drop against heat flux for G=5.6 kg/m^{2}s with distilled water

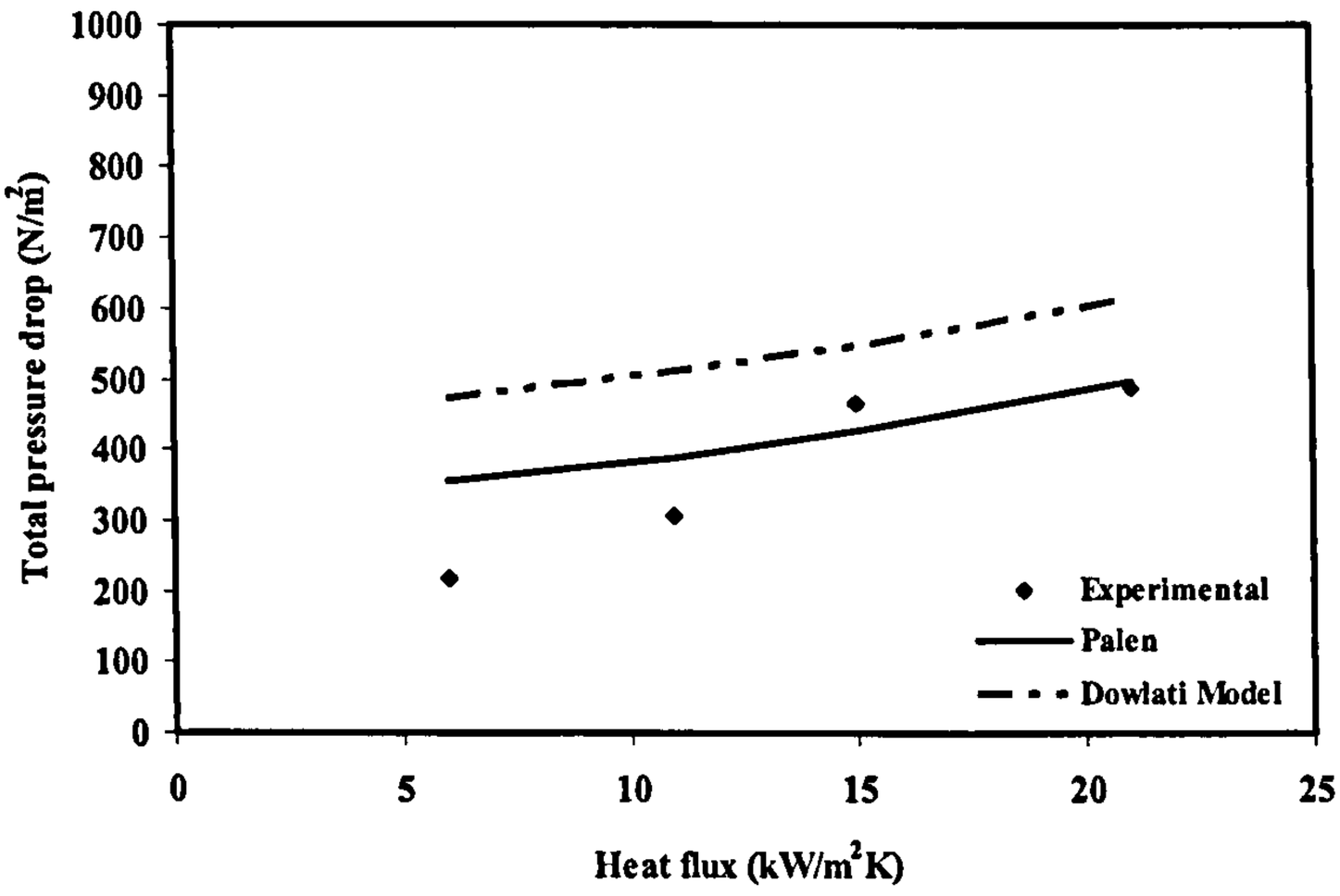

Figure 4.81 Comparison of total pressure drop against heat flux for G=10.6 kg/m^{2}s with distilled water

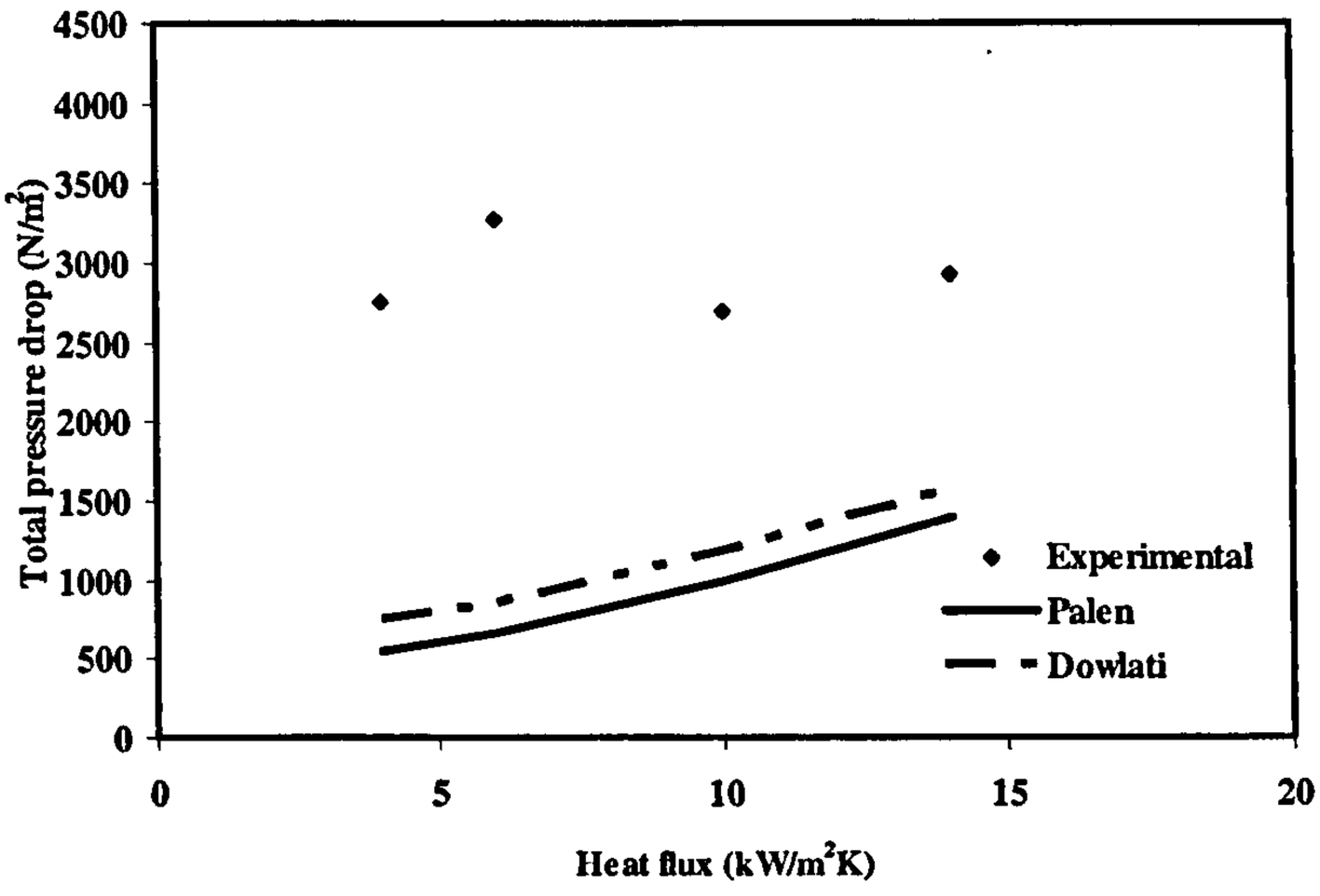

Figure 4.82 Comparison of total pressure drop against heat flux for G=13.1 kg/m^{2}s with R-113

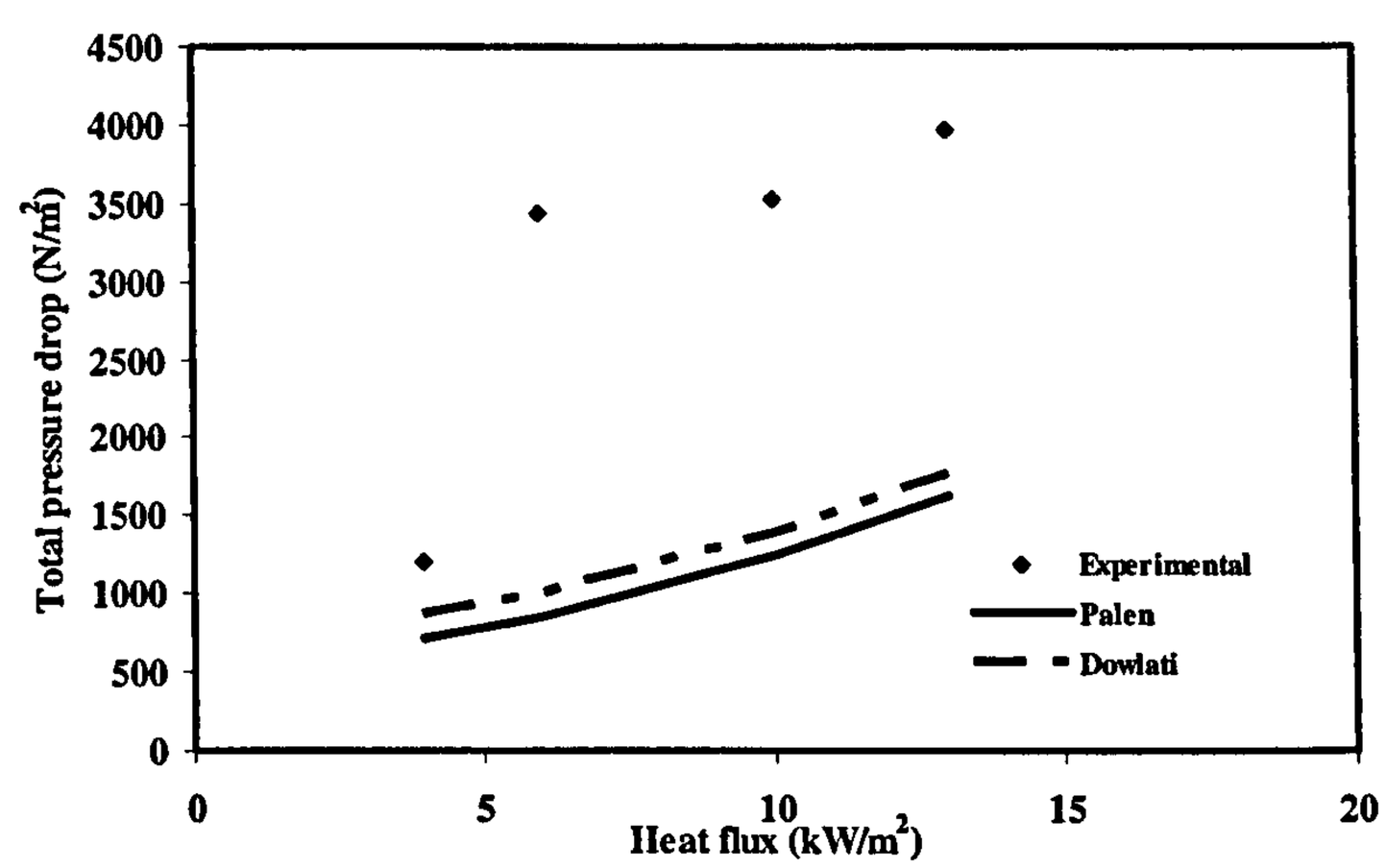

Figure 4.83 Comparison of total pressure drop against heat flux for G=19.7 kg/m^{2}s with R-113

4.6 Heat transfer mechanisms from photographic studies

It was necessary to supplement the temperature readings obtained in the previous sections with information about two-phase flow within the tube bundles. This allowed links between the fluid flow and the heat transfer from the tubes in the bundle to be established. High

speed photographic studies were used to take photos of the motion of the bubbles through the compact tube bundle. As discussed in the experimental programme, there was a glass window at the front and back of the test section. The high speed video camera was able to capture the mechanism occurring on column one of the bundle since it was impossible to capture the process in the central column. As such it was approximated that the glass and the front tubes could be regarded as another column. The regime of boiling observed in the bundle arrangement was divided into;

- Bubbly flow
- Nucleate boiling
- Confined flow

At low heat flux of 6 kW/m^2, and the mass flux of 10.6 kg/m^2s, fewer bubbles were generated on the tube. The pictures showed that only a small portion of the tubes were covered with bubbles and these bubbles were small in size whilst some of them tend to occupy the spaces between the tubes. More bubbles tend to rise up the bundle at moderate to heat flux of 15 and 21 kW/m^2 and the bubbles deformed on the surface of the tube or enveloping a portion of it. Surface tension played a role and it could be suggested that the bubbles have to deform through the small spaces in between the tubes. As the heat flux was increased the bubbles from the lower tube translates through the spacing in between the tubes to have influence on the upper tubes. At the heat flux of 21 kW/m^2, more bubbles are generated and this covered portions of the tubes. It is suggested that confinement of the bubbles has an influence on the heat transfer coefficient. Typical pictures at heat fluxes of 6, 11, 15 and 21 kW/m^2 are shown in Figure 4.84 to Figure 4.86. There were variations of the bubble sizes as it traverses from one tube to the other with both time and space. Typical photos shown in Figure 4.84 for q=6 kW/m^2 showed bubbles growing on tubes and covering portions. Analysis of bubble 'A' from t=0.0 sec to t=30ms showed that the diameter of the bubble had increased in size from 2 mm to 4 mm within this time interval. Unlike large diameter bundles the bubbles observe here are greater than the diameter of the tube. Bubble 'A' has moved from tube 4 to tube 5. Clearly the picture also showed that the bubble is held up in between the tubes. Similarly, bubble 'B' also showed an increase of

growth from 4 to 5mm in diameter and 5 to 7 mm in height. An extension of bubbles for q=15 and 21 kW/m^2 is shown in Table 4.5 and Table 4.9.

Time(sec)	d_a (mm)	h_a(mm)	d_b (mm)	h_b (mm)
0.0000	7	6	8	7
0.0042	8	7	9	7
0.0083	7	6	10	8
0.0125	7	6	8	8

Table 4.8 Growth of bubbles at q=15 kW/m^2 with distilled water

It could be deduced from the above, that bubbles grow as it travels up the bundle. There was also a deformation of the size. Confined bubbles were observed between tubes numbered 2 and 3 the height accounts for the micro layer evaporation within the bundle.

Time (sec)	d_a (mm)	h_a(mm)	d_b (mm)	h_b (mm)
0.0000	15	5	6	8
0.0042	16	4	17	10
0.0083	17	6	13	8
0.0125	23	8	13	9

Table 4.9 Growth of bubbles at q=21 kW/m^2 with distilled water

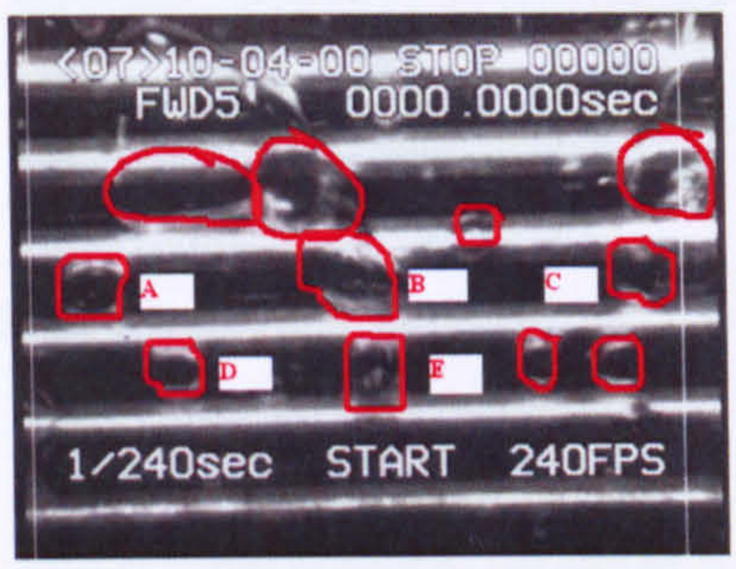

t= 0.000sec

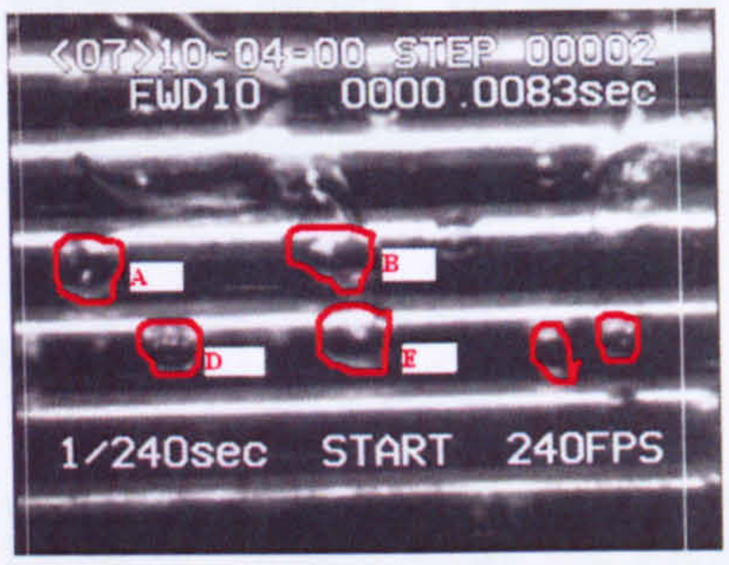

t=0.0083sec

t=0.0042sec

t=0.0125sec

Figure 4.84: Photos of bubbles at q=6 kW/m^2 at G= 10.6 kg/m^{2}s with distilled water. (Scale; 1mm: 1mm)

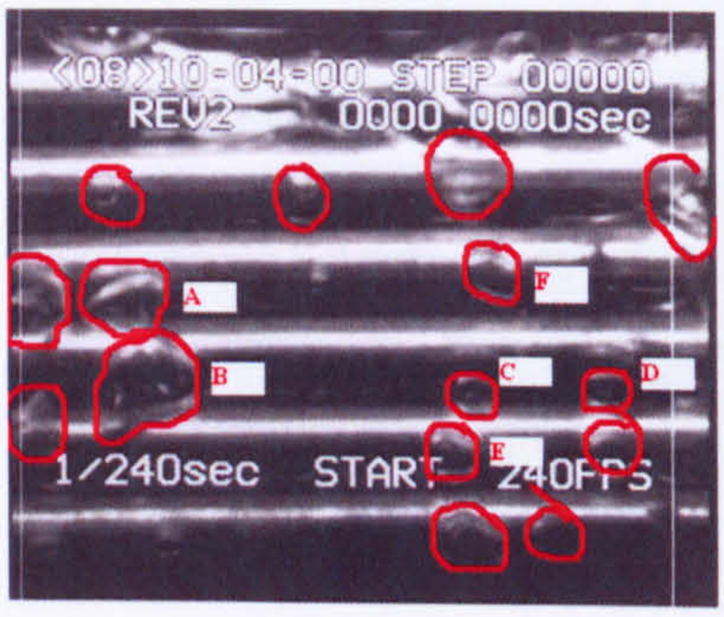

t=0.000sec

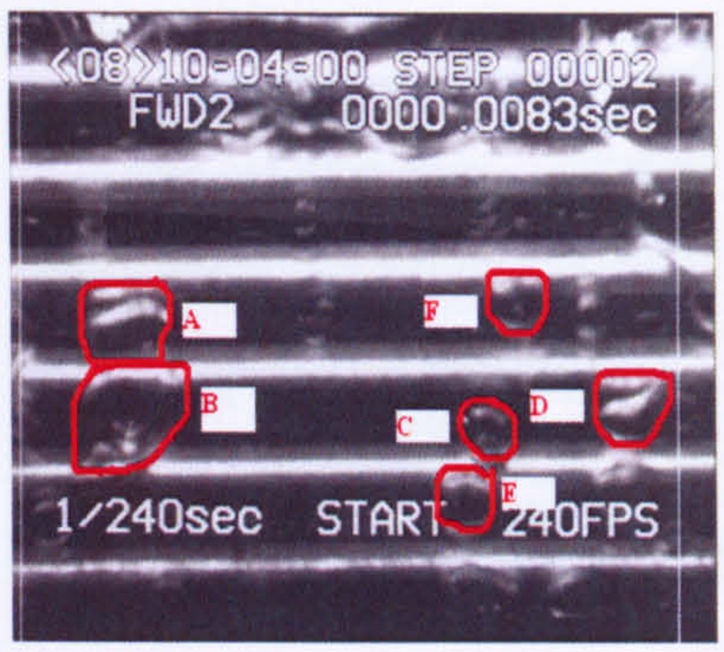

t=0.0083 sec

t=0.0042 sec

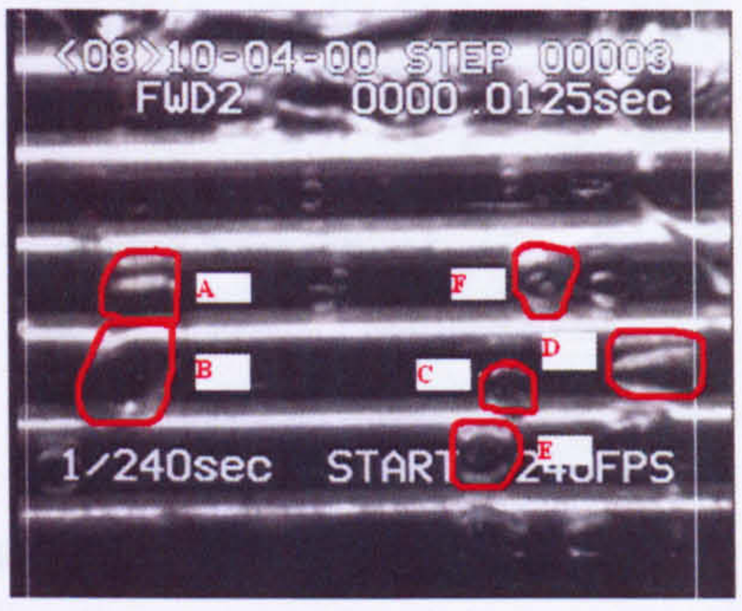

t=0.00125 sec

Figure 4.85 Photos of bubbles at q=15 kW/m^2 at G=10.6 kg/m^{2}s with distilled water (Scale; 1mm: 1mm)

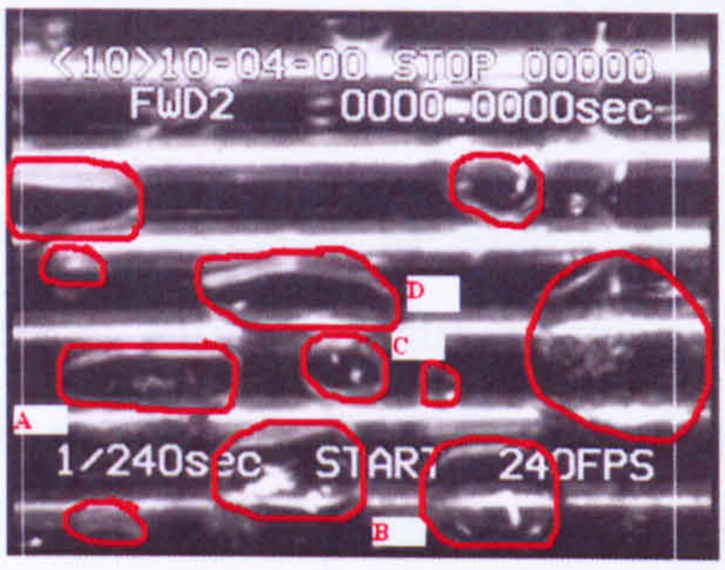

t=0.000 sec

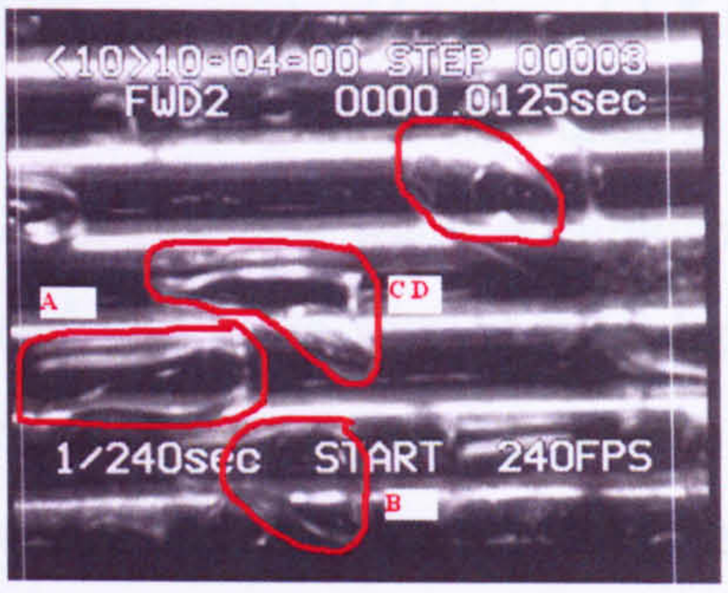

t=0.0125 sec

t=0.0042 sec

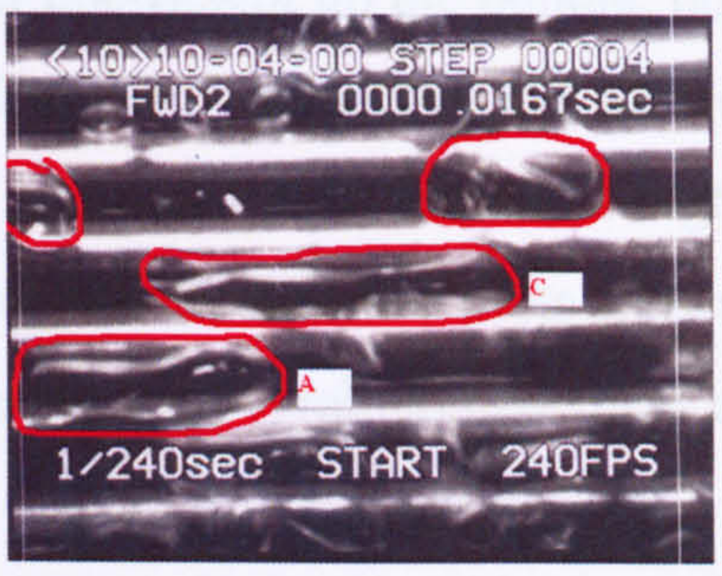

t=0.0167 sec

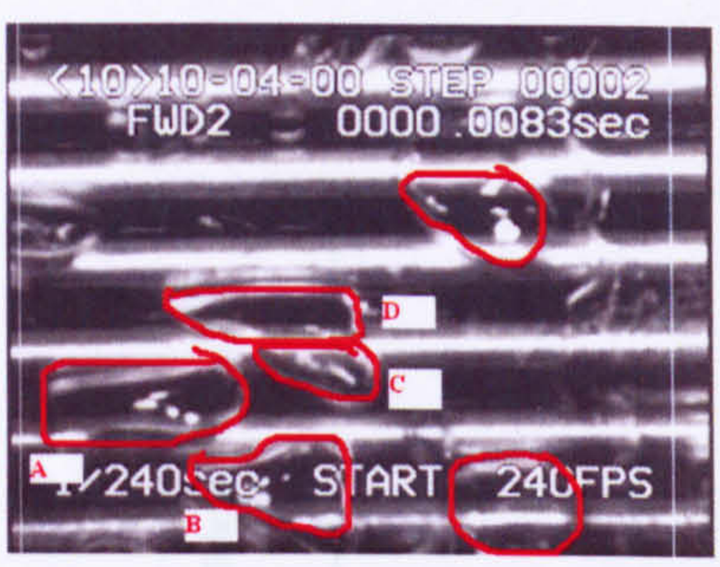

t=0.0083

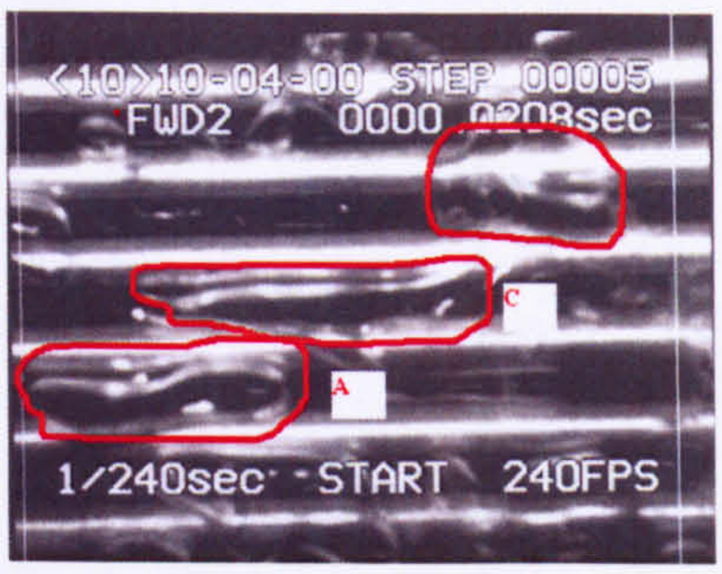

t=0.0208 sec

Figure 4.86 Photos of bubbles at q= 21 kW/m^2 with G=10.6 kg/m^{2}s with distilled water (Scale; 1mm: 1mm)

4.7 Comparison with the results of Gupta [65]

Gupta [65] investigated a tube bundle of diameter 19.05 mm with p/d ratios of 1.5 and 3 using distilled water as working fluid in a 5×3 arrangement. The mass flux used in their work was identical to what is reported in this thesis for distilled water at atmospheric pressure, with heat flux in the range of 10-40 kW/m^2 and mass flux of 0-10 kg/m^{2}s. Their results obtained are compared with experimental results showed in Figure 4.87 and Figure 4.88. It could be deduced from the plots that the compact tube bundle was more enhanced compared to the results of Gupta [65]. The effect of mass flux was clearly indicated for the mass flux of G=5.6 and 10.6 kg/m^{2}s. It was observed that the Gupta [65] results showed an increase in heat transfer coefficient up the bundle, but this was quite opposite in the compact tube bundle. The result confirms the theoretical conception that the local heat transfer coefficient in a compact tube bundle is higher at low vapour quality compared to a large diameter tube bundle. The two plots shows that the gap between the tubes is less significant compared to the overall compactness of the bundle.

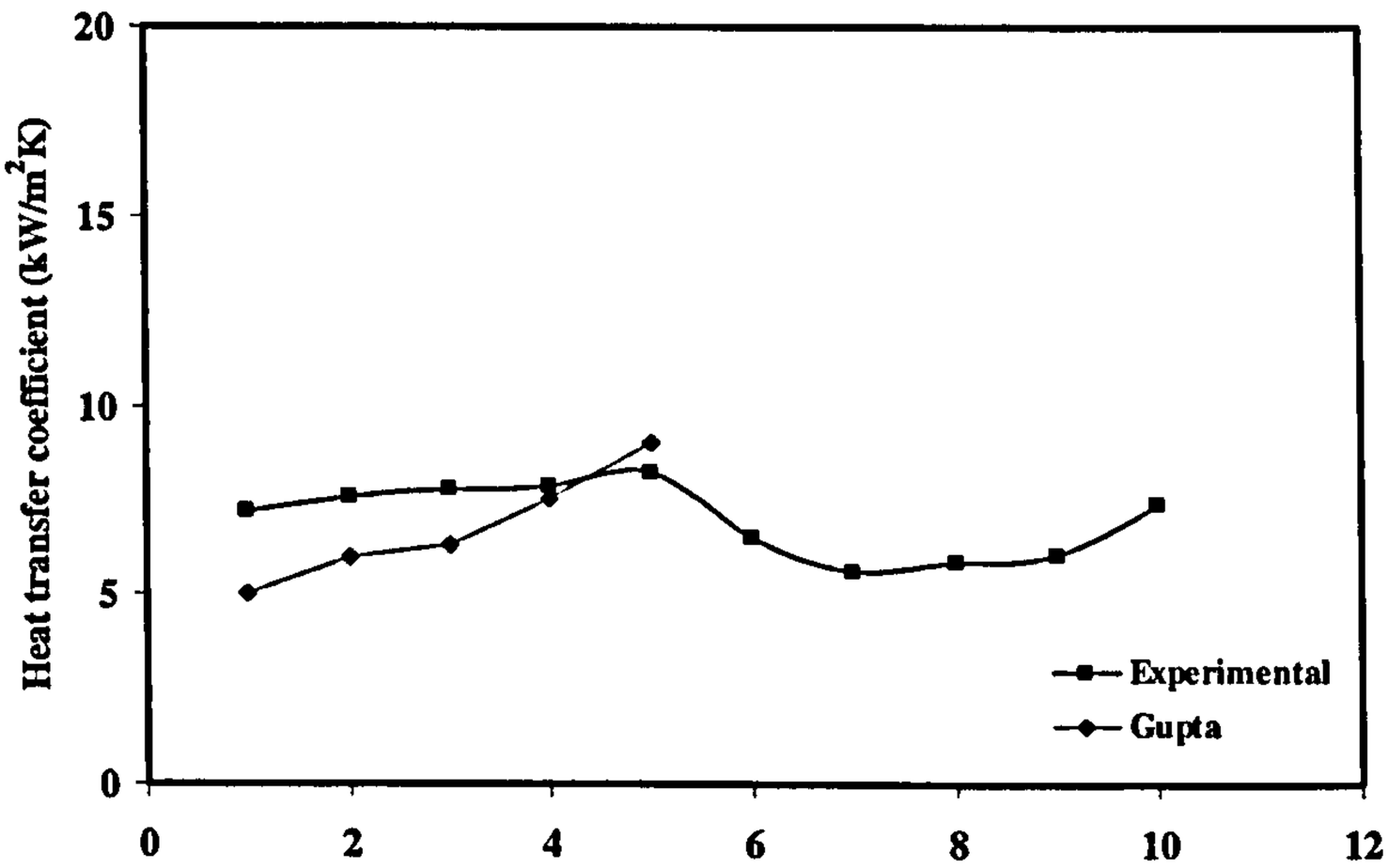

Figure 4.87 Comparison of experimental results with data from Gupta [65] for G=10.6 kg/m^{2}s and q=11 kW/m^2.

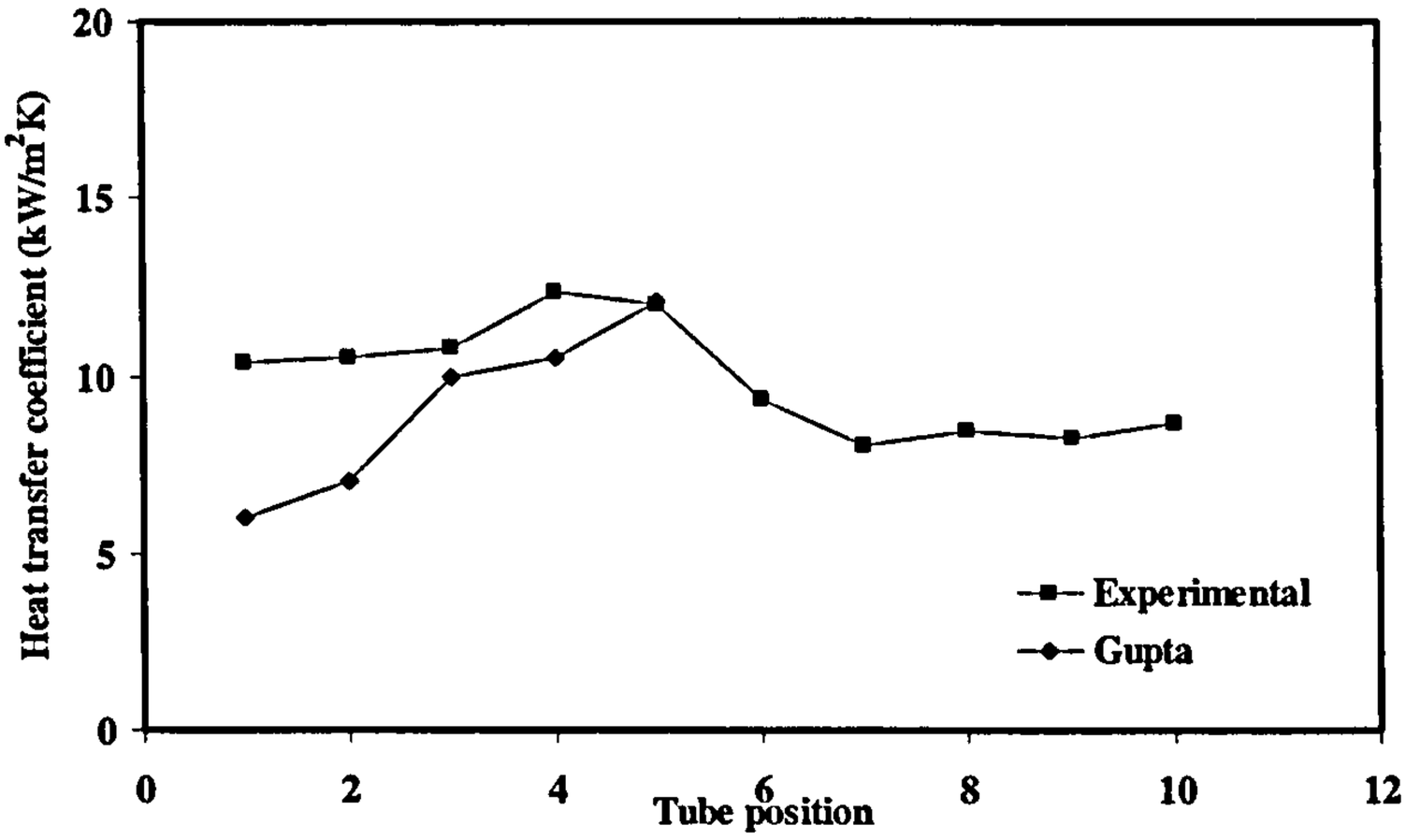

Figure 4.88 Comparison of experimental results with data from Gupta [65] for G=10.6 kg/m^{2}s and q=21 kW/m^2 with distilled water.

4.8 Concluding remarks

An experimental study has been carried out for single tubes and twin tubes in pool boiling. The following remarks are made;

- Results indicated that the boiling mechanism occurring on small tubes were different as the presence of translating bubbles accounted for the heat transfer

- Correlations that have been developed for large diameter tubes and flat plates have been tested against experimental results and none of these was able to satisfactorily predict the experimental results for the working fluids that were used

- Results obtained for the twin tube arrangement also showed that the presence of the tube below acting as vapour generator enhanced the heat transfer coefficient of the upper tube. It is suggested that the thermal boundary layer of the upper tube was disrupted as a result of the bulk movement of bubbles and also translating bubbles from the lower tube.

- The heat transfer coefficient within a compact tube bundle has been discussed and it has been shown that the effect of quality is minimal on the results. The

results showed a strong dependence on the applied heat flux for all the working fluids. Photographic studies showed that bubbles moving up the bundle are confined and these affect the heat transfer coefficient on upper tubes.

Chapter 5

THEORETICAL CONSIDERATIONS

5.1 Introduction

The chapter will discuss various aspects of heat transfer mechanisms that are pertinent during pool boiling as well as flow boiling outside small diameter tubes. It is a generally accepted fact that models that have been developed for macro channels cannot be applied with confidence to boiling heat transfer in compact arrangement. The work discussed here is of pioneering nature and as such ideas derived from large tubes boiling as well as boiling in the inside of micro channels are extended here. The confinement number has been developed for boiling heat transfer in micro channels and Cornwell and Kew [106] suggested a value of 0.50 above which the effect of gap size becomes significant. This approach is extended to compact tube bundles to investigate the effect of bubbles on a tube within the bundle. The twin tube results obtained in Chapter 4 are also analysed as to the effect of bubble size and its variation on the upper tube. It is suggested that the enhancement observed on the upper tube was due to translating bubbles from the lower tube. Analysis of a bubble past a tube is presented and discussed in relation to the experimental results. An attempt would be made to reconcile the mechanisms occurring in the compact tube bundle and the twin tube arrangement.

In summary this chapter will consider the following points in relation to the deductions made from experimental results in Chapter 4;

- Confinement number as applied to a compact tube bundle
- Film thickness under a growing bubble
- Analysis of a bubble past a tube under constant temperature
- Transient analysis of a bubble past a tube

5.2 Confinement number

Confinement number has been used to differentiate the differences between macro and micro channels. Cornwell and Kew [106] has defined confinement number based on the surface tension forces and fluid properties as ;

$$C_o = \frac{\sqrt{\left(\sigma / g(\rho_l - \rho_g)\right)}}{d} \tag{5.1}$$

where d is the hydraulic diameter.

Several investigators have reported the importance of confinement number during two-phase flow within a tube. The confinement number relates to the buoyancy force and the surface tension force on a bubble. Thus increasing confinement number increases the influence of surface tension. Some works of previous authors are discussed in relation to its applicability to this work.

Wallis [120] reported the effect of rise velocity on the bubble in a vertical circular tube. He presented three equations which depended on whether surface tension, viscosity or inertia is the dominant forces on a bubble. The condition for the bubble to be restricted by the effect of surface tension was given by the Eotvos number as;

$$N_{EO} = \frac{gd^2(\rho_l - \rho_g)}{\sigma} < 3.37 \tag{5.2}$$

Equation (5.2) may be arranged to give;

$$d < 1.84\left[\frac{\sigma}{g(\rho_l - \rho_g)}\right]^{1/2} \tag{5.3}$$

Thus the confinement number is given as;

$$C_o > 1/1.84 \tag{5.4}$$

It could be concluded that for confinement number greater than 0.543, bubbles of diameter been equal to tube diameter will be motionless in a vertical tube.

In a related study, Wallis and Makkendry [121], reported the counter-current flow of gas and liquid does not occur if the tube diameter given by the dimensionless expression (5.4), is less than 2. They developed an equation which is given as;

$$d^* = \frac{d}{\left[g\left(\rho_l - \rho_g\right)/\sigma\right]^{1/2}} \tag{5.5}$$

It is observed from the Equation (5.5) that d^* is the reciprocal of the confinement number, which is consistent with Equation (5.4) and gives a confinement number of 0.5.

Boundurant and Westwater, [122] investigated the boiling heat transfer from a closely spaced fins. At smaller spacing there was interaction between bubbles and the fins. Using the expressions developed by Kutadeladze [123] for bubble departure diameter which was given as;

$$d_b = 0.02\theta\left[\frac{\sigma}{g\left(\rho_l - \rho_g\right)}\right]^{1/2} \tag{5.6}$$

It could be deduced that confinement would be dominant if,

$$\frac{\left[\sigma/\left(g\left(\rho_l - \rho_g\right)\right)\right]^{1/2}}{s_f} > \frac{1}{0.02\theta} \tag{5.7}$$

where θ is the contact angle of the fluid in degrees and s_f is the fin spacing . The contact angles for common fluids such as water has been reported by Thome [124] to be in the range of 25°-90°

Yao and Chun [125] investigated the boiling heat transfer in a confined annulus with distilled water, Freon 113 and acetone at atmospheric pressure with gap sizes of 0.32, 0.8 and 2.58 mm. They reported that the boiling curve varied with the Bond number, defined in terms of the gap size δ,

$$Bo = \frac{\delta}{\left[\sigma / \left(g\left(\rho_l - \rho_g\right)\right)\right]^{1/2}} \tag{5.8}$$

They observed that the effect of confinement was significant when the gap size reduces and as such Bond number was unity or less, thus for confinement to be significant $C_o >$ 0.5.

The confinement that has been developed for boiling heat transfer in small tubes and channels is extended to the compact arrangement used in this thesis. A still photographic camera was used to capture the movement of a cylindrical bubble through the bundle using distilled water. Observation showed that when the liquid is stationary bubbles can be trapped below the tube which is shown in Figure 5.1.

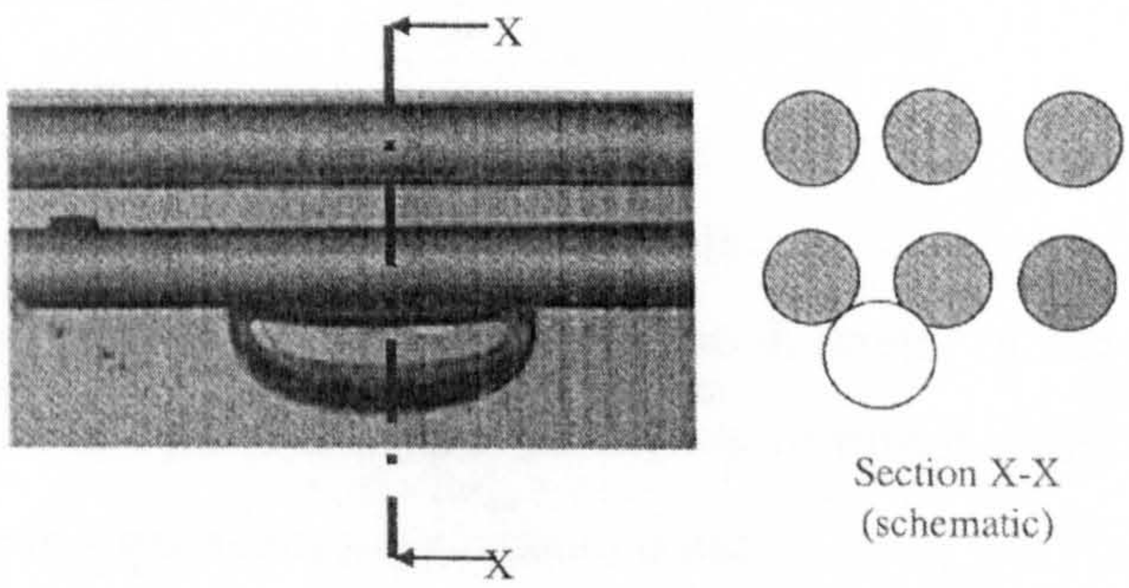

Figure 5.1 Stationary bubble below tube bundle .Kew , Adom and Cornwell [67]

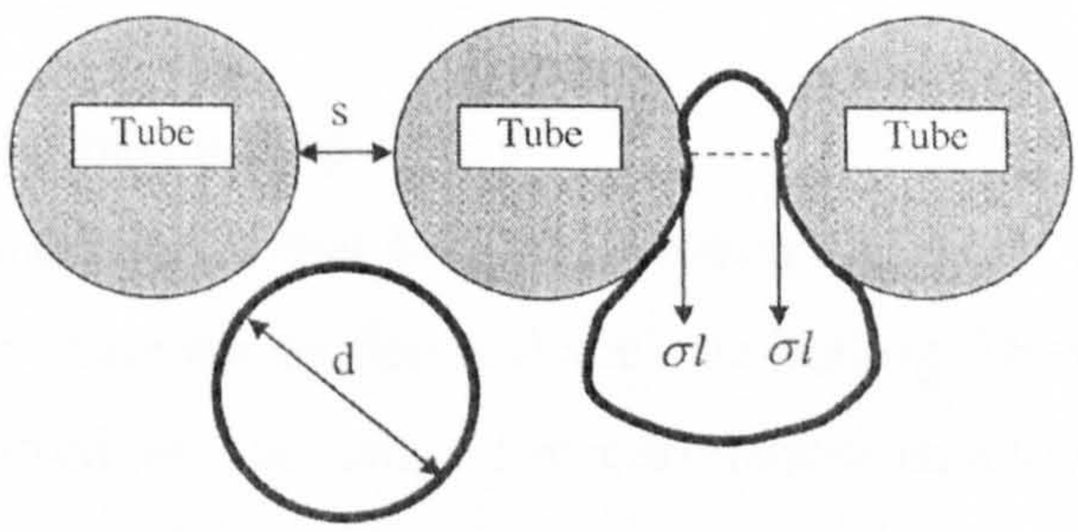

Figure 5.2 Schematic representation of bubbles supported within a compact tube bundle. Kew , Adom and Cornwell [67]

The bubbles shown in Figure 5.2 are approximated to be rising from the lower tube and are regarded as a cylinder with length *l*. The bubbles must be distorted in order to pass through the spacing s between the tubes.

The buoyancy force acting on the bubble is given as;

$$F_b = \frac{\pi d^2}{4} g(\rho_l - \rho_g) l \tag{5.9}$$

The downward component is the surface tension force;

$$F_s = 2\sigma l \tag{5.10}$$

Equating the two forces yields;

$$d = \frac{\sqrt{\sigma / (\rho_l - \rho_g) g}}{0.63} \tag{5.11}$$

If the spacing between the tubes is larger than the diameter of the bubble then the effect of surface tension on the motion of the bubbles is minimal, otherwise the condition for which confinement is significant may be stated as;

$$C_o = \frac{\sqrt{\sigma / g(\rho_l - \rho_g)}}{s} > 0.63 \tag{5.12}$$

5.3 Heat transfer mechanism

The heat transfer mechanism that has been observed in large tube is predominantly a combination of two phase convection and nucleate boiling. The Chen [18] superposition model has been used as the basis for correlation development. This correlation developed for in tube boiling has over the years been applied to boiling outside tube bundles with modifications made to the suppression and enhancement factors. Such methods were adapted by Hwang and Yao [63], Steiner and Taborek [126] and more recently Webb and Gupte [90]. This same model for boiling inside large tubes has been applied to the development of models for the mini and micro channels.

The mechanism of heat transfer over large tube bundles has been generally accepted to be that sliding bubbles as reported by Cornwell [44] and also two-phase convection was responsible for the enhancement observed at higher tubes within a kettle reboiler.

5.3.1 Nucleate boiling component

Various correlations have been developed for the pool boiling heat transfer coefficient for a flat plate or a horizontal tube. Experimental results obtained in this work for small diameter tubes are used in the development of a model.

The results obtained are of the form;

$$\alpha_{npb} = Cq^n \qquad (5.13)$$

These correlations have been summarized in Table 4.1. The exponent n in equation (5.13) lies between 0.5 and 0.7 for large tube diameters and flat plates. The constant C depends on the fluids properties such as the critical pressure, surface finish, and molecular mass. The literature reviewed indicated that flow boiling across a tube or a tube bundle the nucleate boiling component is suppressed by the velocity of the fluid. Due to suppression, Equation (5.13) is recast as;

$$\alpha_{nb} = S\alpha_{npb} \qquad (5.14)$$

where 'S' is the suppression factor

5.3.2 Sliding bubble mechanism

Nakajima [49] observed that large bubbles of the size of the clearance between the tube bundle used in their experimental set up heat transfer was analysed using the linear conduction through the thin film which is analogous to that developed by Cornwell and Schuler [44], the difference been that the sizes of bubbles observed. The work of Cornwell and Schuler [44] using photographic studies outside tube bundle revealed multiple of small bubbles which grows rapidly and slides on the side of the tube as shown in Figure 5.3.

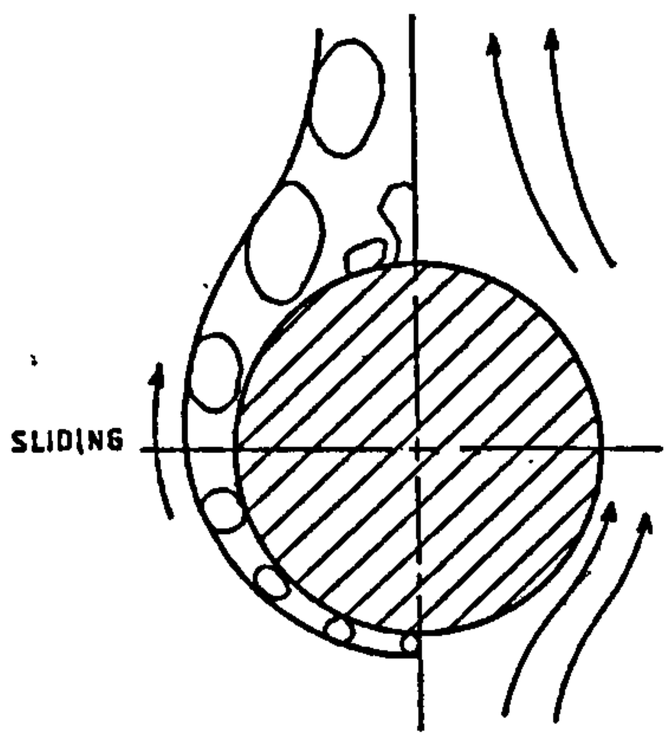

Figure 5.3 Sliding bubble over a large tube, Cornwell and Schuler [44]

Heat is transferred by linear conduction through a film that is laid beneath a bubble which is given as;

$$\alpha_{sb} = \frac{k_l}{\delta} \tag{5.15}$$

The film thickness in the above expression remains relatively constant during the passage. For small diameter tubes, the photographic study reported in Chapter 4 for single tubes has confirmed that for tube diameter of 3.0mm the sliding bubble mechanism is minimal and it cannot account for the total heat transfer coefficient.

5.3.3 Forced Convection

Forced convection has been found to be an important component in most boiling heat transfer analysis. In flow boiling it has been found to contribute to the heat transfer coefficient. It depends on factors such as quality and local liquid velocity. The heat transfer coefficient for single phase is given by the Dittus-Boelter correlation as;

$$\alpha_l = 0.023 \frac{k_l}{d} \mathrm{Re}_l^{0.8} \mathrm{Pr}_l^{0.4} \tag{5.16}$$

where the liquid Reynolds number is given as;

$\mathrm{Re}_l = \dfrac{Gd(1-x)}{\mu_l}$; and Prandtl number is given as;

$$\Pr = \frac{\mu C_p}{k_l}$$

The convective component is given as;

$$\alpha_c = F\alpha_l \tag{5.17}$$

The enhancement F takes into consideration the effect of turbulence and velocity of vapour bubbles induced during the flow. Several correlations are available in the literature which have been established for the factor F such as those of Chen [18], Webb and Chien [90] and Steiner et al [126].

5.3.4 Combination of heat transfer mechanism

The heat transfer mechanism observed from the experimental and photographic studies for the upper tube is a combination of nucleate boiling, sliding bubbles and convective heat transfer coefficient. The heat transfer mechanisms could be written as;

$$\alpha = f\left(\alpha_{nb}, \alpha_{cv,} \alpha_{tf}\right) \tag{5.18}$$

The variables could be determined from appropriate boiling correlations.

5.3.5 Heat transfer due to natural convection

Natural convection has to be considered at areas where there is no nucleate boiling. The area available for natural convection decreases as the nucleation site density increases. The natural convection component is assumed to be zero since boiling takes place at fully developed nucleate boiling.

5.4 Void fraction

Models for two-phase flow can be used to compare the difference between the liquid and vapour velocities. The homogeneous model is a particular flow model in which the phase velocities are considered to be the same. This approach is used to estimate the void fraction in the compact tube bundle to compare it with experimental results. The homogeneous model void fraction for the two phase flow is given as;

$$\varepsilon = \frac{1}{1+\left(\frac{u_g}{u_l}\frac{1-x}{x}\frac{\rho_g}{\rho_l}\right)} \tag{5.19}$$

For homogeneous flow the phase velocities are equal, the void fraction becomes

$$\varepsilon = \frac{1}{1+\left(\frac{1-x}{x}\frac{\rho_g}{\rho_l}\right)} \tag{5.20}$$

The experimental values of void fraction were determined from sample pictures that were obtained using the high speed video camera. It was difficult to experimentally measure the void fraction from the test section, but photos of the third column could be used as a basis in the evaluation of the void fraction and compares it with correlations that have been developed for large tube bundles. A systematic approach was used to estimate the portion of tubes covered with vapour bubbles to the ratio of the total area of the third column. Some two-phase void fraction correlations that have been used by several authors in the estimation of the void fraction are discussed. The commonest are those of Premoli, Zivi and Chisholm. The correlation for Premoli [127] et al is given by;

$$\varepsilon = \frac{1}{1+\left(S\frac{1-x}{x}\frac{\rho_g}{\rho_l}\right)} \tag{5.21}$$

Zivi's [128] correlation for the void fraction is given as;

$$\varepsilon = \frac{1}{1+\left(\frac{1-x}{x}\right)\left(\frac{\rho_g}{\rho_l}\right)^{2/3}} \tag{5.22}$$

The Chisholm [129] correlation is given as;

$$S = \left[1-x\left(1-\frac{\rho_l}{\rho_g}\right)\right]^{1/2} \tag{5.23}$$

For all the models shown above the differences lies in the estimation of the slip ratio S. These models are used to estimate the void fraction in the compact tube bundle. The total thermodynamic quality is used in all the calculations that are presented. Thus the heat transfer coefficient increases with quality up the bundle which is the case for a large tube bundle. This analysis does not tie to the experimental results, as the heat

transfer increases to tube position number four then a sudden drop in heat transfer coefficient as the quality increases. Therefore it is suggested that there is micro layer evaporation as the possible heat transfer mechanism.

5.5 Twin tube

The model presented here attempts to investigate the enhancement observed on the upper tube of a twin tube arrangement. It is also the intention to apply similar arguments for a compact tube bundle which was discussed earlier in the chapter.

The model presented here is given as;

$$\alpha = p\alpha_{tf} + (1-p)\alpha_{nb} \tag{5.24}$$

where α is the heat transfer coefficient for the upper tube, α_{nb} is the nucleate boiling heat transfer coefficient at the appropriate heat flux and α_{tf} is the heat transfer coefficient through a thin film laid down by translating bubbles originating from the lower tube. Analysis from the experimental results indicates the heat transfer of the upper tube is enhanced by translating bubbles from the lower bubbles up to a particular value equating the point where the heat flux q yields a total enveloping of the tube. It is suggested that this is due to the effect of bubbles from the lower tube passing over the upper tube. The model assumes that the translating bubbles envelop a portion p of the length of the tube and heat is transferred by nucleate boiling from a fraction *(1-p)*. The factor p may be applied instantaneously to a length of the tube or represent the proportion of the time during which a single point is traversed by translating bubbles.

Under boiling conditions without the presence of the lower tube the total heat transfer coefficient is given by the nucleate boiling alone;

$$\alpha_{nb} = S\alpha_{npb} \tag{5.25}$$

The value of α may be more than α_{nb} (as immediately after the passage of the translating bubble while a layer of liquid is evaporating under the bubble) or less than α_{nb} (as later in the passage when the liquid layer has evaporated away or when the intensity of the passing bubbles precludes sufficient liquid reaching the tubes, typically at high heat

flux). The enhancement Δα of boiling on the upper tube over that of pure nucleate boiling is given by;

$$\Delta\alpha = p(\alpha_{tf} - \alpha_{nb}) \tag{5.26}$$

It has been shown in the previous section that there is suppression of nucleate boiling when a tube is undergoing pure pool boiling. It is therefore logical to include terms that would account for the suppression as well as enhancement due to the turbulence caused by passing vapour bubbles. The model is then given as;

$$\alpha_{total} = (S\alpha_{nb} + \alpha_{conv})(1-p) + p\alpha_{tf} \tag{5.27}$$

Therefore the enhancement on the upper tube is given as;

$$\Delta\alpha = p\lfloor\alpha_{tf} - S\alpha_{npb} - \alpha_{cv}\rfloor + \alpha_{cv} \tag{5.28}$$

Thus the above equation takes into account the turbulence of bubbles as it translates on the tubes. It is also recognizable that the nucleate boiling coefficient is suppressed and it has also been accounted for.

5.5.1 Determination of p from photographic studies

It is assumed that the tube is covered by bubbles from lower tube and the heat transfer coefficient through the film contributes to the total enhancement on the upper tube. *p* was determined from analysis of photos obtained from experimental work. *p* could be determined from either time or space model and sample photos used showed a variation of bubbles with time. Typical *p* against time is shown in Figure 5.4

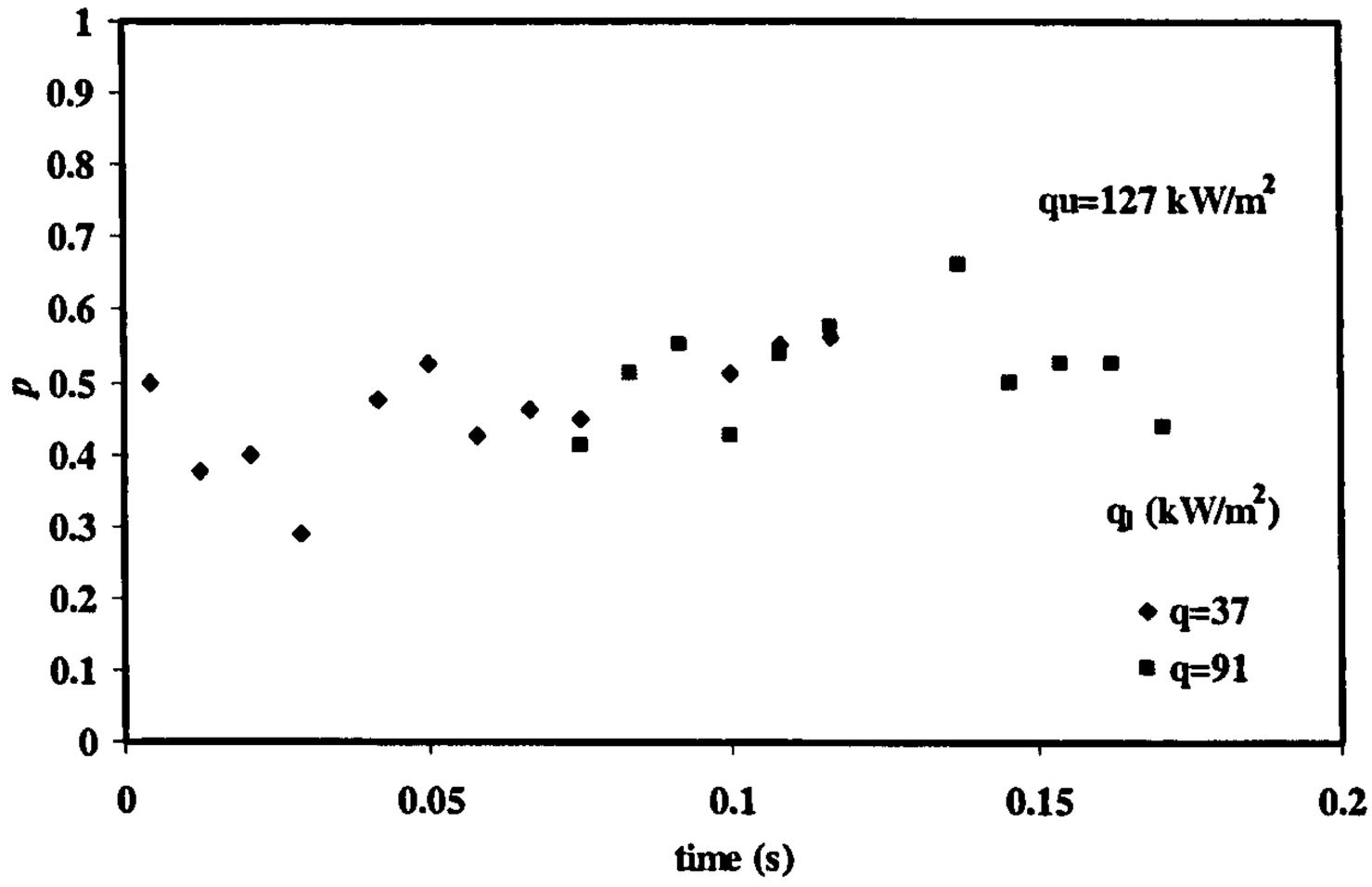

Figure 5.4 Variation of p with time for 3.0 mm tube with distilled water.

5.5.2 Film Thickness

Sliding bubble has been accounted for the mechanism of heat transfer on a large tube by Cornwell and Schuler [44] using photographic studies. Studies by Addlessee [82] as shown in the literature review has film thickness of the order of 200-300μm. This work corroborated by Kenning, Buttress et al [84] shows that the thickness is between 50-70μm on a vapour under an inclined plane. The proceeding paragraph illustrates the derivation of the film thickness under the bubble at a given time, with the assumption that there is no nucleate boiling under the film.

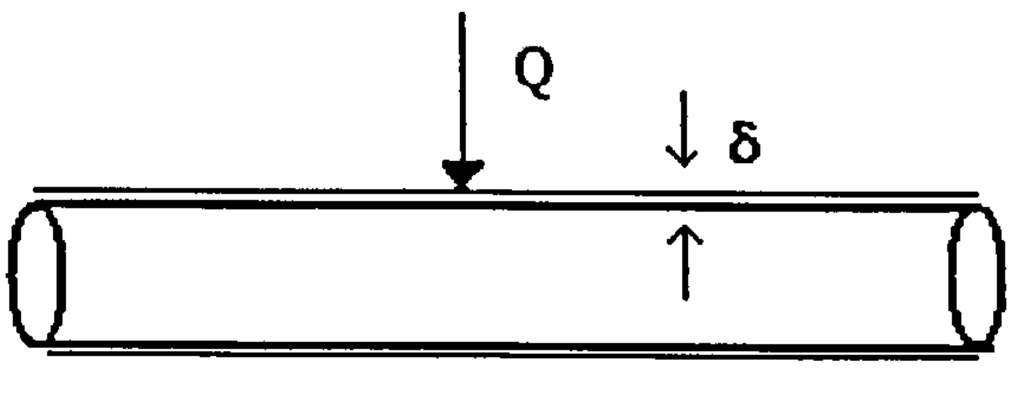

Figure 5.5 Schematic representation of a tube with a passing bubble.

For heat flow through the film as shown in Figure 5.5, the heat flow through the bubble is given as;

$$Q = -\frac{dm_l}{dt} h_{fg} = -\rho_f A \frac{d\delta}{dt} h_{fg} \tag{5.29}$$

Also

$$Q = q_{if} A \tag{5.30}$$

Equating Eq (5.29) and Eq.(5.30) we have ;

$$d\delta = -\frac{q_{if}}{\rho_f h_{fg}} dt \tag{5.31}$$

The heat flux density through the film is by linear conduction such that;

$$q_{if} = \frac{-k_f \Delta T}{\delta} \tag{5.32}$$

Substituting equation (5.32) into equation (5.31), we have;

$$\int_{\delta_i}^{\delta} \delta d\delta = \int_0^t \frac{k_f \Delta T}{\rho_f h_{fg}} dt \tag{5.33}$$

this gives film thickness as a function of time as;

$$\delta^2 = \delta_i^2 - \left(\frac{2\Delta T k_f}{\rho_f h_{fg}} \right) t \tag{5.34}$$

Substituting typical values into the equation (5.35) for distilled water ΔT=5K, δ_i=50μm, k_f=0.681W/mK, ρ_f=958kg/m^3 and h_{fg}=2257000J/kg. The time of 0.0083s used in the equation is typical passing period that was obtained using the high speed video camera;

$$\delta = \left((50 \times 10^{-6})^2 - \frac{2 \times 5 \times 0.681 \times 0.0083}{958 \times 2257000} \right)^{0.5} = 49.94 \mu m$$

The analysis shown in Figure 5.6 based on equation (5.34) shows that the film thickness does not change significantly during the passage of a bubble with time; actually it is approximately equal to the initial film thickness.

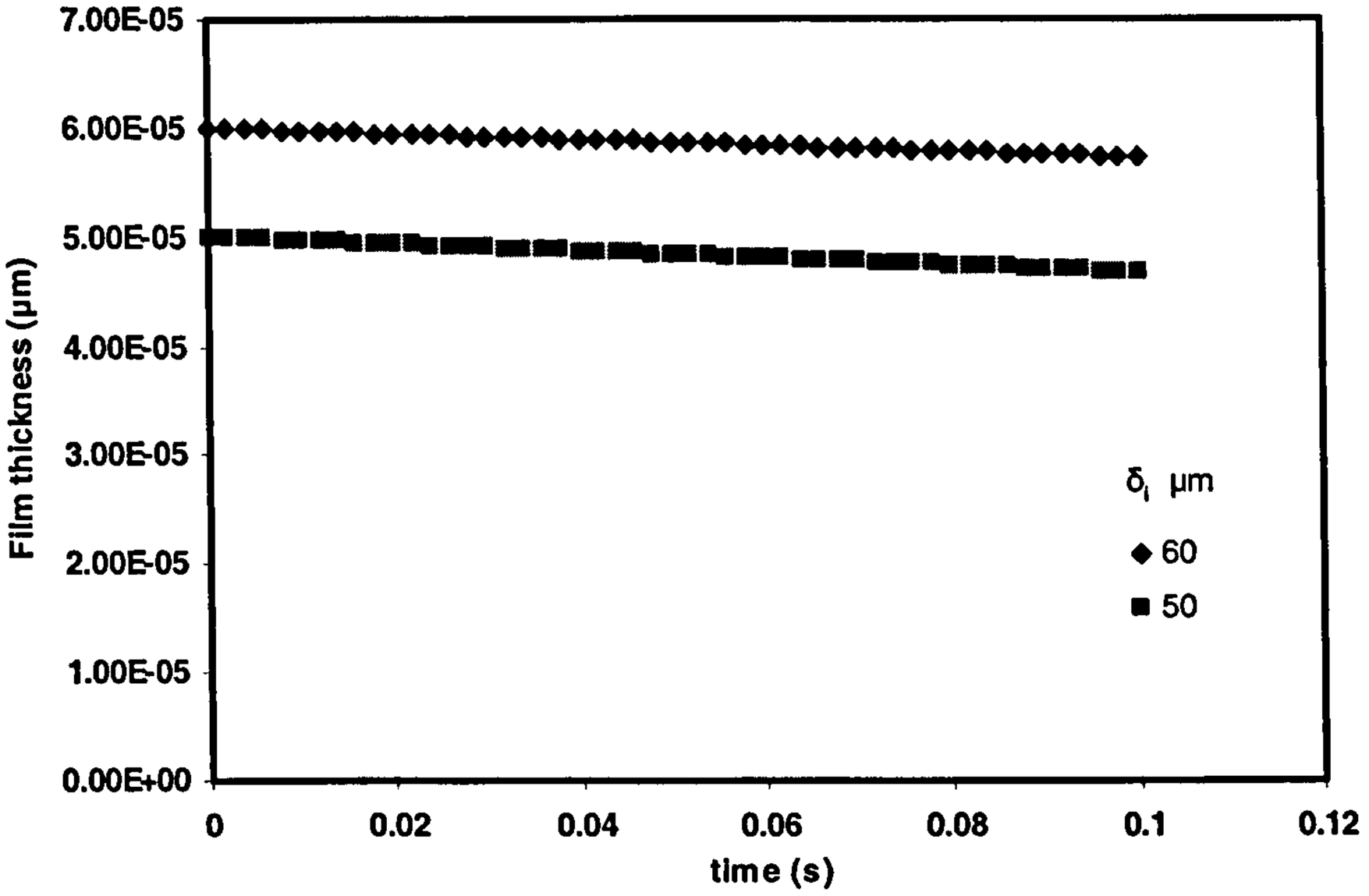

Figure 5.6 Variation of film thickness with time for distilled water.

The dryout time occurs when the film thickness is zero, thus using equation (5.34) δ equals zero, gives;

$$t_d = \frac{\delta^2{}_i \rho_f h_{fg}}{2\Delta T k_f} \tag{5.35}$$

Substituting typical values of the properties of distilled water into equation (5.35) gives;

$$t_d = \frac{\left(50\times10^{-6}\right)^2 \times 958 \times 2257000}{2\times5\times0.681} = 0.7940s$$

Extrapolating from the graphs shown in Figure 5.6 it is clear that under the conditions observed in the experiment for the twin tube, dryout was not achieved and the theory supports this. Analysis of bubble which translates over a tube is presented in the proceeding section to determine the effect of steady state and transient effects.

5.6 Constant temperature difference

This section deals with the analysis of a bubble past a tube where a bubble translates past a section of the tube. The section present the amount of heat transferred within a

cubic bubble, the growth of the bubble and also the average heat transfer coefficient through the bubble. For the purpose of this analysis we assume that the temperature difference between the film and the heater surface is constant. The following assumptions are made;

- The tube is isotropic i.e. the thermal conductivity, density does not change with position.

- The liquid film remains attached to the wall of the tube.

- The thickness of the film is very small compared to the diameter of the tube.

The heat flux across the thin film is then obtained as;

$$q_{tf} = \frac{-k_f \Delta T}{\left[\delta_i^{\,2} - \left(\frac{2\Delta T k_f}{\rho_f h_{fg}}\right) t\right]^{1/2}} \tag{5.36}$$

For this analysis it is assumed that the bubble grows owing to the evaporation of micro layer only. This assumptions means that transient cooling of the heater surface during growth, the consideration of vapour at the outer parts of the bubble and the sensible heat content of the micro layer are all ignored. A cubical bubble (Figure 5.7) of size *s* passing over a tube is analysed.

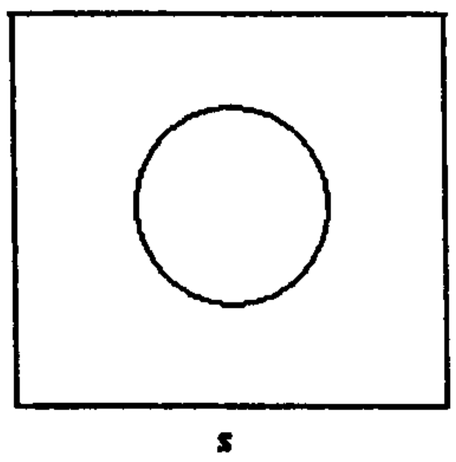

Figure 5.7 End view of cubical bubble of initial size *s* on the surface of a tube.

The expression for the heat flow to the bubble then becomes (assuming a cubic bubble) proceeds as;

$$Q = qAdt \tag{5.37}$$

The heat transferred to the bubble

$$Q = \rho h_{fg} \frac{dV}{dt} \tag{5.38}$$

where dV is change in volume of the bubble and q is average heat transfer rate through the film during the passage time of the bubble. The area of the bubble in contact with the tube is given as;

$A = \pi Ds$ and the volume as;

$V=s^3$ then

$$\frac{dV}{ds} = 3s^2$$

Substituting A, Q and q into equation (5.38) we have;

$$qdt = \frac{3\rho h_{fg} sds}{\pi D} \tag{5.39}$$

Integrating the equation above we have;

$$\int \frac{-k_f \Delta T}{\left[\delta^2{}_i - \left(\frac{2\Delta T k_f t}{\rho_f h_{fg}}\right)\right]^{0.5}} dt = \int_{si}^{sf} \frac{3\rho h_{fg} sds}{\pi D} \tag{5.40}$$

$$\left[\rho_f h_{fg}\left(\delta^2{}_i - \left(\frac{2\Delta T k_f t}{\rho_f h_{fg}}\right)\right)^{1/2}\right] = \frac{3\rho_f h_{fg}}{2\pi D}\left[s^2{}_f - s^2{}_i\right]$$

$$\left[\delta^2{}_i - \frac{2\Delta T k_f t}{\rho_f h_{fg}}\right]^{1/2} = \frac{3}{2\pi D}\left[s^2{}_f - s^2{}_i\right]$$

The final size of the bubble is given as;

$$s^2{}_f = s^2{}_i + \frac{2\pi D}{3}\left[\delta^2{}_i - \left[\frac{2\Delta T k_f t}{\rho_f h_{fg}}\right]\right]^{1/2} \tag{5.41}$$

Equation (5.42) shows an increase of bubble growth size with time which is shown in Figure 5.8. The plot is for a fixed size of bubble of initial size 0.003m and using the properties of distilled water. There is a decrease in size of the bubble due to the micro layer evaporation under the bubble. In effect the area of the bubble in contact with the tube reduces. This is in contrast to the case where the bubbles coalesce on the tube which results in the growth of the bubble.

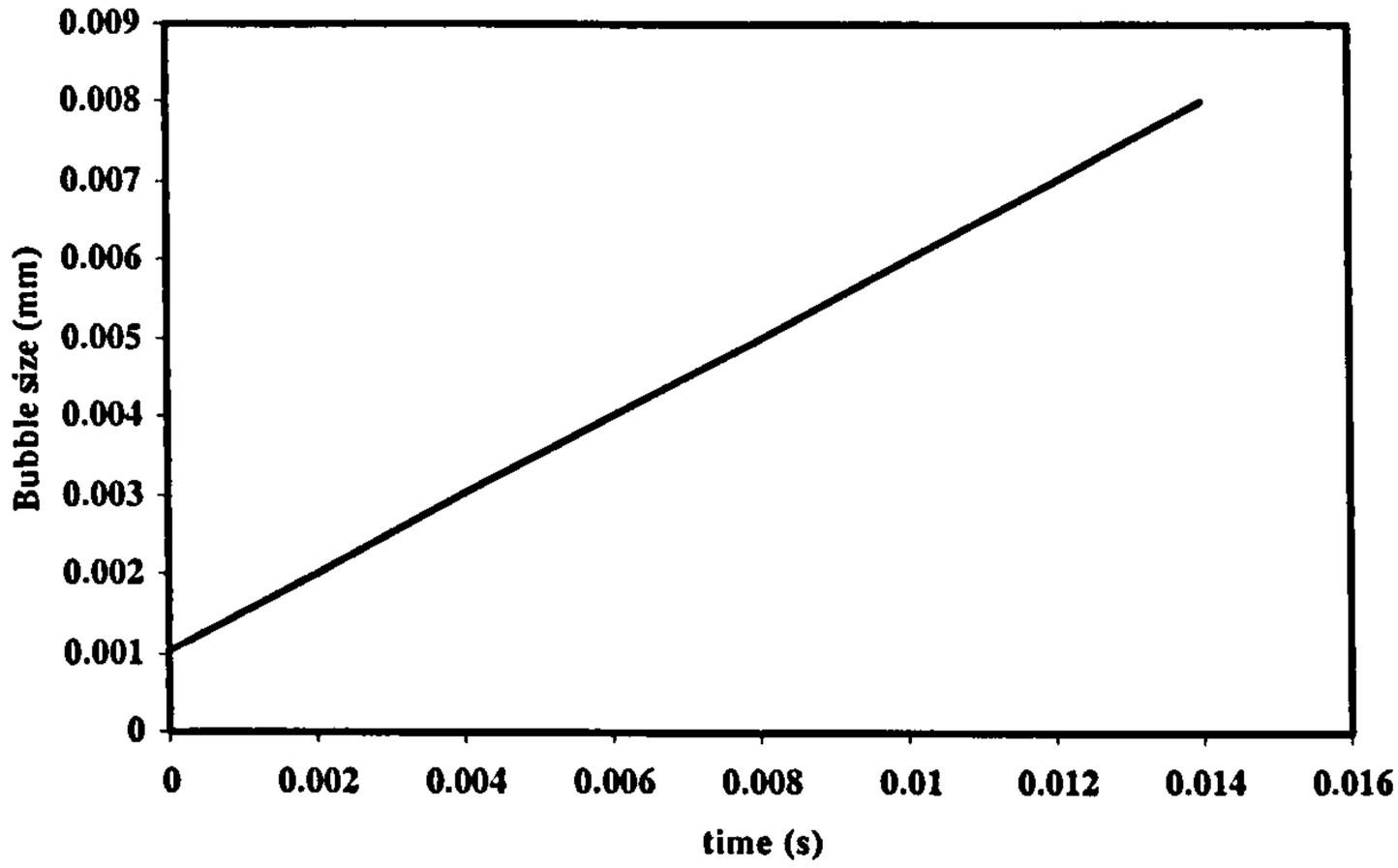

Figure 5.8 Variation of cubical bubble growth with time using Equation (5.42.)

The average heat transfer coefficient across the film is then written as;

$$\alpha_m = \frac{\int_{ti}^{tf} Q dt}{t_f \pi d s \Delta T} \tag{5.42}$$

The numerator of the above integral is given as;

$$\int Qdt = \int q_{if} * Adt = \int \frac{-k_f \Delta T}{\left[\delta_i^2 - \left(\frac{2\Delta T k_f t}{\rho_f h_{fg}}\right)\right]^{1/2}} \times \pi D \left[s_i^2 + \frac{2\pi D}{3} \left[\delta_i^2 - \left(\frac{2\Delta T k_f t}{\rho_f h_{fg}} \right)^{1/2} \right]^{1/2} \right]^{1/2} dt$$

$$\int Qdt = \rho_f h_{fg} \left[s_i^2 + \frac{2}{3}\pi D \left(\delta_i^2 - \frac{2\Delta T k_f t}{\rho_f h_{fg}} \right)^{1/2} \right]^{3/2} \qquad (5.43)$$

Using initial bubble size of equal to the tube diameter of 3mm and the properties of distilled water in Equation (5.44) the plot of average heat transfer coefficient during the passing period of a bubble over the tube yields a plot in as shown in Figure 5.9. The plots shows mean heat transfer coefficient which increases with time.

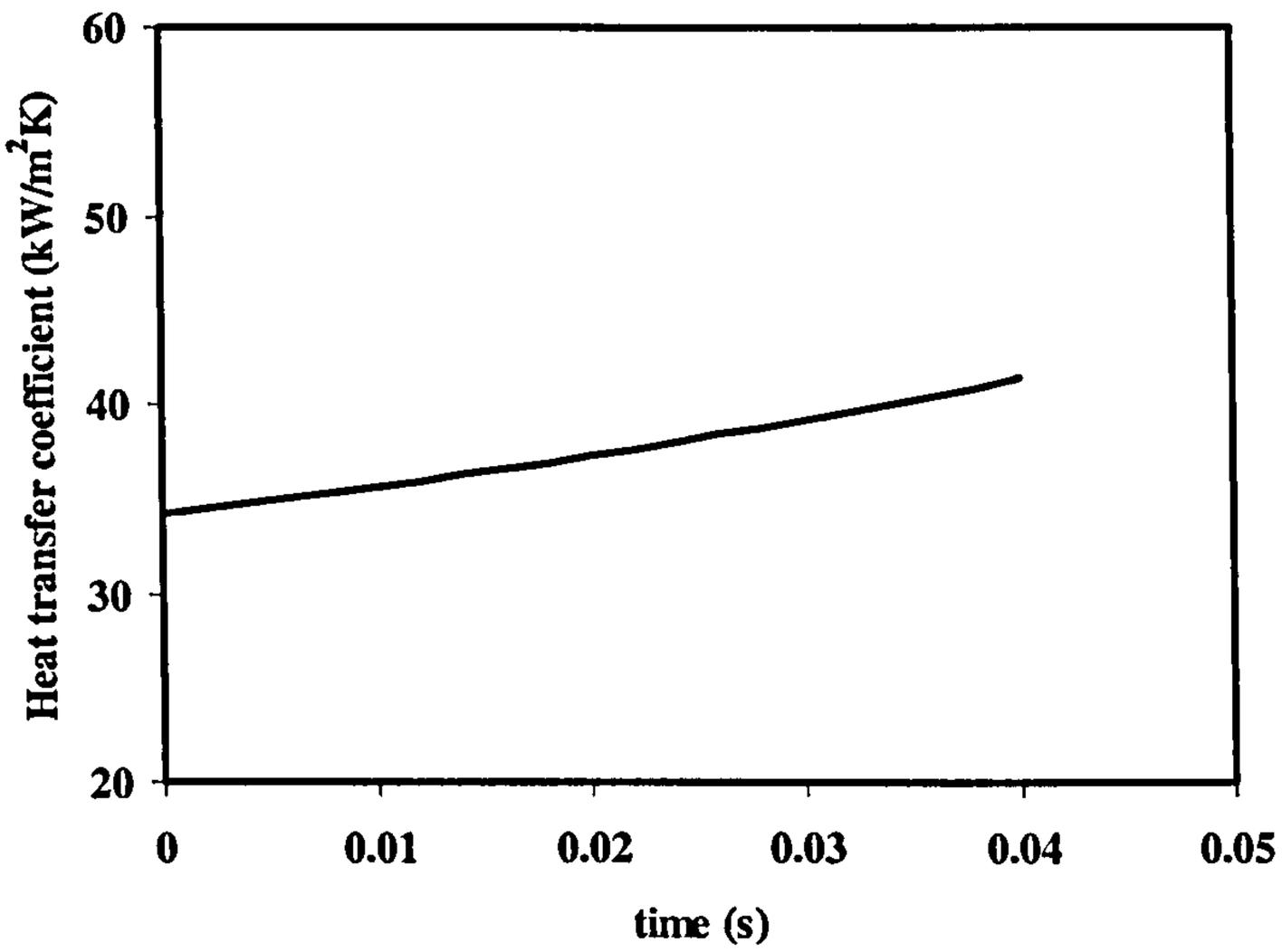

Figure 5.9 Variation of mean heat transfer coefficient using Equation (5.43) for distilled water.

5.6.1 Spherical bubble

Thu section considers the analysis for the condition where the bubble is spherical instead of cubic in nature that translates over the tube under which there is thin film

evaporation. In this case the bubble is almost central to the sphere i.e. they flow around if too much to side. Initial bubble diameter is D. Photographic studies of Cornwell and Schuller [44] and also Williams and Messler in water indicates the advancing angle of around 90° implying the mean angle of 60°. Hence a value of 90° for distilled water in the present analysis for all the fluids.

The volume of the bubble;

$$V = \frac{\pi D^3}{6} \tag{5.44}$$

The diameter of the bubble is then given as;

$$D = 2r\sin\theta_m \tag{5.45}$$

where θ_m, is mean liquid contact angle,

Area in contact with tube;

$$A = \pi dD = 2rD\pi\sin\theta_m \tag{5.46}$$

The volume of the bubble is then;

$$V = \frac{4}{3}\pi r^3 \sin^3\theta_m;$$

Rate of change of bubble volume with radius is;

$$\frac{dV}{dr} = 4\pi r^2 \sin^3\theta_m \tag{5.47}$$

The bubble radius at any time t is;

$$\frac{\rho h_{fg}\sin^2\theta_m}{d}\left(r^2 - r_i^2\right) = \rho h_{fg}\left(\delta_i^2 - \left(\frac{2\Delta T k_f t}{\rho_f h_{fg}}\right)\right)^{1/2}$$

$$r^2 = r_i^2 + \frac{d}{\sin^2\theta_m}\left(\delta_i^2 - \left(\frac{2\Delta T k_f t}{\rho_f h_{fg}}\right)\right)^{1/2} \tag{5.48}$$

The total energy through the thin film under the spherical bubble is given as;

$$Q = \rho_f h_{fg}\left[r_i^2 + \frac{d}{\sin^2\theta_m}\left(\delta_i^2 - \frac{2\Delta T k_f t}{\rho_f h_{fg}}\right)^{1/2}\right]^{3/2} \tag{5.49}$$

Hence the average heat transfer coefficient is given as;

$$\alpha_m = \frac{\rho_f h_{fg}\left[r_i^2 + \frac{d}{\sin^2\theta_m}\left(\delta_i^2 - \frac{2\Delta T k_f t}{\rho_f h_{fg}}\right)^{1/2}\right]^{3/2}}{at\pi d\Delta T} \tag{5.50}$$

Figure 5.10 shows a tube in which a constant heat flux is applied. The consideration is based on a portion of the tube covered with vapour bubble at temperature T_s (saturation temperature) and the other portion covered with liquid. The liquid portion is also at a saturation temperature of T_s. This is analogous to a tube with a portion of it surrounded by vapour and the other portion with liquid. Theoretical consideration shows that the heat transfer coefficient of the vapour side is higher compared to the liquid portion. The portion of the tube covered with vapour depends on the applied heat flux and as such it can be assumed that portion of the tube covered with vapour bubbles is p. Thus p varies from zero to unity.

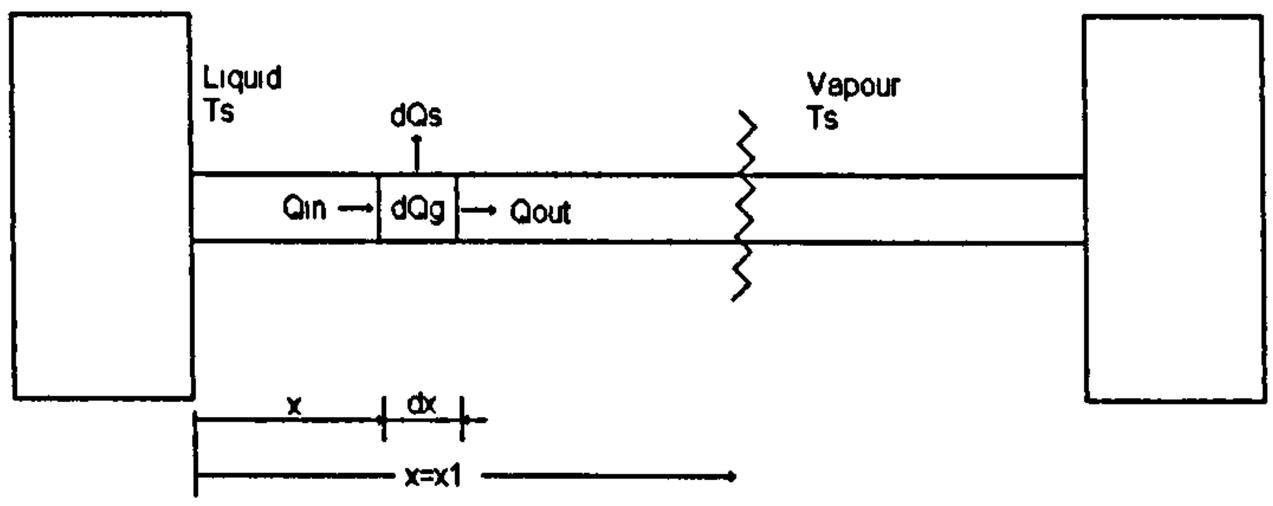

Figure 5.10 A diagram showing a tube with a portion covered with vapour and liquid.

Assumptions

- Longitudinal conduction on the tube is negligible

- The tube is isotropic i.e. the thermal conductivity, density does not change with position

- The liquid film remains attached to the wall of the rod

Heat flow into the element is given as;

$$Q_{in} = -kA\frac{dT}{dx} \tag{5.51}$$

And out of the element by;

$$Q_{out} = -kA\left[\frac{dT}{dx} + \frac{d^2T}{dx^2}dx\right] \tag{5.52}$$

Heat generated within the element is given as;

$$dQ_g = q_g A dx \tag{5.53}$$

The heat transferred by the element through the liquid and vapour section is given as;

$$dQ_s = \alpha_l P(T - T_s)dx \tag{5.54}$$

$$dQ_s = \alpha_v P(T - T_s)dx$$

Applying the conservation of energy gives;

$$Q_{out} - Q_{in} = dQ_g - dQ_s \tag{5.55}$$

Substituting gives a 2nd order ordinary differential equation as;

$$-\frac{d^2T}{dx^2}+\frac{q_g}{k}-\frac{\alpha P}{kA}(T-T_s)=0 \tag{5.56}$$

If $m^2=\frac{\alpha P}{kA}$ and $\Delta T=T-T_s$, and $G=\frac{q_g}{k}$

It follows that;

$$\frac{d^2\Delta T}{dx^2}=G-m^2\Delta T \tag{5.57}$$

The above differential equation is applicable to both the liquid part and the vapour portion. The general solution of this differential equation is;

$$\Delta T=A+Be^{-mx}+Ce^{mx} \tag{5.58}$$

Using the method of undetermined coefficients we have $A=-q_g/km^2$, the solution then becomes;

$$\Delta T=-\frac{q_g}{km^2}+Be^{-mx}+Ce^{mx} \tag{5.59}$$

Boundary conditions were obtained as;

$\Delta T_l(\infty)=\Delta T_l$ $\Delta T_v(\infty)=\Delta T_v$, where $\Delta T_l=q/\alpha_l$ and $\Delta T_v=q/\alpha_v$

$\Delta T_l(0)=\Delta T_v(0)=\Delta T_o$

Using the boundary conditions gives;

$C=0$, and $B=(\Delta T_o-\frac{q_g}{km^2})$

Substituting the constants into Equation (5.59) gives;

$$\Delta T = -\frac{q_g}{km^2} + \left(\Delta T_o + \frac{q_g}{km^2}\right)e^{-mx} \tag{5.60}$$

The boundary condition at x=0 is as follows;

$$\frac{d\Delta T}{dx_{x=0}} = \frac{d\Delta T}{dx_{b=0}} \tag{5.61}$$

From Equation (5.60) the equilibrium temperature could be determined by applying the vapour and liquid section which leads to;

$$\frac{d\Delta T}{dx_{x=0}} = -m_l\left[\Delta T_o + \frac{q_g}{km^2{}_l}\right] \tag{5.62}$$

$$\frac{d\Delta T}{dx_{xv=o}} = -m_v\left[\Delta T_o + \frac{q_g}{km^2{}_v}\right] \tag{5.63}$$

The expression for the equilibrium temperature is given as;

$$\Delta T_o = \frac{q_g}{k}\left[\frac{1}{m_v} - \frac{1}{m_l}\right] \times \left[\frac{1}{m_l - m_v}\right] \tag{5.64}$$

Equation (5.64) is used to determine the equilibrium temperature. Typical values that were used in generating Figure 5.11 are that of the properties of distilled water. The heat transfer coefficient of the vapour section was chosen arbitrary as α_v=60 kW/m^{2}K, α_l=15kW/m^{2}K q=37 kW/m^2. The plot shows that that the vapour section gives a high heat transfer coefficient which corresponds to a low wall superheat compared to the liquid section.

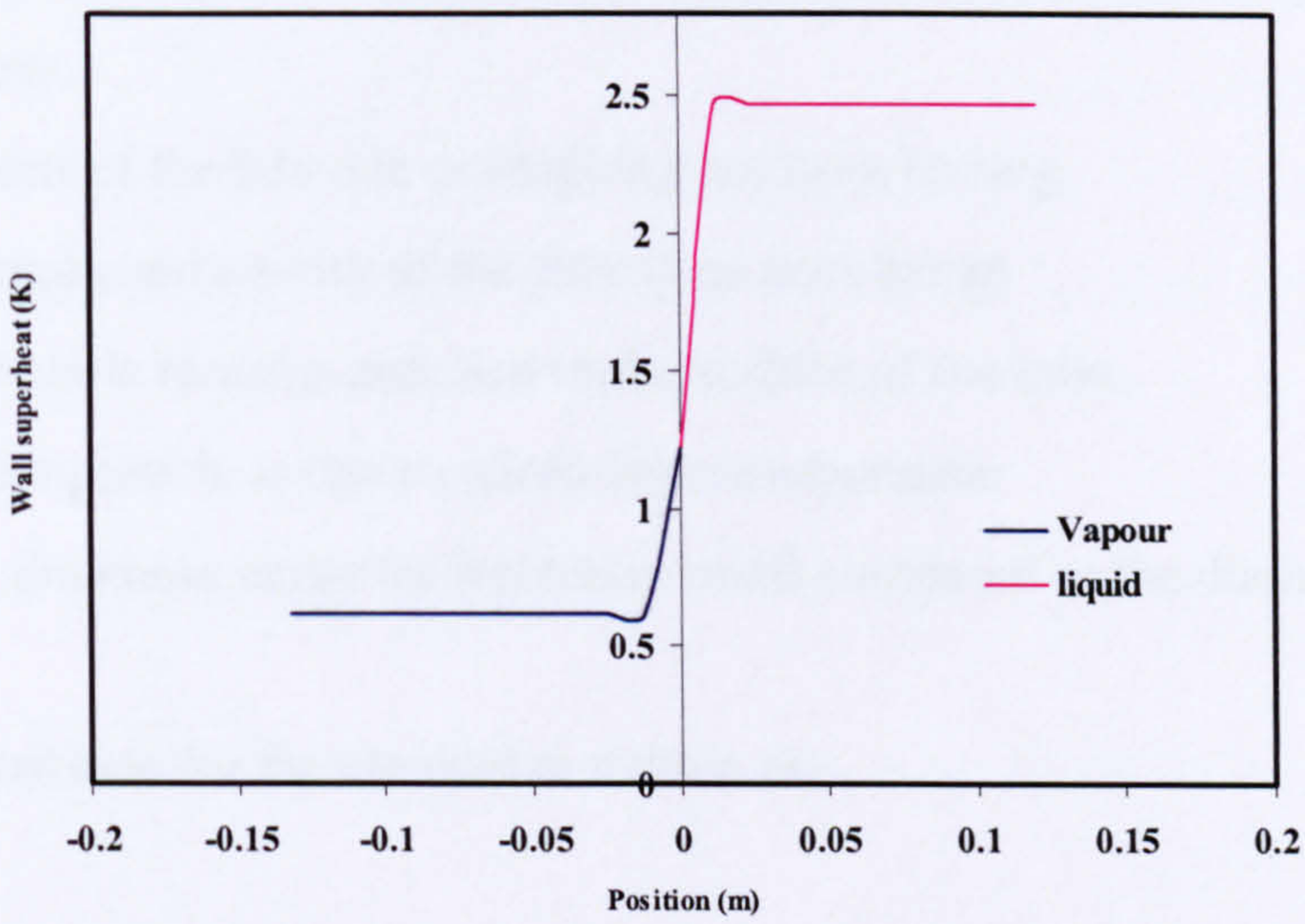

Figure 5.11 Variation of temperature difference with position on a tube based on Equation (5.65)

5.6.2 Transient analysis of a bubble

The transient analysis is to investigate effect of time on the bubble growth. This will be approached by considering it from the finite difference method. The approach is an extension of the theory introduced for the constant temperature in the previous section. The variation of the wall superheat during the passage of a typical bubble is the point of interest. It must be emphasised here that the heat transfer coefficient of the other portions where nucleate boiling is taking place.

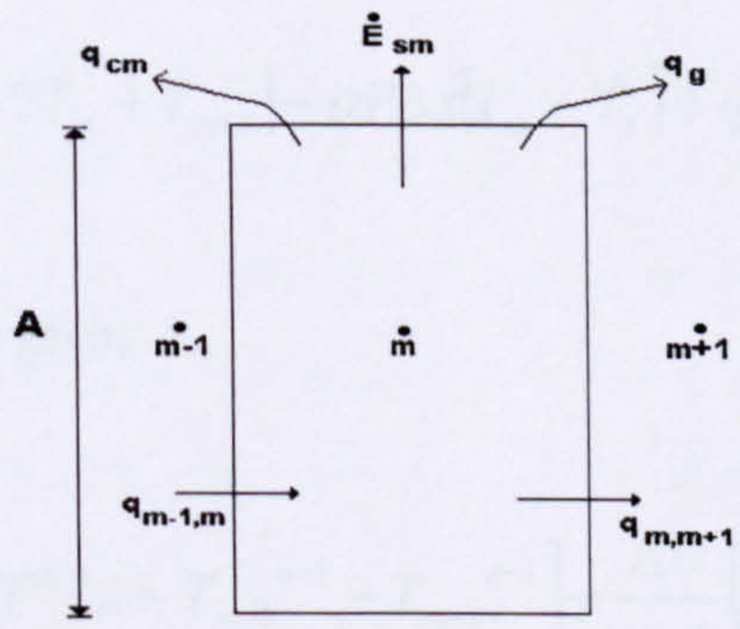

Figure 5.12 Finite element analysis of a bubble past a tube

The following assumptions are made with respect to the transient analysis shown in Figure 5.12 are;

- Portions of the tube are undergoing nucleate boiling
- Thermal conductivity of the tube does not change
- The bubble remains attached to the surface of the tube
- Bubble growth is due to micro-layer evaporation
- Film thickness under the bubble is small compared to the diameter of the tube

The energy balance for the element is written as;

$$q_{m-1,m} + q_g^{"} = q_{m,m+1} + E_{sm} + \alpha P \Delta x (T_s - T_{sat}) \tag{5.65}$$

The energy entering the element is obtained as;

$$q_{m-1,m} = kA \frac{T_{m-1} - T_m}{\Delta x} \tag{5.66}$$

And that leaving the element is;

$$q_{m,m+1} = kA \frac{T_m - T_{m+1}}{\Delta x} \tag{5.67}$$

$$E_s = \rho c A \Delta x \frac{dT_m}{d\theta} \tag{5.68}$$

Substituting into the energy balance Equation (5.65) gives;

$$\rho c A \Delta x \frac{dT_m}{d\theta} = \frac{kA}{\Delta x}[T_{m-1} - 2T_m + T_{m+1}] - \alpha P \Delta x [T_m - T_s] + q_g^{"} A \Delta x \tag{5.69}$$

This may be arranged to give;

$$T_m^{\,n} = T^{n-1}{}_m - \frac{k\Delta\theta}{\rho c \Delta x^2}\left[2T^{n-1}{}_m - T_{m-1}^{\,n-1} - T_{m+1}^{\,n-1}\right] + \frac{\Delta\theta}{\rho c A}\left[q_g^{"} - \alpha \pi d T_m^{\,n-1}\right] \tag{5.70}$$

The transient analysis based on the above equation is shown in Figure 5.13. The boundary conditions used in Figure 5.13, are bubble size of 3mm α_l =2kW/m^{2}K, α_v=15 kW/m^{2}K and q=19 kW/m^2. The plot shows that once the tube is at a fixed heat flux and

bubbles past a portion p, the there is a drop in the temperature difference and this corresponds to a high heat transfer coefficient, which depends on the time the bubble leaves the tube surface. The time frame used was 0.1 ms for the analysis. A typical frame from photographic studies showed 8.3 ms, which implies that for this analysis, typical temperature difference of 6.7K was observed at t=10ms.

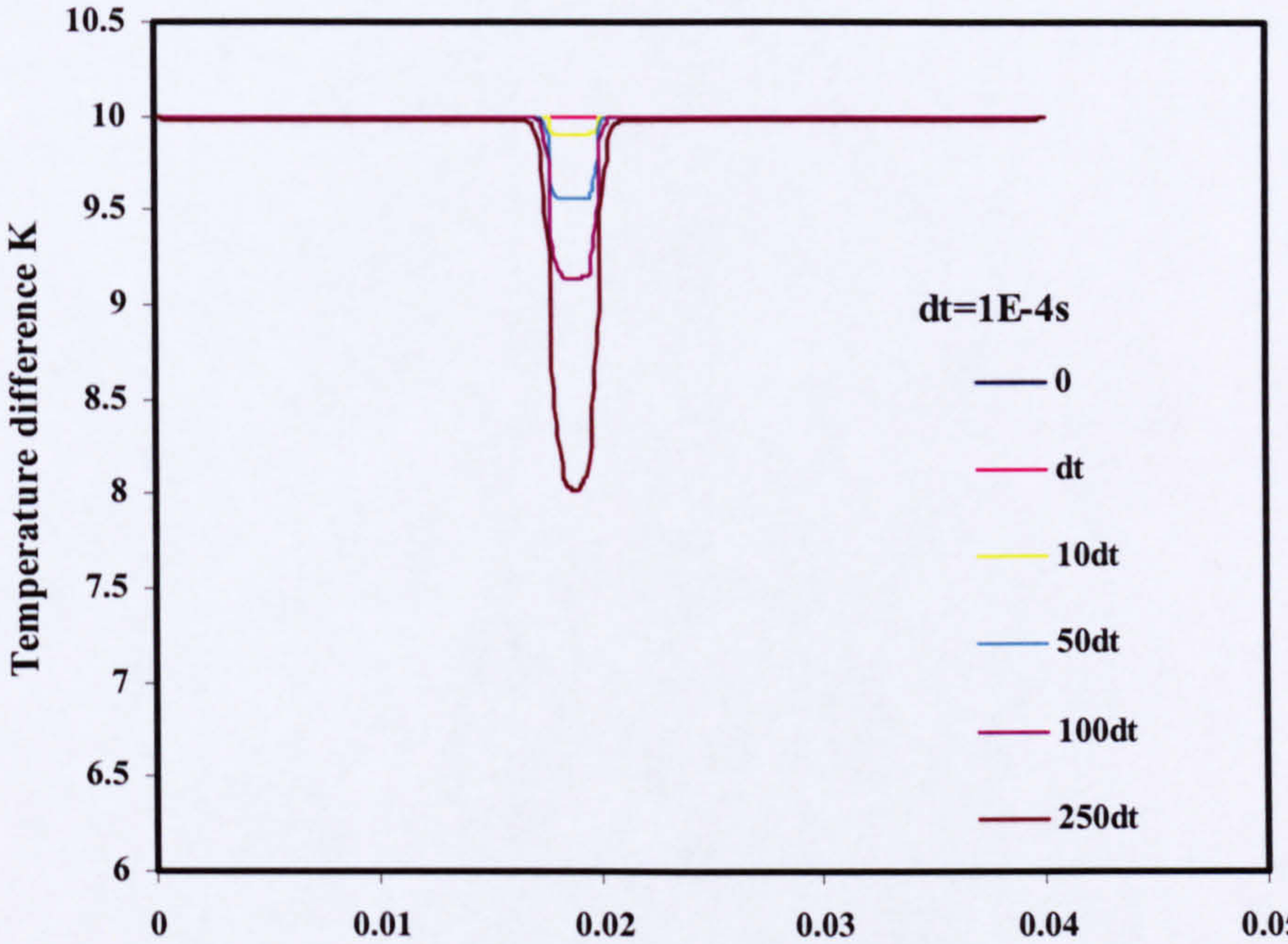

Figure 5.13 Variation of temperature difference with position for a bubble past a tube based on Equation (5.70).

Studies by Jacobi and Thome [110] and Thome, Dupont et al [111] developed a theoretical model to predict the boiling heat transfer inside a micro channel. Their model reviewed in Chapter 2 showed that the heat transfer coefficient is time dependent and depends on the micro layer evaporation under a passing bubble. This approach is similar to the theoretical concept developed, the difference been the area /portion of tube covered by the passing bubbles.

5.7 Concluding remarks

The theory presented in this Chapter has considered the possible heat transfer mechanism responsible in the set up. The following remarks are made;

- For the confinement number Co to be significant the value must be greater than 0.63. This value is in agreement with the Co derived for distilled water and R-113 except Flutec PP1

- Steady state analysis of the film under the bubbles showed that the film thickness does vary with time

- It has also been observed from the photographic studies that the bubbles translating past the tube at higher heat fluxes are larger than the diameter of the tube

- Dryout time of the bubble has been estimated using the typical conditions of water at nominal atmospheric pressure, and it is shown that within the limiting conditions of the bubble, a value of 0.79s was estimated. In fact this value of t_d is greater than values used or estimated using experimental and theoretical values

Chapter 6

DISCUSSION OF RESULTS AND COMPARISON WITH THEORY

6.1 Introduction

Experimental results for the twin tube and tube bundle have been presented in Chapter 4. The theoretical concept that has been introduced in Chapter 5 is analysed in relation to experimental results and deductions are made. Selected correlations such as Chen [18], Bennet et al [87], Steiner and Taborek [126], Hwang and Yao [63], and Gupte and Webb [91] that have been developed and applied to large tube bundles are compared with experimental results obtained and the effect of confinement introduced in Chapter 5 will be discussed. The Thome, Dupont et al [111] three-zone model described in Chapter 5 hypothesised that the dominant mechanism in the heat transfer in micro channels was that of thin film evaporation through a passing bubble. This model is modified and is used to compare the experimental results obtained from the tube bundle. It must be emphasised here that the Thome, Dupont et al [111] model has been developed for micro channels and the geometries for the compact tube bundle is quite different from those inside tubes. The chapter concludes by commenting on the macro models compared to the Thome, Dupont et al [111] model.

6.2 Twin-tube analysis

The results obtained from the twin tube have been presented in Chapter 4 and it was shown that the upper tube heat transfer was enhanced due to the presence of the lower tube bubbles. Results for distilled water at a typical heat flux of 37, 61, 91, 127 kW/m^2 showed this cyclical variation of the amount of space covered on the upper tube. The theory presented in Chapter 5 proposed a concept which has been developed based on the experimental results. The term p in the model varies with time and position. Thus at any time of the motion of the bubbles, p would vary. From the results presented the time effect is argued to be consistent with the experimental results. The nucleate boiling term was observed to be occurring on portions of the tube whiles translating bubbles laid a film, it is also assumed that there is no nucleate boiling occurring under the bubbles, but it is purely an evaporative process which causes the enhancement of heat transfer coefficient. p was determined from the analysis of at least 5 photos to determine the area covered with bubbles from Equation (6.1) given as;

$$p = \frac{p_1 + p_2 + p_3 + \ldots . p_n}{l} \qquad (6.1)$$

where p_1, p_2, p_3 and p_n are the portions covered by bubbles from the lower tube on the upper tube respectively. This estimate is compared with values determined from the equation (5.29) using the heat transfer measurements. The results shown in Figure 6.1 to Figure 6.2 shows that the estimates using the heat transfer analogy is higher than those obtained from the photos.

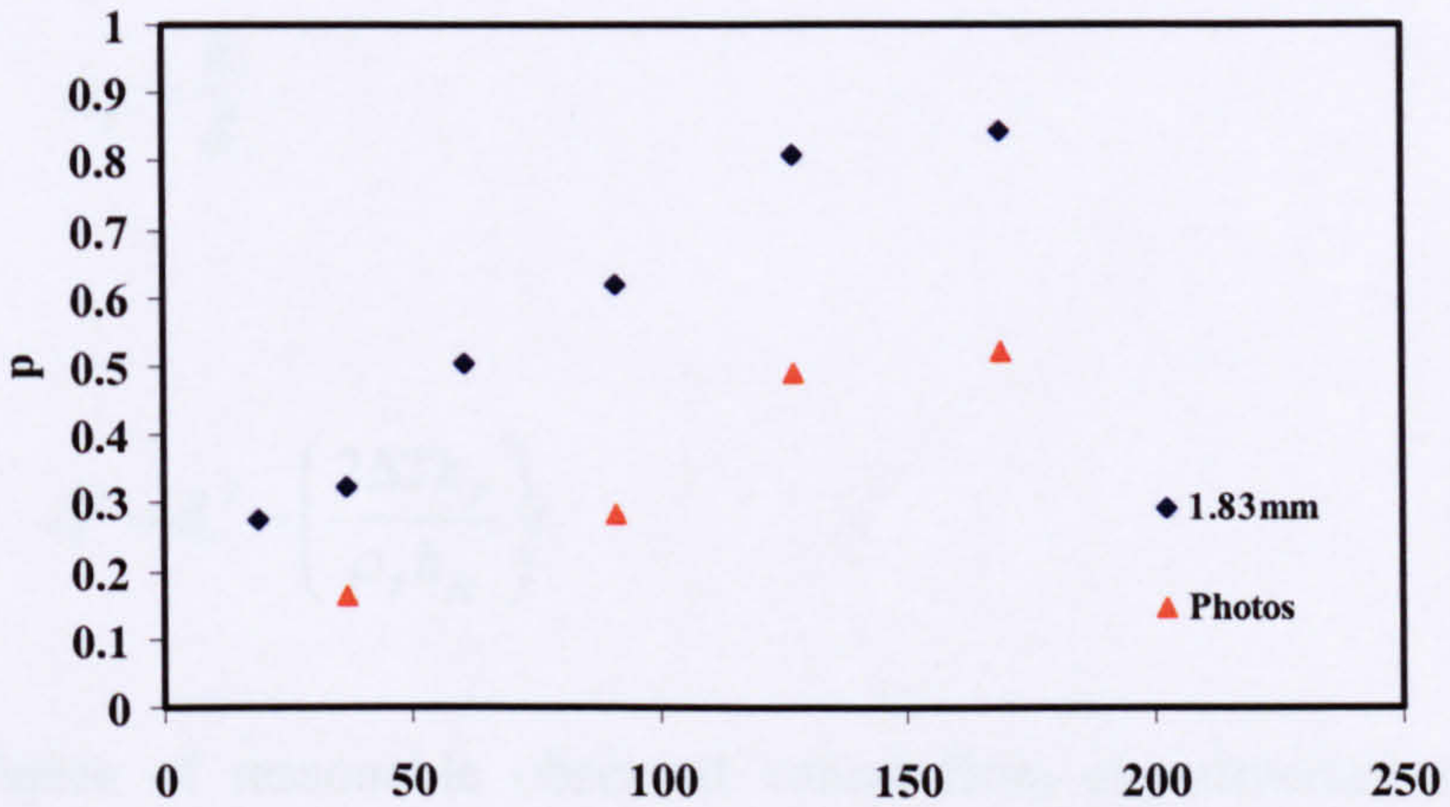

Figure 6.1: Variation of p from Equation (5.27) with heat flux for the 1.83 mm tube with distilled water.

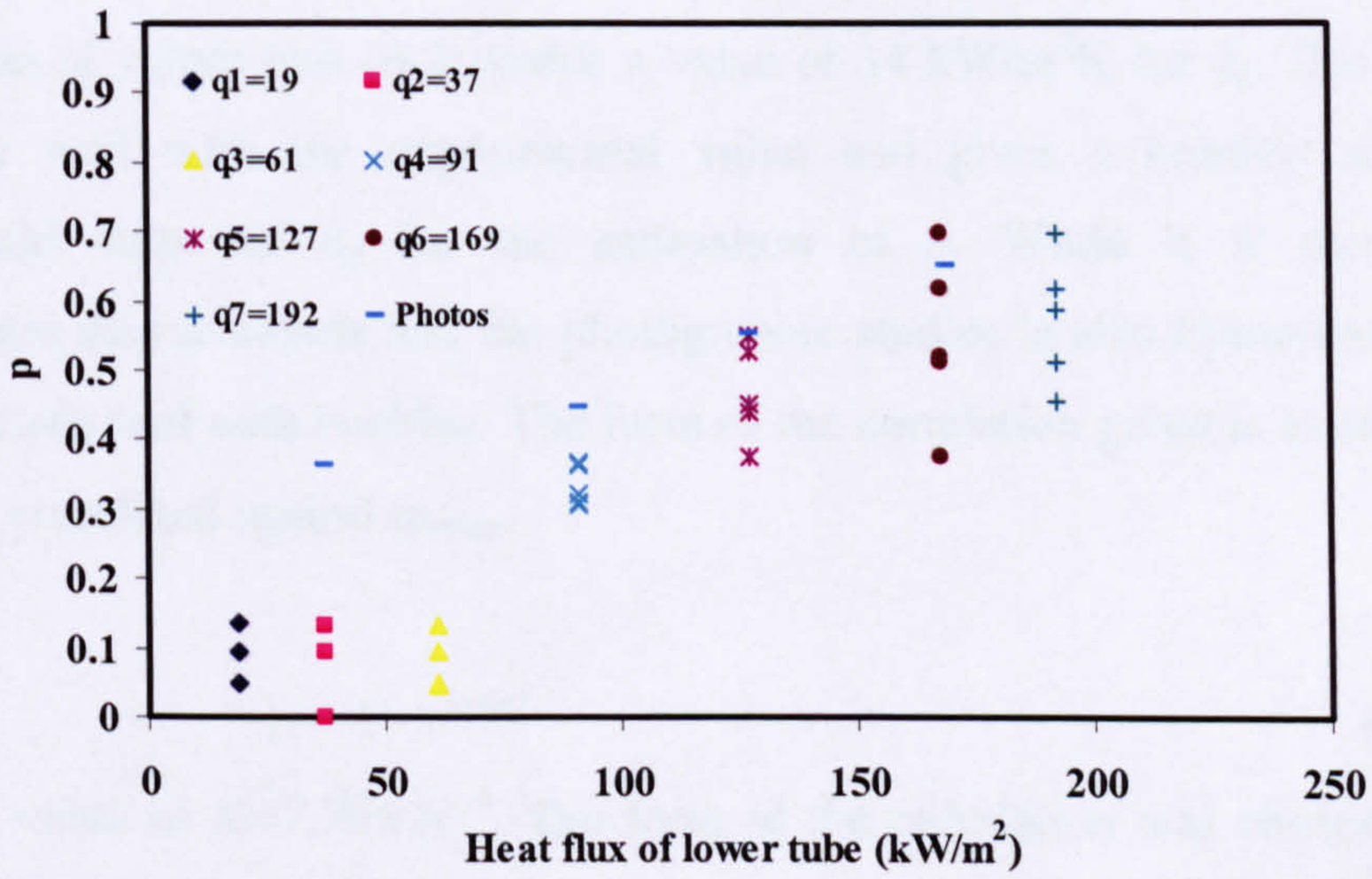

Figure 6.2 Variation of p from Equation (5.27), with heat flux for the 3.0 mm tube with distilled water

The experimental analysis allows the estimation of p by the following reasoning. Enhancement has been shown to be zero at heat flux of about 125 kW/m^2 at all values of the lower tube heat flux. Since the observation indicates p is not zero, then at this point $\alpha_{tf}=\alpha_{nb}$ and for lower tube q=0 kW/m^2 yields approximately $\alpha_{tf}=14\ kW/m^2K$. The value of α_{tf} is also estimated by theoretical consideration of the film under the bubbles for this part of the tube. It is assumed that the heat transfer due to translating bubbles on the same tube is essentially through a thin film rather than that under sliding bubbles. Chapter 5 of the thesis showed that the analysis of the conduction of heat flow through such a thin film thickness δ is given as;

$$\alpha_{tf} = \frac{k}{\delta} \tag{6.2}$$

where

$$\delta^2 = \delta_i^2 - \left(\frac{2\Delta T k_f}{\rho_f h_{fg}}\right) t \tag{6.3}$$

From substitution of reasonable observed values from experimental and also from previous work on sliding bubbles it is evident that for small diameter tubes $\delta_i=\delta$. That is the film suffers very little change due to evaporation during the short passage time of the enveloping bubble. Hydrodynamic analysis of the initial thickness under a bubble on a surface in distilled water by Addlessee and Kew [130] and Kenning [84] have established this to be about 50μm under the boiling conditions at 1 atmosphere. Substitution of values into (6.2) yields a value of 14 kW/m^{2}K for $\alpha_{tf.}$ This corresponds reasonably well with the experimental value and gives a comfort in using this experimental value of α_{tf} for the estimation of p. While it is recognized that experimental data available and the photographic studies is also limited as to diameter of the tube covered with bubbles. The form of the correlation given is as shown in (6.4) have been correlated against q_{lower}.

$$p = 1 - e^{(-Kq)} \tag{6.4}$$

where the value of $K=7.79\times10^{-6}$. The form of the correlation was chosen to meet the requirement that q=0, p=0 and q=infinity, p=1. A comparison between the theoretical estimation of p and from photographs is shown in Figure 6.3.

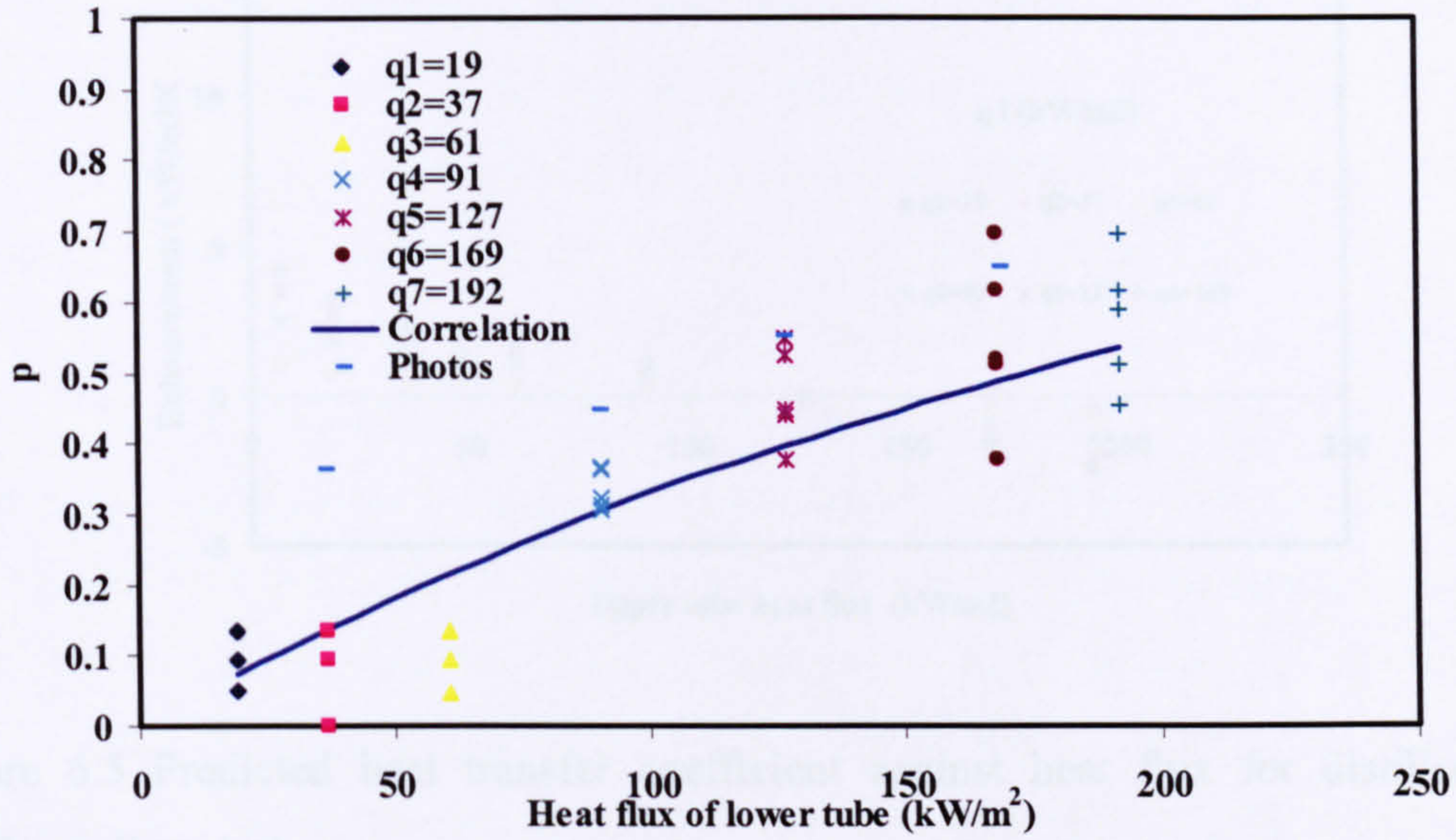

Figure 6.3 Variation of p with the heat flux for 3.00mm tube with distilled water

The semi-theoretical determination of the portion p shown in equation (6.3) is used to compare the experimental determined values as shown in Figure 6.4 and Figure 6.5 for the 2.32mm and 3.00mm tubes. There is a general agreement of the theory introduced in Chapter 5 with experimental values, but more data is necessary to generalise the theory and also to account for the effect of turbulence convection.

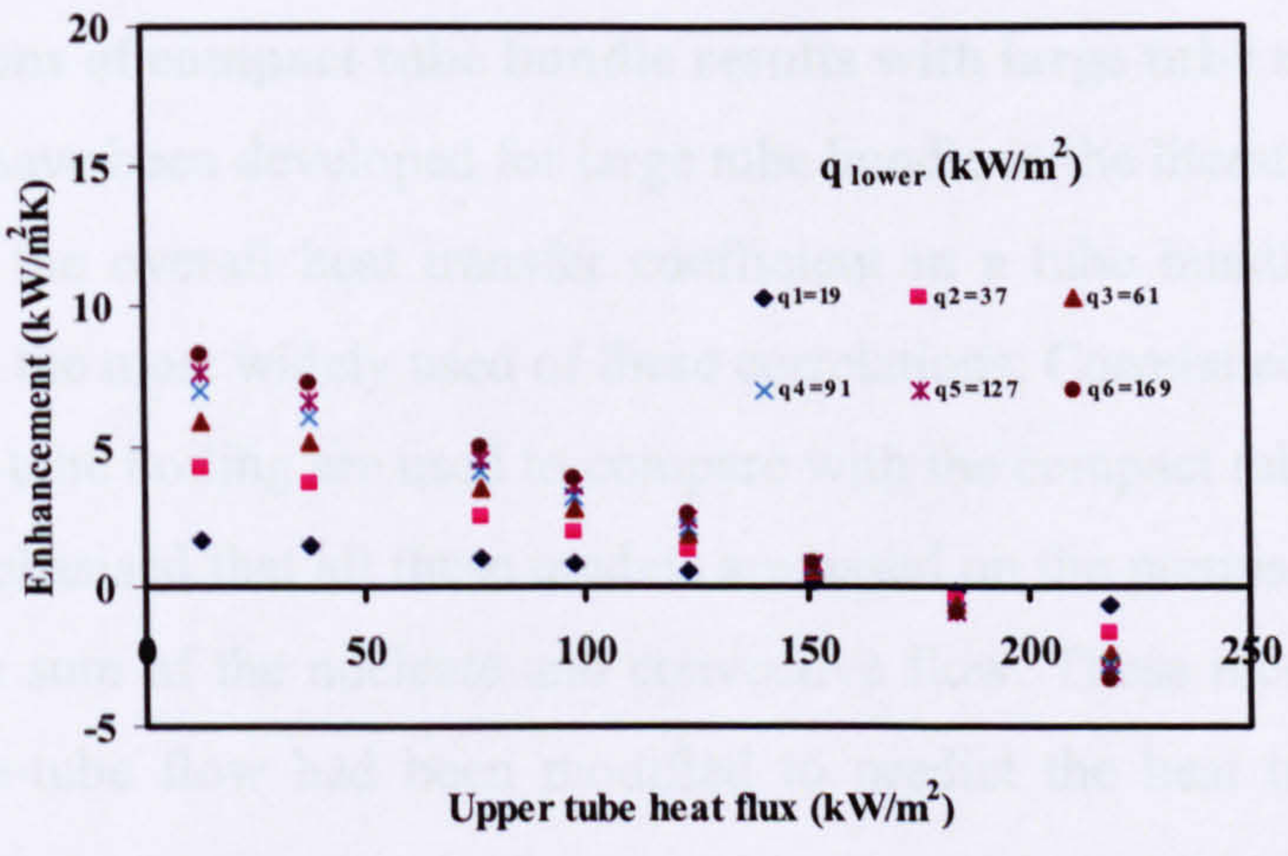

Figure 6.4 Predicted heat transfer coefficient against heat flux for distilled water (2.32mm diameter)

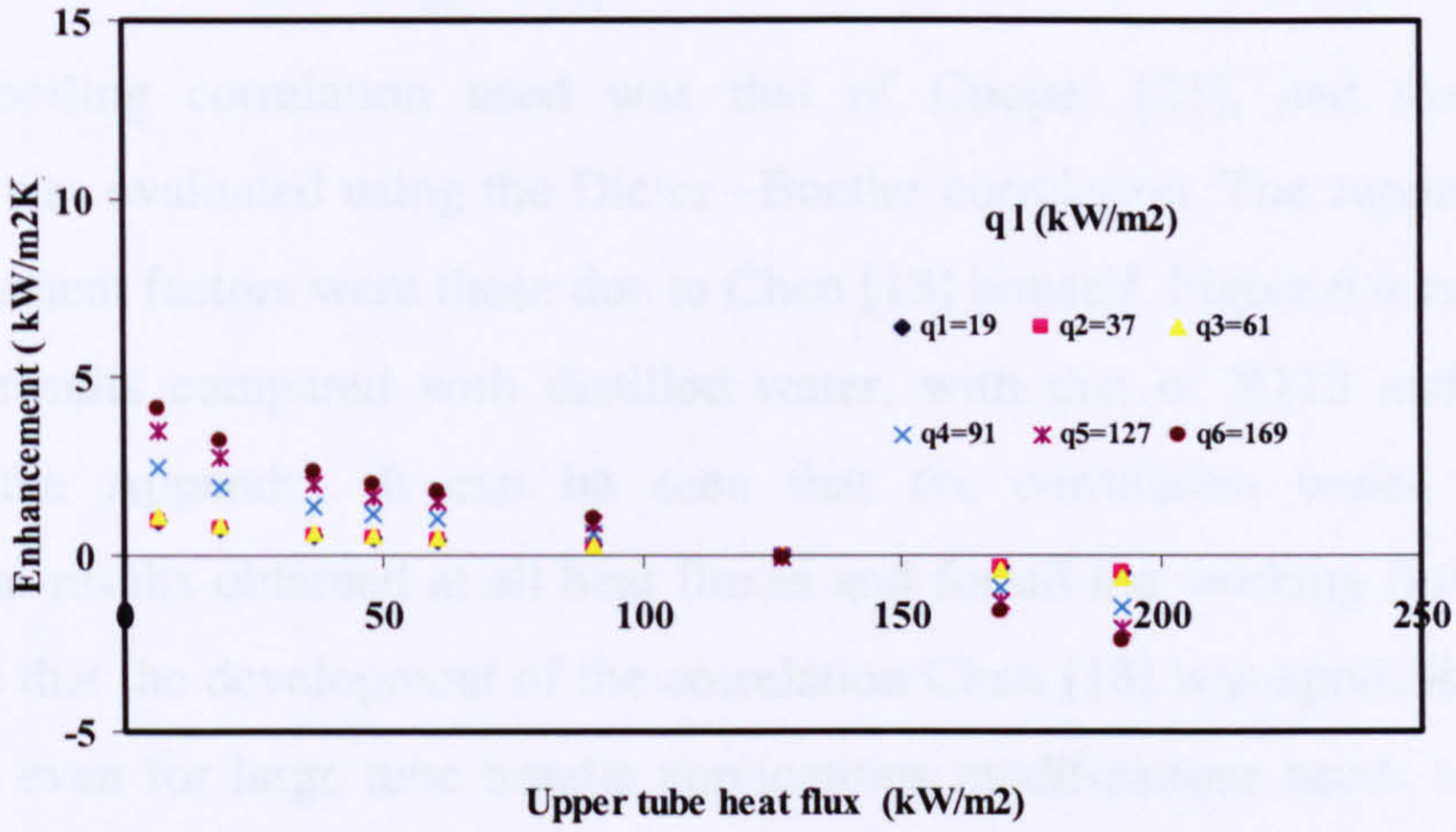

Figure 6.5 Predicted heat transfer coefficient against heat flux for distilled water (3.00mm diameter).

The twin-tube analysis has showed that the heat transfer enhancement due to bubbles from below could not account for the entire process but the turbulent convection also has an effect. This is clearly seen in Figure 6.4 and Figure 6.5 as the value of the heat transfer coefficient due to the thin evaporation is less, and as it there is no correlation that could account for the turbulence observed by the rising bubbles. It has been realised that a better high speed camera with higher number of frames would have captured the details of every passing bubble to determine the actual bubble size.

6.3 Comparisons of compact tube bundle results with large tube models

Various models have been developed for large tube bundle in the literature to predict the local as well as the overall heat transfer coefficient in a tube bundle. The literature review presented the most widely used of these correlations. Correlations that have been developed for in-tube boiling are used to compare with the compact tube bundle results. It is must be emphasised that all these models are based on the premise that the boiling heat transfer is a sum of the nucleate and convective flow. These models even though developed for in-tube flow had been modified to predict the heat transfer results in kettle reboilers.

Chen's correlation [18]

The traditional Chen's [18] correlation has been reviewed in the literature review of Chapter 2. Typically it is written as;

$$\alpha = S\alpha_{nb} + F\alpha_c \qquad (6.5)$$

The pool boiling correlation used was that of Cooper [21], and the convective component was evaluated using the Dieter –Boetler correlation. The suppression factor and enhancement factors were those due to Chen [18] himself. Figure 6.6 and Figure 6.7 shows the results compared with distilled water, with that of R113 and Flutec PP1 shown in the Appendix. It can be seen that the correlation under predicts the experimental results obtained at all heat fluxes and for all the working fluids. It is also argued here that the development of the correlation Chen [18] was applicable to in-tube boiling and even for large tube bundle applications modifications needs to be done in order to predict the results within a reasonable limit. Another possibility is the evaluation of the nucleate pool boiling heat transfer coefficient, since the pool boiling occurring on a small diameter tube is different from that of large tube, the Cooper [21] correlations needs modification. Suppression factor was developed for turbulent boundary layer and therefore cannot be applied to boiling nucleation in laminar flows.

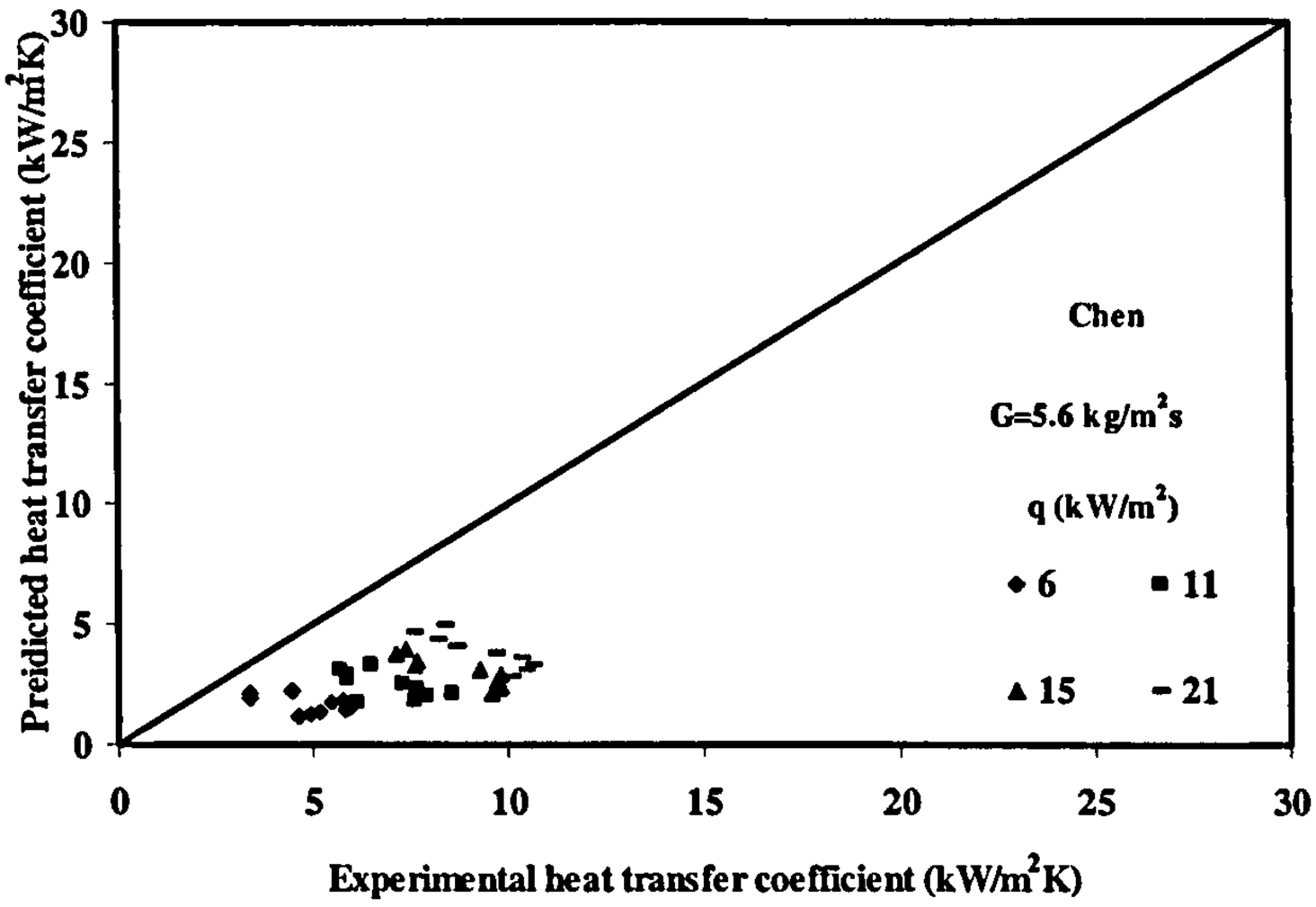

Figure 6.6 Predicted heat transfer coefficient using Chen [18] against experimental data for distilled water at G=5.6 kg/m^{2}s

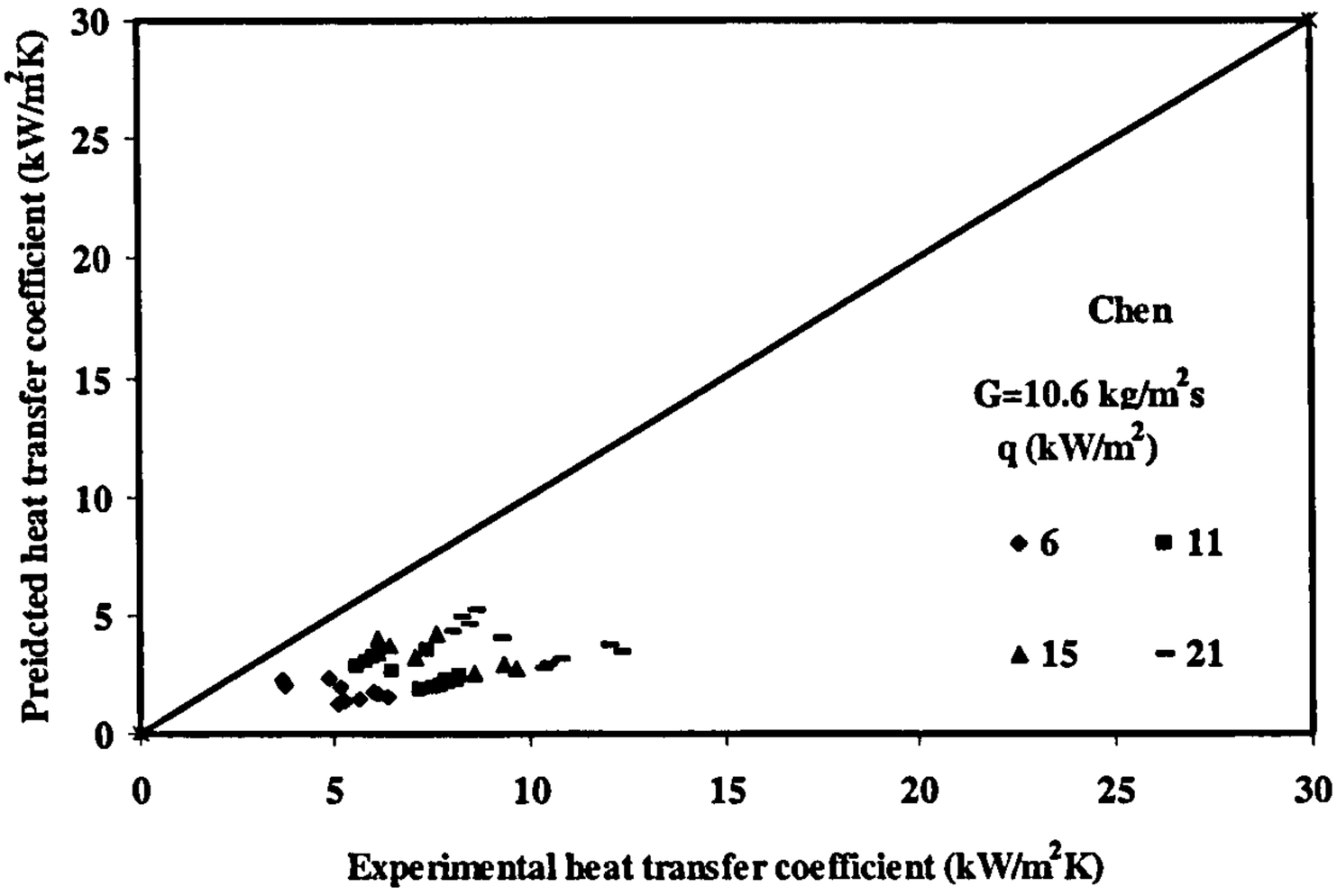

Figure 6.7 Predicted heat transfer coefficient using Chen [18] against experimental data for distilled water at G=10.6 kg/m^{2}s

Bennet and Chen [87]

The suppression factor was modified in the Chen [18] correlation, but the nucleate pool boiling was due to that of Cooper [21] correlation, and the enhancement factor was that of Chen [18]. The modification was based on a correlation developed for the suppression factor. It is based on the turbulent boundary layer approach. Typical results are shown in Figure 6.8 and Figure 6.9 for distilled water. The Bennet [87] correlation for the suppression factor is given in Equation (6.6) as;

$$S = \frac{k_l}{F\alpha_c\beta}\left[1-\exp\left(\frac{-F\alpha_c\beta}{k_l}\right)\right] \tag{6.6}$$

$$\beta = 0.041\sqrt{\left(\frac{\sigma}{g(\rho_l-\rho_g)}\right)} \tag{6.7}$$

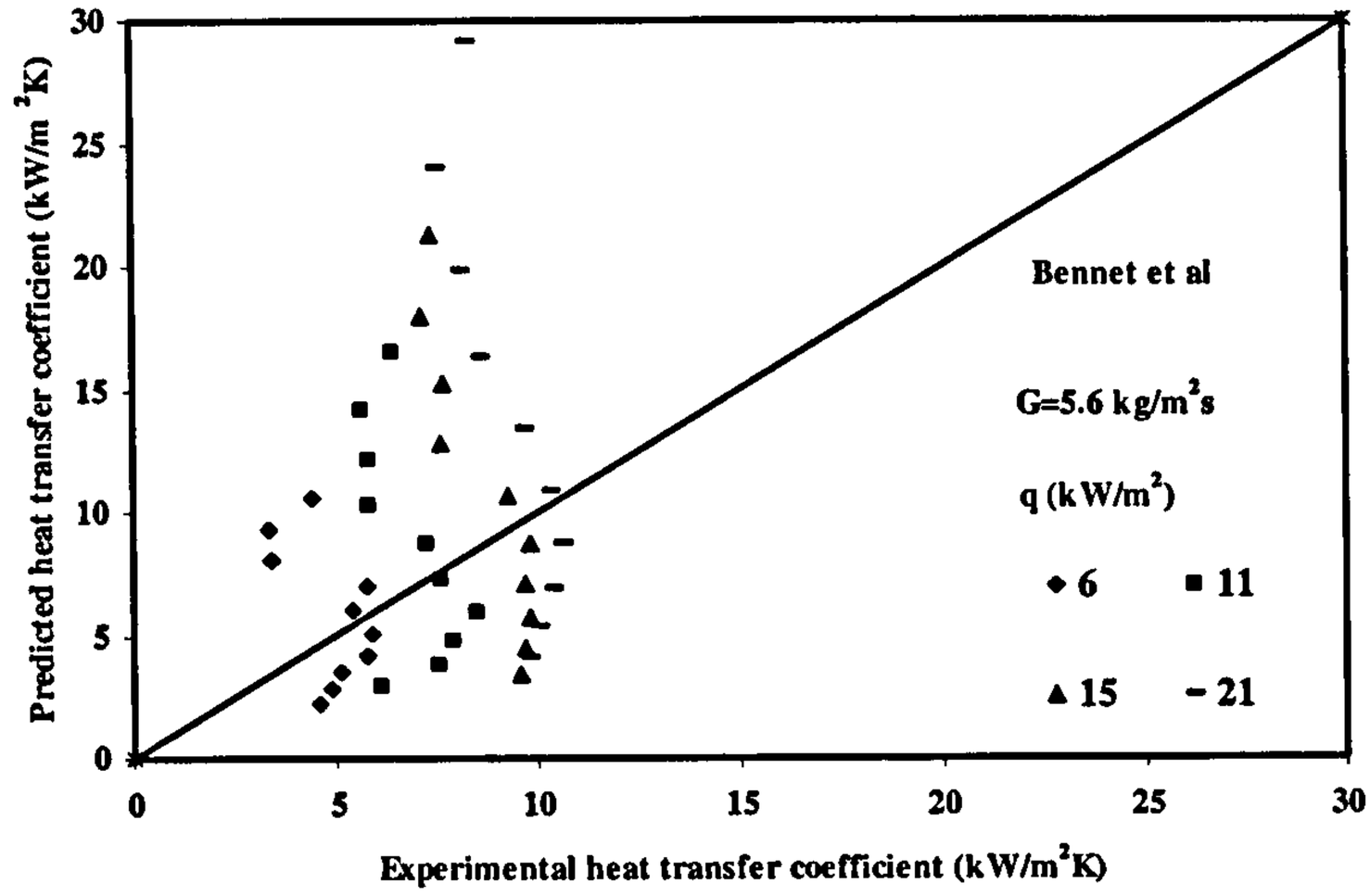

Figure 6.8 Predicted heat transfer coefficient using Bennet et al [87] against experimental data for distilled water at G=5.6 kg/m^{2}s

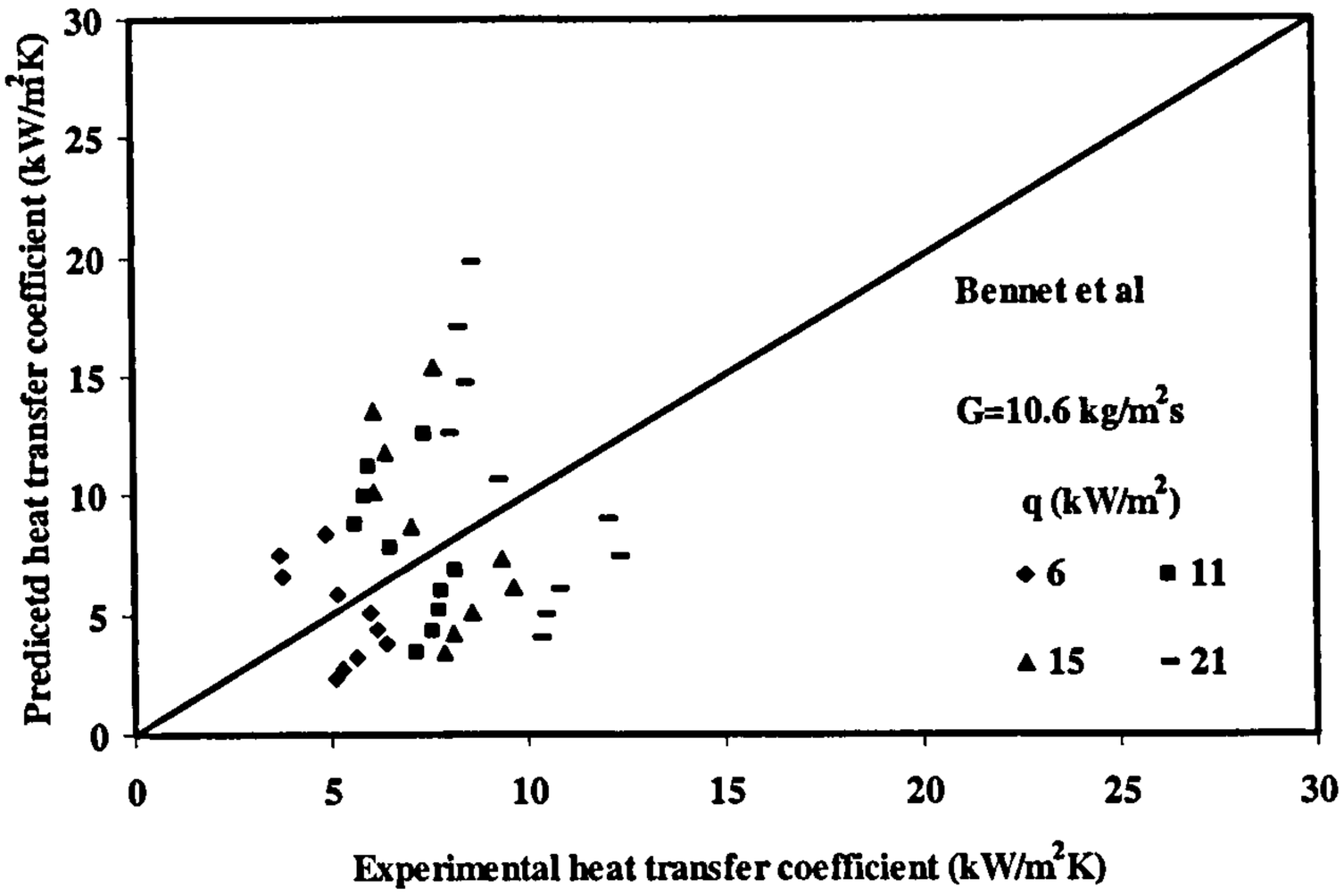

Figure 6.9 Predicted heat transfer coefficient using Bennet et al [87] against experimental data for distilled water at G=10.6kg/m^{2}s

Steiner and Taborek [126]

The Steiner and Taborek [126] model assumes a value of unity for the suppression factor using the superposition model developed by Chen [18]. This model was developed purposely for boiling inside a vertical tube. An asymptotic approach was used in the development of a correlation with the asymptote set to a value of 2. The correlation was compared with the experimental results and it did not show any

satisfactory agreement (Figure 6.10 and Figure 6.11). This might be due again to the usage of the Cooper [21] boiling correlation for the nucleate boiling component. It must be noted that the Reynolds number used in this approach are far higher than that used in this experimental programme. The enhancement factor was given as;

$$F = \left[(1-x)^{1.5} + 1.9x^{0.6} \left(\frac{\rho_l}{\rho_g} \right)^{0.35} \right]^{1.1} \tag{6.8}$$

Using the above equation higher values of enhancement factor was obtained which indicates the boiling mechanism is dependent on the vapour quality.

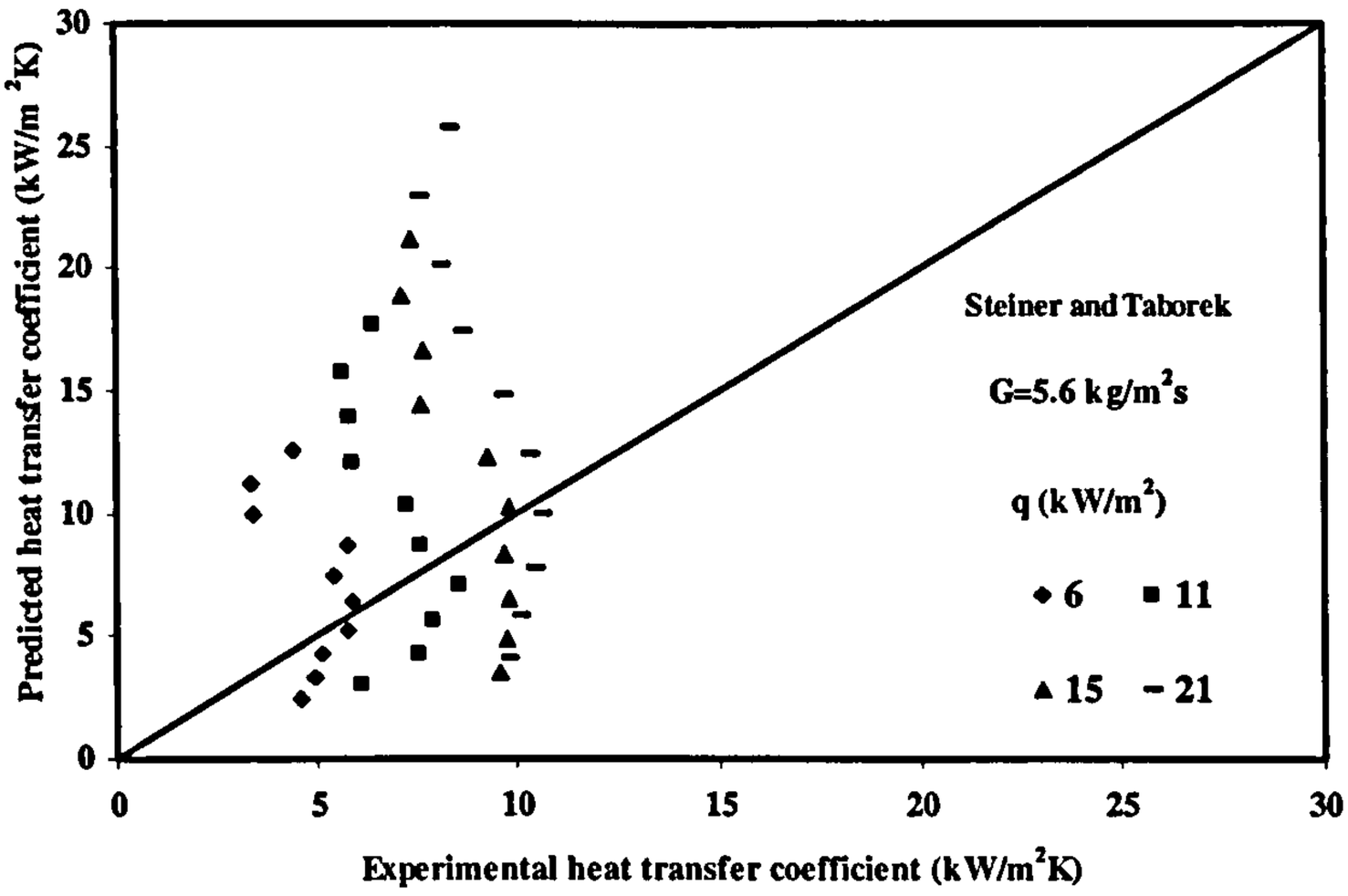

Figure 6.10 Predicted heat transfer coefficient using Steiner and Taborek [126] against experimental data using for distilled water at G=5.6 kg/m^{2}s

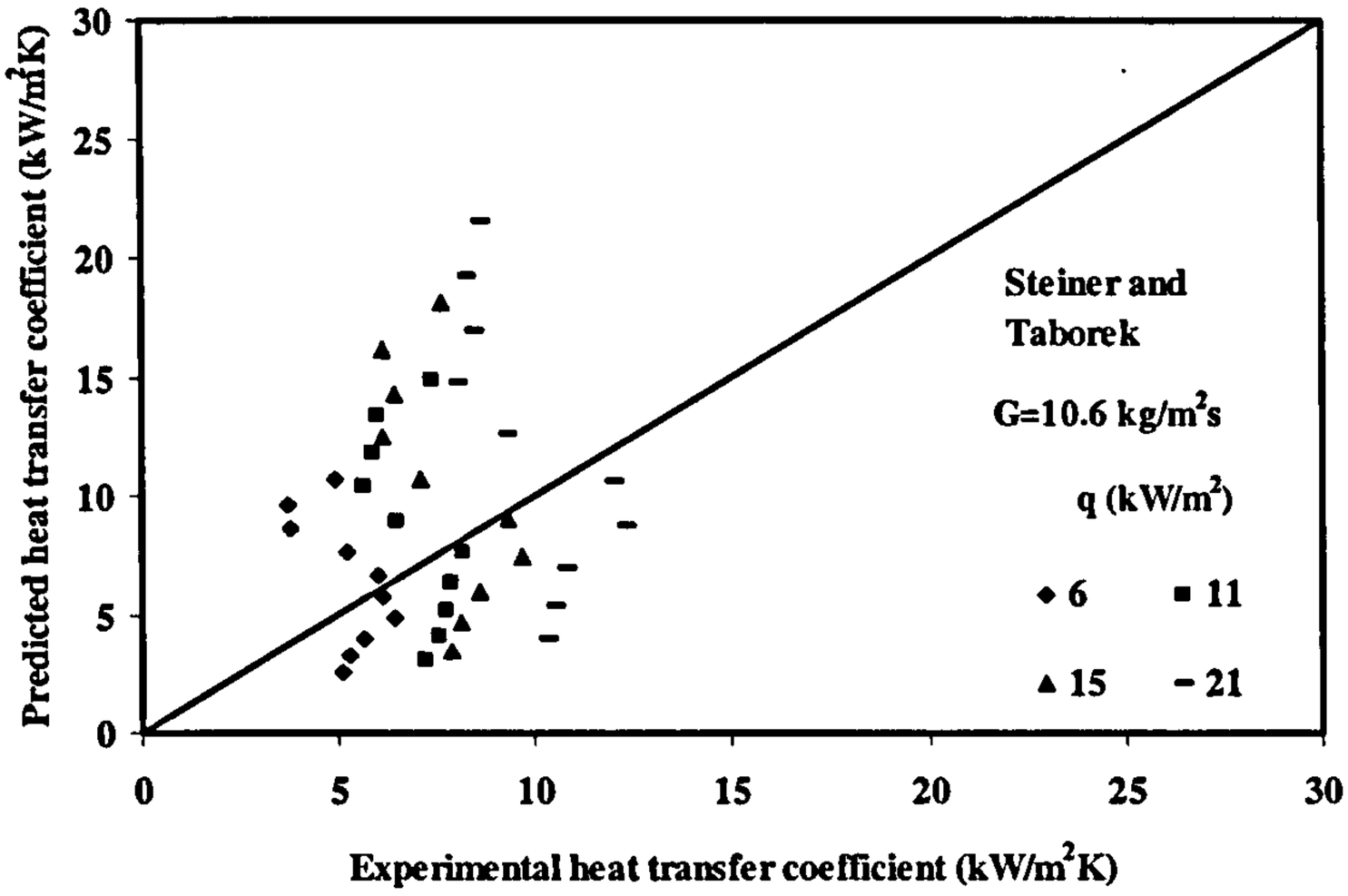

Figure 6.11 Predicted heat transfer coefficient using Steiner and Taborek [126] against experimental data for distilled water at G=10.6 kg/m^{2}s

Hwang and Yao [63]

The Hwang and Yao [63] model was also a modification to the Chen [18] superposition model. The suppression factor used was based on the Bennet [87] and Chen [18] approach, and they developed their own expression for the enhancement factor. They developed an expression for the nucleate pool boiling component which has been described in Chapter 2 with the enhancement factor been that of Polley et al. The plots in Figure 6.12 and Figure 6.13 showed that this model under predicts the experimental results. The geometry used in Polley was different from that of Hwang and Yao [63], even though the correlation predicted their results within a deviation of 33 %. There is also a difference between the geometry of Hwang and Yao [63] and the present experimental studies in terms of the range of parameters investigated. The prediction by the Hwang model shows a relative constant value for all the heat flux and mass flux range tested.

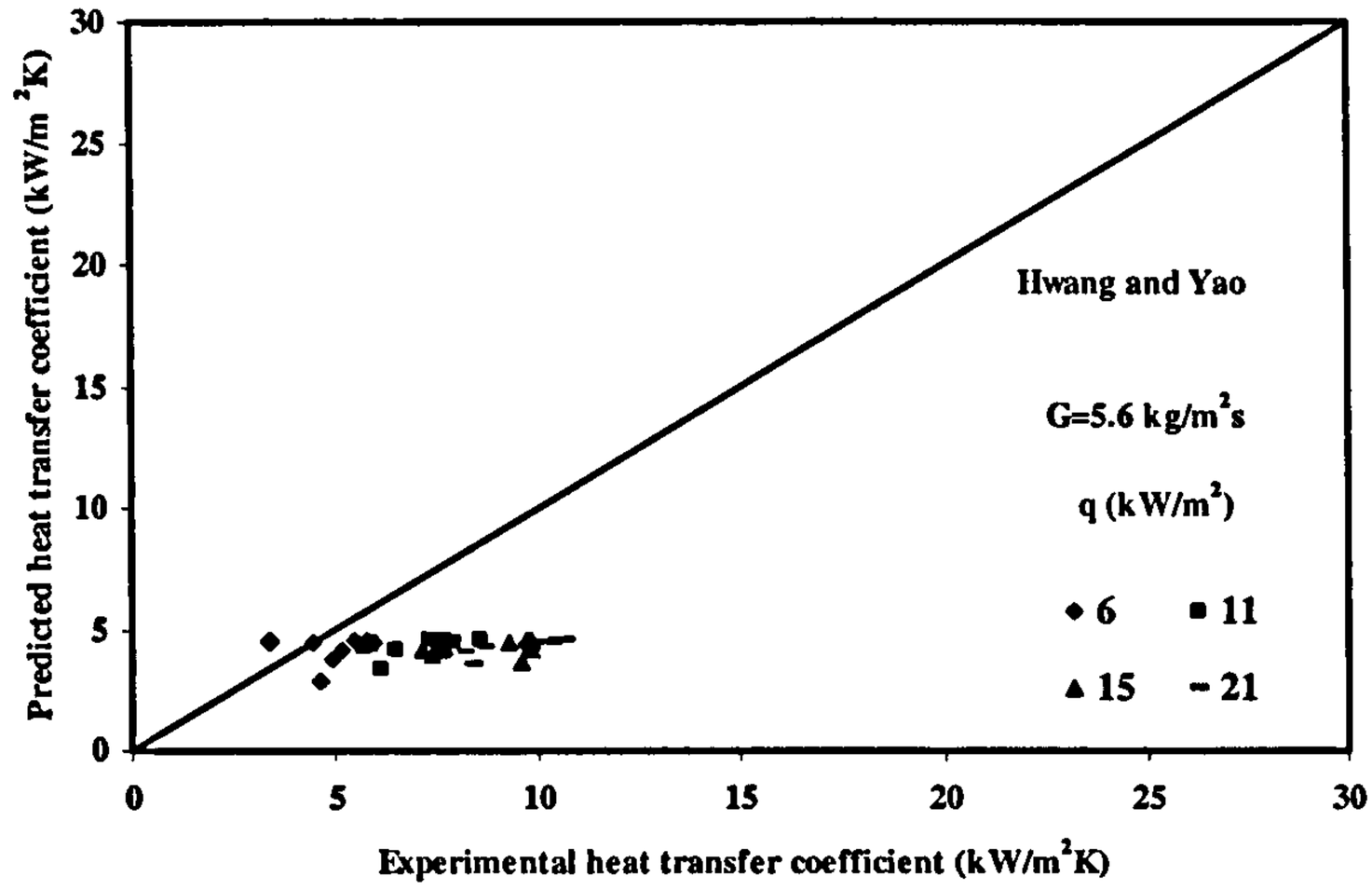

Figure 6.12 Predicted heat transfer coefficient using Hwang and Yao [63] against experimental data for distilled water at G=5.6 kg/m^{2}s

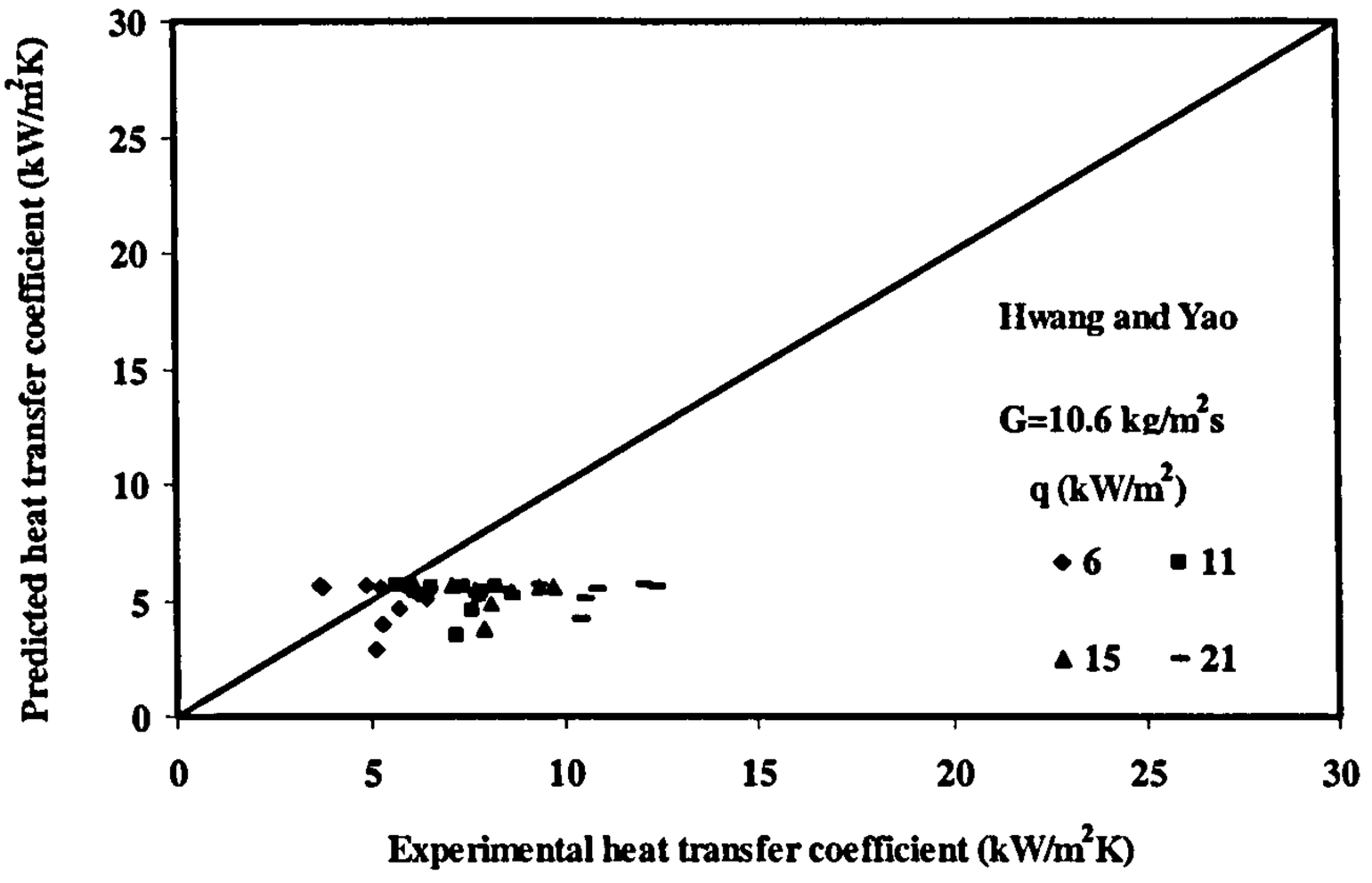

Figure 6.13 Predicted heat transfer coefficient using Hwang and Yao [63] against experimental values for distilled water at G=10.6 kg/m^{2}s

Gupte and Webb [91]

Webb and Gupte [91] developed a model based on their own experimental data for boiling heat transfer in their bundle. They used the asymptotic model with n=3 to analyse their data, but a value of 2 is chosen in this analysis. They developed their own enhancement factor from their results. Referring to the data for distilled water, this model showed the reasonable values of heat transfer coefficient compared to all the

other models. The Webb and Gupte [90] model showed an increase of heat transfer coefficient with quality and it is largely dependent on heat flux. Compared to (Figure 6.14 and Figure 6.15) the result this is quite opposite as the experimental results showed only an increase in heat transfer coefficient and then a drop as quality increases. It has been suggested is due to the effect of confinement.

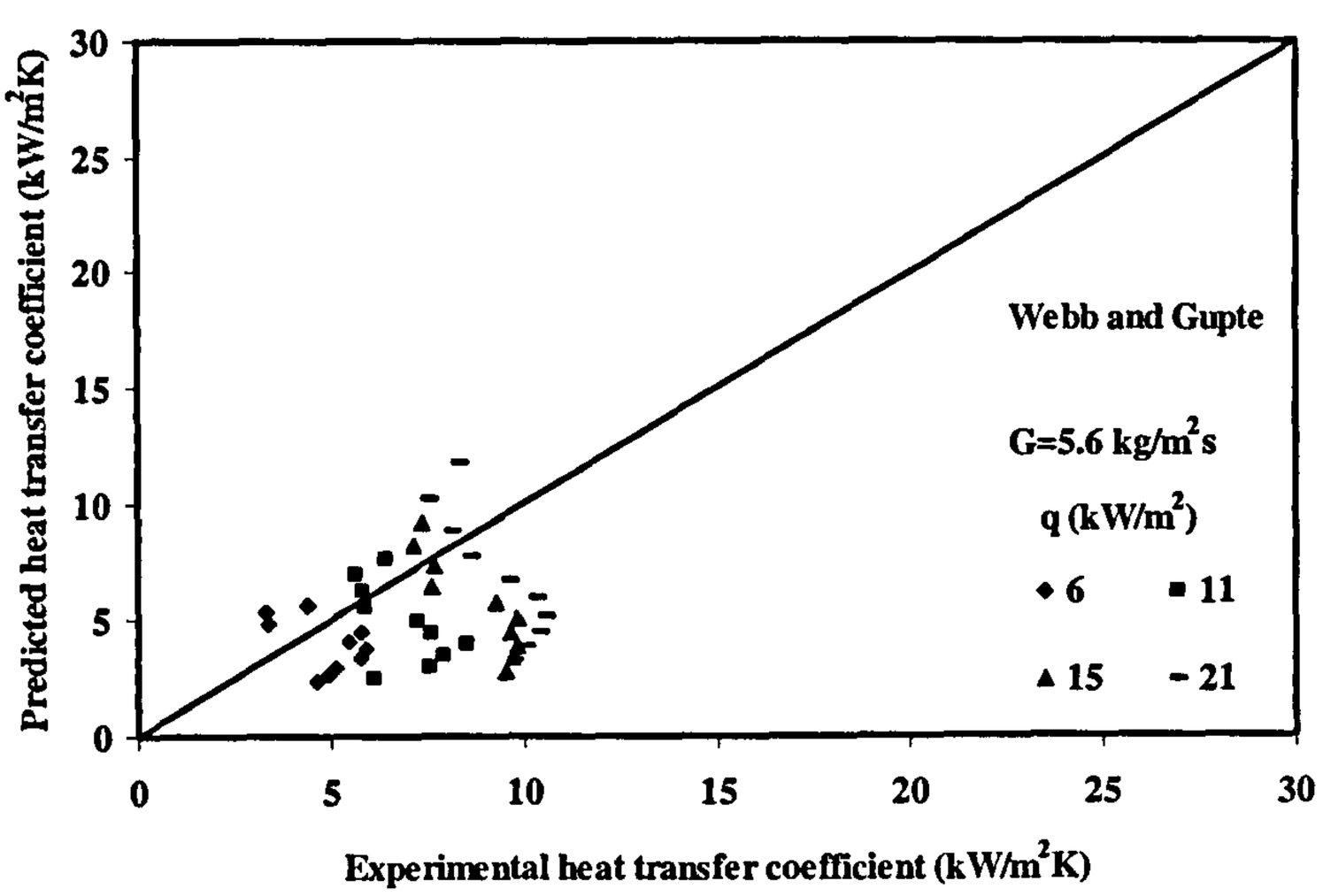

Figure 6.14 Predicted heat transfer coefficient using Gupte and Webb [91] against experimental data for distilled water at G=5.6 kg/m^{2}s

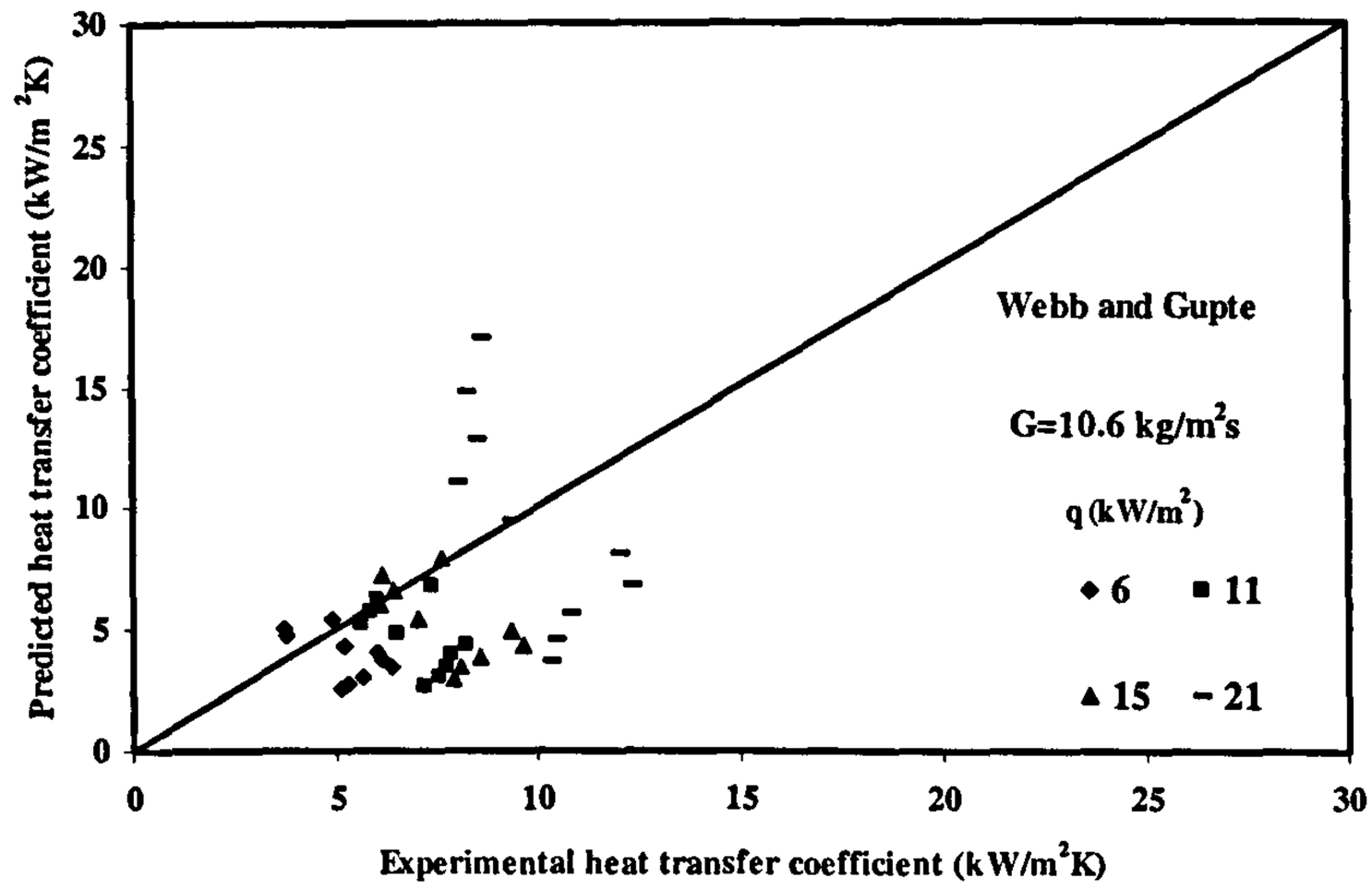

Figure 6.15 Predicted heat transfer coefficient using Gupte and Webb [91] against experimental data for distilled water at G=10.6 kg/m^{2}s

6.4 Comment on the Root Mean Square analysis of large tube models

Root Mean Square analysis have been carried out for all the models used as shown in Table 6.1 to Table 6.3 for distilled water, R-113 and Flutec PP1 respectively. The RSME was evaluated for each heat flux and the average obtained for a given mass flux. With distilled water, the Chen [18] model showed the highest deviation from the experimental results of 0.66 (66%) for all the mass flux tested. This is predominantly due to the convective nature of the model. Hwang and Yao [63] model showed the least deviation with a value of 33%. This was due to probably co-incidence as the geometry of their model as well as the test conditions and parameters were different. Experiential results showed a decrease in heat transfer coefficient at higher tubes. The models of Bennet and Chen [87], Webb et al [90] and Steiner and Taborek [126] all showed on the average a deviation of 40%.

Correlations	**G=5.6 kg/m^{2}s**	**G= 10.6 kg/m^{2}s**	**G=16.70 kg/m^{2}s**	**G=22.20 kg/m^{2}s**	**G=27.8 kg/m^{2}s**
Chen [18]	0.63	0.62	0.65	0.69	0.71
Steiner and Taborek [126]	1.05	0.80	0.66	0.48	0.45
Bennet et al [87]	1.06	0.61	0.57	0.44	0.44
Gupte and Webb [91]	0.43	0.57	0.49	0.42	0.44
Hwang and Yao [63]	0.44	0.30	0.28	0.30	0.33

Table 6.1: Root Mean Square Error Analysis with distilled water

Referring to Table 6.2 for the RMS for R113 as the working fluid, the data clearly shows that maximum deviation again was due to that of Chen [18]. The Hwang and Yao [63] model gave the least deviation. Furthermore, all the macro models gave an average of more than 50% for the R113 as the working fluid. Similar trends were observed in the data for the Flutec PP1 shown in Table 6.3.

Correlations	G=13.1 kg/m^{2}s	G= 19.7 kg/m^{2}s	G= 32.8 kg/m^{2}s
Chen [18]	0.57	0.65	0.61
Steiner and Taborek [126]	0.50	0.59	0.56
Bennet et al [87]	0.44	0.56	0.52
Gupte and Webb [91]	0.52	0.61	0.57
Hwang and Yao [63]	0.49	0.57	0.48

Table 6.2: Root Mean Square Error Analysis with R-113

Correlations	G=17 kg/m^{2}s	G= 26 kg/m^{2}s
Chen [18]	0.52	0.49
Steiner and Taborek [126]	0.98	1.02
Bennet et al [87]	1.05	1.15
Gupte and Webb [91]	0.82	0.77
Hwang and Yao [63]	0.92	1.39

Table 6.3: Root Mean Square Error Analysis with Flutec PP1

The models developed for the large tube bundles as presented could not predict the experimental results using the compact tube bundle. The assumptions that were used in the models were that the convective boiling was the dominant mechanism and was responsible for the heat transfer coefficient. The recent developed three-state model developed by Thome, Dupont et al [111] for boiling in mini channels would be attempted to compare with our results in the proceeding section.

6.5 The three-state model of Thome, Dupont et al [111]

The Thome, Dupont et al [111] model was reviewed in Chapter 2 of this thesis. The model was developed to predict the dynamic and local time averaged heat transfer coefficient in micro and mini channels. The model hypothesised that thin film evaporation was responsible for high heat transfer coefficients in micro channel compared to the large tube models that are mainly dependent on nucleate boiling and two-phase convective mechanism. This model is relevant to the work presented as it postulates that the dominant heat transfer is through the confined bubble which is in conformity to the results presented. The photographic studies showed that the bubbles are confined to the spaces in between tubes.

The model was given as;

$$\alpha(z)=\frac{t_l}{\tau}\alpha_l+\frac{t_{film}}{\tau}\alpha_{film}(z)+\frac{t_{dry}}{\tau}\alpha_v(z) \tag{6.9}$$

The authors defined three parameters that were obtained using published database; they are the minimum film thickness of the liquid film, the pair frequency of the bubbles generation and the correction factor. The initial film thickness was determined using the Moriyama and Inoue film thickness prediction method. The model was used in the comparison of experimental data (Dupont [131]) made up of 1591 data points for R-11, R-12, R-113, R-123, R-134a, R-141b and CO_2. Based on the data points used a recommendation was made on the general values of the parameters. The minimum film thickness, optical frequency was given as;

$$\delta_{\min}=0.3\mu m$$

$$f_{opt}=\left(\frac{q}{q_{ref}}\right)^{1.74} Hz$$

The reference heat flux was given as the function reduced by using the method developed by Cooper [21] for pool boiling correlations which was obtained as;

$$q_{ref}=3328\left(\frac{P_{sat}}{P_{crit}}\right)^{-0.5}$$

The constant used in the correction of the film thickness was obtained as;

$$C_{\delta\infty}=0.29$$

The model presented above was modified to compare it with the experimental data obtained in this thesis. It is recognised that the boiling heat transfer inside mini channel is quite different from that of outside a compact tube bundle. Features that needed modifications were the initial film thickness, analytical determination of the bubble generation frequency and the end film thickness. Since geometry of the three-state model is different from that of our bundle, the diameter d is taken as the minimum clearance or space between the tubes which is 1.5mm. However the confinement numbers that were developed in this thesis for the working fluids are in the same range as that of the published data used in the development of the three-state model.

The following modification was made for all the working fluids shown in Table 6.4.

Fluid	$C_{\delta o}$	d (mm)	δ_o (μm)	n
Distilled water	0.20	1.50	0.90	1.74
R-113	0.29	1.50	0.30	1.74
Flutec PP1	0.29	1.50	0.90	2.00

Table 6.4: Parameters used in Thome , Dupont et al [111] three-state model

The plots shown in Figure 6.16 to Figure 6.25, shows the general trend of the model, but there was an over prediction of the heat transfer coefficient. It is emphasised here that the model development did not consider distilled water and Flutec PP1 as part of the data base and as such the film thickness and bubble generation values used has effect on the heat transfer coefficient. One short fall of the model was the exclusion of any nucleate boiling component. The model also assumed that elongated bubbles are already formed prior to entering the channel, and does not include inception of elongated bubbles. The results in the photographic showed that bubble from the lower tube grow in length as it moved from one tube to the other and there was variation of bubble size with respect to time and position. Also nucleate boiling was observed to exist on the tubes but the duration of it existence was minimal.

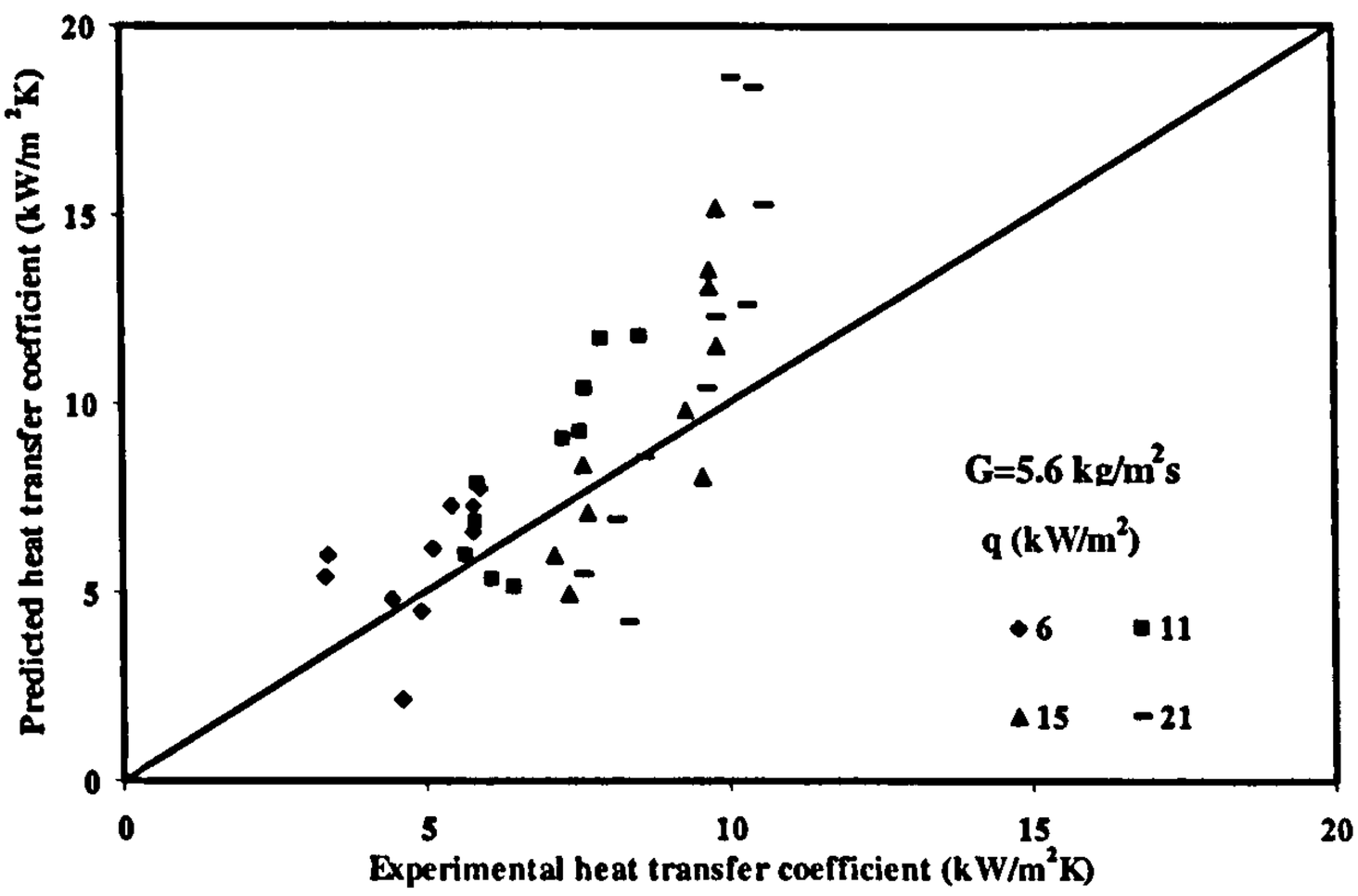

Figure 6.16 Predicted heat transfer coefficient using Thome, Dupont et al [111] against experimental data for distilled water at G=5.6 kg/m^{2}s

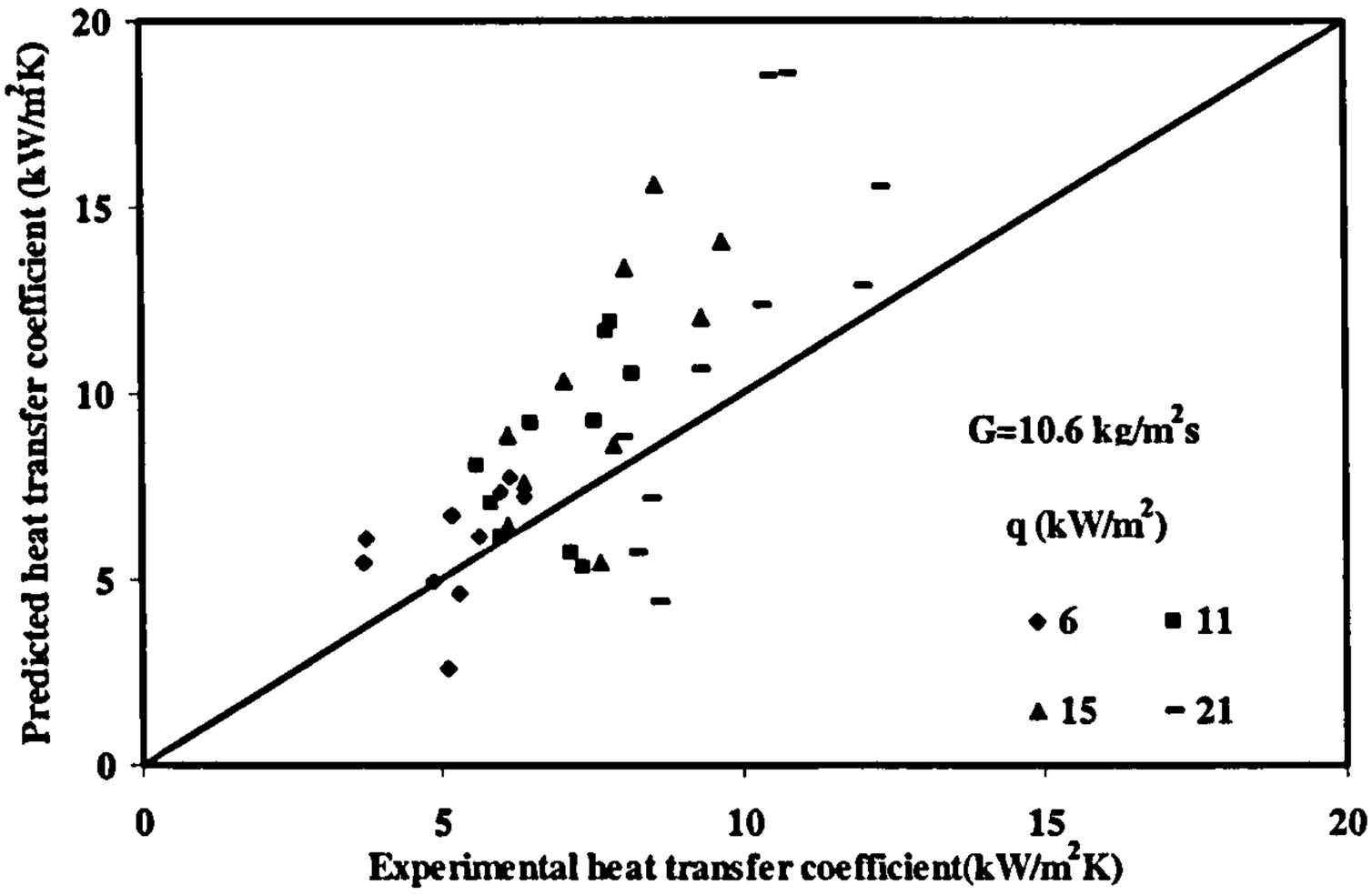

Figure 6.17 Predicted heat transfer coefficient using Thome, Dupont et al [111] against experimental data for distilled water at G=10.6 kg/m^{2}s

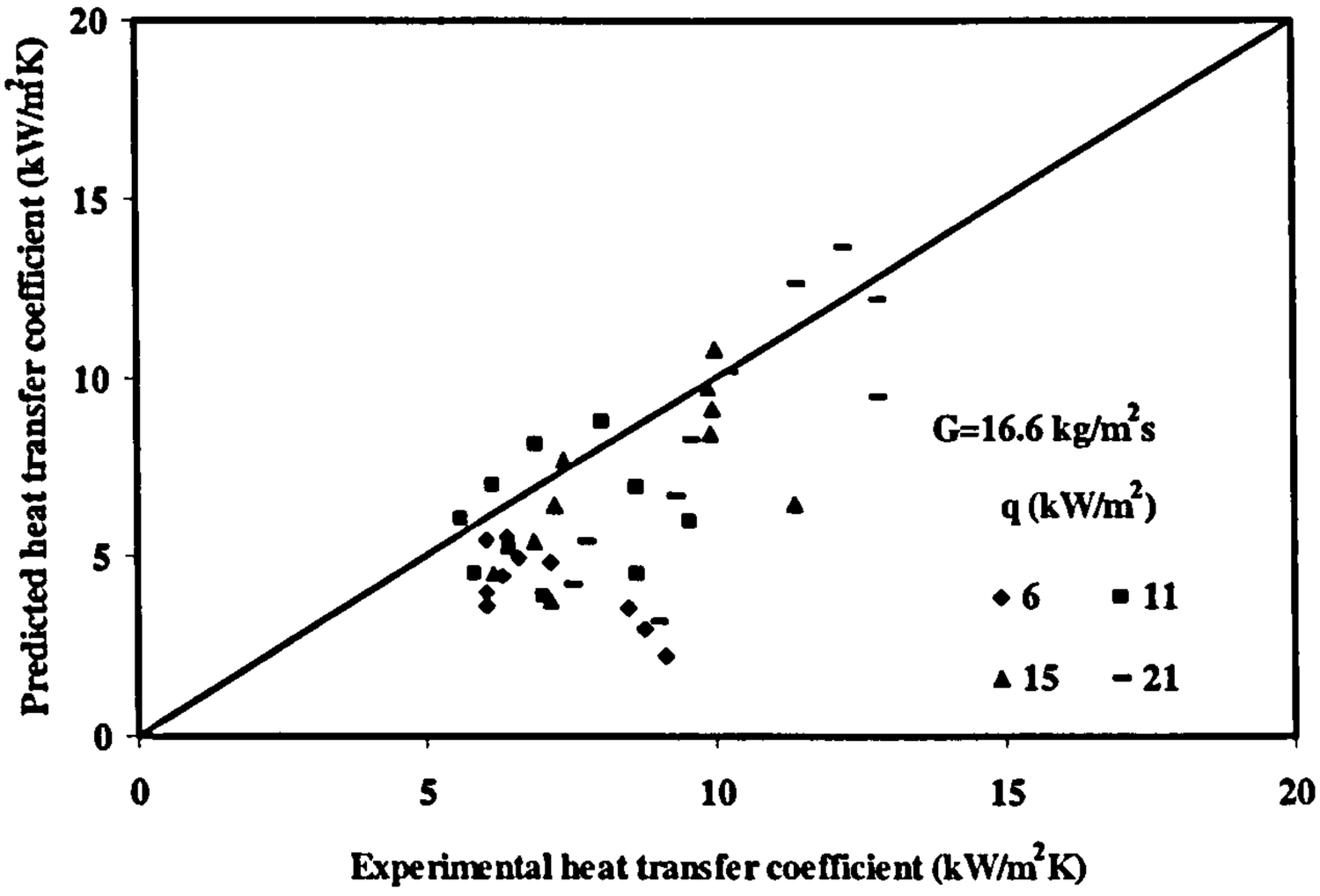

Figure 6.18 Predicted heat transfer coefficient using Thome, Dupont et al [111] against experimental data for distilled water at G=16.6 kg/m^{2}s

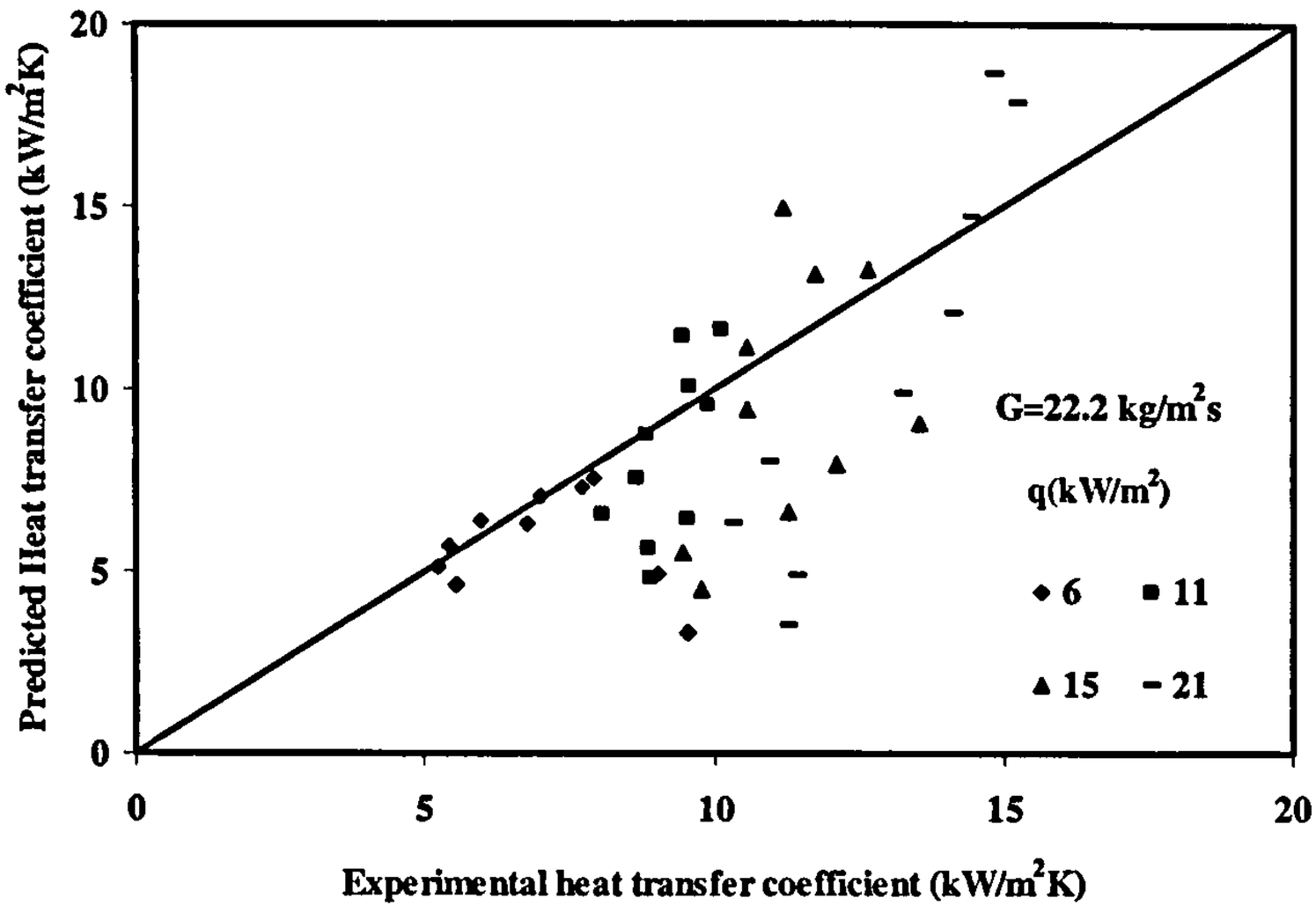

Figure 6.19 Predicted heat transfer coefficient using Thome, Dupont et al [111] against experimental data for distilled water at G=22.20 kg/m^{2}s

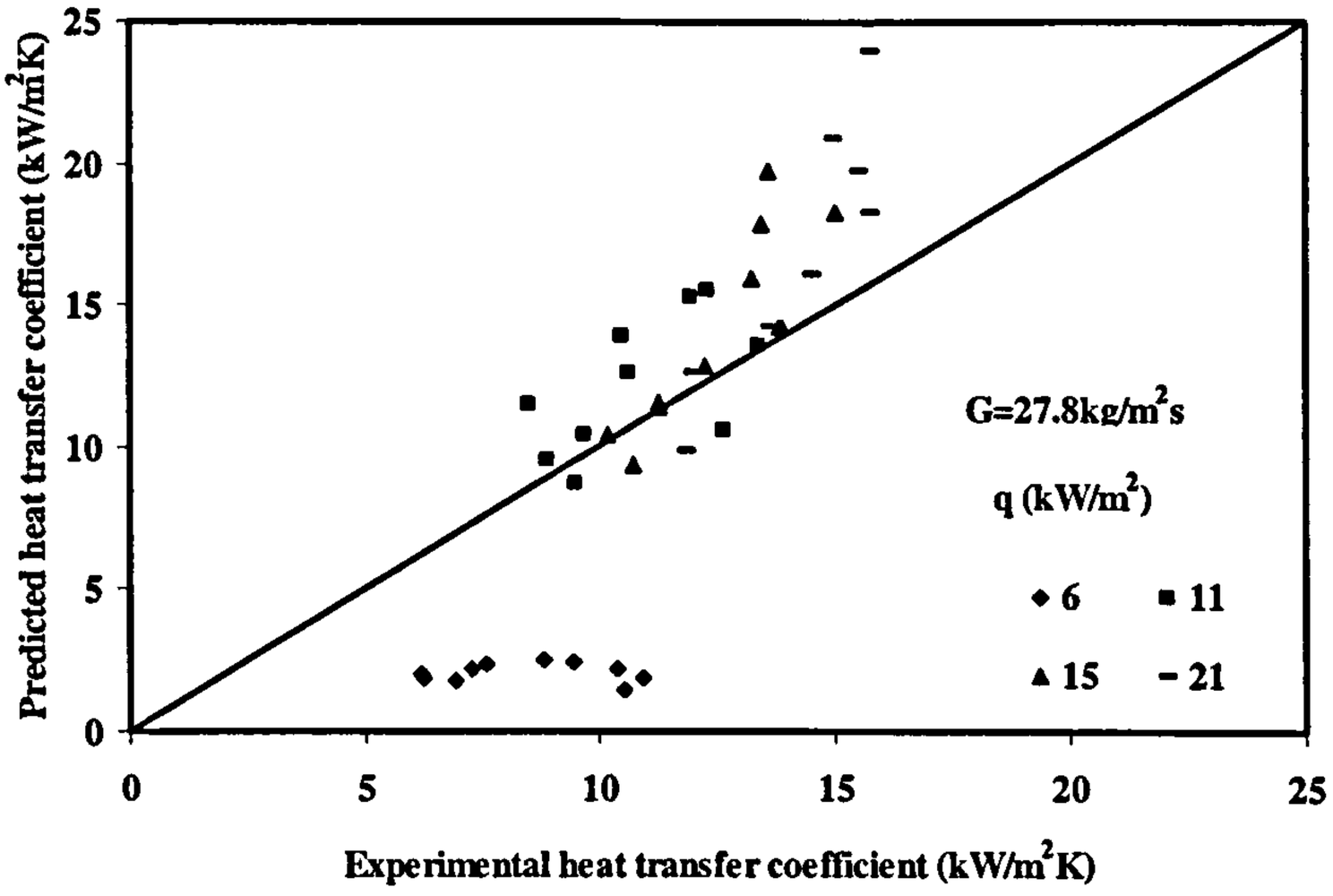

Figure 6.20 Predicted heat transfer coefficient using Thome, Dupont et al [111] against experimental data for distilled water at G=27.8 kg/m^{2}s

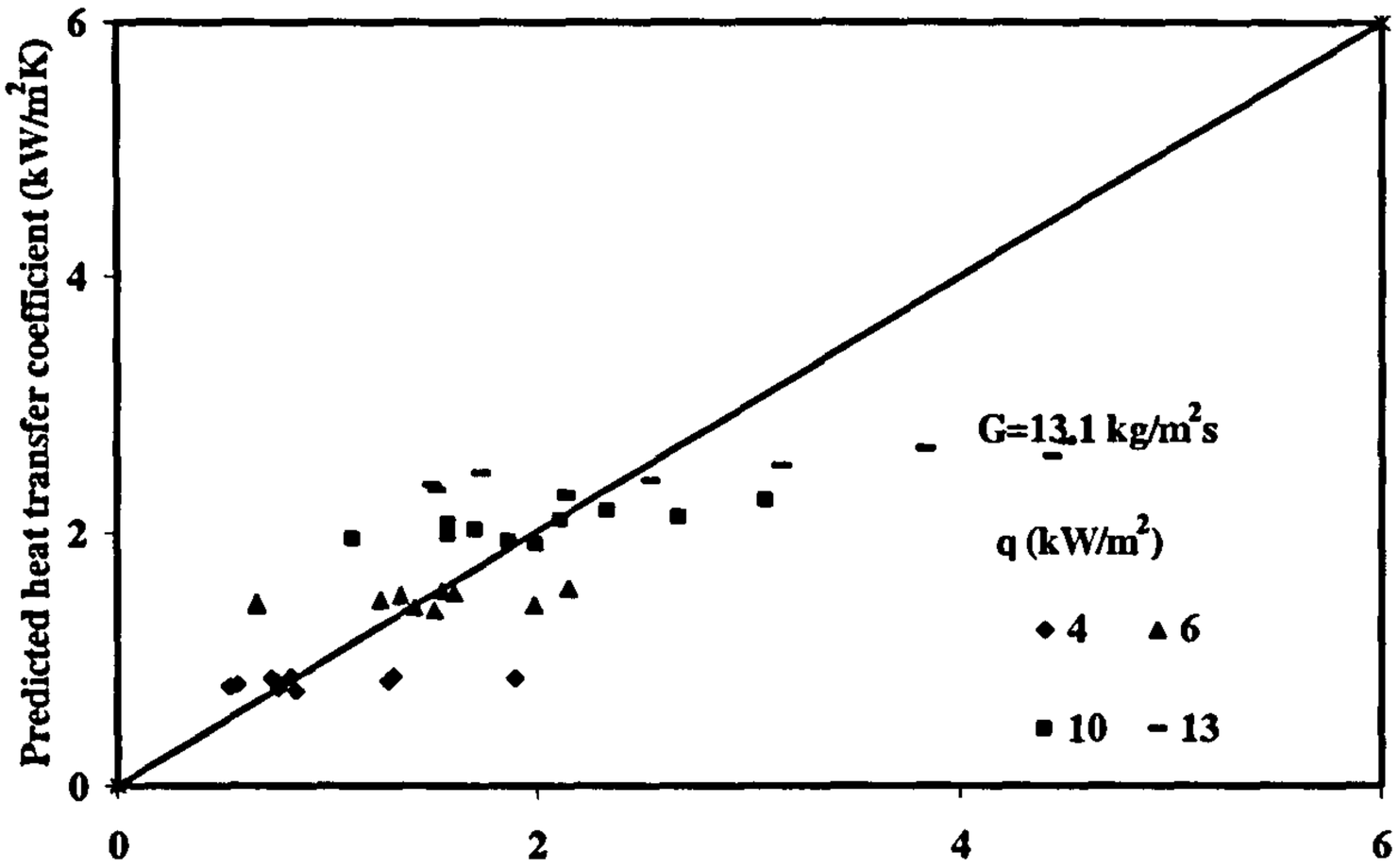

Figure 6.21 Predicted heat transfer coefficient using Thome, Dupont et al [111] against experimental data for R113 at G=13.1 kg/m^{2}s

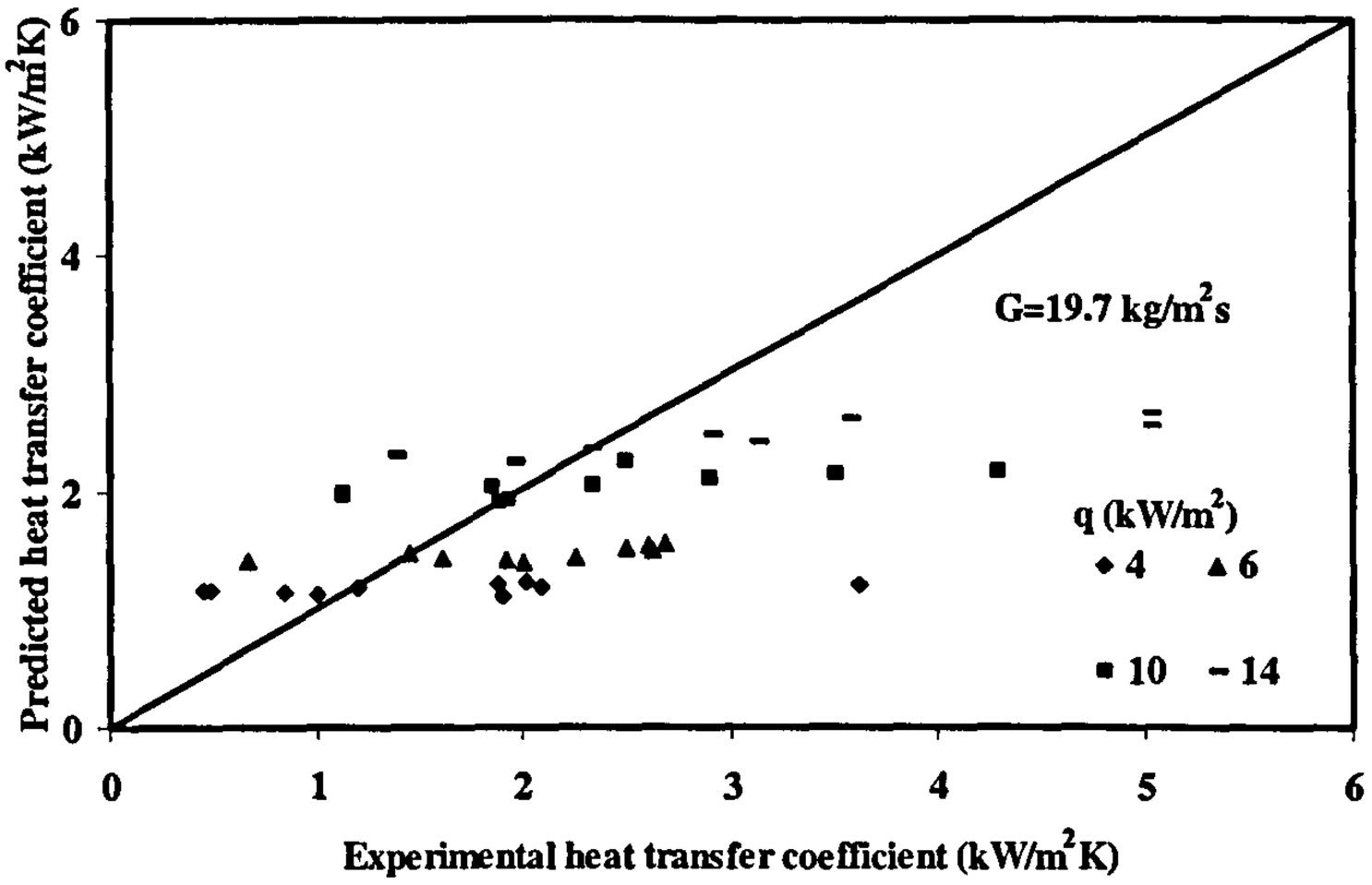

Figure 6.22 Predicted heat transfer coefficient using Thome, Dupont et al [111] against experimental data for R113 at G=19.7kg/m^{2}s

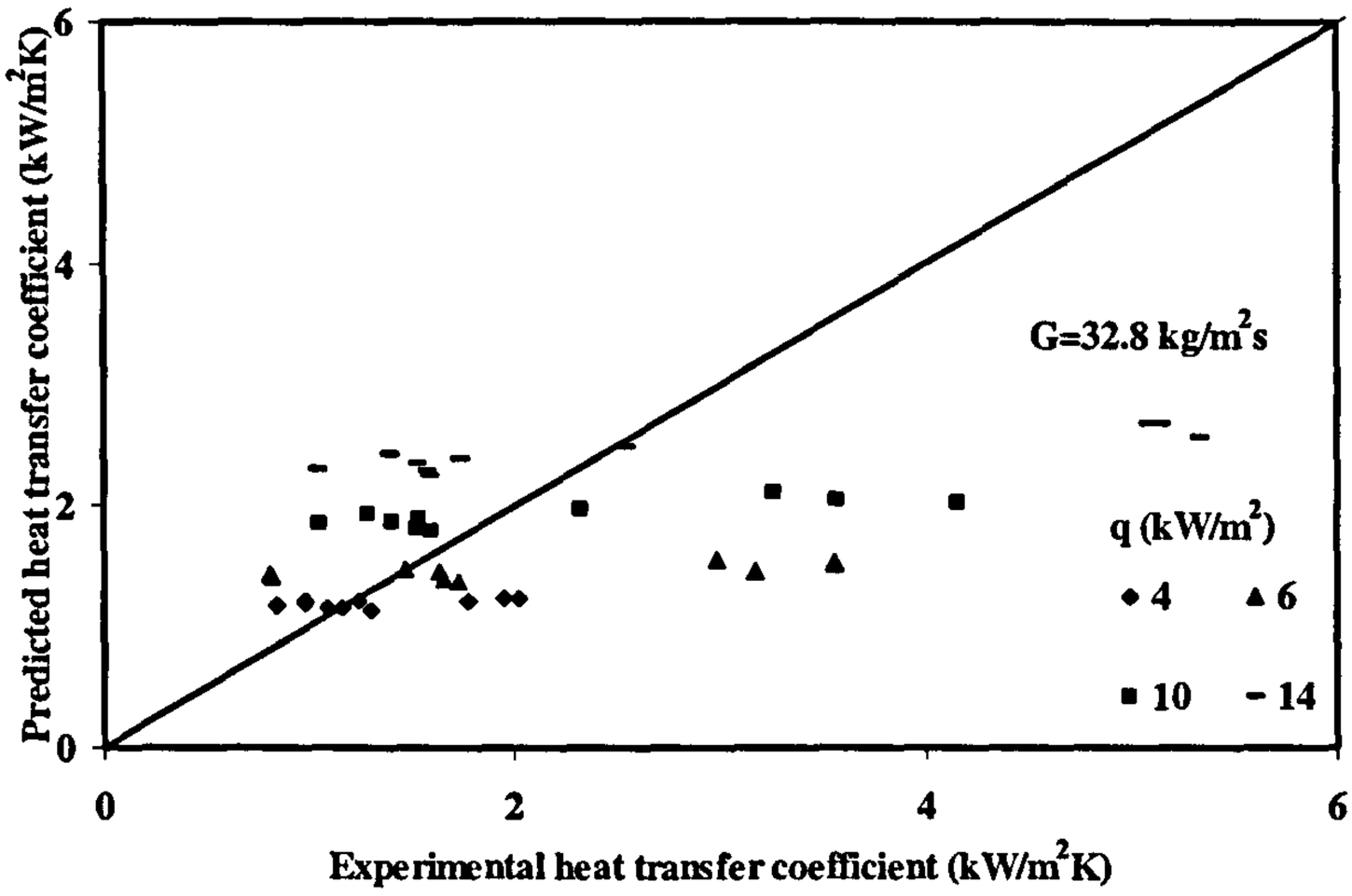

Figure 6.23 Predicted heat transfer coefficient using Thome, Dupont et al [111] against experimental data for R113 at G=32.8 kg/m^{2}s

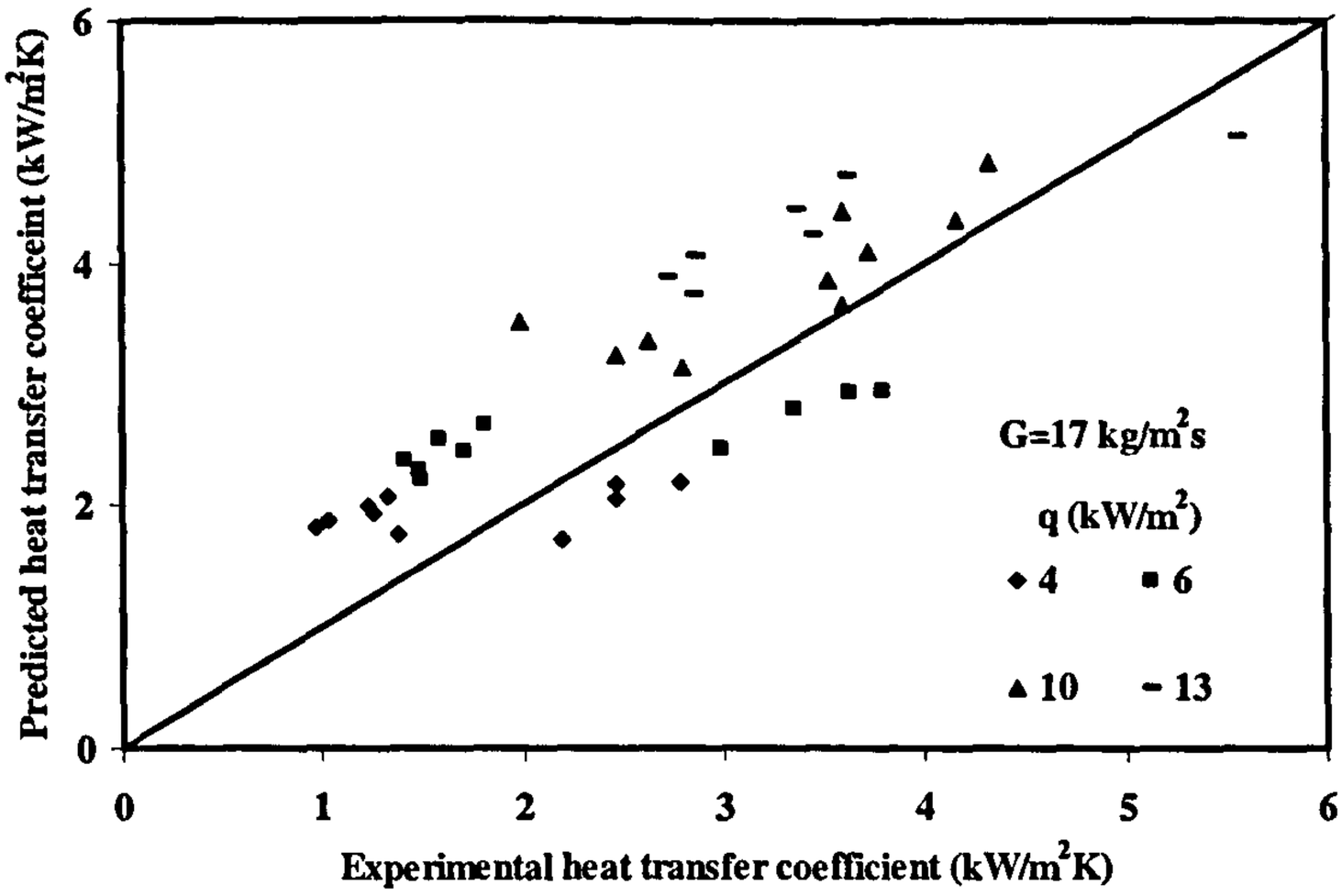

Figure 6.24 Predicted heat transfer coefficient using Thome, Dupont et al [111] against experimental data for Flutec PP1 at G=17 kg/m^{2}s

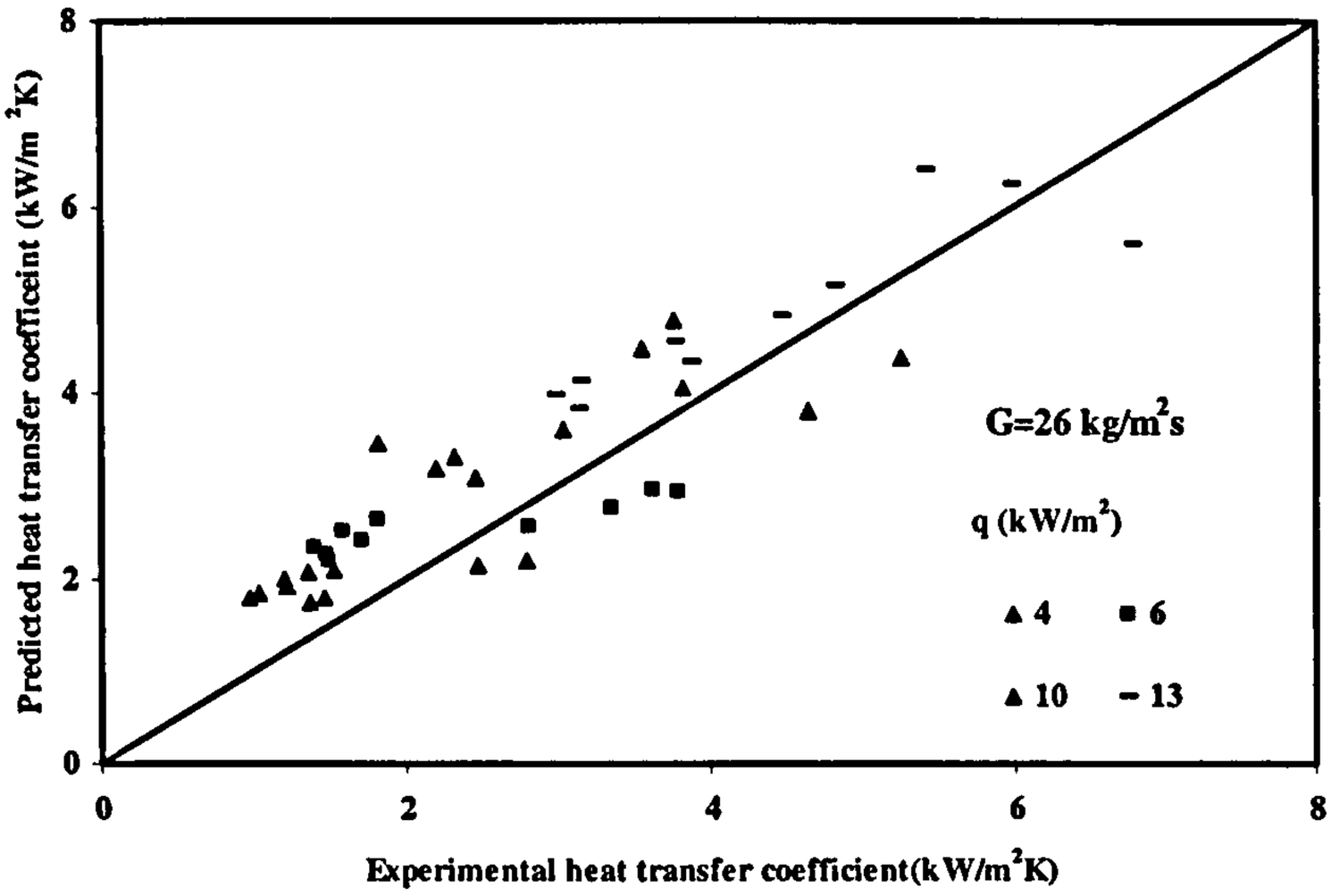

Figure 6.25 Predicted heat transfer coefficient against experimental values using Thome, Dupont et al [111] at G=26 kg/m^{2}s with Flutec PP1

The results obtained from the experimental studies are plotted in the form of heat transfer coefficient against vapour qualities for the working fluids shown in Figure 6.26 -Figure 6.29. It could be inferred from the plots that the heat transfer coefficient showed an increase within vapour qualities of 0 and 0.2 using the Thome, Dupont et al [111] correlation. Thus there is a reasonable agreement between the experiment and the Thome, Dupont et al [111] model at very low vapour quality. This is contrary to the models developed using the Chen's [18] approach for boiling in large diameter tubes. These models showed increase in heat transfer coefficient even at low vapour qualities.

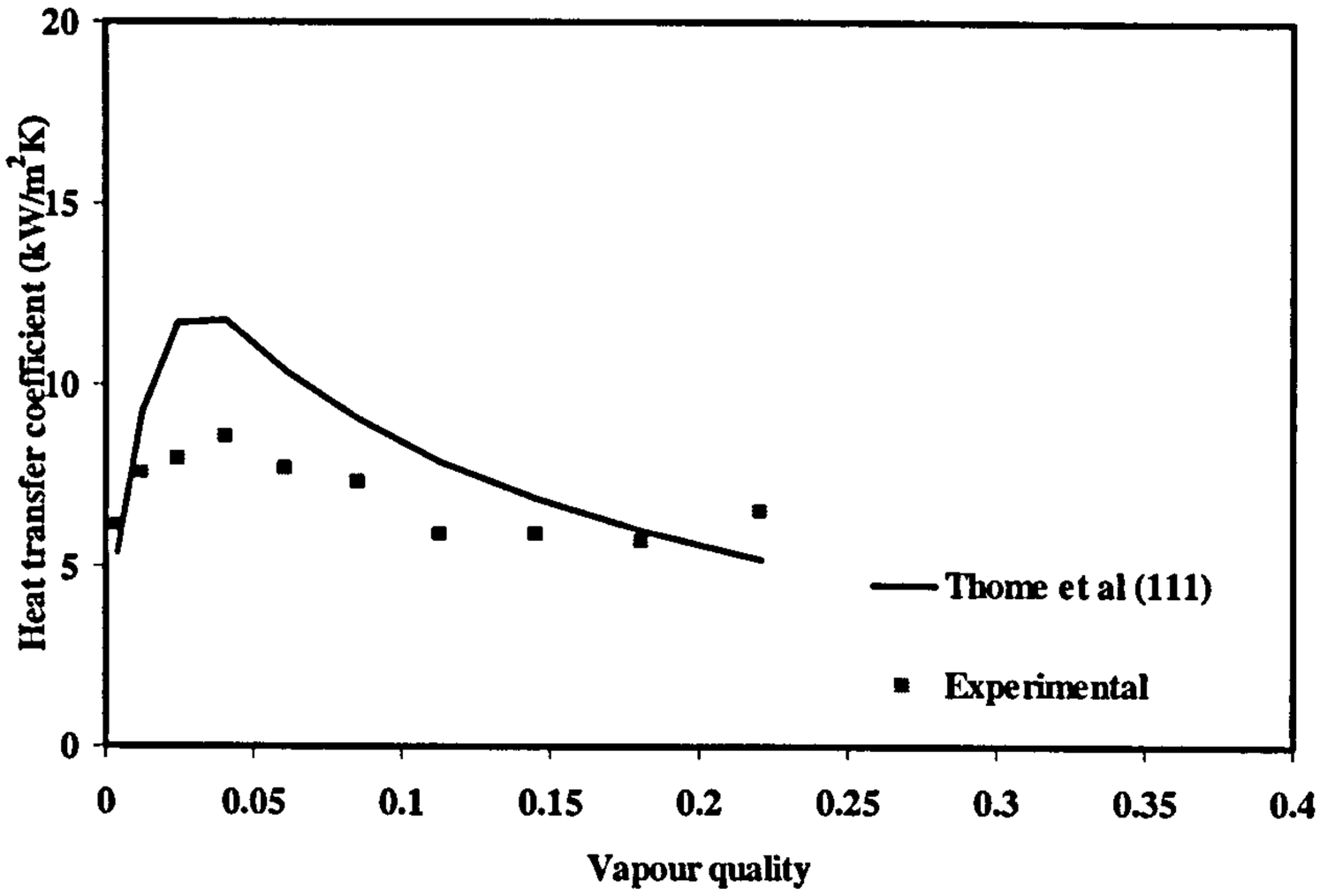

Figure 6.26 Predicted heat transfer coefficient using Thome, Dupont et al [111] against vapour quality for distilled water at G=5.6 kg/m^{2}s, q=11kW/m^2

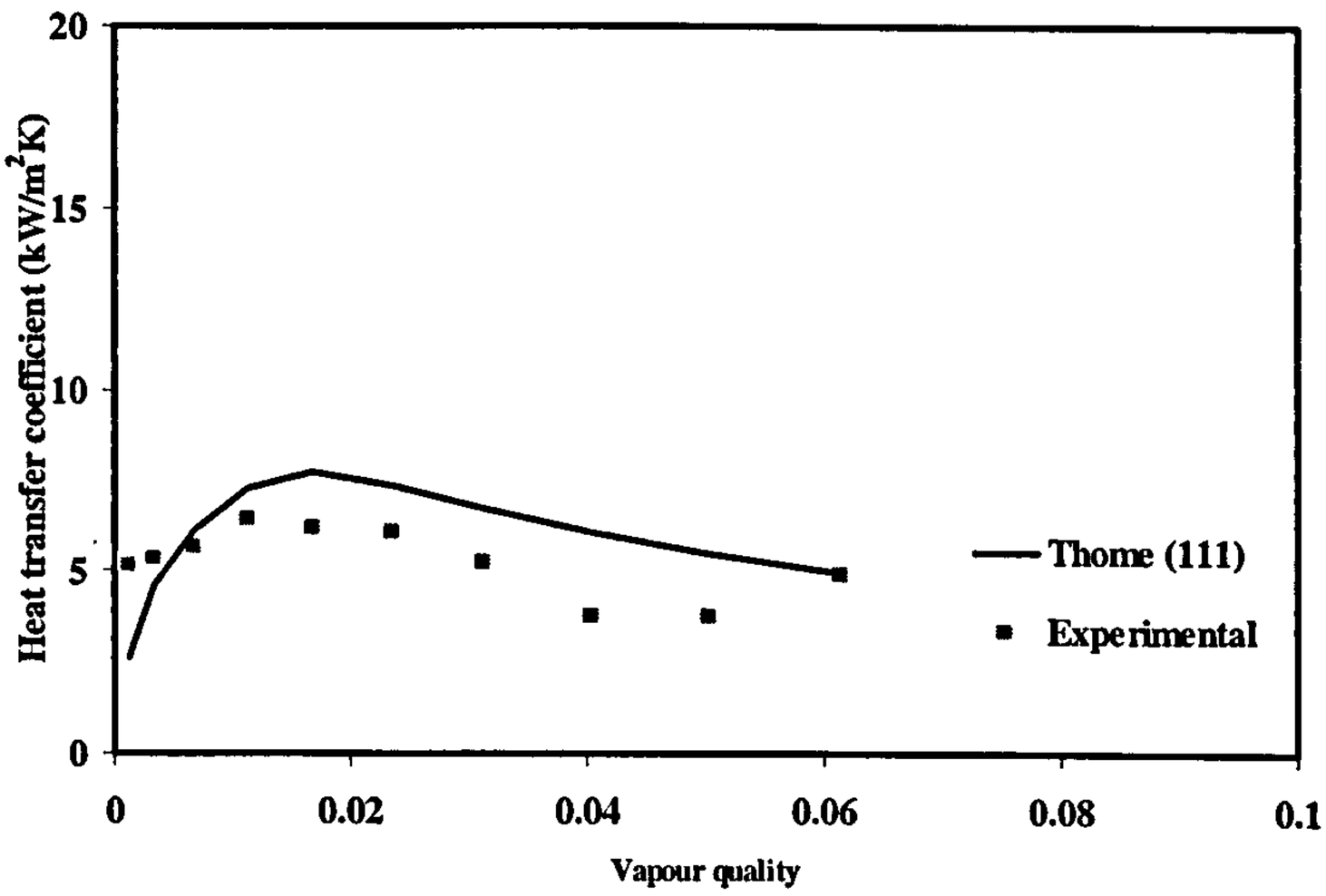

Figure 6.27: Predicted heat transfer coefficient using Thome, Dupont et al [111] against vapour quality for distilled water at G=10.6 kg/m^{2}s , q=6 kW/m^2

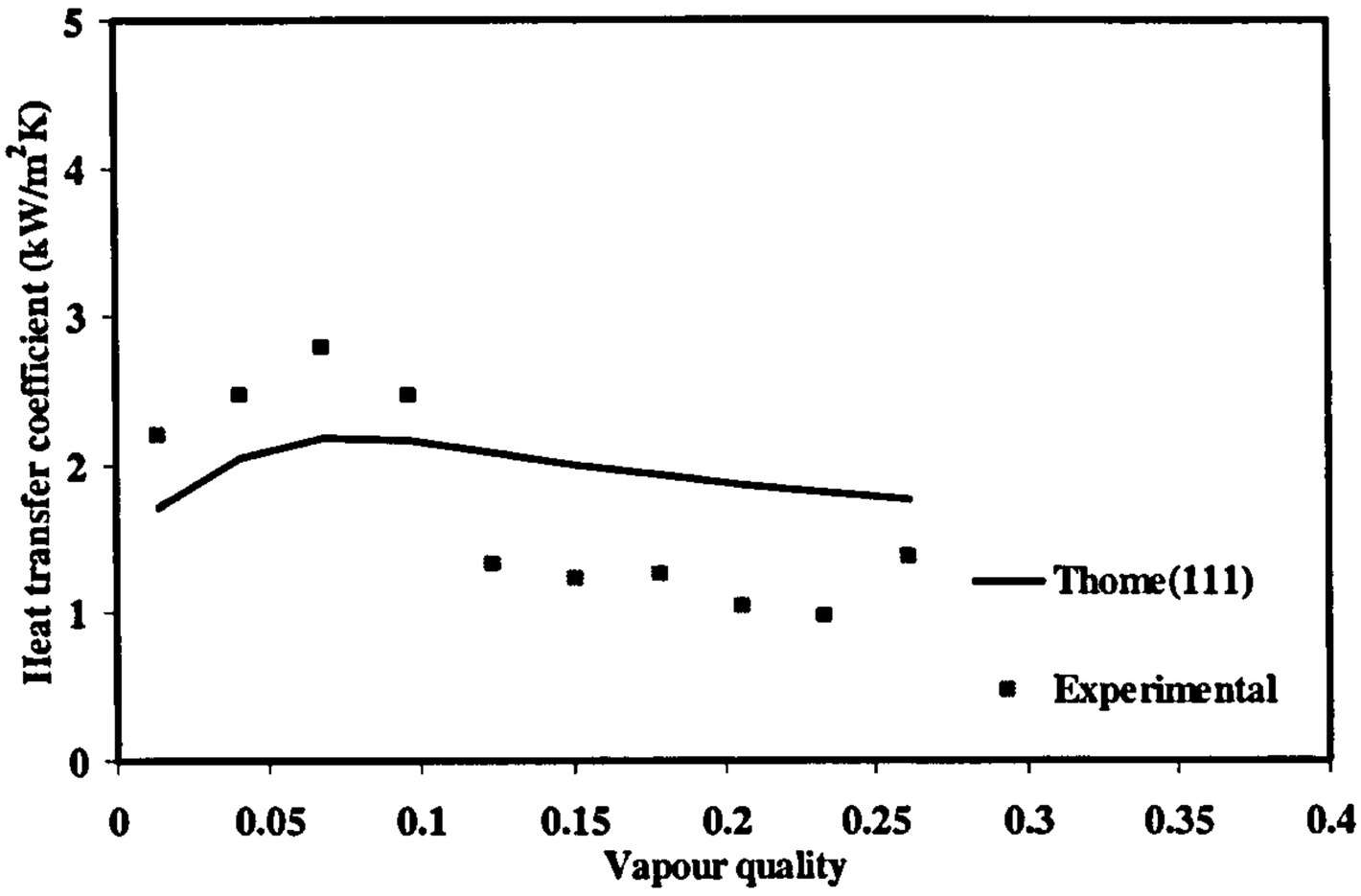

Figure 6.28 Predicted heat transfer coefficient using Thome, Dupont et al [111] against vapour quality for Flutec PP1 at G=17 kg/m^{2}s , q=4 kW/m^2

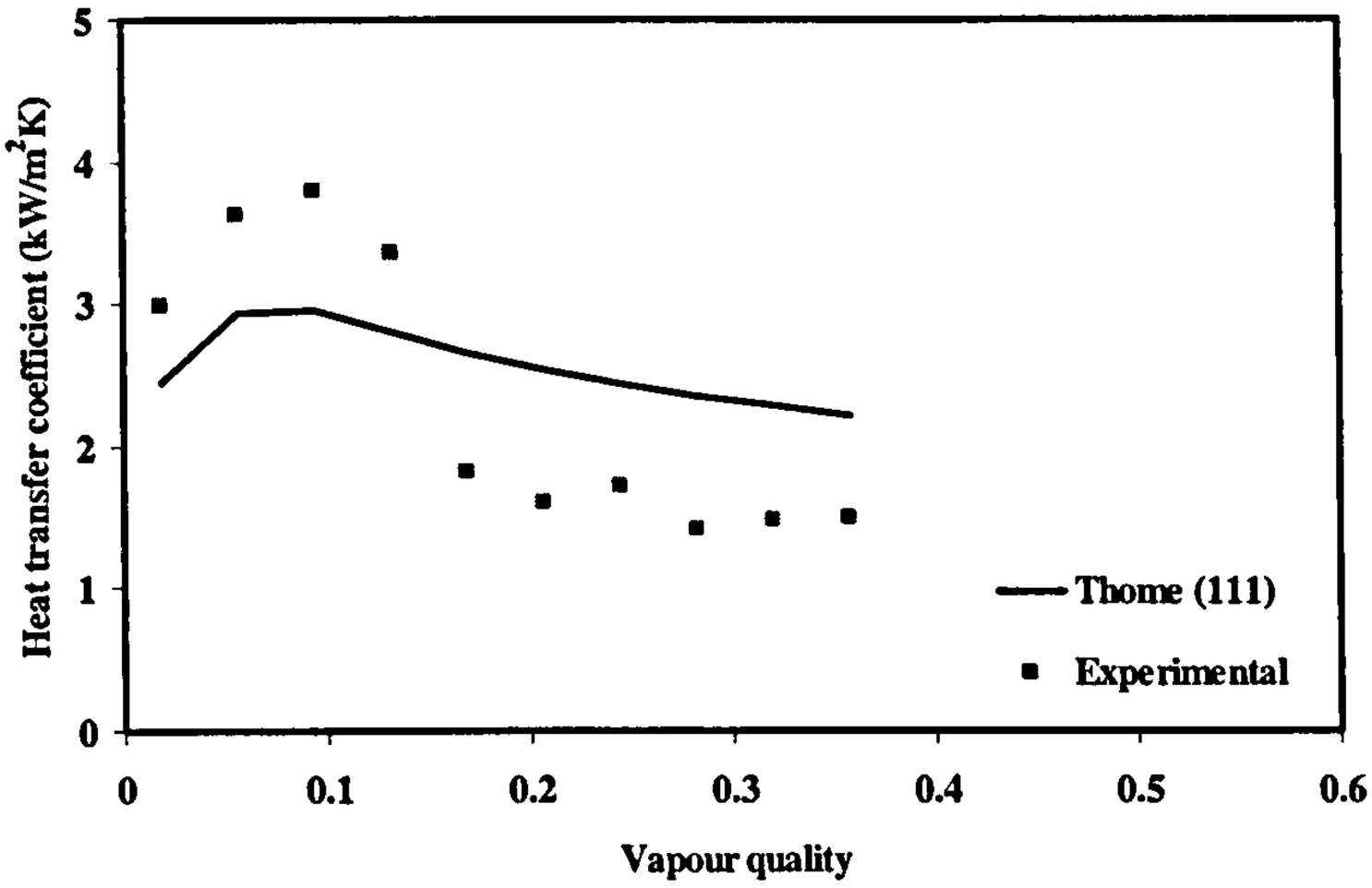

Figure 6.29 Comparison of heat transfer coefficient using Thome, Dupont et al [111] at G=17 kg/m^{2}s with experimental results using Flutec PP1 at q=6 kW/m^2

6.5.1 Comment on the Thome, Dupont et al [111] three-state model

The model of Thome, Dupont et al [111] is quite different from those that were described for large tubes, as it presented the elongated (confined bubble) as the dominant mechanism for the enhanced heat transfer coefficient in micro channels. The modified correlation assumed that the heat transfer coefficient due to the vapour and liquid slugs are negligible, effectively only the thin film would be considered. Table 6.5

to Table 6.7 shows the RSME analysis for the comparisons using distilled water, R-113 and Flutec PP1. Clearly the model predicts the results far better than the macro models for distilled water and R-113.

G(kg/m^{2}s)	RMSE
5.6	0.35
10.6	0.36
16.6	0.37
22.2	0.33
27.8	0.42

Table 6.5: Root Mean Square Error Analysis with Thome, Dupont et al [111] using distilled water

G(kg/m^{2}s)	RMSE
13.1	0.38
19.7	0.49
32.8	0.43

Table 6.6: Root Mean Square Error Analysis with Thome, Dupont et al [111] using R-113

G(kg/m^{2}s)	RMSE
17	0.38
26	0.39

Table 6.7: Root Mean Square Error Analysis with Thome, Dupont et al [111] using Flutec PP1

6.6 Concluding remarks

A comparison has been made between the experimental results and established large tube correlations. The following remarks are made;

- It has been established from the experimental results that the correlations developed for large tube bundles are inadequate in their prediction. It is also

argued that the nucleate boiling correlations need a better model for small diameter tubes

- The confinement number introduced in Chapter 5 has an effect on the results when the working fluid was distilled water. The model developed by Thome, Dupont et al [111] showed good agreement with the experimental results.

- The three-state model is similar in reasoning to the theoretical conception developed in Chapter 5 of this thesis. The similarities lies in the fact that both models considered the thin film evaporation as the dominant mechanism which accounts for the heat transfer coefficient

- The differences between the three-state model and the theoretical conception within the thesis are that no nucleate boiling was considered, no account was made for the effect of turbulence convection. An account of the film thickness using water was not included in the development of the model.

- It is therefore suggested that more data is needed in the development of an appropriate model that would evaporation though the thin film

Chapter 7

CONCLUSIONS AND RECOMMENDATIONS

7.1 Introduction

Advancement in process intensification has shifted attention from traditional heat exchanger equipment such as kettle reboilers, shell and tube heat exchangers which have been used extensively in industry for decades. The reliable design models have made it difficult for heat transfer engineers to adapt to more modern and compact design approaches which invariably save cost in terms of energy saving and low inventory. As a result, an experimental programme has been carried out to investigate the effect of diameter in a compact arrangement to differentiate it from traditional kettle reboilers. Data obtained from such an investigation could be used in the generation of a reliable CFD model for researchers and designers. In order to facilitate these objectives, an experimental investigation has been carried out for tube diameters in the range of 1.83-3.00mm using distilled water, Flutec PP1 and R-113 at nominal atmospheric pressure for pool and flow boiling heat transfer. Two rigs, were designed, Rig I for nucleate pool boiling and Rig II for convective flow boiling over a compact bundle with pitch to diameter ratio of 1.5.

7.2 Conclusion for twin–tube

The following conclusions are made for the single tube and twin-tube experimental work;

- Pool boiling correlations developed for large tubes and plates cannot be used with confidence in predicting heat transfer coefficient on small diameter tubes. The sliding bubbles that accounts for enhancement on large diameter tubes (8-50mm) diminishes as the diameter approaches 3.00mm
- The pool boiling experiment using single tubes diameters showed inconsistencies in the heat transfer coefficient as the diameter was reduced from 3.00mm to 2.32mm and 1.83mm

- From the twin-tube analysis, it has been shown that the enhancement on the upper tube is due to a combination of heat transfer mechanisms namely; translating bubbles and turbulent convection

7.3 Conclusion for compact tube bundle

Test in a compact tube bundle arrangement showed a variation in the heat transfer coefficient up the bundle for all the working fluids used. The following conclusions are drawn;

- The confinement number defined for in tube boiling for micro channels was extended to be applicable for boiling in compact bundles and was shown to be significant (C_o>0.63).

- Confined or elongated bubbles have been shown to be a significant mechanism in compact bundle compared to the nucleate boiling. Thin-film evaporation is responsible for the heat transfer coefficient observed in the tube bundle.

- The modified Thome, Dupont et al [111] correlation was able to predict the results to within on average 35% which supports the hypothesis that the heat transfer coefficient in micro channels was that of thin film evaporation under a passing bubble.

- Flow visualisation showed that the dominant regime at medium heat flux was that of confined bubble.

7.4 Future work and recommendations 0

Future work on boiling over small diameter tube bundles should include investigating the effects of the following;

- Pitch to diameter ratio and tube diameter

- Pressure drop across the tube bundle

- Wide range of heat and mass flux

- Effect and variation of bundle geometry from in-line to staggered arrangement

- Large data bank is required to permit the determination of constants used in the modified model derived here

Much work has been carried out over the past century on the pool and flow boiling heat transfer from large diameter tube bundles and it has been generally understood that nucleate and convective boiling are the dominant mechanisms responsible for the heat transfer. Thus modelling approaches have been based on this premise, which could not be used to predict data when micro or mini channels are used. Presently there are few studies on boiling in a compact tube bundle. In fact, more investigations are needed to fully complement the studies carried out in this thesis in order to apply it to the development of new and novel ideas in the areas of process intensification, electronic cooling and the design of compact heat exchangers.

REFERENCES

1. Kandlikar, G.S., ed. *Hand book of phase change: Boiling and Condensation.* 1999, Taylor and Francis.
2. Jakob, M. and W. Linke, *Der Warmeubergang von einer waagerechten Platte an siedendes Wasser.* Forsch Ingenieurwes, 1933. **4**: p. 75-81.
3. Rohsenow, W.M., *A method for correlating heat transfer data fro surface boiling of liquids.* Trans. ASME, 1952. **74**: p. 969-976.
4. Forster , H.K. and N. Zuber, *Dynamics of vapour bubbles and boiling heat transfer.* AIChE, 1955. **1**: p. 474-478.
5. Han, C.Y. and P. Griffith, *The mechanism of heat transfer in nucleate pool boiling .Part I,II.* Int. J. Heat Mass Transfer, 1965. **8**: p. 887-904,905-914.
6. Beer, H., *Contribution of heat transfer to boiling.* Progr. Heat Mass Transfer, 1969. **2**: p. 311-370.
7. Moore, F.D. and R.B. Messler, *The measurement of rapid surface temperature fluctuations during nucleate boiling.* AIChE, 1961. **7**: p. 620-624.
8. Van Stralen, S. and R. Cole *Boiling Phenomenon.* 1979: McGraw- Hill,N.Y.
9. Frost, W. and C.J. Kippenham, *Bubble growth and heat transfer mechanism in the forced convection boiling of water containing a surface active agent.* Int. J. Heat Mass Transfer, 1967. **10**: p. 931-949.
10. Costas Tsouris and J.V. Porcelli. *Process Intensification-Has it really come?* 2003.
11. Whalley, P.B., *Boiling , Condensation and Gas-Liquid Flow.* 1987, Oxford University Press.
12. Hesselgreaves, J.E., *Compact Heat Exchangers: selection ,design and operation.* 1 ed. 2001: Elsvier Science Ltd. 398.
13. Nukiyama, S., *The maximum and minimum values of the heat transmitted from metal to boiling water at atmospheric pressure.* Int. J Heat and Mass Transfer, 1934. **9**: p. 1419-1433.
14. Akin, G.A. and W.H. McAdams, *Boiling heat transfer in natural convection evaporators.* Ind. Engng Chem, 1939. **31**: p. 487-491.
15. Bakhru, N. and J.H. Leinhard, *Boiling from Small Cylinders.* Int. J. Heat Mass Transfer, 1972. **15**: p. 2011-2025.
16. Elrod, W.C., *Boiling Heat Transfer Data at Low Heat Flux.* ASME.J .Heat Transfer, 1967. **109**: p. 235-243.

17. Wege, M.E. and M.K. Jensen, *Boiling heat transfer from a horizontal tube in an upward Flowing two phase cross flow.* ASME. J .Heat Transfer, 1984. **106**: p. 849-855.
18. Chen, J.C., *Correlation from boiling heat transfer to saturated fluids in convective flow.* I &EC Design. Develop., 1966. **5**(3): p. 322-329.
19. Yilmaz, S., J.W. Palen, and J. Taborek. *Enhanced boiling surfaces as single tubes and tube Bundles.* in *20th AIChE/ASME National heat Transfer Conf.* 1981.
20. Chung-Biau Chou and D.-C. Lu, *Pool boiling of R22,R-124 and R-134a on a plain tube.* Int. J.Heat Mass Transfer, 1997. **40**(7): p. 1657-1666.
21. Cooper, M.G., *Heat transfer rate in saturated nucleate boiling.* Advance Heat Transfer, 1984. **Vol. 16**: p. 157-239.
22. Gupta, S.C., S.K. Agarwal, and B.S. Varshney. *Nucleate pool boiling heat transfer from a horizontal heated cylinder to saturated liquids with radial flow agitation.* in *Convective flow and pool boiling conference.* 1997. Kloster, Germany.
23. Kumar, S., B. Mohanty, and S.C. Gupta, *Boiling heat transfer from a vertical row of horizontal tubes.* Int. J. Heat Mass Transfer, 2002. **Vol. 45**: p. pp. 3857-3864.
24. Ribatski and Jabardo, *Experimental Study on nucleate Boiling of halocarbon refrigerants on cylindrical surfaces.* Int. J. Heat Mass Transfer, 2003. **46**: p. 4439-4451.
25. Stephan, K. and M. Abdelsalam, *Heat Transfer Correlations for Natural Convection Boiling.* Int.J.Heat Mass Transfer, 1980. **23**: p. 73-87.
26. Cornwell, K. *The influence of diameter on nucleate boiling.* in *7th International Heat Transfer Conference.* 1982. Munich and published as "Heat Transfer 1982".
27. Cornwell, K. and S.D. Houston, *Nucleate Pool Boiling on horizontal tubes: a convection based correlation.* Int. J. Heat Mass Transfer, 1994. **Vol. 37**(1): p. 303-309.
28. Kang, M.-G., *Experimental Investigation of Tube length effect on Nucleate Pool Boiling heat transfer.* Annals of Nuclear Energy, 1998. **25**(4-5): p. 295-304.
29. Kew, P.A. and S.D. Houston, *The effect of diameter on boiling heat transfer from the outside of small horizontal tubes.* Trans IChemE, 2002. **Vol.80**(A): p. 278-283.

30. Kaupmann, P., D. Gorenflo, and A. Luke. *Pool Boiling heat transfer on horizontal tubes with different diameters.* in *Boling 2000,Phenomena and Emerging applications.* 2000. Alaska: Begell House.

31. Cornwell, K. and P.A. Kew. *Boiling on Column of Horizontal Wires.* in *8th UK National Heat Transfer Conference.* 2000. Oxford.

32. Das, S., K, N. Putra, and S. Kabelac, *An experimental investigation of pool boiling on narrow horizontal tubes.* Experimental Heat Transfer, 2004. **17**: p. 131-146.

33. Hahne, E. and K. Shi, *How to obtain boiling heat transfer coefficients for tubes from wire experiements.* Int. Comm of Heat and Mass Transfer, 1993. **20**: p. 361-373.

34. Cornwell, K., P.A. Kew, and S.D. Houston. *Boiling in Compact Shell and Tube Bundles.* in *5th International Conference on Boiling Heat Transfer.* 2003. Montego Bay, Jamaica.

35. Schuller, R.B. and K. Cornwell. *Dryout on the Shell -Side of Tube Bundles.* in *IChem E Symposiom series.* 1984.

36. Cornwell, K., *Thermal Optimization of Refrigeration Evaporators.* Proceedings f Institute of Refrigeration Engineers, 1991. **88**: p. 26-35.

37. Cornwell , K., *A new approach to determination of boiling heat transfer coefficients outside tube bundles.* Heat Transfer 1992, 1992. **1**: p. 51-64.

38. Pioro, I.L. *Boiling heat transfer characteristics of thin liquid layers in a horizontally flat two-phase thermosyphon.* in *10th International Heat Pipe Conference.* 1997. Stuggart, Germany.

39. Mostinski, I.L., *Calculation of heat transfer and critical heat flux in boiling liquids based on the law of corresponding states.* Teploenergetica, 1963. **Vol. 10**(4,): p. 66-71.

40. Labuntsov, D.A., *Heat transfer problems with nucleate boiling of liquids.* Thermal Engineering, 1972. **19**(9): p. 21-28.

41. Gorenflo, D., *Pool boiling.* VDI-Heat Atlas, VDI-Verlag, Dusseldorf, 1993.

42. Gorenflo, D., P. Sokol, and S. Caplanis, *Pool boiling heat transfer from single plain tubes to various hydrocarbons.* Int. Journal of Refrigeration, 1990. **13**: p. 286-292.

43. Chun, M.-H. and M.-G. Kang, *Effects of heat exchanger tube parameters on nucleate pool boiling heat transfer.* ASME.J .Heat Transfer, 1998. **120**: p. 468-476.

44. Cornwell, K. and R.B. Schuller, *A study of boiling outside a tube bundle using high speed photography.* Int.J.Heat Mass Transfer, 1982. **35**(5): p. 683-690.
45. Collier, J.G. and J.R. Thome, *Convective boiling and condensation.* 1994: Oxford Science Publications.
46. Palen, J.W., A. Yarden, and J. Taborek, *Characteristics of boiling outside large scale multi tube bundles.* AIChE Symposium, 1972: p. pp. 50-61.
47. Myers, J.E. and D.L. Katz, *Boiling coefficients outside horizontal tubes.* Heat Transfer Symposium Series No. 5,1953, 1953(5): p. 107-114.
48. Wall, K.W. and E.L. Park Jnr, *Nucleate boiling of n-pentane, n-hexane and several mixtures of the two from various tube arrays.* Int. J. Heat Mass Transfer, 1978. **Vol. 21**: p. pp. 73-75.
49. Nakajima, I.J., *Boiling heat transfer outside horizontal tubes.* Heat Transfer Japanese Research, 1978. **7**(2): p. 1-24.
50. Leong, L.S. and K. Cornwell, *Heat Transfer Coefficients in a Reboiler Tube Bundle.* IChemE, 1979.
51. Scoones, D.J., *Boiling on plain and low finned tube bundles, PhD Thesis*, in *Mechanical Engineering*. 1986, Heriot-Watt University: Edinburgh.
52. Rebrov, P.N., V.G. Bukin, and G.N. Danilova, *A correlation for local heat transfer coefficients of heat transfer in boiling of R12 and R22 refrigerants on multirow bundles of smooth tube.* Heat Transfer-Soviet Research, 1989. **21**(4): p. 543-548.
53. Danilova, G.N., V.A. Dyundin, and A.G. Soloviyov, *Heat transfer in boiling of R717 and R22 refrigerants on multirow tube bundles.* Heat Transfer Soviet Research, 1992. **24**(7): p. 889-893.
54. Fujita, Y., H. Ohta, et al. *Boiling heat transfer on horizontal tube bundles,*. in *Proc. Heat Transfer Science and Technology*. 1987. Beijing, China.
55. Fujita, Y., *Heat Transfer in Nucleate Boiling Outside Tube bundles-Prediction for Tube Bundle Effect.* Heat Transfer Japanese Research, 1990. **Vol.1**(2): p. pp. 25-40.
56. Jensen, M.K. and J.T. Hsu, *A parametric study of Boiling Heat Transfer in a Horizontal Tube Bundle.* ASME.J .Heat Transfer, 1988. **Vol.110**: p. 976-981.
57. Grant, I.D.R. and J.A.R. Henry, *Tests on Small Kettle Reboiler.* Heat Exchangers for Two-Phase Applications, 1983. **HTD 27**: p. 41-45.
58. Hsu , J.T., C.S. Lin, and M. Jensen, *Boling heat transfer mechanisms in a horizontal tube bundle.* Experimental Heat Transfer, 1993. **6**: p. 259-271.

59. Robinson, D.M. and J.R. Thome, *Local bundle boiling heat transfer coefficients on a plain tube bundle.* HVAC&R research, 2004. **10**(1): p. 33-51.

60. Yilmaz, S. and Westwater, *Effect of Velocity Heat transfer to Boiling Freon-113.* Journal of Heat Tranfer, 1981.

61. Singh, R.L., J.S. Saini, and H.K. Varma, *Effect of cross flow in boiling heat transfer of water.* Int.J Heat and Mass Transfer, 1983. **26**: p. 1882-1885.

62. Fink, J., E.S. Gaddis, and A. Vogelpol. *Forced convection boiling of a mixture f Freon -11 and Freon 23 flow normal to a cylinder.* in *7th International Heat Transfer Conference.* 1982. Munich.

63. Hwang, T.H. and S.C. Yao, *Forced convective boiling in horizontal tube bundles.* Int.J.Heat Mass Transfer, 1986. **29**(5): p. 785-794.

64. Chen, J.C., *A correlation for boiling heat transfer to saturatedfluids in convective flow.* ASME paper 63-HT-34, 1963.

65. Gupta, A., *Enhancement of boiling heat transfer in a 5*3 tube bundle* Int.J Heat and Mass Transfer, 2005. **48**: p. 3763-3772.

66. Cornwell, K., J.G. Einarsson, and P.R. Andrews. *Studies on boiling in tube bundles.* in *8th International Heat transfer Conference,* . 1986. San Francisco,: Hemisphere.

67. Kew, P.A., E. Adom, and K. Cornwell *Heat flux controlled boiling in confined spaces.* in *13th International Conference on Heat and Mass Transfer* 2006. Sydney, Australia.

68. Ivanov, O.P., V.O. Mamchenko, and A.L. Yemel Yanov, *Boiling and condensation of refrigerants on bundles of smooth horizontal tubes of a two phase thermosyphon.* Heat Transfer Soviet Research, 1988. **210**(3): p. 289-293.

69. Slesarenko, V.N., A.Y. Rudakova, and G.A. Zakharov, *Effects of operating conditions and tube boiling geometry on boiling heat transfer.* Heat Transfer Soviet Research, 1982. **14**(2): p. 119-123.

70. Hsu, J.T. and M.K. Jensen, *Effect of Pitch to diameter ratio on cross flow boiling inline tube bundle.* Collected papers in Heat transfer -ASME, 1988: p. 239-245.

71. Marto, P.J. and C.L. Anderson, *Nucleate Boiling Characteristics of R-113 in a Small Tube Bundle.* ASME.J .Heat Transfer, 1992. **114**(2): p. 425-433.

72. Gupta A, J.S. Saini, and H.K. Varma, *Boiling heat transfer in small horizontal tube bundles at low cross-flow velocities.* Int.J.Heat Mass Transfer Vol.38 No 4, 1995. **38**(4): p. 599-605.

73. King, M.K. and M. Jensen, eds. *Local heat transfer and flow patterns distributions in a kettle reboiler.* Two-phase flow modelling and experimentation, ed. G.P. Celata and R.K. Shah. 1995. 1289-1296.

74. Fujita, Y., *Effects of tube bundles on Nucleate Boiling and Critical heat flux.* Heat Transfer -Asian Research, 1998. **27**(4): p. 312-325.

75. Hahne, E., C. Qiu-Rong, and R. Windisch, *Pool Boiling experiments on finned tubes -an experimental study.* Int. J. Heat Mass Transfer, 1991. **Vol. 34**(8): p. 2071-2079.

76. Zhen-Hua Liu and Y.-H. Qiu, *Enhanced Boiling heat transfer in restricted spaces of a compact tube bundle with enhanced tubes.* Applied Thermal Eng., 2002. **22**: p. 1931-1941.

77. Liu, Z.-H. and E. Ishibashi, *Enhanced boiling heat transfer of Water/salt mixtures in the restricted space of the compact tube bundle.* Heat Transfer Engineering, 2001. **22**(3): p. 4-10.

78. Qui, Y.-H. and Z.-H. Liu, *Boiling heat transfer of water on smooth tubes in a compact staggered tube bundle.* Applied Thermal Engineering, 2004. **24**: p. 1431-1441.

79. Cornwell, K., *The Influence of bubbly flow on boiling from a tube bundle.* Int. J. Heat Mass Transfer, 1990. **Vol.33**(12): p. 2579-2584.

80. Cornwell, K. *The Role of Sliding Bubbles on tube bundles.* in *9th Int. Heat Transfer Conf.* 1990. Jerusalem: Hemisphere.

81. Cornwell, K., S.D. Houston, and A.J. Adlesee. *Sliding Bubbles heat transfer on a tube under heating and cooling conditions.* in *Proceedings of Engineering Foundation on Pool and Flow Boiling*. 1992. Santa Barbara,California.

82. Addlesee, A.J. and K. Cornwell, *Liquid film thickness above a bubble rising under an inclined plate.* Trans IChemE, 1997. **75, Part A,**: p. 663-667.

83. Adlesee, A.J. and K. Cornwell, *Liquid film thickness above a bubble rising under an inclined plate.* Trans IChemE, 1997. **75,Part A**: p. 663-667.

84. Kenning, D.B.R., O.E. Butress, and Y. Yan. *Heat Transfer to a sliding Bubble.* in *Proc. UEF Conference, Boiling 2000 :Phenomena and Emerging Applications,*. 2000. Alaska: Begell House.

85. Adlesee, A.J. and P.A. Kew, *Development of the liquid film above a sliding bubble.* Trans IChemE, 2002. **80 Part A**: p. 272-277.

86. Palen, J.W. and C.C. Yang, *Circulation Boiling Model for analysis of kettle and internal rebolers.* Heat Exchangers for Two-Phase applications, 1983. **HTD-27**: p. 55-61.

87. Bennet, L., M.W. Davis, and B.L. Hertzler, *The suppresion of saturated nucleate boiling by forced convective flow.* AIChE Symposium, 1980. **76**(199): p. 91-103.

88. Cornwell, K., N.W. Duffin, and R.B. Schuller. *An experimental Study of the effects of fluid flow on boiling within a kettle reboiler tube bundle,Paper No. 80-HT-45.* in *ASME/AIChE National Heat transfer Conference.* 1980. Orlando.

89. Zukauskas, A., *Heat transfer from tubes in cross flow.* Advances in Heat Transfer, 1972. **8**: p. 93-160.

90. Webb, R.L. and L.-H. Chien, *Correlations of convective vaporisation on banks of plain tubes using refrigerants.* Heat Transfer Eng . 1994. **15**(3): p. 57-69.

91. Gupte, N.S. and R.L. Webb, *Shellside Boiling in Flooded Refrigerant Evaporators II Enhaced tubes.* HVAC&R research, 1995. **1**(1): p. 48-60.

92. Ishihara , K., J.W. Palen, and J. Taborek, *Critical review of correlations for predicting two-phase flow pressure drop across tube banks.* Heat Transfer Eng . 1980. **1**(3): p. 23-32.

93. Cornwell, K. and D.J. Scoones, *Analysis of low quality boiling on plain and low finned tube bundles.* Heat Transfer, IMechE Mechanical Engineering Publications, 1988. **1**: p. 21-32.

94. Cornwell, K. and L.S. Leong, *On the analysis of low quality flow boiling.* Int.J.Heat and Fluid Flow, 1979. **1**: p. 63-69.

95. Brisbane, T.W.C., I.D.R. Grant, and P.B. Whalley, *A Prediction Method for Kettle Reboiler Performance.* ASME, 1980.

96. Whalley, P.B. and D. Butterworth, *A Simple method for calculating the recirculating flow in a vertical thermosyphon and kettle reboilers.* Heat Exchangers for Two-Phase Applications, 1983. **HTD 27**: p. 47-53.

97. Jensen, M.K., *A model for the recirculating flow in a kettle reboiler.* AIChE Symposium, 1988. **84**(263): p. 114-119.

98. Kumar, S., A. Jain, et al., *Recirculation model of a kettle reboiler.* Int. J Heat and Mass Trasnfer, 2003. **46**: p. 2899-2909.

99. Ishibashi, E. and K. Nishikawa, *Saturated boiling heat transfer in narrow spaces.* Int.J Heat and Mass Trasnfer, 1969. **12**: p. 863-894.

100. Fujita, Y., H. Ohta, et al., *Nucleate boiling heat transfer and critical heat flux in narrow space between rectangular surfaces.* Int.J. Heat and Mass Trasnfer, 1988. **31**(2): p. 229-239.

101. Hung, Y.-H. and S.C. Yao, *Pool boiling heat transfer in narrow horizontal annular crevices.* ASME Journal of Heat Transfer, 1985. **107**: p. 656-662.

102. Kang, M.-G. and Y.-H. Han, *Effects of annular crevices on pool boiling heat transfer.* Nuclear Engineering and Design, 2002. **213**: p. 259-271.

103. Kang, M.-G., *Effects of pool subcooling on boiling heat transfer in a vertical annulus with closed bottom.* Int. J Heat and Mass Transfer, 2005. **48**: p. 225-263.

104. Chen, L., Y.S. Tian, and T.G. Karayianis, *The effect of tube diameter on vertical two-phase flow regimes in small tubes.* Int. J Heat and Mass Transfer, 2006. **49**: p. 4420-4230.

105. Kew, P.A. and K. Cornwell *Correlations for the predictions of boiling heat transfer in small diameter channels.* Applied Thermal Eng., 1997. **17**(8-10): p. 705-715.

106. Cornwell , K. and P.A. Kew. *Boiling in Small Parallel Channels.* in *Proc. CEC Conference on Energy Efficiency in Process Technology.* 1993. Athens: Elsvier Applied Sciences.

107. Thome, J.R., *Boiling in microchannels: a review of experiment and theory.* International Journal of Heat and Fluid Flow, 2004. **25**: p. 128-139.

108. Webb, R.L. and N.S. Gupte, *A critical review for convective Vaporization in tubes and tube banks.* Heat transfer Eng Vol 13 no 3, 1992. **13**(3): p. 58-81.

109. Liu, Z. and R.H.S. Winterton, *A general correlation for saturated and subcooled flow boiling in tubes and annuli, based on a nucleate boiling equation.* Int.J Heat and Mass Transfer, 1991. **34**(11): p. 2759-2766.

110. Jacobi, A.M. and J.R. Thome, *Heat transfer model for evaporation of elongated bubble flows in microchannels.* Journal of Heat Transfer, 2002. **124**: p. 1131-1136.

111. Thome, J.R., V. Dupont, and A.M. Jacobi, *Heat transfer model for evaporation in microchannels: Part I: presentation of the Model.* Int. J. Heat Mass Transfer, 2004. **47**: p. 3375-3385.

112. Huo, X., L. Chen, et al., *Flow boiling and flow regimes in small diameter tubes.* Applied Thermal Eng., 2004. **24**: p. 1225-1239.

113. Andrews, P.R. and K. Cornwell, *Cross-sectional and longitudinal heat transfer variations in a reboiler tube bundle section.* Chemical Engineering Research Design, 1987. **65**.

114. Scoones, D.J., D. Morris , and K. Cornwell *Analysis of of flow boiling data from a tube bundle.* 1986. HTFS Research symposium.

115. Memory, S.B., S.V. Chilman, and P.J. Marto, *Nucleate Pool Boiling of a Turbo-B bundle in R-113.* ASME.J .Heat Transfer, 1994. **116**(3): p. 670-678.

116. Churchill, S.W., *Heat Exchanger Design Handbook.* 1983.

117. Houston, S.D. and K. Cornwell, *Heat Transfer to solid sliding bubbles on a tube under evaporating and non-evaporating conditions.* Int.J.Heat Mass Transfer, 1996. **39**(1): p. 211-214.

118. Boinnet, P., *Heat transfer from small tubes.* 2006.

119. Dowlati, R., M. Kawaji, and A.M.C. Chan, *Two-phase crossflow and boiling heat transfer in horizontal tube bundles.* Journal of Heat Transfer, 1996. **118**: p. 124-131.

120. Wallis, G.B., *One dimensional two-phase flow.* 1969: McGraw Hill.

121. Wallis, G.B. and S. Makkenchery, *The hanging film phenomenon in vertical annular two-phase flow.* Transaction of ASME Journal of Fluids Engineering, 1974.

122. Boundurant, D.L. and J.W. Westwater *Performance of transverse fins for boiling heat transfer.* Chemical Engineering Progress, 1971. **67**(113): p. 30-37.

123. Kutateladze, S.S., *Principle equations of thermodynamics of nucleate boiling.* Heat Transfer Soviet Research, 1981. **13**(3): p. 1-14.

124. Thome, J.R., *Enhanced boiling heat transfer.* 1990: Hemisphere,Washington D.C.

125. Yao, S.-C. and Y. Chang, *Pool boiling heat transfer in a confined space.* Int.J Heat and Mass Trasnfer, 1983. **26**(6): p. 841-848.

126. Steiner, D. and J. Taborek, *Flow boiling heat transfer in vertical tubes correlated by asymptotic model.* Heat Transfer Eng . 1992. **13**(2): p. 43-69.

127. Primoli, A., D. Francesco, and A. Prina. *An empirical correlation for evaluating two-phase mixture density under adiabatic conditions.* in *European Two-Phase Group Meeting, Milan.* 1970.

128. Zivi, S.M., *Estimation of steady -state steam void fraction by means of principle of minimum entropy production.* Journal of Heat Transfer, 1964. **86**: p. 247-252.

129. Chisholm, D., *An equation for velocity ratio in two-phase flow.* 1972, NEL, 535.

130. Addlesee, A.J. and P.A. Kew, *Development of the liquid film above a sliding bubble.* Trans IChemE, 2002. **80 Part A,pp.272-277.**

131. Dupont, V., J.R. Thome, and A.M. Jacobi, *Heat transfer model for evaporation in microchannels. Part II : comparion with data base.* Int.J Heat and Mass Transfer, 2004. **47**: p. 3387-3401.

APPENDIX

APPENDIX A: UNCERTAINTY ANALYSIS

This appendix analysis the uncertainty analysis for all the data reduction during the course of the experimental work.

Uncertainty in heat transfer area

Heat transfer area is given as;

$$A = \pi dl \tag{A. 1}$$

The uncertainty is obtained from;

$$\Delta A = \left[\left(\frac{\partial A}{\partial d} \right)^2 \Delta d^2 + \left(\frac{\partial A}{\partial l} \right)^2 \Delta l^2 \right]^{1/2} \tag{A. 2}$$

$$\Delta A = \left[(\pi l)^2 \Delta d^2 + (\pi d)^2 \Delta l^2 \right]^{1/2} \tag{A. 3}$$

Uncertainty in Cross sectional Area of tube

The cross sectional area of the tube is given as;

$$A_x = \pi \left(r_o^2 - r_i^2 \right) \tag{A. 4}$$

$$\Delta A_x^2 = \left(\frac{\partial A_x}{\partial r_o} \right)^2 \Delta r_o^2 + \left(\frac{\partial A_x}{\partial r_i} \right)^2 \Delta r_i^2 \tag{A. 5}$$

where,

$$\frac{\partial A}{\partial r_o} = 2\pi r_o$$

$$\frac{\partial A}{\partial r_i} = -2\pi r_o$$

Uncertainty in heat generated within the tube

$$q_g = \frac{Q}{A_x l} \tag{A. 6}$$

$$\Delta q_g{}^2 = \left(\frac{\partial q_g}{\partial Q}\right)^2 \Delta Q^2 + \left(\frac{\partial q_g}{\partial A}\right)^2 \Delta A^2 + \left(\frac{\partial q_g}{\partial l}\right)^2 \Delta l^2 \tag{A. 7}$$

Where,

$$\frac{\partial q_g}{\partial Q} = \frac{1}{Al}$$

$$\frac{\partial q_g}{\partial A} = \frac{-Q}{A^2 l}$$

$$\frac{\partial q_g}{\partial l} = \frac{-Q}{Al^2}$$

Uncertainty power input

$$Q = I^2 R \tag{A. 8}$$

$$\Delta Q = \left[\left(\frac{\partial Q}{\partial I}\right)^2 \Delta I^2 + \left(\frac{\partial Q}{\partial R}\right)^2 \Delta R^2\right]^{\frac{1}{2}} \tag{A. 9}$$

$$\Delta Q = \left[2IR\Delta I^2 + I^2 \Delta R^2\right]^{1/2} \tag{A. 10}$$

Uncertainty in heat flux

The heat flux is given as;

$$q = \frac{Q}{\pi dl} \tag{A. 11}$$

The uncertainty becomes;

$$\Delta q = \left[\left(\frac{\partial q}{\partial Q} \right)^2 \Delta Q^2 + \left(\frac{\partial q}{\partial d} \right)^2 \Delta d^2 + \left(\frac{\partial q}{\partial l} \right)^2 \Delta l^2 \right]^{1/2} \qquad \text{(A. 12)}$$

$$\Delta q = \left[\left(\frac{1}{\pi d l} \right)^2 \Delta Q^2 + \left(\frac{Q}{\pi d^2 l} \right)^2 \Delta d^2 + \left(\frac{Q}{\pi d l^2} \right) \Delta l^2 \right]^{1/2} \qquad \text{(A. 13)}$$

Heat transfer coefficient

Heat transfer coefficient is given by;

$$\alpha = \frac{q}{T_{wall} - T_{sat}} \qquad \text{(A. 14)}$$

The uncertainty in the heat transfer coefficient is given as ;

$$\Delta \alpha = \left[\left(\frac{\partial \alpha}{\partial q} \right)^2 \Delta q^2 + \left(\frac{\partial \alpha}{\partial \Delta T} \right)^2 \Delta T^2 \right] \qquad \text{(A. 15)}$$

where

$$\frac{\partial \alpha}{\partial q} = \frac{1}{\Delta T}$$

$$\frac{\partial \alpha}{\partial \Delta T} = \frac{-q}{\Delta T^2}$$

Calculation of Wall temperature of tube

The temperature of the inside wall of the tube is measured from the thermocouple. The surface temperature of the tube is analysed by considering the internal heat generated within the cylinder.

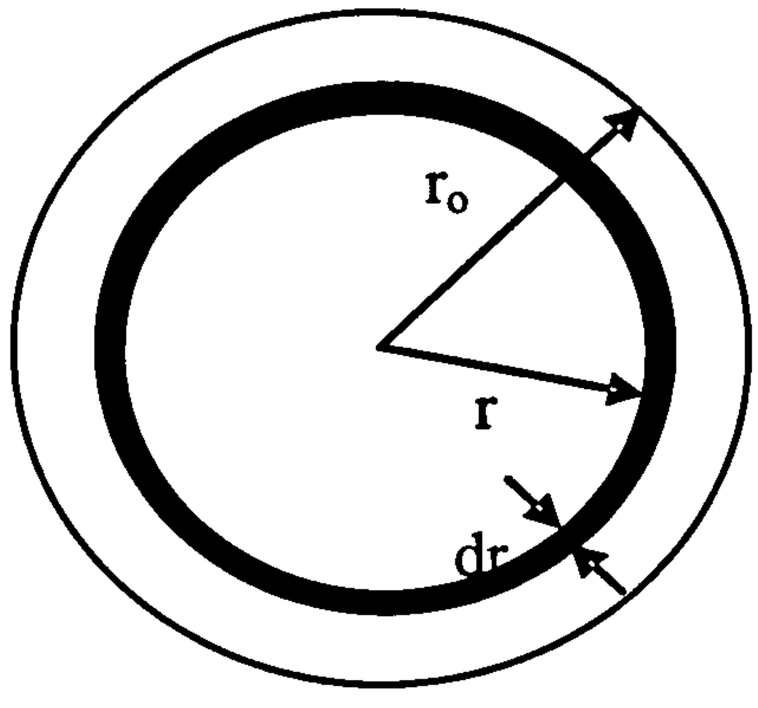

Figure A. 1: Cross section of a tube

For steady state radial conduction with no variation of the temperature profile along the tube .the energy balance may be written in the form;

$$\frac{d}{dr}r\left(\frac{dT}{dr}\right)+\frac{qr}{k}=0 \qquad \text{(A. 16)}$$

$$T=\frac{-qr^2}{4k}+c_1\ln r+c_2 \qquad \text{(A. 17)}$$

The boundary conditions are;

$$\frac{dT}{dr}(r_i)=0 \qquad \text{(A. 18)}$$

$$c_1=\frac{qr^2}{2k}\,T_i=T \text{ at } r_i$$

Therefore,

$$T_i=\frac{-qr_i^2}{4k}+\frac{qr_i^2}{2k}\ln r_i+c_2 \qquad \text{(A. 19)}$$

$$c_2=T_i+\frac{qr^2{}_i}{2k}\left(\frac{1}{2}-\ln r_i\right)$$

Then we have,

$$T_{wall} = \frac{-qr_o^{\,2}}{4k} + \frac{qr_i^{\,2}}{2k}\ln r_o + T_i + \frac{qr_i^{\,2}}{2k}\left(\frac{1}{2} - \ln r_i\right) \qquad \text{(A. 20)}$$

$$T_{wall} = T_i - \frac{qr_o^{\,2}}{2k}\left[\frac{1}{2} - \frac{r_i^{\,2}}{r_o^{\,2}}\ln r_o - \frac{r_i^{\,2}}{2r_o^{\,2}} + \frac{r_i^{\,2}}{r_o^{\,2}}\ln r_i\right]$$

$$T_{wall} = T_i - \frac{qr_o^{\,2}}{2k}\left[\frac{1}{2}\left(1 - \frac{r_i^{\,2}}{r_o^{\,2}}\right) + \frac{r_i^{\,2}}{r_o^{\,2}}\ln\frac{r_i}{r_o}\right] \qquad \text{(A. 21)}$$

The wall superheat is given as;

$$\Delta T = T_i - \frac{qr_o^{\,2}}{2k}\left[\frac{1}{2}\left(1 - \frac{r_i^{\,2}}{r_o^{\,2}}\right) + \frac{r_i^{\,2}}{r_o^{\,2}}\ln\frac{r_i}{r_o}\right] - T_w \qquad \text{(A. 22)}$$

According to Coleman and Steele, the uncertainty in the wall superheat is given;

$$d(\Delta T) = \left[\left(\frac{\partial \Delta T}{\partial T_i}\right)^2 \Delta T_i^{\,2} + \left(\frac{\partial \Delta T}{\partial T_w}\right)^2 \Delta T_w^{\,2} + \left(\frac{\partial \Delta T}{\partial q}\right)^2 \Delta q^2 + \left(\frac{\partial \Delta T}{\partial r_i}\right)^2 \Delta r_i^{\,2} + \left(\frac{\partial \Delta T}{\partial r_o}\right)^2 \Delta r_o^{\,2}\right]^{1/2}$$

Effect of PTFE on the surface temperature

Using the equation for the conduction through a cylinder, the effect of the PTFE on the wall temperature could be determined. The thickness of the PTFE is negligible and the thermocouple measures the internal temperature at r=0. Thus,

$$T_{in} = T_i - \frac{qr_o^{\,2}}{4k_{ptfe}}$$

$T_{in} = T_i - \dfrac{qr_o^{\,2}}{4k_{ptfe}}$, using a radius of 1.5 mm

$$T_{in} = T_i - \frac{5.625\times10^{-7} q_g}{k_{ptfe}}$$

The volume of the tube is calculated as $1.19\times10^{-7}m^3$, therefore the above equation becomes,

$$T_{in} = T_i - \frac{6.29\times10^{-14} q}{k_{ptfe}}$$

Calculation thermodynamic quality

The total thermodynamic quality is estimated from the energy balance as;

$$x = \frac{m_v}{m_l} \tag{A. 23}$$

where

$$m_v = \frac{30\times q\times \pi dl}{h_{fg}} \tag{A. 24}$$

and m_l is the mass flow rate of the fluid

Similarly, tube by tube quality was estimated which is given as;

$$m_v = \frac{3\times n\times q\times \pi dl}{h_{fg}} \tag{A. 25}$$

where n is the number of tubes in a row.

The uncertainty on the thermodynamic quality is given as;

$$\Delta x^2 = \left(\frac{\partial x}{\partial m_v}\right)^2 \Delta m_v^2 + \left(\frac{\partial x}{\partial m_l}\right)^2 \Delta m_l^2 \tag{A. 26}$$

where

$$\frac{\partial x}{\partial m_v} = \frac{1}{m_l} \text{ and } \qquad \frac{\partial x}{\partial m_l} = \frac{m_v}{m_l^2}$$

Calculation of uncertainty analysis using sample readings

Typical reading obtained from the test rigs are used to compute the error in each of the parameters used in the thesis.

Inside diameter of tube d_i=2.4 mm

Outside diameter d_o=3.0 mm

Length of tube l=85 mm

Current I=20 A, Voltage V=0.4883 V, T_{in}=101.4 K,

Uncertainty in length, Δl=0.01mm

Uncertainty in diameter Δd=0.01mm

Uncertainty in current, ΔI=0.1 A

Uncertainty in voltage, ΔV=0.001V

From equation (A.21), T_s=101.25 K

The uncertainties in the parameters used in the thesis are

The error in the inside temperature is ΔTin =0.1 K

From equation (A.3), $\Delta A_s = 2.672 \times 10^{-6} m^2$

From equation (A.5), $\Delta A_x = 1.207 \times 10^{-9}\ m^2$

From equation (A.23), ΔT_{diff} =0.1417 K

From equation (A.13), Δq =0.0776 kW/m^2

From equation (A.15), $\Delta\alpha = 1.185\ kW/m^2K$

$$\text{Heat flux}, q = \frac{20 \times 0.4883}{3.142 \times 0.003 \times 0.085} = 12.18 kW/m^2$$

$$\text{Heat transfer coefficient}, \alpha = \frac{12.18}{101.25 - 99.8} = 8.4 kW/m^2K$$

There percentage error in the heat transfer coefficient is 14%

APPENDIX A2: CALIBRATION RESULTS

Differential pressure transducer

The differential pressure transducer used in the Rig II is an RS model, capable of measuring pressure in the range of 0-5psi. The calibration was done by connecting a plain tube to one port of the transducer with the other port open to the atmosphere. The tube is filled with water to a height and the output of the transducer is connected logged on to a data logger. The height of the water is reduced and the corresponding voltage signal obtained on the logger. The calibration is repeated twice on different dates to ensure repeatability of results. Results obtained from the calibration is as shown in Fig A.2

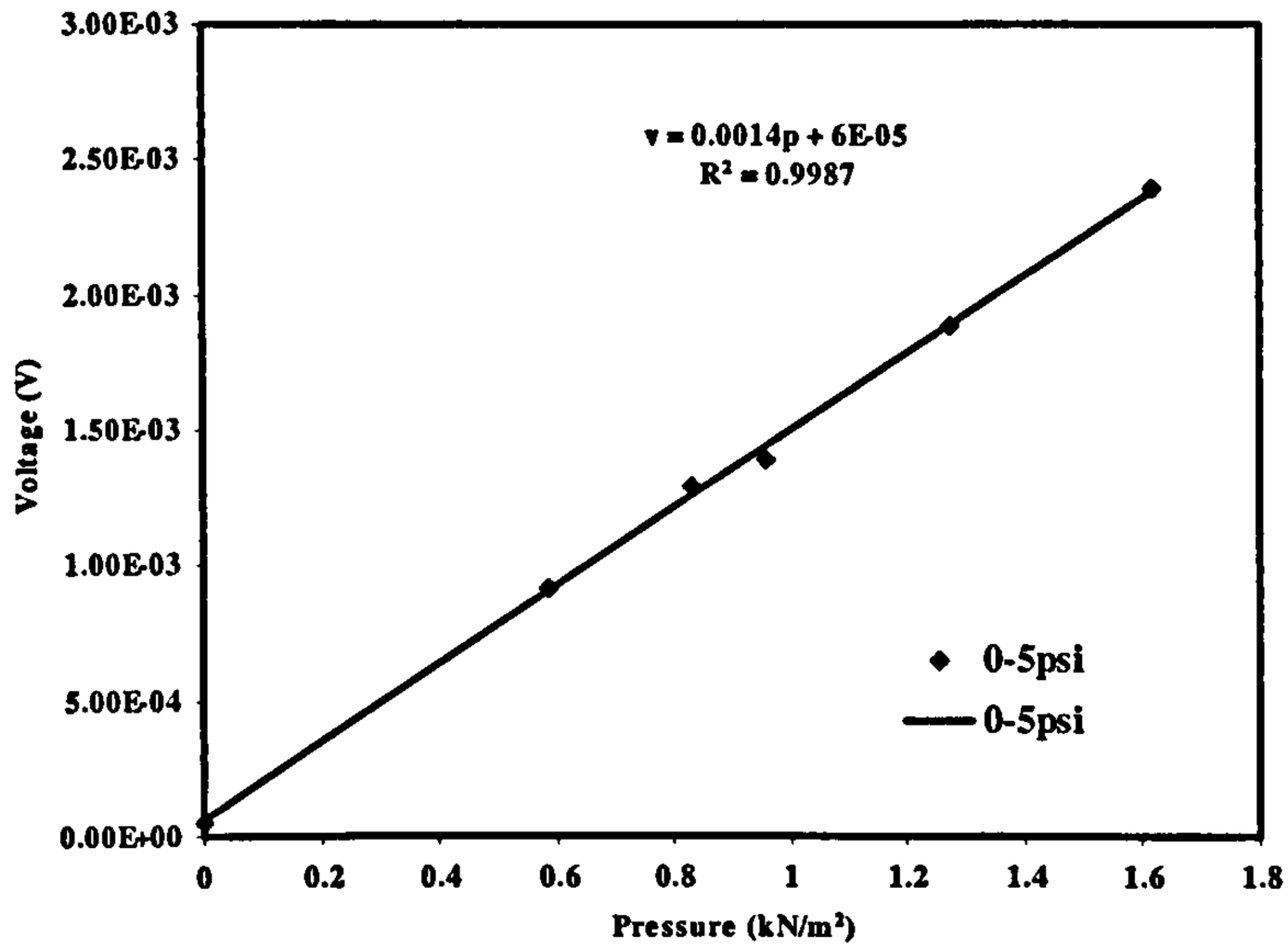

Figure A. 2: Calibration of pressure transducer

Rotameter Calibration

The flow meter connected in the rig II is calibrated to ensure accurate measurement. The fluid tank was heated to 98 °C, whiles the pump was switched on to pump the liquid through the flow meter to an empty beaker. A beaker was used to collect the amount of working fluid for every 60 seconds. The flow meter was adjusted for values at 0.2, 0.3 and 0.4litres and in each case the corresponding amount of fluid collected was noted in the given time. The test was repeated and results obtained are shown in Fig. A3.

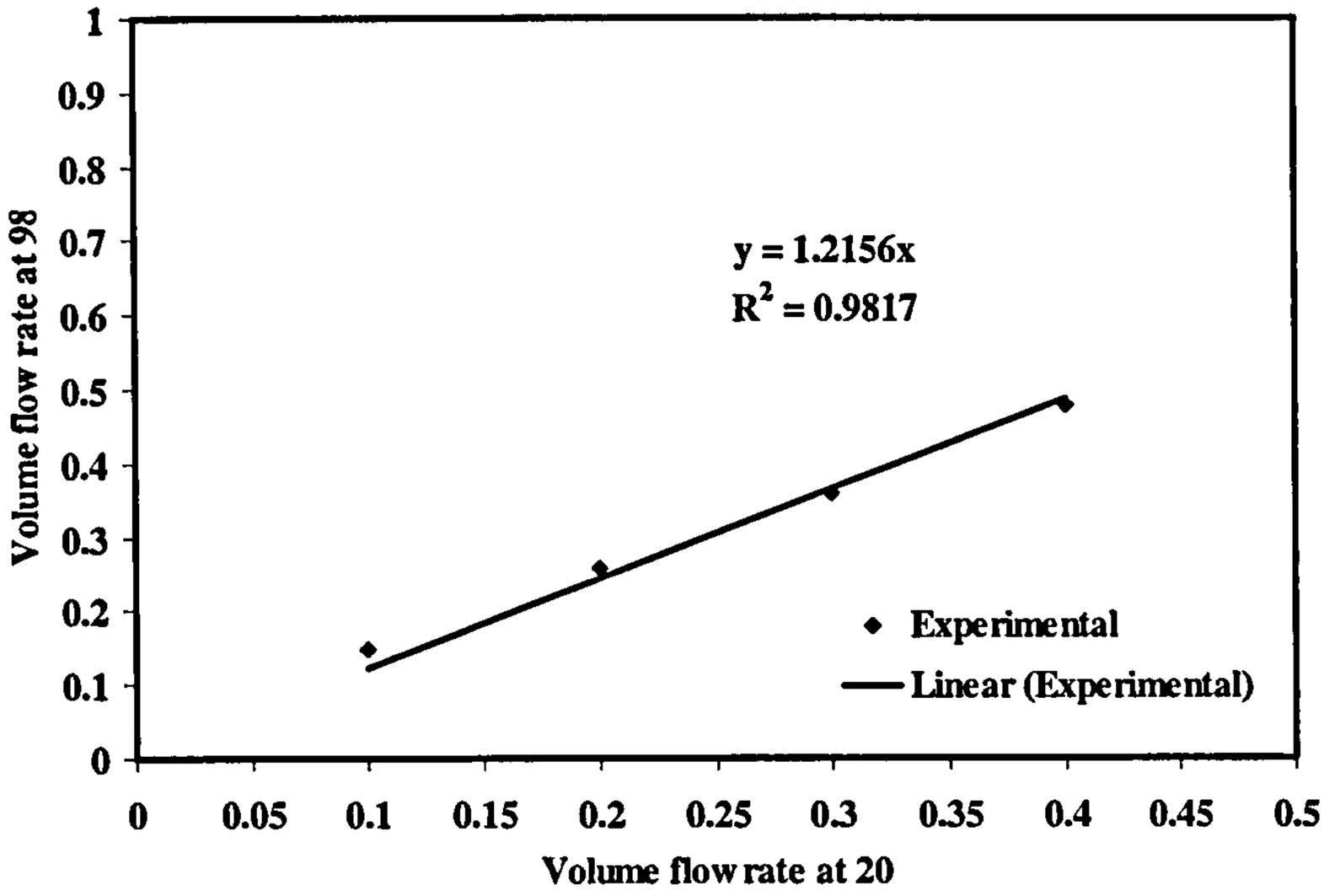

Fig A.3 : Plot of water at 98°C against water at 20°C using the flow meter.

The calibration for the other working fluids were obtained by using a standard correlation using the data on the weight of the float, density of float, density of fluid and viscosity of the working fluid.

The correlation was given as for s a size 7 stainless steel float as;

$$I = \log\left(\frac{\rho_{float} \times \rho_{fluid}}{m_{float} \times \left(\rho_{float} - \rho_{fluid}\right)^{0.5} \times k_1 \times \mu}\right)$$

$$F_t = k_2 \times \left(m_{float} \times \left(\frac{\rho_{float} - \rho_{fluid}}{\rho_{float} \times \rho_{fluid}}\right)\right)^{0.5}$$

$$f = F_t \times Scale\ (l/min)$$

where k_1 and k_2 are constants that depends on the float type and in this case they are 0.147 and 0.679 respectively.

Sample calculations using the above expressions were used to obtain the flow rates for the working fluids used as shown in Table A.1 and A.2

Size 7 Metric, SS float, 20°C, R113`

Scale Reading	0.10	0.20	0.30	0.40	0.50	0.60	0.70	0.80	0.90
l/min	0.07	0.16	0.24	0.31	0.39	0.47	0.55	0.63	0.78

Table A.1: Flow rate using R113

Size 7 Metric, SS float, 20°C, distilled water

Scale Reading	0.10	0.20	0.30	0.40	0.50	0.60	0.70	0.80	0.90
l/min	0.10	0.20	0.31	0.41	0.51	0.61	0.72	0.82	0.92

Table A.2: Flow rate using distilled water

Thermocouple details

The thermocouples used for the experimental work were type K. The thermocouples were inserted into the tube which was filled with a sealant to maintain an adiabatic condition. The thermocouples were calibrated by using an ice bath and a hot water bath. The hot water bath was heated in steps of 10 degrees to 80 degrees, whilst the average of three mercury thermometers was used to determine the temperature of the hot water. The thermocouples were then connected to the Easyest data logger where readings were stored for the estimation of the surface temperature of the tube. Temperature readings that were obtained by the thermocouples were converted to voltages as shown in Fig A.4.

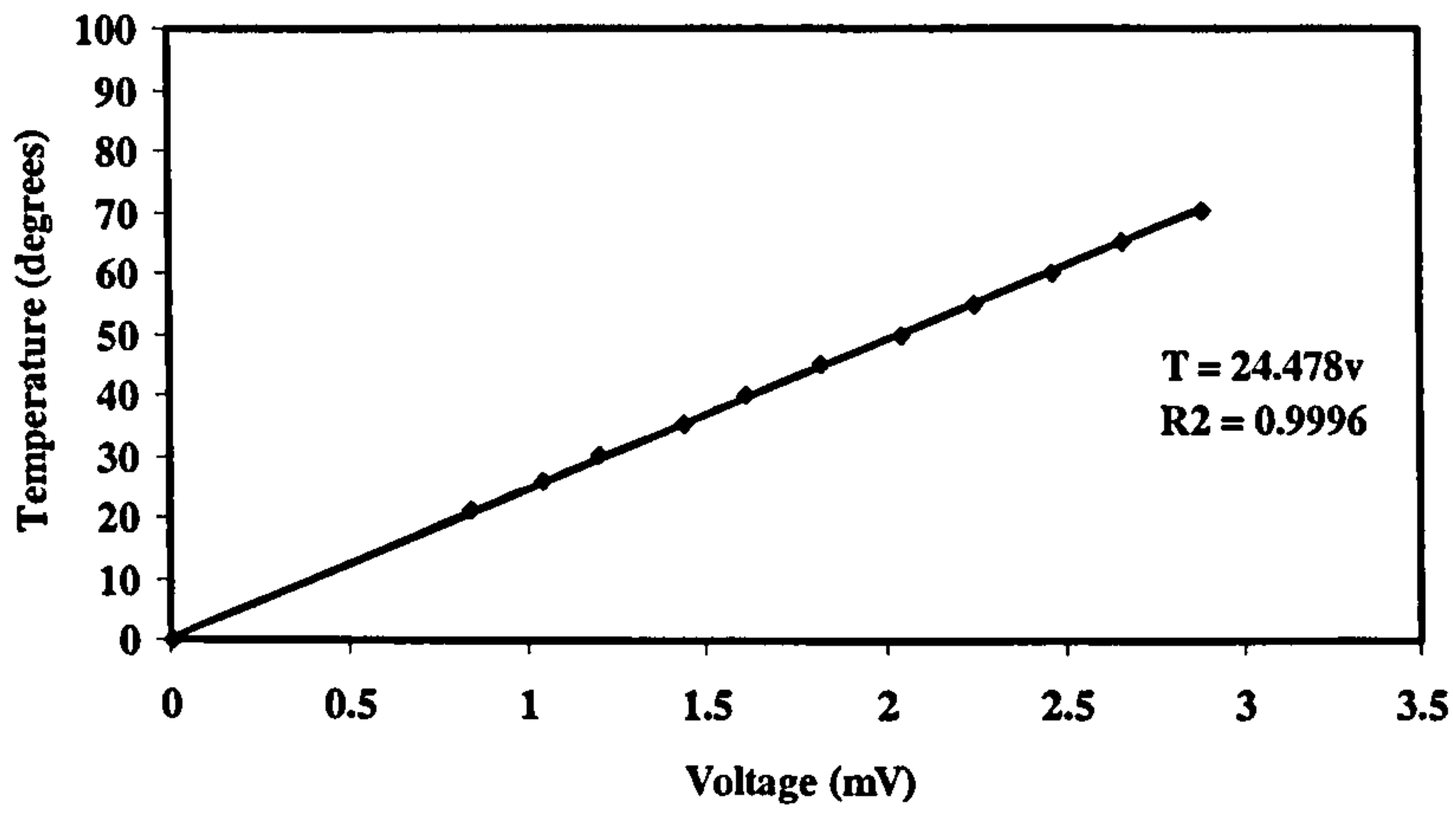

Figure A.4. : Sample calibrated thermocouple readings

Simple Ohm's law experiment was used to obtain the resistance of the stainless steel used for the experiment. The experiment was obtained by passing current through a length of the tube (100mm) and recording the corresponding voltage across the tube. Results obtained are shown in Figure A.5. This resistance as expected changes with the length of the tube and as such it was used in the computation of the heat flux for the

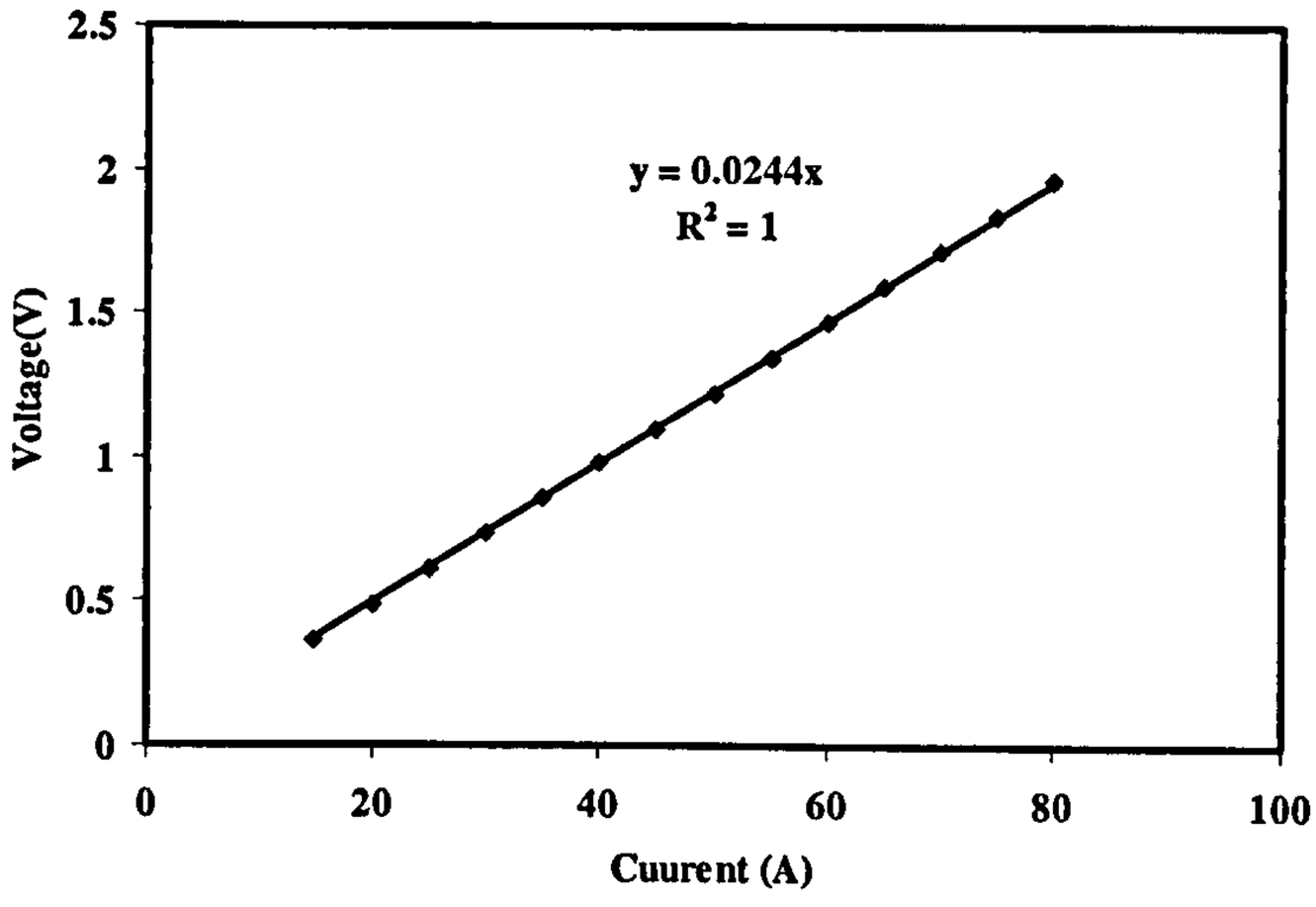

Figure A.5: Plot of voltage against current for stainless steel tube

APPENDIX A3: PROPERTIES OF WORKING FLUIDS

Fluid	Boiling Point (°C)	Density (kg/m^3)		Latent heat (J/kg)	Viscosity (mPas)		Thermal conductivity (W/mK)	Molecular mass	Critical pressure (bar)	Specific heat capacity	Surface Tension (N/m)
		Liquid	Vapour		Liquid	Vapour					
Water	100	958	0.598	2257000	0.276	0.012	0.681	18	221	4200	0.0589
R113	47.8	1508	7.44	144000	0.516	0.011	0.0705	187.39	34	984	0.0147
Flute PP1	57	1582	13.5	85500	0.425	0.0011	0.632	338	18	1200	0.0083

Table A. 1: Properties of the fluids used in this thesis

APPENDIX B: SAMPLE CALCULATION FOR POOL BOILING CORRELATIONS

MOSTINKI

The Mostinki's correlation is given as

$$\alpha_{nb} = 0.1061 q^{0.7} p_c^{0.69} F(p) \qquad \text{(B. 1)}$$

$$F(p) = 1.8 p_r^{0.17} + 4 p_r^{1.2} + 10 p_r^{10}$$

For water we show the sample calculation used

Critical pressure is 221 bar, there for the reduced pressure pr=p/p_{cr}

$$P_r = \frac{1}{221} = 4.5248 \times 10^{-3}$$

$$F_P = 1.8\left[4.5248 \times 10^{-3}\right]^{0.17} + 4\left[4.5248 \times 10^{-3}\right]^{1.2} + 10\left[4.5248 \times 10^{-3}\right]^{10} = 0.725010$$

The nucleate boiling expression is given as;

$$\alpha_{nb} = 0.106 \times \left[221 \times 10^5\right]^{0.69} q^{0.7} \times 0.7250$$

$$\alpha_{nb} = 3.186 q^{0.7}$$

CORNWELL CORRELATION

$$Nu = AF(p)\mathrm{Re}^{0.67}{}_b \,\mathrm{Pr}^{0.4} \qquad \text{(B. 2)}$$

where A=9.7$(p_c)^{0.5}$ with p_c in bar

$$F(p) = 1.8 p_r^{0.17} + 4 p_r^{1.2} + 10 p_r^{10} \qquad \text{(B. 3)}$$

The function of the reduced pressure is the same as that of Mostinki's correlation above.

The constant A is given as;

$$A = 9.7 \times [221]^{0.5} = 144.2$$

The Reynolds number is given as;

$$\mathrm{Re} = \frac{qd}{\mu h_{fg}} = \frac{q \times 0.003}{2257000 \times 2.76 \times 10^{-4}} = 4.8159 \times 10^{-6} q$$

Prandtl number $\mathrm{Pr} = \dfrac{\mu C_p}{k} = \dfrac{2.76 \times 10^{-4} \times 4200}{0.61} = 1.7022$

Substituting into the equation gives;

$$Nu = 144.2 \times 0.7251 \times [4.8159 \times 10^{-6} q]^{0.67} \times [1.7022]^{0.4} = 0.03541 q^{0.67}$$

$$\frac{\alpha d}{k} = 0.03541 q^{0.67}$$

$$\alpha_{nb} = 8.03872 q^{0.67}$$

COOPER CORRELATION

The Cooper correlation is given as;

$$\alpha = A P_r^{(0.12 - \log \varepsilon)} (-\log P_r)^{-0.55} M^{-0.5} q^{0.6667} \qquad \text{(B. 4)}$$

The reduced pressure is the same as that calculated for the Mostinki's correlation.

Using a conservative value of A=40, M=18 for water, we have

$$\alpha = 40\left[4.524\times10^{-3}\right]^{(0.12-\log 1)}\left(-\log 4.5248\times10^{-3}\right)^{-0.55}\times18^{-0.5}\times q^{0.667} \quad \text{(B. 5)}$$

$$\alpha = 3.08717q^{0.667}$$

APPENDIX C: TUBE BUNDLE SAMPLE CALCULATIONS

In this section, sample calculations for all the correlations used in comparing our experimental results are presented. The properties of the fluid (distilled water) that are essential to the computation of the heat transfer coefficient using the large tube correlations are shown in Table C.1

Parameter	**Calculated Values**
G	5.6(kg/m^{2}s)
q	6 (kW/m^2)
Tube no	10
Thermodynamic quality (x)	0.1215
Density of fluid	958 kg/m^3
Density of vapour	0.598 kg/m^3
Viscosity of liquid	2.76 ×10^{-4} Pas
Diameter	0.003 m
Surface tension	5.89×10^{-2} (N/m)
Latent heat of vaporization	2257000 (J/kg)
Acceleration due to gravity	9.81 (m/s^2)
Thermal conductivity (k_l)	0.681(W/mK)

Table C.1: Parameters used in Appendix C

1.0 CHEN CORRELATION

The Chen correlation is given as

$$\alpha = S\alpha_{nb} + F\alpha_{cv} \qquad \text{(C. 1)}$$

The Reynolds number is given as

$$\mathrm{Re}_l = \frac{Gd(1-x)}{\mu_l} = \frac{5.66\times 0.003\times(1-0.1215)}{2.76\times 10^{-4}} = 53.156$$

The forced convective component is given as;

$$\alpha_{cv} = 0.023\frac{k}{d}\mathrm{Re}_l^{0.8}\,\mathrm{Pr}_l^{0.4} = 0.023\times\frac{0.681}{0.003}\times 53.156^{0.8}\times 1.707^{0.4} = 0.1553 kW/m^2 \quad \text{(C. 2)}$$

$$S = \frac{1}{1+2.53\times10^{-6}\,\mathrm{Re}_l^{1.17}} = \frac{1}{1+2.53\times10^{-6}\times 53.156^{1.17}} = 0.9997$$

Enhancement factor,

$$F = 2.35\left[\left(\frac{1}{X_{tt}}\right)+0.213\right]^{0.736} = 7.845$$

Nucleate pool boiling is due that of Cooper is 1.0233 kW/m^{2}K from Appendix B.

The total two phase heat transfer coefficient is given as;

$$\alpha = 0.9997\times 1.0233 + 0.1553\times 7.8465 = 2.24 kW/m^2\mathrm{K}$$

2.0 BENNET AND CHEN

The suppression factor for the Bennet correlation is given as;

$$S = \frac{k_l}{F\alpha_c\beta}\left[1-\exp\left(\frac{-F\alpha_c\beta}{k_l}\right)\right] \quad \text{(C. 3))}$$

$$\beta = 0.041\sqrt{\left(\frac{\sigma}{g(\rho_l-\rho_g)}\right)} = \left[\frac{5.89\times10^{-2}}{9.81(958-0.598}\right]^{0.5}\times 0.041 = 1.0267\times10^{-4}$$

Substituting into Equation (C.3)

$$S = 0.5157$$

Using the enhancement factor from Chen, the total heat transfer coefficient is given as;

$$\alpha = 7.845 \times 1.2781 + 0.9999 \times 1.0223 = 11.05 kW / m^2 K$$

3.0 STEINER AND TABOREK CORRELATION

The Steiner and Taborek correlation is given as;

$$\alpha = \left[(F\alpha_c)^n + (\alpha_{nb})^n \right]^{1/n} \qquad \text{(C. 4))}$$

The nucleate boiling is due that of Cooper' calculated in Appendix B, whereas the enhancement factor is due that calculated from;

$$F = \left[(1-x)^{1.5} + 1.9 x^{0.6} \left(\frac{\rho_l}{\rho_g} \right)^{0.35} \right]^{1.1} = \left[(1-0.1215)^{1.5} + 1.9 \times 0.1215^{0.6} \left(\frac{958}{0.598} \right)^{0.35} \right]^{1.1} = 9.7877$$

Substituting values into (C4) to obtain;

$$\alpha = \left[(9.7877 \times 1.278)^2 + 1.0233^2 \right]^{1/2} = 12.5 kW / m^2 K$$

4.0 HWANG AND YAO

$$\alpha = S\alpha_{nb} + F\alpha_{cv} \qquad \text{(C. 5))}$$

$$\alpha_{nb} = 0.2086 q^{0.75} \qquad \text{(C. 6))}$$

$$\alpha_l = \alpha_{fc} \left[1 - X_{loc} \right]^{0.6} \qquad \text{(C. 7))}$$

$$\varepsilon_m = \frac{0.833 X_{loc}}{X_{loc} + (1 - X_{loc}) \left(\rho_g / \rho_f \right)} = \frac{0.833 \times 0.1215}{0.1215 + (1 - 0.1215) \left(\frac{0.598}{958} \right)} = 8.30 \times 10^{-1}$$

$$R^* = \frac{d}{2} \left[\frac{\sigma}{g(\rho_f - \rho_g)} \right]^{-1/2} = \frac{0.003}{2} \left[\frac{5.89 \times 10^{-2}}{9.81(958 - 0.598)} \right]^{-1/2} = 8.5610^{-3}$$

$$Y = 0.0205\left(\frac{d}{R^*}\right) = 0.0205\left(\frac{0.003}{8.56\times10^{-3}}\right) = 7.18\times10^{-3}$$

$$F = \left(\frac{1}{1-\varepsilon}\right)^{0.744} = \left(\frac{1}{1-8.3\times10^{-1}}\right)^{0.744} = 3.7299$$

$$\alpha = (1-0.1215)^{0.6}\times1.27 = 1.1825\,\mathrm{kW/m^2K}$$

$$S = \frac{k}{F\alpha_l Y}\left[1-\exp\left(\frac{-F\alpha_l Y}{k}\right)\right]$$

$$S = \frac{6.88\times10^{-1}}{3.7299\times7.18\times10^{-3}}\left[1-\exp\left(\frac{-3.7229\times1.1825\times10^{3}\times7.18\times10^{-3}}{6.18\times10^{-3}}\right)\right] = 2.15\times10^{-2}$$

Substituting values into equation (C6)

$$\alpha = 2.15\times10^{-2}\times1.0233 + 3.7299\times1.1825 = 4.4kW/m^2K$$

5.0 GUPTE AND WEBB CORRELATION

The asymptotic model developed by Webb and Gupte is given as;

$$\alpha = \left[(F\alpha_{cv})^n + (\alpha_{nb})^n\right]^{1/n} \qquad \text{(C. 8))}$$

Martinelli parameter is calculated as;

$$X_{tt} = \left(\frac{\mu_f}{\mu_g}\right)^{0.1}\left(\frac{\rho_g}{\rho_l}\right)^{0.5}\left(\frac{1-x}{x}\right)^{0.9} = \left(\frac{2.76\times10^{-4}}{1.2\times10^{-5}}\right)^{0.1}\left(\frac{0.598}{958}\right)^{0.5}\left(\frac{1-0.1215}{0.1215}\right)^{0.9} = 0.2016$$

$$\phi_l = 1+\frac{8}{X_{tt}}+\frac{1}{X_{tt}^{\ 2}} = 1+\frac{8}{0.2016}+\frac{1}{0.2016^2} = 65.2873$$

The enhancement factor is given as;

$$F = C_1\left[\frac{\phi_l[P_r+1]}{2}\right]^{c_2} = 1\left[\frac{65.2873(1.707+1)}{2}\right]^{0.327} = 4.3185$$

The single phase heat transfer coefficient is given by;

$$Nu = c\,\mathrm{Re}^m\,\mathrm{Pr}^{0.36} = 0.900\times(60.24)^{0.4}\times 1.707^{0.36}$$

Substituting values into (C8) gives;

$$\alpha = \left[(4.3185\times 1.2781)^2 + 1.0233^2\right]^{1/2} = 5.6\,kW/m^2K$$

6.0 THOME MODEL

$$\alpha(z) = \frac{t_l}{\tau}\alpha_l + \frac{t_{film}}{\tau}\alpha_{film}(z) + \frac{t_{dry}}{\tau}\alpha_v(z) \qquad \text{(C. 9))}$$

The time periods used in the above model were given as;

$$t_l = \frac{\tau}{1+\frac{\rho_l}{\rho_v}\frac{x}{1-x}} = \frac{39.2}{1+\frac{958}{0.598}\frac{0.1215}{1-0.1215}} = 0.17644s,$$

$$t_g = \frac{\tau}{1+\frac{\rho_v}{\rho_l}\frac{1-x}{x}} = \frac{39.1094}{1+\frac{0.598}{958}\frac{1-0.1215}{0.1215}} = 39.1094s$$

and

$$t_{dry\,film}(z) = \frac{\rho_l h_{fg}}{q}[\delta_o(z)-\delta_{\min}] = \frac{958\times 226000}{6000}\left[1.95\times10^{-6}-9\times10^{-7}\right] = 3.79\times10^{-1}s,$$

$$U_p = G_{total}\left[\frac{x}{\rho_v}+\frac{1-x}{\rho_l}\right] = 5.66\times\left[\frac{0.1215}{0.598}+\frac{1-0.1215}{958}\right] = 1.1556m/s$$

$$B_o = \frac{\rho_l d}{\sigma} = \frac{958\times1.5\times10^{-3}}{5.89\times10^{-2}} = 32.5844$$

The average heat transfer coefficient through the elongated bubble was obtained as;

$$\frac{\delta_o}{d} = C_{\delta_o}\left(3\sqrt{\frac{\nu_l}{U_p d}}\right)^{0.84}\left[\left(0.07Bo^{0.41}\right)^{-8} + 0.1^{-8}\right]^{-1/8}$$

$$= 1.5\times10^{-3}\times0.29\left(3\times\sqrt{\frac{2.88\times10^{-7}}{1.1556\times1.5\times10^{-3}}}\right)\left[\left(0.07\times32.584^{0.41}\right)^{-8} + 0.1^{-8}\right]^{-1/8} = 1.95\times10^{-6}$$

$$\delta(z,t) = \delta_o(z) - \frac{q}{\rho_l h_{fg}}t = 1.95\times10^{-6} - \frac{6000}{958\times2257000}\times3.79\times10^{-1} = 9.00\times10^{-7}$$

Substituting values into (C9) gives;

$$\alpha_{film}(z) = \frac{k_l}{\delta_o - \delta_{end}}\ln\left(\frac{\delta_o}{\delta_{end}}\right)$$

$$= \frac{0.681}{1.95\times10^{-6} - 9\times10^{-7}}\ln\left(\frac{1.95\times10^{-6}}{9\times10^{-7}}\right) = 5.01 kW/m^2K$$

$$\alpha(z) = \frac{3.79\times10^{-1}}{39.2}\times5.02 = 4.8 kW/m^2K$$

The heat transfer coefficients due to the vapour and liquid slugs are negligible.

APPENDIX D1: COMPARISON OF RESULTS WITH DISTILLED WATER

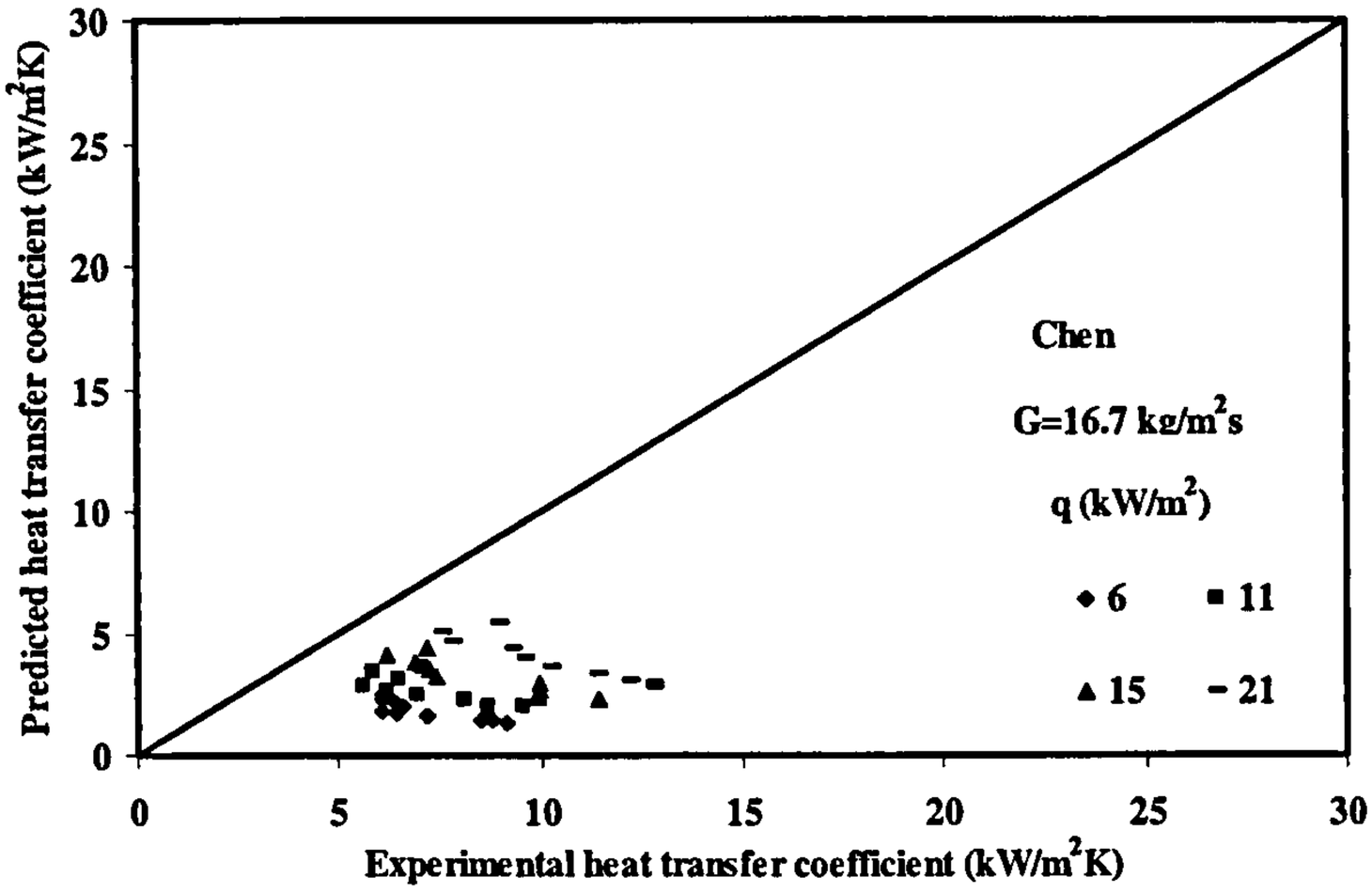

Figure D. 1 Comparison of predicted heat transfer using Chen against experimental data for distilled water for G=16.7 kg/m^{2}s

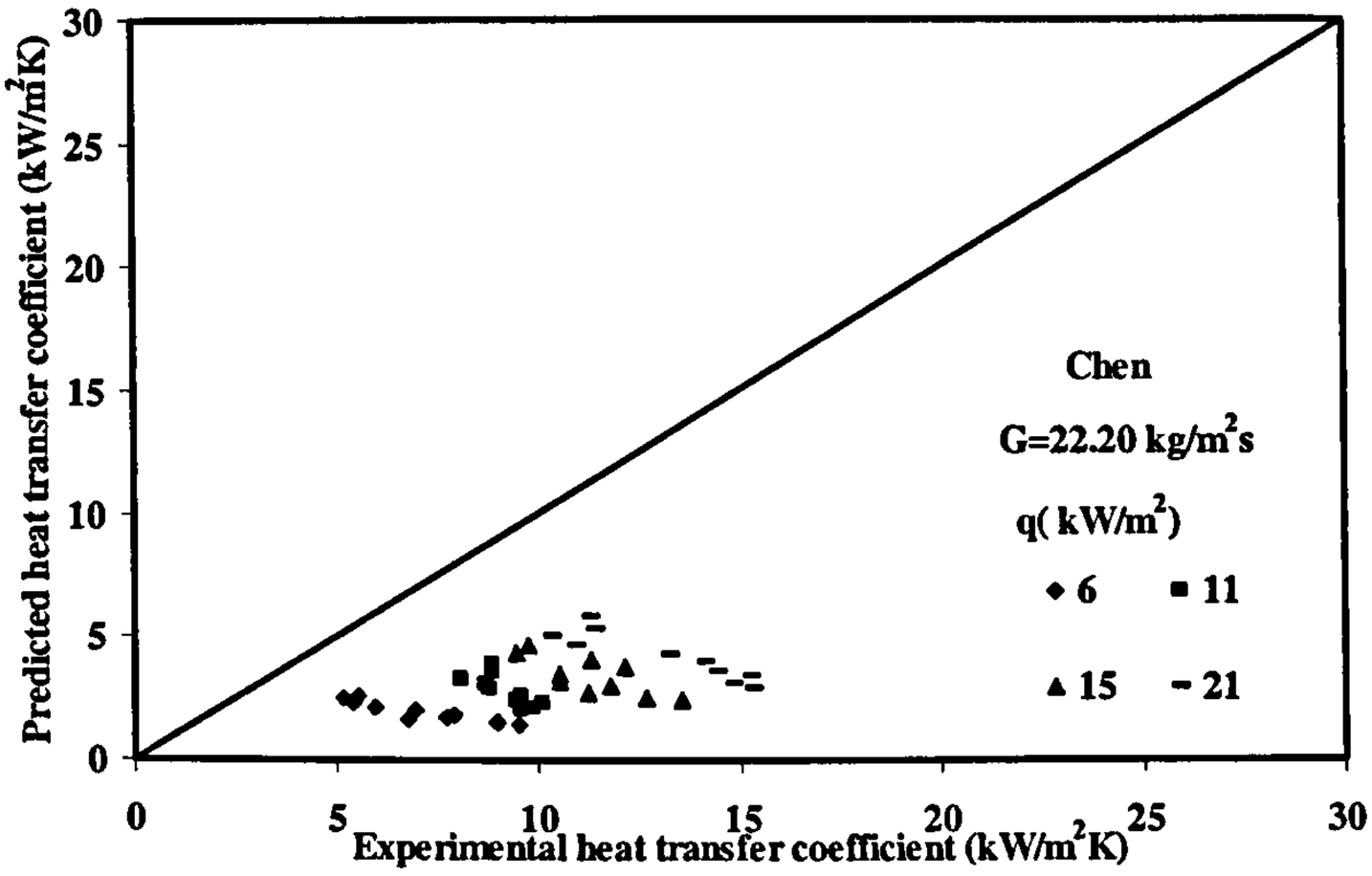

Figure D. 2 Comparison of predicted heat transfer coefficient with experimental results with Chen for distilled water for G=22.20 kg/m^{2}s.

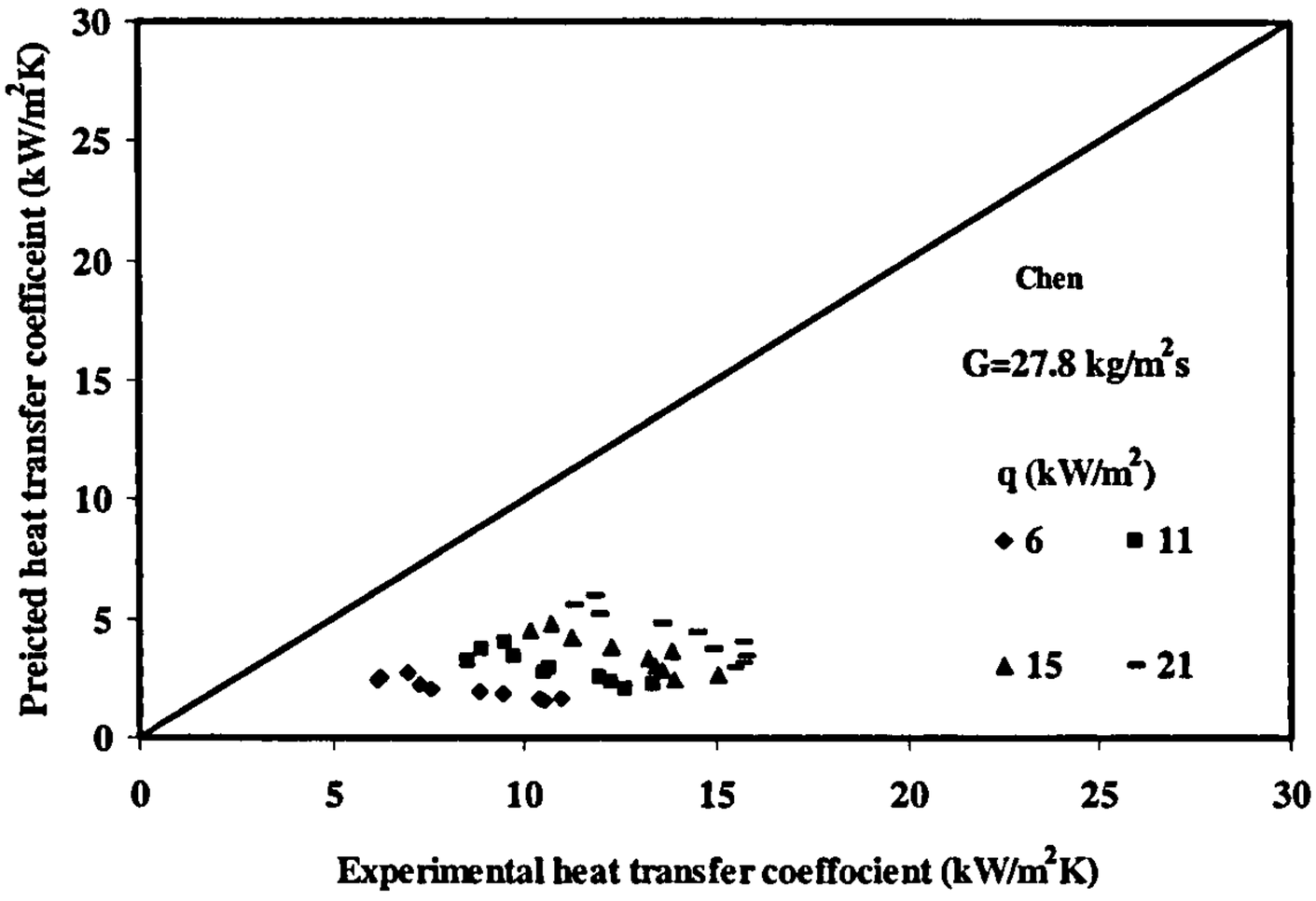

Figure D. 3 Comparison of predicted heat transfer coefficient with experimental results with Chen for distilled water for G=27.8 kg/m^{2}s.

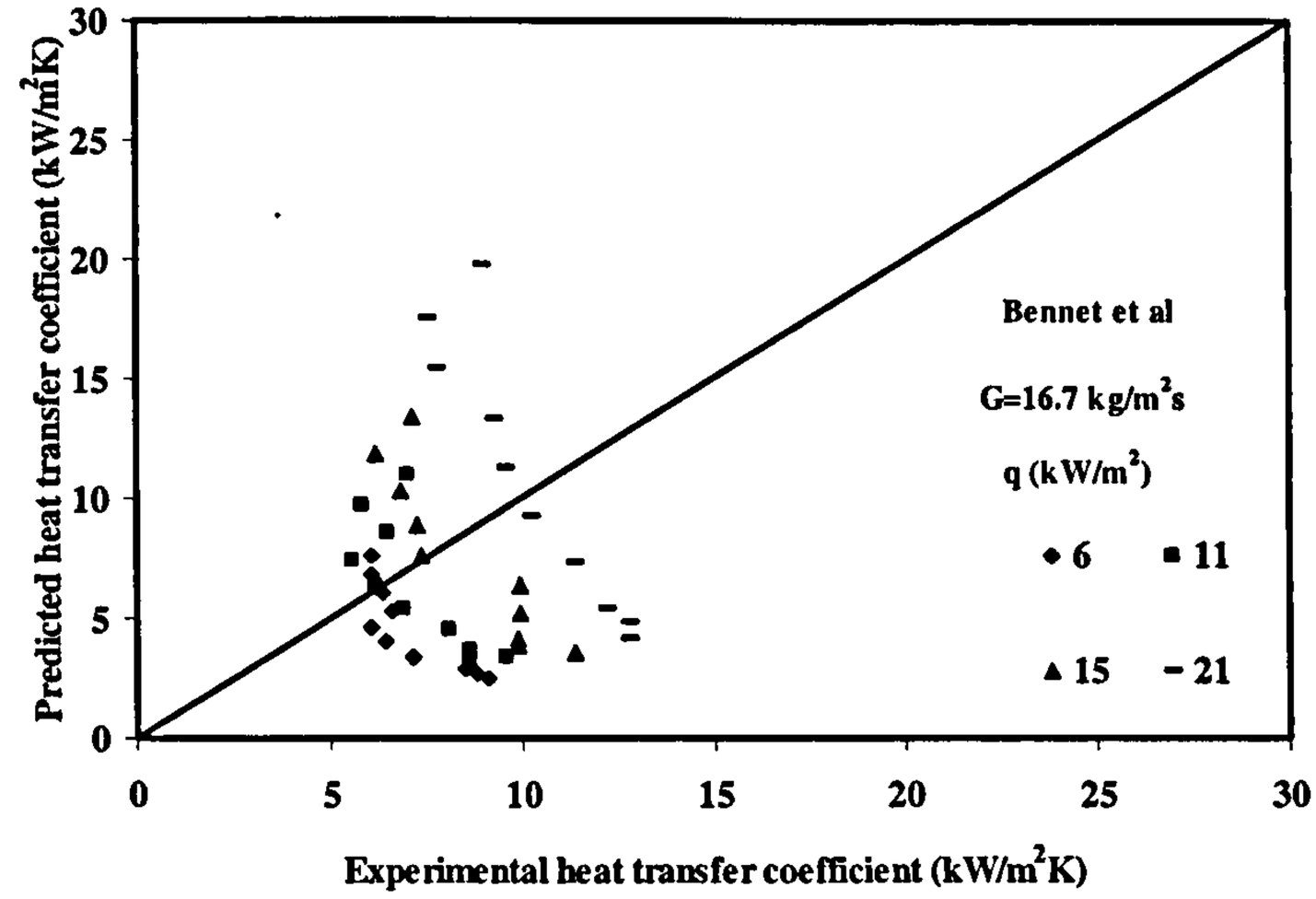

Figure D. 4 Comparison of predicted heat transfer coefficient with experimental results with Bennet et al for distilled water for G=16.7 kg/m^{2}s.

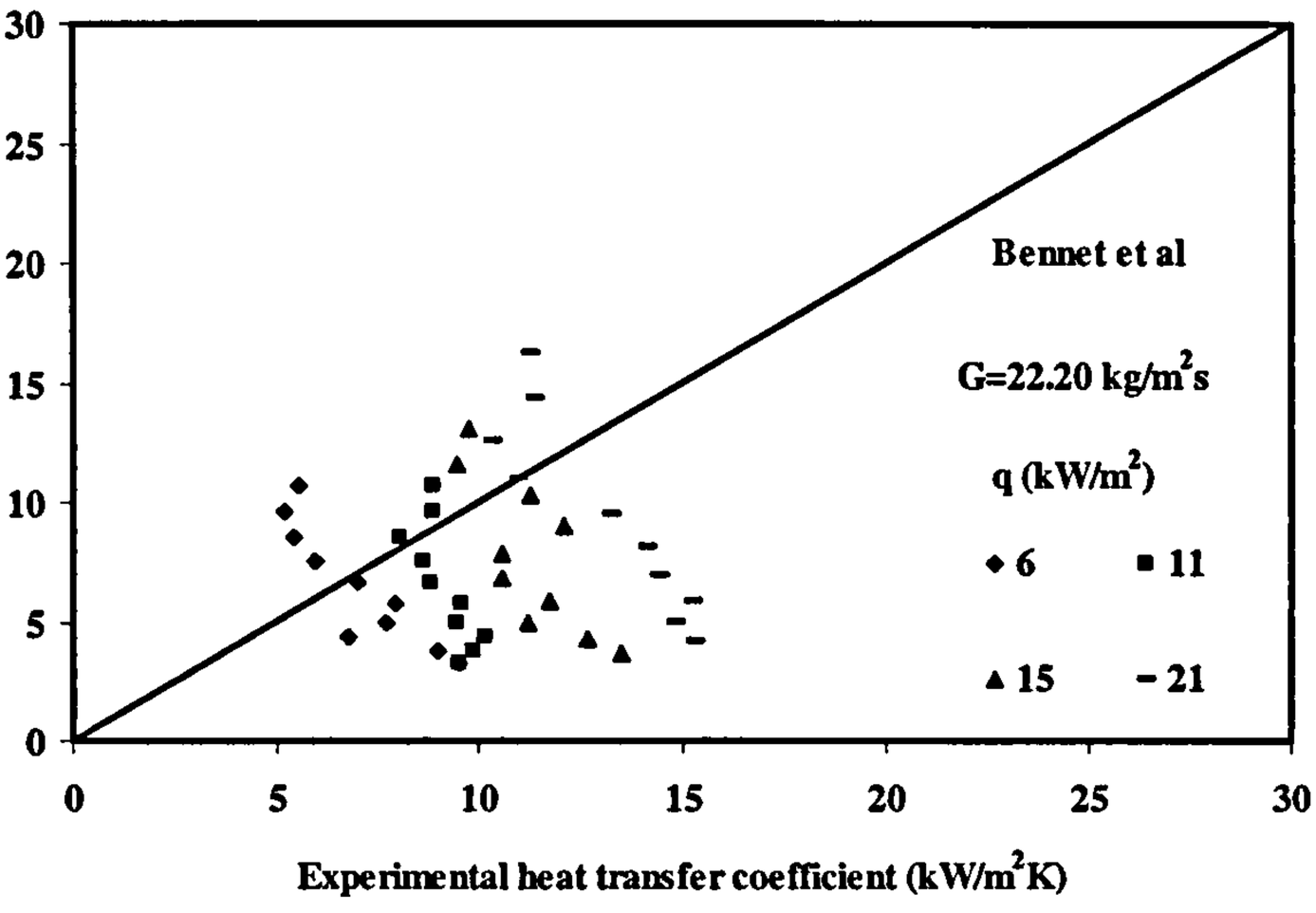

Figure D. 5 Comparison of predicted heat transfer coefficient with experimental results with Bennet et al for distilled water for G=22.20 kg/m^{2}s.

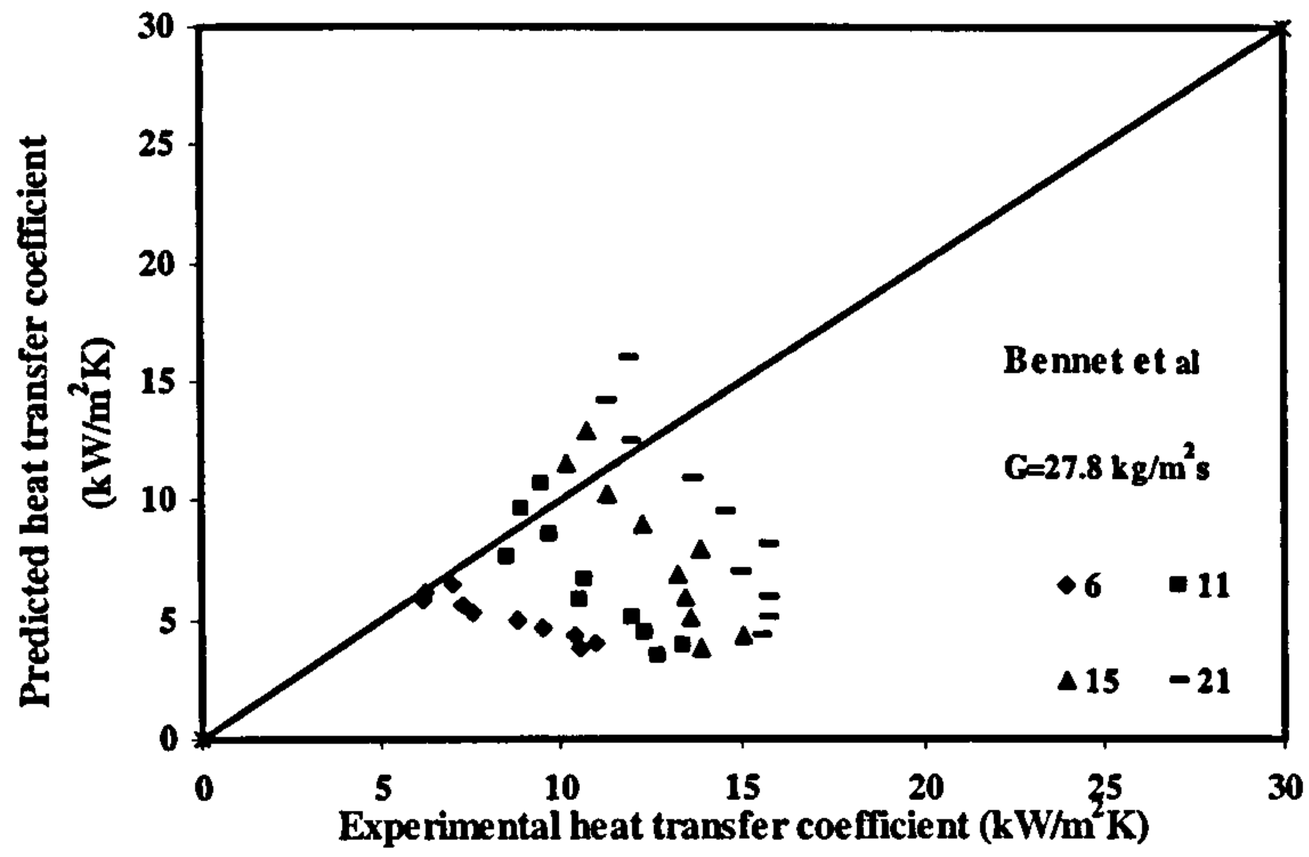

Figure D. 6 Comparison of predicted heat transfer coefficient with experimental results with Bennet et al for distilled water for G=27.8 kg/m^{2}s.

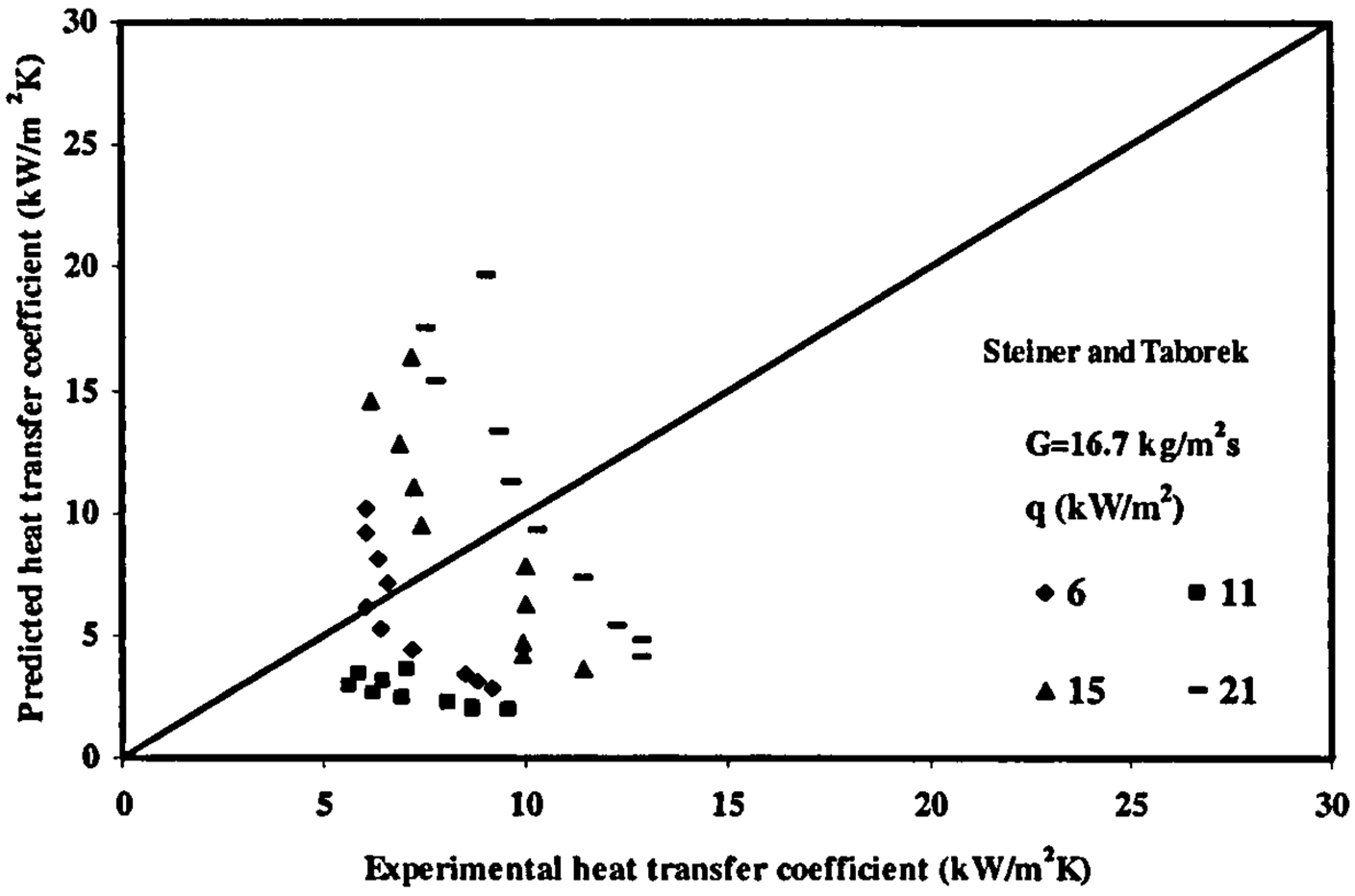

Figure D. 7 Comparison of predicted heat transfer coefficient with experimental results with Steiner and Taborek for distilled water for G=16.7 kg/m^{2}s.

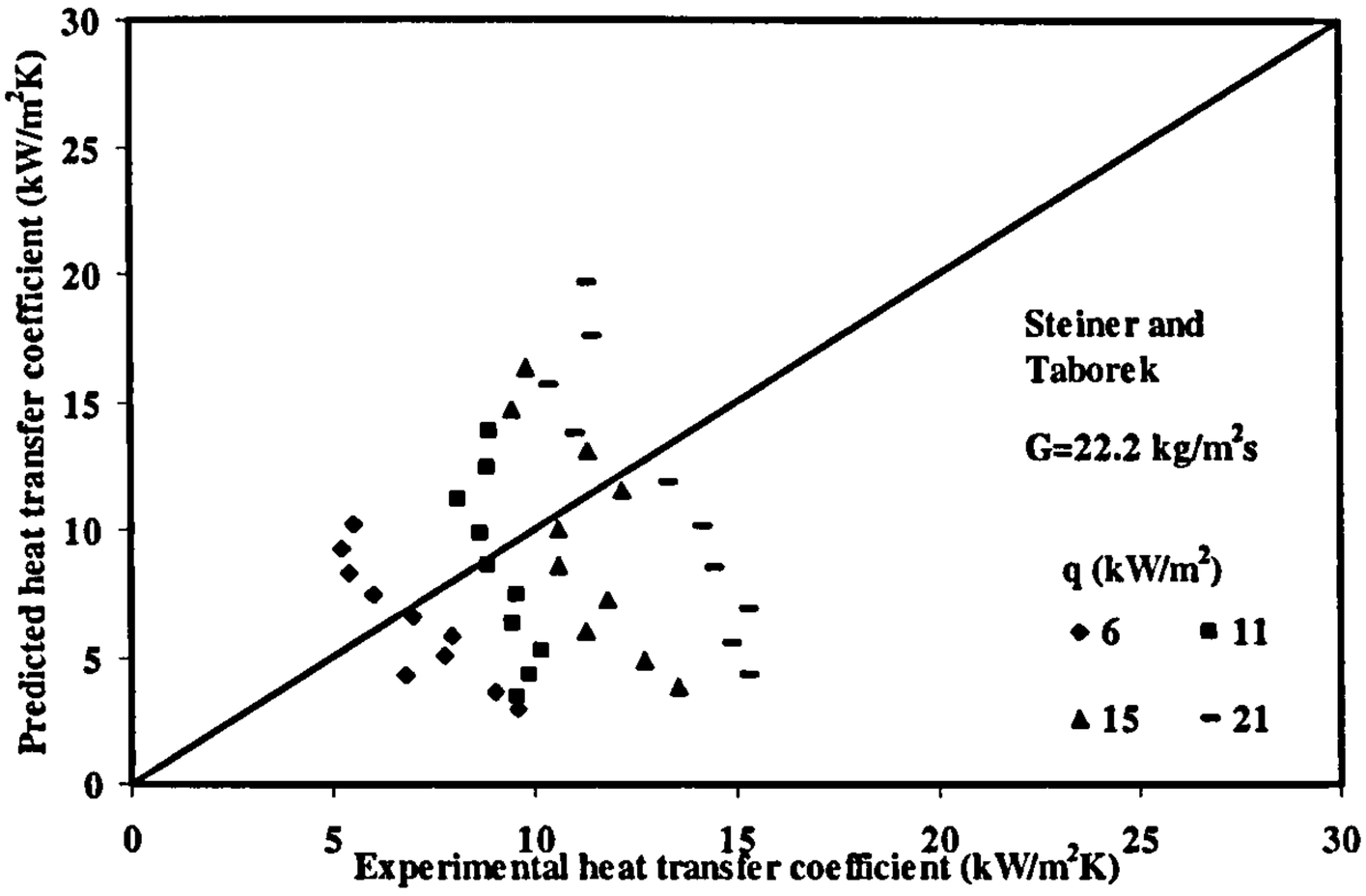

Figure D. 8 Comparison of predicted heat transfer coefficient with experimental results with Steiner and Taborek for distilled water for G=22.2 kg/m^{2}s.

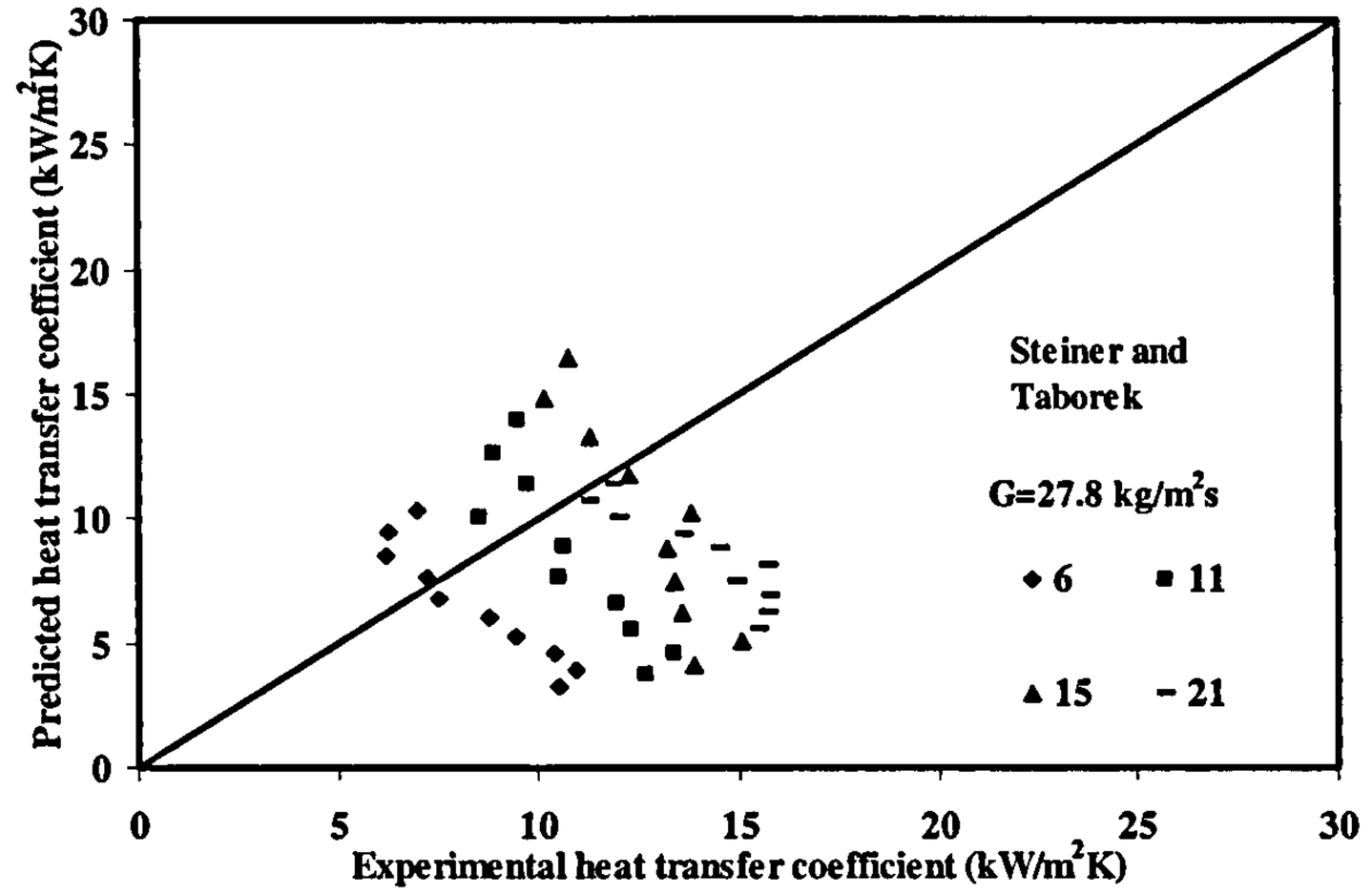

Figure D. 9 Comparison of predicted heat transfer coefficient with experimental results with Steiner and Taborek for distilled water for G=27.8 kg/m^{2}s.

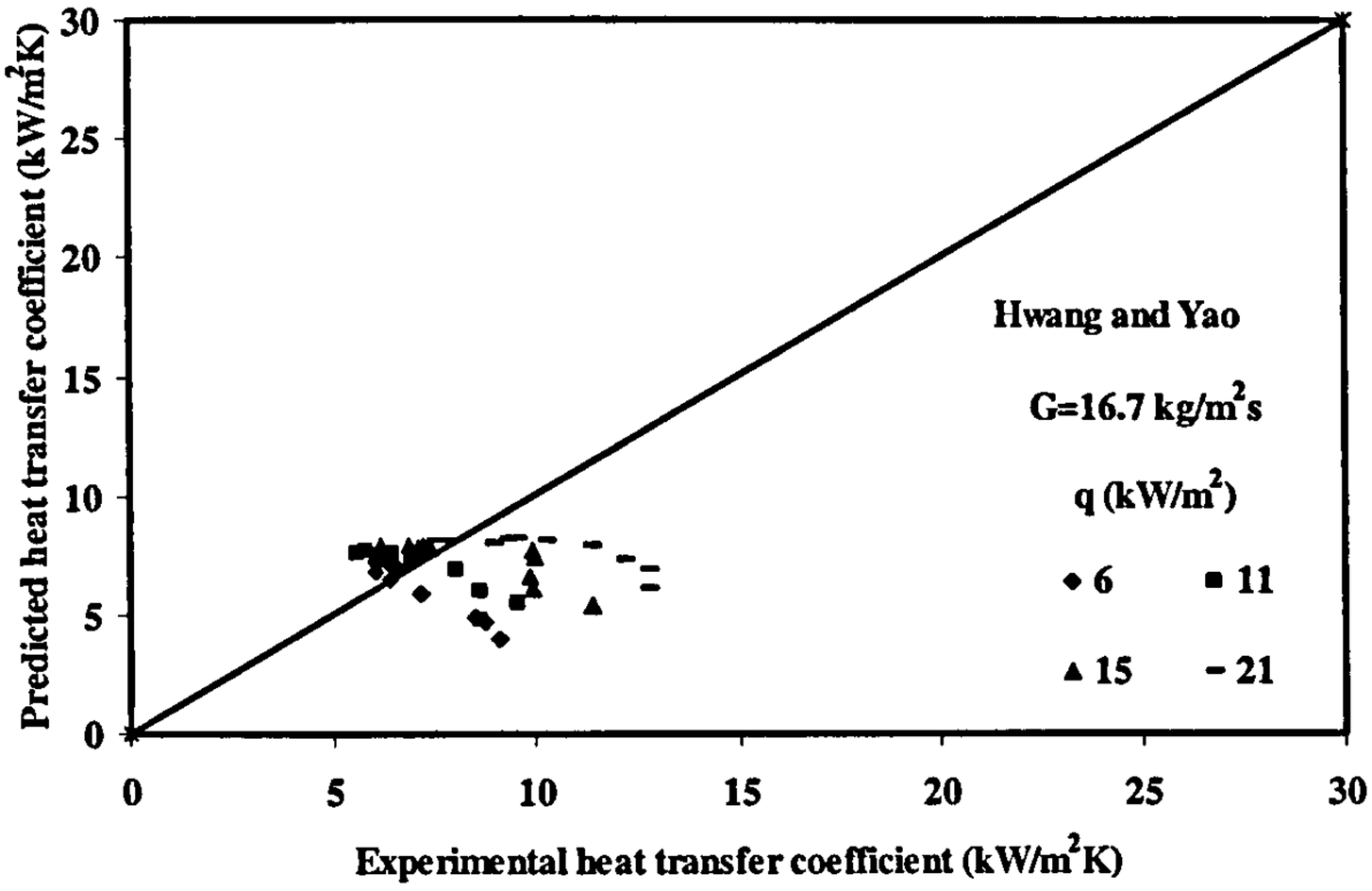

Figure D. 10 Predicted heat transfer coefficient using Hwang and Yao against experimental data for distilled water for G=16.7 kg/m^{2}s

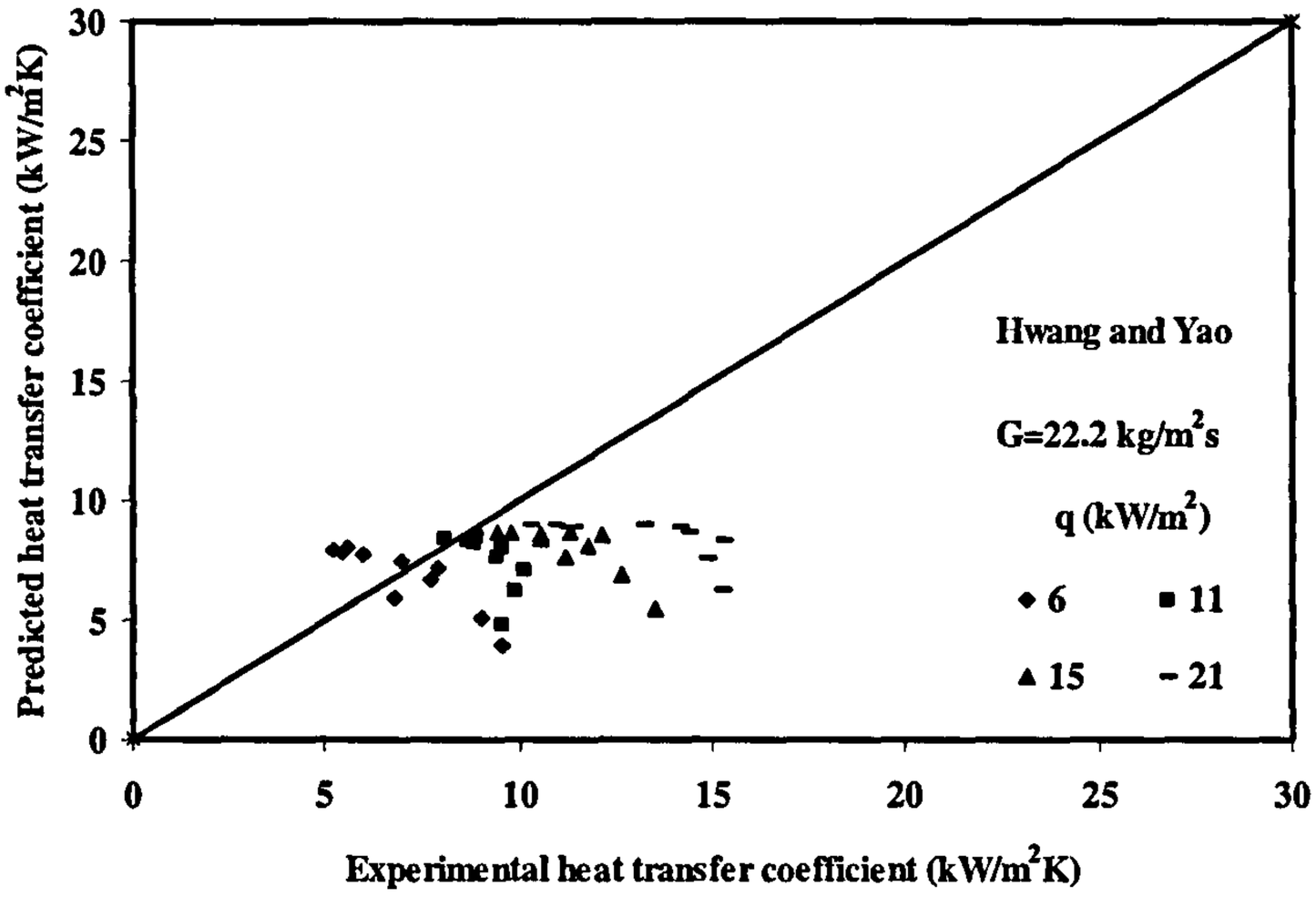

Figure D. 11 Comparison of predicted heat transfer coefficient with experimental results with Hwang and Yao for distilled water for G=22.20 kg/m^{2}s

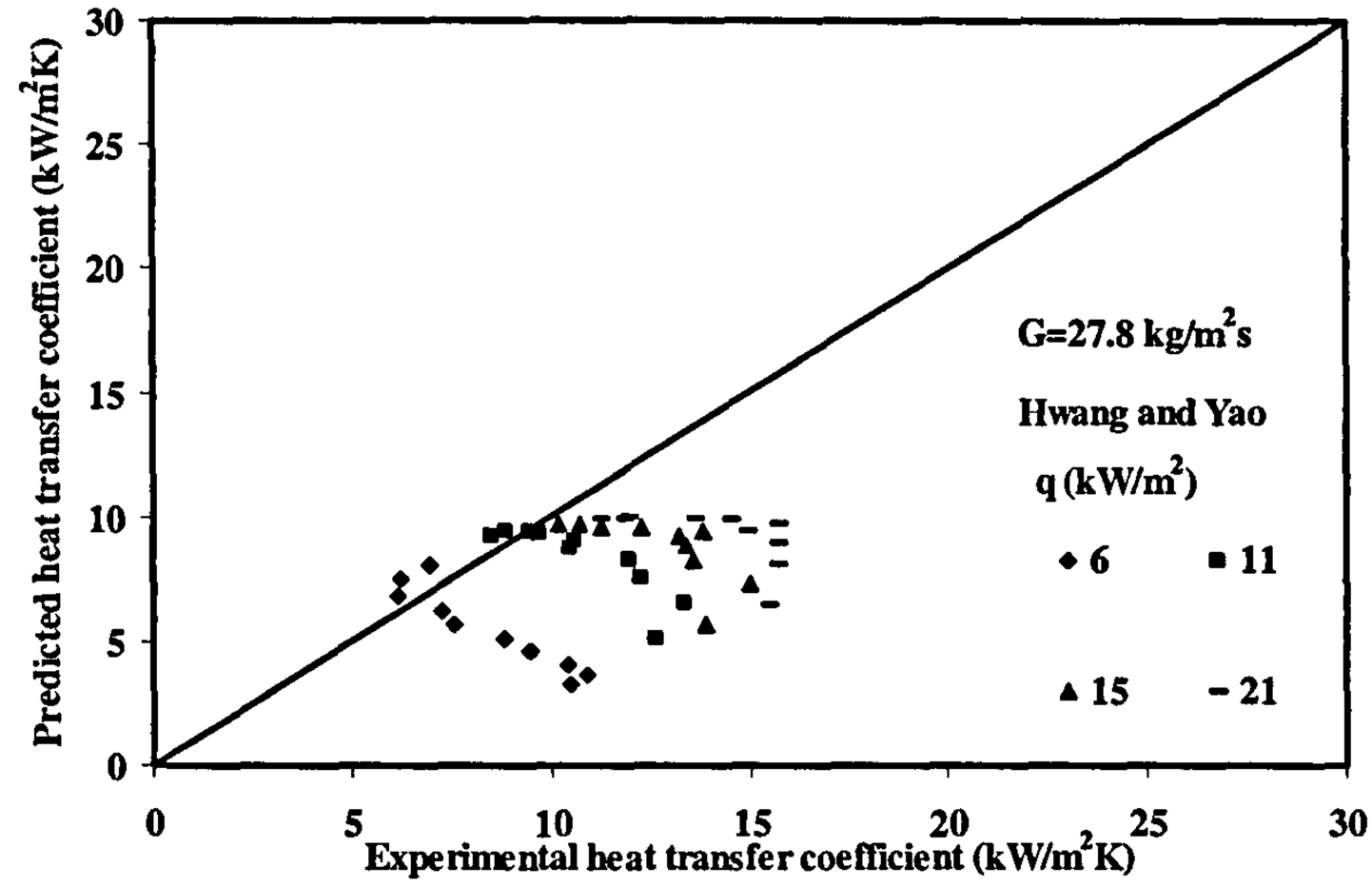

Figure D. 12 Comparison of predicted heat transfer coefficient with experimental results with Hwang and Yao for distilled water for G=27.8 kg/m^{2}s.

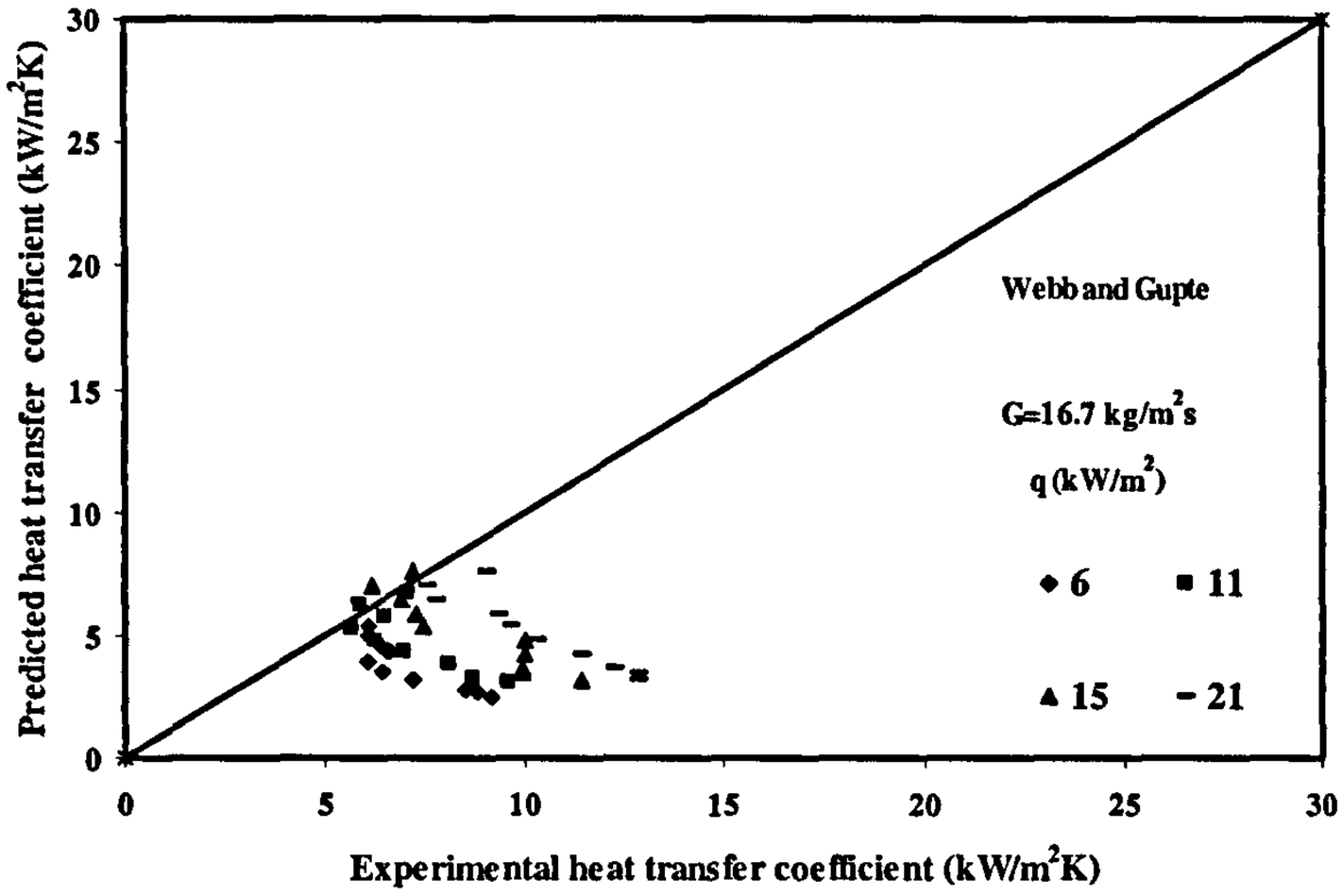

Figure D. 13 Comparison of predicted heat transfer coefficient with experimental results with Webb and Gupte for distilled water for G=16.7 kg/m^{2}s.

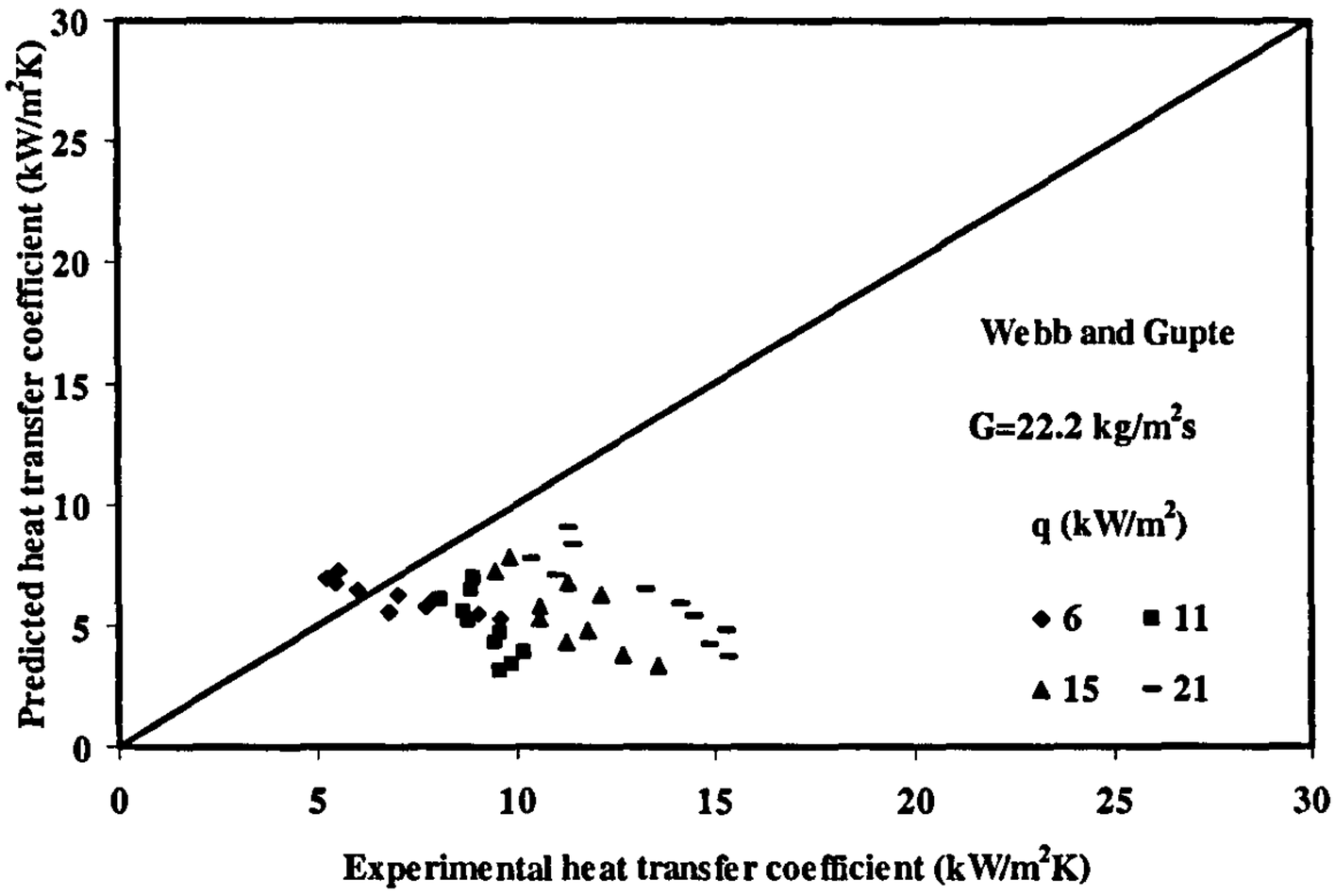

Figure D. 14 Comparison of predicted heat transfer coefficient with experimental results with Webb and Gupte for distilled water for G=22.2 kg/m^{2}s.

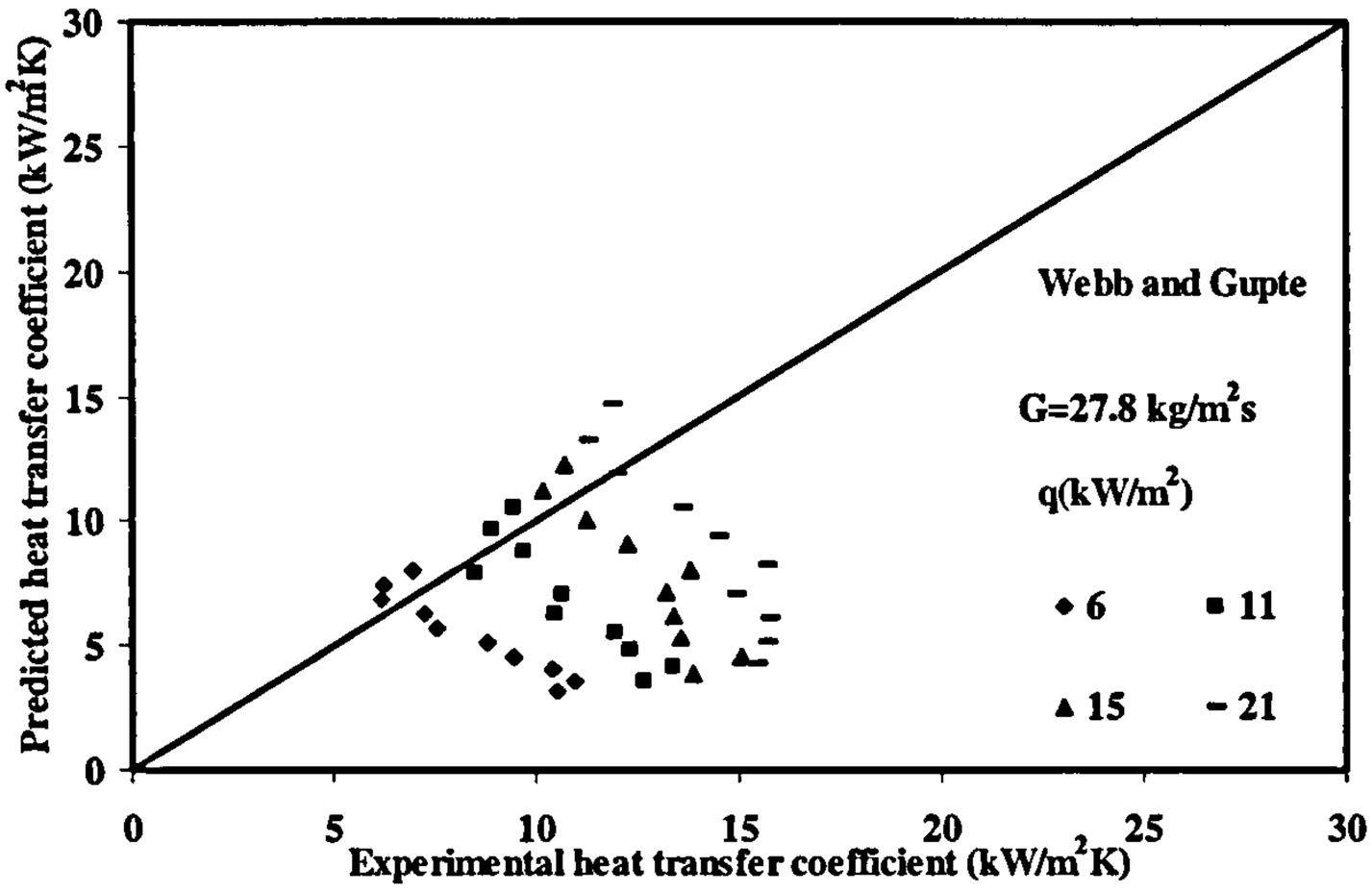

Figure D. 15 Comparison of predicted heat transfer coefficient with experimental results with Gupte and Webb for distilled water for G=27.8 kg/m^{2}s.

APPENDIX D2: COMPARISON OF RESULTS WITH R113

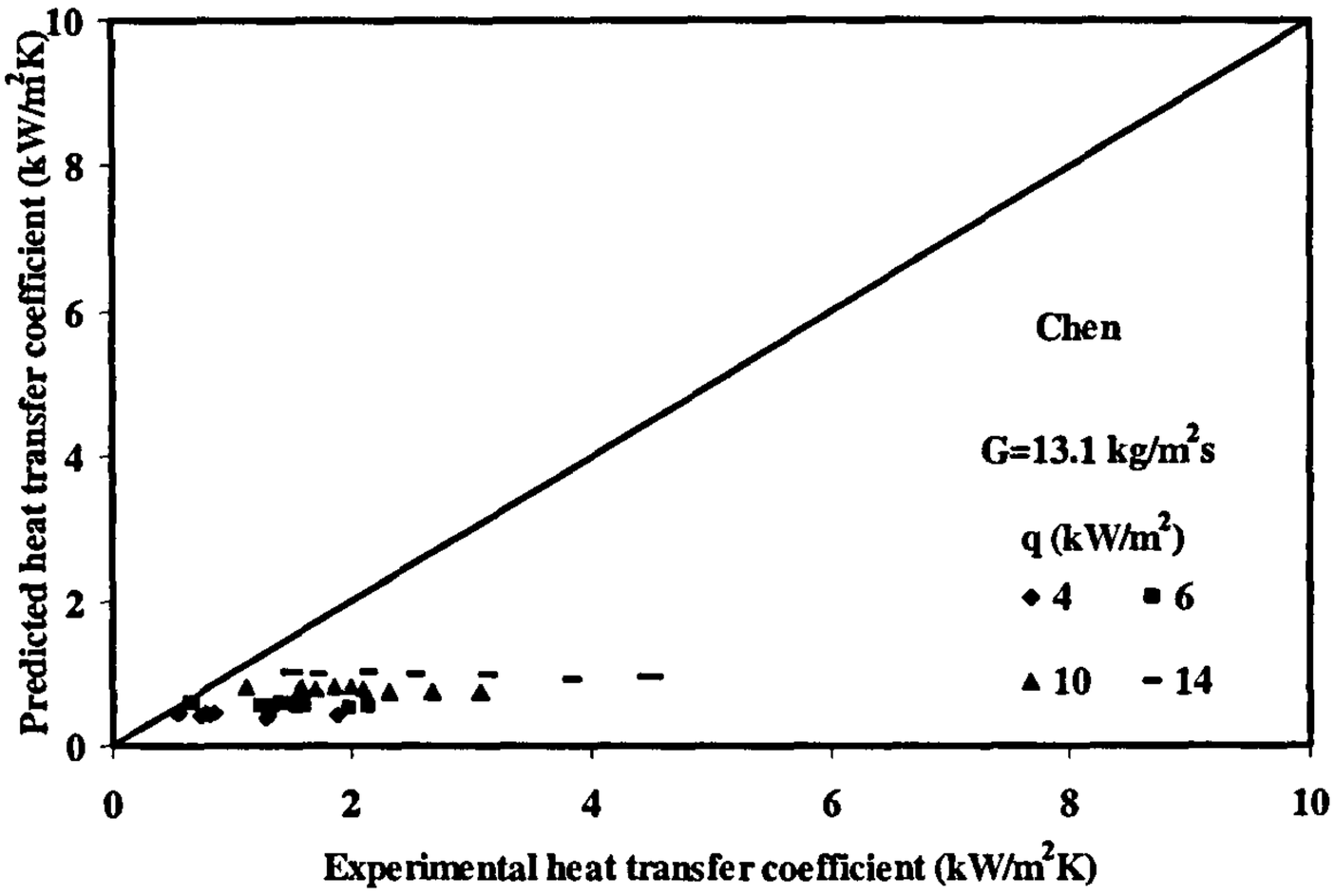

Figure D. 16 Comparison of predicted heat transfer coefficient with experimental results with Chen for R113 for G=13.1 kg/m^{2}s.

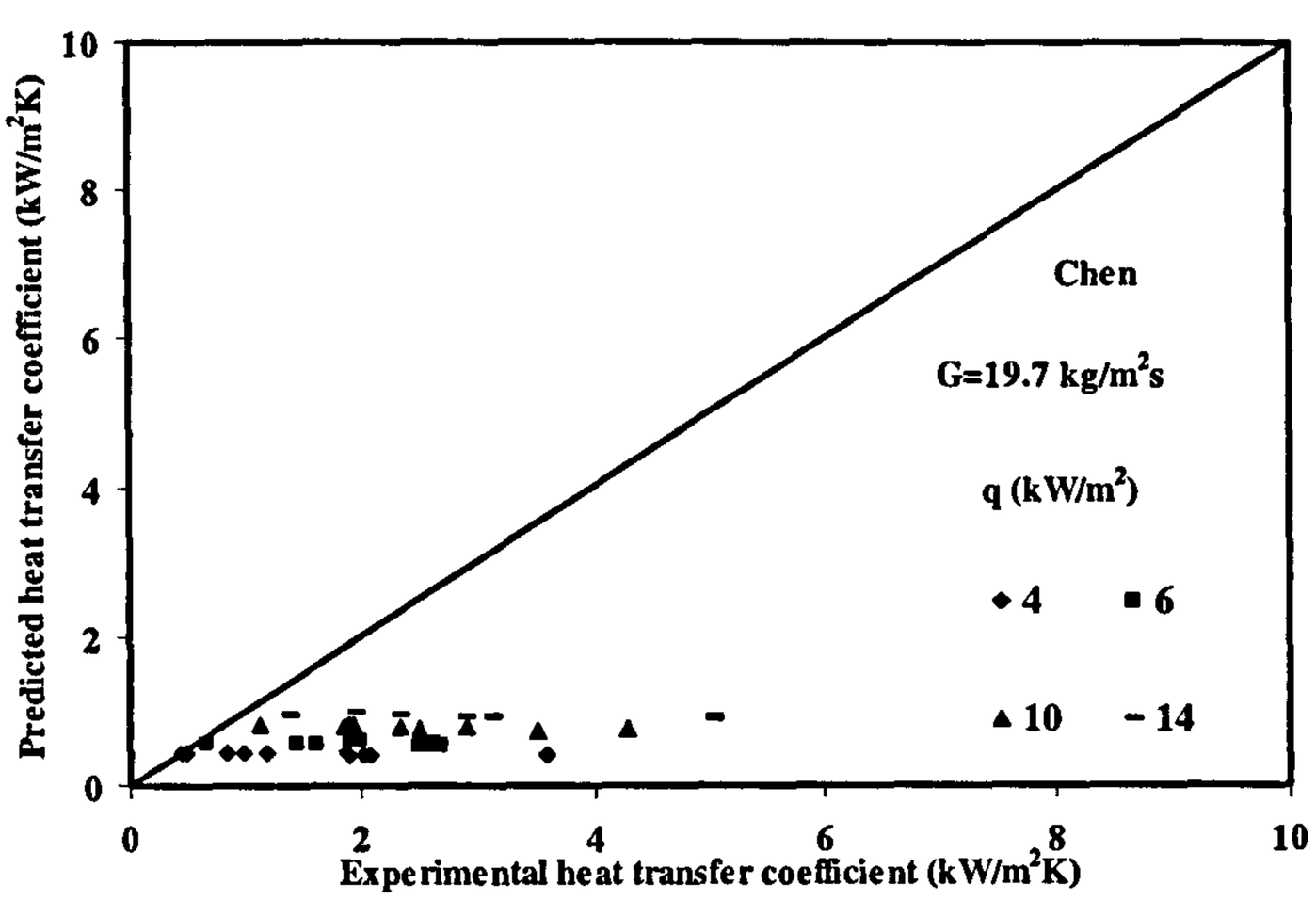

Figure D. 17 Comparison of predicted heat transfer coefficient with experimental results with Chen for R113 for G=19.7 kg/m^{2}s.

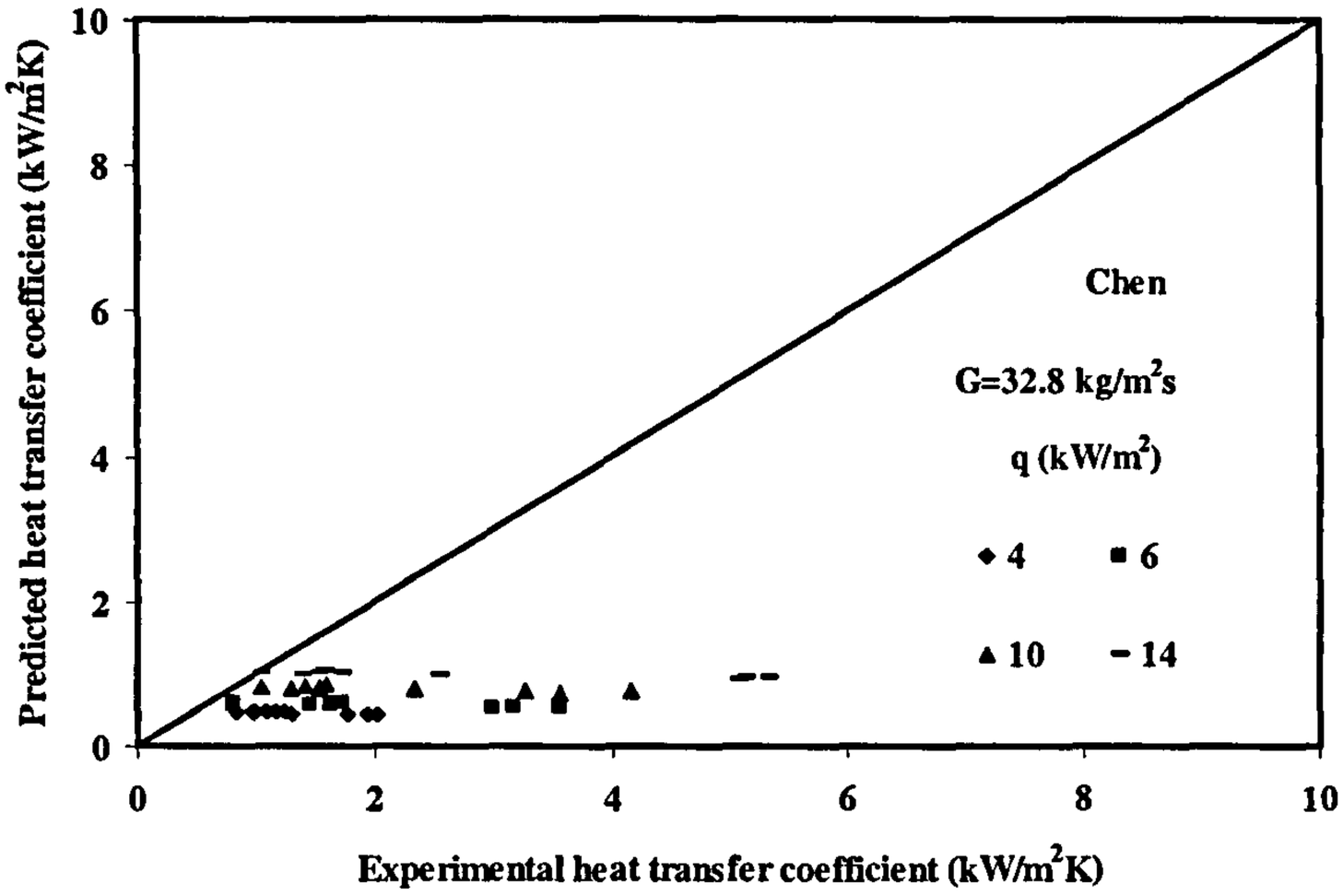

Figure D. 18 Comparison of predicted heat transfer coefficient with experimental results with Chen for R113 for G=32.8 kg/m^{2}s.

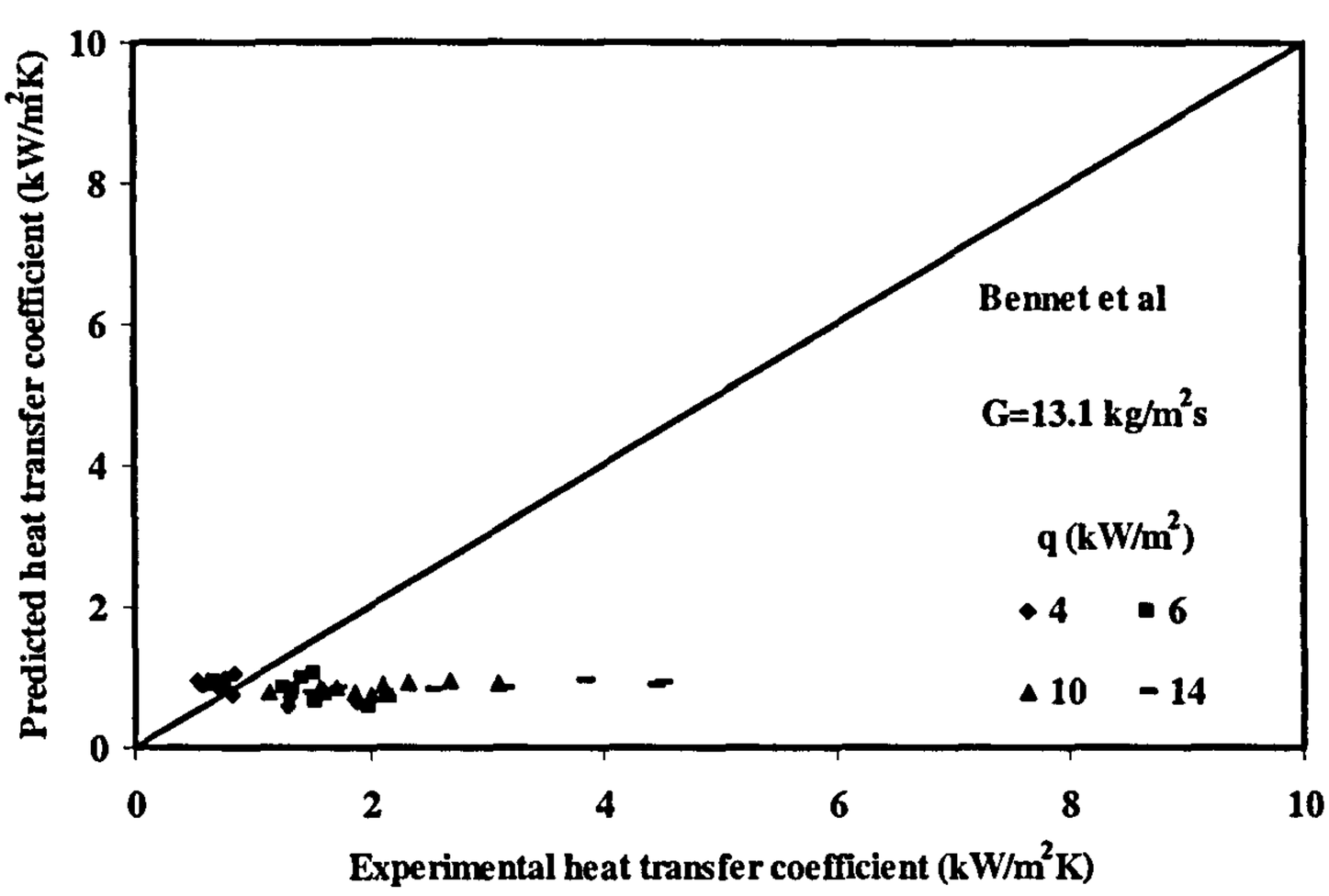

Figure D. 19 Comparison of predicted heat transfer coefficient with experimental results with Bennet et al for R113 for G=13.1 kg/m^{2}s.

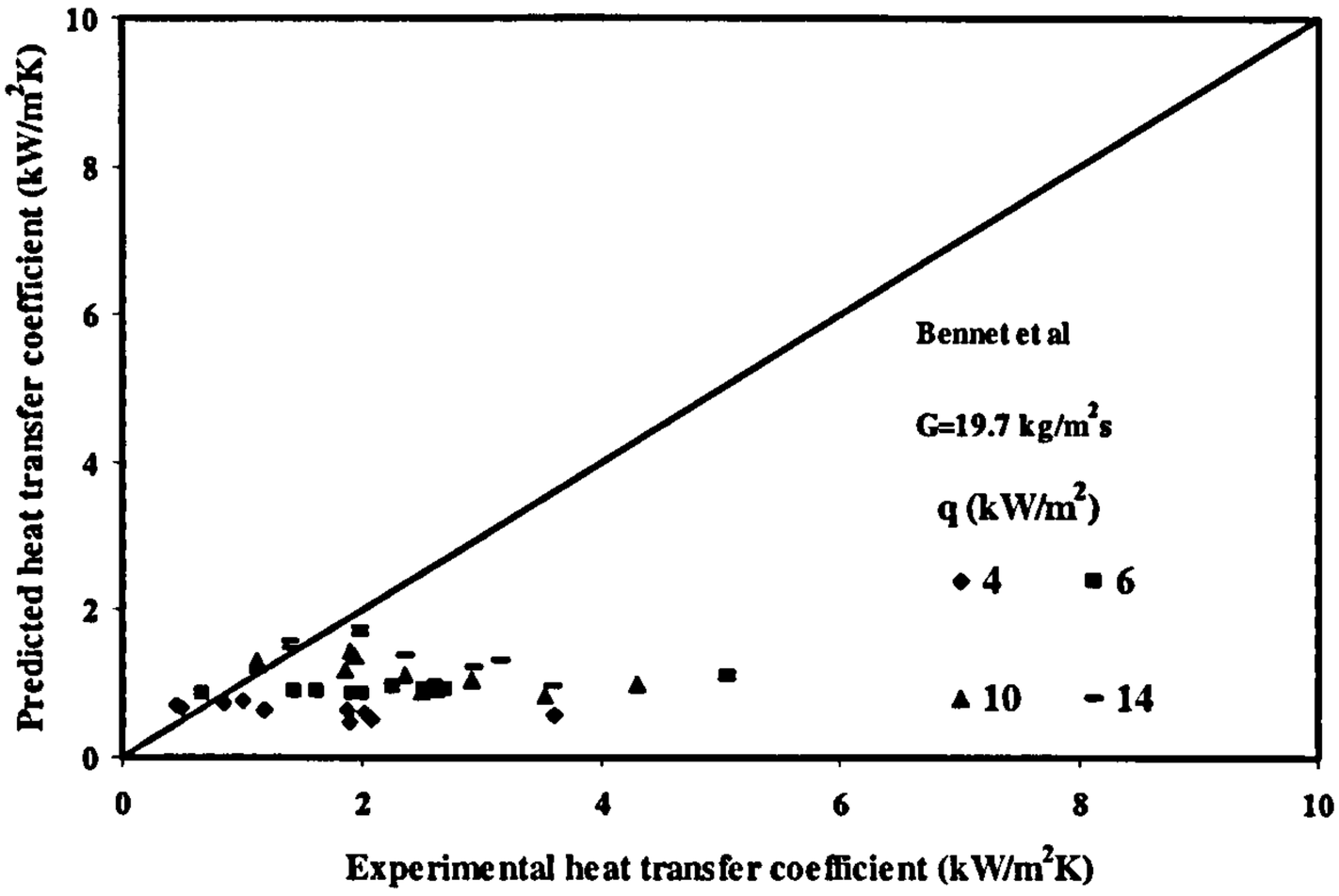

Figure D. 20 Comparison of predicted heat transfer coefficient with experimental results with Bennet et al for R113 for G=19.7 kg/m^{2}s.

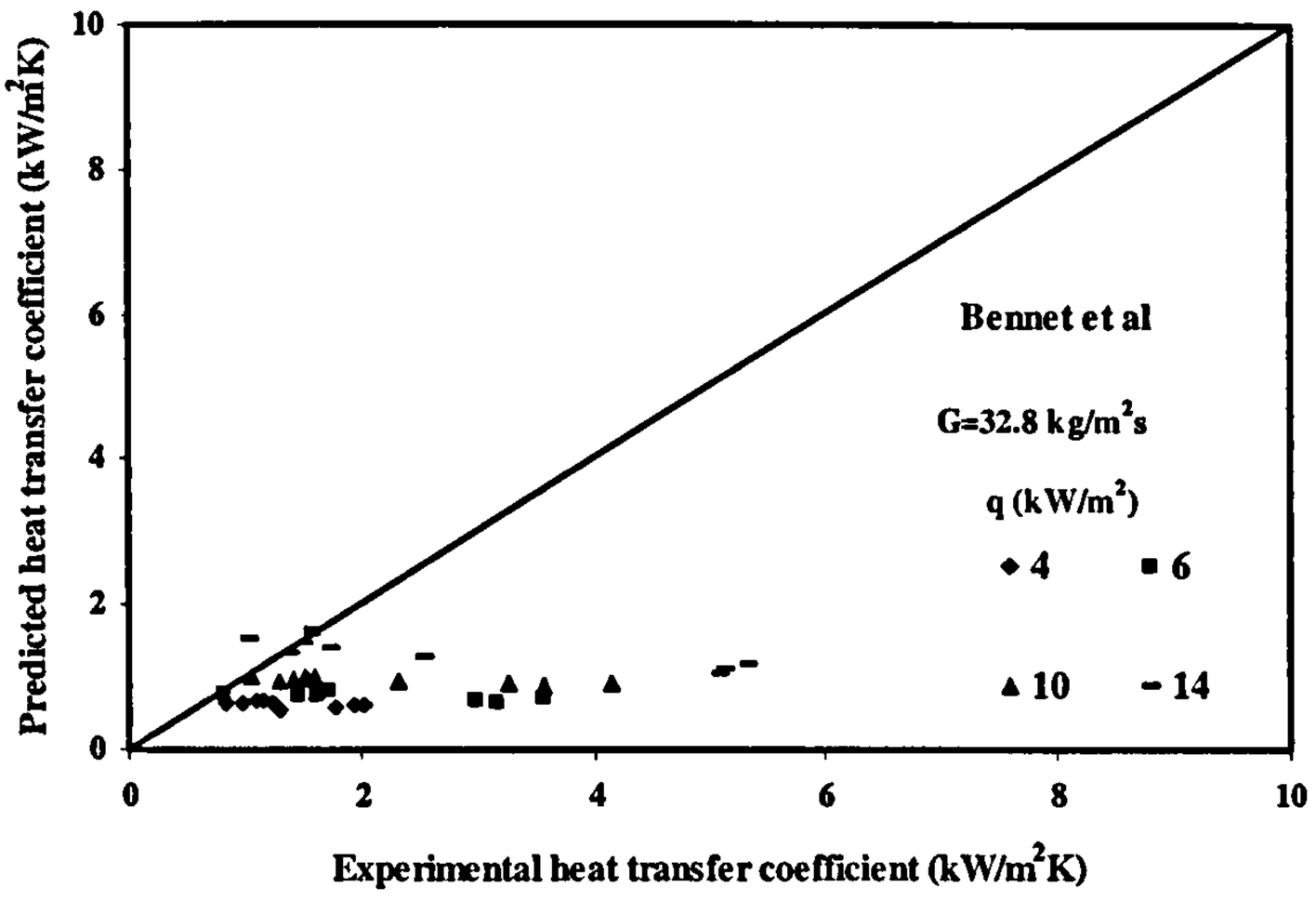

Figure D. 21 Comparison of predicted heat transfer coefficient with experimental results with Bennet et al for R113 for G=32.8 kg/m^{2}s.

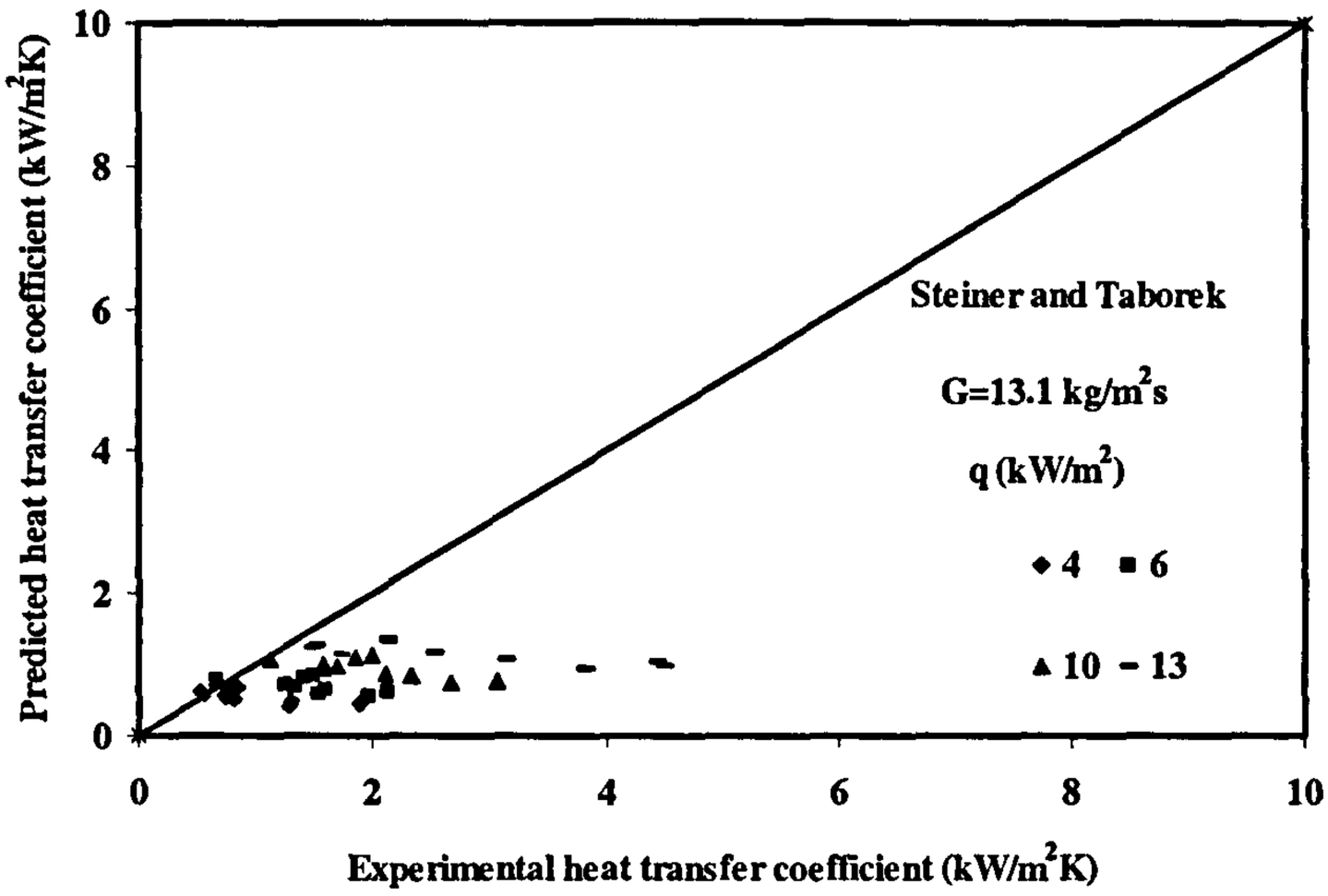

Figure D. 22 Comparison of predicted heat transfer coefficient with experimental results with Steiner and Taborek for R113 for G=13.1 kg/m^{2}s.

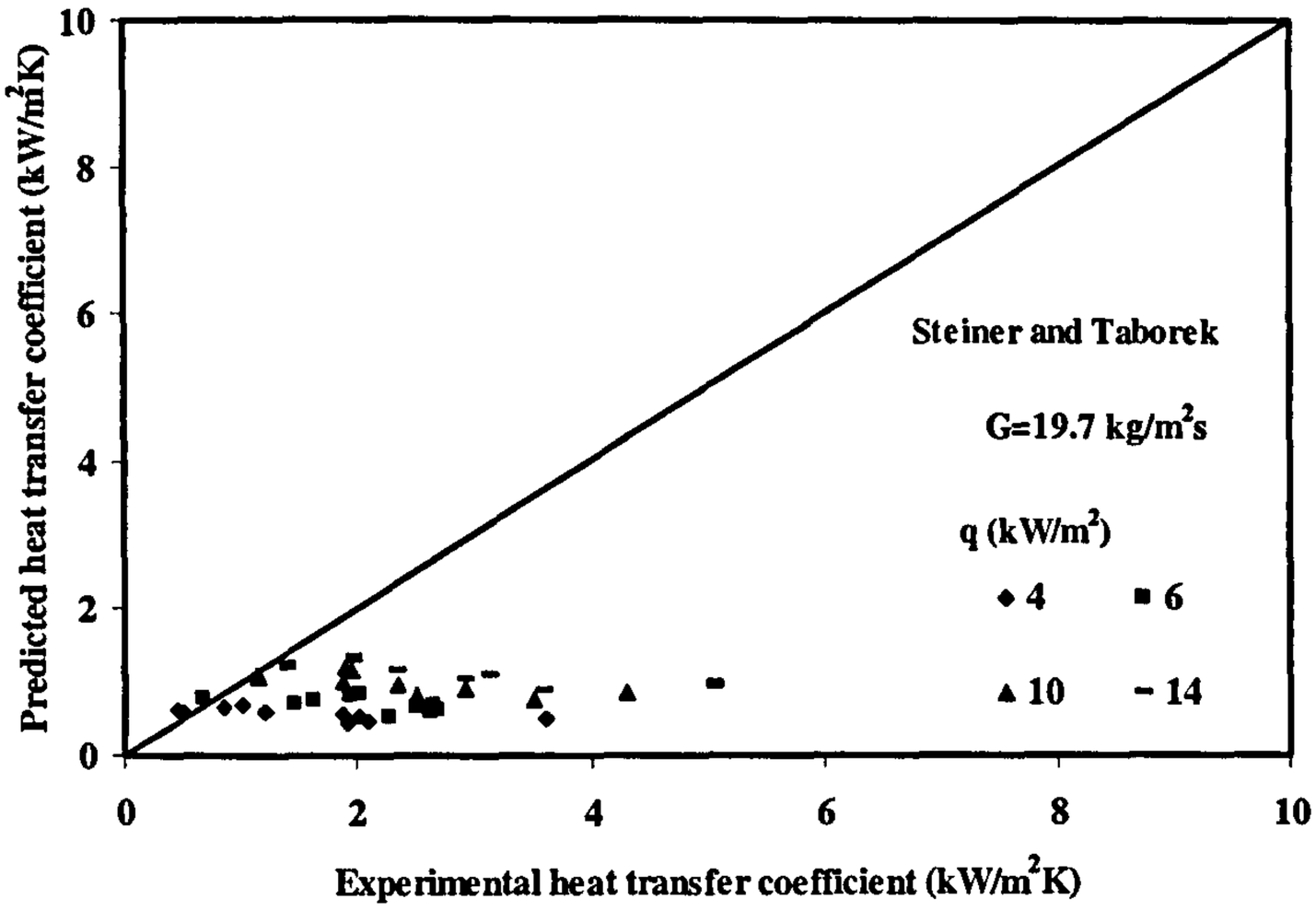

Figure D. 23 Comparison of predicted heat transfer coefficient with experimental results with Steiner and Taborek for R113 for G=19.7 kg/m^{2}s.

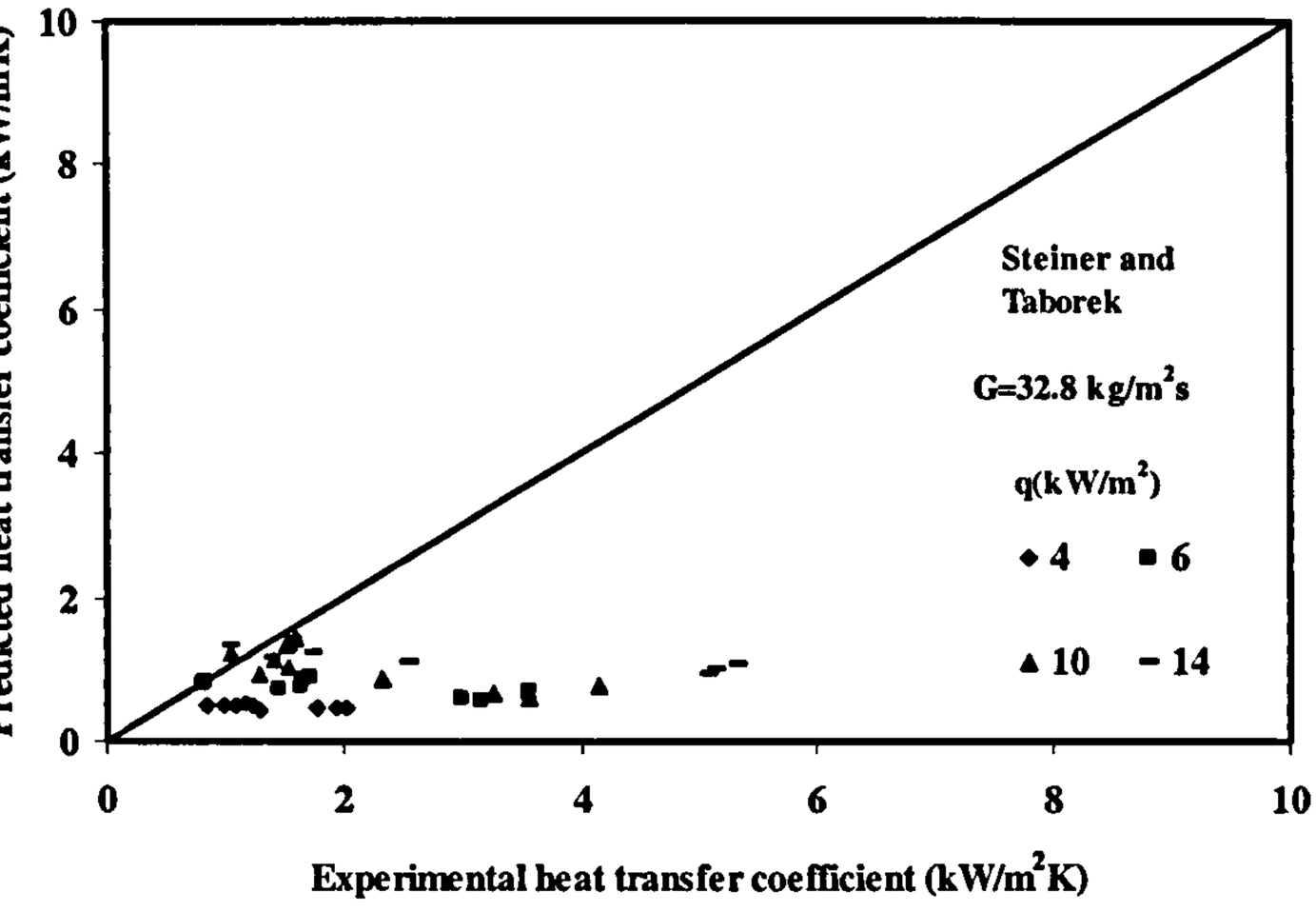

Figure D. 24 Comparison of predicted heat transfer coefficient with experimental results with Steiner and Taborek for R113 for G=32.8 kg/m^{2}s.

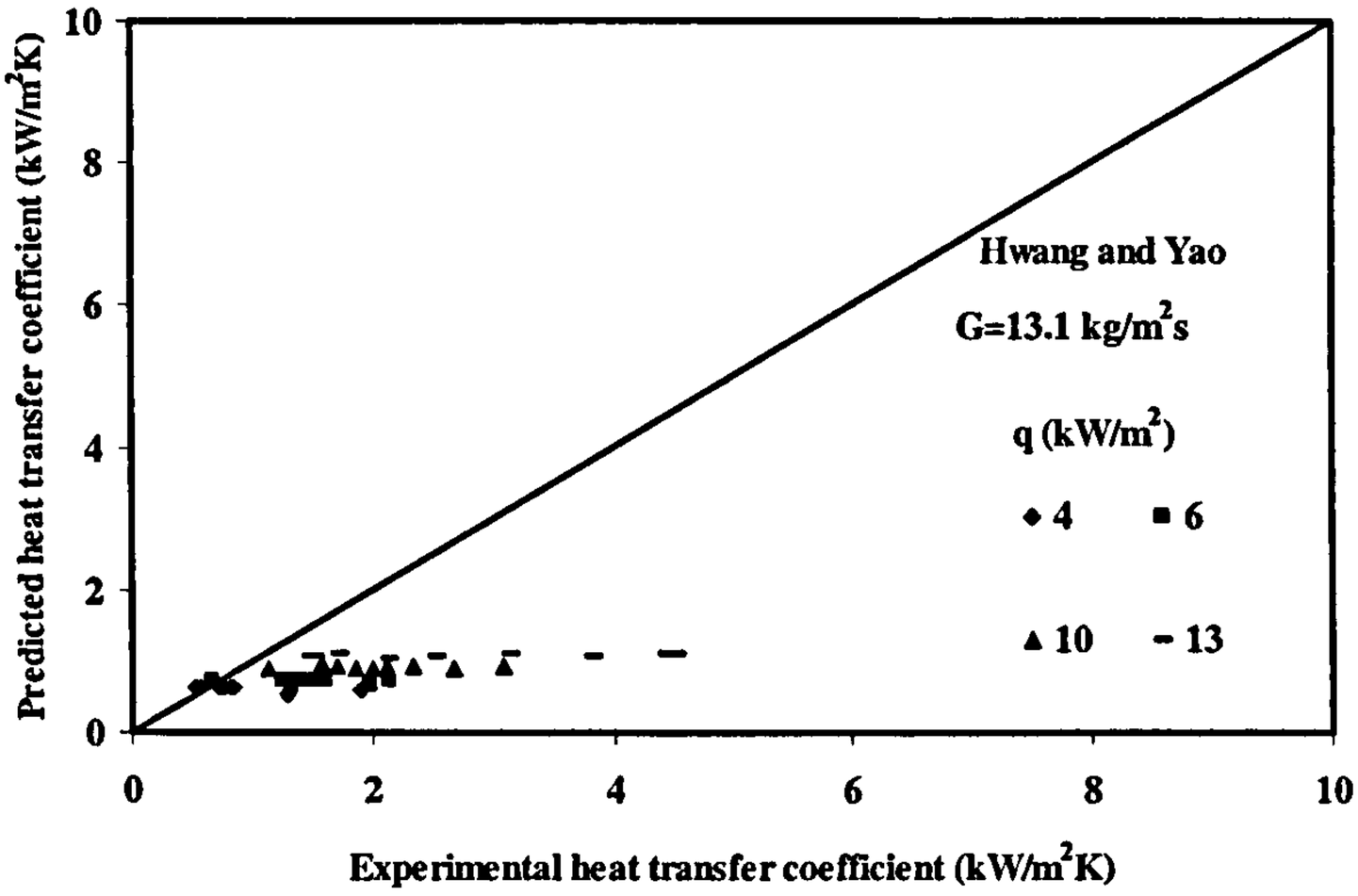

Figure D. 25 Comparison of predicted heat transfer coefficient with experimental results with Hwang and Yao for R113 for G=13.1 kg/m^{2}s.

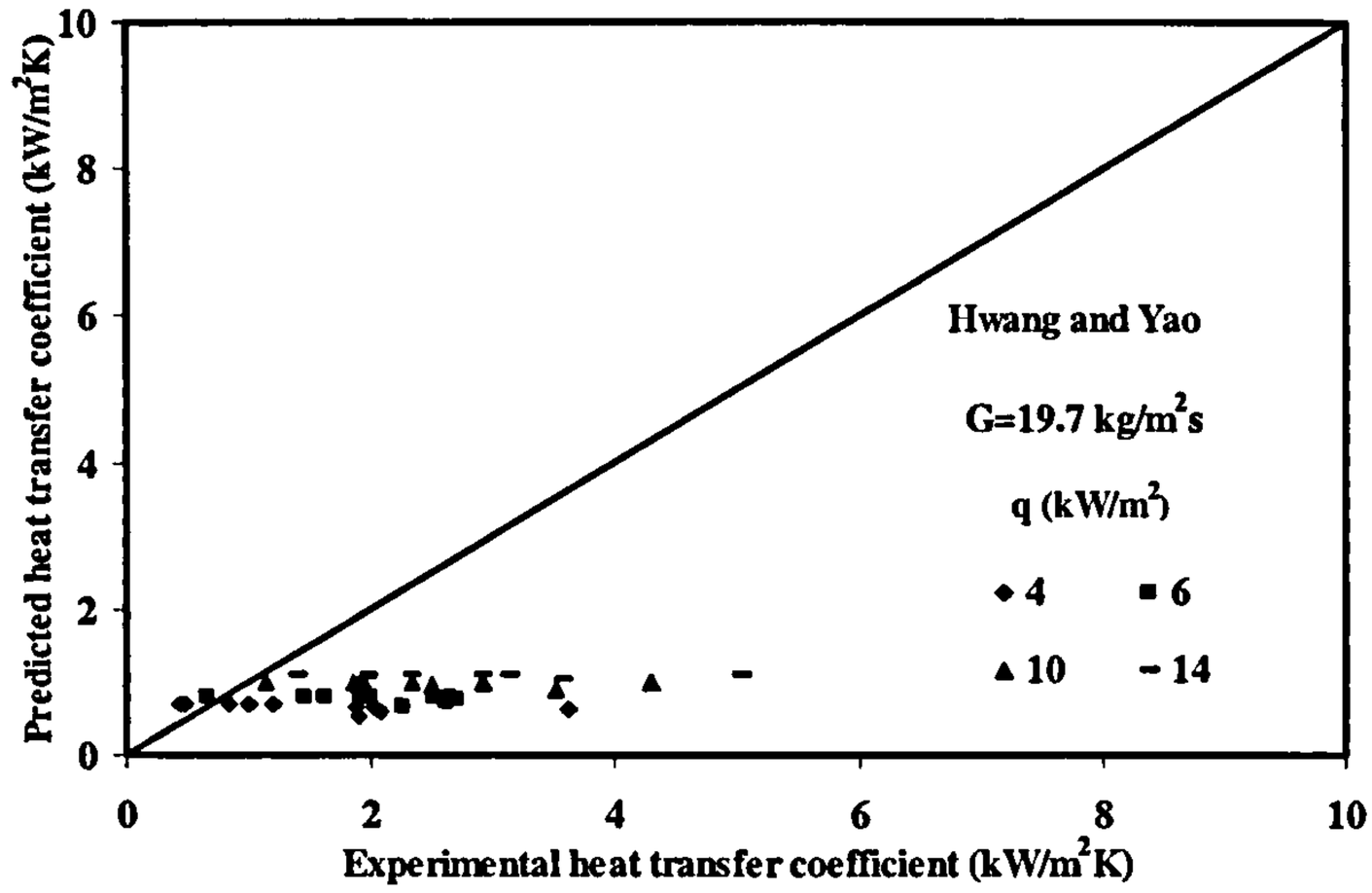

Figure D. 26 Comparison of predicted heat transfer coefficient with experimental results with Hwang and Yao for R113 for G=19.7 kg/m^{2}s.

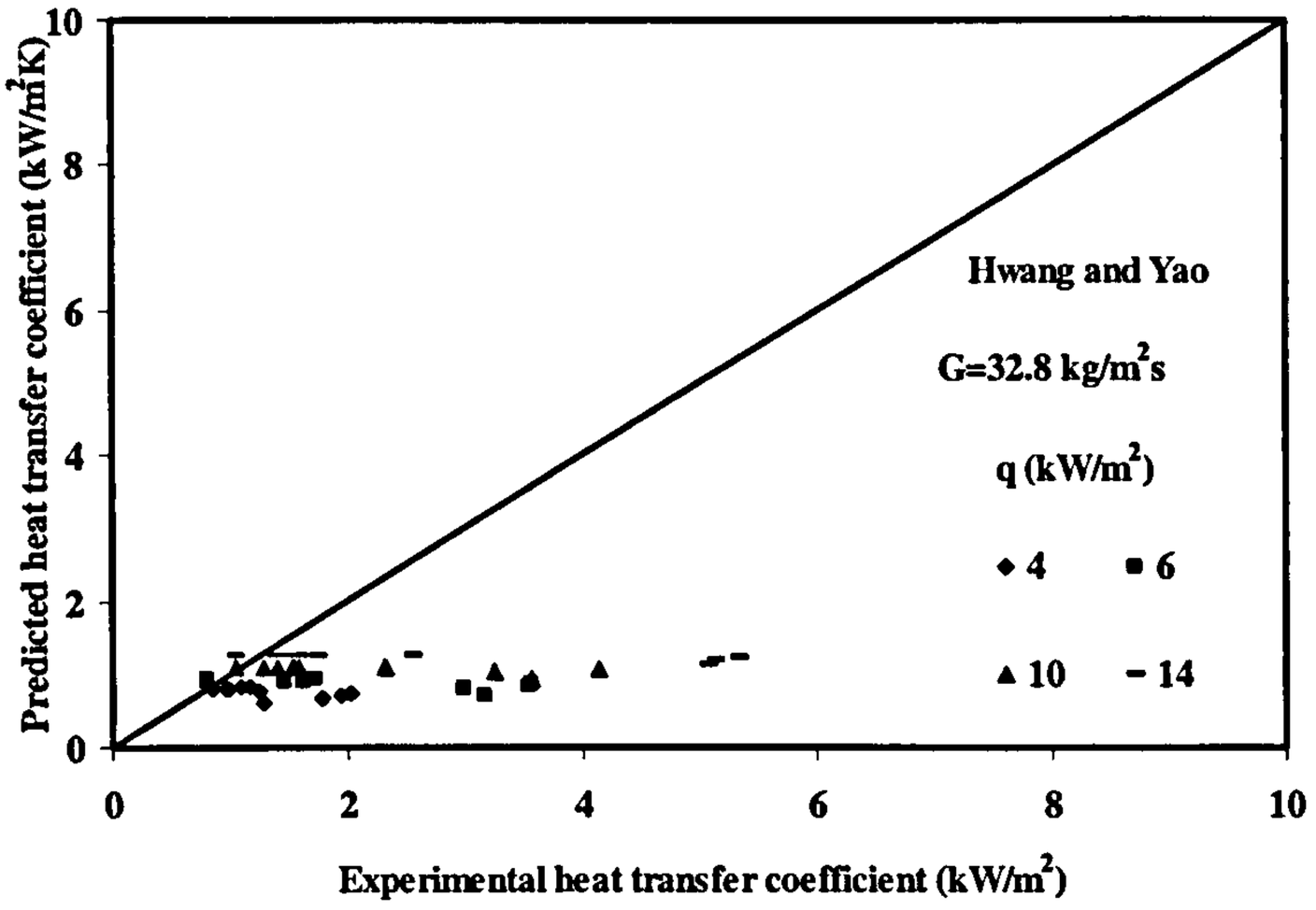

Figure D. 27 Comparison of predicted heat transfer coefficient with experimental results with Hwang and Yao for R113 for G=32.8 kg/m^{2}s.

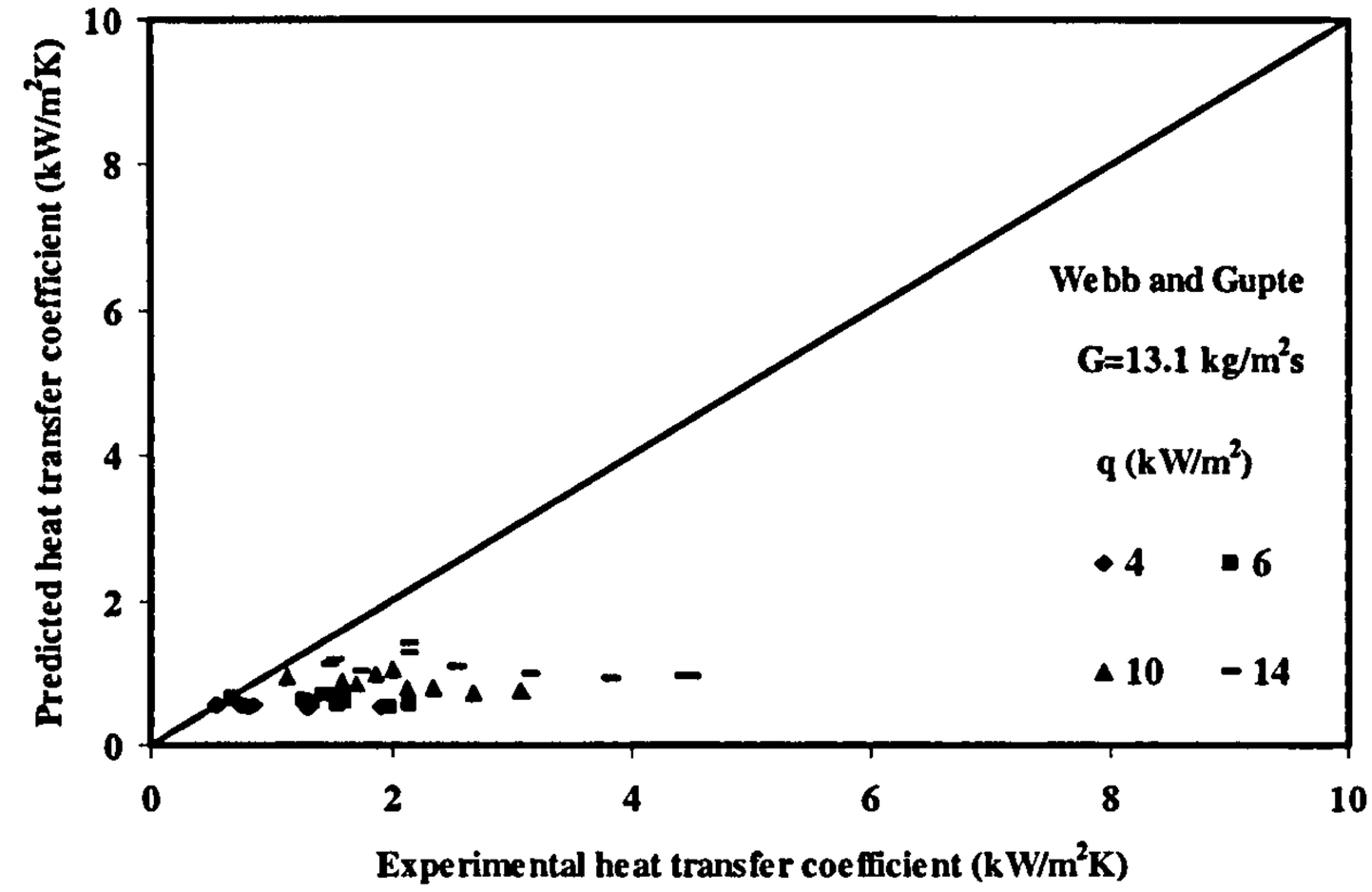

Figure D. 28 Comparison of predicted heat transfer coefficient with experimental results with Gupte and Webb for R113 for G=13.1 kg/m^{2}s.

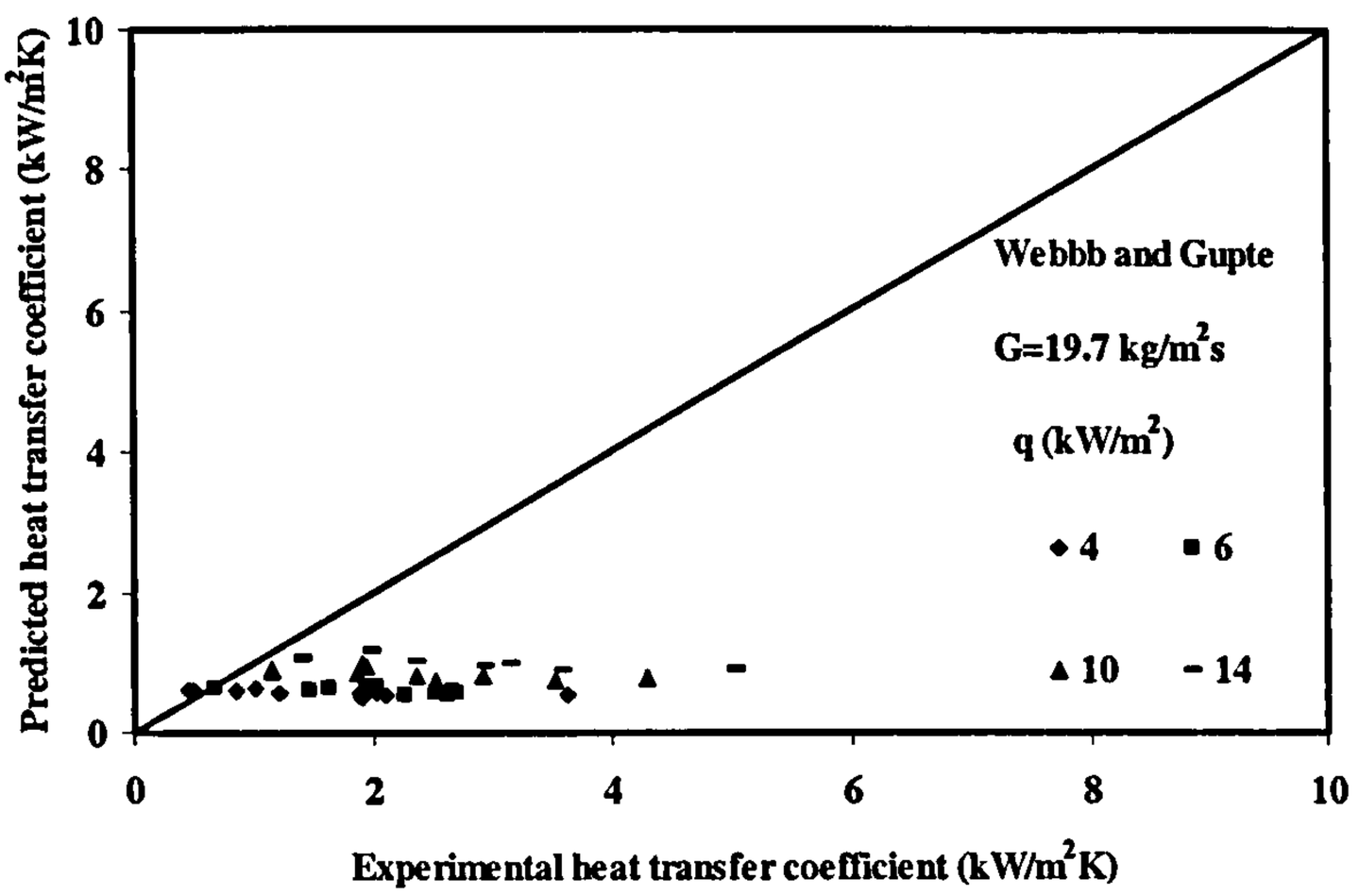

Figure D. 29 Comparison of predicted heat transfer coefficient with experimental results with Gupte and Webb for R113 for G=19.7 kg/m^{2}s.

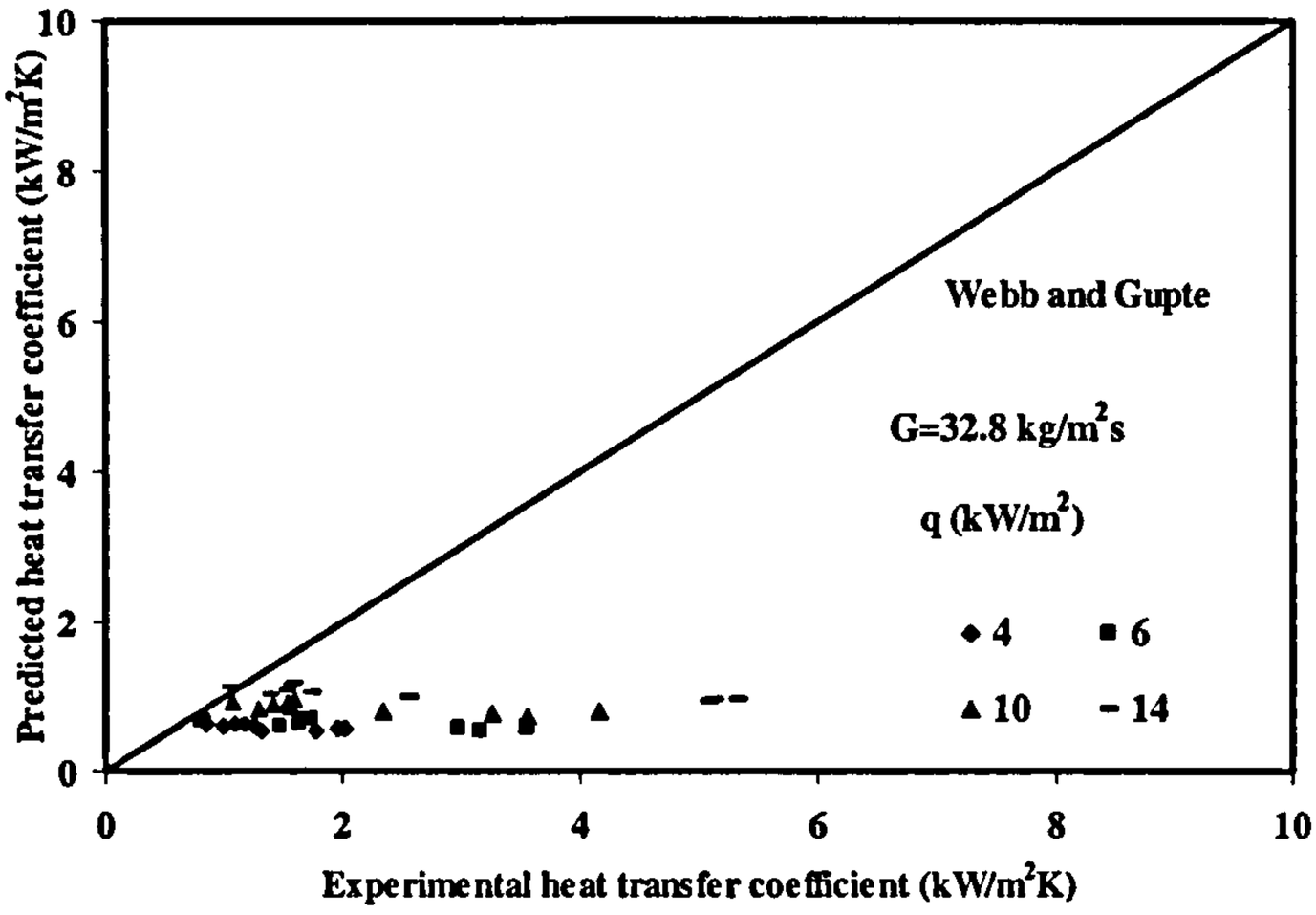

Figure D. 30 Comparison of predicted heat transfer coefficient with experimental results with Gupte and Webb for R113 for G=32.8 kg/m^{2}s.

APPENDIX D3: COMPARISON OF RESULTS WITH FLUTEC PP1

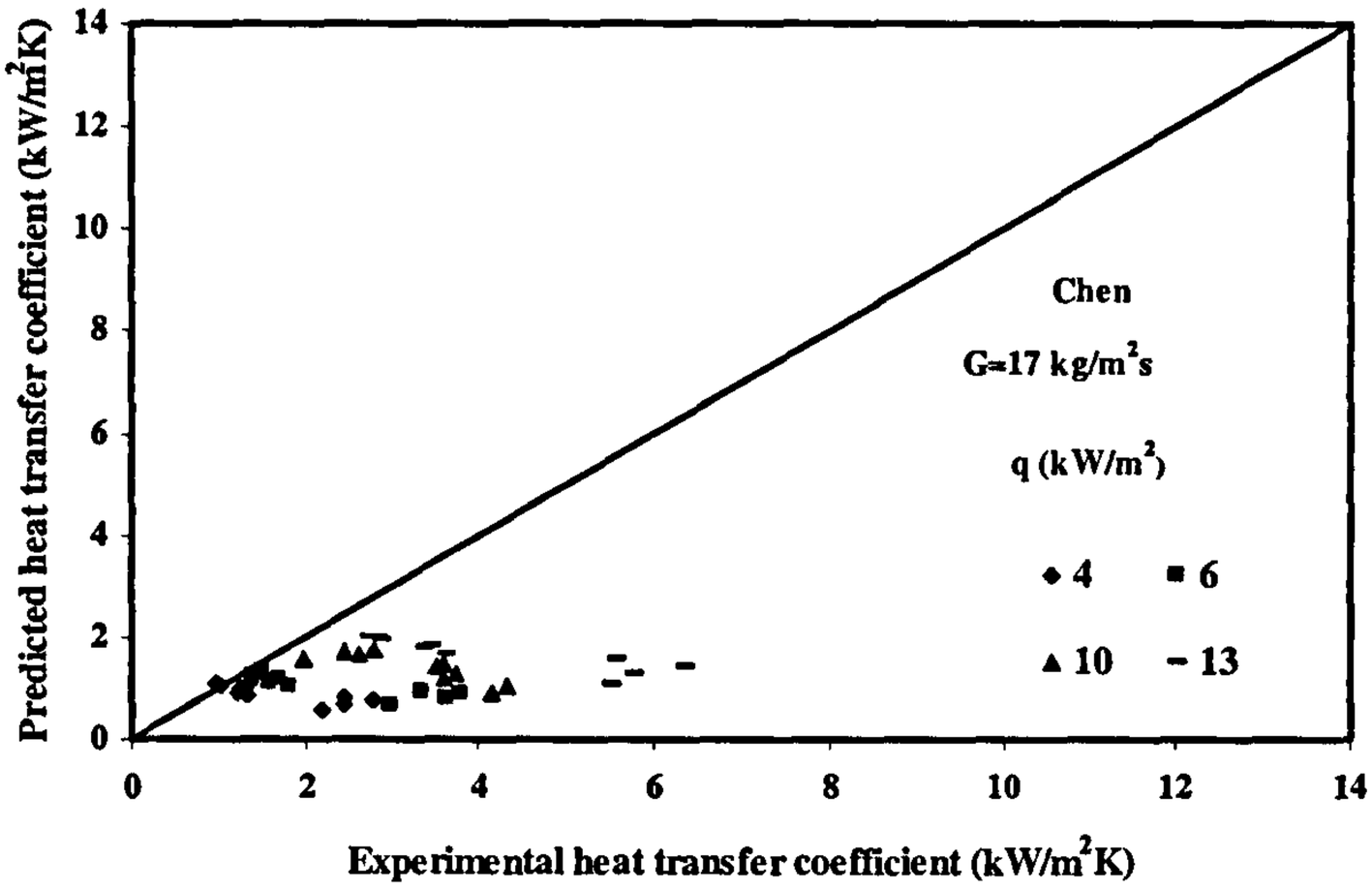

Figure D. 31 Comparison of predicted heat transfer coefficient with experimental results with Chen for Flutec PP1 for G=17 kg/m^{2}s.

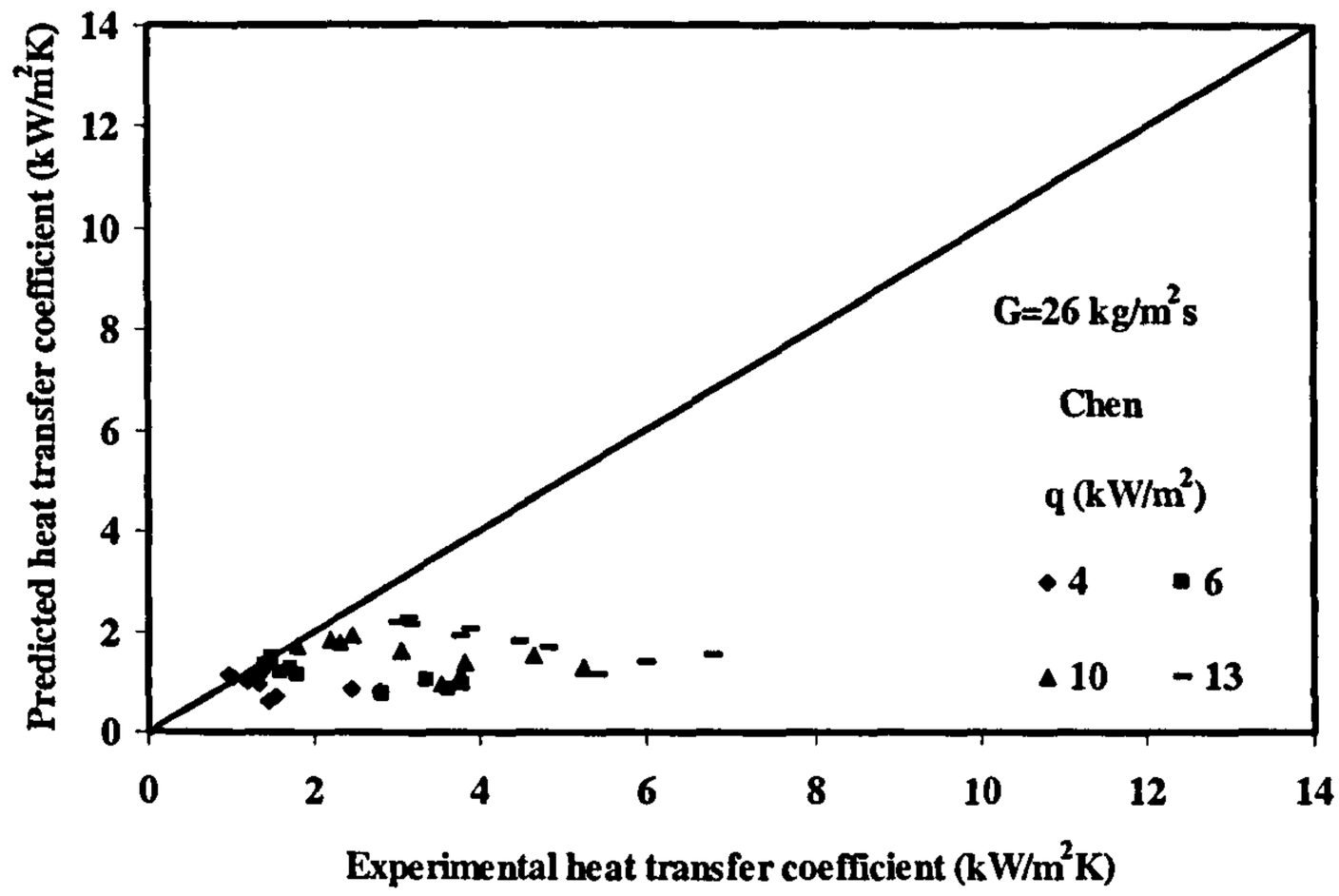

Figure D. 32 Comparison of predicted heat transfer coefficient with experimental results with Chen for Flutec PP1 for G=26 kg/m^{2}s.

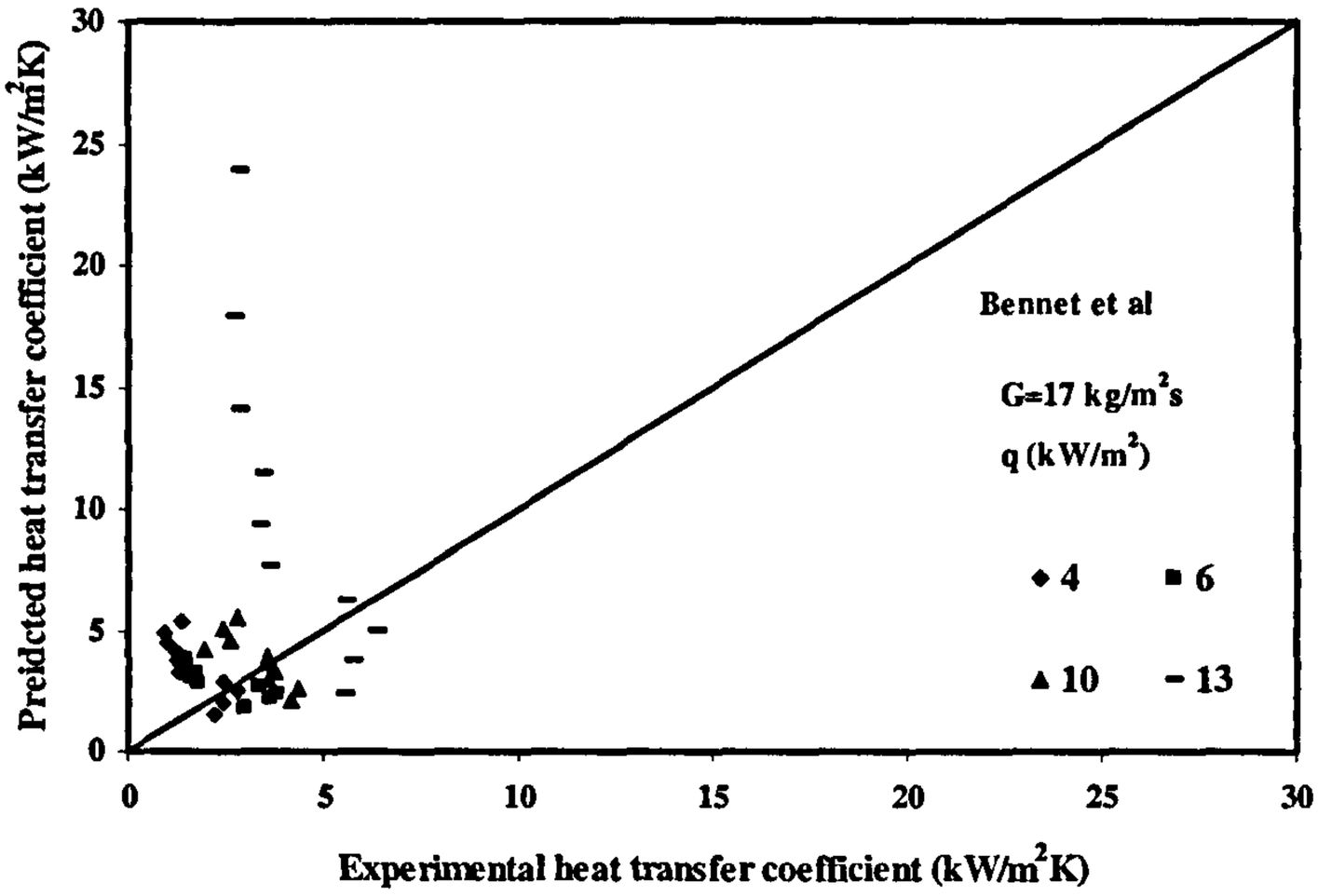

Figure D. 33 Comparison of predicted heat transfer coefficient with experimental results with Bennet et al Flutec PP1 for G=17 kg/m^{2}s

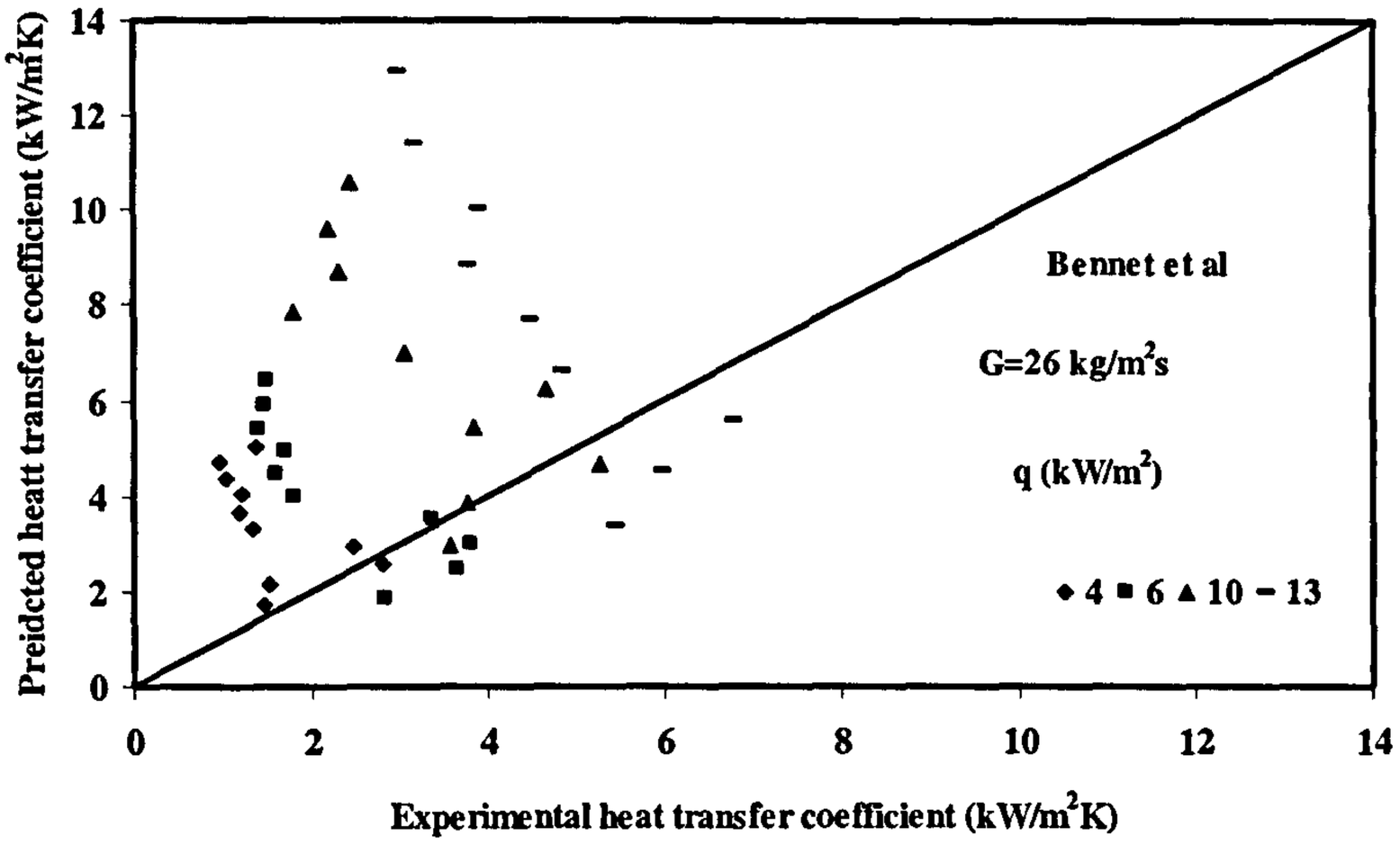

Figure D. 34 Comparison of predicted heat transfer coefficient with experimental results with Bennet et al Flutec PP1 for G=26 kg/m^{2}s

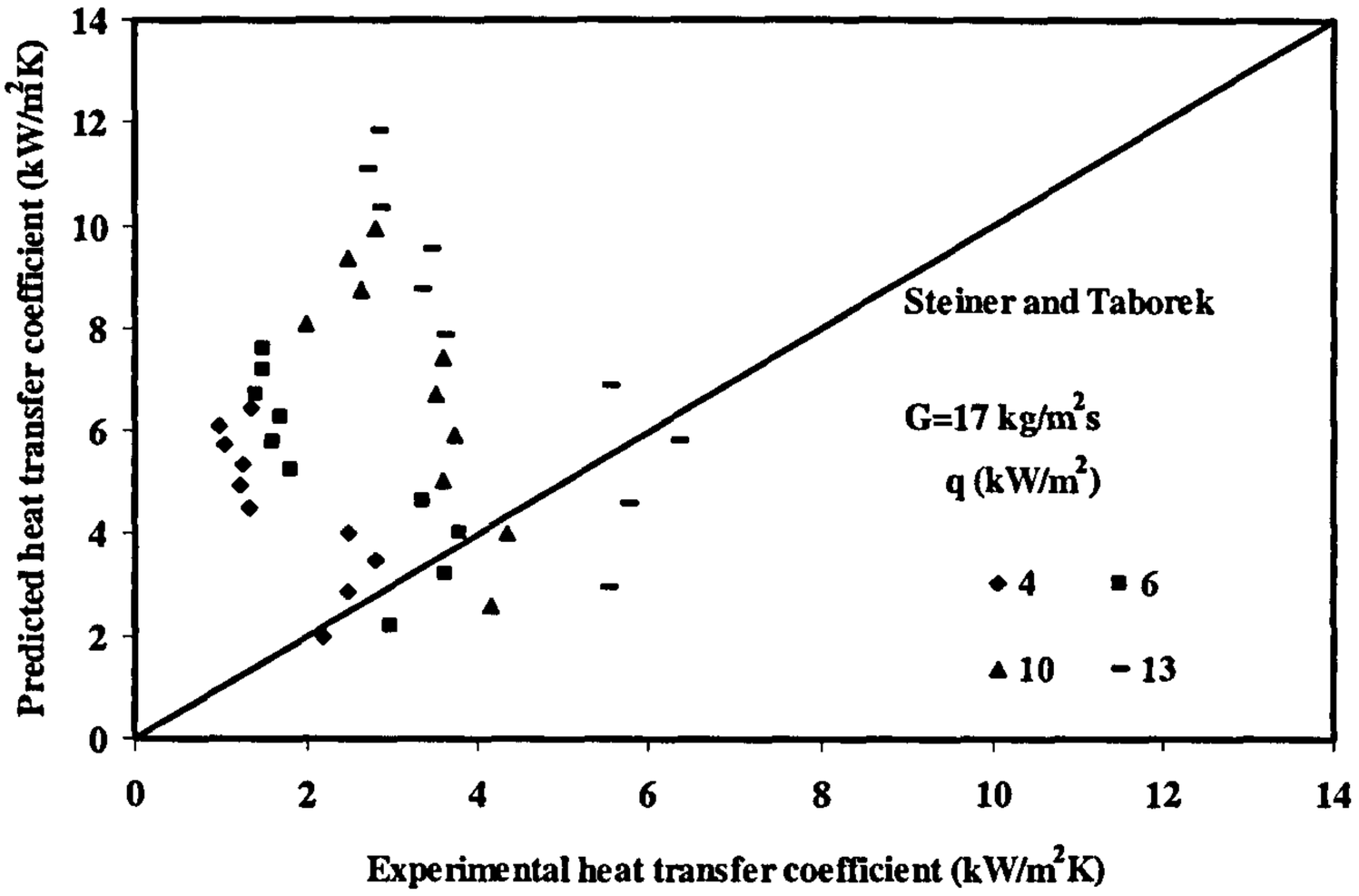

Figure D. 35 Comparison of predicted heat transfer coefficient with experimental results with Steiner and Taborek for Flutec PP1 for G=17 kg/m^{2}s

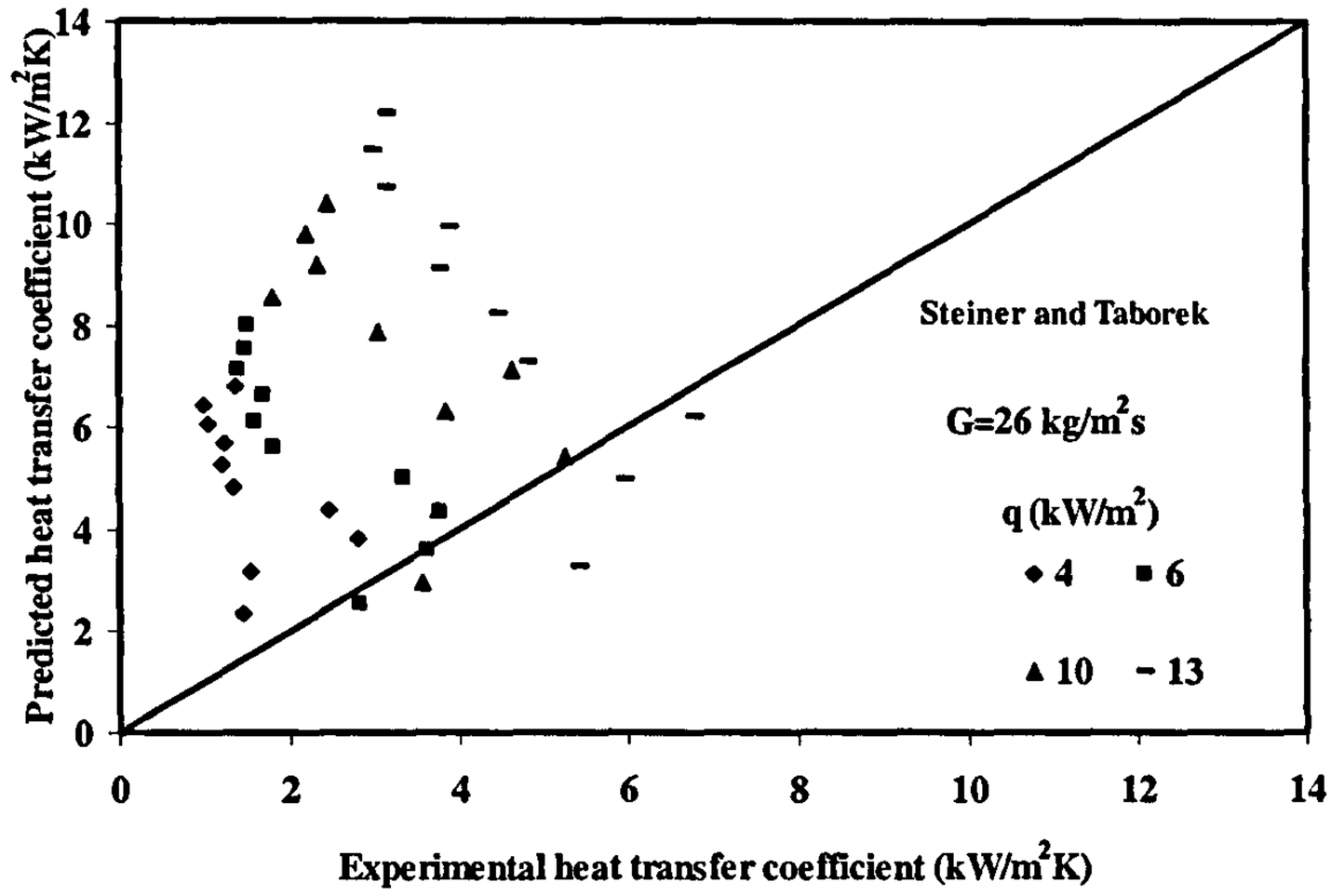

Figure D. 36 Comparison of predicted heat transfer coefficient with experimental results with Steiner and Taborek for Flutec PP1 for G=26 kg/m^{2}s

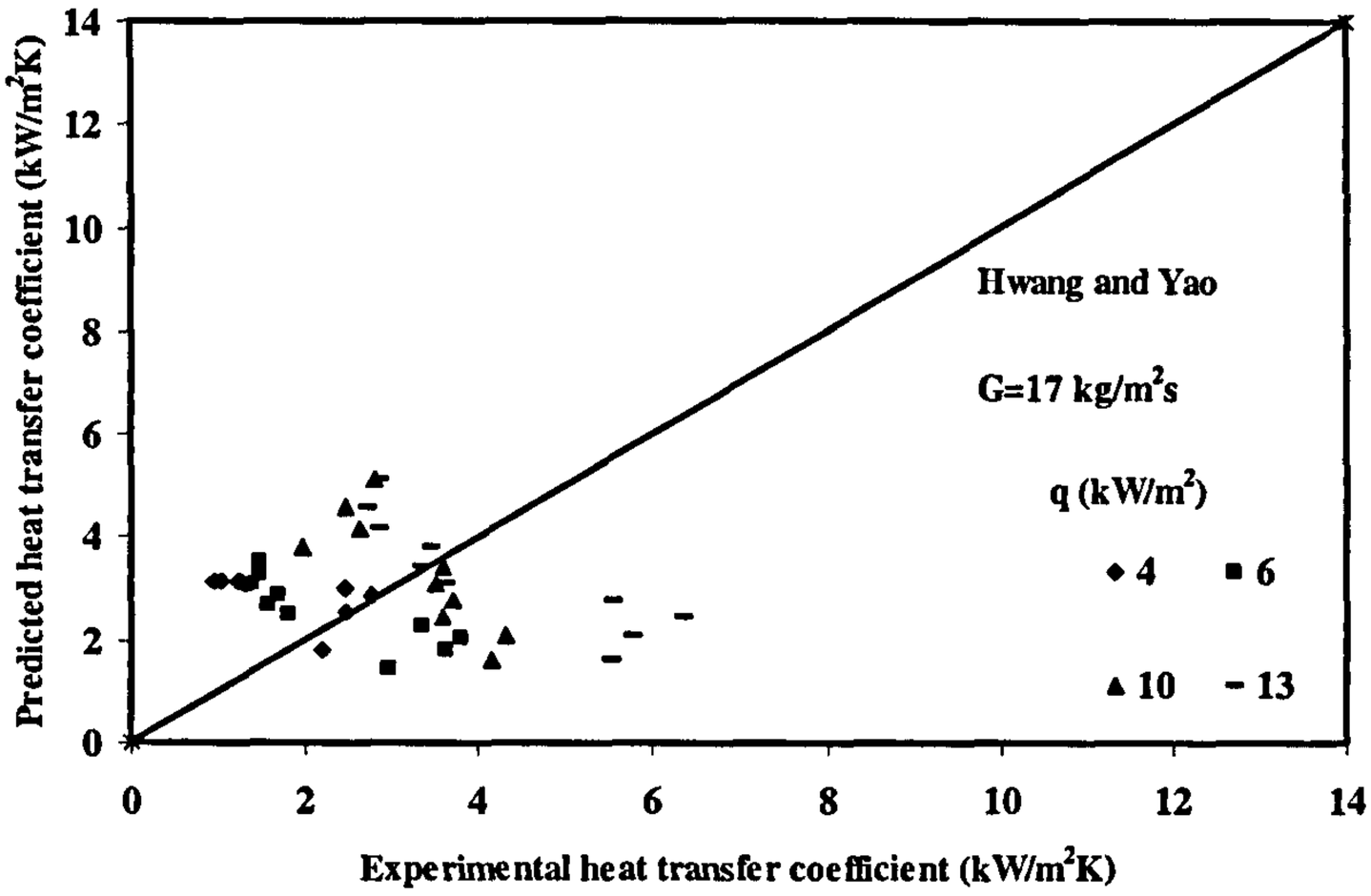

Figure D. 37 Comparison of predicted heat transfer coefficient with experimental results with Hwang and Yao for Flutec PP1, G=17 kg/m^{2}s.

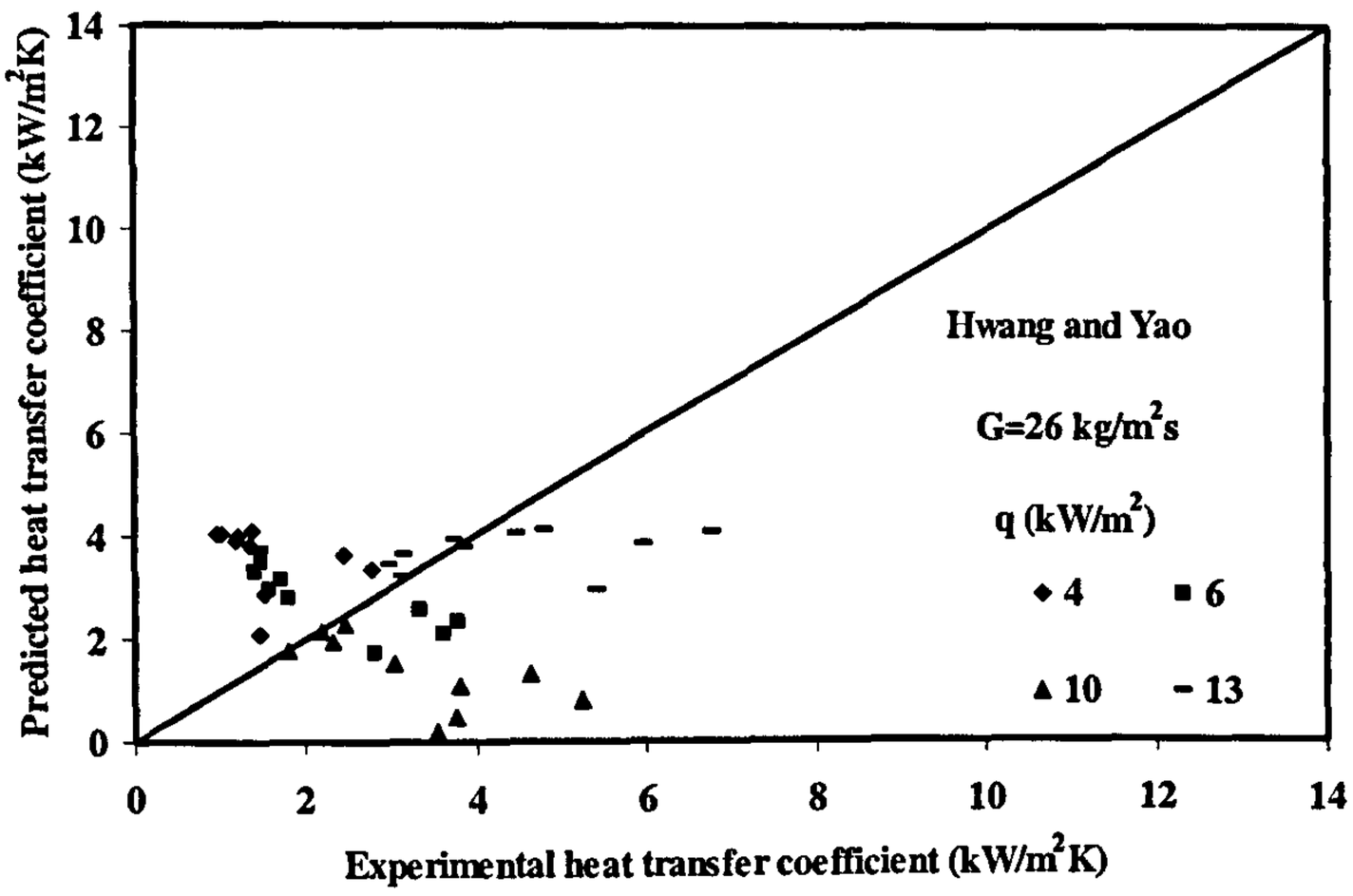

Figure D. 38 Comparison of predicted heat transfer coefficient with experimental results with Hwang and Yao for Flutec PP1, G= 26 kg/m^{2}s.

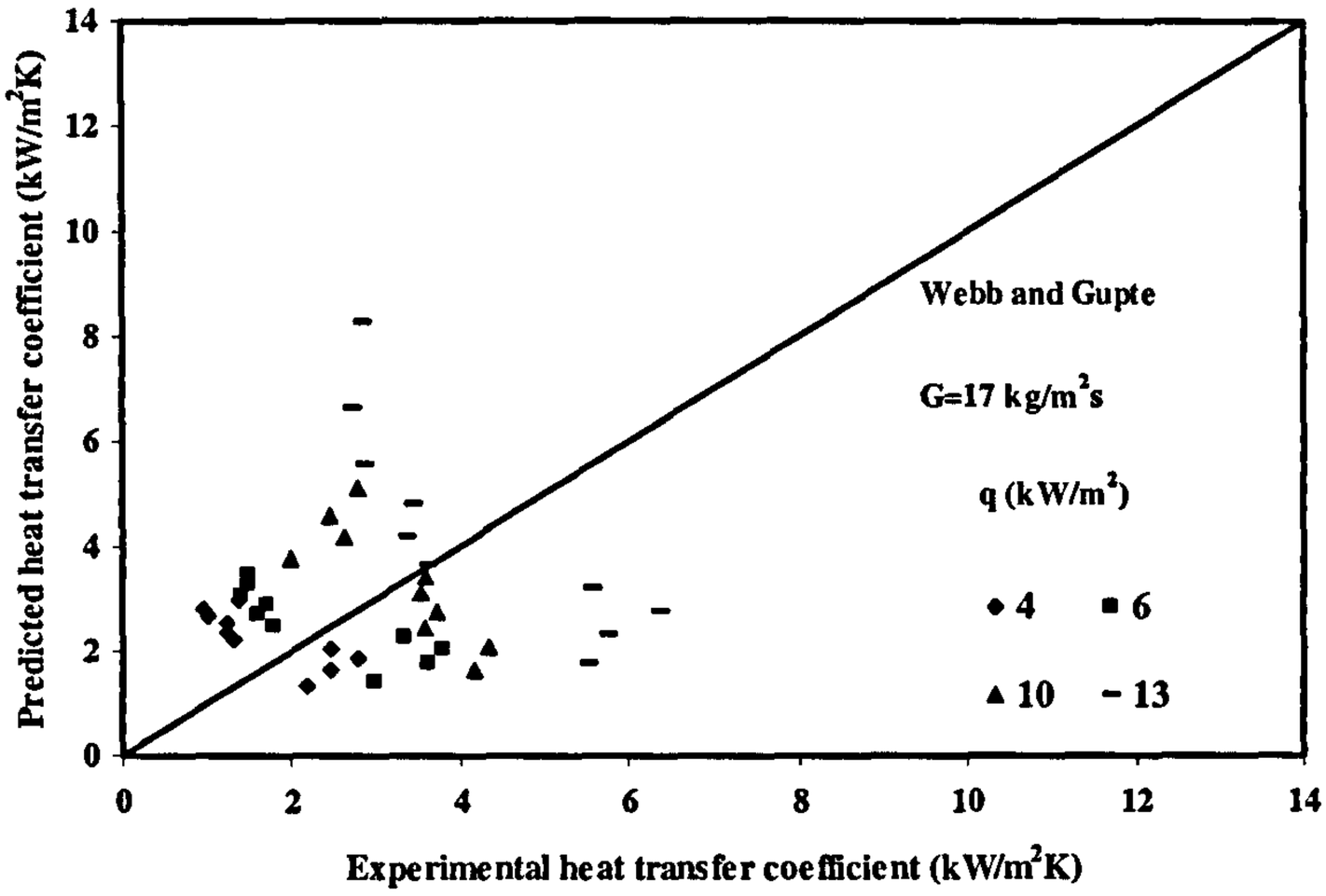

Figure D. 39 Comparison of predicted heat transfer coefficient with experimental results with Gupte and Webb for Flutec PP1, G=17 kg/m^{2}s.

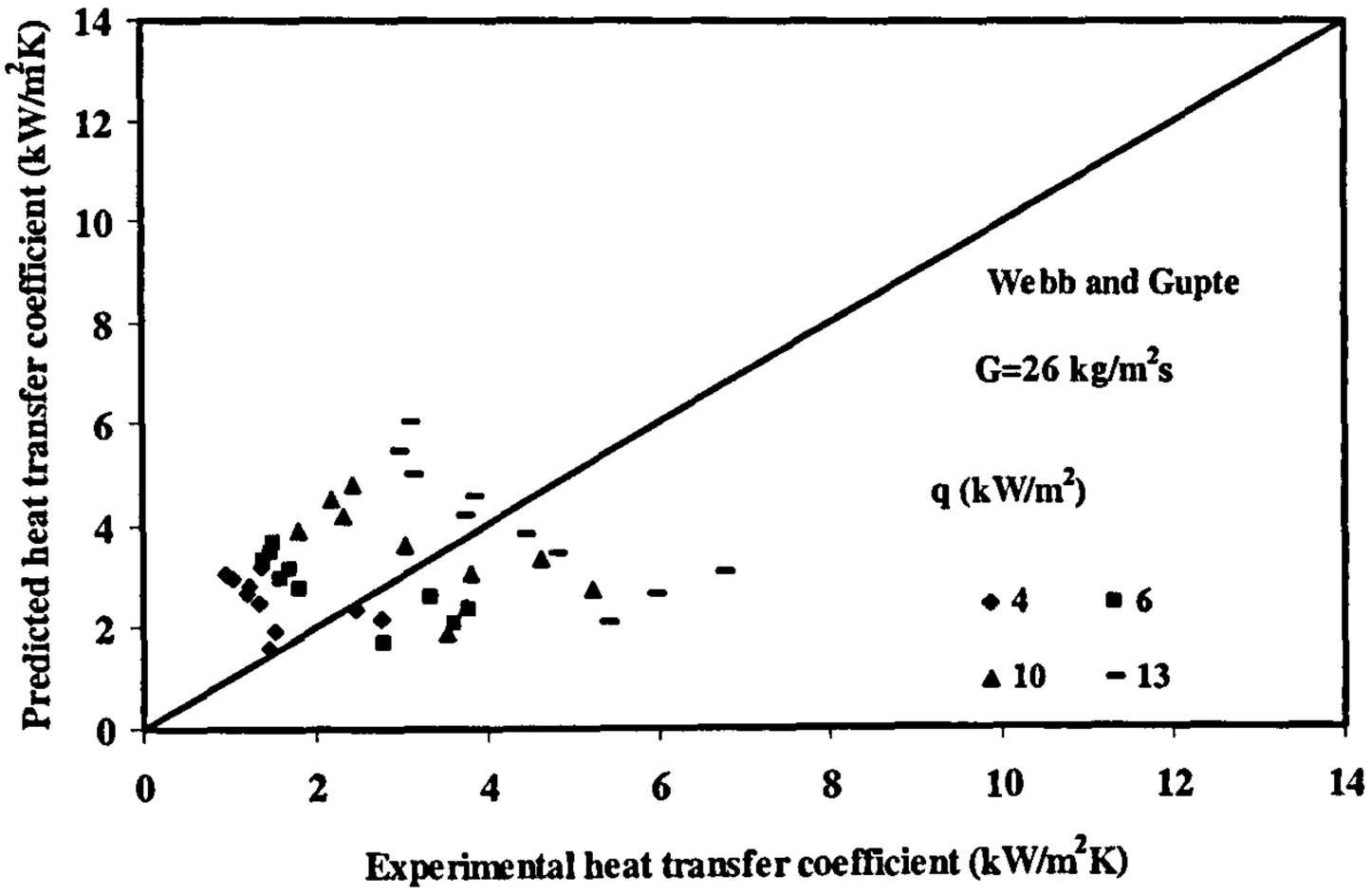

Figure D. 40 Comparison of predicted heat transfer coefficient with experimental results with Gupte and Webb for Flutec PP1, G= 26 kg/m^{2}s.

APPENDIX E: HIGH SPEED VIDEO PHOTOGRAPH

Figure E. 1 Lower tube at 127 kW/m^2 with upper at 37 kW/m^2 at t=0.0 s

Figure E. 2 Lower tube at 127 kW/m^2 with upper at 37 kW/m^2 at t=0.05 s

Figure E. 3 Lower tube at 127 kW/m^2 with upper at 37 kW/m^2 at t=0.0542 s

Figure E. 4 Lower tube at 127 kW/m^2 with upper at 37 kW/m^2 at t=0.0625 s

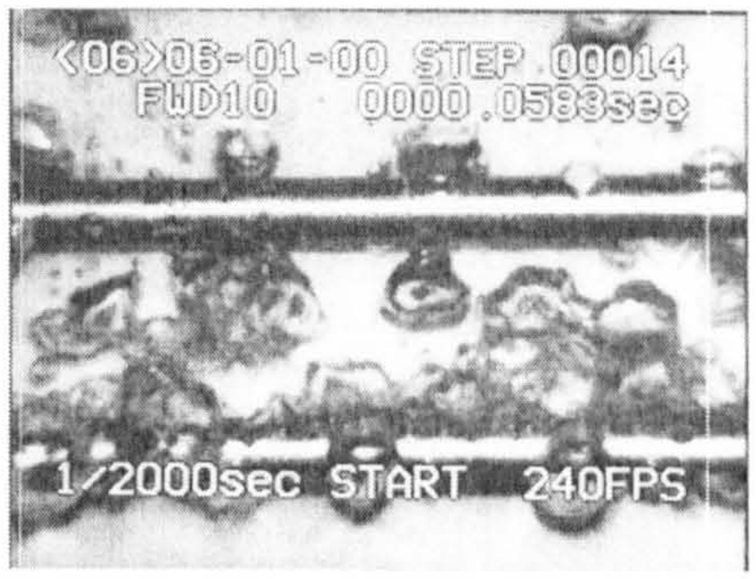

Figure E. 5 Lower tube at 169kW/m^2 with upper at 37 kW/m^2 at t=0.0583 s

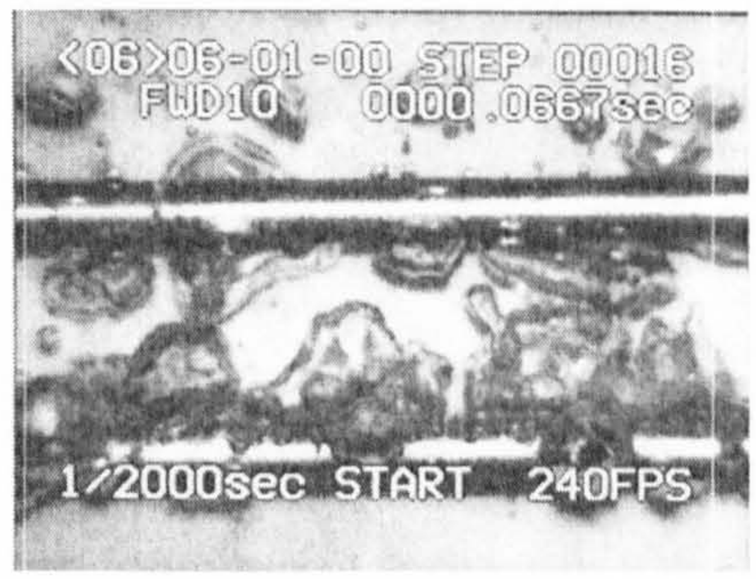

Figure E. 6 Lower tube at 169kW/m^2 with upper at 37 kW/m^2 at t=0.0667 s

Figure E. 7 Lower tube at 127 kW/m^2 with upper at 91 kW/m^2 at t=0.00 s

Figure E. 8 Lower tube at 127 kW/m^2 with upper at 91 kW/m^2 at t=0.0208 s

Figure E. 9 Lower tube at 127 kW/m^2 with upper at 91 kW/m^2 at t=0.0292 s

Figure E. 10 Lower tube at 127 kW/m^2 with upper at 91 kW/m^2 at t=0.0292 s

Figure E. 11 Lower tube at 127 kW/m^2 with upper at 91 kW/m^2 at t=0.0625 s

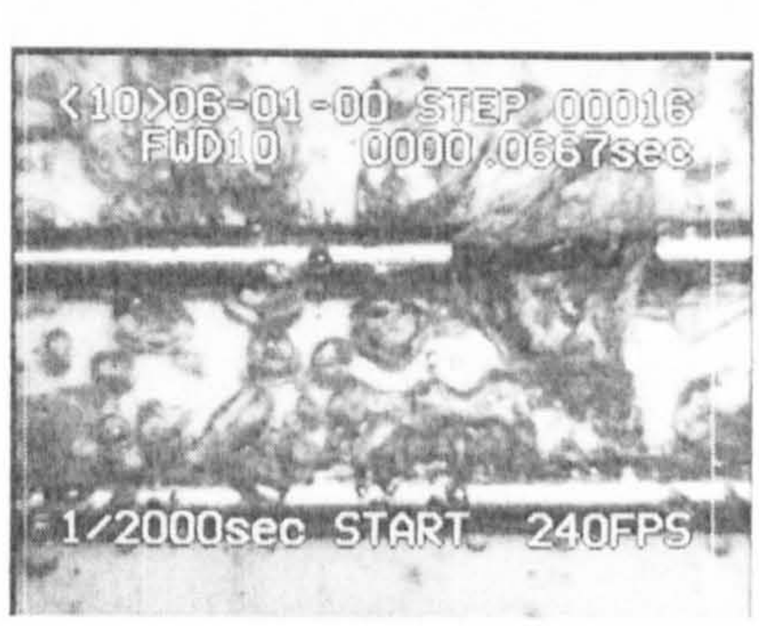

Figure E. 12 Lower tube at 127 kW/m^2 with upper at 91 kW/m^2 at t=0.0667 s

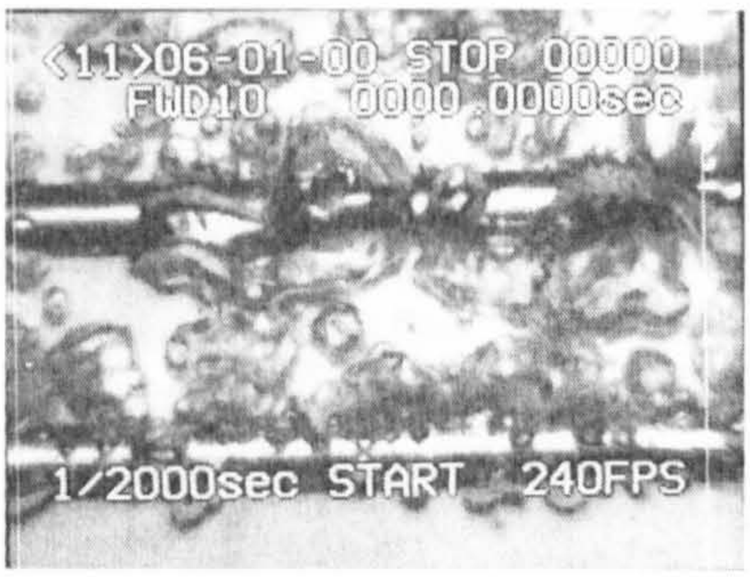

Figure E. 13 Lower tube at 169kW/m^2
with upper at 91 kW/m^2 at t=0.00s

Figure E. 14 Lower tube at 169kW/m^2
with upper at 91 kW/m^2 at t=0.0125s

Figure E. 15 Lower tube at 169 kW/m^2
with upper at 91 kW/m^2 at t=0.0167s

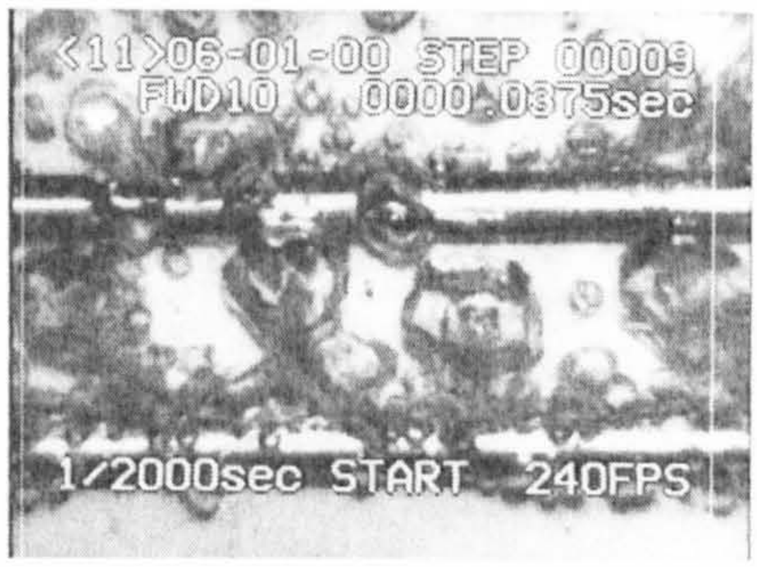

Figure E. 16 Lower tube at 169 kW/m^2
with upper at 91 kW/m^2 at t=0.0375s

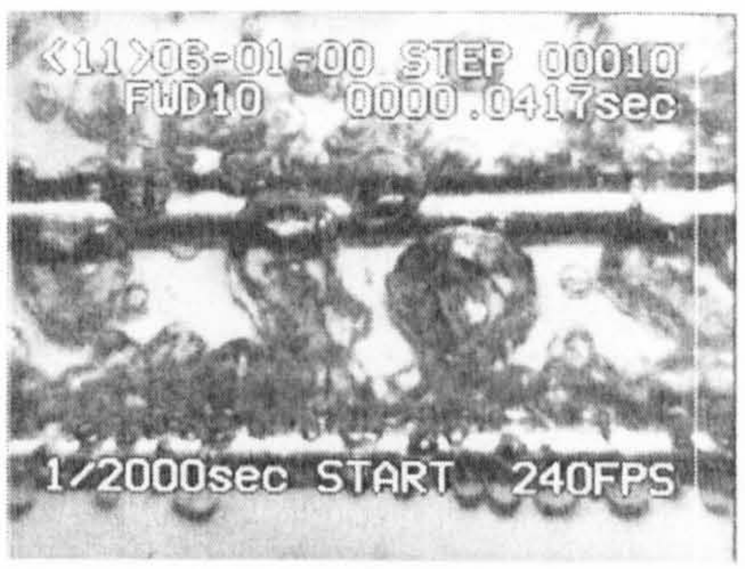

Figure E. 17 Lower tube at 169 kW/m^2
with upper at 91 kW/m^2 at t=0.0417s

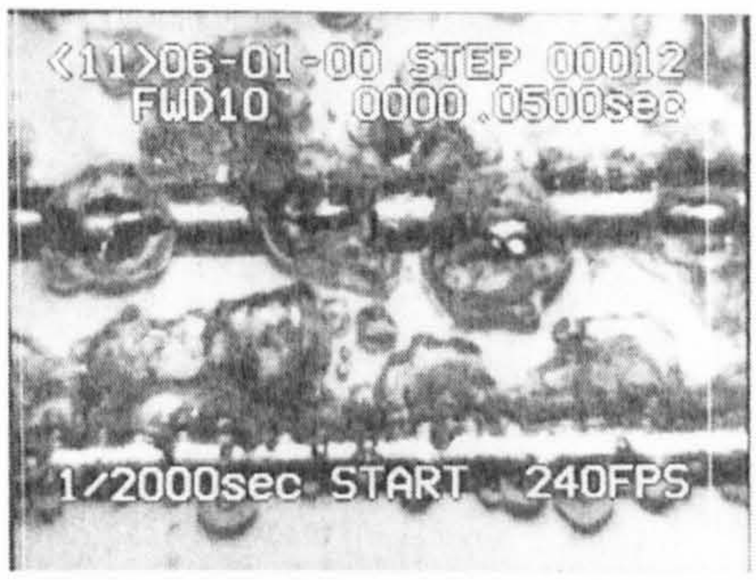

Figure E. 18 Lower tube at 169 kW/m^2
with upper at 91 kW/m^2 at t=0.050s

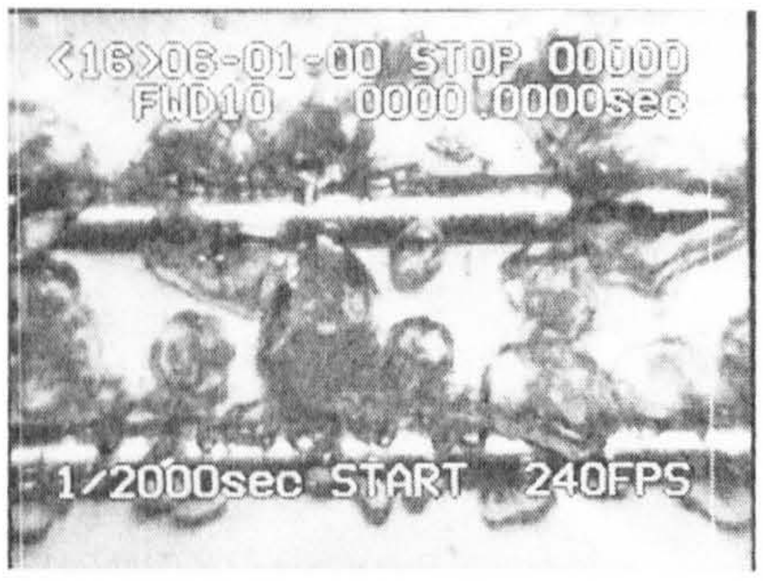

Figure E. 19 Lower tube at 169 kW/m^2 with upper at 127 kW/m^2 at t=0.00s

Figure E. 20 Lower tube at 169 kW/m^2 with upper at 127 kW/m^2 at t=0.0125s

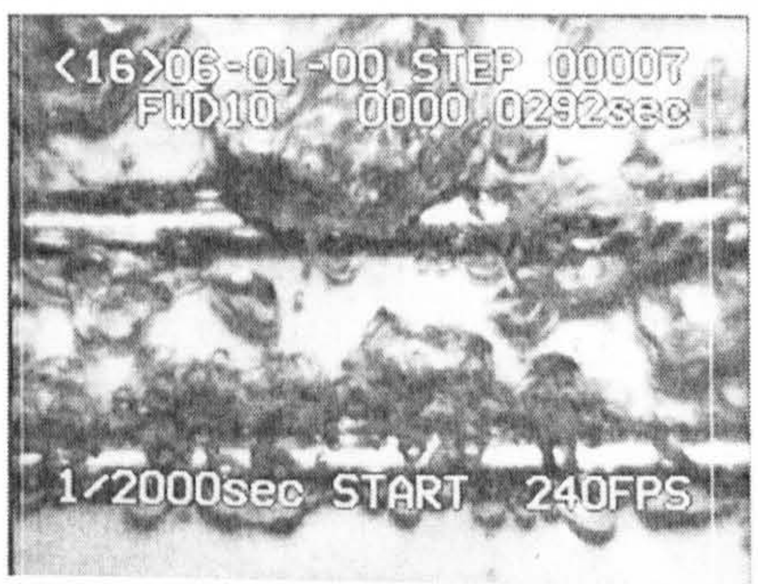

Figure E. 21 Lower tube at 169 kW/m^2 with upper at 127 kW/m^2 at t=0.0292s

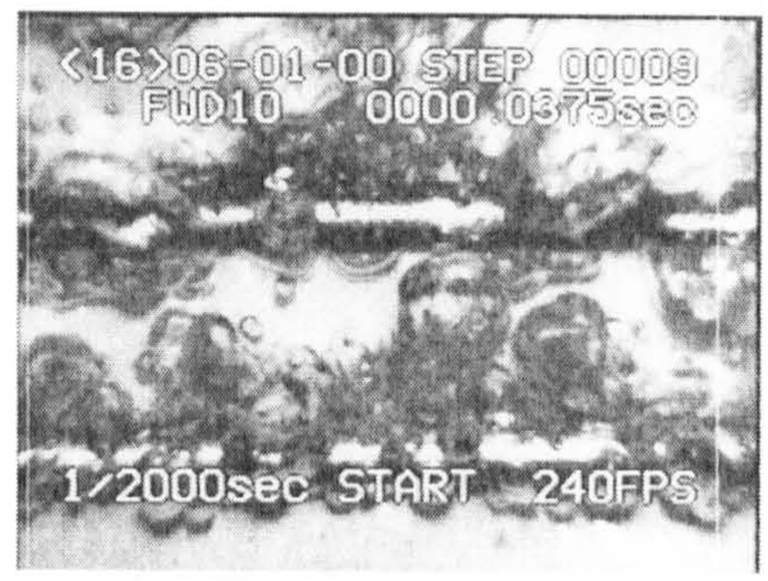

Figure E. 22 Lower tube at 169 kW/m^2 with upper at 127 kW/m^2 at t=0.0375s

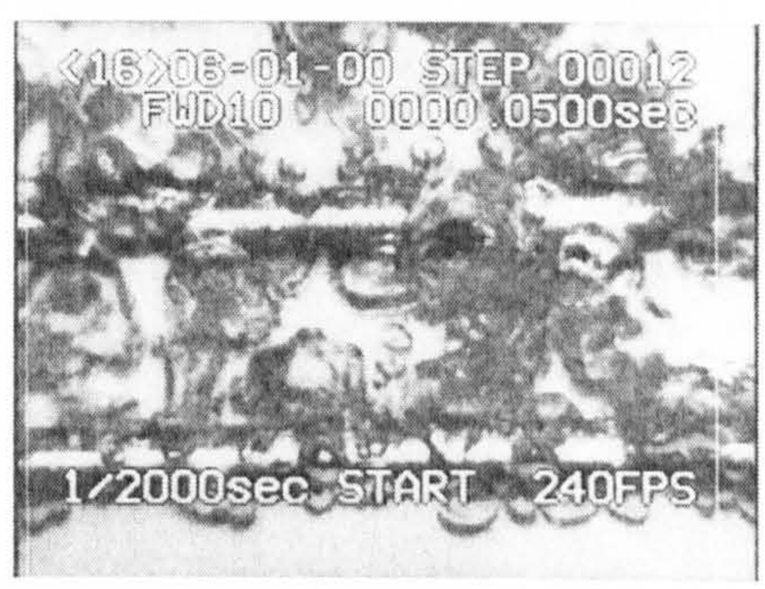

Figure E. 23 Lower tube at 169 kW/m^2 with upper at 127 kW/m^2 at t=0.05s

Figure E. 24 Lower tube at 169 kW/m^2 with upper at 127 kW/m^2 at t=0.0583s

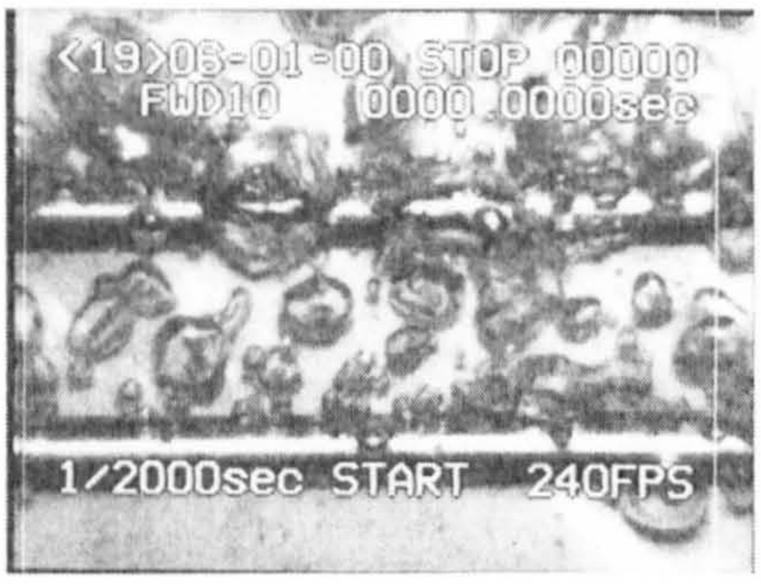

Figure E. 25 Lower tube at 91 kW/m^2 with upper at 169 kW/m^2 at t=0.00s

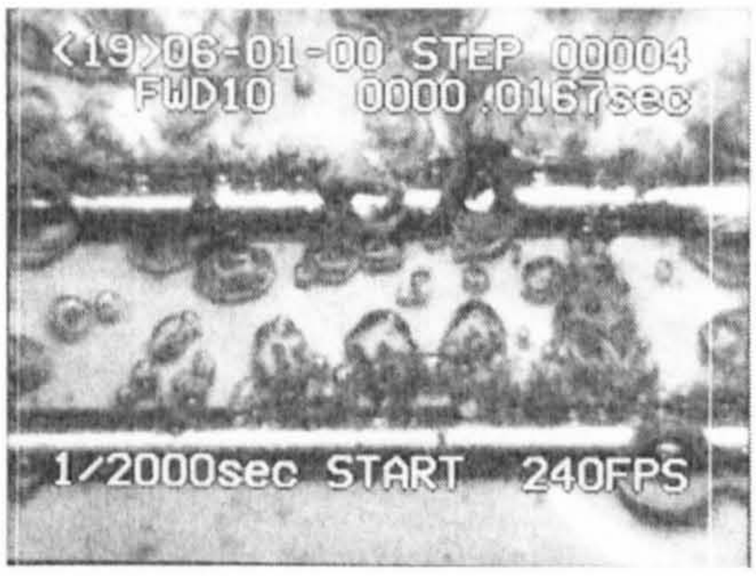

Figure E. 26 Lower tube at 91 kW/m^2 with upper at 169 kW/m^2 at t=0.0167s

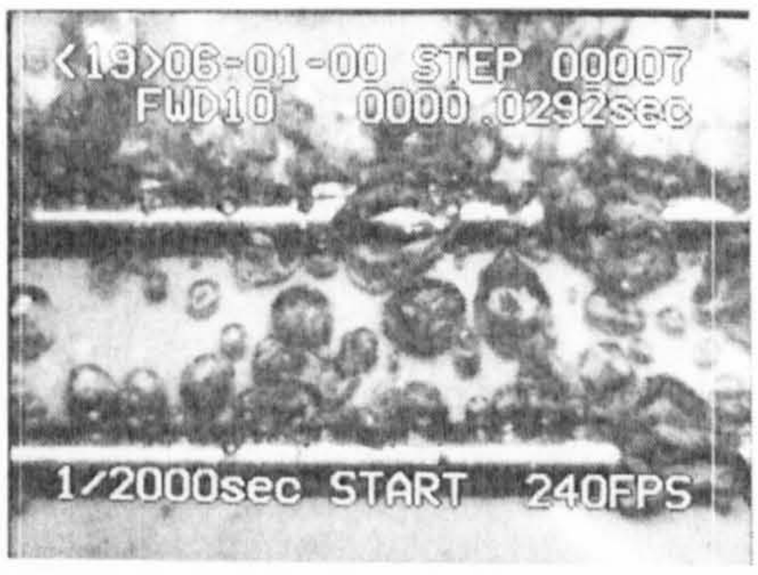

Figure E. 27 Lower tube at 91 kW/m^2 with upper at 169 kW/m^2 at t=0.0292s

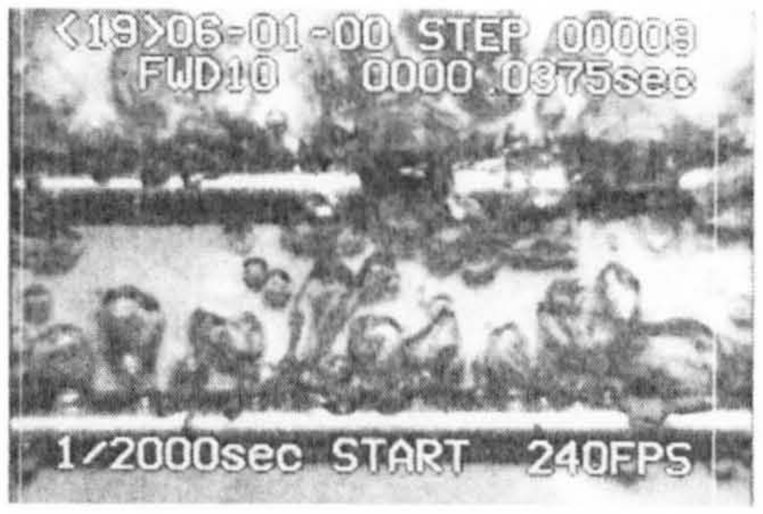

Figure E. 28 Lower tube at 91 kW/m^2 with upper at 169 kW/m^2 at t=0.0375s

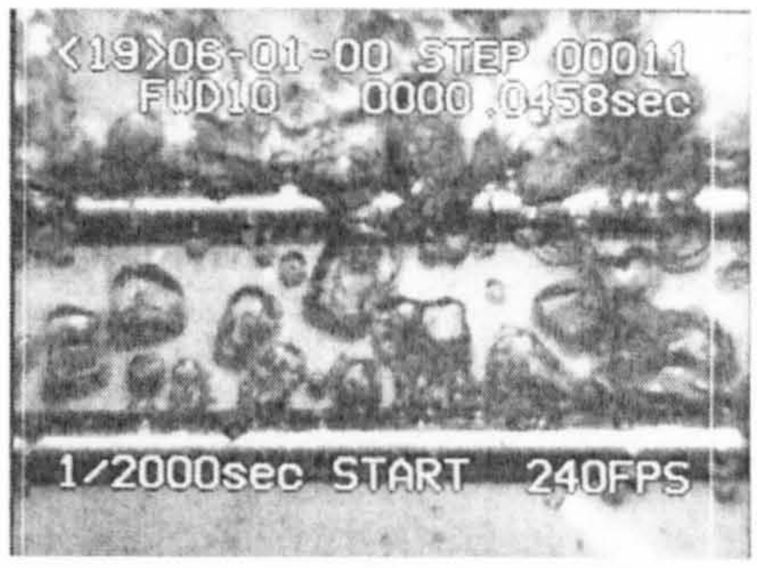

Figure E. 29 Lower tube at 91 kW/m^2 with upper at 169 kW/m^2 at t=0.0458s

Figure E. 30 Lower tube at 91 kW/m^2 with upper at 169 kW/m^2 at t=0.0542s

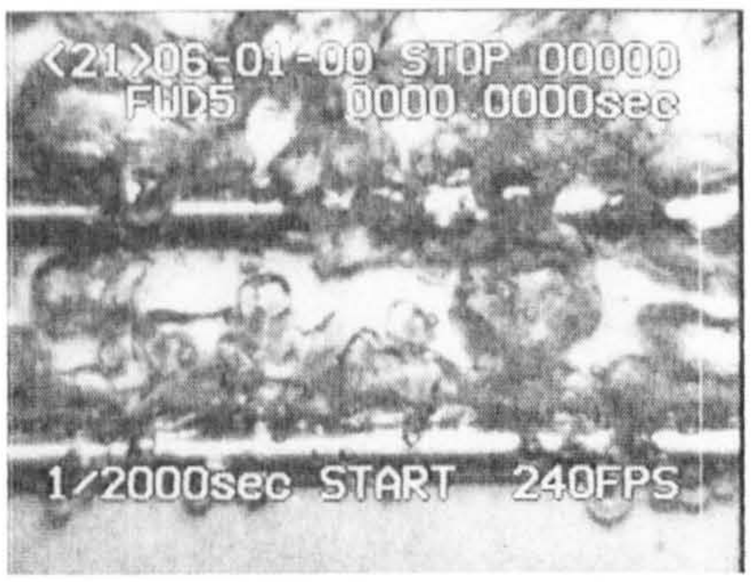

Figure E. 31 Lower tube at 169 kW/m^2 with upper at 169 kW/m^2 at t=0.00s

Figure E. 32 Lower tube at 169 kW/m^2 with upper at 169 kW/m^2 at t=0.0125s

Figure E. 33 Lower tube at 169 kW/m^2 with upper at 169 kW/m^2 at t=0.0208s

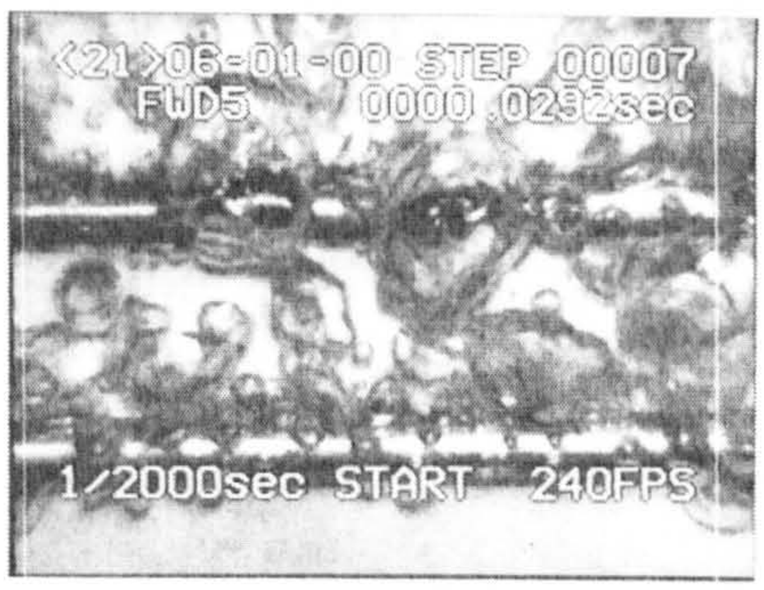

Figure E. 34 Lower tube at 169 kW/m^2 with upper at 169 kW/m^2 at t=0.0292s

Figure E. 35 Lower tube at 169 kW/m^2 with upper at 169 kW/m^2 at t=0.0375s

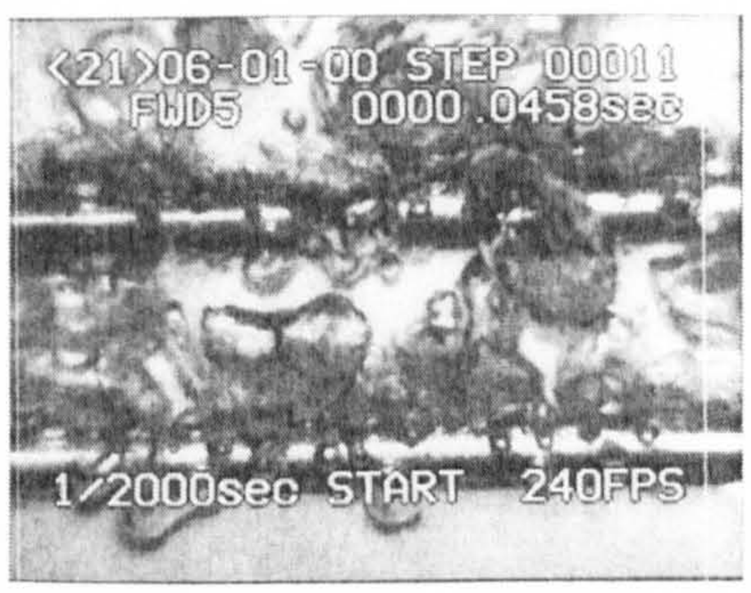

Figure E. 36 Lower tube at 169 kW/m^2 with upper at 169 kW/m^2 at t=0.0458s